Sustainable Procedures for Cellulose Derivatizations and Renewable Thermoset Materials

Zur Erlangung des akademischen Grades eines

DOKTORS DER NATURWISSENSCHAFTEN

(Dr. rer. nat.)

von der KIT-Fakultät für Chemie und Biowissenschaften

des Karlsruher Instituts für Technologie (KIT)

genehmigte

DISSERTATION

von

M. Sc. Jonas Wolfs

aus Wiesbaden

1. Referent: Prof. Dr. Michael A. R. Meier
2. Referent: Prof. Dr. Joachim Podlech

Tag der mündlichen Prüfung: 27.04.2023

Für meine Eltern,

Petra und Leo Wolfs

„Alle Wissenschaftler versuchen, an der Pyramide menschlichen Wissens weiterzubauen. Ich hoffe, dass ich einen kleinen Stein dazutun konnte.“

Stephen Hawking

Declaration of Authorship

Die vorliegende Arbeit wurde von Juni 2020 bis März 2023 unter Anleitung von Prof. Dr. Michael A. R. Meier am Karlsruher Institut für Technologie (KIT) angefertigt.

Hiermit versichere ich, dass ich die Arbeit selbständig angefertigt, nur die angegebenen Quellen und Hilfsmittel benutzt und mich keiner unzulässigen Hilfe Dritter bedient habe. Insbesondere habe ich wörtlich oder sinngemäß aus anderen Werken übernommene Inhalte als solche kenntlich gemacht. Die Satzung des Karlsruher Instituts für Technologie (KIT) zur Sicherung wissenschaftlicher Praxis habe ich beachtet. Des Weiteren erkläre ich, dass ich mich derzeit in keinem laufenden Promotionsverfahren befinde und auch keine vorausgegangenen Promotionsversuche unternommen habe. Die elektronische Version der Arbeit stimmt mit der schriftlichen Version überein und die Primärdaten sind gemäß Abs. A (6) der Regeln zur Sicherung guter wissenschaftlicher Praxis des KIT beim Institut abgegeben und archiviert.

Karlsruhe, 25.05.2023

_____

Jonas Wolfs

Danksagung

Ich möchte mich bei allen Personen bedanken, die mir diesen Weg ermöglicht haben und mich während dieser Arbeit unterstützt haben.

Zuerst möchte ich mich bei dir, **Mike**, für die Aufnahme in deinen Arbeitskreis und das entgegengebrachte Vertrauen bedanken. Du hast mich zu jeder Zeit unterstützt, sowohl fachlich als auch persönlich, wofür ich dir sehr dankbar bin. Außerdem danke ich dir für deine offene, persönliche Art, die ein sehr angenehmes und produktives Arbeitsumfeld geschaffen hat.

I would like to thank you, **Mats**, for the amazing opportunity to join your group at KTH for three months. I appreciate the great collaboration and thank you for the scientific discussions as well as the plenty information about Stockholm and Sweden in general. Additionally, I want to thank **all the people from the coatings division** for welcoming me so nicely in your group and for the great events we spent together. I also want to thank you, **Iuliana** for the great collaborative time in Stockholm and the amazing friendship that developed during that time. You really made my time in Sweden unforgettable.

Ich möchte mich auch bei dem Karlsruhe House of Young Scientists (**KHYS**) bedanken für die finanzielle Förderung meines dreimonatigen Forschungsaufenthaltes an der KTH in Stockholm.

Ich möchte mich außerdem bei allen Kollegen in meinem Arbeitskreis bedanken. Ihr habt für eine großartige Arbeitsatmosphäre gesorgt und ich bin dankbar für eure Hilfsbereitschaft zu jeder Zeit. Ihr habt meine tägliche Arbeit unglaublich bereichert. Besonders möchte ich meinen Sitznachbarn im Büro danken: **Clara**, für deine zahlreichen hilfreichen Ratschläge (sowohl fachlich, als auch überfachlich), aber auch die gemeinsamen Klimastreiks, Kulturküchenbesuche und die vielen Momente, in denen wir gemeinsam gelacht haben, **Bohni**, für deine Hilfsbereitschaft, die vielen gemeinsamen Fahrradtouren und die unzähligen Essensbestellungen nach der Arbeit. **Caitlyn,** your positive energy every morning made every day at work start in a good mood. Außerdem möchte ich dir, **Maxi**, dafür danken, dass ich damals so freundlich im Arbeitskreis

aufgenommen wurde, für die vielen Ratschläge, wenn ich nicht weiterwusste und für die Freundschaft, die sich daraus entwickelt hat mit mittlerweile unzähligen Kochabenden. Nicht zuletzt danke ich auch insbesondere **Anja**, **Michi**, **Pete**, **Roman**, **Dani**, **Luis**, **Qianyu** und **Timo** für die gemeinsame Zeit im Arbeitskreis und die vielen Dinge, die wir gemeinsam erlebt haben.

Vielen Dank an **Clara**, **Timo**, **Pete**, **Roman**, **Iuliana**, **Eren** und **Marc** für das Korrekturlesen meiner Arbeit und auch der Manuskripte während der Promotion. Außerdem möchte ich mich bei **Lisa Wanner**, **Olga Matveyeva**, **Patrick Kern** und **Fabio Reuter** für die Unterstützung im Labor bedanken und bei **Katharina Elies**, **Hans Weickenmeier**, **Daniel Zimmermann**, **Marcel Häringer**, **Karolin Kohnle**, **Birgit Huber** und **Meryem Akdemir** für die durchgeführten Messungen meiner Proben.

Besonderer Dank gebührt meinen Freunden **Fred**, **Mauro** und **Nick** für eure Unterstützung zu jeder Zeit und eure zahlreichen Besuche hier in Karlsruhe, insbesondere während der schwierigen Lockdown-Zeiten. Ihr habt mich immer bestärkt und zur richtigen Zeit für Ablenkung gesorgt, wofür ich euch sehr dankbar bin.

Bedanken möchte ich mich auch bei meiner Tante **Renate** für die Unterstützung und den Zusammenhalt während der gesamten Zeit. Außerdem möchte ich mich bei meinem Schwager **Christoph** für die wertvollen Ratschläge bedanken.

Der wichtigste Dank gilt meiner Familie, meiner Schwester **Lisa**, und vor allem meinen Eltern **Petra** und **Leo**. Ihr habt mir diesen Weg ermöglicht und ich wusste dabei, dass ich mich immer auf euch verlassen kann. Ich möchte euch von ganzem Herzen dafür danken, dass ihr mich zu jeder Zeit unterstützt habt und mir immer Rückhalt gegeben habt.

Abstract

In the last few decades, synthetic polymeric materials have fundamentally changed our daily life due to their appealing material properties in many aspects as well as their low-cost production. However, most of these polymers are entirely petroleum-based, and their production cannot be considered sustainable, not only due to the depletion of fossil resources. The utilization of renewable resources for polymer synthesis has therefore become a major interest. At the same time, several more aspects need to be considered for the design of more sustainable synthetic pathways like the prevention of waste products, the use of benign reagents, and the reduction of auxiliaries (e.g. solvents). The *Twelve Principles of Green Chemistry* summarize these factors and were used as the guiding framework in this work for the development of novel procedures for the synthesis of polymeric materials based on renewable resources.

First, a novel cellulose acetylation process using the DMSO/DBU/CO_2 switchable solvent system was developed without the need of any additional catalyst or activation step. Vinyl acetate was used as a more benign acetylation agent under mild conditions and the straightforward recyclability of all employed components was demonstrated with high recycling ratios (87.0–98.9%). Compared to the industrially applied heterogeneous *Acetic Acid Process*, less cellulose backbone degradation due to the non-acidic conditions was found (M_n = 35 kDa vs. 12 kDa) and a direct synthesis of cellulose acetates with lower degrees of substitution was possible due to the homogeneous conditions by simply adjusting the equivalents of acetylation agent.

Related to this, a method for the degree of substitution determination of cellulose acetates, butyrates, laurates, and benzoates using ATR-FTIR spectroscopy was established applying a novel non-linear correlation approach.

The DMSO/DBU/CO_2 switchable solvent system was further used for the development of a tandem reaction approach for cellulose derivatization applying a single catalyst for three consecutive transformations. In this procedure, cellulose was first solubilized and then functionalized with four different isothiocyanates, which were formed *in situ via* a catalytic sulfurization of isocyanides with elemental sulfur. This one-pot process was shown to be beneficial in terms of efficiency as well as sustainability compared to a stepwise synthesis, with recycling ratios ranging from 79.1 to 95.6% for the employed components.

By extending this approach to castor oil as a natural polyol, novel thionourethane thermoset materials could be synthesized. An additional solvent for this process could completely be prevented as castor oil was found to act in a dual role: as the solvent for the isothiocyanate formation and subsequently react quantitatively as the polyol component in the thionourethane thermoset formation. The kinetics of these two steps were studied in detail *via* real-time IR measurements, and the thermoset crosslinking step was found to be thermally triggerable after quantitative formation of the diisothiocyanate, which enabled high control over the curing process of the system.

Zusammenfassung

Synthetische Polymere haben aufgrund ihrer in vielerlei Hinsicht attraktiven Materialeigenschaften sowie ihrer kostengünstigen Herstellung in den letzten Jahrzehnten unser tägliches Leben grundlegend verändert. Die meisten dieser Polymere basieren jedoch vollständig auf Erdöl und ihre Herstellung kann aufgrund der Erschöpfung dieser fossilen Ressourcen und weiterer Aspekte nicht als nachhaltig angesehen werden. Die Nutzung nachwachsender Rohstoffe für die Polymersynthese ist daher inzwischen von besonderem Interesse. Gleichzeitig müssen mehrere weitere Aspekte für die Gestaltung nachhaltigerer Synthesewege berücksichtigt werden, wie die Vermeidung von Abfallprodukten, die Verwendung von unbedenklichen Reagenzien und die Reduzierung von Hilfsstoffen (z. B. Lösungsmitteln). In diesem Zusammenhang wurden die *zwölf Prinzipien der grünen Chemie* verfasst, welche in dieser Arbeit als Leitlinien für die Entwicklung neuartiger Verfahren zur Synthese polymerer Materialien auf Basis nachwachsender Rohstoffe dienen.

Zunächst wurde ein neuartiges Cellulose Acetylierungsverfahren unter Nutzung des DMSO/DBU/CO_2 schaltbaren Lösungsmittelsystems ohne die Notwendigkeit eines zusätzlichen Katalysators oder Aktivierungsschrittes entwickelt. Vinylacetat wurde als umweltfreundlicheres Acetylierungsmittel unter milden Bedingungen verwendet, und ein einfaches Recycling aller verwendeten Komponenten wurde mit hohen Recyclingquoten (87,0–98,9%) gezeigt. Im Vergleich zum industriell angewandten heterogenen *Eisessigverfahren* wurde ein geringerer Abbau des Celluloserückgrats aufgrund der nicht-sauren Bedingungen festgestellt (M_n = 35 kDa vs. 12 kDa). Eine direkte Synthese von Celluloseacetaten mit niedrigeren Substitutionsgraden aufgrund der homogenen Bedingungen konnte durch einfaches Anpassen der Äquivalente an Acetylierungsmittel ermöglicht werden.

Mit Bezug hierzu wurde eine neue Methode zur Bestimmung des Substitutionsgrades von Celluloseacetaten, -butyraten, -lauraten und -benzoaten mittels ATR-FTIR-Spektroskopie unter Anwendung eines neuartigen nichtlinearen Korrelationsansatzes etabliert.

Das DMSO/DBU/CO_2 schaltbare Lösungsmittel wurde des Weiteren zur Entwicklung eines Tandem-Reaktionsansatz zur Cellulose-Derivatisierung genutzt, der einen einzigen Katalysator für drei aufeinanderfolgende Umwandlungen verwendet. Bei diesem Verfahren wurde Cellulose zunächst gelöst und dann mit vier verschiedenen Isothiocyanaten funktionalisiert, die *in situ* über eine katalytische Sulfurierung von Isocyaniden mit elementarem Schwefel gebildet wurden. Dieses Eintopfverfahren erwies sich hinsichtlich Effizienz und Nachhaltigkeit als vorteilhaft gegenüber einer schrittweisen Synthese und ermöglichte Recyclingquoten der eingesetzten Komponenten von 79,1 bis 95,6%.

Durch Erweiterung dieses Ansatzes auf Rizinusöl als natürliches Polyol wurden neuartige Thionourethan-Duroplaste synthetisiert. Ähnlich wie beim vorherigen Ansatz für die Cellulosefunktionalisierung wurden die funktionellen Isothiocyanatgruppen *in situ* über eine katalytische Sulfurierung von Isocyaniden mit elementarem Schwefel erzeugt, jedoch bei diesem Ansatz ohne die Notwendigkeit eines zusätzlichen Lösungsmittels. Es wurde festgestellt, dass Rizinusöl als Lösungsmittel für die Isothiocyanatbildung fungiert und anschließend als Polyolkomponente in der Thionourethan-Duroplastbildung vollständig reagiert. Die Kinetik dieser beiden Schritte wurde im Detail durch Echtzeit-IR-Messungen untersucht, und es wurde festgestellt, dass der Duroplast-Vernetzungsschritt thermisch auslösbar ist, nachdem das Diisothiocyanat quantitativ gebildet wurde, was eine hohe Kontrolle über den Aushärtungsprozess des Systems ermöglicht.

Table of Contents

1 Introduction

The use of chemical reactions has in the past led to significant developments and increases in wealth for humans: from the discovery of fire, through metallurgy, to the synthesis of complex pharmaceuticals today. The industrial synthesis of fertilizers has helped alleviate hunger in large parts of our planet with at the same time growing population. Today, chemical technologies are being optimized to such a high level that humanity could reach unprecedented prosperity. Nowadays, in the developed part of the world, almost all basic needs are not only covered, but a wide range of luxury products, such as clothing and cosmetics, are also abundantly available. Many of these products are primarily based on a few basic chemicals produced on massive scales from petroleum. These fossil resources require millennia to regenerate, while the resulting materials often have a much shorter lifespan, sometimes as short as a few minutes for single-use plastic materials. In this context, the term “sustainability” plays a key role, which, for example, the UN Commission on Environment and Development defined in the “Brundtland Report” in 1987 as “a development that meets the needs of the present without comprising the ability of future generations to meet their own needs”.[1] The transition to sustainable development is one of the critical tasks of today’s generation. Fundamental changes must be made in almost every branch of today’s society and economy to achieve this goal. The main challenge is to find ways to sustain modern wealth while minimizing environmental impact, which demands extensive efforts in research and technological development. A transition to *Green Chemistry* is necessary concerning the chemical sector, which strives to work at the molecular level to contribute to sustainability. Especially in one of the biggest branches of the chemical industry, the production of polymeric materials (better known as plastics), significant changes need to be fulfilled as more than 90% of the produced polymers in 2021 were fossil-based.[2] Plastic materials exhibit very appealing properties, making them almost unavoidable in modern life, and are therefore produced in massive amounts (390.7 million tons in 2021).[2] For the transition to sustainable use of polymeric materials, the industrial sector has to reduce and recycle plastic materials wherever possible. People must handle plastic materials sustainably and dispose them correctly. Lastly, modern

chemistry must develop new synthetic procedures for polymeric materials by applying the principles of green chemistry, which is the main objective of this thesis.[3–5]

2 Theoretical Background

Nowadays, polymeric materials are one of the most important materials with various applications ranging from packaging to high-performance applications in lithium-ion batteries.[6–10] Due to their broad palette of applications, appealing properties, and mostly low-cost, the annual polymer production reached 390.7 million tons in 2021 and is expected to increase even further.[2] More than 90% of the produced polymers in 2021 were fossil-based, which leads to major concerns, as petroleum is not renewable and cannot be considered sustainable.[2] Therefore, more sustainable procedures and concepts, based on renewable resources and improved processes, need to be developed to meet the long-term demand and ensure wealth for humanity. The following chapters describe the connection between chemistry and sustainability, which is the basis for research on sustainable polymeric materials.

2.1 Sustainable and Green Chemistry

The field of sustainable chemistry is a comparably young branch of research, with its starting point in the late 1980s.[11] Before that time, the interest of the chemical industry sector was mainly focused on economic development with continuous increases in efficiency, scale, and output. Today's chemical sector is almost entirely based on fossil resources, as these are available in vast amounts at comparably low costs.[12–15] Fossil resources in the chemical sector are used not only as an energy source, but also as a resource: different kinds of crackers (for instance thermal or steam cracking) convert petroleum into simpler organic molecules, which are then used to synthesize nearly every bulk chemical.[16–19] These bulk chemicals are then used in different intermediates to produce almost every commercially available chemical product, ranging from plastic materials to fertilizers and from detergents to pharmaceutics.[20]

Due to the diminishing supply of these non-renewable resources and the increasing awareness of environmental aspects, a major transformation of the chemical sector is necessary to achieve sustainable development.[21–24] Therefore, the research interest in sustainable chemistry started to increase in the early 1990s with the aim to find technological solutions to counter the high dependency on fossil resources. The substantial increase in scientific publications of sustainable chemistry relative to the overall

number of publications in chemistry from 1990 to 2022 can be seen as a clear indicator of a growing interest in sustainable chemistry (**Figure 1**).

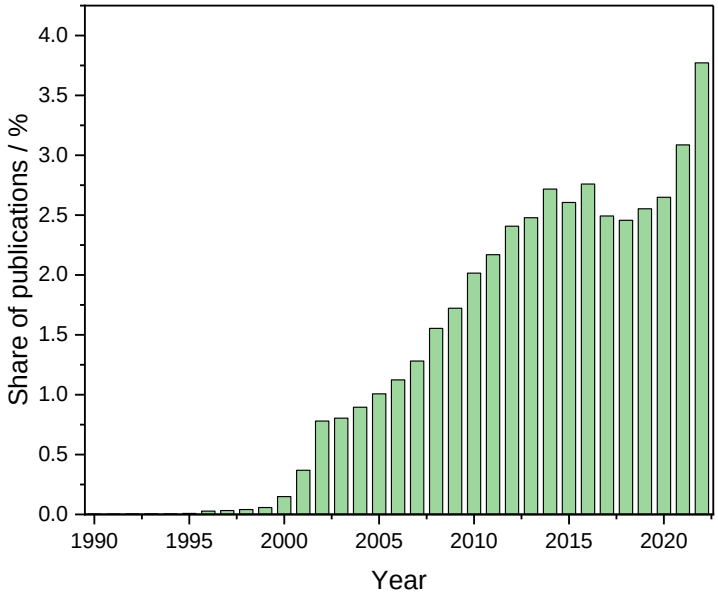

Figure 1 *Visualization of the share of publications of sustainable chemistry in the field of chemistry (according to the search result of the term "sustainable chemistry" relative to the search term "chemistry" using the search engine SciFinder®).*

The term "Green Chemistry" was defined as the "design of chemical products and processes to reduce or eliminate the use and generation of hazardous substances" in the 1990s and was substantially influenced by Paul Anastas and John C. Warner, who formulated the "Twelve Principles of Green Chemistry" (**Table 1**).[3–5] These principles were intended as a guiding framework to help chemists tune their protocols and research toward sustainability. These guidelines for green chemistry do not just encourage researchers to use renewable resources, but instead motivate them by careful planning of chemical syntheses and molecular design to reduce adverse consequences.[4] Thereby, the whole process life-cycle from the raw material used to the efficiency and safety of the reaction, as well as the safety, toxicity, and biodegradability of products and used reagents, are taken into account. The twelve principles were later summarized into the more convenient and memorable mnemonic PRODUCTIVELY by Tang *et al.*[25] Additionally, the three main points about the green chemistry framework were summarized by Anastas *et al.* in 2009 to: "1) Green Chemistry designs across all stages of the chemical life-cycle; 2) Green Chemistry seeks to design the inherent nature of the chemical products and processes to reduce their intrinsic hazard; and 3) Green Chemistry works as a cohesive system of principles or design criteria.[4]

Table 1 *The twelve principles of green chemistry as published by Anastas and Warner in 1998.*[3]

	The Twelve Principles of Green Chemistry
1	**Prevention:** It is better to prevent waste than to treat or clean up waste after it is formed.
2	**Atom Economy:** Synthetic methods should be designed to maximize the incorporation of all materials used in the process into the final product.
3	**Less Hazardous Chemical Syntheses:** Wherever practical, synthetic methodologies should be designed to use and generate substances that possess little or no toxicity to human health and environment.
4	**Designing Safer Chemicals:** Chemical products should be designed to preserve efficacy of function while reducing toxicity.
5	**Safer Solvents and Auxiliaries:** The use of auxiliary substances (e.g. solvents, separation agents, etc.) should be made unnecessary whenever possible and, when used, innocuous.
6	**Design for Energy Efficiency:** Energy requirements should be recognized for their environmental and economic impacts and should be minimized. Synthetic methods should be conducted at ambient temperature and pressure.
7	**Use of Renewable Feedstocks:** A raw material or feedstock should be renewable rather than depleting wherever technically and economically practicable.
8	**Reduce Derivatives:** Unnecessary derivatization should be minimized or avoided, if possible, because such steps require additional reagents and can generate waste.
9	**Catalysis:** Catalytic reagents are superior to stochiometric reagents.
10	**Design for Degradation:** Chemical products should be designed so that at the end of their function they break down into innocuous degradation products and do not persist in the environment.
11	**Real-Time Analysis:** Analytical methodologies need to be further developed to allow for real-time, in-process monitoring and control prior to the formation of hazardous substances.
12	**Inherently Safer Chemistry:** Substances and the form of a substance used in a chemical process should be chosen to minimize the potential for chemical accidents, including releases, explosions, and fires.

2.1.1. Metrics for Sustainable Chemistry

Sustainability depends on many factors, some of which are “soft factors”, which are difficult to be quantified. However, to compare different chemical processes with each other, it is necessary to introduce metrics that can be used to make decisions about various aspects concerning sustainability. For this reason, scales were developed to examine different sustainability factors concerning chemical procedures or chemical reactions in general.[26] B. Trost introduced the concept of atom economy (*AE*) in 1991, which focuses on the molecular level of chemical reactions to achieve sustainability.[27,28] It quantifies the atom count of the starting materials incorporated into the desired product. A reaction in which few atoms of the reactants appear in the product intrinsically produces many side products and generates waste, which makes the reaction less efficient already on the very first level, without considering other factors like solvents, energy consumption, or yield. Therefore, this concept is the first sustainability metric to look at when a novel reaction is planned.

$$AE = \frac{M_{\text{product}}}{\sum_i M_{i,\text{starting materials}}} \tag{1}$$

Consequently, an ideal reaction concerning the atom economy would have *AE* = 1 (or 100%), whereas *AE* = 0 (or 0%) means that none of the starting materials are being incorporated into the desired product.

Another commonly used metric to evaluate the sustainability of a reaction is the environmental factor (*E*-factor), which R. Sheldon introduced in 1992.[11,29] The *E*-factor is defined as the actual amount of waste produced, including everything but the desired product. It considers the yield, reagents, solvent losses, all process aids, and in principle, even fuel.[11]

$$E-\text{factor} = \frac{\sum m_{\text{starting materials}} - m_{\text{product}}}{m_{\text{product}}} \tag{2}$$

The higher the *E*-factor value, the more waste is produced in the examined reaction or process and therefore has a higher negative environmental impact. The ideal *E*-factor is *zero*, meaning no waste is generated during the reaction. Due to the practically very easy applicability of the *E*-factor, just from the knowledge of the raw materials' weight

and the weight of the products, the *E*-factor could be easily implemented in the chemical industry. Typical *E*-factors of different segments in the industry are presented in **Table 2**.

Table 2 *Typical E-factors of different segments in the chemical industry. Adapted from Sheldon et al.*[11]

Industry segment	Product / t a^{-1}	*E*-factor
Oil refining	10^6–10^8	<0.1
Bulk chemicals	10^4–10^6	<1–5
Fine chemicals	10^2–10^4	5–50
Pharmaceuticals	10–10^3	25–100

It can be concluded that, especially in the fine chemical and pharmaceutical industries, a far larger environmental impact is generated, which is a direct consequence of the products produced in these segments that are more complicated molecules requiring multi-step syntheses. The generated waste can often be reduced by developing more step economic procedures, as stated by e.g. Wender *et al.*[30] Sheldon defined the *E*-factor to have one exception from the calculation: water that is used in the process (but not water that is formed in the reaction).[11] The reason is that the inclusion of water can lead to exceptionally high *E*-factors, making meaningful comparisons of processes difficult. This can be seen in the examples of three different fermentation reactions, as presented in **Table 3**.

Table 3 *E-factors of some exemplary fermentation reactions according to Sheldon.*[31]

Product	*E*-factor	*E*-factor (incl. water)
Citric acid	1.4	17
Bioethanol	1.1	42[a]
Rec. insulin	6600	50 000

[a] Additionally includes CO_2

The major contribution to the *E*-factor often comes from solvent losses. However, in research, solvent losses (i.e., solvent recovery ratios) were often not reported, which made the comparison concerning the sustainability of newly developed procedures

almost impossible. Therefore, Roschangar *et al.* proposed two new *E*-factor derivatives: i) the “simple *E*-factor” (*sEF*, equation (*3*)), and ii) the “complete *E*-factor” (cEF, equation (*4*)).[32] The *cEF* accounts for all process materials, including water, which is different from the classic *E*-factor, and furthermore does not consider recycling due to competitive region-specific waste economics associated with energy recovery and treatment options.[32,33] The *sEF* discounts water and solvents in general, which is more appropriate for early development phase assessments and can therefore be seen as a metric on a development level between the *AE* and the *E*-factor.

$$sEF = \frac{\sum m_{\text{raw materials}} + \sum m_{\text{reagents}} - m_{\text{product}}}{m_{\text{product}}} \tag{3}$$

$$cEF = \frac{\sum m_{\text{raw materials}} + \sum m_{\text{reagents}} + \sum m_{\text{solvents}} + \sum m_{\text{water}} - m_{\text{product}}}{m_{\text{product}}} \tag{4}$$

The actual commercial *E*-factor falls somewhere between *sEF* and *cEF* and can be calculated as soon as reliable data for solvent losses and solvent recycling ratios are available.[33] Generally, the *E*-factor does not consider the toxicity of reactants or products, which can be seen as the major drawback of the *E*-factor as a sustainability metric. However, it still is a simple to apply and meaningful measure for a first basic evaluation of the efficiency and sustainability of a given process.

Several more approaches exist as extensions or alternatives to the atom economy and the *E*-factor, such as the actual atom economy (*AAE*), which corrects the *AE* by the obtained yield of the reaction.[34–36] Constable *et al.*[37] from Glaxo Smith Kline (GSK) introduced the reaction mass efficiency (*RME*), which is defined as the mass of the product obtained divided by the total mass of reactants in the stoichiometric equation (equation (*5*)) and is expressed as a percentage value.[31]

$$RME = \frac{M_{\text{product}}}{\sum_i M_{\text{I,starting materials}} \times \text{molar ratio}} \times \text{yield} \tag{5}$$

A disadvantage of the AAE and the RME compared to the AE is that they cannot be determined without any experimental work, yet they provide a more accurate, not a theorized value.

Another metric is the mass intensity (*MI*), introduced by the GSK group[38] and is sometimes also related to the process mass intensity (*PMI*). It is defined as the total mass of materials used in a process divided by the mass of the product obtained.[39] This practically results in: *MI* = *E*-factor + 1, meaning that the ideal *MI* is 1 as compared to 0 for the *E*-factor. The mass productivity was suggested by the same authors of the *MI* and is defined as the reciprocal *MI*. These alternative metrics did not establish a particular advantage over the *AE* and the *E*-factor, which is why those two measures are most widely used in the field of sustainable chemistry research. The *AE* and the *E*-factor are complementary green metrics, as the *AE* can be used as a quick tool before conducting any experiments, and the *E*-factor as a measure of the total waste formed in practice.

A comprehensive approach for the assessment of the environmental impact of a product is determined by the Life Cycle Assessment (LCA).[40–47] This concept is widely accepted in the industry and is associated with all stages of the process, from raw material extraction and processing to recycling or final disposal. The procedures for conducting LCAs are included in the environmental management section of the International Organization for Standardization (ISO). These provide the general principles and framework of the method and outline the “requirements and guidelines”. For example, in ISO 14040, LCA was defined as: “LCA studies the environmental aspects and potential impacts throughout a product's life (i.e., cradle-to-grave) from raw material acquisition through production, use, and disposal. The general categories of environmental impacts needing consideration include resource use, human health, and ecological consequences.“[48] The thorough calculation of the overall impact on the environment for a particular product using LCA is an essential measure for evaluating and optimizing manufactured products. However, such a thorough analysis is not always feasible or necessary at the research stage, which is why the *AE* and *E*-factor remain the most widely used metrics in the literature.

2.1.2. Renewable Feedstock

Today, about 13% of the consumed crude oil in the US is used to produce industrial chemicals.[49,50] This is, after the transportation sector, the largest consumer of fossil crude oil. Therefore, a transition to renewable alternatives needs to be fulfilled in the chemical industry to sustain itself in the long term. Many abundant bioresources could serve as a renewable feedstock for the chemical industry.[51] However, from a chemical perspective, most renewable feedstocks are highly functionalized molecules compared to fossil feedstocks, which mainly consist of saturated hydrocarbons. Therefore, a significant challenge in this context is to provide new tools for converting renewables into a broad palette of organic compounds.[50] One promising approach for this is a petroleum refinery-like system called “biorefinery”, which is a facility that integrates biomass conversion processes to produce fuels and different platform chemicals from biomass.[52–55] The biorefinery concept is analogous to today's petroleum refineries, which produce numerous petroleum-derived chemical products and fuels. Industrial biorefineries were identified as the most promising opportunity to create a new bio-based industry. By producing a high number of products, a biorefinery can take advantage of differences in biomass components and intermediates and maximize the value derived from the biomass feedstock.[56] Recent research focuses on biomass gasification (e.g., wood, wood waste, corn stover, switchgrass, straw, or agricultural waste) with temperature, pressure, and oxygen to produce syngas (mainly CO and H_2),[57,58] which can be used to feed the conventional resource streams of the chemical industry, for example methanol production, an important commodity chemical for producing many other goods.

The most used renewable feedstocks in the chemical industry for non-fuel applications include plant oils, polysaccharides (e.g., cellulose and starch), sugars, lignin, and others (**Scheme 1**). From these renewable raw materials, fine chemicals, pharmaceuticals, coatings, or packaging materials can be produced after the corresponding chemical processing.[58]

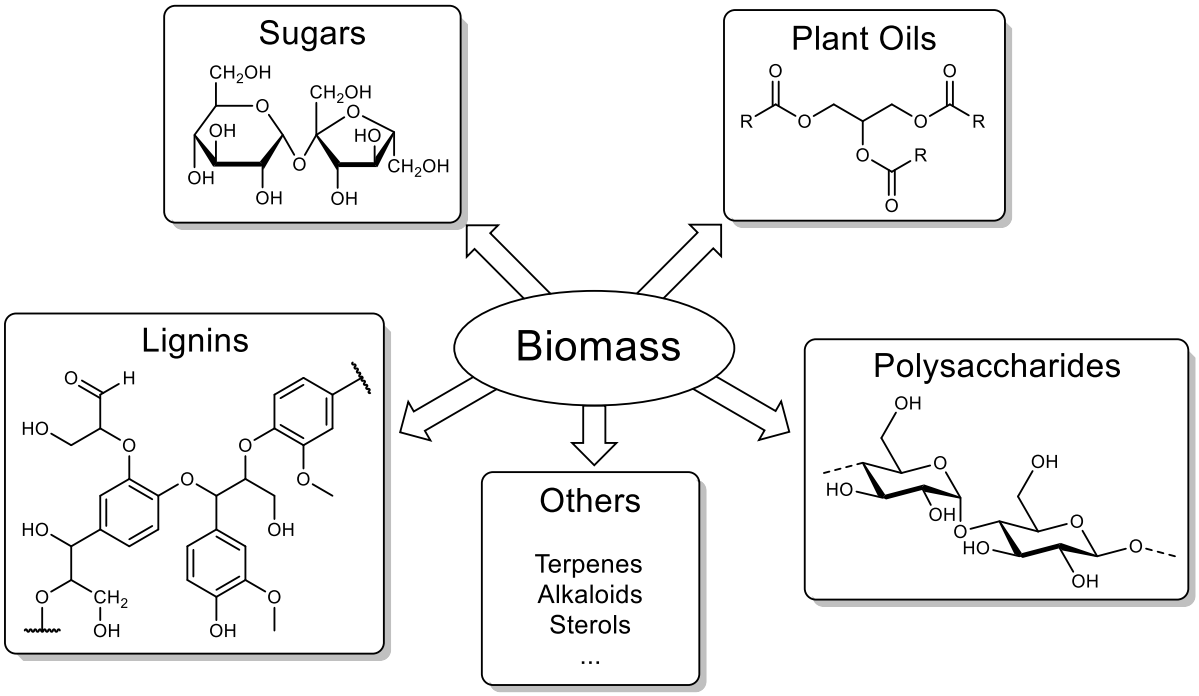

Scheme 1 *Plant-derived renewable raw materials in the chemical industry for non-fuel applications.*

Plant oils play one of the most important roles as a renewable raw material for the chemical industry (in Germany, 30% of the used renewable raw materials were plant oils).[58] These are mainly used to produce, e.g., surfactants, cosmetic products, or lubricants.[58] Plant oils are generally composed of triglycerides, which are tri-esters of glycerol and three fatty acids (**Figure 2**) with varying compositions depending on the plant as well as factors like the season, crop, and growing conditions.[59] The fatty acids can generally be categorized into two groups: saturated and unsaturated, with saturated fatty acids only containing carbon-carbon single bonds. In unsaturated fatty acids, carbon-carbon double bonds are present. The degree of unsaturation (besides other factors like the carbon chain length and the stereochemistry of the double bond) has a major influence on the physical and chemical properties.[59] Oils like coconut or palm kernel oil are mainly composed of saturated C_{12} and C_{14} fatty acids and are, therefore, most important for producing surfactants. Other oils like linseed oil are primarily composed of unsaturated fatty acids (linoleic acid and linolenic acid, **Figure 2**) and find for instance application in the chemical industry for the production of linoleum (floor covering) by oxidative polymerization in mixtures with other vegetable oils, wood flour or cork, limestone, and pigments on a carrier fabric made of jute.[60] The application of

plant oils in polymer science is expected to play an essential role during the 21st century in synthesizing polymers from renewable resources.[59,61] Plant oils and their derivatives are already used today as polyols for synthesizing polyurethanes as a substitute for petroleum-derived polyols.

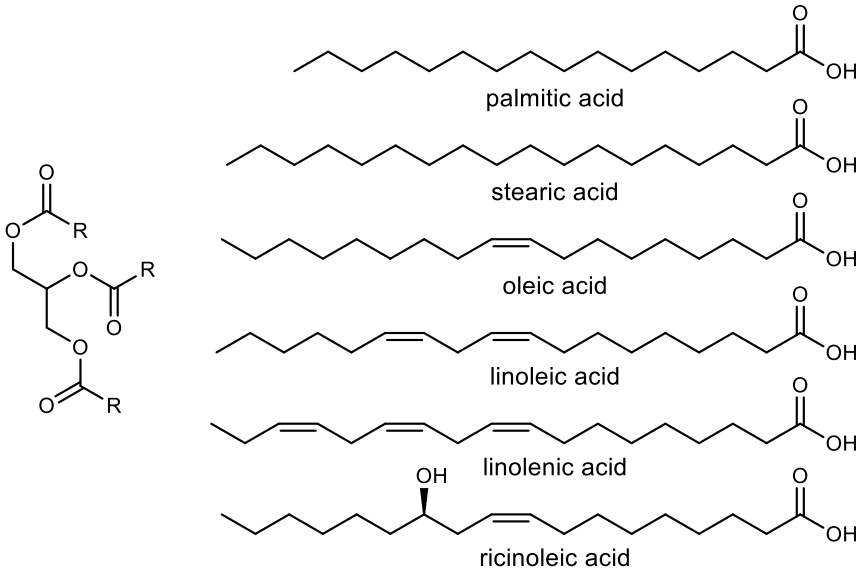

Figure 2 *Chemical structure of triglycerides with a selection of typical fatty acids occurring in natural plant oils.*

Therefore, plant oils with a high degree of unsaturation (like canola, soybean, linseed, sunflower, or corn) are epoxidized and then reacted with, e.g., methanol to prepare polyols (**Figure 3a**).[59,62] Depending on the degree of unsaturation of the individual plant oil, the resulting degree of epoxidation, and consequently the OH value, different crosslinking densities can be obtained with, e.g., methylene diphenyl isocyanate (MDI) as the diisocyanate component. This results in different T_gs and tensile strengths of the thereof derived PUs, with the general trend of higher T_g and higher tensile strength with higher crosslinking densities. Linseed oil, for example, with a comparably high degree of unsaturation, results in a polyol with comparably higher hydroxyl value and, therefore, in a thermoset with higher T_g and tensile strength if compared to other plant oil-derived polyurethane thermosets from, e.g., sunflower or canola oil based on MDI as determined by Petrović *et al*.[62] Polyols derived from plant oils are promising bio-based alternatives to existing polyols, but still two derivatization steps (epoxidation and ring-opening) are necessary to obtain the desired polyol. An alternative, not needing any prior derivatization step, is castor oil (**Figure 3b**), which can be considered the

only commercially available polyol directly produced by nature.[63] Concerning the direct utilization of castor oil as a polyol in polyurethane synthesis, it has some advantages, like water resistance and flexibility, but also disadvantages, such as comparably low functionality.[63,64] However, a higher hydroxyl value can be obtained by reacting castor oil with, e.g., glycerol, which leads to a more rigid thermoset when crosslinked with, e.g., MDI.

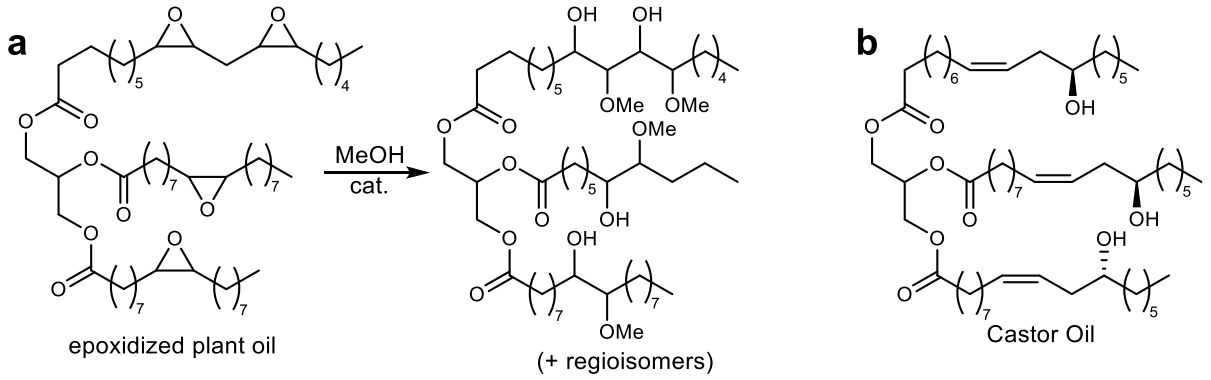

Figure 3 a *Polyol synthesis approach from epoxidized plant oil.*[62] ***b*** *Representative structure of castor oil as a triglyceride composed of three ricinoleic acid units.*

One of the most important processes using renewable resources is bioethanol production *via* fermentation. In 2021, global bioethanol production reached 27.3 billion gallons, compared to 22.4 billion gallons in 2011.[65] For the production, crops like sugar cane, hemp, corn, sugar beet, or wheat are used, which makes ethanol production compete with the food supply and raises ethical conflicts.[66] Consequently, research focuses on the implementation of lignocellulosic substances for the production of bioethanol from agricultural wastes. However, this process still has several challenges, as the material must be appropriately pretreated to ensure a complete delignification and an effective fermentation process. Nevertheless, the use of lignocellulosic materials for bioethanol production has great potential. It has been estimated that 442 billion liters of bioethanol could be produced from lignocellulosic biomass and that total crop residue and wasted crops can produce 491 billion liters of bioethanol per year, which is about 16 times more than the world bioethanol production now.[67,68] Bioethanol is today mainly used as a fuel additive, but it also shows high potential as a platform molecule in the chemical industry. For instance, it can be used in other fermentative processes to produce acetic acid or in a dehydration reaction for the production of ethylene.[69,70] In countries with cheap bioethanol availability, ethylene is already today produced in relevant

amounts by dehydration. Still, steam cracking of petroleum is by far the primary source of ethylene today.[71] Many industrial processes exist with excellent efficiencies, but the starting materials are mostly petroleum-derived, which makes the overall procedure unsustainable. One example is the production of vinyl acetate (**Scheme 2**).

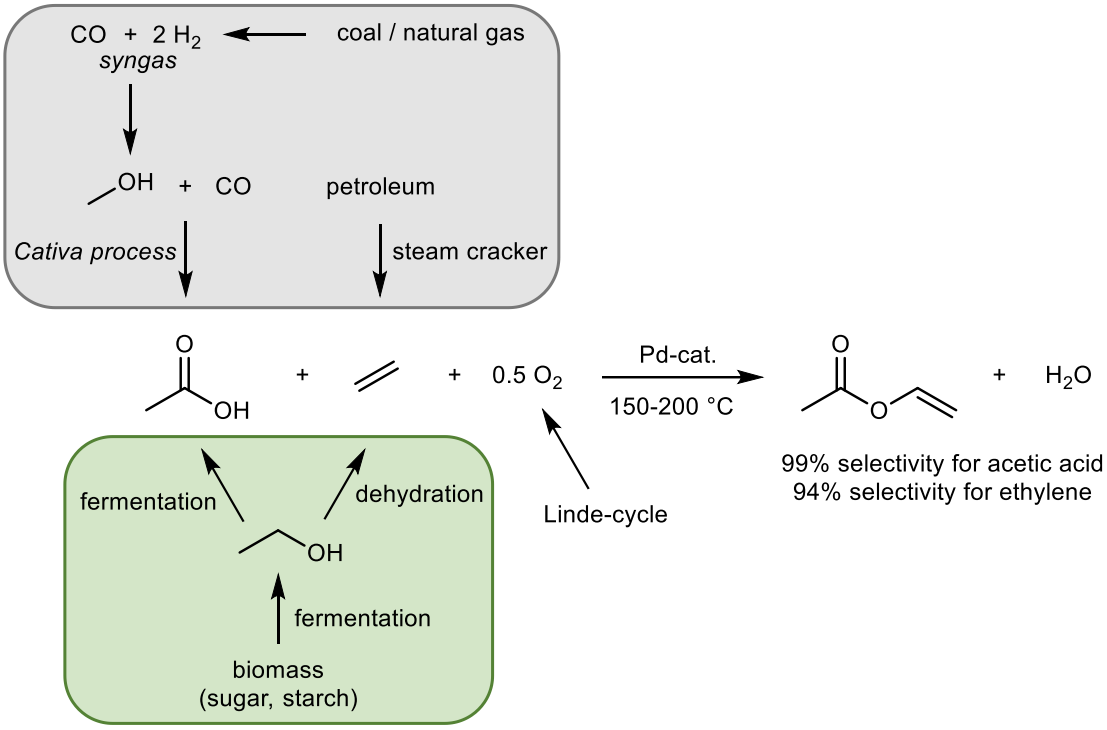

Scheme 2 *Industrial synthesis of vinyl acetate from fossil resources (red) and possibilities from renewable resources (green).*[69–73]

It is mainly produced by the ethylene-based process (ca. 70% of worldwide production).[72] In this gas-phase process, ethylene reacts with acetic acid and oxygen in a palladium catalyst-containing fixed-bed reactor, resulting in vinyl acetate and water with a selectivity of 94% for ethylene and 98–99% for acetic acid.[71,72] This makes vinyl acetate production very efficient, but as described before, ethylene and acetic acid also need to be originated from a sustainable resource for an entirely sustainable process. However, the industry chooses the cheapest way to produce these two compounds, which is mainly the carbonylation of methanol for acetic acid and steam cracking for ethylene.[69,70] With methanol mainly produced from syngas,[73] the industrial synthesis of vinyl acetate today is entirely based on fossil resources (red box in **Scheme 2**). However, with the described potential of biomass conversion to platform molecules like acetic acid or ethylene, many processes, like the production of vinyl acetate, can be transformed entirely bio-based.

2.2 Cellulose

Cellulose is the most abundant biopolymer on earth and is considered an almost inexhaustible source of biomass, with an annual production of approximately 1.5×10^{12} tons.[74] It is formed by the repeated connection of D-glucose units, making it a highly functionalized, linear, rigid homopolymer, which is hydrophilic, chiral, biodegradable, and possible to be chemically modified in numerous ways.[75]

Cellulose was isolated for the first time by the French chemist Anselme Payen in 1837.[74,76] He described the biopolymer as the resistant fibrous solid that remains after treatment of various plant tissues with acids and ammonia, followed by the extraction with water, alcohol, and ether. Subsequent employment of elemental analysis yielded the molecular formula $C_6H_{12}O_5$, thus determining the isomerism to starch. The structure was then confirmed by Dumas *et al.* in 1839 and named "cellulose" due to its property being the main constituent of wooden cells (French: *cellules*).[77] Cellulose being a polymer was first elucidated by Hermann Staudinger in 1920.[78] He found, by acetylation and deacetylation of cellulose, that its structure does not just consist of an aggregation of glucose units, instead being linked together covalently forming long molecular chains (polymers). The cellulose structure is composed of β-1,4-linked D-glucopyranose units (**Figure 4**) with *n* representing the degree of polymerization.

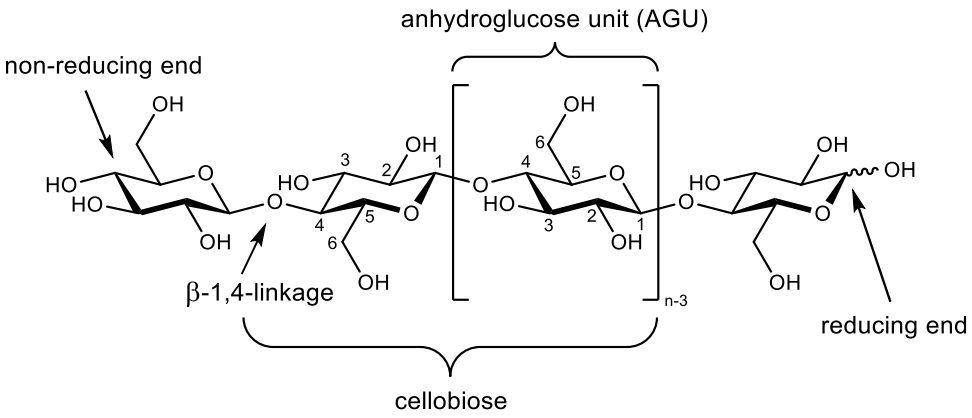

Figure 4 *Chemical structure of cellulose.*

The β-1,4-linkage between the monomeric units is an acetal moiety, which enables the chemical categorization of cellulose as a polyacetal. The repeating unit of cellulose, i.e. β-1,4-linked D-glucopyranose units, are usually termed anhydroglucose unit (AGU), as two glucose units are β-1,4-connected *via* a condensation reaction under elimination

of one equivalent water. The polymeric structure of cellulose comprises two ends: one non-reducing end and one reducing end. The reducing end is the hemiacetal moiety, which is in equilibrium with the corresponding aldehyde in its ring-opened form and can therefore be oxidized (giving it the name reducing end). The non-reducing end is the 4-position of a cyclic D-glucopyranose unit bearing a secondary alcohol functional group and cannot ring-open in this position. The reducing end allows for a selective chemical modification, a so-called end-functionalization primarily investigated with cellulose nanocrystals (CNCs).[79–81] The degree of polymerization (DP) of cellulose (*n* in **Figure 4**) varies with the origin and treatment of the raw material (some typical values are presented in **Table 4**). From *in vitro* synthesized cellulose samples, it was found that β-1,4-linked D-glucopyranose units start to offer the characteristic properties of cellulose at a DP between 20–30.[74,82]

Table 4 *Typical DP for different cellulose types as reported by Klemm et al.*[74]

Cellulose type	Degree of polymerization (DP)
Cotton	800–10 000
Bacterial cellulose	800–10 000
Wood pulp	300–1 700
Regenerate fibers	250–500
Microcrystalline cellulose	150–300

Microcrystalline cellulose can be produced from other types of cellulose by treatment with mineral acids.[83–86] The linking acetal moiety in cellulose is susceptible to hydrolysis under acidic conditions, leading to partial depolymerization under the abovementioned conditions. However, due to the strong intra- and intermolecular interactions *via* hydrogen bonds between the polymer backbones, cellulose is remarkably resistant to hydrolysis, even under acidic conditions. Therefore, partial cleavage of the acetal moieties preferentially takes place in the amorphous regions compared to the crystalline regions, as the intra- and intermolecular interactions *via* hydrogen bonds are weaker in the amorphous regions. Accordingly, the previously mentioned depolymerization in the amorphous regions of cellulose under acidic conditions results in a relative increase in crystallinity. Therefore, microcrystalline cellulose has a lower DP and a higher degree of crystallinity compared to natural sources of cellulose. Due to its more defined

structure, higher homogeneity over different batches, and high purity, microcrystalline cellulose has become an important model cellulose source in research. Nowadays, four general pathways for the synthesis of cellulose exist, which are the *in vivo* synthesis from plants, the *in vivo* synthesis from bacteria, algae, and fungi, as well as two different *in vitro* synthesis approaches, which are the biotechnological synthesis using recombinant enzymes, and the fully synthetic approach *via* ring-opening polymerizations (**Scheme 3**).

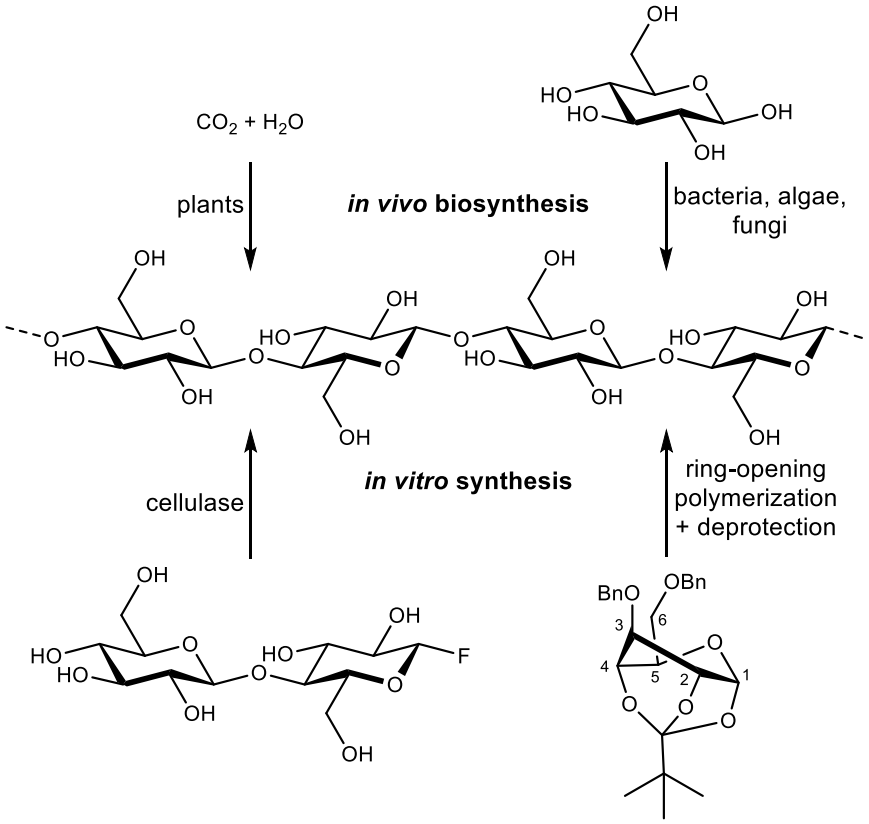

Scheme 3 *Four general pathways for the synthesis of cellulose. Adapted from Klemm et al.*[74]

The most dominant pathway is the synthesis of cellulose from plants, especially wood, where it forms a natural composite material with lignin and other polysaccharides like hemicellulose. In the seed hairs of cotton, cellulose is naturally available in its almost pure form. Certain bacteria, algae, and fungi were found to produce cellulose, and research over the last decades showed that cellulose biosynthesis had been part of cyanobacteria metabolism for over 3.5 billion years.[74,87,88] The first *in vitro* synthesis of cellulose *via* a cellulase-catalyzed mechanism was reported in 1991 by Kobayashi *et al.* based on cellobiosyl fluoride (**Scheme 3**).[89–91] The first fully chemosynthetic approach

towards cellulose was carried out *via* ring-opening polymerization of a benzyl protected α-D-glucose orthopivalate in 1996 (**Scheme 3**).[92]

2.2.1. Cellulose as a Raw Material

The predominant occurrence of cellulose is in the form of wood combined with other polysaccharides (e.g., hemicelluloses) and lignin at varying amounts. An exemplary representation of two common types of hemicellulose and an idealized structure of lignin is shown in **Scheme 4**b.

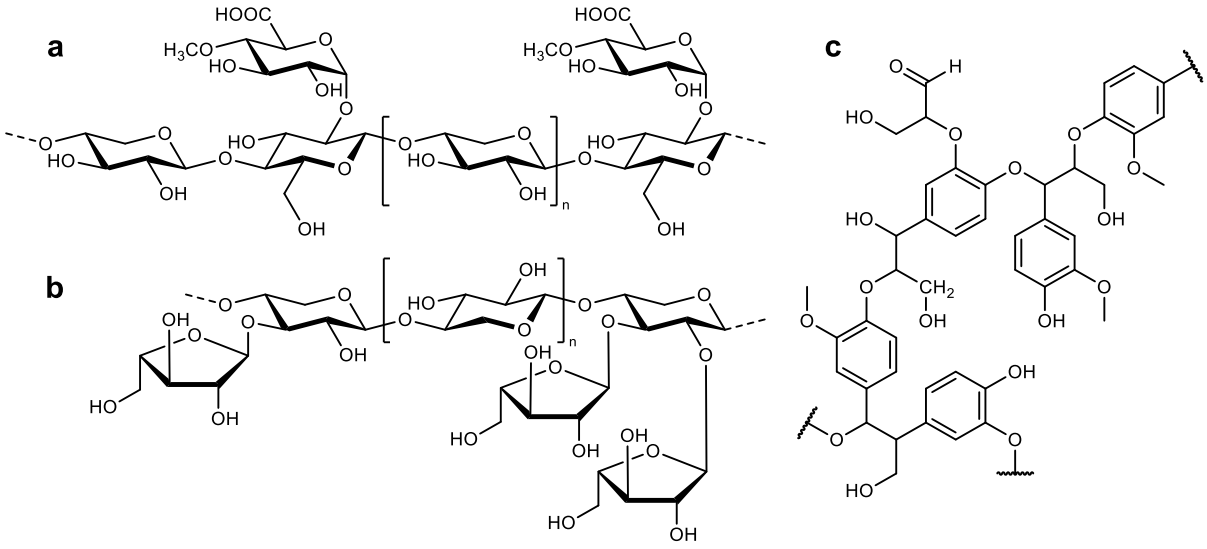

Scheme 4 a+b *Structure of two representative types of hemicellulose, 4-O-methylglucoronoxylan (**a**), and arabinoxylan (**b**), as reported by Heinze et al.[93]* ***c*** *Representative, idealized excerpt of a lignin structure.*

Cellulose is also present in many other sources, like agricultural residues, grasses, water plants, and basically every other plant. This makes cellulose a promising raw material, as it is not competing with food or feed. However, wood pulp remains the primary source for processing cellulose, which is mainly used for producing paper and cardboard.[74] Approximately 6% of the total isolated cellulose pulp (around 9.2 million tons in 2021) was used to synthesize cellulose derivatives, like cellulose esters and cellulose ethers or applied for cellulose regeneration processes to produce regenerate fibers and films.[94] Cellulose in its unmodified form is an environmentally friendly raw material due to its bio-compatibility, bio-degradability, and the fact that it is completely bio-based – properties that most other polymeric materials nowadays do not fulfill,

leading to environmental challenges. Different sources and their composition concerning hemicellulose and lignin content are shown in **Table 5**. Cotton has the highest cellulose content with marginal amounts of lignin and hemicellulose. This considerably facilitates the purification and isolation process and is, therefore, one of the preferred sources in theory. However, the high land and water demand for cotton cultivation makes it unattractive to isolate cellulose, especially considering that numerous agricultural residues such as rice, wheat straw or sugarcane bagasse exist, which can also be used for the isolation of cellulose. These are produced in large amounts and can be considered as abundant waste materials.

Table 5 *Composition of some typical cellulose-containing raw materials, adapted from Heinze et al.*[93]

Source	Cellulose (%)	Lignin (%)	Hemicellulose (%)	Extracts (%)
Hardwood	43–47	16–24	23–25	2–8
Softwood	40–44	25–32	25–29	1–5
Bagasse	40	20	30	10
Cotton	95	1	2	0.4
Hemp	70	6	22	2
Jute	71	13	14	2
Sisal	73	11	14	2
Rice straw	43	20	33	<1
Wheat straw	58–73	16–23	25–31	3–5.8

Implementing the mentioned waste materials as a resource for isolating cellulose enables the production of materials with considerably higher economic value. Cellulose can also be employed as a raw material for producing different fine chemicals, biofuels, and platform molecules in biorefineries (**Scheme 5**). These chemo-catalytical conversions occur via direct liquefaction, gasification, aqueous-phase reforming, or pyrolysis.[95] A major challenge remains the targeted synthesis of these compounds, as a mixture of many different compounds is usually obtained, which mostly leads to a demanding separation procedure. Therefore, much research is performed on this topic to develop selective processes with an emerging trend in integrating catalytic thermochemical conversions with selective hydrogenolysis and hydrogenation.[95–98] One example of a comparably selective process is the production of levoglucosenone as a platform

chemical (**Scheme 5**). It was discovered as a product of the thermal decomposition of cellulose in 1970.[99] Its production is now optimized to yields of up to 51% *via* solvent-assisted pyrolysis in the presence of sulfuric acid.[100] The production of levoglucosenone from a wide range of cellulosic biomass was commercialized by the Australian company Circa in the Furacell process. Huber *et al*. presented a method for synthesizing 1,6-hexanediol from levoglucosenone, which can be used as a building block for, e.g., the synthesis of polyesters, polycarbonates, or polyurethanes.[101]

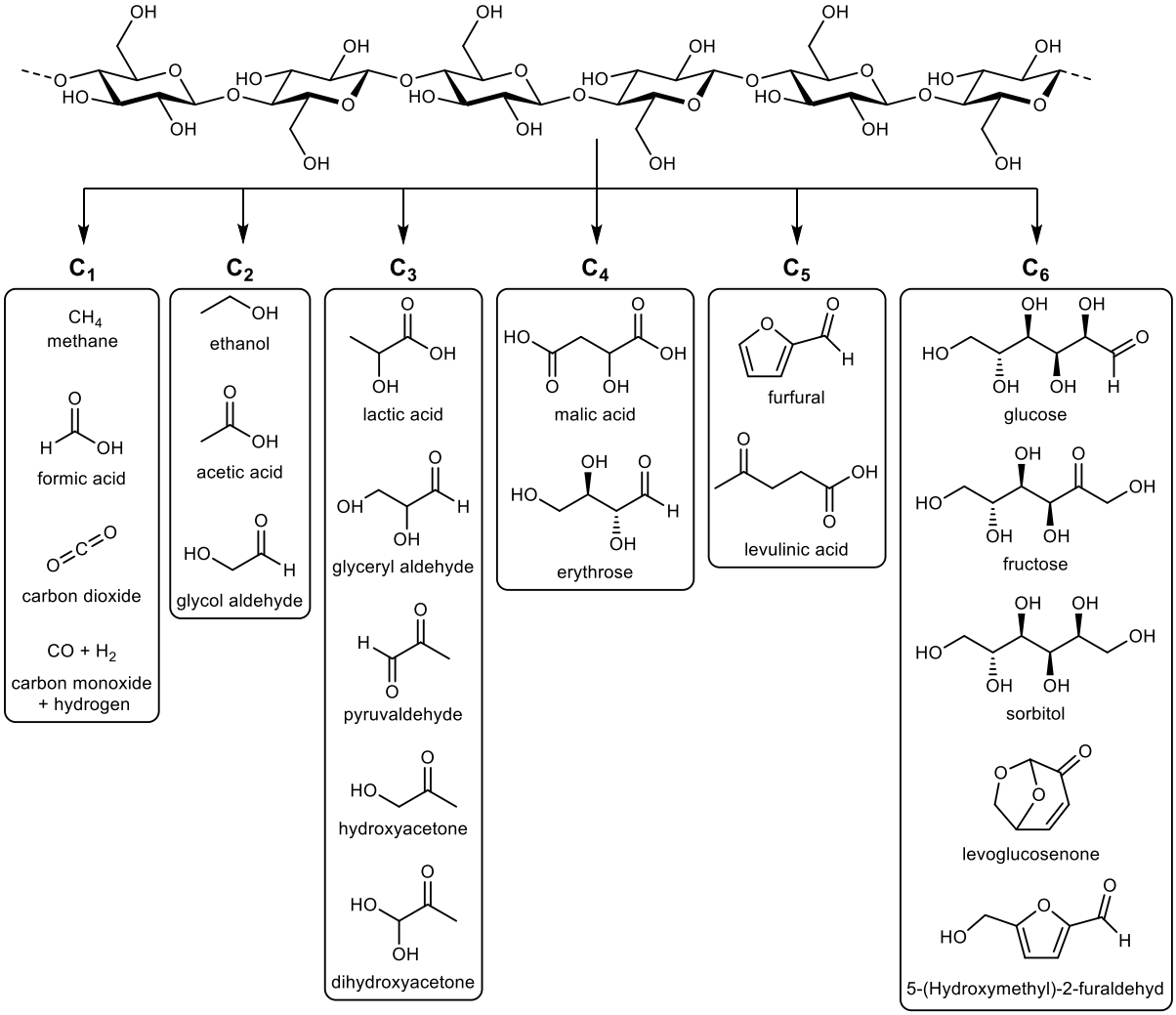

Scheme 5 *Possible platform molecules derived from cellulose or lignocellulosic biomass. Partially adapted from Beltramini et al.[95]*

All the described properties of cellulose merged with its manifold potential uses (directly or transformed into smaller building blocks in biorefineries) renders cellulose a promising raw material for the increasing demand for environmentally friendly and bio-based materials.

2.2.2. Isolation of Cellulose

The most common source for cellulose remains wood, and to isolate the cellulose fibers, the hemicellulose, and lignin must be removed. This is performed in so-called pulping procedures, either mechanically or by chemical treatments. In both cases, the wood is first chopped into smaller wood chips, which can then be used as an easier-to-handle raw material with increased surface area.[93]

In mechanical pulping procedures, the wood is usually first treated with steam, and then the fibrous material is separated by abrasive refining or grinding. However, this method cannot remove lignin quantitatively, which influences the overall properties of the pulp, i.e. its color. The mechanical pulp can be treated with bleach to increase brightness, but it remains less light stable and tends to yellowing due to the oxidation of the remaining lignin. This pulp is, therefore, primarily used for paper with a relatively short lifespan, like newspapers or brochures.

In chemical pulping, the cellulose is isolated by making the other components soluble, which can then be removed. Nowadays, chemical pulping is the dominant method, accounting for 77% of the globally produced cellulose pulp.[102] The most important chemical pulping processes are the Kraft pulping, sulfite pulping, and soda pulping, out of which the Kraft pulping is the dominant method with 95%.[102] The reason is that pulp from the Kraft process results in stronger fibers, is less dependent on the wood raw material, and has an efficient chemical recovery process. In a typical procedure, the wood chips are heated in an aqueous solution of sodium hydroxide, and sodium sulfide ("white liquor") to a cooking temperature of around 170 °C for 3–4 h.[102] Lignin is extensively degraded under these conditions, resulting in water-soluble compounds, which can then be removed from the remaining solid. The first step of the main degradation reaction of lignin in Kraft pulping is the formation of a quinone methide structure (**Scheme 6**). Subsequently, a hydrogen sulfide anion adds to the quinone methide intermediate as a strong nucleophile and then initiates the cleavage of the β-*O*-4'-bond under the formation of a thiirane (**Scheme 6**).[102]

Pulps of high purity are required to produce cellulose derivatives or cellulose regenerate fibers. This highly pure pulp is called dissolving pulp and is composed of more than

90% pure cellulose. Wood-derived cellulose accounts for about 85–88% of dissolving pulp; the majority of the rest comes from cotton.[93]

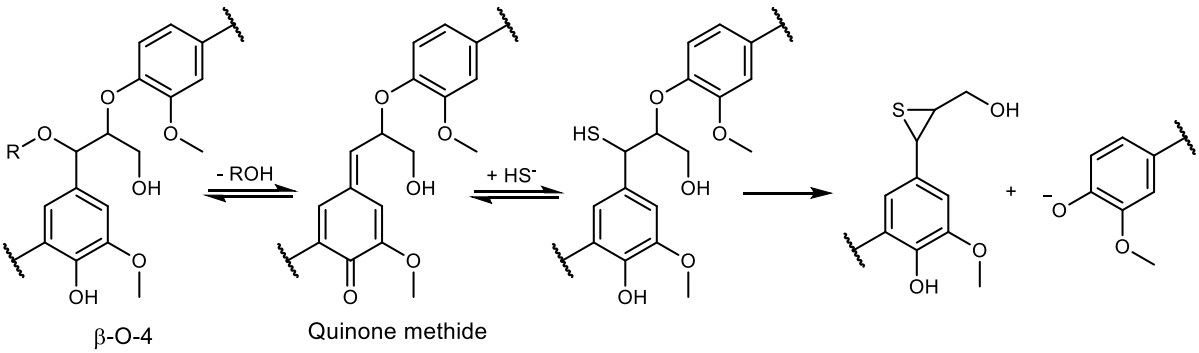

Scheme 6 *Reaction scheme for the cleavage of phenolic β-O-4 structures in lignin during Kraft pulping according to Ek et al.[103]*

A more recent approach to chemical pulping is the so-called organosolv pulping, in which different organic solvents are used to remove lignin and hemicellulose. This process was patented by Theodor Kleinert in 1968[104] and includes solvents like methanol, ethanol, acetone, butanol, ethylene glycol, and formic acid at temperatures of up to 220 °C under increased pressure.[105]

2.2.3. Dissolution and Regeneration

The insolubility of cellulose in water as well as most other common organic solvents, such as acetone, chloroform, or cyclohexane, is a very appealing property on the one hand, as it makes cellulose a very inert material, but very challenging on the other hand for chemical modifications or regeneration approaches. Advanced solvents or solvent systems are necessary for the dissolution of cellulose. Generally, the dissolution of cellulose can be categorized into two groups: 1) derivatizing and 2) non-derivatizing solvents. Historically, cellulose-dissolving systems were all based on the derivatizing approach. The solubilization of cellulose using “Schweizer’s reagent” ($[Cu(NH_3)_4](OH)_2$) can be considered as one of the first approaches for a derivatizing solubilization of cellulose, described in 1857.[106] The solubilized cellulose could then be regenerated by the addition of an acid. Using this system, cellulose could be extracted from wood pulp, cotton, and other cellulose sources and was used to produce regenerated cellulose

fibers (rayon). Another derivatizing method that became predominant for the regeneration of cellulose is the so-called viscose process. In this solubilization approach, the hydroxyl groups of cellulose react with CS_2 in alkali solution, forming a xanthogenate functionality. This ionic moiety interrupts the hydrogen bonds between the chains, enabling the dissolution of the derivatized cellulose (**Scheme 7**). Analogously to the "Schweizer's reagent", the cellulose precipitates upon treatment with an acidic solution under the regeneration of CS_2. To produce viscose fibers (rayon), the solubilized cellulose is extruded through spinnerets into a precipitation bath consisting of an aqueous sulfuric acid solution. The resulting fibers were marketed as artificial silk due to their similar feel and texture. Using the same process, but making sheets instead of fibers, results in a product marketed as "cellophane". This transparent foil was useful for food packaging due to its appealing property of repelling air, oils, and liquid water, while being permeable to gaseous water. Furthermore, cellophane is compostable, biodegradable, and bio-based as it is produced from cellulose. However, due to their less expensive production, petroleum-based polymeric foils soon replaced cellophane as a packaging material. One of the major drawbacks of the viscose process is the toxicity related to the CS_2 and the considerable amount of waste generated during the procedure. Therefore, in 2000 the CarbaCell process was introduced, which utilizes urea (which is far less toxic than CS_2) under alkaline conditions to form a soluble cellulose carbamate derivative (**Scheme 7**).[107,108] Non-derivatizing solvents are the second category, which can be applied for cellulose solubilization and can generally be described as polar enough solvents to interrupt the intra- and intermolecular hydrogen bonds between the cellulose chains. The most common non-derivatizing solvents are dimethyl sulfoxide-tetrabutylammonium fluoride (DMSO-TBAF),[109,110] *N*,*N*-dimethylacetamide-lithium chloride (DMAc-LiCl),[111–114] and *N*-methyl morpholine *N*-oxide (NMMO).[115] From these three examples, NMMO has especially gained interest, as it is used for the Lyocell process, which was developed in the 1980s and later brought to industrial application.[116] This process is used similarly to the viscose process for producing regenerated cellulose fibers, but is considered beneficial as this process is comparatively simple and is practically free from emissions as the solvent can almost quantitatively be recovered.[74] Another class of solvents for cellulose dissolution, which also belongs to the non-derivatizing category, are ionic liquids (ILs), defined as organic salts with a melting point below 100 °C.

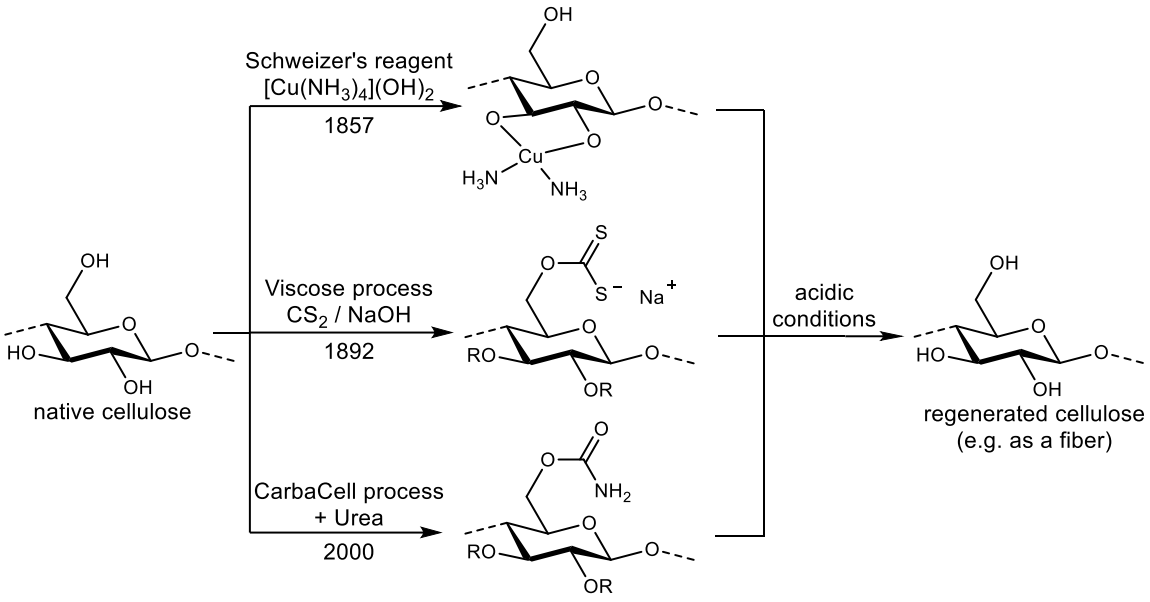

Scheme 7 *Three different derivatizing cellulose solubilization procedures for producing regenerated cellulose products.*

They generally share the properties of high thermal and chemical stability, non-flammability, and intrinsically low vapor pressure. Due to their typically bulky, non-symmetric organic cations and bulky anions, crystallization is hindered, which results in a comparably low melting temperature (**Scheme 8**).[117–119]

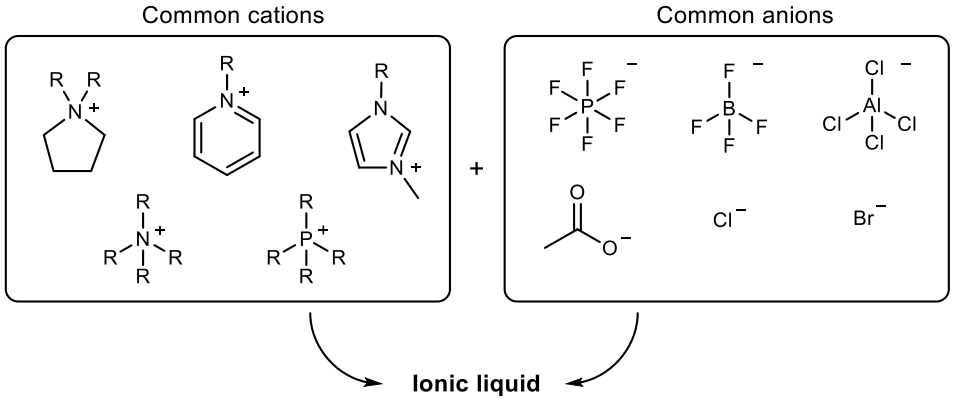

Scheme 8 *Examples of typical ionic liquids compositions (cations and anions).*

Graenacher was the first to report about ionic liquids in 1934,[120] even though they were not classified as ionic liquids at that time. Most ionic liquids are quaternary ammonium salts with different types of counterions. Differently substituted methylimidazolium salts are especially common, like 1-butyl-3-methylimidazolium chloride (BMIMCl), 1-allyl-3-methylimidazolium chloride (AMIMCl),[121,122] or 1-ethyl-3-methylimidazolium acetate

(EMIMOAc).[123–125] However, the main limitation of ILs is their expensive multi-step synthesis and easy contamination when used for derivatization reactions, resulting in a challenging recycling procedure as high boiling impurities accumulate over time.[126,127] Furthermore, some anions of ionic liquids are reactive in certain combinations, like for example in the case of 1-ethyl-3-methylimidazolium acetate, the acetate anion tends to react with cellulose, forming cellulose acetates.[128]

In 2005, Jessop *et al.* presented a system in which a non-ionic liquid can be turned into an ionic liquid with drastically higher polarity by introducing CO_2 (**Scheme 9**).[129]

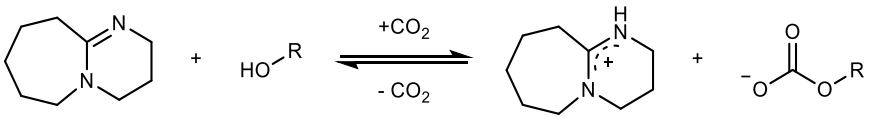

Scheme 9 *The "switching" of the switchable solvent system from non-ionic to ionic with CO_2 as demonstrated by Jessop et al.*[129]

He used an alcohol in a 1:1 molar ratio with the organic superbase 1,8-diazabicyclo-[5.4.0]-undec-7-ene (DBU) at room temperature and a pressure of one atmosphere of CO_2. This treatment was shown to convert the alcohol to a carbonate anion and the DBU to a protonated amidinium cation. Upon the removal of CO_2, this system could be returned to its non-ionic state and therefore showed a reversible and switchable character, which highly influenced the polarity of the solvent. This system was introduced to "facilitate organic syntheses and separations by eliminating the need to remove and replace solvents after each reaction step.[129]

This concept of the switchable solvent system was then applied for cellulose dissolution simultaneously by Jerome *et al*.[130] and Xie *et al*.[131] in 2013. In the approach presented by Xie *et al.*, the system was applied, as demonstrated by Jessop *et al*., with an alcohol component, which forms the ionic liquid together with DBU.[131] This ionic liquid was then shown capable of solubilizing cellulose in the presence of DMSO as a co-solvent. Therefore, this procedure can be categorized as a non-derivatizing approach, similar to the solubilization approaches applying "classic", non-switchable ionic liquids. Jerome *et al*., on the other hand, showed that cellulose could also be solubilized without the need for an additional alcohol.[130] In this case, the hydroxyl groups of

the cellulose itself form the carbonate anion, which then interrupts the intra- and intermolecular hydrogen bond interactions and leads to a DMSO-soluble derivative (**Figure 5**).

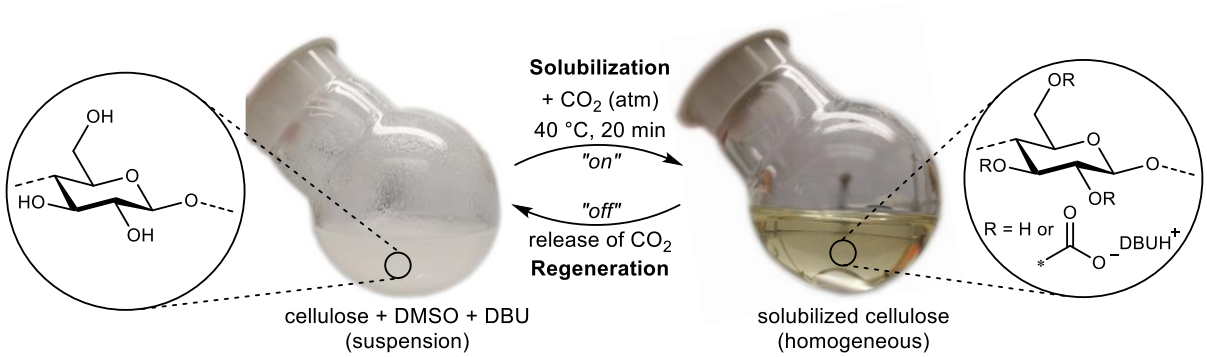

Figure 5 *Dissolution of cellulose in the DMSO/DBU/CO_2 switchable solvent system.*

The formation of the ionic cellulose carbonate structure was confirmed by Meier *et al*. *via* infrared spectroscopic analyses and the trapping of the *in situ* formed carbonate with benzyl bromide and methyl iodide as electrophiles, forming the corresponding cellulose benzyl carbonate and cellulose methyl carbonate, respectively.[132] In 2021, Bialik *et al.* additionally confirmed the formation of cellulose carbonates *via* direct evidence from nuclear magnetic resonance spectroscopy.[133] Upon the removal of CO_2 (by degassing with nitrogen, argon, air, or simple long-time storage at room temperature), the cellulose was shown to precipitate and could reversibly be solubilized again by the addition of CO_2.[130,134] The previously described switchable solvent system shows a remarkable chemical analogy to the industrially applied viscose process, as the thio-analog of carbon dioxide, i.e., CS_2, is used in this process, forming a cellulose xanthogenate structure instead of a carbonate. Beneficial compared to the viscose process is the fact that CO_2 can be considered as a waste material, is less toxic, and the regeneration of cellulose can be easier achieved by simple degassing or precipitation from an anti-solvent without the necessity of an acid as in the case of the viscose process. Compared to classic ionic liquids, the switchable solvent system was demonstrated to work under milder conditions (room temperature vs. commonly elevated temperatures above 90 °C) and the solubilization process to be more rapid (20 min vs. several hours in the case of most ionic liquids).[122,126] Furthermore, pretreatment of cellulose to form alkaline cellulose is not necessary. DMSO is categorized as a “usable” solvent by most sustainability-focused solvent selection guides with only minor issues

concerning reactivity and stability.[135,136] With its non-volatility, ease of purification, and low toxicity, DMSO can be considered a more sustainable solvent than DMAc or most ILs, which commonly need multi-step syntheses, increasing the cost and environmental impact. DBU, which is frequently used in the switchable solvent system, is an effective organocatalyst for many other syntheses. Thus, DBU was shown to fulfill a dual role for cellulose derivatizations by being part of the solubilization process and acting simultaneously as a derivatization catalyst in several cases.[137–144] All of these beneficial properties make the switchable solvent system a powerful, versatile, and potentially more sustainable alternative to existing cellulose solvents and make it attractive not just for the regeneration of cellulose but also for chemical modifications of cellulose. It was also demonstrated in numerous publications that other organobases than DBU can be used, like DBN, TBD, MTBD, TMG, P2-Et, or DABCO.[130,138,145,146] Slightly different conditions need to be applied then, like other dissolution temperatures or an increased pressure of CO_2.

2.2.4. Cellulose Derivatives and their Application

Cellulose has been used for thousands of years in the form of wood, cotton, and other plant fibers as an energy source, building material, and for clothing.[74] However, cellulose as a raw material for chemical modifications only ranges back about 180 years. The first cellulose derivative synthesized on an industrial scale was cellulose nitrate, initially synthesized from cotton applying a mixture of nitric and sulfuric acid to form so-called “gun cotton,” which was used starting from 1845 as a substitute for black powder.[147] The production on an industrial scale, however, was stopped in 1847 because of its rapid catalytic decomposition and high flammability, which led to multiple plant explosions.[147] The problem of rapid decomposition could be solved in 1866 by F. Abel by thoroughly washing the nitrocellulose to remove the adhering acids.[148] This was the starting point for military importance as gun powder. Nitrocellulose was the first thermoplastic material called celluloid (together with camphor as a plasticizer), which was initially used as a substitute for ivory in producing billiard balls. Within the following years, additional applications, for example as optical films in photography and cinematography, were established until they were replaced by the less flammable cellulose

acetate.[147] Today, several different derivatizations for cellulose exist, but the commercially by far most important cellulose derivatives are cellulose esters and cellulose ethers.[93] Since cellulose is insoluble in water and all common organic solvents, derivatization reactions, especially on an industrial scale, are usually performed in heterogeneous systems. Herein, the derivatization starts in the amorphous regions of the cellulose polymer, which are accessible to the reagents. As the reaction proceeds, new reactive centers become accessible so that all parts of the cellulose eventually get functionalized. However, this results in a non-statistical distribution of functional groups along the polymer backbone, if not high degrees of substitution are targeted. In some cases, the cellulose becomes soluble as it reaches a certain degree of substitution, thus subsequently reacting to completion in a homogeneous phase. A prominent example of this type of derivatization reaction is the industrial synthesis of cellulose acetate *via* the *Acetic Acid Process*.

2.2.4.1. Cellulose Esters

Theoretically, cellulose can be functionalized with an unlimited number of organic acids, resulting in an unlimited number of possible cellulose esters. In practice, however, these possibilities are drastically limited by the complex nature of the cellulose polymer. Highly esterified cellulose is, therefore, only produced from selected aliphatic acids. Industrially, cellulose acetate, cellulose acetate propionate, and cellulose acetate butyrate are the most important products manufactured on an industrial scale for over 90 years.[147] Out of these, cellulose acetate is the most important derivative and was produced industrially mainly via two different processes: the *Methylene Chloride Process* (also known as the *Dormagen Process*) and the *Acetic Acid Process* (**Scheme 10**). However, today only the *Acetic Acid Process* is still of industrial relevance.[149]

For the *Acetic Acid Process*, cellulose is suspended in glacial acetic acid, with the addition of 2–15% (by mass) of sulfuric acid as a catalyst and an excess of 10–40% acetic anhydride (based on a targeted peracetylation).[150–152] The reaction starts heterogeneously and continues in homogeneous phase, as the partially acetylated cellulose becomes soluble in glacial acetic acid. Finally, this results in cellulose triacetate with a

degree of substitution (DS) between 2.8–3.0.[153] In this heterogeneous cellulose functionalization approach, the cellulose must always be perfunctionalized, as otherwise inhomogeneously substituted cellulose acetate would be obtained. This can be explained by the nature of the heterogeneous reaction, in which the hydroxyl groups only become accessible to the reactant as the reaction proceeds from the outside to the inside of the fiber or particle, first reacting in amorphous regions. This causes irreproducible product characteristics, with an inhomogeneous distribution of the functional groups along the chain, making it unsuitable for commercial processing.[93,153,154]

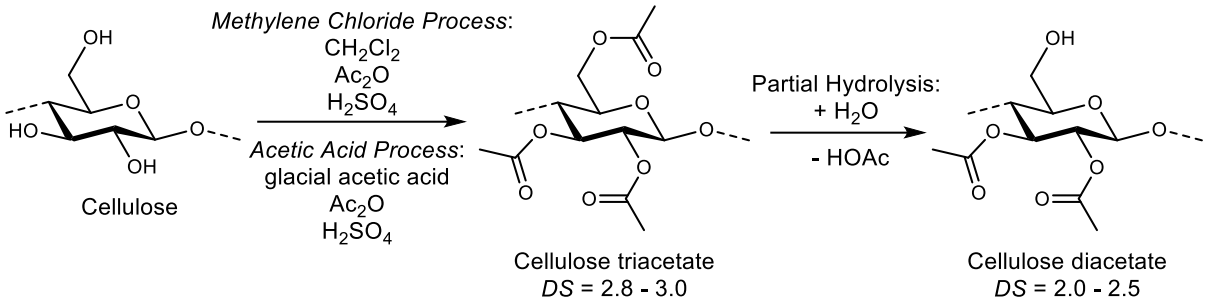

Scheme 10 *Industrial synthesis of cellulose diacetate via the Acetic Acid Process and the Methylene Chloride Process.*

The limited solubility of the resulting cellulose triacetate was a considerable obstacle to its industrial application for a long time after its discovery. These solubility issues could be solved in 1904 by Miles and Eichengrün by synthesizing an acetone-soluble secondary cellulose acetate by subsequent partial hydrolysis of the primary cellulose triacetate.[147] This partial hydrolysis of the resulting peracetylated cellulose triacetate still takes place today in the industrial *Acetic Acid Process*. This is achieved by adding water after the reaction mixture becomes completely homogeneous. The amount of water and stirring time depends on the targeted final DS of the cellulose acetate. Typically, cellulose diacetates with a DS of 2.0–2.5 are produced, as the cellulose acetate is soluble in acetone in this range of functionalization.

Due to the acidic condition during the acetylation reaction, partial cleavage of the polymeric main chain is unavoidable in this process, as the acetal moiety in the cellulose backbone is prone to hydrolysis under acidic conditions, which leads to a significant decrease in molecular weight of the polymer (**Scheme 11**). In some cases, where a lower molecular weight is desired, this can be seen as a positive side effect. However,

mostly this degradation reaction results in challenges, as the material properties of the final cellulose acetate strongly depend on the molecular weight.

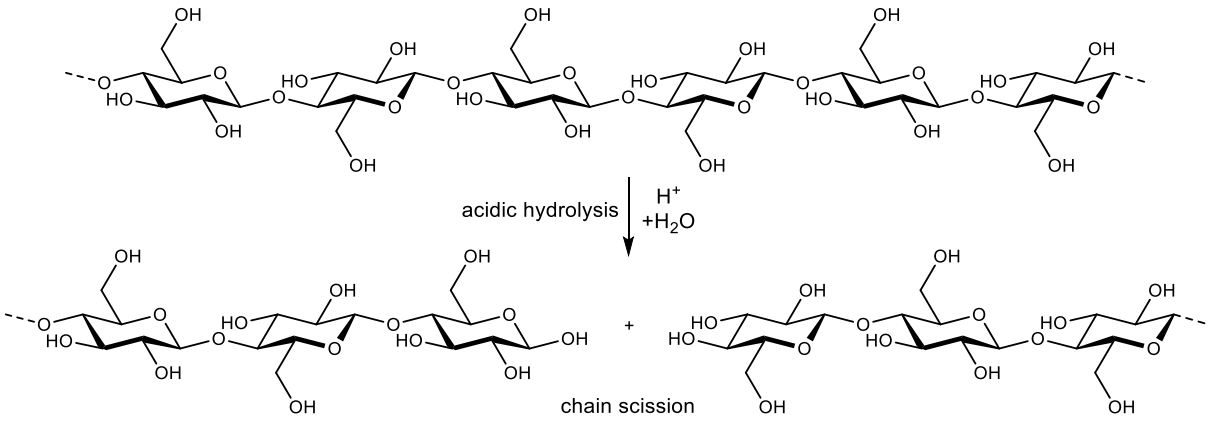

Scheme 11 *Chain scission of cellulose under acidic conditions via acidic hydrolysis of a linking acetal moiety.*

In the *Methylene Chloride Process* developed by Bayer, the acetic acid in the *Acetic Acid Process* is substituted by methylene chloride. This substitution mainly has two advantages: 1) allowing for reflux cooling during the exothermic esterification reaction, which guarantees better temperature control, and 2) methylene chloride is a better solvent for cellulose triacetate than acetic acid, which enables the use of lower catalyst concentrations leading to an inherent quality improvement. However, quality improvements in flake quality in the competing *Acetic Acid Process* circumvented these advantages and alongside the higher productivity, thus led to the closure of the last *Methylene Chloride Process* plant in 2003.[151]

Cellulose acetate has various applications: one of the leading applications since its mass production started was the fiber market. Fibers made from cellulose acetate share many properties with viscose derived fibers, but behave differently when exposed to heat, as viscose resists heat, whereas cellulose acetate is prone to melting. Moreover, acetate fibers exhibit a smooth, satiny texture, which makes them a good substitute for silk. However, today less than 1% of the world's fiber production is related to cellulose acetate, as cheaper polyester fibers have mainly replaced it.[155] Besides the fiber market, cellulose acetate is also used in the field of plastic materials, membranes for separation technologies, or cigarette filters.[74,150,153,156–161] Another important application was the use of cellulose acetate as optical films, which replaced the initial

films that were based on nitrocellulose due to its lower flammability. However, it was found that the films start to deteriorate upon long-time storage, especially under humid and warm conditions, which was termed the “vinegar syndrome”. It is caused by a partial cleavage of acetyl moieties in the material, forming acetic acid. This degradation is an auto-catalytic process, as acids catalyze the deacetylation. Any initial residues of acetic acid from the production starts this degradation, which underlines the importance of thorough washing of the material.

Homogeneous derivatizations of cellulose have been investigated by many researchers in the last few years (**Table 6**).

Table 6 *Overview of homogeneous cellulose acetylation approaches in different solvent systems and with varying acetylation reagents.*

Solvent	Reactant	Conditions	Ref.
[AMIM]Cl	Acetic anhydride	80–100 °C, 2–23 h	[121,122]
[C_4MIM]Cl + pyridine	Acetic anhydride	80 °C, 2 h	[126]
[C_4MIM]Cl	Acetyl chloride	80 °C, 2 h	[126]
[EMIM]OAc/DMSO	Isopropenyl acetate	80 °C, 0.1–16 h	[125,162]
[DBNH]OAc	Acetic anhydride	70 °C, 2 h	[163]
[DBNH]OAc	Vinyl acetate	70 °C, 2 h	[163]
[DBNH]OAc	Isopropenyl acetate	70 °C, 2 h	[163]
DMSO/MeOH/DBU/CO_2	Acetic anhydride	80 °C, 3 h	[144]
DMSO/DBU/CO_2	Acetic anhydride	80 °C, 5 h	[137]
DMSO/DBU/CO_2	Vinyl acetate	60 °C, 4 h	[140]

They require solvents, which should be prevented in terms of sustainability, if not urgently necessary. However, homogeneous cellulose derivatizations also offer several benefits, which can compensate for using solvents, especially if the applied solvents can be recovered sufficiently. Homogeneous derivatizations generally enable better control over the DS by adjusting the reactant's equivalents and a homogeneous functionalization along the polymer chain with commonly milder reaction conditions.[164] This means that the DS in homogeneous derivatization reactions can, in most cases, be controlled directly, which is beneficial compared to heterogeneous procedures like the *Acetic Acid* or *Methylene Chloride Process*, as in these cases first complete acetylation

has to be performed with partial deacetylation in a second step. Additionally, over-stoichiometric amounts of reactant are needed, and the harsh acidic conditions lead to partial cellulose backbone degradation, as explained before. In many homogeneous derivatizations, basic or neutral conditions can be applied, which prevents acetal hydrolysis and therefore does not decrease the molecular weight. Homogeneous acetylations of cellulose were demonstrated to be possible with various acetylation agents in different solvent systems, as summarized in **Table 6**.

Besides the most relevant cellulose acetates, only mixed cellulose esters of cellulose acetate propionate and cellulose acetate butyrate have attained notable importance on a commercial scale. Cellulose esters of higher acids are usually more challenging to prepare, as the anhydrides of these acids are less reactive due to the high degree of steric hindrance.[147] Therefore, many research approaches were pursued to synthesize higher cellulose esters or cellulose esters with certain functionalities in the ester carbon chain, such as carbon-carbon double bonds. These cellulose esters are, in most cases, only accessible *via* homogeneous procedures because of the before-mentioned lower reactivity. Several recent approaches for synthesizing different cellulose esters are summarized in **Scheme 12**. One approach from these concerning sustainability should be highlighted here: the synthesis of fatty acid cellulose esters (FACEs) in the DMSO/DBU/CO_2 switchable solvent system utilizing high oleic sunflower oil.[138] This procedure is beneficial concerning sustainability because the reagent does not have to be synthesized. Instead, it is directly derived from nature. Furthermore, no additional catalyst was necessary, as the DBU, used for cellulose solubilization, also acts as a transesterification catalyst. In some approaches, in which functional cellulose esters (with terminal carbon-carbon double bonds) are synthesized, additional post-functionalization could be applied. For example, Meier *et al.* used thiol-ene click reactions for the post-functionalization of cellulose 10-undecenoates.[165]

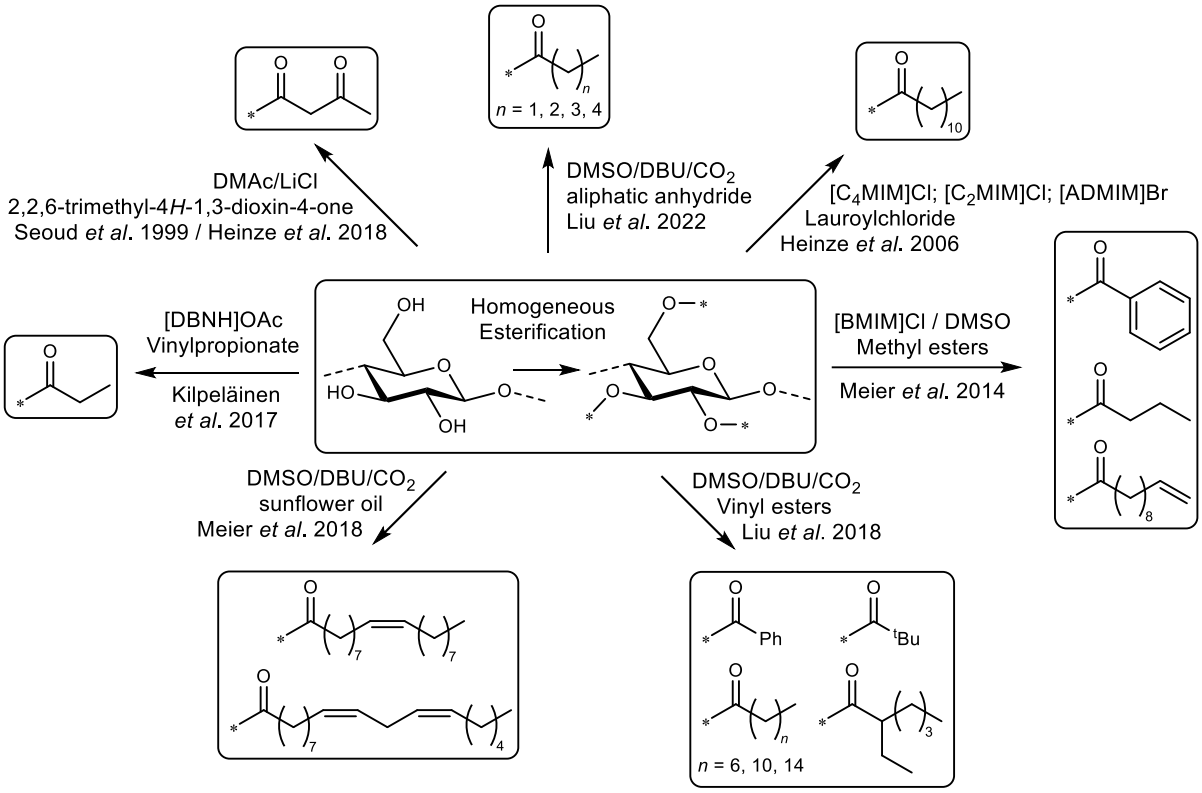

Scheme 12 *Overview of recently described homogeneous esterification reactions in different cellulose solvents.*[126,138,141,163,165–168]

2.2.4.2. Cellulose Ethers

Cellulose ethers are an important class of cellulose derivatives with various applications as thickeners, suspending agents, water-binders, film formers, protective colloids, or glue in the food, paint, paper, cosmetics, pharmaceutical, adhesive, printing, textile, or building material industries.[93] Their general properties of water-solubility, low toxicity, high economic efficiency, easy handling, and good availability make cellulose ethers very attractive for many applications. The worldwide production of cellulose ethers was estimated to be around 650 000 t in 2018.[93] The commercially most important cellulose ethers are methyl cellulose (MC), ethyl cellulose (EC), hydroxyethyl cellulose (HEC), hydroxypropyl cellulose (HPC), carboxymethyl cellulose (CMC), various mixed cellulose ethers consisting of the aforementioned substituents and all of these in varying degrees of substitution and/or ratios (for mixed ethers). This broad palette enables the industry to finely tune the properties of the resulting cellulose ethers for the specific

requirements and also explains the wide range of possible applications of cellulose ethers.

The etherification reactions of cellulose on an industrial scale are usually carried out heterogeneously. During these processes, the cellulose remains in a fibrous or particulate form during the whole reaction. Due to the strong intra- and intermolecular interactions *via* hydrogen bonds, the cellulose has to be activated beforehand, reducing these interactions and enabling a reaction with the etherifying reagent. In almost all cases, this activation is performed with an aqueous sodium hydroxide solution, leading to a strong cellulose swelling. In many cases, an organic diluent is added, which effectively suspends and disperses the cellulose, acts as a heat-transfer medium during the reaction, and facilitates the recovery of the reaction product. Commonly used diluents in this context are *iso*-propyl or *tert*-butyl alcohol, acetone, toluene, or dimethoxyethane.[93,169–171] The synthesis pathways of the industrially most produced cellulose ethers are shown in **Scheme 13**.

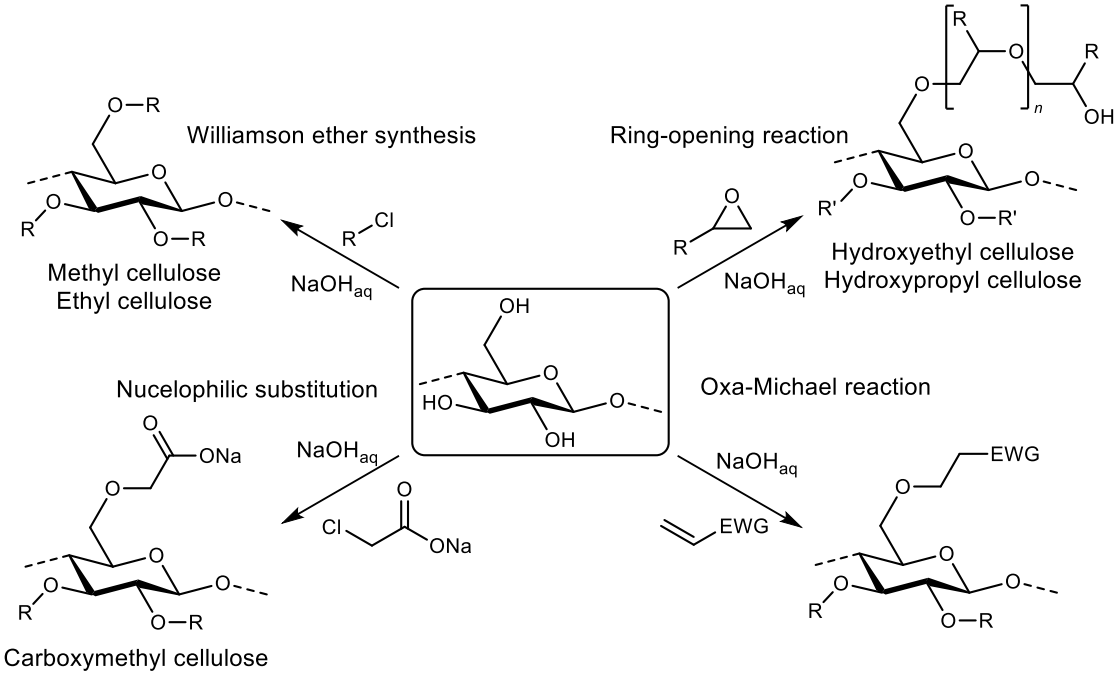

Scheme 13 *Synthesis pathways for the most important commercial cellulose ethers.*

All of these are based on the activation of cellulose with sodium hydroxide, followed by heterogeneous modification. Methyl and ethyl cellulose are formed *via* a Williamson ether synthesis with the corresponding alkyl halide (usually methyl chloride and ethyl chloride are used).[93,172] For the production of hydroxyethyl cellulose and hydroxypropyl

cellulose, epoxides are employed, which react in a ring-opening reaction with the hydroxyl groups of the activated cellulose. In these derivatization reactions, partial polymerizations can be observed analogously to grafting-from approaches (**Scheme 13**). However, these polymerization reactions usually only occur to a small extent due to the high number of available hydroxyl groups along the cellulose backbone. Another commercially very relevant cellulose ether (sales worldwide approx. 230 000 t) is carboxymethyl cellulose, categorized as an ionic cellulose ether and used for applications like binder or thickener in the food, laundry detergent, and pharmaceutical industry.[172] It is produced by the reaction with chloroacetic acid *via* a nucleophilic substitution in the α-position. Another commercially relevant class of derivatization is the reaction with compounds bearing an activated double bond in an oxa-michael addition type reaction. A common example of this type of derivatization is the reaction with acrylonitrile to form cyanoethyl cellulose. Homogeneous cellulose etherification reactions are not as important as homogeneous cellulose esterification reactions, not even regarding lab-scale syntheses.[93] One reason is that the very polar polymer cellulose is transferred to a far less polar derivative during the reaction. Consequently, the very polar solvents used for cellulose derivatization, like ionic liquids or DMAc/LiCl, cannot solubilize the formed product, and the cellulose derivative, therefore, precipitates during the reaction. Another issue is the solubility of the activating agent (NaOH), which is, in most cases, needed to increase the hydroxyl groups' nucleophilicity for the subsequent nucleophilic substitution reaction. Nevertheless, there are numerous examples of etherification reactions in homogeneous phase.[173–179] For example, cellulose was dissolved in LiCl/1,3-dimethyl-2-imidazolidinone (DMI), activated with sodium hydroxide, and then reacted with methyl iodide for the homogeneous synthesis of methyl cellulose.[177]

2.2.4.3. Other Cellulose Derivatives

Cellulose esters and cellulose ethers are the most relevant cellulose derivatives, and the only cellulose derivatives produced on a large industrial scale. Nevertheless, several other approaches for the derivatization of cellulose with advanced functional properties exist. Some of these other types of derivatizations are described in this chapter. Oxidation of cellulose can be performed in numerous ways, resulting in the introduction of carboxy, aldehyde, or keto groups. Concerning the resulting product properties, selective oxidation with regard to regioselectivity and the functional group is desirable. In this context, two main procedures became established: the selective oxidation of the primary hydroxyl group at the 6-position of the AGU and the oxidative cleavage of the secondary hydroxyl groups in 2 and 3 positions, forming the 2,3-dialdehyde cellulose (**Scheme 14**).

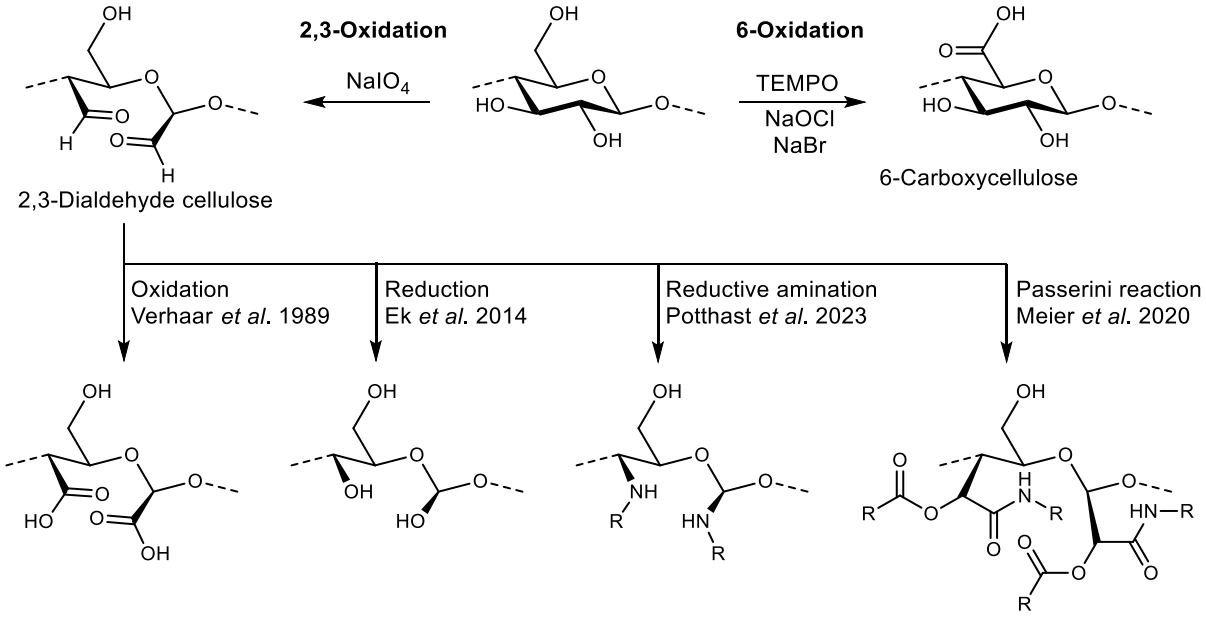

Scheme 14 *Two selective oxidation procedures for the synthesis of 6-carboxy cellulose and 2,3-dialdehyde cellulose and subsequent modification approaches of 2,3-dialdehyde cellulose.*[180–183]

Nooy *et al*. presented the oxidation system 2,2,6,6-tetramethylpiperidine-*N*-oxyl (TEMPO) with NaOCl and NaBr in 1994 for the selective oxidation of primary hydroxyl groups in polysaccharides to the corresponding polyuronic acid, which was the starting point for the TEMPO-mediated oxidations of cellulose.[184] The selectivity was very high concerning the primary hydroxyl oxidation with moderate backbone degradation.[185–187]

By optimization of the reaction conditions, it was found that the lowest depolymerization of amorphous cellulose occurs at a constant pH value of 10 at T = 4 °C.[188] The high selectivity of the TEMPO-mediated reaction was verified by computational investigations on the mechanism.[189]

The oxidation of cellulose with periodate, forming the 2,3-dialdehyde cellulose (**Scheme 14**) has received considerable interest because of the manifold subsequent reaction possibilities of the aldehyde groups. For example, subsequent oxidation of the aldehyde groups with sodium chlorite/hydrogen peroxide yields the 2,3-dicarboxy cellulose, which shows high calcium-binding capacity and bio-degradability, while the disodium salt showed typical properties of a polyelectrolyte.[180,190,191] Another example is the post-modification of 2,3-dialdehyde cellulose *via* the Passerini three-component reaction utilizing different renewable carboxylic acids and commercially available as well as renewable isocyanides in an aqueous medium.[183] Recently, a novel reductive amination approach with 2-picoline borane was reported to generate novel thermoplastic materials with tunable glass transition temperatures.[182]

In recent years, click chemistry reactions were applied to cellulose modifications. Sharpless coined the term click chemistry, and these reactions are defined as being experimentally simple, needing no protection from oxygen, requiring only stoichiometric amounts of starting materials, and do not generate byproducts (or byproducts that can be removed easily).[192] Some examples of click reactions are 1,3-dipolar cycloadditions of an azide and a triple bond (Huisgen reaction), photoinitiated thiol-ene reactions, thia-Michael additions, or [4+2] cycloaddition reactions (Diels-Alder reaction and others). As cellulose has none of the required functional groups necessary for these types of reactions, previous derivatization must be performed. Therefore, esterification and etherification reactions were utilized to introduce a triple bond containing substituents.[193–196] Heinze *et al.* reported a derivatization of cellulose in DMAc/LiCl with *p*-toluenesulfonyl chloride (TsCl), followed by a substitution with sodium azide or propargylamine. The resulting cellulose derivatives were then coupled *via* the 1,3-dipolar cycloaddition (Huisgen reaction) in an aqueous medium and $CuSO_4$ as the catalyst (**Scheme 15**).[197]

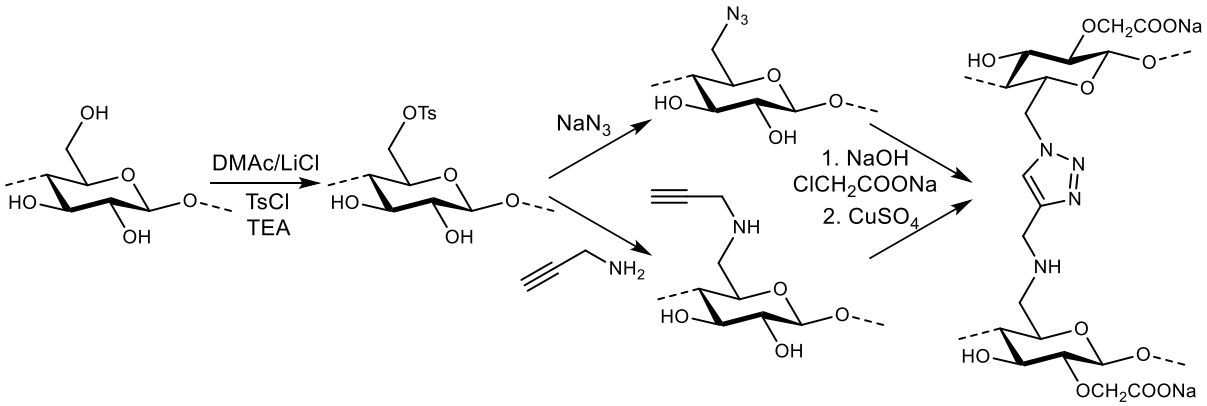

Scheme 15 *Cellulose derivatization and consecutive click reaction coupling via 1,3 dipolar cycloaddition of an azide and a triple bond as reported by Heinze et al.*[197]

2.2.4.4. Degree of Substitution Determination

Cellulose bears three hydroxyl groups per anhydroglucose repeating unit, which can be derivatized. Depending on the procedure, conditions, type of reactant, and reactant equivalents, different degrees of substitution can be obtained. Generally, the value can range from 0 (native, unmodified cellulose) to 3 (completely derivatized). The DS, the type of derivatization (i.e. the substituent), and the degree of polymerization usually have the greatest impact on the resulting properties of the derivatized cellulose sample. Especially the strong influence of the DS on the properties of the material can be seen by, for example, the solubility characteristics of cellulose acetate with different DS, as shown in **Table 7**. Slight variations in the average DS strongly influence the solubility and other material properties such as water sorption or thermal properties. Therefore, precise control over the DS in synthesizing cellulose derivatives is necessary, and a reliable determination method is thus compulsory.

Table 7 *Typical solubility of cellulose acetates with different DS.*[147]

DS	Chloroform	Acetone	2-Methoxyethanol	Water
3.0–2.8	Soluble	x	x	x
2.7–2.2	x	Soluble	x	x
1.8–1.2	x	x	Soluble	x
0.9–0.6	x	x	x	Soluble
<0.6	x	x	x	x

For this purpose, several DS determination methods have been developed up to the present day. The most common method for cellulose esters is the titration method, which is based on hydrolysis in an alkaline solution with subsequent titration as a quantification method of ester moieties.[121,198–200] However, this method is limited to the class of cellulose esters and is further a destructive method, very time- and labor-intensive, and requiring comparably large sample amounts. Alternatively, ^{1}H and ^{13}C NMR spectroscopy is a compelling method for DS determination, as it is a direct, non-destructive method applicable to a broad range of cellulose derivatives.[122,123,206,207,125,126,139,201–205] One of the main limitations of this method is the necessity for solubilization, which is especially challenging for cellulose derivatives with a low DS, which are often insoluble in common organic solvents. Furthermore, it is limited to cellulose derivatives with substituents whose signals in the ^{1}H NMR spectrum do not overlap with those of the AGU protons, typically used as the reference for DS calculations. Another method for DS determination *via* NMR spectroscopy involves derivatization of the unreacted hydroxyl groups of the cellulose sample with 2-chloro-4,4,5,5-tetramethyl-1,3,2-dioxaphospholane (2-Cl-TMDP, which is a phosphorous-containing reactant), followed by quantitative ^{31}P NMR spectroscopy (**Scheme 16**).

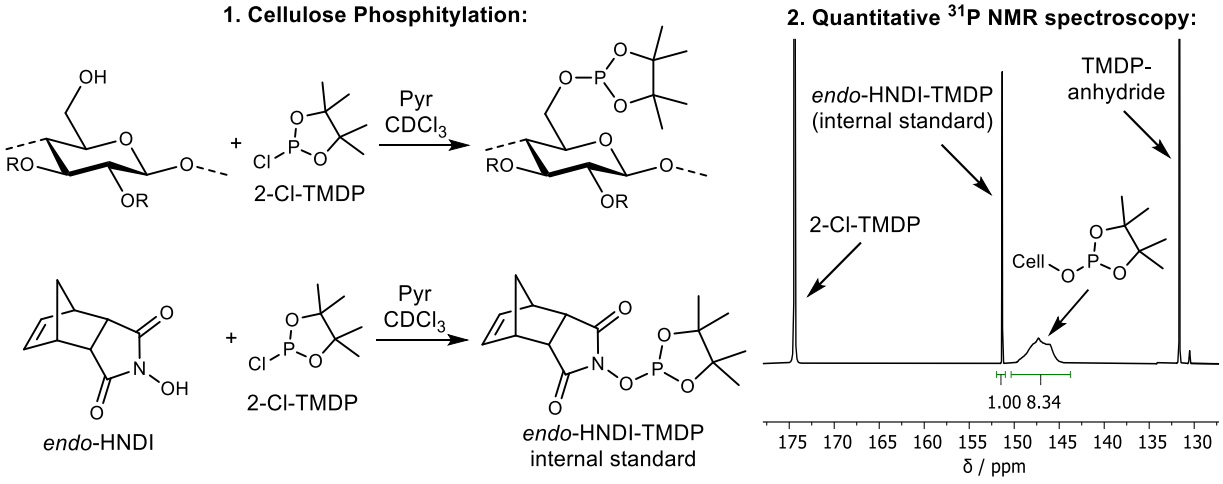

Scheme 16 *Phosphitylation of cellulose derivatives and endo-HNDI (as internal standard) with 2-chloro-4,4,5,5-tetramethyl-1,3,2-dioxaphospholane for the DS determination via ^{31}P NMR spectroscopy.*

This method was introduced by Kilpeläinen *et al*.[208] in 2010 and was initially proposed as a DS determination method for chloroform-soluble cellulose esters. However, several examples demonstrated the applicability to almost any class of cellulose derivative,

with the prerequisite of chloroform solubility being expanded by adjusting the derivatization procedure.[138,143,146,209–211] For example, by increasing the pyridine content, which then acts as the solvent and the basic catalyst simultaneously.

Solubility issues, in combination with time-consuming sample preparation, remain the major limitation of this method. Further procedures for DS determination involving gas chromatography,[212,213] UV-Vis spectroscopy,[214] or elemental analysis[183,201,215,216] were developed, but every technique has its limitations concerning either solubility, applicability, or precision. Fourier transform infrared (FTIR) spectroscopy is a promising and often-used technique for analyzing cellulose derivatives, as solid samples can be analyzed without pretreatment, preventing the necessity of solubilization.[217] In prior research applying transmission FTIR spectroscopy for DS determination, a linear relationship between the carbonyl band absorbance area and the DS was observed when commercial cellulose triacetate was used in different mass ratios relative to the used KBr to simulate different DS values of cellulose acetate.[214] This technique was shown to facilitate the construction of a calibration curve, as no different cellulose acetates with regularly spaced DS need to be synthesized. However, the examined samples need to be precisely weighed and homogeneously distributed in the KBr disc in the form of a fine powder to gain precise results. Especially cellulose acetates with lower DS (<1.5) cannot be easily ground to a fine powder due to their elastic consistency.[214] The requirement of a homogeneous KBr pellet with a precisely weighed sample mass can be avoided by referencing the arising carbonyl band in the IR spectrum against a vibrational signal unaffected by the acetylation. Cheng *et al*. referenced the carbonyl vibration of the acetyl group to the C-O stretching vibration of the cellulose backbone with mixtures of microcrystalline cellulose and cellulose triacetate to simulate cellulose acetates with DS ranging from 1.80 to 2.85 and observed a curvilinear relationship between the DS and the carbonyl band absorbance intensity.[218] A similar curvilinear relationship was found by Melo *et al.* for the DS determination of cellulose acetates *via* ATR-FTIR spectroscopy monitoring the O-H stretching vibration referenced to the C-O stretching vibration.[219] Zhang *et al*. referenced the carbonyl band against the bridge oxygen antisymmetric stretching signal of the cellulose backbone for acetylated cellulose nanocrystals with a DS between 0.46–1.84 and observed a linear relationship with

increasing DS.[220] ATR-FTIR spectroscopy has the advantage of easier sample preparation compared to transmission FTIR spectroscopy devices, as no KBr disc has to be produced. It can be concluded that there is no gold standard for cellulose DS determination, which can be applied to all cellulose derivatives as every DS determination method has its limitations. Therefore, a set of different methods needs to be investigated and applied to the individual sample to fit its specific needs, and if possible, two independent methods should be applied.

2.3 Sulfur-Based Reactions

Sulfur is the 10th most abundant element and can be found almost everywhere - in meteorites, the ocean, the earth's crust, the atmosphere, and in practically all plants and animals.[221] It is the element with the most known allotropes, the most stable of these being alpha-sulfur, which is an odorless, pale yellow, brittle solid at room temperature consisting of S_8 rings in an orthorhombic lattice.[221] It can be found both in its native form and in metal sulfide ores and often occurs naturally in the vicinity of volcanoes and hot springs.[221] Today, it is mainly obtained as a side-product from the oil-refining industry and was produced at an estimated amount of 80 million tons in 2021.[222] This globally produced amount exceeds the commercial demand. Thus, most sulfur mines around the world have closed down and sulfur deposits grow rapidly.[223] Therefore, a lot of research has been performed in the last years dealing with the utilization of elemental sulfur for value-added products and materials. In its elemental form, sulfur is the most atom-efficient building block concerning the incorporation of sulfur into organic molecules. It, therefore, enables the design of inherently greener chemical processes if used as a sulfurizing reagent compared to other alternatives, such as phosphorus pentasulfide, Lawesson's reagent, carbon disulfide, or thiophosgene, which are at the same time a lot more toxic, reactive, and therefore more challenging to handle. Thus, the utilization of elemental sulfur fulfills many aspects of the Twelve Principles of Green Chemistry and enables the development of more sustainable chemical procedures.

2.3.1. Isothiocyanates

Isothiocyanates are the thio-analogues of isocyanates and therefore share many properties with this class of functional group. In nature, isothiocyanates can be found in, e.g., cruciferous vegetables like broccoli, cabbage, or cauliflower and were suggested to have anti-cancer activity by inducing cycle arrest in the cell, which leads to apoptosis.[224–226] Isothiocyanates in plants are generated by an enzymatic reaction from glucosinolates, primarily upon tissue damage, releasing, e.g., allyl, benzyl, or phenethyl isothiocyanate.[227,228] Isothiocyanates were also shown to have considerable antiproliferative and antibacterial activity, which could make them useful in food preservation.[229–231] They were recently also applied for labeling proteins *via* covalent binding to lysine or cysteine residues.[232–235] Isothiocyanates are also widely used in organic chemistry and generally react with nucleophiles and participate in cycloadditions, leading to various heterocycles.[236]

Similar to the synthesis of isocyanates from an amine and phosgene, the classic synthesis of isothiocyanates is performed with an amine and thiophosgene (**Scheme 17**, **A**).[237–240] This reaction is very efficient, but undesirable due to the high toxicity related to thiophosgene and the low functional group compatibility.[241] Another often used synthetic pathway is the utilization of carbon disulfide with amines (**Scheme 17**, **B**).[242–245] Very time-efficient pathways were reported using carbon disulfide, but often vast amounts of chemical waste are produced in these procedures, as over-stoichiometric amounts of carbon disulfide and base are necessary.[245] Fujiwara *et al*. presented a method for synthesizing isothiocyanates from isoselenocyanates with elemental sulfur in 1991 (**Scheme 17**, **C**).[246] The Se-S exchange reaction was found to occur quantitatively in the presence of a tertiary amine base with yields of up to 99%.[246] One year later, the same authors showed a similar method, but from isotellurocyanates instead of isoselenocyanates, which can both be generated *in situ* from an isocyanide with the respective metal.[247] However, other than in the case of isoselenocyanate, the *in situ* generated isotellurocyanate could not be confirmed as an intermediate due to the high reactivity of isotellurocyanates. It was shown that in the case of isoselenocyanates, the Se-S exchange is the rate-determining step, whereas, in the case of tellurium, the isotellurocyanate formation from tellurium and isocyanide is rate-determining.[247] How-

ever, selenium and tellurium are both toxic and should therefore be prevented, if possible. Another catalytic transformation from isocyanides with disulfides and thallium(I) salts were reported by Okano *et al.* in 1977 (**Scheme 17**, **D**).[248] A method utilizing thiourea with a nitrile oxide was demonstrated by Baxendale *et al*. in 2013 *via* a 1,3-dipolar cycloaddition to an unstable 1,4,2-oxathiazoline intermediate with subsequent rearrangement and elimination of urea, forms the desired isothiocyanate (**Scheme 17**, **E**).[249] However, the instability of the nitrile oxide leads to many side-products, which makes this approach less attractive. A promising approach is the decomposition of thiocarbamates, dithiocarbamates, or thioureas with various reagents, but it has to be taken into consideration that the thiocarbamate/thiourea has to be synthesized beforehand, which limits the overall applicability as thiocarbamates and thioureas themselves are usually synthesized from isothiocyanates (**Scheme 17**, **F**).[250–255] Approaches with thiocarbonyl transfer reagents for the synthesis of isothiocyanates from amines can be applied with compounds like di-(2-pyridyl)thionocarbonate (**Scheme 17**, **G**).[256,257] Another possibility is the formation of isothiocyanates from the oxo-analogue with thionation agents like the Lawesson's reagent (**Scheme 17**, **H**). This was even reported to be possible under solvent-free conditions,[258] but isocyanates are usually synthesized from amines and phosgene, which decreases the overall applicability and sustainability of this pathway.

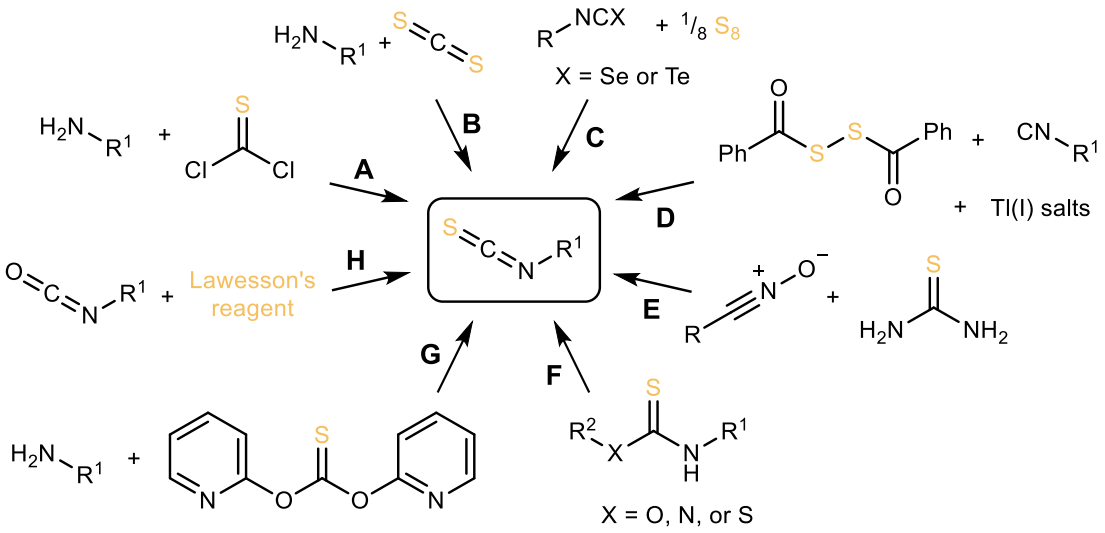

Scheme 17 *Synthetic accessibility of isothiocyanates.*[241]

The formation of isothiocyanates applying elemental sulfur can generally be considered more appealing, as these reaction procedures are typically more atom efficient.[231]

Besides the presented isothiocyanate formation from isoseleno-/telluro-cyanates with elemental sulfur, two more main approaches for the synthesis of isothiocyanates applying elemental sulfur can be found in the literature: First, the reaction of carbenes with sulfur generating thiocarbonyl compounds (e.g., thiophosgene in the case of dichlorocarbene), which directly reacts to an isothiocyanate in the presence of a primary amine (**Scheme 18**). These carbenes are usually generated *in situ* (e.g., from chloroform under basic conditions), and the subsequent mechanism for the formation of the thiocarbonyl compound is based on a nucleophilic attack of the sulfur on the electrophilic carbene (similar to the mechanism shown in **Scheme 19 a**).[259–262] The *in situ* generated thiocarbonyl compound reacts with a primary amine to the corresponding isothiocyanate (**Scheme 18**), which can subsequently react with a second equivalent of primary amine to the corresponding symmetric thiourea.

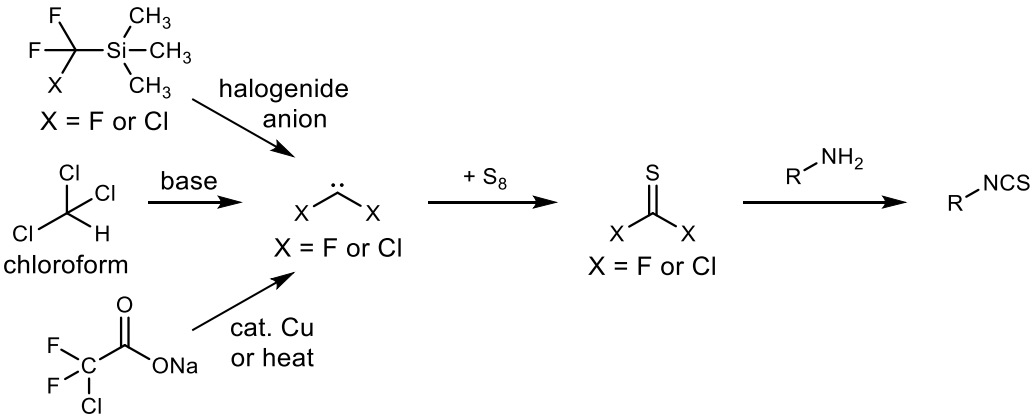

Scheme 18 *Synthesis of isothiocyanates from dihalocarbenes and elemental sulfur with different in situ generation methods for dihalocarbenes.*[259–262]

The second approach for the synthesis of isothiocyanates applying elemental sulfur involves the sulfurization of isocyanides, which recently gained more attention. Two different mechanistic pathways were proposed for this reaction: i) the sulfur-activated pathway, in which the isocyanide acts as the electrophile in its carbenoid structure (**Scheme 19 a**), and ii) the isonitrilium pathway, in which the isocyanide acts as the nucleophile (**Scheme 19 b**).[263] Research studies by Al-Mourabit *et al*., Meier *et al*., and Ábrányi-Balogh *et al*. strongly support the sulfur-activated mechanism, in which the isocyanide reacts as the electrophilic carbenoid with the activated polysulfide anion acting as the nucleophile.[231,263–266] This mechanism is possible under the application of a base and enables milder conditions with fewer side reactions compared to the

thermal activation without a base, which is supposed to proceed *via* the isonitrilium pathway.[231] When a primary or secondary amine is applied as the sulfur-activating base, this amine subsequently reacts with the formed isothiocyanate, resulting in a multicomponent reaction of isocyanide, amine, and sulfur, forming the corresponding thiourea with the amine component acting in a dual role in this transformation (as explained in **chapter 2.3.2** and in **Scheme 22**).[265]

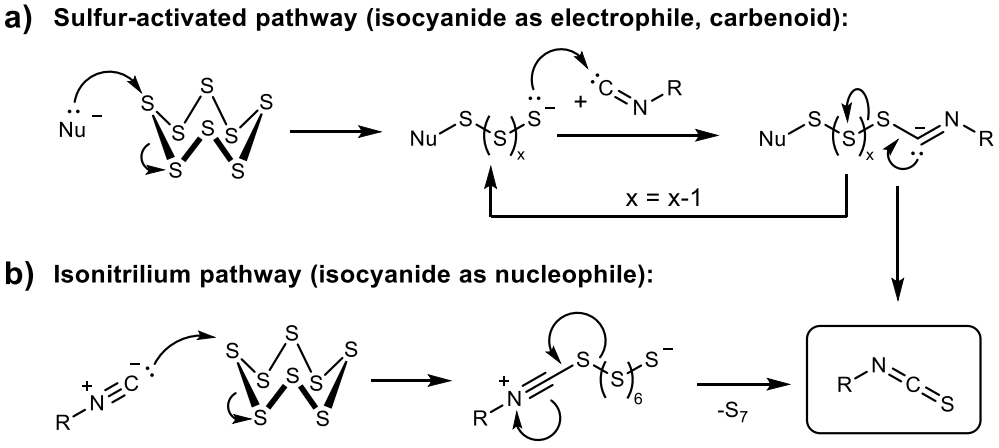

Scheme 19 *Proposed mechanisms for the formation of isothiocyanates via sulfurization of isocyanides with elemental sulfur.*[265,266]

2.3.2. Sulfur-based Multicomponent Reactions (SMCRs)

Multicomponent reactions (MCRs) are defined as reactions in which three or more compounds react to form a product, which consists of most of the atoms of the used starting material, typically resulting in high atom economies.[267–269] Their modular character enables a vast amount of possible products, thus this class of reactions is often used in combinatorial chemistry.[270] Multicomponent reactions can be categorized as a subclass of one-pot reactions, which enable a secondary transformation of an *in situ* generated compound without isolation in the same flask. This allows for shorter reaction times and typically more straightforward work-ups with less waste generation compared to the corresponding step-wise synthesis, which is beneficial both synthetically and in terms of sustainability.[268,269] Since the introduction of the Strecker synthesis in 1850 for the formation of α-amino acids,[271] many more multicomponent reactions were introduced, for example, the Mannich reaction,[272] Hantzsch reaction,[273] or isocyanide-

based MCRs like the Passerini[274] and Ugi reactions.[275–277] The inexpensive, inodorous, and nontoxic characteristics of sulfur make it a desirable substrate for MCRs to access both highly diverse and complex organic structures.[278,279]

The first reported elemental sulfur-based multicomponent reaction is the Willgerodt-Kindler reaction, discovered in 1923 by Kindler as a refinement of the Willgerodt reaction.[280] The original Willgerodt reaction involves the synthesis of terminal (thio)amides from alkyl ketones with ammonium sulfide and ammonium hydroxide.[281,282] Kindler discovered that elemental sulfur and ammonia could be used instead of ammonium sulfide, which reduces the typical reaction temperature from >160 °C to 100 °C.[280] The scope of the reaction increased even further after discovering that primary and secondary amines could be used instead of ammonia, resulting in the corresponding substituted amide (**Scheme 20**).[283]

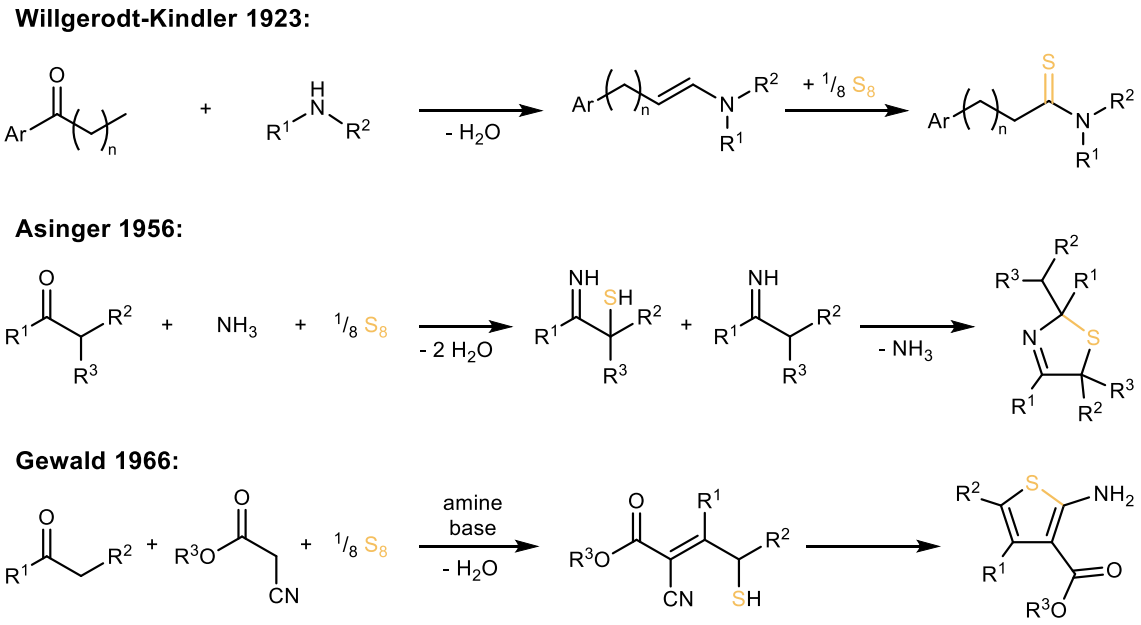

Scheme 20 *Overview of three sulfur-based multicomponent reactions.*

Another very established sulfur-based multicomponent reaction is the Asinger reaction, which was discovered in 1956.[284] It consists of the reaction of a ketone with ammonia and elemental sulfur, resulting in a substituted 3-thiazoline heterocycle (**Scheme 20**). Unlike the Willgerodt-Kindler reaction, the Asinger reaction readily proceeds at room temperature, and it is industrially used for the synthesis of 2-isopropyl-5,5-dimethyl-3-thiazoline, which is an intermediate in the production of D-penicillamine, an α-amino

acid used for the treatment of Wilson's disease,[285] cystinuria,[286] idiopathic pulmonary fibrosis,[287] and scleroderma.[288,289]

A third example of a sulfur-based multicomponent reaction is the Gewald reaction, in which an aldehyde or ketone reacts with an α-cyanocarbonyl compound and elemental sulfur forming a substituted 2-aminothiophene (**Scheme 20**).[290] The first step of this reaction involves a Knoevenagel condensation of the methylene-activated α-cyano-carbonyl compound with the aldehyde or ketone. The subsequent mechanism is not entirely understood but ultimately results in the corresponding thiophene derivative. Alternatively to the utilization of elemental sulfur, an α-mercapto aldehyde or ketone can be used in the Gewald reaction and the Asinger reaction.

The utilization of inorganic elemental sulfur in organic multicomponent reactions has achieved remarkable development in recent years, demonstrated by recent examples in the literature, as shown in **Scheme 21**.

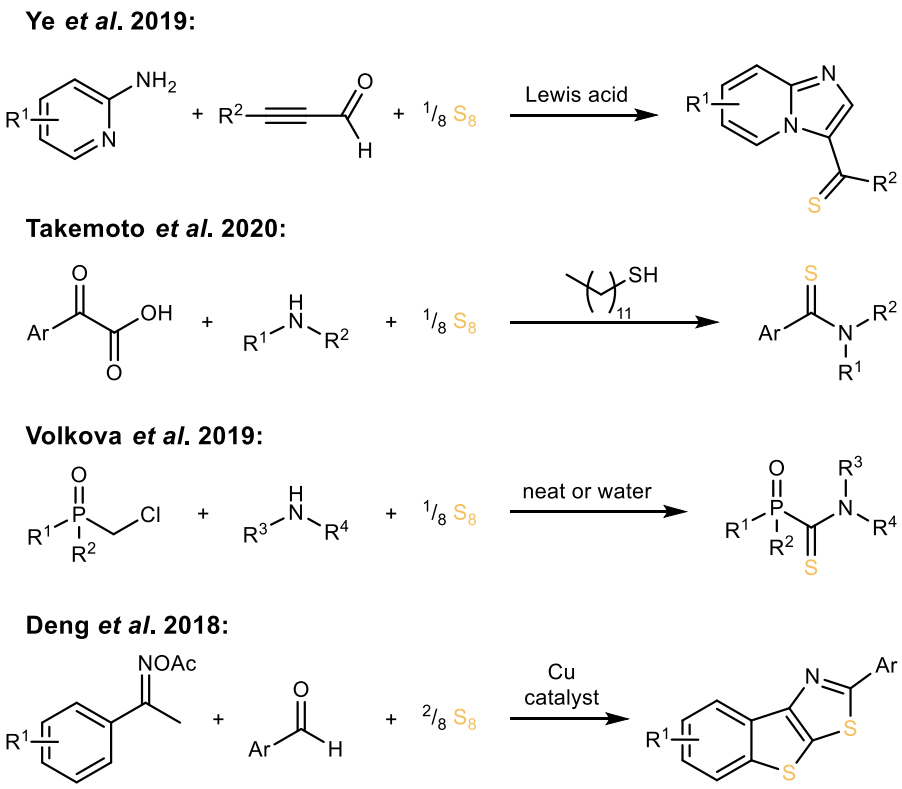

Scheme 21 *Overview of recent examples of sulfur-based multicomponent reactions.*[278]

A three-component annulation reaction of 2-aminopyridines with ynals and elemental sulfur was presented by Ye *et al.* with $Sc(OTf)_3$ as the Lewis acid catalyst in this reac-

tion.[278,291] This annulation resulted in imidazo[1,2-a]pyridine thiones and was demonstrated for 37 examples. A thioacylation of amines with α-keto acids and elemental sulfur was demonstrated by Takemoto *et al.* in 2020.[278,292] *n*-Dodecanethiol was used as the solvent for this reaction, as it is capable of solubilizing elemental sulfur and therefore facilitates the sulfur activation. Yields of up to 97% could be achieved in this transformation under very mild reaction conditions (room temperature, **Scheme 21**). A metal-free procedure to a wide range of phosphoryl thioamides from chloromethylphosphine oxides was presented by Volkova *et al.* in 2019.[293] This reaction was demonstrated for 30 examples in water as the solvent or under neat conditions and resulted in yields of up to 99%. A bis-heteroannulation of aromatic ketoxime acetates with aromatic aldehydes and elemental sulfur resulting in fused thieno[3,2-d]thiazoles were demonstrated by Deng *et al*. in 2018.[294] The reaction proceeded under copper catalysis, and the resulting thiophene-fused polycyclic compounds were expected to find application in optoelectronic materials.

Recently, elemental sulfur was implemented in isocyanide-based multicomponent reactions. A first example was demonstrated by Al-Mourabit *et al.* in 2014 for the synthesis of asymmetric thioureas from isocyanides, amines, and elemental sulfur.[265] The amine acts in a dual role in this approach: First, it activates the sulfur *via* a nucleophilic attack, forming a polysulfide chain, as shown in **Scheme 19**. This was postulated to form an intermediate isothiocyanate by reaction with the isocyanide, which then reacts with the amine initially used to activate the elemental sulfur in a nucleophilic addition, resulting in the final thiourea compound (**Scheme 22**). The two substituents of the thiourea are determined by the isocyanide, as well as the amine, which enables the targeted synthesis of asymmetric thioureas under mild conditions and high yields of up to 99%.[265] Ábrányi-Balogh *et al.* then showed in 2019 the possibility of using alcohols or thiols instead of amines for this multicomponent reaction, resulting in thio- or dithiocarbamates.[263] The alcohol (or thiol) component was found not to be basic enough to activate sulfur and thus an additional base had to be used to form the intermediate isothiocyanate (**Scheme 22**). Sodium hydride was found to be the most effective base in this context, resulting in the highest yields of up to 94% for the optimized conditions. Ábrányi-Balogh *et al.* were able to isolate the intermediately formed isothiocyanate

when Cs_2CO_3, DIPEA, or NaOEt were used as the base, which confirmed the isothiocyanate as the intermediate of this reaction. Meier *et al.* then investigated the formation of the isothiocyanate without subsequent derivatization and tuned the reaction concerning sustainability (**Scheme 22**).[266] Optimized conditions enabled the synthesis of isothiocyanates with DBU as the base in catalytic amounts (down to 2 mol%), compared to the approach of Ábrányi-Balogh *et al.*, in which the base had to be added in (over-)stoichiometric amounts.

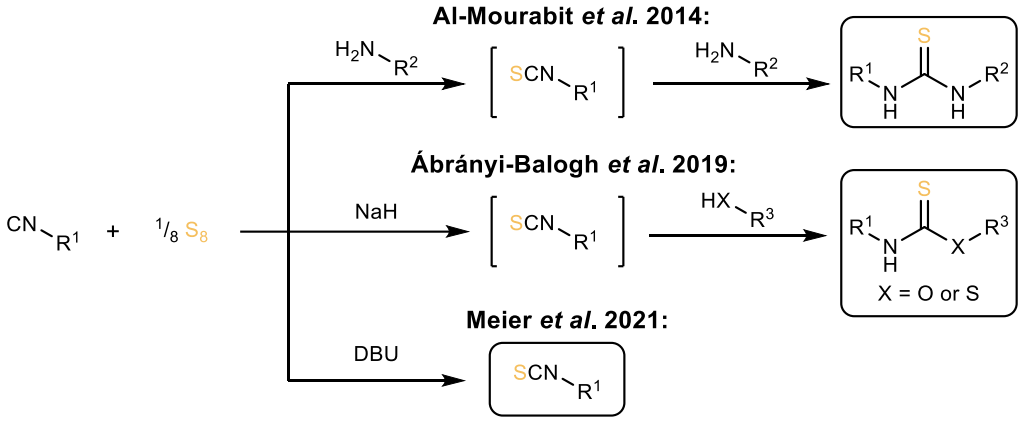

Scheme 22 *Isocyanide-based multicomponent reactions with elemental sulfur and a recent example of an organobase-catalyzed isothiocyanate formation.*

Meier *et al.* furthermore demonstrated that the formation of isothiocyanates is possible in benign solvents such as γ-butyrolactone (GBL) or Cyrene™ under mild conditions (40 °C). Moreover, this procedure is beneficial compared to other methods (see **Scheme 17**) as the reaction has 100% atom economy, utilizes elemental sulfur, and prevents highly toxic reagents like thiophosgene or Lawesson's reagent.

2.3.2.1. SMCRs in Polymer Chemistry

A clear transition from simple plastic materials to diverse functional materials for advanced applications has occurred in polymer science.[295] Recently, in the early 2000s, first reports about monomer preparation *via* multicomponent reactions and subsequent polymerizations were published. Meier *et al*. fulfilled one of the most important landmarks in this field in 2011, when they introduced multicomponent reactions as a polymerization approach to polymer science.[296] The Passerini three-component reaction based on renewable monomers was used to form novel polyesters with amide moieties in their sidechain. The previously mentioned advantages of MCRs, like the mild conditions, high efficiency, and excellent diversity of product structures, can also be transferred to polymer sciences.[277]

Combining these numerous benefits with the versatility and cost-effectiveness of elemental sulfur makes SMCRs even more attractive in the field of polymer chemistry. Therefore, a lot of exciting research was recently performed in this field, as demonstrated by a selection of SMCRs for polymer synthesis in **Scheme 23**.

Kanbara *et al*. demonstrated a possible application of the Willgerodt-Kindler reaction of dialdehydes and diamines with elemental sulfur to prepare polythioamides.[297] This three-component reaction was applied to several different dialdehyde/diamine combinations affording various polythioamides in moderate to good yields. Based on the experimental observations, an initial polycondensation affording the intermediate Schiff base polymer, followed by a subsequent nucleophilic attack of polysulfide anions to the azomethine units, was postulated as the mechanism for this type of polymerization.[297] Finally, the structure, solubility, and thermal properties of three selected polythioamides were compared to analogous polyamides, which resulted in generally better solubility with generally lower thermal stability in TGA measurements for polythioamides compared to their oxo-analogue. In 2015, Tang *et al.* presented another approach towards polythioamides *via* an SMCR using a diyne instead of the dialdehyde as shown by Kanbara *et al*.[298] This multicomponent reaction can also be categorized as a Willgerodt-Kindler reaction, but in a modified variation. Modern versions of the Willgerodt-Kindler reaction showed that alkynes could be used alternatively to aldehydes or ketones to form thioamides.[283] In 2018, the same group then presented an isocyanide-based multicomponent reaction applying elemental sulfur to synthesize

polythioureas (**Scheme 23**) based on the SMCR reported by Al-Mourabit in 2014 (**Scheme 22**).[265,299]

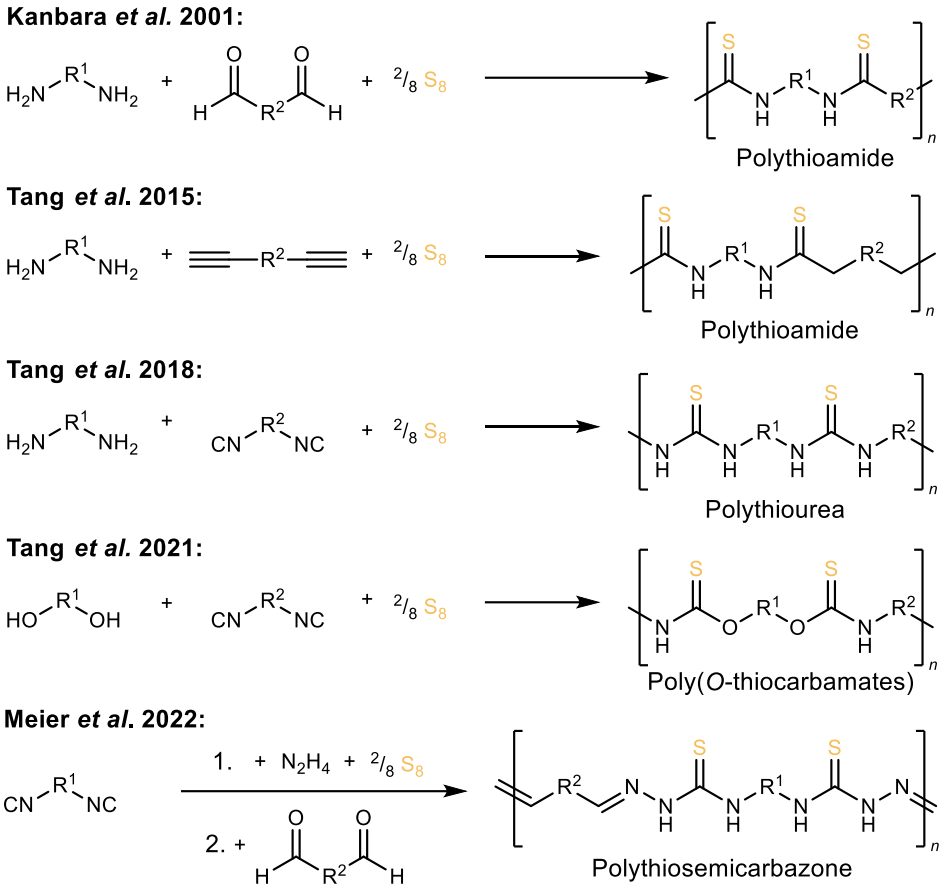

Scheme 23 *Overview of elemental sulfur-based multicomponent reactions for polymerizations via step-growth procedures.*

This SMCR was shown to proceed at room temperature without any catalyst (as the amine autocatalyzes the reaction) with 100% atom economy. A library of 16 different polythioureas was synthesized, and molecular weights of up to M_w=242 500 g mol^{-1} could be obtained with yields as high as 95%.[299]

After Ábrányi-Balogh *et al.* presented the formation of (di-)thiocarbamates from isocyanides with (dithiols) diols and elemental sulfur (**Scheme 22**), this novel SMCR was then applied to polymer chemistry by Tang *et al*. in 2021 for the formation of multifunctional poly(*O*-thiocarbamates) as shown in **Scheme 23**.[300] Seven different poly(*O*-thiocarbamates) were synthesized with yields of up to 95% and the polymers were found

to exhibit high refractive indices. Incorporating tetraphenylethene moieties into the polymer backbone structure enabled the use as fluorescent sensors to detect Hg^{2+} ions with a proven selectivity over interferences by Pb^{2+}, Au^{3+}, and Ag^{+} ions.[300]

In 2022, Meier *et al.* presented the reaction of diisocyanides with elemental sulfur and hydrazine forming stable dithiosemicarbazides, which were subsequently reacted with dialdehydes resulting in polythiosemicarbazones (**Scheme 23**).[301]

These very recent findings demonstrate the versatility and some first applications that can be expected from sulfur-containing polymers synthesized *via* efficient SMCRs and thus shows the importance of more research in this field.

3 Aim

The development of truly sustainable polymeric materials is urgently needed due to the increasing environmental problems, in combination with the depletion of fossil resources. In this context, renewable polymers like cellulose-based cellophane, cellulose acetate, or celluloid remain promising. They are not only bio-based, but also show very appealing material properties and are, in some cases, biodegradable. However, due to the inert nature of cellulose as a substrate, reactive and toxic reagents, often in over-stoichiometric amounts, are needed for the chemical derivatization, thus lowering the overall sustainability of many processes. This demonstrates that besides the renewability aspect, several more factors need to be considered for the development of a sustainable polymer product.

Related to this, Anastas and Warner introduced the *Twelve Principles of Green Chemistry* in 1998,[3] which since then acted as the primary guidelines for the design of sustainable chemical procedures. They include the design of safer procedures, the prevention of toxic compounds, the use of renewable feedstocks, high atom economies, high energy efficiency, and the prevention of waste. However, the fulfillment of all these requirements is a major challenge and can only be achieved through clever design of the synthetic procedures themselves, for example by the implementation of atom-efficient tandem reactions into the polymer synthesis process. Tandem reactions inherently fulfill many aspects of green chemistry, as multiple consecutive reaction steps are coupled in a one-pot procedure, preventing the exposure to intermediate products and the necessity of isolation and purification, thus intrinsically increasing the efficiency and sustainability.

This work aims for the development of novel procedures for the sustainable synthesis of polymeric materials, in which as many of the *Twelve Principles of Green Chemistry* as possible should be implemented. This was performed based on two promising renewable substrates: (i) cellulose as the most abundant renewable biopolymer on earth and (ii) castor oil as a renewable polyol that is directly derived from nature.

4 Results and Discussion

In this chapter, the results of this thesis are presented and discussed in detail. It is subdivided into 4 parts: in chapter 4.1, a novel synthetic approach is described to obtain cellulose acetates from cellulose and vinyl acetate in the DMSO/DBU/CO_2 switchable solvent system, offering benefits compared to existing procedures concerning the resulting material properties and sustainability aspects. Chapter 4.2 deals with a novel method for the determination of the degree of substitution of cellulose esters *via* ATR-IR spectroscopy. In chapter 4.3, a new concept is introduced that combines a tandem reaction approach with cellulose dissolution and functionalization. In this approach, the reactants (isothiocyanates) are generated *in situ* in the DMSO/DBU/CO_2 switchable solvent system *via* a sulfurization of isocyanides with elemental sulfur without the addition of any additional catalyst (the DBU present in the system acts as the catalyst for the formation of the reactant). Finally, in chapter 4.4, the before-investigated reaction (sulfurization of isocyanides with elemental sulfur to form isothiocyanates) was applied to another completely bio-based substrate: castor oil. In this unprecedented approach, diisothiocyanates were formed with castor oil acting as the solvent for the formation of the diisothiocyanates and then in the second step acting as the reactant (as a polyol), to form novel thionourethane thermosets.

4.1 A More Sustainable Cellulose Acetate Synthesis Approach

This chapter is based on previously published results by the author of this thesis:

Wolfs, J.; Meier, M. A. R. A More Sustainable Synthesis Approach for Cellulose Acetate Using the DBU/CO_2 Switchable Solvent System. *Green Chem.* **2021**, *23* (12), 4410–4420.[140]

Text, figures, and data are reproduced from this article and were partially edited and extended with permission from the Royal Society of Chemistry.

Abstract

Cellulose acetate is one of the most important cellulose derivatives and commercially mainly produced using the Acetic Acid Process, in which over-stoichiometric amounts of acetic anhydride and concentrated acetic acid is used to obtain cellulose triacetate. A subsequent partial hydrolysis is necessary to achieve evenly substituted cellulose acetates with lower degrees of substitution. Homogeneous acetylations in ionic liquids or other cellulose dissolving solvent systems often offer milder conditions with the possibility of a one-step synthesis of cellulose acetates with lower degrees of substitution by simply adjusting the equivalents of the acetylation agent. Here we show an efficient homogeneous cellulose acetylation process without the need of any additional catalyst or activation step using the DBU/CO2 switchable solvent system. Vinyl acetate was used as a more benign acetylation agent under mild conditions and straightforward recyclability of all employed components was demonstrated with high recycling ratios (87.0–98.9%). Less cellulose backbone degradation compared to a cellulose acetate sample synthesized by the Acetic Acid Process from the same cellulose source was shown by size exclusion chromatography (M_n=35 kDa vs. 12 kDa), which resulted in improved mechanical properties of solvent casted foils. Other homogeneous procedures reported so far (e.g. in ionic liquids) reached lower degrees of substitution, needed additional catalysts, proved to be less advantageous in terms of recycling, or required more reactive acetylation agents. Our results thus demonstrate a cellulose acetylation method with full focus on sustainability, efficiency, and applicability, resulting in an *E*-factor of 1.92 for the overall process.

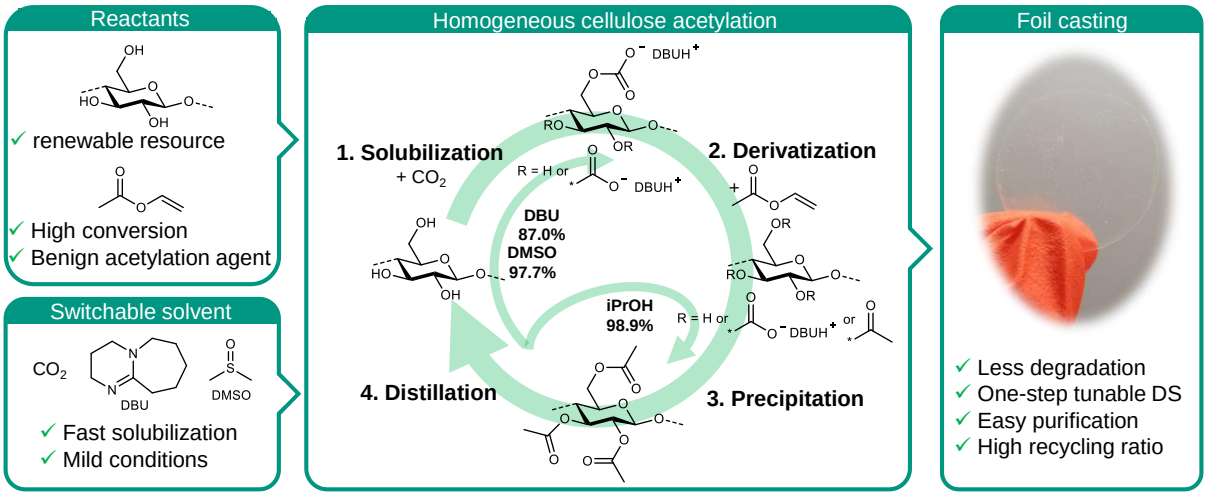

Cellulose Dissolution and Derivatization

For the homogeneous acetylation investigated herein, cellulose was first dissolved using the DBU/CO_2 switchable solvent system with the optimized conditions as reported by our group in 2018.[132] Therefore, all cellulose samples were dried under vacuum for 24 h at 100 °C to remove water, possibly causing deviations in the exact ratio of cellulose to the acetylating agent and furthermore minimizing the risk of potential side reactions. The dried cellulose was first suspended in dry DMSO at 40 °C in the presence of DBU (3 eq. per anhydroglucose unit (AGU)) and then solubilized under stirring by bubbling CO_2 into the suspension for 20 min. These very mild conditions and the rapid dissolution contribute to several benefits in terms of sustainability and efficiency compared to classic ionic liquids, which often need elevated temperatures and several hours for complete dissolution of the cellulose.[122,126] For the derivatization reaction, a calculated amount of vinyl acetate was added slowly to the solution in order to prevent local precipitation of the cellulose. The temperature was then elevated to 60 °C ensuring a rapid reaction, but at the same time prevents the vinyl acetate (b.p. 72 °C) from evaporating (steps 1 and 2, solubilization and derivatization, in **Scheme 24**).

The use of vinyl acetate has several benefits compared to acetic anhydride as an acetylating agent: First, the formed vinyl alcohol byproduct immediately tautomerizes to acetaldehyde, which evaporates due to its low boiling point (b.p. 20 °C), shifting the chemical equilibrium to the product side. This ensures high conversions, reducing the amount of reactant needed and thus makes the synthesis more efficient. Second, the

acetaldehyde does not react or form a salt with DBU, keeping the concentration and therefore the catalytic activity high, even at low temperatures. When anhydrides are used, the formed acid byproduct forms a salt with DBU, reducing its catalytic activity as reported by Liu *et al*.[141] Third, the evaporation of acetaldehyde during the reaction facilitates the subsequent recycling process of the DMSO/DBU mixture. If anhydrides are used as acetylation agents, the formed DBU salt ([DBUH][OAc] in the case of acetic anhydride) commonly needs to be neutralized (with e.g. NaOH) and then extracted to recover the DBU.[137] This additional step leads to generation of more waste, consequently increasing the environmental footprint and cost. Instead, the captured acetaldehyde can be used for other reactions (especially from larger scale acetylations with vinyl acetate), as acetaldehyde is a bulk chemical needed for many industrial processes. Moreover, as already described in the introduction, vinyl acetate is a more sustainable and less toxic alternative to acetic anhydride.

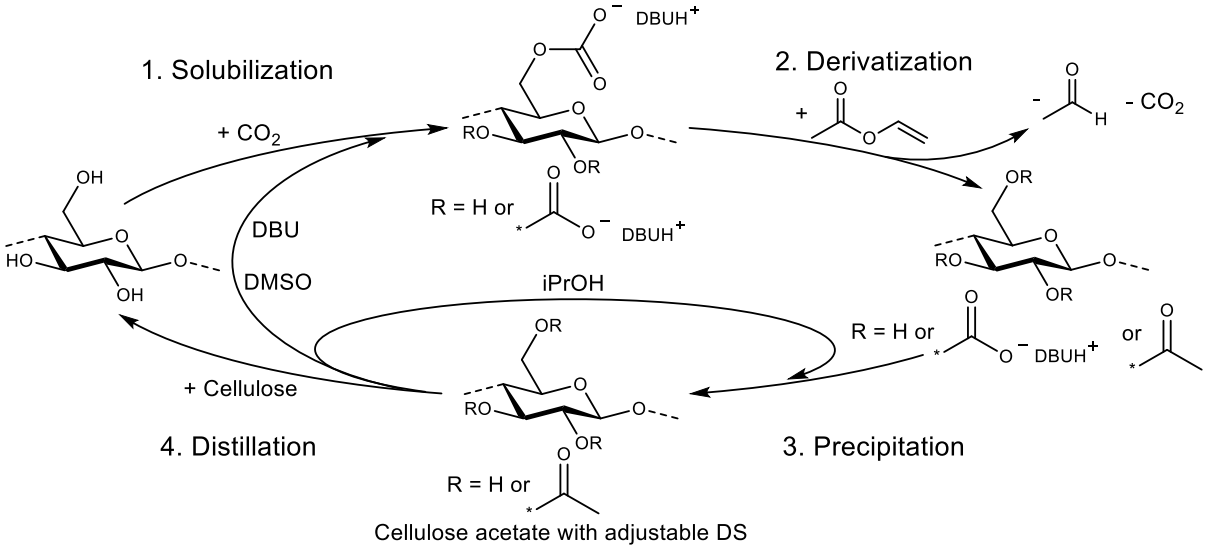

Scheme 24 *Dissolution and activation of cellulose in a DBU/CO_2 switchable solvent system with subsequent acetylation using vinyl acetate and recycling of the solvents.*

A linear correlation between the DS values determined via ^{31}P NMR analysis and the relation of integrals from the ATR-IR spectra was shown by Kilpeläinen *et al*.[211] Therefore, ATR-IR spectroscopy was used to optimize the reaction time by monitoring the integrals of the decreasing O-H stretching vibration signal at 3390 cm^{-1}, the increasing signal of the carbonyl stretching vibration at 1728 cm^{-1} and the increasing intensity of the C-O stretching vibration of the acetyl moiety at 1230 cm^{-1}. All signals were normal-

ized to the intensity of the C-O stretching vibration of the AGU at 1025 cm^{-1} for a relative comparison of the achieved DS, as the intensity of this signal is not significantly affected by the acetylation. It was observed that almost maximal conversion was reached after 240 min (**Figure 6**). To prevent side reactions, which can potentially lower the DMSO/DBU recycling rate, all acetylations were thus terminated after 240 min.

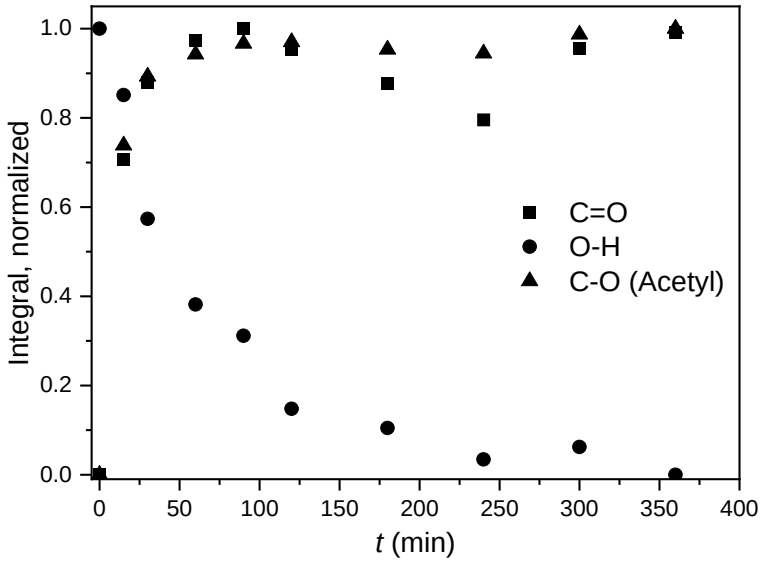

Figure 6 *Normalized integrals of the characteristic vibrations over time in the homogeneous cellulose acetylation using vinyl acetate from the respective ATR-IR signals, referenced to the AGU C-O stretching vibration signal.*

Purification of the synthesized cellulose acetate samples was performed by precipitation from an anti-solvent. Methanol, ethanol, and isopropanol are commonly used antisolvents for cellulose acetate synthesized using a homogeneous approach, but optimization studies revealed significantly lower DS values when methanol or ethanol were used. A partial transesterification of cellulose acetate with methanol/ethanol catalyzed by DBU, which is still present in the precipitation mixture, was assumed. Precipitation of a reaction mixture (3 eq. vinyl acetate per AGU, 4 h at 60 °C) from methanol, ethanol and isopropanol with subsequent stirring for 30 min revealed a lower DS for the samples precipitated from methanol ($DS_{^1H}$=1.73) and ethanol ($DS_{^1H}$=2.12) compared to the sample precipitated from isopropanol ($DS_{^1H}$=2.43) as determined by ^1H NMR spectroscopy (Experimental Section, **Figure S28**).

To confirm a possible heterogeneous deacetylation by transesterification catalyzed by DBU, a purified cellulose acetate sample ($DS_{^1H}$=2.43) was subsequently stirred in

methanol, ethanol, and isopropanol with 3 eq. of DBU per AGU for 12 h at room temperature. The resulting suspension was filtered, the solids were analyzed by ATR-IR spectroscopy and the filtrate by ^{1}H NMR spectroscopy, respectively. ATR-IR spectroscopy confirmed the deacetylation as the characteristic bands (C=O at 1728 cm^{-1}, C-O at 1230 cm^{-1} and C-H at 1025 cm^{-1}) of the acetyl moiety decreased and the O-H band at around 3390 cm^{-1} increased relative to the C-O vibration of the AGU at 1025 cm^{-1} (**Figure 7**) when methanol or ethanol was used as antisolvent. For the sample stirred in isopropanol, no significant decrease of the acetyl signals or increase of the O-H signal was detected.

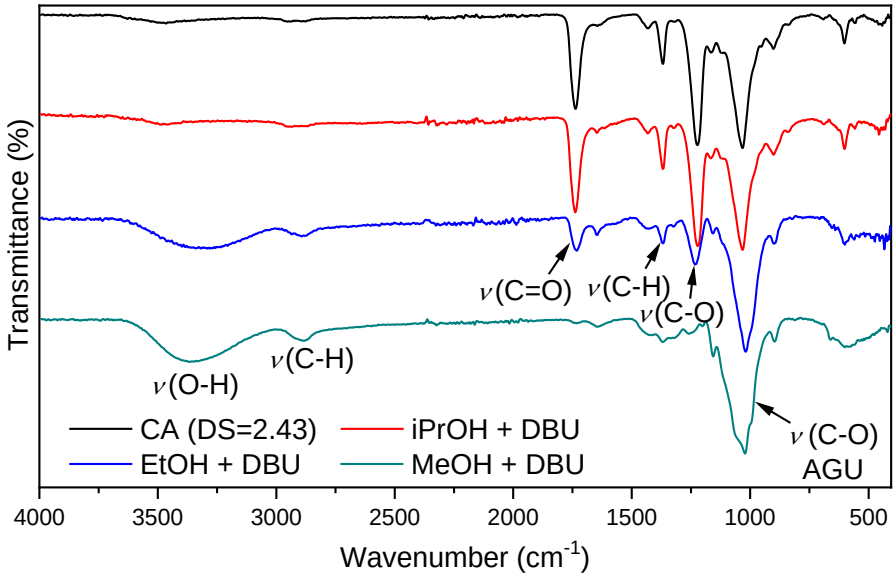

Figure 7 *ATR-IR spectra of a purified CA sample (DS_{1H} = 2.43, black) and this sample stirred in iPrOH (red), EtOH (blue), and MeOH (green) with DBU for 12 h at r.t., filtered and dried.*

The filtrates analyzed by ^{1}H NMR spectroscopy showed the formation of the respective transesterification products (methyl acetate and ethyl acetate) when methanol or ethanol was used (Experimental Section, **Figure S29**), which confirms a transesterification and deacetylation of cellulose acetate in methanol and ethanol when DBU is present. In contrast, the formation of isopropyl acetate was not observed by ^{1}H NMR spectroscopy when cellulose acetate was stirred in isopropanol in the presence of DBU.

Cellulose acetates with different DS values were synthesized by varying the equivalents of vinyl acetate using the optimized reaction and work-up procedure (**CA-1**–**CA-7**, **Table 8**, **Figure 9**).

Table 8 *Summary of the synthesized cellulose acetates and the DS obtained using different eq. of vinyl acetate (VA).*

Sample	Cellulose type[b]	Eq.VA	Yield[d]	Conversion[d]	DS_{1H}	DS_{31P}	DS C_6[f]	DS C_3[f]	DS C_2[f]
CA-1	MCC	1.0	91%	quant.[e]	1.02	1.04	-	-	-
CA-2	MCC	1.5	91%	97%	1.45	1.47	-	-	-
CA-3	MCC	2.0	91%	85%	1.70	1.73	0.80	0.71	0.22
CA-4	MCC	2.5	84%	87%	2.17	2.18	0.90	0.87	0.40
CA-5	MCC	3.0	92%	79%	2.36	2.50	0.89	0.95	0.67
CA-6	MCC	3.5	98%	74%	2.59	2.52	-	-	-
CA-7	MCC	4.5	99%	65%	2.94	2.97	0.98	0.97	1.02
CA-FP	FP	4.5	91%	59%	2.66	2.44	-	-	-
CA-HET[a]	MCC	12.9[c]	91%	23%	2.92	2.96	-	-	-
CA-REC	MCC	2.5	95%	92%	2.29	2.32	-	-	-
CA-REC2	MCC	3.0	99%	80%	2.40	2.42	-	-	-

[a]Synthesized via a heterogeneous acetylation route analogously to the *Acetic Acid Process*. [b]MCC=micro crystalline cellulose, FP=filter paper. [c]Acetic anhydride used as acetylating agent. [d]Calculated based on the DS_{1H}. [e]Quantitative conversion assumed based on a calculated conversion of 102%. [f]Calculated from ^{13}C NMR method with peak deconvolution based on the DS_{31P}.

The DS of the prepared CAs was determined by reacting the free hydroxyl groups of the respective CA sample with the phosphitylating agent 2-chloro-4,4,5,5-tetramethyl-1,3,2-dioxaphospholane (2-Cl-TMDP) to yield phosphite esters, which can be detected quantitatively via ^{31}P NMR spectroscopy. By integration of these signals and comparison with the phosphitylated internal standard *endo-N*-hydroxy-5-norbornene-2,3-dicarboximide (*endo*-HNDI-TMDP), the average DS can be calculated according to a procedure introduced by Kilpeläinen *et al*.[208] (Experimental Section, equation (*18*)).

Almost full conversion of the acetylating agent was observed for the synthesis of CAs with lower DS (Entry **CA-1** to **CA-4**, **Table 8**), whereas a 1.5-fold excess of vinyl acetate per hydroxyl group (4.5 eq. per AGU) was needed to obtain a per-*O*-acetylation of cellulose (Entry **CA-7**, **Table 8**).

Compared to other homogeneous acetylation reactions reported so far (acetylation with isopropenyl acetate in 1-ethyl-3-methyl-imidazolium acetate[123]), less equivalents of acetylating agent was required to obtain peracetylation. Higher DS could be obtained with less acetylating agent (compared to acetylation with acetic anhydride in 1-

allyl-3-methylimidazolium chloride[121,122] or acetylation with acetic anhydride in 1,5-diazabicyclo(4.3.0)non-5-enium acetate[198]). Acetylation in the DBU/CO_2 switchable solvent system using acetic anhydride[137] generally reached lower DS with higher loadings of reactant (DS=2.89, DS=2.27 and DS=1.78 for 5, 4 and 3 eq. per AGU) demonstrating the high efficiency of vinyl acetate as a mild and less toxic acetylating agent in this solvent system with the benefit of an easier solvent recycling due to the *in situ* evaporation of the formed acetaldehyde byproduct as already explained before. Kilpeläinen *et al*.[211] demonstrated an acetylation of cellulose in the ionic liquid 1,5-diazabicyclo[4.3.0]non-5-ene acetate with vinyl acetate as acetylating agent under comparable reaction conditions, but the conversion remained low (DS=1.58 with 3 eq. of VA).

The acetaldehyde side product formed during the acetylation reaction could be captured in a cold trap (-50 °C) when a slight flow of argon was applied, as confirmed by ^{1}H NMR spectroscopy (**Figure 8**). However, vinyl acetate was also captured in significant amounts due to its relatively high vapor pressure at the reaction temperature of 60 °C.

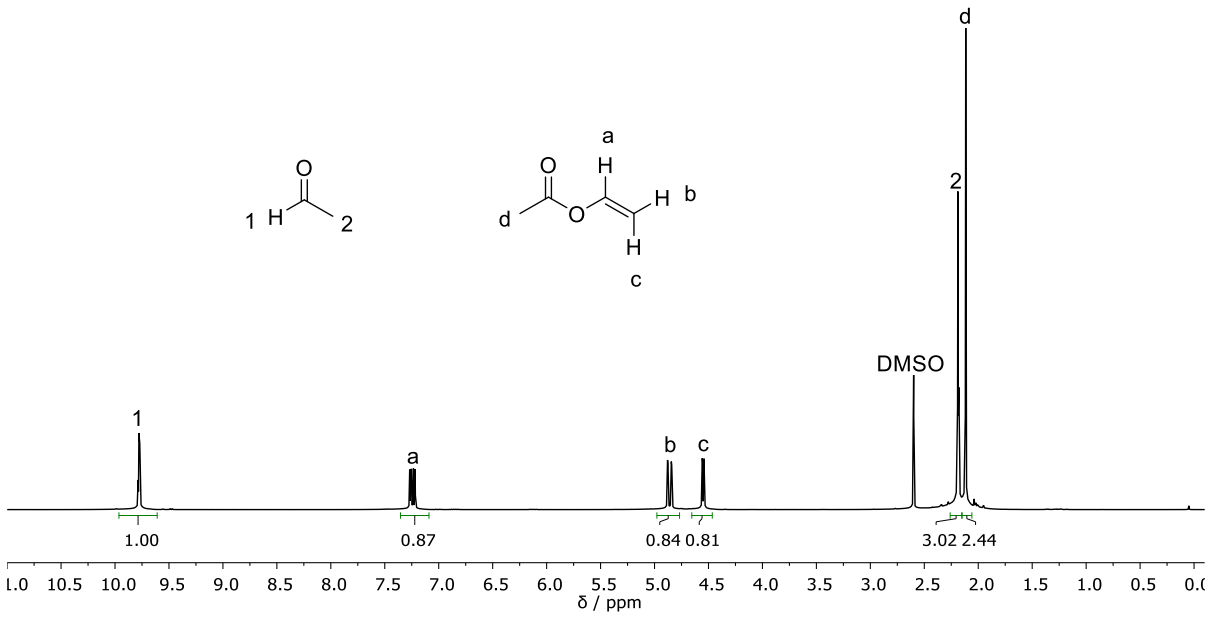

Figure 8 *^{1}H NMR ($CDCl_3$) spectrum of the acetaldehyde byproduct with unreacted vinyl acetate and DMSO captured in a -50 °C cold trap attached to the reaction flask.*

On an industrial scale with the use of more advanced fractionating columns, this can certainly be prevented, and acetaldehyde could be captured in high purity for a use in other processes. This reduces the amount of waste produced, further increasing the

sustainability and efficiency. To proof the versatility of this system, filter paper was also used as a cellulose source and acetylated successfully (**CA-FP**, **Table 8**).

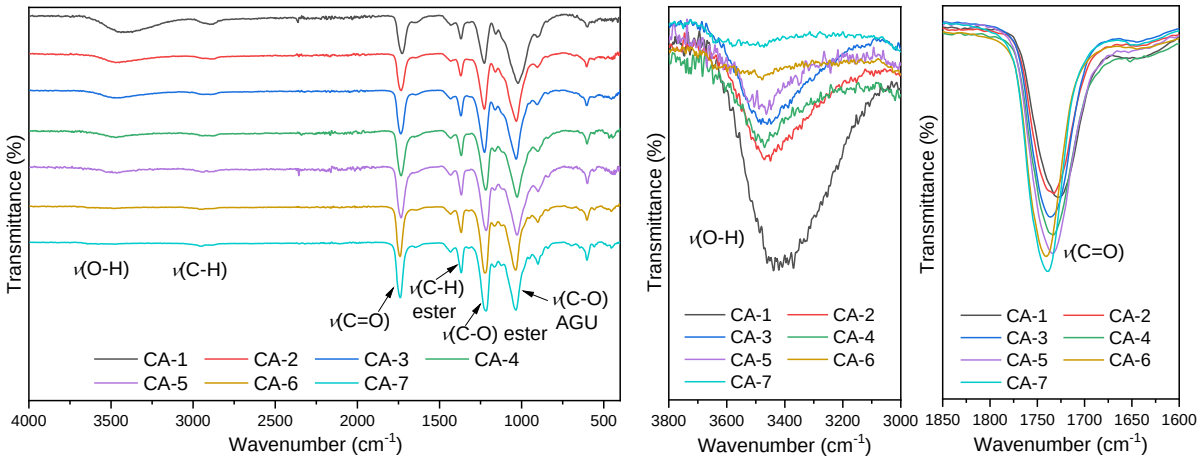

Figure 9 *ATR-IR spectra (left) and expanded views of the O-H stretching vibration (middle) and C=O stretching vibration (right) for* ***CA-1*****–*****CA-7****.*

A per-*O*-acetylated CA sample using the *Acetic Acid Process* was also synthesized (**CA-HET**) as a reference material in a modified protocol according to Malm *et al*.[152] from the same cellulose source as in the homogeneous acetylation using the DBU/CO_2 switchable solvent system. Size exclusion chromatography measurements of the two samples reveals significantly higher molecular weight for **CA-7** synthesized using the DBU/CO_2 switchable solvent system (M_n=35 kDa) compared to **CA-HET** synthesized by the *Acetic Acid Process* (M_n=12 kDa) as shown in **Figure 10a**.

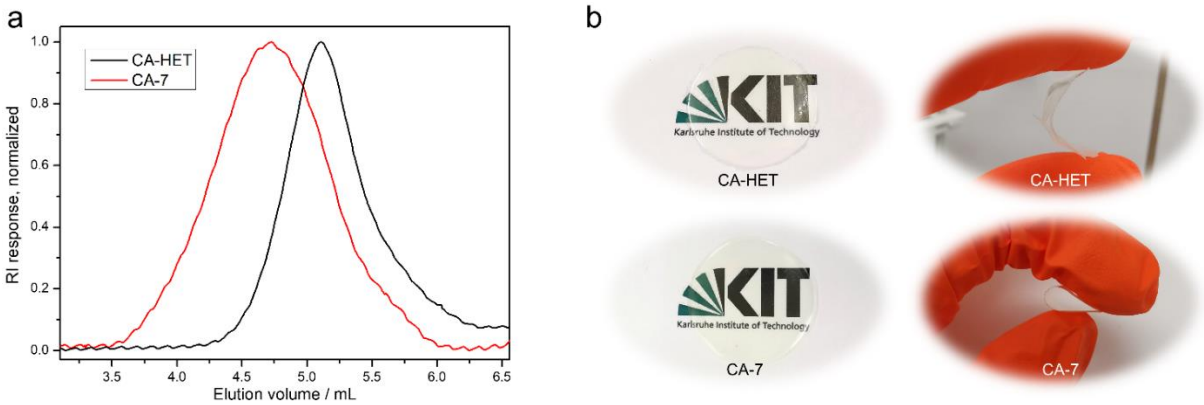

Figure 10 a *Size exclusion chromatography traces of cellulose triacetate synthesized by the heterogeneous acetylation using acetic anhydride (****CA-HET****,* DS_{31P}*=2.96,* M_n*=12 kDa) and the homogeneous route using vinyl acetate (****CA-7****,* DS_{31P}*=2.97,* M_n*=35 kDa).* M_n *were extrapolated from a PMMA standard.* ***b*** *Photographs of* ***CA-HET*** *and* ***CA-7*** *foils with bending tests of the material.*

This validates the distinctly milder acetylation conditions using this solvent system with less degradation of the cellulose backbone.

Furthermore, significant deacetylation was observed for **CA-HET** after 2.5 months storage in a closed screw cap vial (30.1% deacetylation, **Figure 11**), which is caused by the literature-known *vinegar syndrome*.[302,303] This degradation process is catalyzed by acids. Therefore, a thorough removal of residual acetic acid is crucial when using the *Acetic Acid Process* for the synthesis of cellulose triacetate. Despite profound washing and no detection of acetic acid in the ^{1}H NMR spectrum, presumably trace amounts of acetic acid remained in the sample causing an accelerated degradation. Contrary, no deacetylation was observed for **CA-7** in the same time frame (**Figure 11**), highlighting another advantage of this procedure.

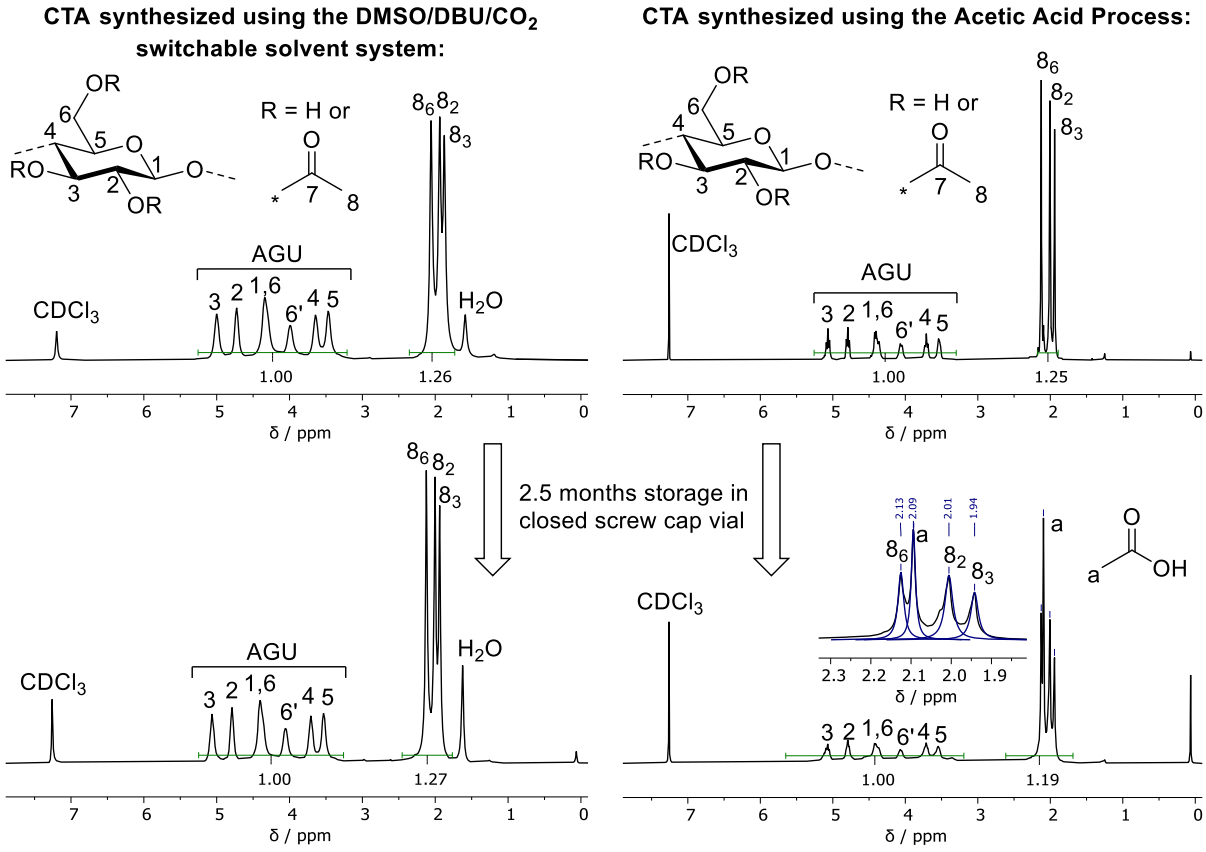

Figure 11 *^{1}H NMR ($CDCl_3$) spectra of **CA-7** before and after 2.5 months storage in a closed screw cap vial. Calculated DS_{1H} (**CA-7**) = 2.94, after 2.5 months: DS_{1H} (**CA-7**) = 2.96 (left two spectra) and **CA-HET** before and after 2.5 months storage in a closed screw cap vial (right two spectra). Peak deconvolution: blue lines in expanded view. Calculated DS_{1H} (**CA-HET**) = 2.92, after 2.5 months: DS_{1H} (**CA-HET**) = 2.04 (30.1% deacetylation).*

Tensile strength measurements were performed for **CA-5**, **CA-6,** and **CA-7**, as their DS was high enough to solubilize in acetone or chloroform, which is a prerequisite to prepare cellulose acetate foils by a solvent casting technique (**Table 9**, **Figure 12**).

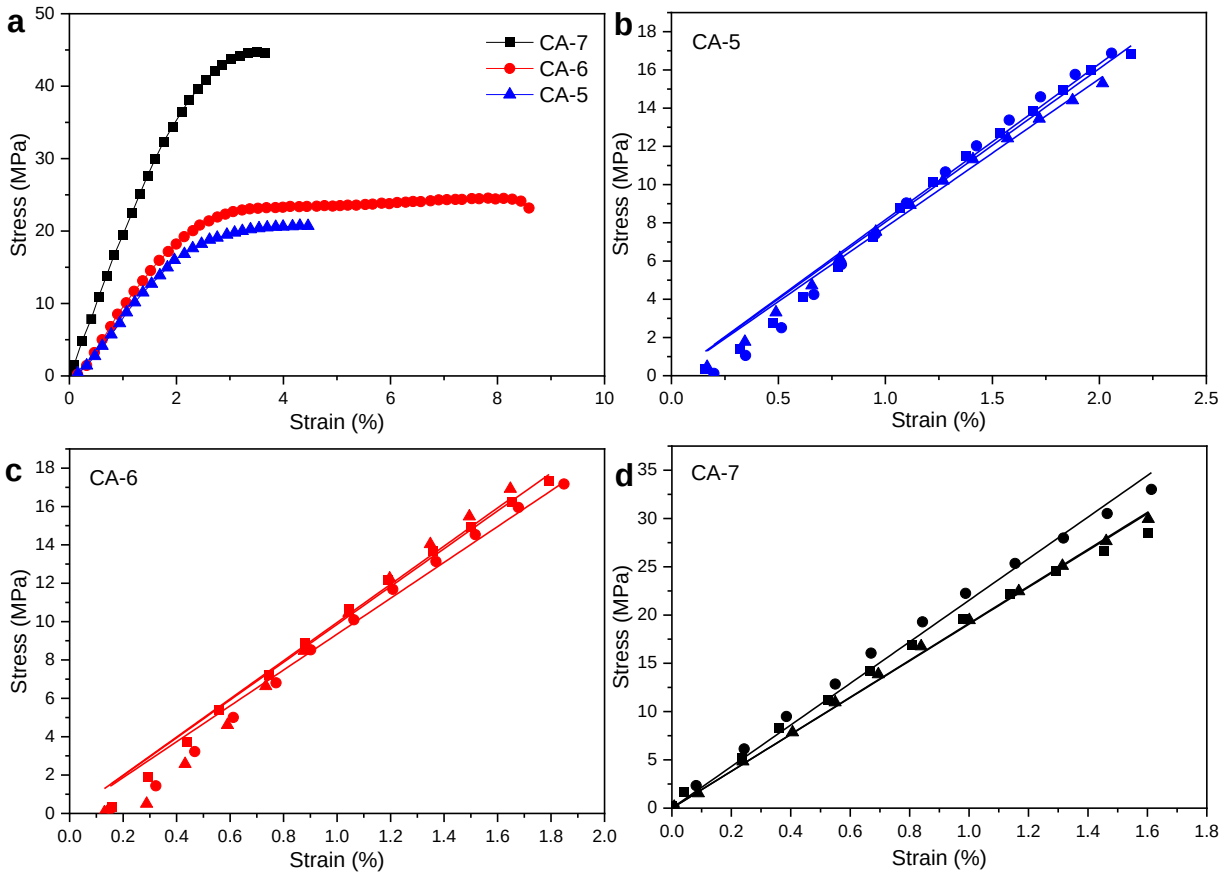

***Figure 12 a** One representative tensile strength measurement of the respective cellulose acetate film prepared by solvent casting. **b** Linear region of three tensile strength measurements with the respective linear fit for the determination of Young's moduli of **CA-5**, **CA-6**, and **CA-7** (**b**, **c**, and **d**).*

A tensile strength measurement of **CA-HET** was planned as a comparison, but the foil was too brittle to be inserted into the instrument. The foils prepared from **CA-7** and **CA-HET** were therefore compared by bending and **CA-HET** started to shatter at low deformation, while **CA-7** could be bent by 180° without breaking as shown in **Figure 10 b**, which indicates considerably better mechanical properties of **CA-7** compared to **CA-HET**, presumably due to its higher M_n. This was also observed by Sookne and Harris comparing the tensile strength of CA films with different number average degrees of polymerization ($\overline{DP_n}$).[304,305] In this report, the tensile strength of a CA film with

$\overline{DP_n}$=43 (corresponding to M_n=12.4 kDa) could not be measured due to its high brittleness, which is in accordance to the results obtained for **CA-HET**. The tensile strength of a comparable sample to **CA-7** with an M_n≈36 kDa showed a tensile strength of approx. 62 MPa, which is higher, but in a comparable range to the ultimate tensile strength measured for **CA-7** (42.9 ± 2.8 MPa). According to Sookne and Harris, tensile strength of CA films increase with higher $\overline{DP_n}$s up to an asymptotic value for CAs with $\overline{DP_n}$>500 (corresponding to M_n>144 kDa).[304] Hence, CAs with higher M_n are desirable, which can be achieved by the herein introduced homogeneous acetylation due to its milder reaction conditions, leading to less degradation of the cellulose backbone compared to the *Acetic Acid Process* as shown in **Figure 10a**. It has to be mentioned that in industrial acetylation processes, dissolving pulp is mainly used as cellulose source, which has a higher M_n compared to microcrystalline cellulose. Partial backbone degradation still leads to cellulose acetate with adequate M_n, but it remains a big challenge for industrial acetylations to reach almost fully substituted cellulose acetate with a sufficiently high $\overline{DP_n}$.[151] The Young's moduli were determined from the linear region of the stress-strain curves. An average value from 3 measurements was determined by using a linear fit and the standard deviation was calculated (**Table 9**, **Figure 12b**–**d**).

Table 9 *Thermal and mechanical characterization of the synthesized cellulose acetates with different DS.*

Sample	$T_{d,5\%}$ / °C	$T_{d,50\%}$ / °C	T_g / °C	Young's modulus / MPa	Ultimate tensile strength / MPa
CA-1	260.7	341.4	-	-	-
CA-2	233.3	350.6	-	-	-
CA-3	280.2	355.3	-	-	-
CA-4	292.0	369.9	190.7	-	-
CA-5	286.7	365.1	188.9	747.1 ± 89.3	19.5 ± 0.9
CA-6	286.4	364.9	190.0	955.9 ± 31.0	22.9 ± 1.1
CA-7	320.0	375.3	183.7	2005.5 ± 105.4	42.9 ± 2.8

The thermal stability of the CAs was determined by thermogravimetric analysis (TGA). The calculated results for $T_{d,5\%}$ and $T_{d,50\%}$ are summarized in Table 9. All samples showed a single major degradation step and an improvement in thermal stability was

observed with an increase of the DS value (**Figure 13**). The onset degradation temperature $T_{d,5\%}$ increased from 260.7 to 292.0 and 320.0 °C for the CAs with a DS_{31P} of 1.04, 2.18 and 2.97, respectively. Analogously, the $T_{d,50\%}$ also increased from 341.4 to 369.9 and 375.3 °C for the same CA samples. A $T_{d,\ onset}$ of 252 °C for a cellulose triacetate sample (DS=2.92) and 224–243 °C for a CA (DS=2.50) was observed by Kamide *et al.*[306], which is lower than the $T_{d,5\%}$ observed for comparable CAs (**CA-7** and **CA-5**, respectively), but shows the same trend with a higher T_d for increasing DS values. Higher thermal degradation temperatures of **CA-7** and **CA-5** could be explained by the absence of any residual acetic acid, which possibly lowers the thermal stability of the material. No glass transition temperature was observed for **CA-1**–**CA-3**, whereas a glass transition was observed for samples **CA-4**–**CA-5** with T_gs ranging from 183.7 to 190.7 °C.

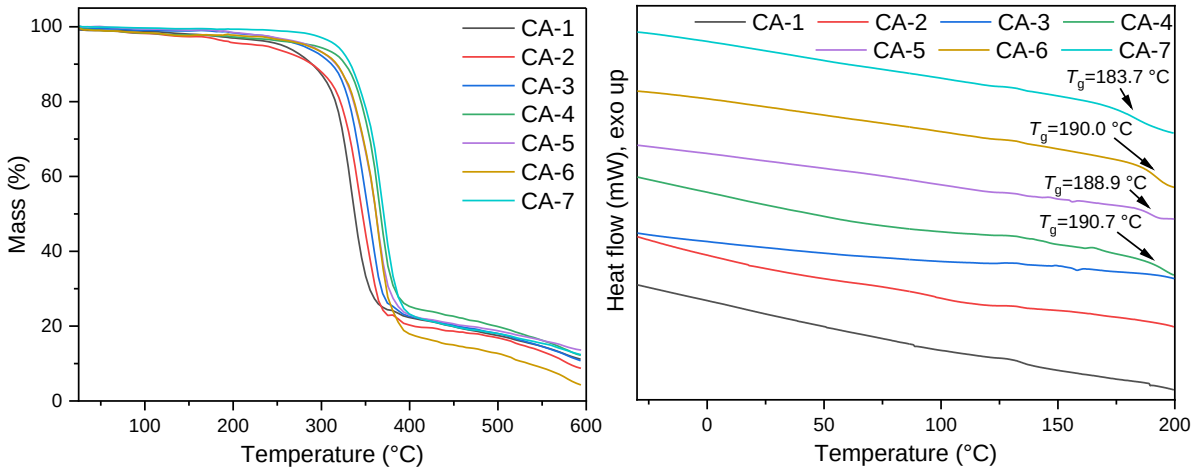

Figure 13 *TGA thermograms of all investigated cellulose acetates (left) and the corresponding DSC plots of* ***CA-1***–***CA-7*** *(right).*

The three hydroxyl groups of cellulose at the C2, C3 and C6 position are known to differ in their reactivity, resulting in a distribution of the acetyl moiety among the three hydroxyl groups for CA samples with a DS<3.[121] The DS for those three individual functionalities was investigated via ^{13}C NMR spectroscopy in an inverse gated decoupling experiment by comparing the integral of the three signals at 169.49 ppm, 169.84 ppm and 170.78 ppm, which can be assigned to the carbonyl carbons of the acetyl moiety at C2, C3 and C6 position, respectively. Due to the overlap of the signals, a peak deconvolution method was used to determine the integrals of the three peaks as

shown in **Figure 14**. Based on the calculated individual DS values, a higher functionalization is obtained for the C6 and C3 position compared to the C2 position for all investigated CA samples. Consequently, the observed order of reactivity for the acetylation is C6-OH > C3-OH > C2-OH. This result is similar to the homogeneous acetylation of cellulose with acetic anhydride in the ionic liquid 1-allyl-3-mathylimidazolium chloride[121] or in the solvent system DMAc-LiCl.[307] In the commercial synthesis of partially substituted CA, the distribution of the acetyl moieties is different from that observed in these homogeneous acetylation reactions because of the deacetylation process: During the partial hydrolytic deacetylation of fully acetylated CA, the C6 position is preferably hydrolyzed, resulting in a lower individual DS at C6 relative to the DS at C3 and C2.[93]

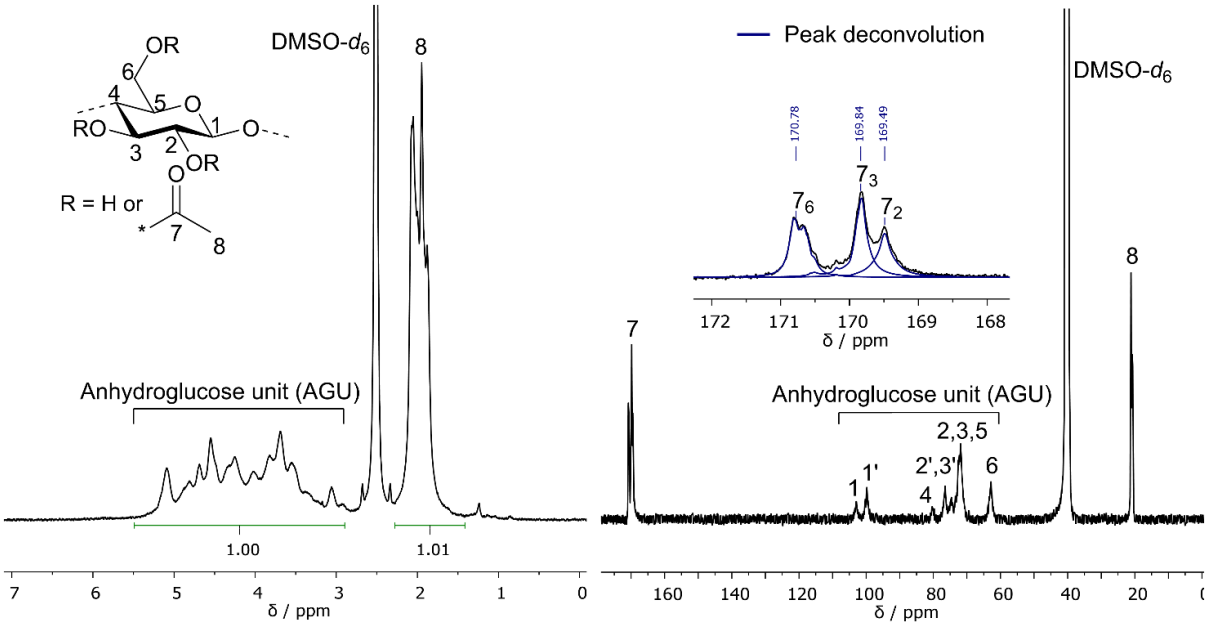

Figure 14 *^{1}H NMR (left, DMSO-d_6 + TFA) and ^{13}C NMR (right, DMSO-d_6) spectra of partially acetylated cellulose acetate (**CA-5**, DS_{31P}=2.50). Peak deconvolution: blue lines in expanded view.*

Different substitution patterns obviously lead to deviations in properties of the material, especially the solubility. In a solubility study, it was found that despite the different substitution pattern, **CA-4** (DS_{31P}=2.18), **CA-5** (DS_{31P}=2.50) and **CA-6** (DS_{31P}=2.52) were soluble in acetone, which is also observed for commercially produced cellulose diacetate (DS of 2.0-2.5) and is an important property for processability (e.g. foil casting) of the material (**Table 10**). For a sustainable homogeneous cellulose acetylation,

recyclability of the solvent and antisolvent used for precipitation is crucial as this account most to the *E*-factor (**Figure 17**). To reduce the influence of sample loss during the process and thus ensuring a more precise recycling ratio determination, a larger batch (**CA-REC**, 4.00 g cellulose) was performed. After precipitation and filtration, a mixture of isopropanol, DMSO and DBU remains to be recycled. Advantageous for the recycling steps is the low number of compounds, which need to be purified. Due to the almost quantitative conversion of vinyl acetate (92%) and the evaporation of acetaldehyde during the reaction, no side product needs to be removed.

Table 10 *Solubility chart of the synthesized cellulose acetates.*

Entry	$CHCl_3$	CH_2Cl_2	Acetone	DMSO	H_2O
CA-1					
CA-2					
CA-3					
CA-4					
CA-5					
CA-6					
CA-7					
CA-FP					

This enables an easier purification by fractional distillation as illustrated in Figure 16. In other procedures, i.e. when acetic anhydride is used as acetylating agent, the acetic acid byproduct forms a salt with DBU, complicating the recovery process.[137,308,309] After recovery of isopropanol in a first fraction, an intermediate fraction containing isopropanol and DMSO (**Figure 16**) needed to be collected to ensure a complete removal of the alcohol. This prevents a partial non-derivative dissolution mechanism with a possible transesterification side reaction of isopropanol with vinyl acetate in a second cycle. Transesterification of methanol with acetic anhydride as acetylation agent in the non-derivative dissolution approach was shown to occur by Liu *et al*.[144] To facilitate the recycling process, DMSO and DBU was then distilled together in a third fraction and the molar composition of the obtained mixture was calculated by comparison of the integrals in the ^{1}H NMR spectrum (equation (6)–(*8*), **Figure 15**).

$$\frac{n_{\mathrm{DBU}}}{n_{\mathrm{DMSO}}} = \frac{\frac{I_{\mathrm{DBU}}}{N_{\mathrm{H,DBU}}}}{\frac{I_{\mathrm{DMSO}}}{N_{\mathrm{H,DMSO}}}} = \frac{I_{\mathrm{DBU}} \times N_{\mathrm{H,DMSO}}}{N_{\mathrm{H,DBU}} \times I_{\mathrm{DMSO}}} \tag{6}$$

$$n_{\mathrm{DMSO}} = \frac{m_{\mathrm{total}}}{M_{\mathrm{DMSO}} + \frac{I_{\mathrm{DBU}} \times N_{\mathrm{H,DMSO}}}{N_{\mathrm{H,DBU}} \times I_{\mathrm{DMSO}}} \times M_{\mathrm{DBU}}} \tag{7}$$

$$n_{\mathrm{DBU}} = \frac{m_{\mathrm{total}}}{M_{\mathrm{DBU}} + \frac{I_{\mathrm{DMSO}} \times N_{\mathrm{H,DBU}}}{N_{\mathrm{H,DMSO}} \times I_{\mathrm{DBU}}} \times M_{\mathrm{DMSO}}} \tag{8}$$

n_{DBU}: amount of substance of DBU in the mixture
n_{DMSO}: amount of substance of DMSO in the mixture
m_{total}: total mass of the mixture
M_{DBU}: molar mass of DBU ($M_{\mathrm{DBU}} = 152.24\ \mathrm{g\,mol^{-1}}$)
M_{DMSO}: molar mass of DMSO ($M_{\mathrm{DMSO}} = 78.13\ \mathrm{g\,mol^{-1}}$)
I_{DBU}: integral of the DBU signal (1.73–1.62 ppm) in the ^{1}H NMR spectrum
I_{DMSO}: integral of the DMSO signal (2.70–2.30 ppm) in the ^{1}H NMR spectrum
$N_{\mathrm{H,DBU}}$: number of protons expected for the DBU signal (1.73–1.62 ppm) in the ^{1}H NMR spectrum
$N_{\mathrm{H,DMSO}}$: number of protons expected for the DMSO signal (2.70–2.30 ppm) in the ^{1}H NMR spectrum

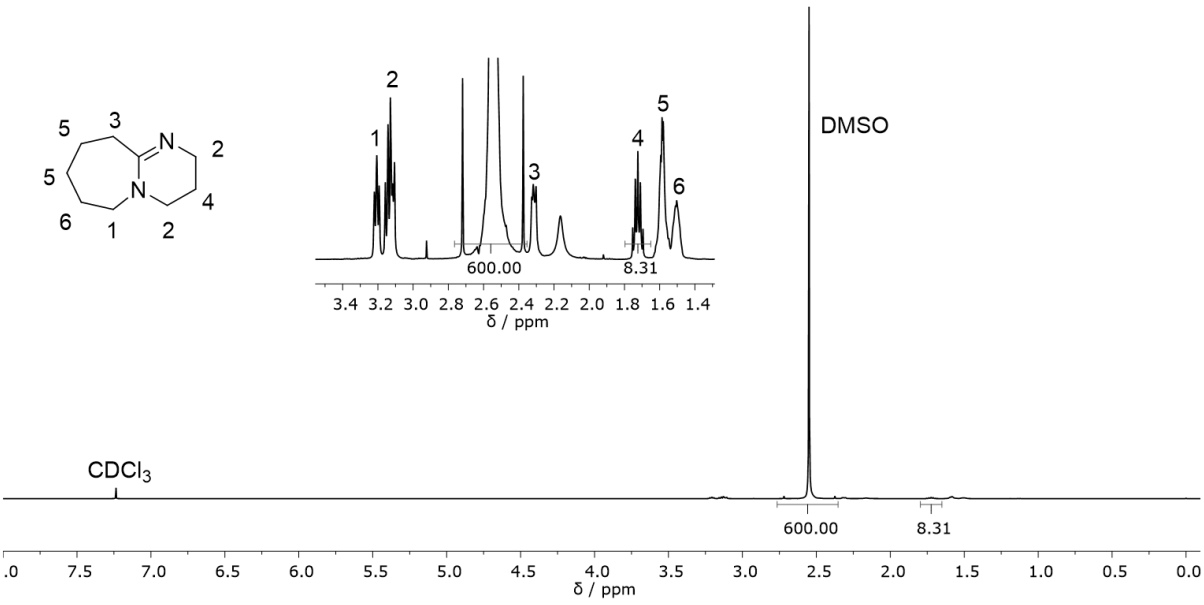

Figure 15 *^{1}H NMR ($CDCl_3$) spectrum of the redistilled DMSO/DBU mixture (3rd fraction).*

Even though minor impurities were detected in the recycled DMSO/DBU fraction, the solvent could be successfully reused in a second cycle for the homogeneous synthesis of **CA-REC2** after adjusting the molar composition by the addition of a calculated

amount of fresh DBU (67 eq. DMSO and 3 eq. DBU for 1 eq. AGU) without prior drying or considerable differences compared to a fresh batch. **CA-REC2** with a DS_{1H} of 2.40 was obtained using the recycled solvents, compared to a DS_{1H} of 2.36 for **CA-5** when fresh solvents were used (**Table 8**).

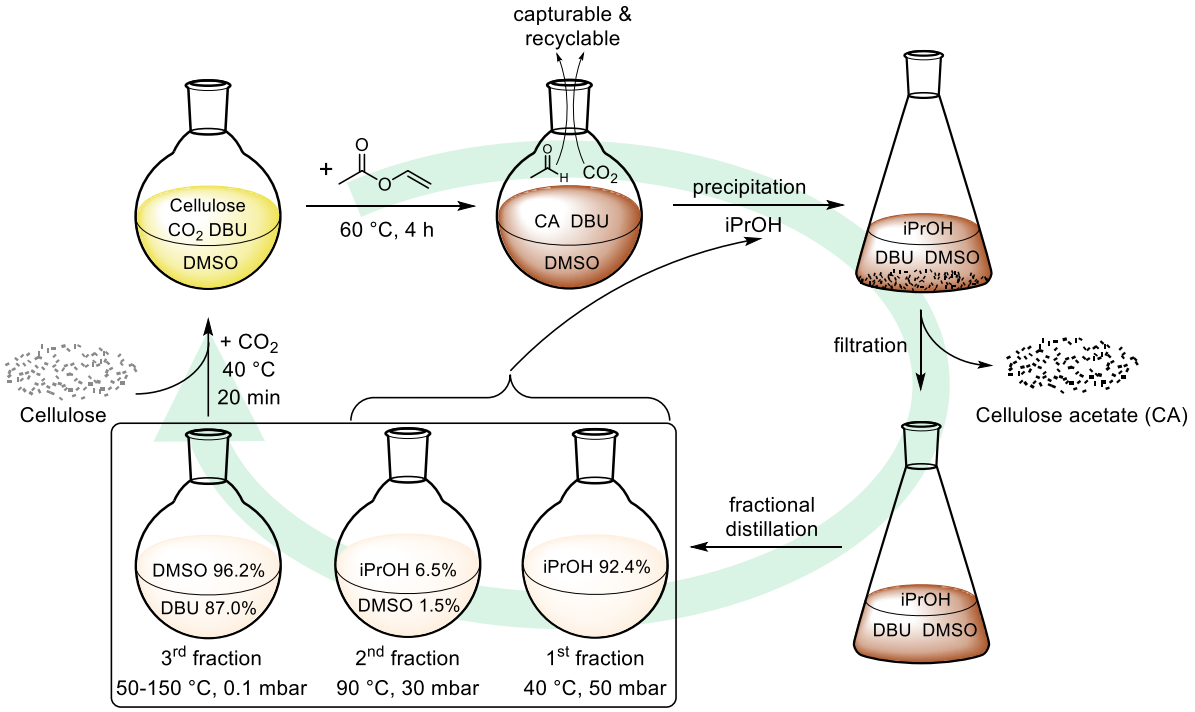

Figure 16 *Scheme for the homogeneous cellulose acetylation and recycling procedure. All recycling ratios given in % are related to the used starting material, respectively.*

The distilled intermediate fraction consisting of isopropanol and DMSO was analyzed for its molar composition, analogously to the mixed DMSO/DBU fraction, by ^{1}H NMR spectroscopy and then added to the pure isopropanol fraction as the low amount of DMSO does not affect the precipitation of cellulose acetate when used in a second synthesis and purification cycle. Including the recovered DMSO and isopropanol from the intermediate fraction, a total recycling ratio of 97.7% DMSO (96.2 + 1.5.% from the intermediate fraction), 87.0% DBU and 98.9% iPrOH (92.4 + 6.5%) was achieved for the first cycle. This is close to the recovery ratio obtained by Xie *et al*. (92% DMSO and 91% DBU) for the acetylation of cellulose with acetic anhydride using the DBU/CO_2 switchable solvent system.[137] However, the recovery of DBU is significantly more complex when acetic anhydride is used, because the solution had to be extracted with ethyl acetate and neutralized with sodium hydroxide to remove the acetic acid byproduct, which generates more waste and consequently decreases the overall sustainability.

The CO_2 used for solubilization was neglected for *E*-factor calculations due to its low impact and complex quantification. Furthermore, on larger scale, it could be recovered as it is released during the functionalization reaction. An *E*-factor of 1.92 was calculated for the overall process, which is in the range of the *E*-factor from industrial syntheses of bulk chemicals (<1–5) as reported by Sheldon.[11] This *E*-Factor is significantly lower (~3 to almost 10 times) than for other reported cellulose acetate synthesis procedures.[310] After calculation of the partial *E*-factor for every single component, it is obvious that the major contribution to the *E*-factor comes from iPrOH, as it contributed 35% to the total *E*-factor in the first cycle and 72% in the second cycle (**Figure 17**, **Figure S27**). We assume that the loss of iPrOH can mainly be explained by evaporation during the work-up procedure due to its comparably high volatility. Working in a closed system using an industrial setup together with a recovery of the used CO_2 and capturing of the acetaldehyde byproduct, an *E*-factor close to 1 should realistically be possible.

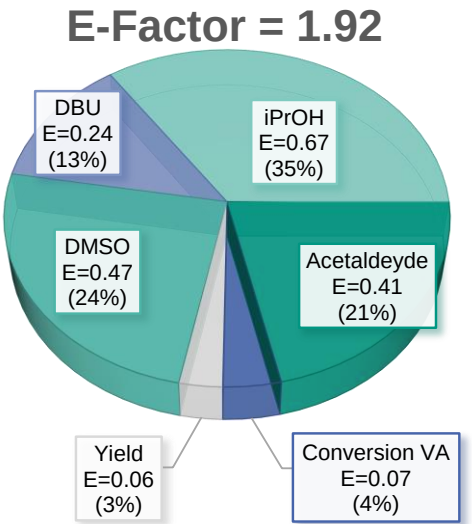

Figure 17 *Pie chart of the partial E-factors for the synthesis of* ***CA-REC*** *(DS_{1H}=2.29) in the first recovery cycle with the respective contribution to the total E-factor in %.*

In order to really evaluate whether this process is also superior over the well-refined *Acetic Acid Process* even after 100 cycles and more on a larger scale, further assessment has to be performed in pilot plants. In particular, the one-step synthesis of cellulose diacetate (DS=2.0–2.5), which typically can only be achieved in a two-step process, with a more benign acetylation agent, mild conditions, high reagent conversion,

low degradation, and easy recycling process with high recovery ratios makes the presented process a very promising and more sustainable alternative to existing procedures.

Conclusion

A sustainable and homogeneous acetylation of cellulose with vinyl acetate was achieved under mild conditions in a CO_2 based switchable solvent. After optimization of the reaction and work-up procedure by monitoring the reaction using Fourier-transform infrared spectroscopy, a set of CAs with different DS ranging from 1.04 to 2.97 were directly synthesized by varying the equivalents of vinyl acetate. The direct synthesis of cellulose diacetates (DS=2.0–2.5) is advantageous over the commercially used *Acetic Acid Process*, in which cellulose triacetate needs to be partially hydrolyzed due to its otherwise inhomogeneous distribution of acetyl groups along the polymeric chain. Higher molecular weight of the synthesized cellulose acetate was maintained when the presented procedure with vinyl acetate was applied, if compared to a sample synthesized via the *Acetic Acid Process* from the same cellulose source (M_n=35 kDa vs. M_n=12 kDa). No additional catalyst was needed, since DBU was already part of the solvent system acting as the transesterification catalyst. In other homogeneous syntheses of cellulose acetate using acetic anhydride (or acetyl chloride) as acetylation agent, the byproduct acetic acid (or HCl) is generated, which forms a salt with DBU and therefore reduces its catalytic activity and complicates the recovery, leading to the generation of more waste. All employed solvents in this system were recovered by simple fractional distillation with recycling ratios of 98.9% iPrOH, 97.7% DMSO and 87.0% DBU with 95% CA yield and a vinyl acetate conversion of 92%, resulting in an *E*-factor of 1.92. A possible capture of the generated acetaldehyde during the functionalization was shown. Thermal properties of the synthesized products were investigated by thermogravimetric analysis and differential scanning calorimetry with degradation temperatures ($T_{d,5\%}$) ranging from 233.3 to 320.0 °C and glass transition temperature (T_g) between 183.7–190.7 °C. Foils from acetone soluble samples were prepared by solvent casting and the mechanical properties were analyzed via tensile strength measurements revealing elastic moduli (*E*) between 747.1–2005.5 MPa and ultimate tensile strength values between 19.5–42.9 MPa depending on the DS of the samples.

4.2 Degree of Substitution Determination of Cellulose Esters *via* ATR-FTIR Spectroscopy

The author planned and evaluated the experiments and developed the non-linear regression approach. F. Clara M. Scheelje gave valuable input to the research work and the evaluations. Olga Matveyeva synthesized parts of the materials library (for details see chapter 6.3.2) under co-supervision of the author and was part of evaluations for the non-linear regression approach.

This chapter is based on previously published results by the author of this thesis:

Wolfs, J., Scheelje, F. C. M., Matveyeva, O., Meier, M. A. R. Determination of the degree of substitution of cellulose esters via ATR-FTIR spectroscopy *J. Polym. Sci.*, **2023**, 1–11.[311]

Abstract

Cellulose derivatives are promising bio-based polymeric materials with possible applications ranging from thickening agents and stabilizers to optical films. The precise determination of the degree of substitution (DS) is crucial, as the DS substantially influences the material properties of such cellulose derivatives. Herein, the applicability of ATR-FTIR for DS determination of cellulose esters was investigated. 16 cellulose acetates with DS ranging from 0.41 to 2.99 were synthesized and three acetyl group-specific vibrational signals were evaluated quantitatively in reference to the cellulose anhydroglucose unit vibration ν(C–O)$_{AGU}$. A non-linear correlation for the absorbance intensity with the DS was observed and the data was fitted based on a newly developed model with correlation coefficients R^2 between 0.958 and 0.998, depending on the evaluated signal. This DS determination method is simple and efficient, since it does not need any prederivatization or extensive sample preparation and can furthermore be applied to non-soluble samples. In order to widen the scope, eight cellulose butyr-

ates, six cellulose laurates and six cellulose benzoates with different DS were synthesized and the DS determination method could be analogously applied to these cellulose esters, but a separate calibration for the different esters was found to be necessary.

Synthesis of Cellulose Acetates with Different DS Values

For the DS determination of cellulose acetates using ATR-FTIR spectroscopy, a calibration needed to be recorded in the first step. Therefore, a range of cellulose acetates with different, evenly spaced DS values were synthesized directly in homogeneous solution using the (previously) established DMSO/DBU/CO_2 switchable solvent system with vinyl acetate as the reactant, as introduced in chapter 4.1 (**Figure 18**).[129,130,132,137,140,141]

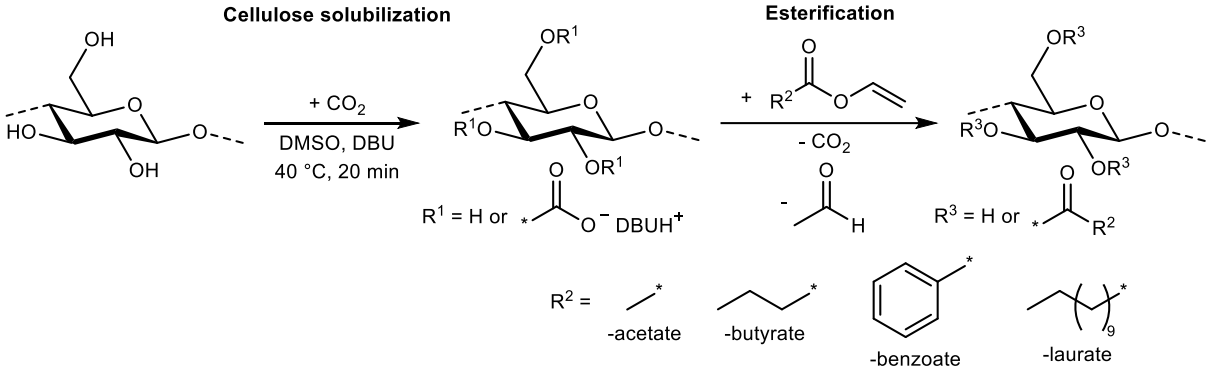

Figure 18. *Synthesis of cellulose acetates, butyrates, benzoates, and laurates with different DS.*

This synthetic route enables a precise and direct control of the DS over a very broad range by simply varying the equivalents of reactants.[140] In this way, 16 cellulose acetates were synthesized and their DS was determined using ^{1}H NMR spectroscopy (DS_{1H}) as shown in **Figure 19a**. Trifluoroacetic acid was used as an additive for the ^{1}H NMR measurements to shift the water signal to lower field, as it otherwise interfered with the signal of the AGU protons, leading to less precise integration. Next, the DS of all cellulose acetates was additionally determined using quantitative ^{31}P NMR spectroscopy after derivatization with a phosphitylation agent, applying the method as reported by Kilpeläinen *et al*. (**Figure 19b**).[208] However, the cellulose acetate samples with lower DS ($DS_{1H} \leq 1.21$) could not be measured using this ^{31}P NMR technique due to solubility issues (**Table 11**).

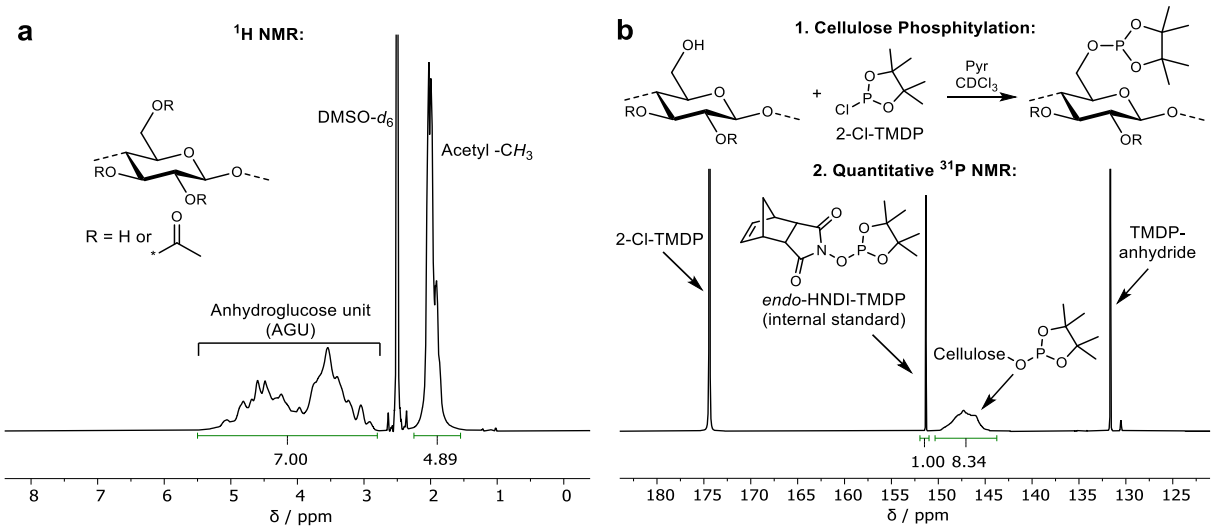

Figure 19. *(**a**) ^{1}H NMR spectrum (DMSO-d_6 + TFA) of an exemplary cellulose acetate with a calculated DS_{1H}=1.63 (**b**) and the ^{31}P NMR spectrum ($CDCl_3$) of the same sample after phosphitylation with a calculated DS_{31P}=1.64. The TMDP-anhydride results from a side reaction with water.*

Table 11. *DS values of all synthesized cellulose acetates applying different determination methods.*

Sample	DS_{1H}	DS_{31P}	$DS_{IR,O-H}$	$DS_{IR,C=O}$	$DS_{IR,C-H}$	$DS_{IR,C-O}$	DS_{IR}
CAc-1	0.41	-[a]	0.24	0.43	0.45	0.36	0.42
CAc-2	0.59	-[a]	0.47	0.57	0.53	0.52	0.54
CAc-3	0.70	-[a]	0.34	0.64	0.71	0.66	0.67
CAc-4	1.11	-[a]	1.12	0.96	1.02	1.03	1.00
CAc-5	1.21	-[a]	0.77	1.12	1.21	1.10	1.15
CAc-6	1.33	1.44	1.60	1.42	1.54	1.39	1.45
CAc-7	1.58	1.58	1.66	1.70	1.76	1.58	1.68
CAc-8	1.63	1.64	1.57	1.63	1.63	1.65	1.64
CAc-9	2.14	2.12	2.26	2.54	2.39	2.21	2.38
CAc-10	2.33	2.31	2.60	2.24	2.23	2.39	2.29
CAc-11	2.36	2.24	2.18	2.60	2.45	2.27	2.44
CAc-12	2.42	2.34	2.24	2.46	2.32	2.21	2.33
CAc-13	2.48	2.41	2.58	2.35	2.35	2.47	2.39
CAc-14	2.55	2.46	2.41	2.94	2.66	2.48	2.69
CAc-15	2.74	2.83	2.99	2.59	2.88	3.04	2.84
CAc-16	2.99	2.96	2.96	3.07	3.08	2.88	3.01

[a] Not determined due to insolubility.

The determined DS_{31P} values of the cellulose acetate samples were considerably close to those determined *via* ^{1}H NMR spectroscopy, as the calculated average relative error between the DS_{1H} and DS_{31P} was 2.7% (**Figure 20**). Both NMR-derived DS values confirm each other and are the basis of the following investigations.

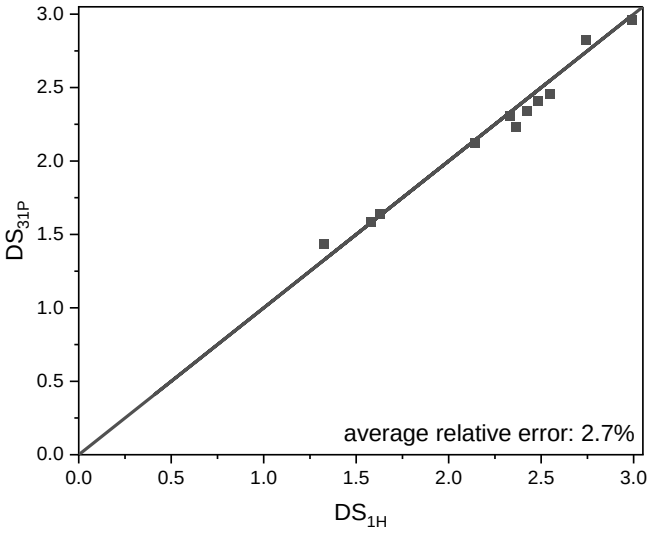

Figure 20 *Determined DS_{31P} plotted against the DS_{1H}.*

DS Determination of Cellulose Acetates via ATR-FTIR Spectroscopy

IR spectra of all cellulose acetate samples were measured using an ATR-FTIR spectrometer, making the measurements more convenient compared to a transmission FTIR instrument, as no KBr pellets need to be prepared. For every synthesized cellulose acetate, five different samples were measured to minimize possible measurement errors. The deviation of five different measurements is exemplarily shown in **Figure 21** (relative standard error for the integrated ν(C=O) signal of CAc-7 = 4.7%).

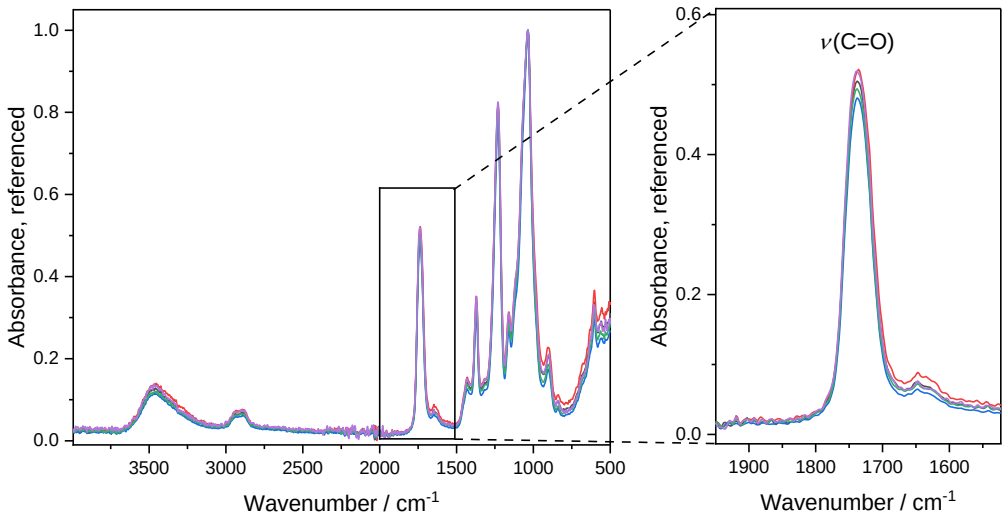

Figure 21 *Overlaid ATR-FTIR spectra of a cellulose acetate sample with DS_{1H}=1.58 (CAc-7, 5 measurements). All spectra are referenced to the $\nu(C–O)_{AGU}$ signal.*

Three main vibrational signals arise in the IR spectrum due to the acetylation of cellulose: the carbonyl stretching vibration ν(C=O) at ca. ν=1740 cm^{-1}, the acetyl C–H deformation vibration δ(C–H) at ca. ν=1370 cm^{-1}, and the acetyl C–O stretching vibration ν(C–O)$_{ester}$ at ca. ν=1220 cm^{-1}. The O–H stretching vibration ν(O–H) at ca. ν=3325 cm^{-1} decreases during the acetylation.

The strongest signal of native cellulose is the C–O stretching vibration of the AGU backbone ν(C–O)$_{AGU}$ at ν=1030 cm^{-1} and the intensity of this signal is assumed to not be affected by the degree of substitution. This signal was therefore chosen as the reference and all other signals were examined relative to it. The trend of an increasing absorbance of the three main acetyl related peaks with an increasing DS in visualized in **Figure 22**. Pure and unmodified MCC was used as the reference substance with DS=0.

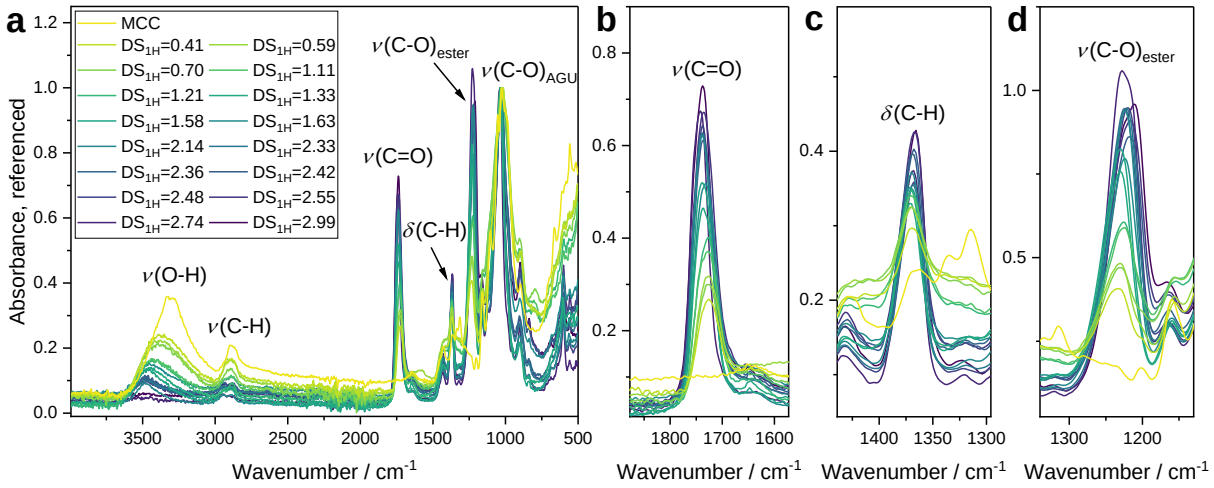

Figure 22. *Overlaid ATR-FTIR spectra of cellulose acetates with different DS values and expanded views of the ν(C=O), δ(C–H), and ν(C–O)$_{ester}$ vibrations of the acetyl moiety.*

The spectrum of native cellulose exhibits a certain absorbance intensity in the wavenumber range of all three acetyl group specific signals (ν(C=O), δ(C–H), and ν(C–O)$_{ester}$), which can be interpreted as the offset (**Figure 23**) and are quantified by the variable *c* in equation (*9*). The absorbance intensity of all cellulose acetate samples of the respective acetyl peaks were plotted against the DS$_{1H}$ and are presented in **Figure 23**. The DS$_{1H}$ was determined in triplicates from three different samples of each cellulose acetate batch and the standard deviation was calculated (error bars in **Figure 23**). The

low deviation (ranging from σ = 0.01 to 0.04) indicates high DS homogeneity within the sample of the synthesized cellulose acetates.

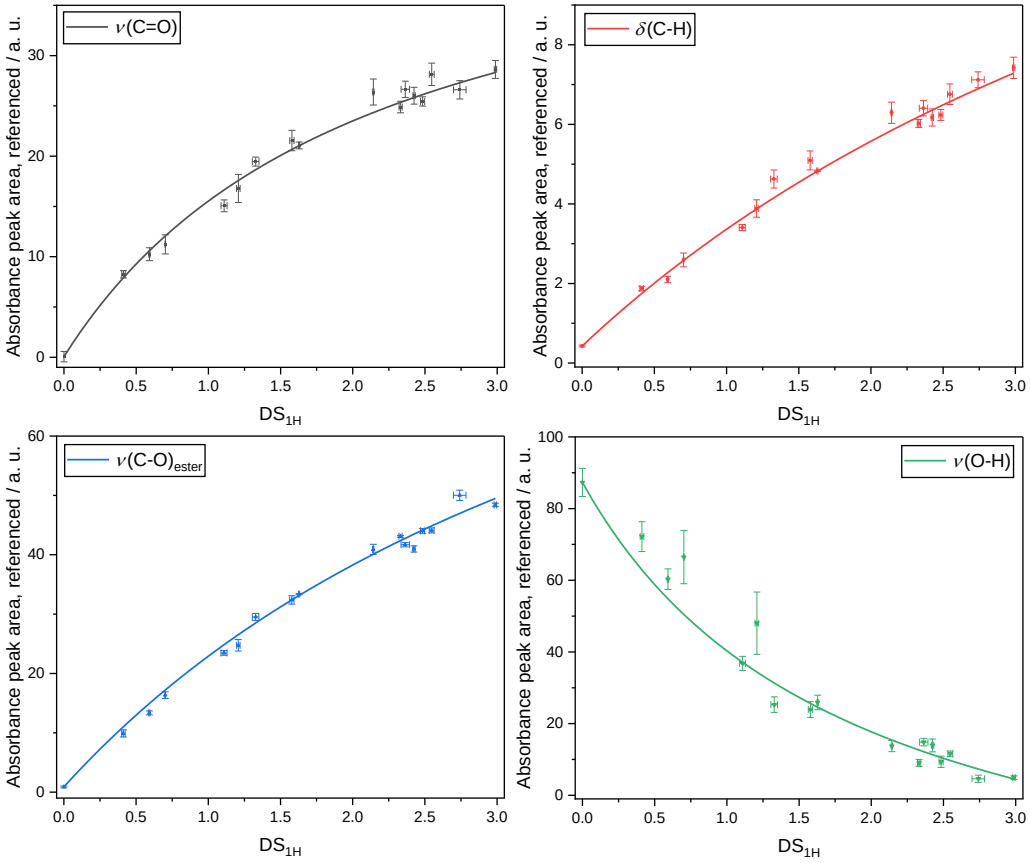

Figure 23. *Absorbance peak area of the respective acetyl signal plotted against the DS_{1H} of cellulose acetate. A non-linear regression was performed based on equation* (9)*. The absorbance of all samples was determined after being referenced to the ν(C–O)$_{AGU}$ vibration. The error bars correspond to the respective standard deviations of a fivefold determination for the absorbance and a triple determination for the DS_{1H}.*

According to Lambert-Beer's law, a linear correlation for the absorbance intensity with increasing DS was expected. However, a curvilinear correlation was observed, which is in accordance with the investigations of Cheng *et al.* for mixtures of cellulose triacetate and MCC to model cellulose acetates in a DS range of 1.80–2.85.[218] In this previous publication, it was assumed that the Lambert-Beer law has its limitations and is only valid for systems with a low dispersion coefficient or at low concentrations.[218] They found a second degree polynomial function to fit best to the observed data and took this as a confirmation of validity ($DS = ar^2 + br + c$, with *r* being the ratio between the individual acetyl signal and the C-O stretching vibration reference signal).[218] Nevertheless, the curvilinear relationship can also be explained by another, in our opinion

more plausible reason: if the reference peak intensity is influenced in a linear manner with increasing DS, which is in contrast to the previously made assumption, the relationship can be explained with equation (*9*).

$$A = \frac{a \times DS}{1 + b \times DS} + c \tag{9}$$

A is the absorbance, *a* is a peak specific constant quantifying to which extent the respective acetyl signal increases with increasing DS, *b* is a constant quantifying to which extent the reference peak is influenced with increasing DS, and *c* is the offset in *A* from zero, which is caused by the cellulose backbone structure. Two plausible scenarios could influence the reference peak in a linear manner as described by equation (*9*): first, the acetyl moieties cause an additional signal that overlaps with the ν(C–O)$_{AGU}$ signal at ca. ν=1030 cm^{-1}, therefore leading to an increase with increasing DS. This correlation is illustrated by a simulation based on modelled IR spectra (**Figure 24**). The simulation in **Figure 24** was performed with the software *Origin 9.8.0.200*. The FT-IR absorbance spectrum of CAc-7 was used as a template and the relevant peaks (ν(O–H), ν(C=O), δ(C–H), ν(C–O)$_{ester}$, and ν(C–O)$_{AGU}$) were fitted applying a gaussian fit (**Equation (10)**). The resulting five fit equations (**Table 12**) were used in the next step to simulate different DS values. The fitted ν(C–O)$_{AGU}$ peak was kept constant, whereas the ν(C=O), δ(C–H), and ν(C–O)$_{ester}$ peaks were linearly increased and the ν(O–H) peak linearly decreased (with the assumption of a linear peak intensity correlation as described by the Lambert-Beer law) and plotted for a calculated DS of 1.0, 1.5, 2.0, and 3.0 (**Figure 24 a-d**). The peak intensities based on the fitted peak equations were calculated in the range of DS=0.0–3.0 in increments of ΔDS=0.05 and plotted against the calculated DS for the ν(C=O), δ(C–H), and ν(C–O)$_{ester}$ signal (**Figure 24 e**).

$$y = y_0 + \frac{A}{w\sqrt{\pi/2}} e^{-2\frac{(x-x_c)^2}{w^2}} \tag{10}$$

Table 12 *Values of the gaussian fit equation for the different peaks for DS=1.0.*

Peak	y_0	x_c	A	w
ν(C–O)$_{AGU}$	0	1030.6	216.8	150.1
ν(C–O)$_{ester}$	0	1228.4	56.6	62.5
δ(C–H)	0	1370.1	15.2	25.3
ν(C=O)	0	1732.3	57.7	67.1
ν(O–H)	0	3450.8	66.7	141.0

Second, the reference peak ν(C–O)$_{AGU}$ can be seen as a sum of all C–O vibrations on the AGU backbone. Therefore, through acetylation, the C–O stretching vibrations in the AGU are likely shifted, which could lead to a narrower peak overlap, resulting in a relative increase of the reference peak. The second assumption is strengthened by the fact that the C–O stretching vibration of the AGU at ν=1030 cm^{-1} becomes narrower with increasing DS (**Figure 22**). With these considerations in mind, the relationship from equation (*9*) was used as the fit equation for a non-linear fit applied to the data as shown in **Figure 23**. The calculated values *a* and *b* from the non-linear fit equation as well as the offset values *c* are summarized in **Table 13**. The DS$_{IR}$ were then calculated based on the obtained results from these calibration curves (**Table 11**) and were plotted against the determined DS$_{1H}$ for a comparison of the two methods (**Figure 25**).

Table 13 *Results of the non-linear fit for cellulose acetate (CAc), cellulose butyrate (CBu), cellulose laurate (CL), and cellulose benzoate (CBz) as well as CAcs based on mixtures of cellulose triacetate and cellulose (CAc-mixtures).*

Cellulose ester	Peak	*a*	*b*	*c*	R^2
CAc	ν(O–H)	-72.310±7.320	0.540±0.094	87.282	0.958
CAc	ν(C=O)	22.738±1.113	0.470±0.048	0.062	0.993
CAc	δ(C–H)	3.414±0.129	0.163±0.028	0.428	0.998
CAc	ν(C–O)$_{ester}$	26.764±0.940	0.216±0.024	0.886	0.998
CAc-mixtures	ν(O–H)	-39.668±1.914	0.147±0.024	87.282	0.992
CAc-mixtures	ν(C=O)	20.077±1.104	0.391±0.049	0.062	0.997
CAc-mixtures	δ(C–H)	5.451±0.392	0.499±0.078	0.428	0.997
CAc-mixtures	ν(C–O)$_{ester}$	28.396±1.275	0.264±0.027	0.886	0.998
CBu	ν(C=O)	22.039±2.794	0.295±0.099	0.062	0.988
CBu	ν(C–O)$_{ester}$	30.098±4.826	0.433±0.154	0.886	0.985
CL	ν(C=O)	16.338±1.121	0.021±0.038	0.062	0.995
CL	ν(C–O)$_{ester}$	12.324±0.849	0.160±0.032	0.886	0.997
CBz	ν(C=O)	24.333±1.875	0.500±0.086	0.062	0.992
CBz	ν(C–O)$_{ester}$	60.093±10.832	1.189±0.324	0.886	0.996

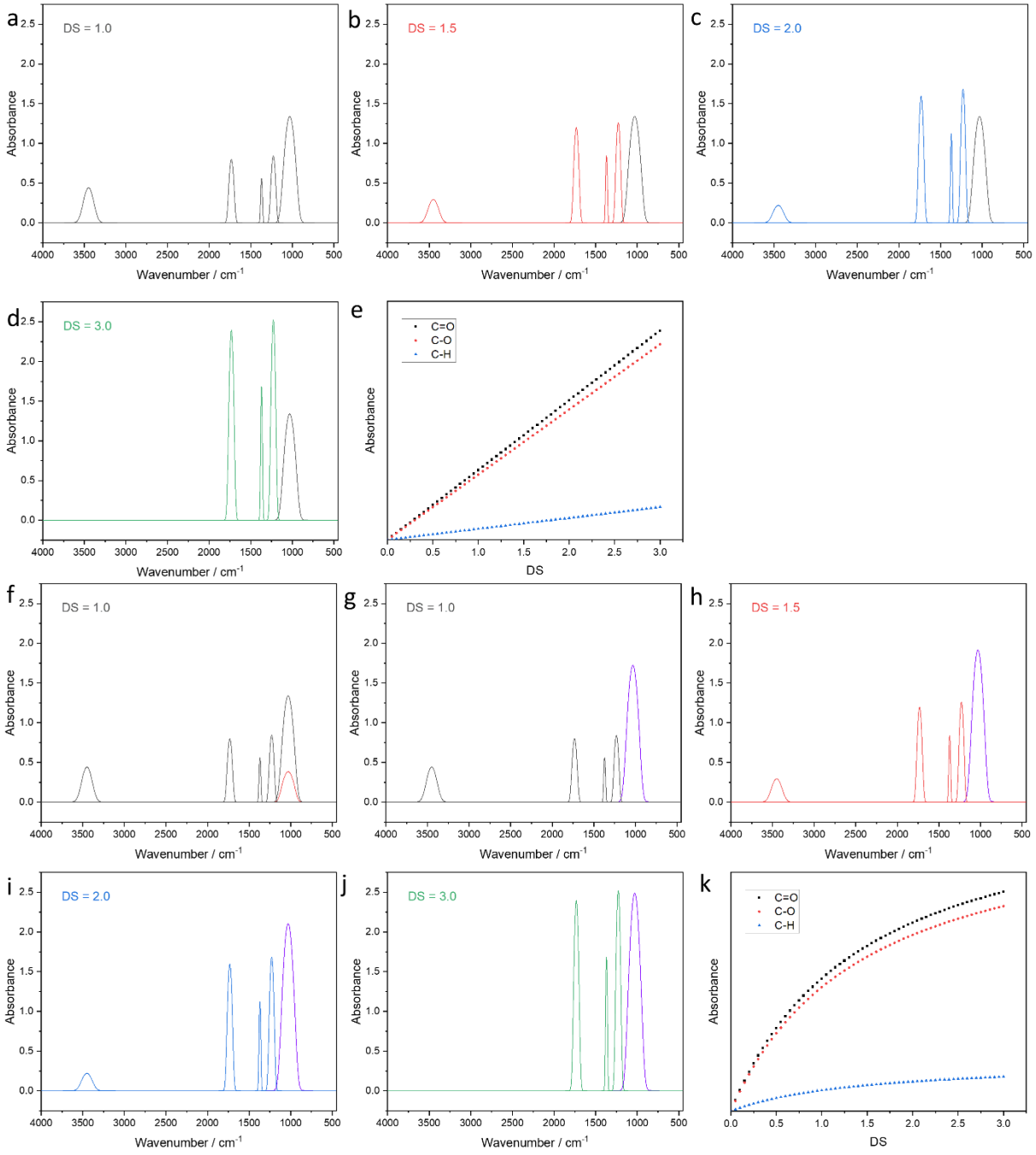

Figure 24 *(a)–(d) Simulated IR spectra of cellulose acetate with different DS, linearly increasing absorbance of the three acetyl signals (C=O, C-H and C-O vibration) with a constant absorbance of the C-O stretching vibration of the AGU as a reference signal. (e) Simulated absorbance intensities based on this model for different DS values. (f) Simulated IR spectrum of cellulose acetate with a DS of 1.0 and a hypothetical peak from the acetyl group (red), which arises at the same wavenumber as the reference peak (C-O stretching vibration of the AGU). (g) Simulated IR spectrum of cellulose acetate with the adjusted reference peak (purple) representing the sum of the two peaks: (black and red in (f)). (h)–(j) Simulated IR spectra of cellulose acetate with increasing DS and a linearly increasing reference peak. (k) Simulated absorbance intensities based on this model for different DS values.*

The comparison shows that the highest average relative error was observed for the evaluation of the O–H stretching vibration, i.e. the $DS_{IR,O\text{-}H}$ in relation to the DS_{1H}. This can be explained by i) the comparably broad ν(O–H) signal, which leads to higher uncertainties and deviations for the integration of the peak, and ii) the ν(O–H) signal is considerably influenced by water, which can be adsorbed to cellulose acetate samples in varying amounts, depending on the individual DS and the time the sample was exposed to (humid) air. Even though all samples were dried at 100 °C under reduced pressure (30 mbar) for 12 h and immediately measured, the ν(O–H) signal resulted in the highest deviations, which is also confirmed by the comparably low correlation coefficient R^2 for the calibration curve of the ν(O–H) signal (**Table 13**). The DS_{IR} were then calculated based on the obtained results from these calibration curves (**Table 11**) and were plotted against the determined DS_{1H} for a comparison of the two methods (**Figure 25**).

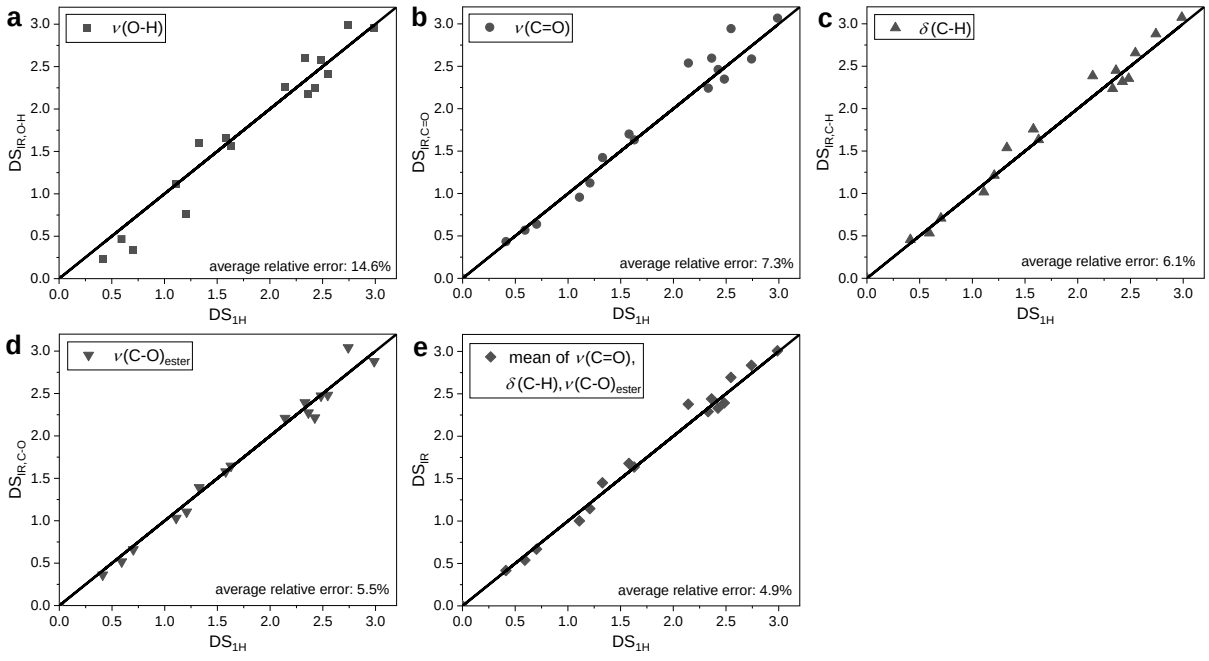

Figure 25. *DS_{IR} determined from the calibration of the respective peak (ν(O–H), ν(C=O), δ(C–H), and ν(C–O)$_{ester}$) compared to the DS_{1H} of all synthesized cellulose acetates.*

The $DS_{IR,O\text{-}H}$ was therefore not considered for further quantitative evaluations. However, in special cases, such as for the determination of historical cellulose acetate objects containing plasticizers (e.g. triphenyl phosphate or diethyl phthalate), the ν(C=O), δ(C–H), and ν(C–O)$_{ester}$ band cannot be used due to overlapping peaks from the plasticizers.

Melo *et al.* demonstrated a successful DS determination of historical objects containing plasticizers using the ν(O–H) signal.[219] Nevertheless, for pure cellulose acetate samples, the ν(O–H) signal was considered unsuitable, as explained before.

The $DS_{IR,C=O}$, $DS_{IR,C-H}$, and $DS_{IR,C-O}$ resulted in similar average relative error values (5.5–7.3%) in relation to the DS_{1H}. It was found that the arithmetic mean of the $DS_{IR,C=O}$, $DS_{IR,C-H}$, and $DS_{IR,C-O}$ results in an even lower average relative error of 4.9% as can be seen in **Figure 25e**. This averaging and thus most efficient use of all information contained in the spectra thus represents the most accurate means of calibration.

Comparison of homogeneous cellulose acetates with mixtures of CTA/MCC

In previous investigations in this field, often mixtures of cellulose acetates (mostly triacetates) with pure, unmodified cellulose were prepared to simulate cellulose acetates with different intermediate DS values.[207,218] These were then used to create calibration curves for cellulose acetate in certain DS ranges. It was often assumed that this procedure is valid, but not confirmed by a suitable comparison to calibrations performed on a broad range of homogeneous cellulose acetate samples with evenly distributed DS values. We thus prepared mixtures of CTA with MCC and compared the obtained data to the dataset we observed from homogeneous cellulose acetates (**Figure 26**). It was found that both methods led to similar results, but the deviations within the fivefold determination for a single sample are considerably higher for the mixtures (with only few exceptions), as can be seen by the error bars, i.e. the standard deviation, in **Figure 26**.

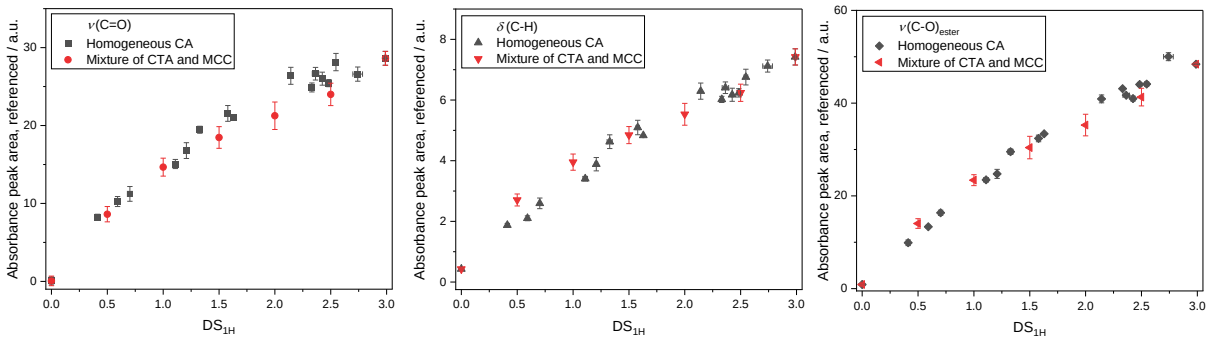

Figure 26 *Comparison of homogeneously synthesized cellulose acetates with mixtures of CTA and MCC.*

This can be explained by the higher heterogeneity within the sample, which consequently leads to deviations during the FTIR measurement, especially in the case of ATR-FTIR instruments as the penetration depth of the evanescent wave into the sample is only in the range of few micrometers.[312] This reduces the statistical effect in the measurement of heterogeneous samples and therefore leads to higher deviations for different measurements.

DS Determination of other Cellulose Esters

The calibration curve obtained from cellulose acetates was assumed to be applicable to other aliphatic or aromatic cellulose esters, as the relevant functional groups monitored via ATR-FTIR remain similar. Therefore, a set of cellulose butyrates, laurates, and benzoates with different DS were synthesized and analyzed analogously as the cellulose acetates (**Figure 27**). All determined DS values are summarized in **Table 14**. The absorbance of the two ester moiety signals $\nu(C–O)_{ester}$ and $\nu(C=O)$ relative to the reference peak $\nu(C–O)_{AGU}$ were investigated and plotted against the DS_{1H} of the respective cellulose esters (**Figure 28**). A fit based on equation (*9*) was performed and the calculated values for *a* and *b* are summarized in **Table 13**. The DS_{IR} values were then calculated based on the calibration curve from cellulose acetate, as well as an individual calibration curve based on the respective cellulose esters (**Table 14**).

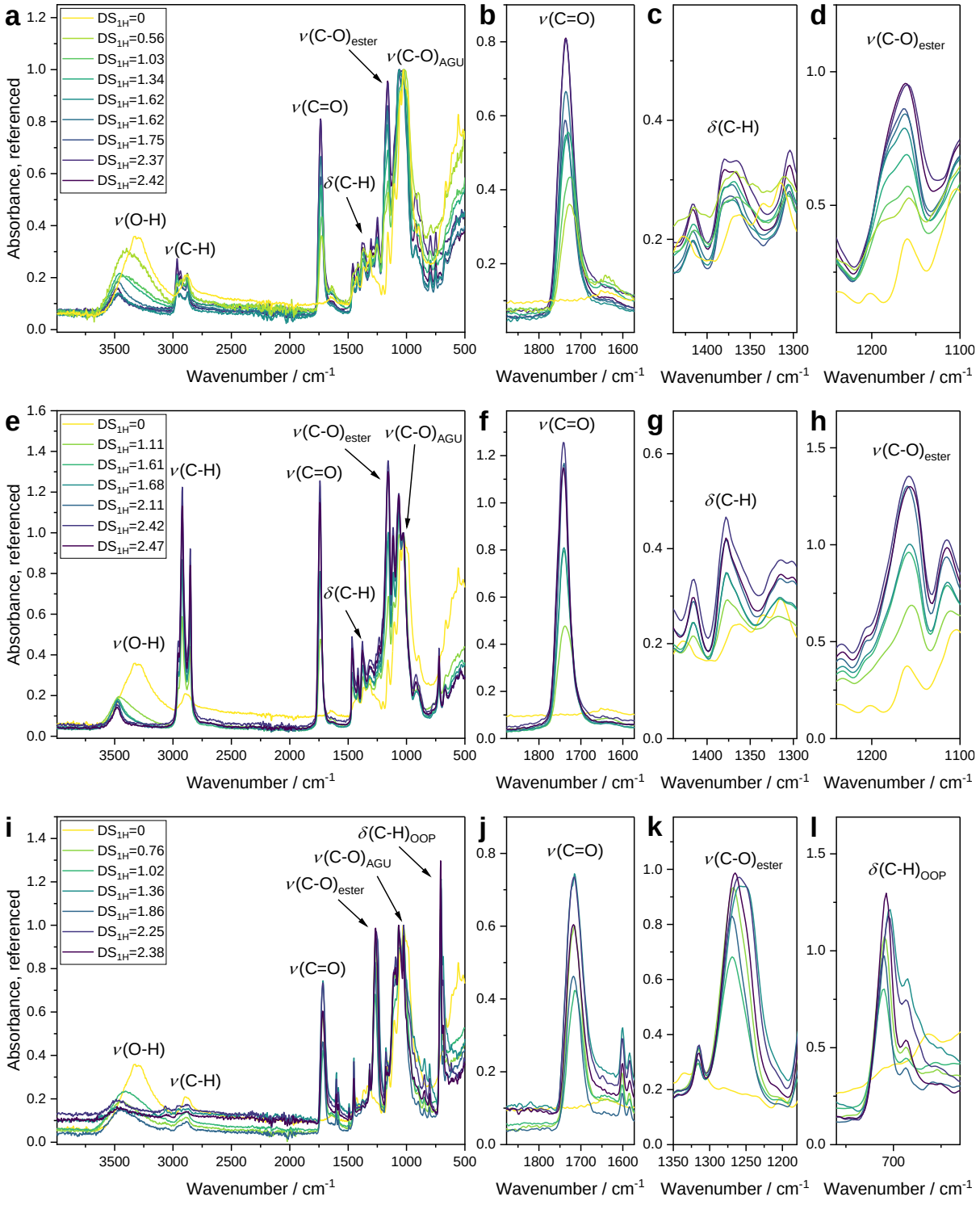

Figure 27 *Overlaid ATR-FTIR spectra of (**a–d**) cellulose butyrate, (**e–h**) cellulose laurate, and (**i–l**) cellulose benzoate with expanded views of the relevant vibration.*

Table 14. *DS values of all synthesized cellulose butyrates (CBu), cellulose laurates (CL), and cellulose benzoates (CBz) applying different determination methods.*

Sample	DS_{1H}	DS_{31P}	$DS_{IR,C-O}$ [b]	$DS_{IR,C=O}$ [b]	$DS_{IR,C-O}$ [c]	$DS_{IR,C=O}$ [c]
CBu-1	0.56	- [a]	0.56	0.62	0.57	0.67
CBu-2	1.03	1.08	0.81	0.96	0.79	1.10
CBu-3	1.34	1.42	1.25	1.47	1.13	1.87
CBu-4	1.62	1.52	1.60	1.45	1.38	1.84
CBu-5	1.62	1.63	1.84	1.77	1.54	2.39
CBu-6	1.75	1.72	1.98	1.45	1.62	1.83
CBu-7	2.37	2.24	2.22	2.39	1.76	3.77
CBu-8	2.42	2.15	2.35	2.38	1.82	3.74
CL-1	1.11	1.13	1.06	1.24	1.07	0.68
CL-2	1.61	1.49	1.65	2.92	1.62	1.29
CL-3	1.68	1.65	1.68	3.05	1.63	1.30
CL-4	2.11	1.83	2.12	6.36	2.05	2.03
CL-5	2.42	2.28	2.55	21.19	2.25	2.49
CL-6	2.47	2.25	2.28	9.09	2.13	2.18
CBz-1	0.76	0.91	0.75	0.80	0.66	1.01
CBz-2	1.02	1.07	1.10	1.18	1.06	1.37
CBz-3	1.36	1.46	1.53	1.65	1.67	1.72
CBz-4	1.86	1.79	1.62	1.74	2.15	1.92
CBz-5	2.25	2.17	2.13	2.29	2.15	1.92
CBz-6	2.38	2.34	2.46	2.65	2.01	1.87

[a] Not determined due to insolubility. [b] Calculated using a calibration based on the respective ester (CBu, CL, CBz). [c] Calculated using the calibration based on cellulose acetate.

The fitted curves were compared to the calibration performed for cellulose acetate and high deviations were obtained for the ν(C=O) vibrational signal (**Figure 28a**). The ν(C–O)$_{ester}$ signal absorbance intensities showed a better correlation to the calibration of cellulose acetate, as shown in **Figure 28b**. The absorbance intensities are differently influenced for every class of cellulose ester, as can be seen from the fitted curves, as well as from the calculated values for *a* and *b* in **Table 13**. A calibration based on the absorbance intensities of cellulose acetate can therefore not be generally applied to other cellulose esters, even if they are aliphatic and do not bear any other functional groups. A separate calibration is necessary in order to achieve sufficiently precise results. This is confirmed by the fact that the calculated $DS_{IR,C-O}$ and $DS_{IR,C=O}$ values based on a calibration from cellulose acetate differ considerably from the DS values determined *via* ^{1}H NMR, ^{31}P NMR, or ATR-FTIR with a calibration based on the respective cellulose ester itself (**Table 14**). Especially for cellulose laurates, unreliable

$DS_{IR,C-O}$ and $DS_{IR,C=O}$ values were obtained when a calibration from cellulose acetate was applied. Generally, the approach of using ATR-FTIR spectroscopy was shown to be applicable to different cellulose esters apart from cellulose acetate, but a separate calibration must be performed for accurate results based on the ν(C–O)$_{ester}$ absorbance intensity.

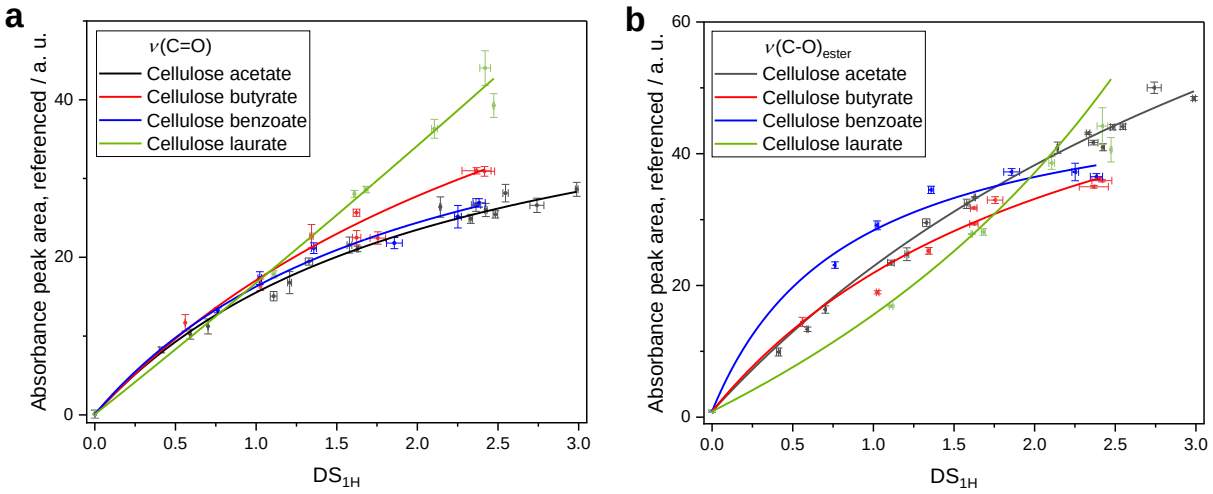

Figure 28. *Non-linear fits of the absorbance intensity of the ν(C–O)$_{ester}$ and ν(C=O) of cellulose butyrate, benzoate, and laurate plotted against the DS_{1H}. The fit of cellulose acetate is shown for comparison, respectively.*

Conclusion

The relationship between the DS and the absorbance intensity of different substituent specific vibrational signals in ATR-FTIR spectra was investigated for four different cellulose esters. 16 cellulose acetates, eight cellulose butyrates, six cellulose laurates, and six cellulose benzoates with varying DS were synthesized, and their respective DS values were determined *via* ^{1}H and ^{31}P NMR spectroscopy. The determined DS was set into relation to the absorbance intensity of the ν(C–O)$_{ester}$, ν(C=O), and δ(C–H) vibration of the ester moiety after referencing these signals to the ν(C–O)$_{AGU}$ of the cellulose AGU. A non-linear correlation was observed and a model was proposed describing this relationship. The presented DS determination method is advantageous in terms of its quick and simple measurement, but especially because of its applicability to non- or poorly soluble samples, as no pretreatment is necessary. As most other DS determination methods rely on soluble samples and the solubility in most cases reduces for cellulose derivatives with lower DS, the presented method is expected to complement existing methods.

4.3 Cellulose Thionocarbamate Synthesis *via* a Tandem Reaction Approach in the DMSO/DBU/CO_2 Switchable Solvent System

This chapter is based on previously published results by the author of this thesis:

Wolfs, J.; Nickisch, R.; Wanner, L.; Meier, M. A. R. Sustainable One-Pot Cellulose Dissolution and Derivatization via a Tandem Reaction in the DMSO/DBU/CO_2 Switchable Solvent System. *J. Am. Chem. Soc.* **2021**, *143* (44), 18693–18702.[201]

The author developed the synthetic procedure, planned and evaluated the experiments, and wrote the manuscript. R. Nickisch gave valuable input to the research work and synthesized the used *n*-dodecylisothiocyanate. L. Wanner synthesized parts of the materials library (for details see chapter 6.3.3) under supervision of the author.

Abstract

New sustainable concepts have to be developed to overcome the increasing problems of resource availability. Cellulose derivatives with tunable material properties are promising bio-based alternatives to existing petroleum-derived polymeric materials. However, the chemical modification of cellulose is very challenging, often requiring harsh conditions and complex solubilization or activation steps. More sustainable procedures towards novel cellulose derivatives are therefore of great interest. Herein, a novel concept combining two approaches is described: i) tandem catalysis and ii) cellulose derivatization applying a single catalyst for three transformations in the DMSO/DBU/CO_2 switchable solvent system. Cellulose was functionalized with four different bio-based isothiocyanates, which were formed *in situ via* a catalytic sulfurization of isocyanides with elemental sulfur, preventing the exposure and handling of isothiocyanates. The degree of substitution of the formed *O*-cellulose thiocarbamates was shown to be controllable in a range of 0.52–2.16 by varying the equivalents of reactants. All obtained

products were analyzed by ATR-IR, ^{1}H, ^{13}C, and ^{31}P NMR spectroscopy, as well as size exclusion chromatography, elemental analysis, differential scanning calorimetry and thermal gravimetric analysis. Finally, the tandem reaction approach was shown to be beneficial in terms of efficiency as well as sustainability compared to a stepwise synthesis and recycling ratios ranging from 79.1% to 95.6% were obtained for the employed components, resulting in an *E*-factor of 2.95 for the overall process.

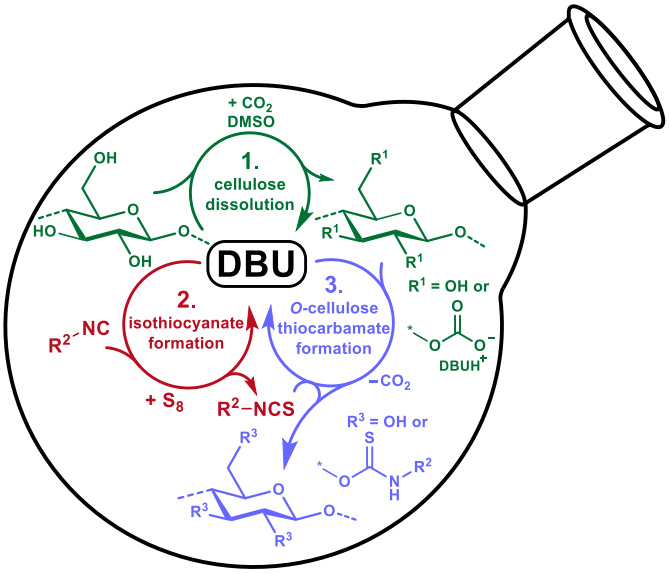

Cellulose Dissolution and Derivatization

Cellulose was dissolved in the DMSO/DBU/CO_2 switchable solvent system applying the optimized conditions as reported by our group in 2018.[132] This enables the dissolution of cellulose under very mild conditions (40 °C, atmospheric pressure) within 20 minutes, which is beneficial, especially compared to ionic liquids, as usually elevated temperatures and several hours for the solubilization of cellulose are required in these cases.[126] Then, as a first proof of concept, a functionalization of cellulose in the DMSO/DBU/CO_2 switchable solvent system with an isothiocyanate was performed as shown in **Scheme 25**. *n*-Dodecyl isothiocyanate was used as a reactant, yielding the corresponding *O*-cellulose-*N*-*n*-dodecyl thiocarbamate (**CD-1, Table 15**).

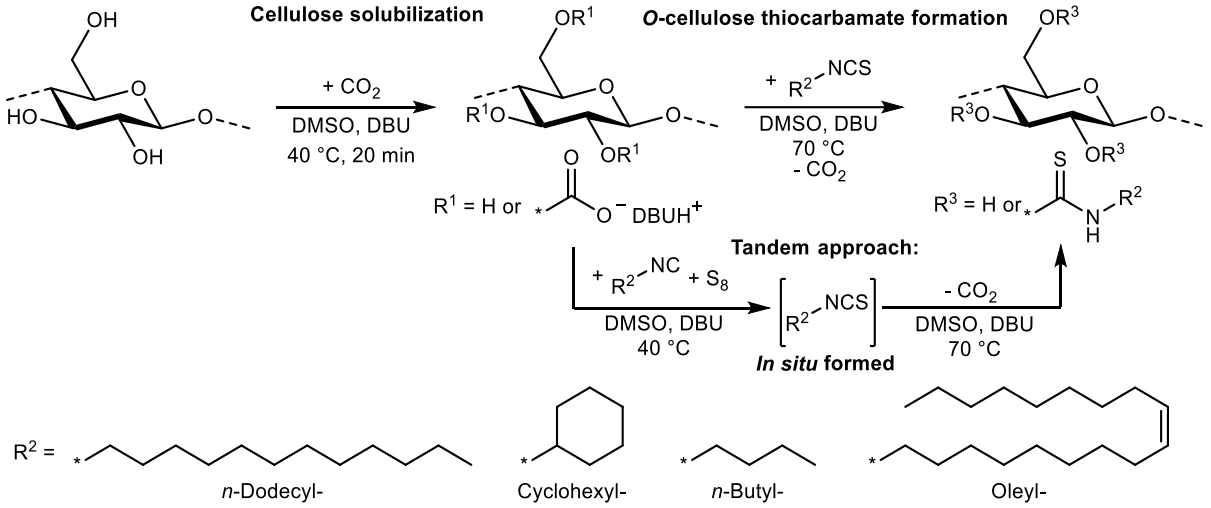

Scheme 25 One-pot cellulose solubilization in the DMSO/DBU/CO_2 switchable solvent system and subsequent derivatization with (*in situ* formed) isothiocyanates resulting in *O*-cellulose thiocarbamates. DBU has to be added only at the beginning of the cellulose solubilization.

Successful derivatization was obtained as confirmed by ^{1}H NMR (**Figure 29**) and ATR-IR spectroscopy (**Figure 38a**). However, an unexpected side reaction took place as indicated by the broad signal at δ=6.62−5.44 ppm in the ^{1}H NMR spectrum and a signal in the IR-spectrum at ν=1709 cm^{-1}, which could not be assigned to any of the *O*-cellulose-*N*-*n*-dodecyl thiocarbamate functionalities.

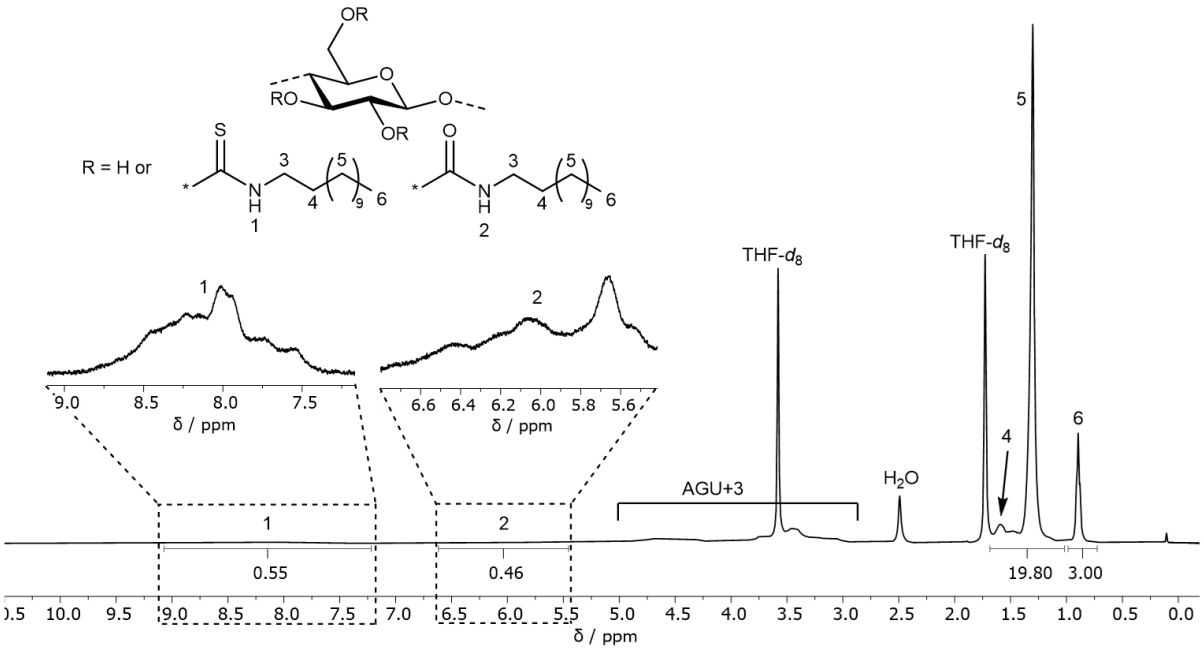

Figure 29 *^{1}H NMR spectrum (THF-d_8) of* ***CD-1****. Integrals referenced to the methyl protons* ***6****.*

Side Reaction Investigation

In order to investigate the side reaction, a model reaction was chosen to facilitate the analytical assessment, as cellulose derivatives are mostly more challenging in their structural evaluation. Cellulose was therefroe substituted by *n*-hexanol as a model alcohol component and reacted with *n*-dodecyl isothiocyanate under the otherwise same reaction conditions. Two main products were formed during this reaction and separated *via* flash column chromatography. ^{1}H NMR spectroscopy revealed the formation of 27 mol% *O*-*n*-hexyl-*N*-*n*-dodecyl carbamate, besides 73 mol% of the expected *O*-*n*-hexyl-*N*-*n*-dodecyl thiocarbamate by a comparison of the integrals of the isolated crude mixture after work-up as shown in **Figure 30**. The unexpected formation of the oxocarbamate was further confirmed by IR and ^{13}C NMR spectroscopy, as well as mass spectrometry (Experimental Section, **Figure S138**–**Figure S141**).

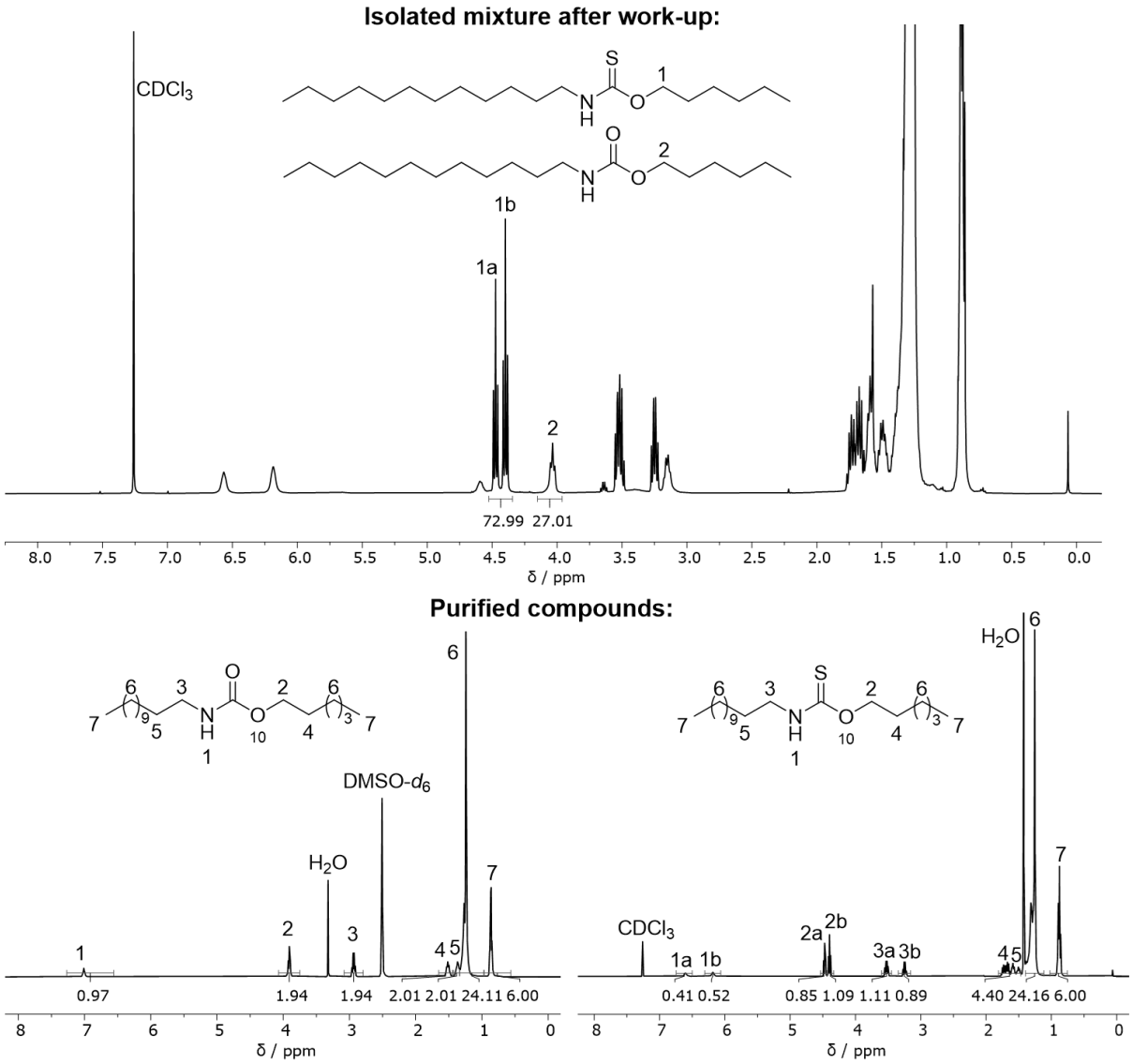

Figure 30 *Top: ^{1}H NMR spectrum ($CDCl_3$) of the crude mixture of O-n-hexyl-N-n-dodecyl thiocarbamate and O-n-hexyl-N-n-dodecyl carbamate for determination of the thio- oxo carbamate ratio. Signals a and b are observed because of the cis/trans isomerism of the thiocarbamate moiety caused by the hindered rotation due to the partial double bond character.*[313] *Bottom: ^{1}H NMR spectra (left: DMSO-d_6, right: $CDCl_3$) of the purified model compounds O-n-hexyl-N-n-dodecyl carbamate (left) and O-n-hexyl-N-n-dodecyl thiocarbamate (right).*

In order to rule out a possible conversion of the formed thiocarbamate to the corresponding oxocarbamate in a second step (as explained for various reaction conditions in the literature),[314–316] the purified *O-n*-hexyl-*N-n*-dodecyl thiocarbamate was stirred under the before applied reaction conditions and worked up analogously. However, the thiocarbamate remained stable over a period of 24 h and no conversion to the corresponding oxocarbamate was observed, indicating formation of the side product during

the reaction and not in a subsequent step. In further investigations, the stability of *n*-dodecyl isothiocyanate was checked in the switchable solvent system in the absence of an alcohol and found a near quantitative formation of *N*,*N*'-didodecylurea (**Scheme 26**).

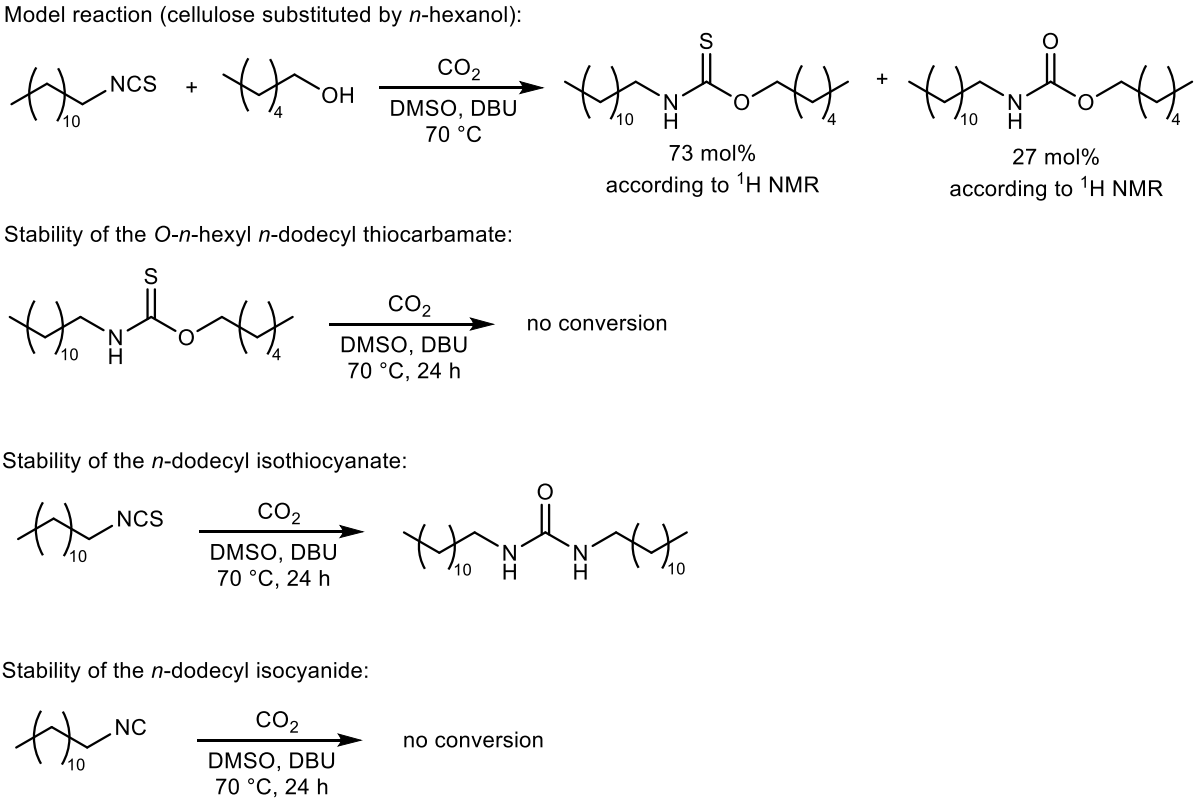

Scheme 26 *Performed control experiments for the side reaction investigation.*

With these findings as summarized in **Scheme 26**, it can be hypothesize that, even though the reaction was performed under inert conditions, small amounts of water could lead to this reaction: The isothiocyanate reacts with water, forming the corresponding thiocarbamic acid, which is unstable and decomposes to an amine and COS. The amine forms a carbamate salt with the CO_2 present in the system and then reacts with another equivalent of amine to the symmetric urea under elimination of one equivalent water as described by e.g. Zhao *et al*.[317] The recovered water keeps the cycle reacting, which explains a near quantitative conversion with just small amounts of water present (**Scheme 27**).

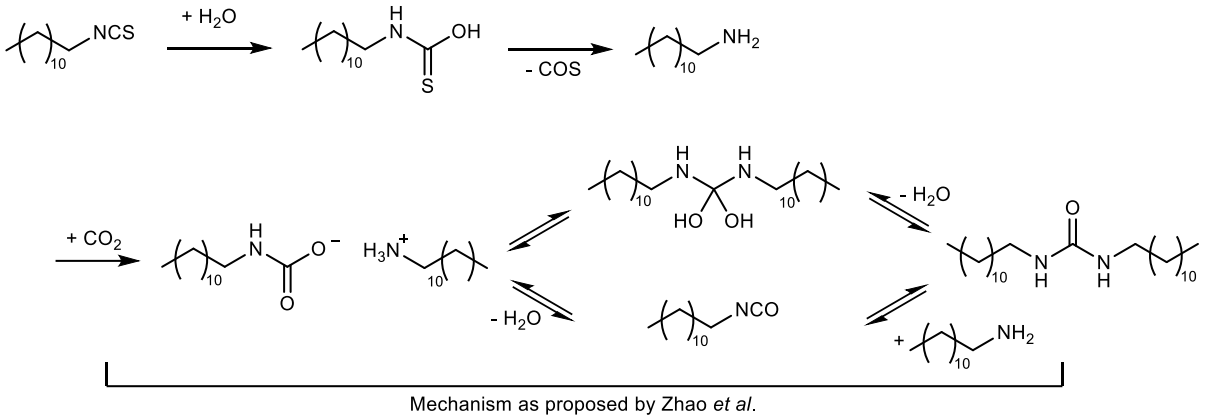

Scheme 27 *Proposed formation of N,N'-didodecyl urea from n-dodecyl isothiocyanate in the switchable solvent system. The formation of the urea from an amine is adapted from Zhao et al.*[317]

Zhao *et al*.[317] proposed this reaction mechanism to proceed *via* an intermediate isocyanate, which could be detected in our investigations. *n*-Dodecylisocyanate was found as an intermediate in low concentration when *n*-dodecylisothiocyanate was heated to 70 °C in the absence of an alcohol in the DMSO/DBU/CO_2 switchable solvent system, as confirmed by gas chromatography measurements (**Figure 31**).

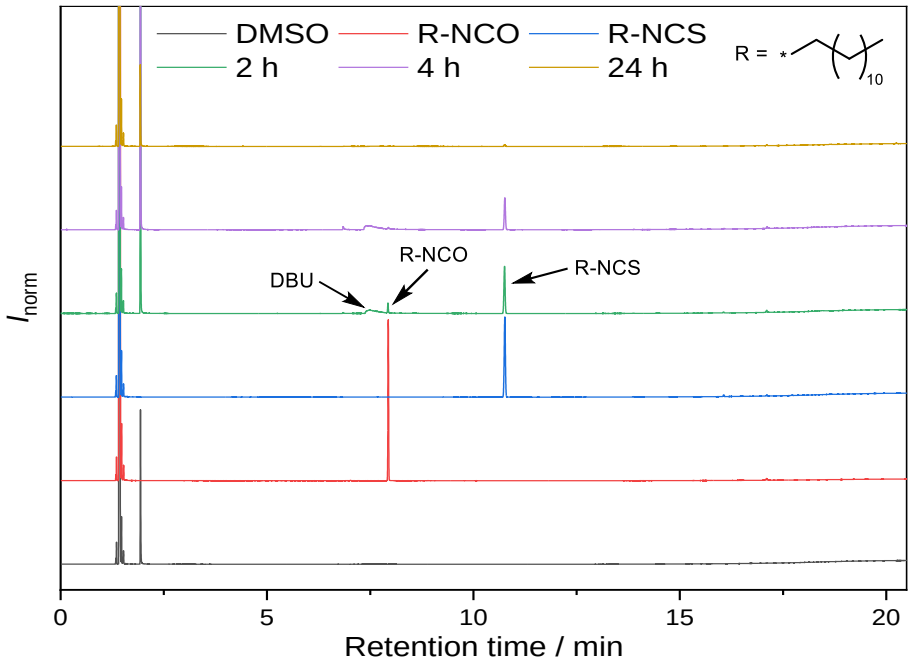

Figure 31 *Stacked GC spectra of the references DMSO, n-dodecylisocyanate, n-dodecylisothiocyanate and the reaction mixture of n-dodecylisothiocyanate in the DBU/CO_2 switchable solvent system at 70 °C after 2, 4, and 24 h. The product (N,N'-didodecylurea) is not detected in these measurements because of its insolubility in ethylacetate.*

This explains the formation of a carbamate when an additional alcohol is present, as in this case. An analogous formation of the oxocarbamate moiety could be confirmed on cellulose samples by a comparison of the observed IR spectra of **CD-1** and a *O*-cellulose-*N*-*n*-dodecyl carbamate sample, which was synthesized using a *n*-dodecylisocyanate (**Figure 32**).

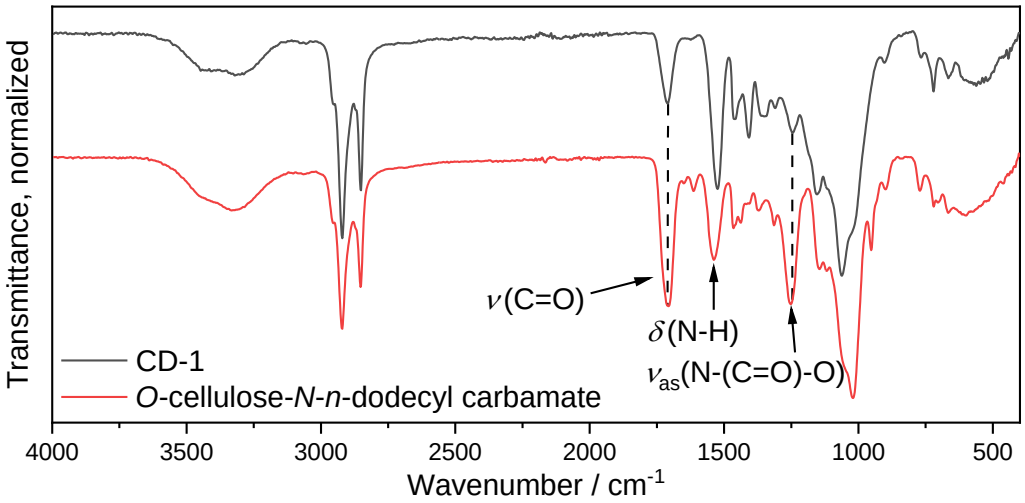

Figure 32 *Comparison of the IR spectra of* ***CD-1*** *and a O-cellulose-N-n-dodecyl carbamate sample, which was synthesized using n-dodecylisocyanate.*

Tandem Reaction Approach

In order to establish a tandem reaction for cellulose functionalization with a triple use of DBU, the isothiocyanate reactant has to be formed *in situ* in the DMSO/DBU/CO_2 switchable solvent system. This *in situ* isothiocyanate formation was achieved by the addition of a suspension consisting of the liquid isocyanide and elemental sulfur to the cellulose solution without the addition of further solvent or DBU. A slow, dropwise addition of the suspension is crucial because higher loadings of sulfur in the reaction mixture leads to the precipitation of cellulose. This can be explained by the necessity of DBU for the sulfur activation forming polysulfide chains or trisulfur radical anions,[266,292,318] which partially withdraws DBU from the DMSO/DBU/CO_2 switchable solvent system, destabilizing the solubilized cellulose carbonate and consequently leads to the precipitation of cellulose. The *in situ* isothiocyanate formation was carried out at 40 °C, but optimization studies showed that a subsequent increase to 70 °C after full addition of the suspension is beneficial to achieve higher conversions of the isothiocyanate to the corresponding *O*-cellulose thiocarbamate. The isothiocyanate was formed

successfully as an intermediate, as confirmed by gas chromatography measurements of the reaction solution. Due to the high reactivity of isothiocyanates, only low amounts could be detected, indicating a rapid conversion to the *O*-cellulose thiocarbamate. This observation is beneficial for the design of safe procedures, which is requested by one of the *Twelve Principles of Green Chemistry*. The reactive and intrinsically noxious isothiocyanate compound is generated *in situ* and immediately reacts with the hydroxyl groups of the cellulose, reducing a potential exposure risk. Even though isothiocyanates are considered reactive, in an attempted heterogeneous functionalization of cellulose with an excess of *n*-dodecylisothiocyanate and the absence of any solvent, no conversion could be detected by IR measurements (**Figure 33**), indicating the necessity of a catalyst and/or solvent for the derivatization reaction.

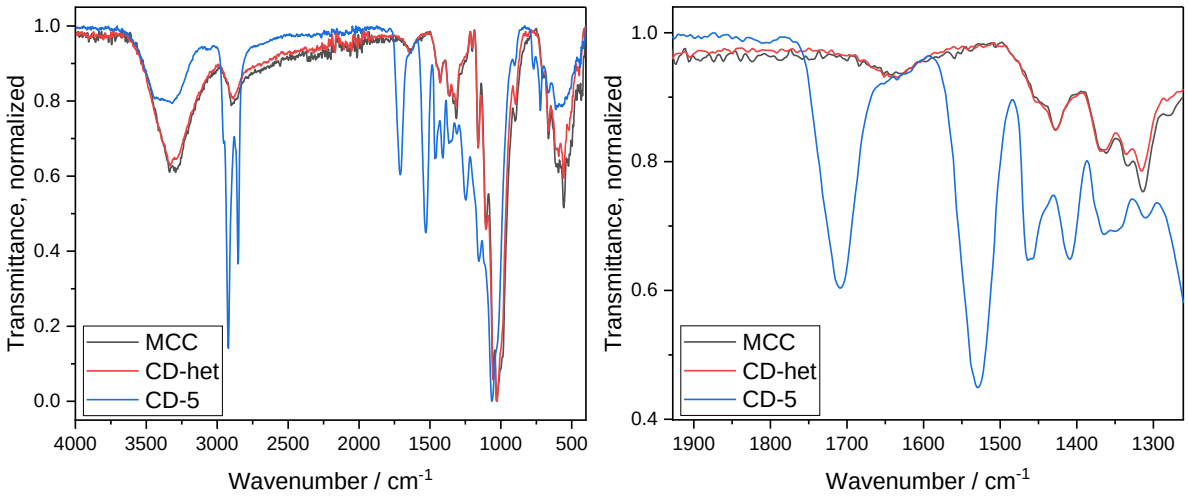

Figure 33 *Overlayed IR-spectra of native cellulose (**MCC**), cellulose after an attempted heterogeneous modification with n-dodecyl isothiocyanate (**CD-het**) and **CD-5** as a comparison.*

The influence of DBU as a catalyst on the third reaction step was further investigated by the same model reaction as already used for the side reaction investigation (reaction of *n*-hexanol with *n*-dodecylisothiocyanate) with varying equivalents of DBU (0–1.0 eq.). The model reactions were screened using gas chromatography and an increase in the formation of *O*-*n*-hexyl-*N*-*n*-dodecyl thiocarbamate was detected with increasing equivalents of DBU, as shown in **Figure 34**, confirming that DBU accelerates this reaction.

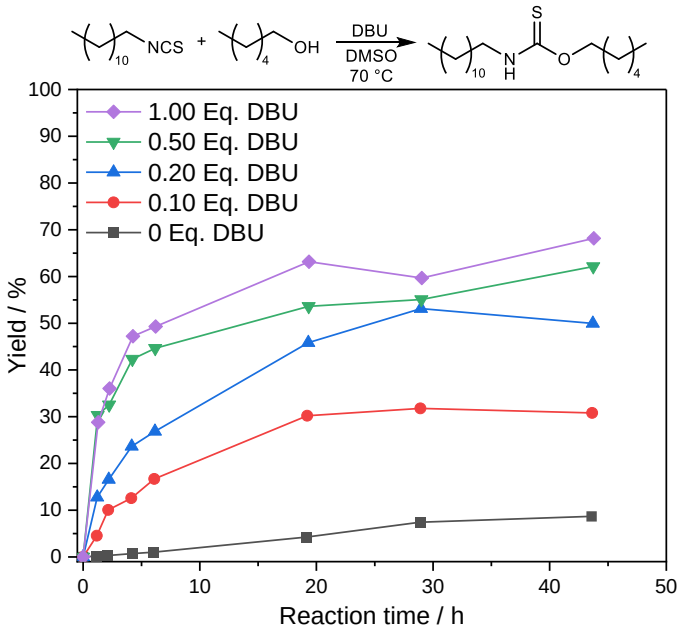

Figure 34 *Reaction screening of the model reaction of n-hexanol with n-dodecylisothiocyanate with different equivalents of DBU. The formation of O-n-hexyl-N-n-dodecyl thiocarbamate was monitored using gas chromatography.*

After having established a fundamental understanding of this new tandem reaction and after having confirmed the triple use of DBU, a set of 16 *O*-cellulose thiocarbamates with four different substituents and different degrees of substitution were synthesized *via* the tandem reaction approach as shown in **Scheme 25** and are summarized in **Table 15**. The herein presented approach can be categorized as a tandem reaction because one catalyst promotes three different mechanisms: 1) partial carbonylation of cellulose[132] leading to dissolution in DMSO, 2) isothiocyanate synthesis by sulfurization of an isocyanide, and 3) cellulose derivatization to the corresponding *O*-cellulose thiocarbamate. As the side reaction forming the oxocarbamate species is potentially caused by water, all reactions were performed under inert conditions. However, a partial oxocarbamate formation could not be suppressed. The mole fraction of thiocarbamate ($x_{S,NMR}$) in the modified cellulose samples was quantified by comparison of the two N-H signal integrals in the ^{1}H NMR spectra (**Figure 29**). Due to the broad signals with low intensity, elemental analysis was used as a second method to verify the determined mole fraction (**Table 15**).

Table 15 *Synthesized O-cellulose thiocarbamates with the thiocarbamate mole fraction determined via elemental analysis and ^{1}H NMR spectroscopy ($x_{S,EA}$ and $x_{S,NMR}$), degree of substitution determined via ^{31}P NMR spectroscopy (DS_{31P}) and elemental analysis ($DS_{EA,NC}$ and $DS_{EA,NH}$), and degradation temperature ($T_{d,5\%}$).*

Sample	Reagent	Eq.[a]	$x_{S,EA}$[b]	$x_{S,NMR}$[c]	DS_{31P}[d]	$DS_{EA,NC}$[e]	$DS_{EA,NH}$[e]	$T_{d,5\%}$ / °C
CD-1	*n*-C_{12}-NCS	3.0	58.4±0.8%	54.5%	1.70	1.67±0.06	1.48±0.17	249.7
CD-2	*n*-C_{12}-NC+S_8	1.0	16.4±0.4%	17.6%	0.52	0.78±0.03	0.75±0.05	222.2
CD-3	*n*-C_{12}-NC+S_8	1.5	33.7±1.0%	40.0%	0.89	0.88±0.03	0.76±0.04	254.6
CD-4	*n*-C_{12}-NC+S_8	2.0	59.4±1.1%	-[f]	1.07	1.17±0.04	1.05±0.11	247.2
CD-5	*n*-C_{12}-NC+S_8	3.0	48.2±5.4%	52.0%	1.56	1.48±0.00	1.34±0.02	247.2
CD-6	*n*-C_{12}-NC+S_8	6.0	73.1±2.3%	69.0%	2.16	2.09±0.22	1.62±0.26	234.7
CC-1	cy-C_6-NC+S_8	2.0	38.9±0.1%	42.1%	1.00	0.93±0.00	0.92±0.00	239.7
CC-2	cy-C_6-NC+S_8	3.0	51.0±0.1%	58.1%	1.20	1.13±0.01	1.21±0.02	239.7
CB-1	*n*-C_4-NC+S_8	2.0	38.8±0.3%	38.8%	1.31	1.26±0.00	1.17±0.01	212.2
CB-2	*n*-C_4-NC+S_8	3.0	68.1±1.4%	67.0%	1.30	1.24±0.03	1.35±0.10	239.7
CO-1	Oleyl-NC+S_8	2.0	61.0±1.2%	-[g]	1.69	1.70±0.07	1.53±0.17	262.2
CO-2	Oleyl-NC+S_8	3.0	66.8±1.5%	-[g]	2.11	2.55±0.29	2.56±0.35	264.7
CD-2wt%	*n*-C_{12}-NC+S_8	3.0	55.6±0.5%	51.6%	1.24	1.27±0.00	1.13±0.04	n.d.
CD-4wt%	*n*-C_{12}-NC+S_8	3.0	71.3±0.2%	64.8%	1.61	1.75±0.00	1.57±0.02	n.d.
CD-5wt%	*n*-C_{12}-NC+S_8	3.0	74.8±0.4%	68.1%	1.59	1.65±0.02	1.45±0.03	n.d.
CD-REC	*n*-C_{12}-NC+S_8	3.0	76.6±0.5%	70.4%	1.47	1.42±0.06	1.44±0.09	n.d.

[a]Equivalents of isothiocyanate/isocyanide per AGU; 1.12 eq. sulfur was used per eq. of isocyanide in the tandem reaction approaches. All samples (except for CD-2wt%, CD-4wt%, and CD-5wt%) were performed with a cellulose concentration of 3 wt%. [b]Mole fraction of thiocarbamate determined *via* elemental analysis. [c]Mole fraction of thiocarbamate determined *via* ^{1}H NMR spectroscopy. [d]Calculated values corrected using elemental analysis data. [e]The error is the standard deviation calculated from two or three measurements, depending on the sample (see Experimental Section **Table 28**). [f]Not determined due to low signal intensity in the ^{1}H NMR spectrum caused by low solubility. [g]Not determined due to overlap with double bond signals.

Despite a low signal intensity in the ^{1}H NMR spectra, the determined ratios were remarkably similar to those calculated from elemental analysis data as shown in **Figure 35a**, revealing that ^{1}H-NMR spectroscopy is a sufficient analysis for determination of the mole fraction for the (thio)carbamate cellulose derivatives. The highest discrepancy was observed for **CD-3**, but the relative deviation remained below 19%. From the x_S data in **Table 15**, a trend can be seen with declining oxocarbamate formation when higher equivalents of reactant were used. In the IR spectrum, the thio- as well as the oxocarbamate moiety cause an increase of the N-H deformation vibration signal at ν=1530 cm^{-1}, whereas only the oxocarbamate moiety causes a C=O stretching vibration signal. By normalization of the IR spectra to the N-H deformation vibration signal instead of the C-O stretching vibration of the AGU, the influence of different degrees of substitution could be eliminated for a relative comparison of the oxocarbamate formation in different samples. As a result, the trend of a declining side reaction ratio

could be confirmed *via* IR spectroscopy by a relative comparison of the C=O signal intensities for samples **CD-2**–**CD-6** as shown in **Figure 35b**. Besides the applied concentration of 3 wt% cellulose in the DMSO/DBU/CO_2 switchable solvent system, a test series with 2, 4, and 5 wt% was performed to investigate the influence of cellulose concentration on the DS and oxocarbamate formation. A lower DS and mole fraction of thiocarbamate was observed at low cellulose concentration (2 wt%, DS_{31P}=1.22), whereas the obtained DS remained stable at 3, 4, and 5 wt% cellulose concentration (DS_{31P}=1.56, 1.61, and 1.59, respectively). Furthermore, the oxocarbamate formation was favored at lower concentrations as presented in **Figure 35c** by an increase of the C=O stretching vibration signal relative to the N-H deformation vibration signal. This trend could be confirmed by the determined thiocarbamate mole fraction (**Table 15**) with $x_{S,NMR}$=51.6, 52.0, 64.8, and 68.1% for 2, 3, 4, and 5 wt% cellulose concentration, respectively. This is beneficial in terms of sustainability, as the reaction provides comparable DS with less side reaction when less solvent is used for the functionalization.

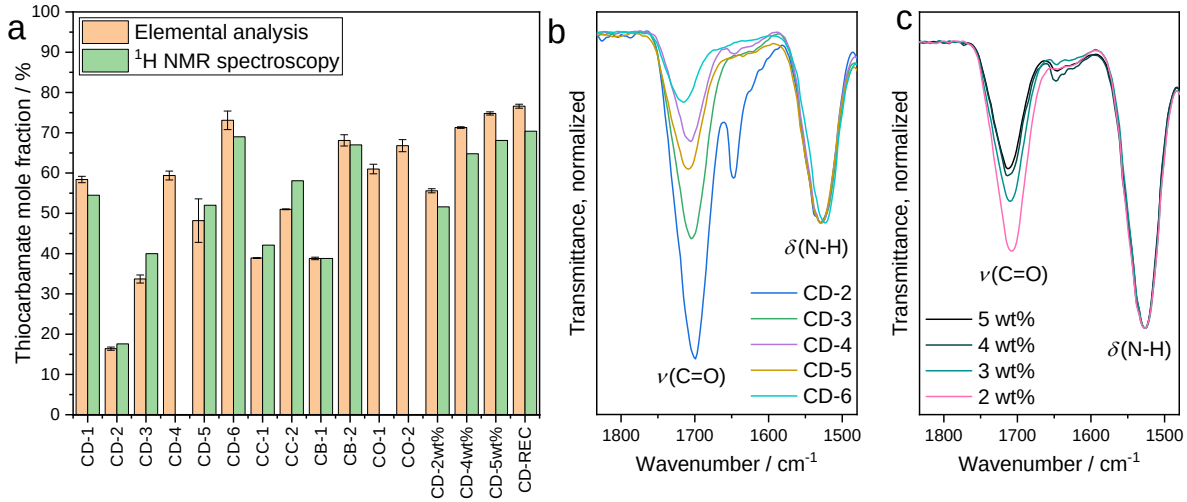

Figure 35 *Bar chart comparison of the thiocarbamate mole fraction (x_S) determined via elemental analysis and ^{1}H NMR spectroscopy. $x_{S,NMR}$ of* ***CD-4*** *could not be determined due to low signal intensity caused by low solubility, $x_{S,NMR}$ of* ***CO-1*** *and* ***CO-2*** *could not be determined due to overlap with double bond signals (**a**). Overlayed IR-spectra of* ***CD-2*****–****CD-6*** *normalized to the N-H deformation vibration for a relative comparison of oxocarbamate formation (**b**). Overlayed IR-spectra of four O-cellulose-N-n-dodecyl thiocarbamate samples synthesized with different cellulose concentrations (5, 4, 3, and 2 wt%) normalized to the N-H deformation vibration for a relative comparison of oxocarbamate formation. 3 eq. n-dodecyl isocyanide were used per AGU in all four batches (**c**).*

The influence of aging on the thiocarbamate mole fraction $x_{S,EA}$ was investigated by storage of sample **CO-2** for 2 months under air. No oxidation of the thiocarbamate

moiety was observed, as the mole fraction remained stable ($x_{S,EA}$=66.8±1.5% vs. 69.1±2.3% after 2 months).

The degree of substitution of the synthesized *O*-cellulose thiocarbamates could not be determined *via* ^{1}H NMR spectroscopy because of overlapping signals from THF-d_8 and H_2O with signals of the AGU protons. Therefore, the DS_{31P} was determined by a procedure introduced by Kilpeläinen *et al*.[208], in which the remaining free hydroxyl groups of the respective cellulose sample are reacted with the phosphitylating agent 2-chloro-4,4,5,5-tetramethyl-1,3,2-dioxaphospholane to yield phosphite esters, which can be detected quantitatively by ^{31}P NMR spectroscopy. To verify the determined DS_{31P}, elemental analysis was used as a second method for DS determination. Using elemental analysis data, the DS can be calculated based on the nitrogen to carbon ratio ($DS_{EA,NC}$) or the nitrogen to hydrogen ratio ($DS_{EA,NH}$) according to equation (*11*) and (*12*).

$$DS_{EA,NC} = \frac{n_{C,AGU} \times \frac{w_N}{M(N)}}{n_{N,S}\frac{w_C}{M(C)} - n_{C,S} \times \frac{w_N}{M(N)}} \tag{11}$$

$$DS_{\mathrm{EA,NH}} = \frac{n_{\mathrm{H,AGU}} \times \frac{w_{\mathrm{N}}}{M(\mathrm{N})}}{n_{\mathrm{N,S}}\frac{w_{\mathrm{H}}}{M(\mathrm{H})} - (n_{\mathrm{H,S}} - n_H) \times \frac{w_{\mathrm{N}}}{M(\mathrm{N})}} \tag{12}$$

w_{H}: mass fraction of hydrogen
w_{C}: mass fraction of carbon
$M(\mathrm{H})$: molar mass of hydrogen $M(\mathrm{H}) = 1.00784\ \frac{\mathrm{g}}{\mathrm{mol}}$
$M(\mathrm{C})$: molar mass of carbon $M(\mathrm{C}) = 12.0107\ \frac{\mathrm{g}}{\mathrm{mol}}$
$M(\mathrm{N})$: molar mass of nitrogen $M(\mathrm{N}) = 14.0067\ \frac{\mathrm{g}}{\mathrm{mol}}$

Any solvent residues or other impurities in the investigated cellulose samples distort the DS measurements drastically, which is why a high purity is essential and thus was proven by ^{1}H NMR spectroscopy (Experimental Section). The measured $DS_{EA,NC}$ and $DS_{EA,NH}$ are in accordance with the determined DS_{31P} in most cases as shown in **Figure 36** by a comparison of the three narrow bars for the individual sample. By comparison of the used equivalents of isocyanide with the obtained DS, the conversion can be determined (**Figure 36**). The highest conversions were observed when oleyl isocyanide was used as the reactant, or when low equivalents (1.0 eq.) of reactant were

chosen (**CO-2**: 85% conversion and **CD-2**: 78% conversion, calculated based on the $DS_{EA,NC}$).

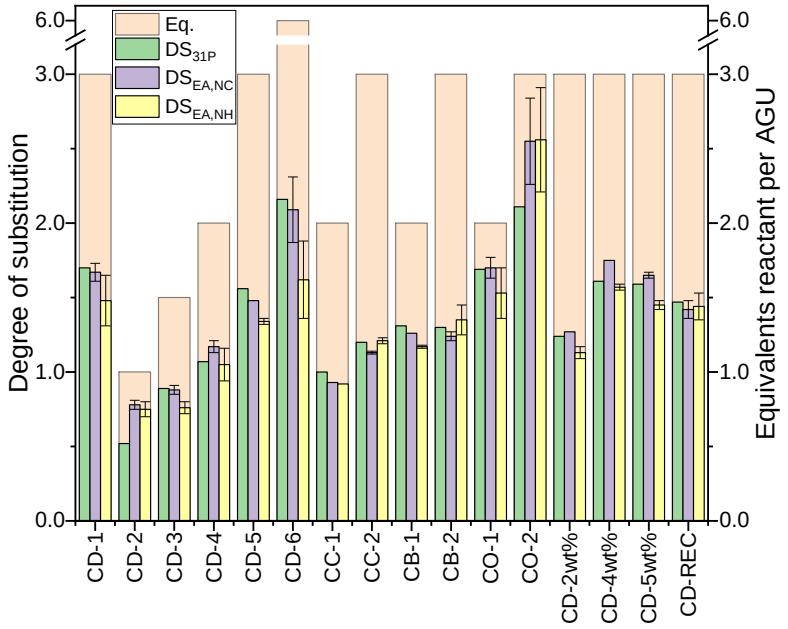

Figure 36 *Bar chart comparison of the degrees of substitution determined via ^{31}P NMR spectroscopy (DS_{31P}) and elemental analysis ($DS_{EA,NC}$, $DS_{EA,NH}$) and the used equivalents of reactant per AGU.*

By comparing the two samples **CD-1** and **CD-5** (**Table 15**), the direct functionalization of cellulose with an isothiocyanate can be compared to the tandem reaction approach under the otherwise same reaction conditions (3.0 eq. reactant). The thiocarbamate mole fraction (58.4±0.8% vs. 48.2±5.4%), as well as the DS_{31P} (1.70 vs. 1.56) is slightly higher when *n*-dodecyl isothiocyanate was used directly, compared to when formed *in situ*. However, since the separate synthesis of *n*-dodecyl isothiocyanate from *n*-dodecyl isocyanide yields 88% product,[266] 3.0 eq of the presynthesized isothiocyanate theoretically correspond to 3.41 eq. isocyanide. This overcompensates the lower obtained DS_{31P}, because a theoretical DS_{31P}=1.82 should be obtained when 3.41 eq. isocyanide were used instead of 3.0 eq in the tandem procedure (linear correlation assumed for the extrapolation, see **Figure 37**). Together with the higher synthetic effort and waste formation of a stepwise synthesis, the tandem reaction approach is beneficial in terms of efficiency as well as sustainability.

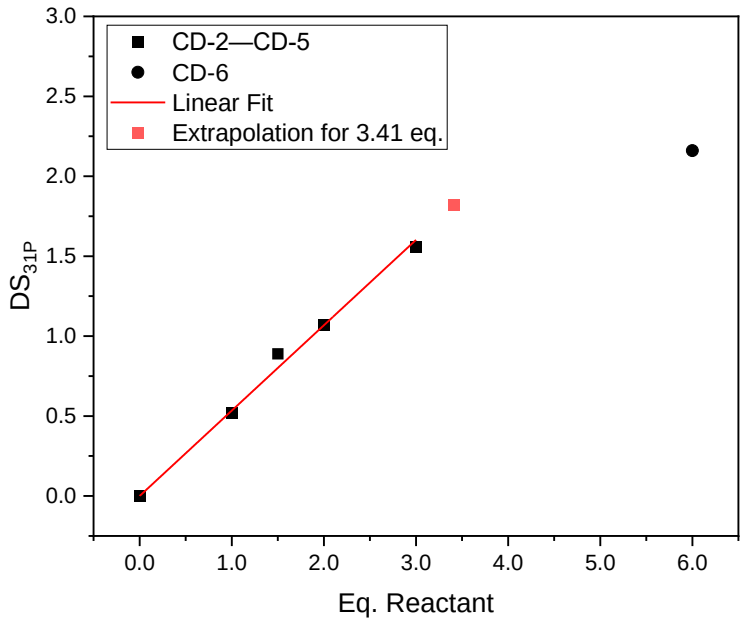

Figure 37 *Linear fit of the DS_{31P} with 0.0–3.0 equivalents of isocyanide reactant and extrapolation of the DS_{31P} with 3.41 eq. of isocyanide (calculated: DS_{31P} = 1.82).*

The degree of substitution of **CD-2**–**CD-6** could be controlled in a range of DS_{31P}=0.52–2.16 by varying the equivalents of isocyanide reactant between 1.0–6.0 eq. per AGU. The successful derivatization was confirmed by ATR-IR spectroscopy as the characteristic thiocarbamate signals of the N-H bending vibration at ν=1530 cm^{-1} and the C=S stretching vibration at ν=1150 cm^{-1} were observed (**Figure 38**). A decrease of the O-H stretching vibration at ν=3360 cm^{-1} and an increase of the N-H bending vibration at ν=1530 $cm^{-.1}$ was found, which confirms the trend of an increasing degree of substitution from **CD-2** to **CD-6**. All spectra were normalized to the C-O stretching vibration of the AGU at ν=1023 cm^{-1} for a relative comparison, as the intensity of this signal is not considerably affected by the derivatization.

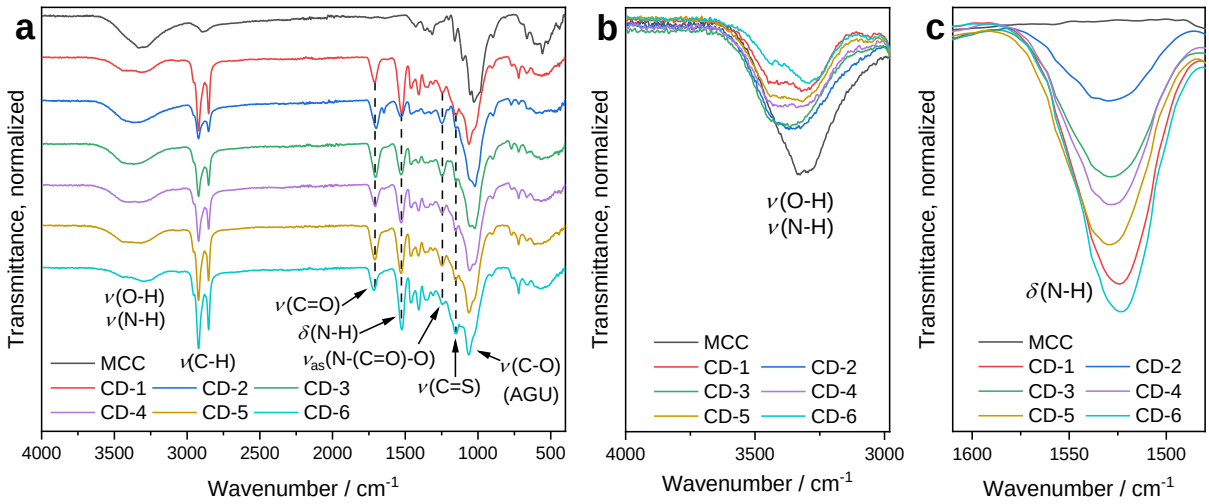

Figure 38. (a) *Stacked IR-spectra and expanded views of the overlayed* ***(b)*** *O-H or N-H stretching vibrations and* ***(c)*** *N-H bending vibration for* ***CD-1–CD-6*** *with MCC as a reference. All spectra were normalized to the signal of the C-O stretching vibration at ν=1023 cm-1. MCC=microcrystalline cellulose.*

Size exclusion chromatography measurements of the *O*-cellulose thiocarbamates revealed a trend of increasing hydrodynamic volume (i.e. decreasing retention time) with an increase of the DS for samples **CD-2**–**CD-4** (**Figure 39**). This correlation is expected due to the increase of the average molecular weight, however this trend does not continue for samples **CD-5**, **CD-6**, and **CD-1** even though the DS increases for these samples. Contrarily, the retention time decreases with an increasing DS in these cases. A possible explanation is that the polymer adapts a more compact shape in solution due to the increased hydrophobicity and the growing interactions of the introduced thiocarbamate side chains, leading to a decrease in hydrodynamic volume.

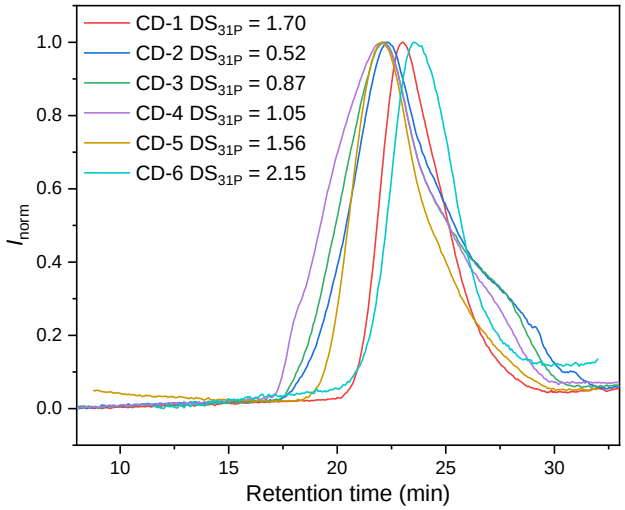

Figure 39. *Size exclusion chromatography traces of* ***CD-1–CD-6*** *recorded in DMAc (0.03 wt% LiCl).*

The thermal stability of the samples was investigated using thermogravimetric analysis (TGA). The calculated results for $T_{d,5\%}$ ranged from 222.2 to 264.7 °C, which was lower than that of native microcrystalline cellulose (319.7 °C). The lower $T_{d,5\%}$ is expected to result from the cleavage of the thiocarbamate moiety, which is indicated by the two-step thermal degradation process (**Figure 40**). In earlier studies, similar behavior was reported for polymers containing thiocarbamate moieties in the side-chain and a thermal decomposition to the corresponding thiol and isocyanate was verified *via* IR spectroscopy and gas chromatography coupled with mass spectrometry.[319] Comparable degradation temperatures of thiocarbamate moieties between 219–228 °C were observed in this study, which further indicates the thiocarbamate cleavage of *O*-cellulose thiocarbamates in a first step.

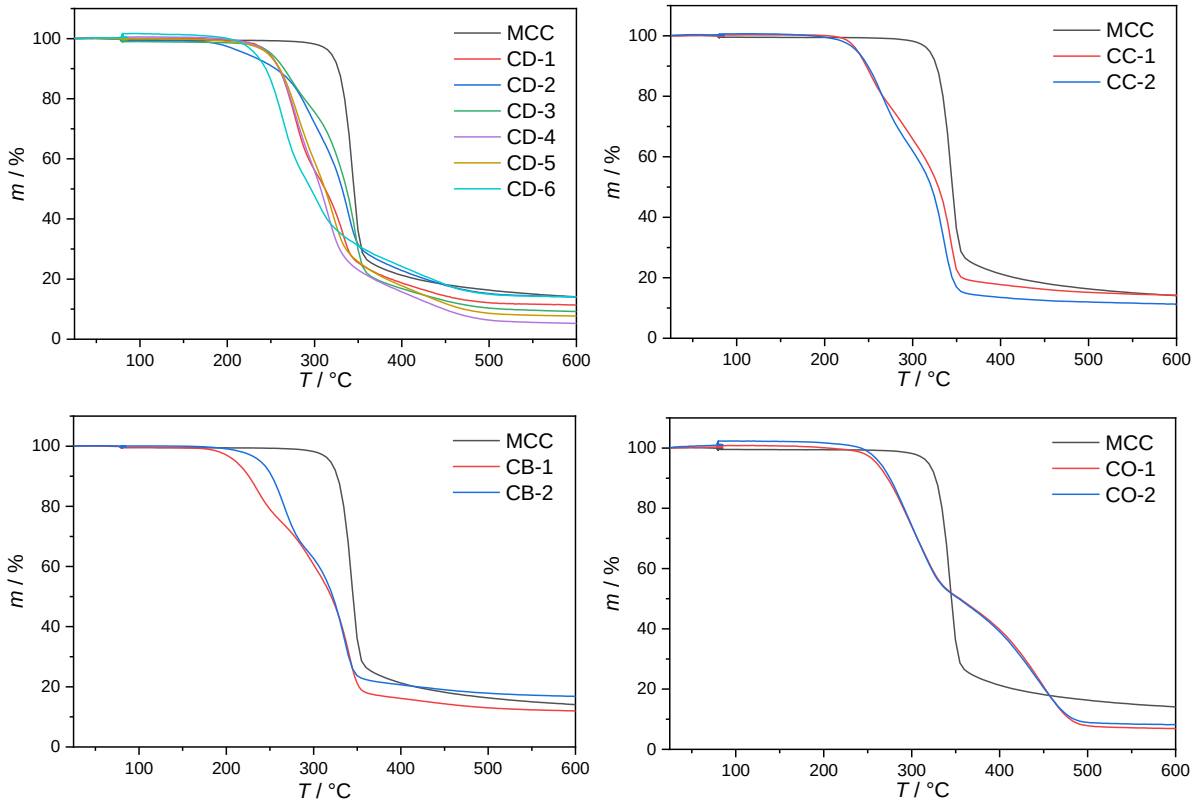

Figure 40 *TGA analysis of the synthesized O-cellulose thiocarbamates with MCC as a reference.*

DSC measurements were performed for the synthesized *O*-cellulose thiocarbamates and no glass transition could be observed in the range of −50 to 200 °C (**Figure 41**). A certain instability in the baseline was found, but no T_g could be found.

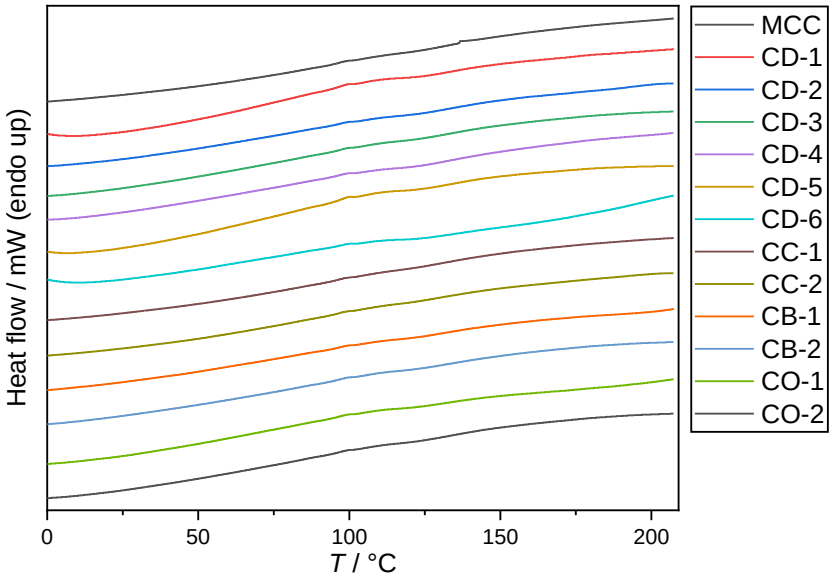

Figure 41 *DSC analysis of the synthesized O-cellulose thiocarbamates and MCC as a reference, second heating step.*

All samples were obtained as white or yellow powdery solids with different solubilities, depending on the substituent as well as the DS. A solubility study (**Table 16**) revealed that all samples were soluble in DMAc + LiBr. No trend between the DS or the substituent on the solubility in DMSO or THF could be concluded.

Table 16 *Solubility chart of the synthesized O-cellulose thiocarbamates.*

Sample	$CHCl_3$	DMSO	THF	DMAc + LiBr
CD-1				
CD-2				
CD-3				
CD-4				
CD-5				
CD-6				
CC-1				
CC-2				
CB-1				
CB-2				
CO-1				
CO-2				
CD-2wt%				
CD-4wt%				
CD-5wt%				
CD-REC				

red = insoulble, green = soluble

For a sustainable cellulose functionalization using a homogeneous approach, recyclability of the solvent and antisolvent is essential, as this accounts most to the generation of waste and thus the *E*-factor. To reduce the influence of sample loss and ensure a more precise recycling ratio determination, the process was scaled up (**CD-REC**, 4.00 g cellulose) and the used components for solubilization and precipitation/purification (DMSO, DBU, and isopropanol) were recycled *via* fractional distillation. Recycling ratios of 91.5% for DMSO, 79.1% for DBU, and 95.6% for isopropanol were obtained, which is close to recovery ratios reported for cellulose acetylations in the DMSO/DBU/CO_2 switchable solvent system by Xie *et al.* (92% DMSO and 91% DBU)[137] or in one of our previous reports (97.7% DMSO, 87.0% DBU, 98.9% isopropanol)[140]. This results in a calculated *E*-factor of 2.95 for the overall process, which is significantly lower (up to 5 times) than reported one-step modifications of cellulose under various conditions.[310] Considering that a separate synthesis of the isothiocyanate reactant solely results in an *E*-factor of 1.22–2.81 (depending on the isothiocyanate)[266] makes the presented tandem reaction approach highly efficient for the synthesis of *O*-cellulose thiocarbamates. The contribution of the individual losses of the different components was evaluated and is summarized in **Figure 42**.

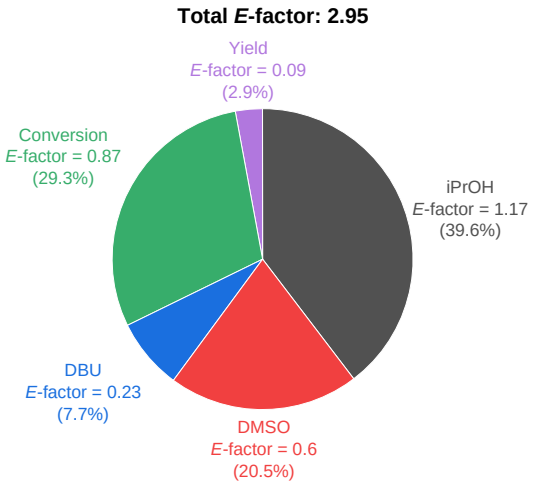

Figure 42 *Pie chart of the different E-factor contributions for the synthesis of* ***CD-REC****.*

The reusability of the recovered DMSO/DBU mixture was subsequently demonstrated by a successful synthesis of an *O*-cellulose-*N*-oleyl thiocarbamate without considerable differences compared to a fresh batch (DS_{31P}=1.63 with 2.0 eq. oleyl isocyanide and redistilled DMSO/DBU compared to **CO-1** with DS_{31P}=1.69) after the molar composition of the redistilled DMSO/DBU fraction was appropriately adjusted by the addition of a calculated amount of fresh DBU.

Conclusion

A novel functionalization approach for cellulose with isothiocyanates providing *O*-cellulose thiocarbamates was achieved in the DMSO/DBU/CO_2 switchable solvent. The isothiocyanate was generated *in situ via* a DBU catalyzed sulfurization of isocyanides with elemental sulfur, resulting in a tandem reaction protodcol for cellulose derivatization with a single catalyst. Besides the expected thionocarbamate formation, a partial formation of an oxocarbamate moiety was observed. This was confirmed by a model reaction, in which cellulose was substituted with *n*-hexanol and reacted with *n*-dodecylisothiocyanate under the otherwise same reaction conditions. The formation of 23 mol% *O*-*n*-hexyl-*N*-*n*-dodecyl carbamate besides 73 mol% of *O*-*n*-hexyl-*N*-*n*-dodecyl thiocarbamate was confirmed by ^{1}H NMR, ^{13}C NMR, and IR spectroscopy, as well as mass spectrometry. The extent of thiocarbamate formation in the synthesized *O*-cellulose thiocarbamates was quantified by ^{1}H NMR spectroscopy and verified *via* elemental analysis as well as IR spectroscopy. The concentration of cellulose in the switchable solvent system was shown to influence the thiocarbamate formation ratio, leading to higher mole fraction of thiocarbamate side chains with less side reaction at higher concentrations. A set of 16 *O*-cellulose thiocarbamates was synthesized with four different substituents and the degree of substitution was shown to be controllable between DS_{31P}=0.52–2.16 by varying the equivalents of reactant with conversions of up to 85%. Thermal properties of the synthesized products were investigated by thermogravimetric analysis and differential scanning calorimetry revealing degradation temperatures ($T_{d,5\%}$) ranging from 222.2 to 264.7 °C and no observable glass transition temperature in a range of −50 to 210 °C. The tandem reaction approach was shown to be beneficial in terms of efficiency as well as sustainability compared to a stepwise synthesis, and the recyclability of the used components was demonstrated with recovery ratios of 91.5% DMSO, 79.1% DBU and 95.6% isopropanol. This results in a calculated *E*-factor of 2.95 for the synthesis of *O*-cellulose thiocarbamates in a novel one-pot tandem procedure, demonstrating the versatility of the DMSO/DBU/CO_2 switchable solvent system for cellulose dissolution and functionalization with a triple catalytic use of DBU.

4.4 Polythionourethane Thermoset Synthesis via Activation of Elemental Sulfur in an Efficient Multicomponent Reaction Approach

This chapter is based on previously published results by the author of this thesis:

Wolfs, J.; Ribca, I.; Meier, M. A. R.; Johansson, M. Polythionourethane Thermoset Synthesis via Activation of Elemental Sulfur in an Efficient Multicomponent Reaction Approach. *ACS Sustain. Chem. Eng.* **2023**, *11* (9), 3952–3962.[320]

The author developed the synthetic procedure, conducted and evaluated the experiments, and wrote the manuscript. I. Ribca gave valuable input to the research work, was part of several discussions, and assisted with analytical measurements.

Abstract

For the transition towards a safer and more sustainable production of polymeric materials, new synthetic concepts need to be developed. Herein, a catalytic, solvent-free synthesis approach for novel thionourethane thermoset materials is described, in which the diisothiocyanate reactant is generated *in situ via* a sulfurization of isocyanides with elemental sulfur, preventing the exposure and handling of the diisothiocyanate. In this one-pot procedure, castor oil fulfills a dual role: i) acting as the solvent for the *in situ* diisothiocyanate synthesis in the first step and ii) reacting as the polyol component in the subsequent thionourethane thermoset formation. The kinetics of the consecutive two-steps were studied in detail *via* real-time IR measurements, and the thermoset crosslinking step was found to be thermally triggerable after the diisothiocyanate reactant is quantitatively formed, enabling high control over the curing process of the system. Differential scanning calorimetry, thermal gravimetric analysis, and rheological measurements were performed to investigate the thermal and mechanical properties of the novel thionourethane thermosets and then compared to analogous polyurethane materials. Our results demonstrate an unprecedented approach for thermoset synthe-

sis *via* an *in situ* reagent synthesis, i.e., the generation of isothiocyanates from isocyanides by catalytic activation of elemental sulfur, and subsequent thermally triggerable thermosetting with a polyol, resulting in materials with appealing properties.

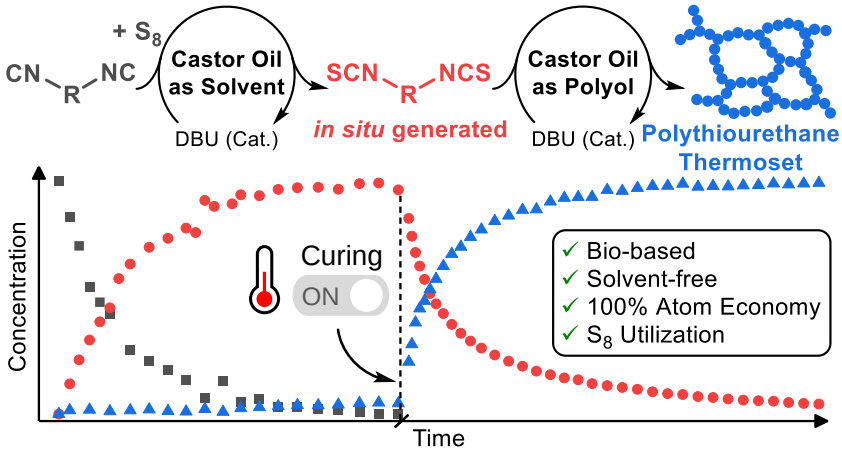

OH-value Determination of Castor Oil and Isocyanide Synthesis

For the synthesis of thionourethane thermosets with *in situ* generation of the diisothiocyanate reactant, a catalytic sulfurization approach of diisocyanides with elemental sulfur was chosen (**Scheme 28**). This reaction is performed in castor oil, which acts as the solvent for the formation of the diisothiocyanate and then as the polyol component in the crosslinking step. To achieve a successful thermoset curing, an exact stoichiometry between the diisothiocyanate and the hydroxyl groups of the polyol (i.e. castor oil) is a prerequisite. Therefore, the hydroxyl value of castor oil was first determined using a derivatizing approach, in which the free hydroxyl groups of castor oil react with 2-chloro-4,4,5,5-tetramethyl-1,3,2-dioxaphospholane to form a phosphite, which can then quantitatively be determined *via* ^{31}P-NMR spectroscopy together with an internal standard (Experimental Section, **Figure S171**). In a triple determination, the OH-value was calculated to OH_S = 2.39±0.02 mmol g^{-1}, which corresponds to a hydroxyl value of *HV* = 134.1±1.2 mg KOH g^{-1}. The determined hydroxyl value is close to values reported in the literature, which range from 102–165 mg KOH g^{-1}, depending on factors like the exact origin and storage time of the individual batch of castor oil.[321–326]

The used diisocyanides were synthesized according to a more sustainable synthesis procedure developed by Meier *et al*.[327] using three bio-based diamines (1,5-diaminopentane, 1,10-diaminodecane, and 1,12-diaminododecane) as well as two common

petroleum-based diamines (1,6-diaminohexane and isophorone diamine). Furthermore, three diisothiocyanates (1,5-diisothiocyanatopentane, 1,6-diisothiocyanatohexane, and isophorone diisothiocyanate) were synthesized according to the procedure of Meier *et al*.[266] in order to compare resulting thionourethane thermosets from presynthesized diisothiocyanates with *in situ* generated diisothiocyanates.[266]

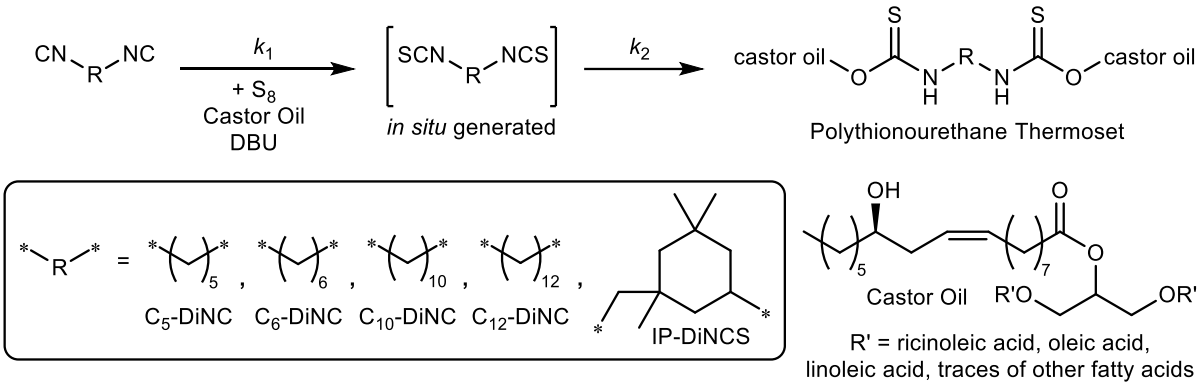

Scheme 28 *Synthesis of Polythionourethane Thermosets Based on Castor Oil with in situ Generation of Diisothiocyanates via Catalytic Sulfurization of Diisocyanides with Elemental Sulfur.*

In Situ Diisothiocyanate Formation

First reactions for the formation of diisothiocyanates from diisocyanides with elemental sulfur and DBU as the base revealed that castor oil is a suitable solvent for this synthesis. The amount of castor oil was chosen to fit a 1:1 stoichiometry of OH groups to the generated isothiocyanate functional groups to ensure a quantitative conversion in the second reaction step. IR spectroscopy was used to monitor the reaction progress, as the isocyanide, isothiocyanate, as well as the resulting thionourethane functional group exhibit distinct signals in the IR spectrum (**Figure 43**). The investigations showed that a heterogeneous synthesis of diisothiocyanates from diisocyanides and elemental sulfur with quantitative conversions is possible according to IR measurements. Furthermore, it was found that the isothiocyanate formation reaction proceeded much faster than the subsequent reaction of the isothiocyanate with the hydroxyl group of castor oil. This behavior is beneficial in multiple ways: first, a faster reaction of the diisocyanide enables a quantitative formation of the diisothiocyanate before the curing takes place, which prevents problems concerning the heterogeneity of the first reaction step with an increase of viscosity or gelation due to the curing. Second, the “activated” mixture can be transferred into a mold of choice after quantitative conversion of the

diisocyanide, and finally, the crosslinking reaction can actively be triggered by an increase in temperature.

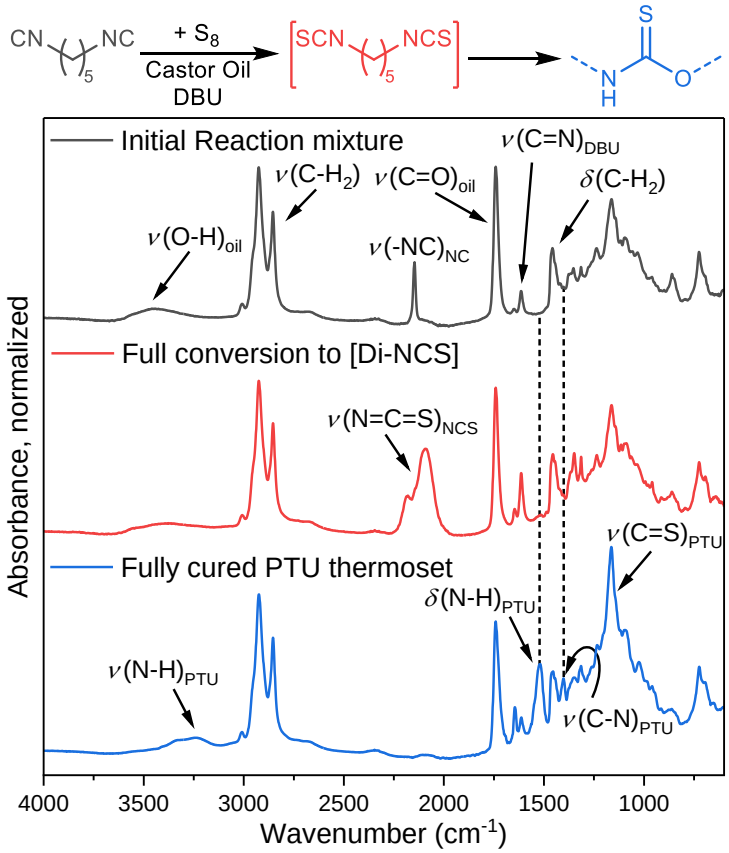

Figure 43 *Stacked IR spectra of the multicomponent reaction of castor oil with 1,5-diisocyano pentane, elemental sulfur, and DBU as organo-base at three stages of the reaction. All spectra were normalized on the* $\nu_{as}(C\text{-}H_2)$ *signal at 2929* cm^{-1}.

Thermoset Synthesis

Investigations on the crosslinking reaction, using presynthesized 1,6-diisothiocyanato hexane (C_6-DiNCS) with castor oil in 1:1 stoichiometry of the isothiocyanate to hydroxyl functional group, resulted in no gelation, even though quantitative conversion of the isothiocyanate functionality was detected *via* IR spectroscopy. It was found that a slight excess of isothiocyanate functional groups over the hydroxyl groups (1.1:1.0) is necessary for the successful curing of the material. This can be explained by two possible side reactions: first, if low amounts of water are present in the reaction mixture, the isothiocyanate group can react with water, forming a thionocarbamic acid, which is unstable and degrades to an amine. This results in a deactivated chain-end, which can be reactivated if a certain excess of diisothiocyanate is present under the formation of an interposed thiourea moiety (**Scheme 29**).

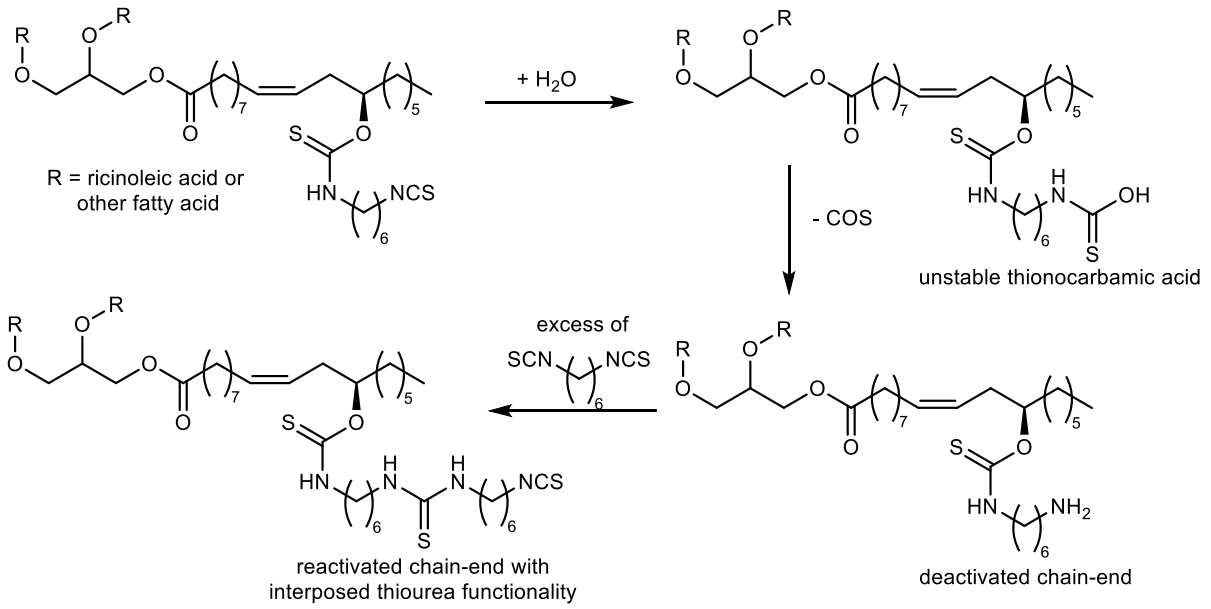

Scheme 29 *Hypothesized deactivation of the active chain end in the presence of water with a subsequent reactivation chain-end with a slight excess of diisothiocyanate under the formation of an interposed thiourea moiety.*

A second explanation could be the partial formation of dimers or trimers of the isothiocyanate functional group, which was reported to be possible under the catalysis of DBU by Taguchi *et al*.[328,329] However, the extent of possible thiourea and/or trimer formation remained lower than the detection limit of the applied analytical methods (i.e. ^{1}H NMR and IR spectroscopy), and could therefore not undoubtedly be confirmed for this system. Furthermore, crosslinking reactions of C_6-DiNCS with castor oil in the absence of DBU at *T*=100 °C did not lead to any detectable thionourethane formation after 48 h reaction time, which indicates the necessity of a base for the reaction. DBU can therefore be considered to act in a dual role, as it catalyzes both reaction steps, i.e. the isothiocyanate formation and the thionourethane formation.[201,266,300] Other organobases (triethylamine, 4-dimethylaminopyridine, 1,4-diazabicyclo[2.2.2]octane, and 1,5,7-triazabicyclo[4.4.0]dec-5-ene) were screened as possible alternatives, but DBU was found to be the most effective candidate in this context.

The full two-step process from 1,5-diisocyanido pentane (C_5-DiNC), S_8, castor oil, and DBU as organo-base with *in situ* generation of the intermediate 1,5-diisothiocyanato pentane (C_5-DiNCS) to the fully cured thionourethane thermoset material was monitored in real-time using IR-spectroscopy. A temperature of *T*=55 °C was chosen for the formation of the C_5-DiNCS in castor oil as a solvent, followed by an increase to *T*=100 °C for the crosslinking reaction after full conversion to the diisothiocyanate was

detected. The progress of the reaction is displayed in **Figure 44a–d** with a decrease of the ν(-NC) signal and a simultaneous increase of the ν(N=C=S) signal in the first 36 min at T=55 °C. Upon heating to T=100 °C, a decrease of the ν(N=C=S) signal with a simultaneous increase of the thionourethane δ(N-H) signal was obtained. All spectra were normalized to the ν_{as}(C-H$_2$) stretching vibration at ν=2929 cm^{-1}, as no change in C-H bonds takes place and the absorbance intensity of this signal is therefore expected to stay constant throughout the reaction.

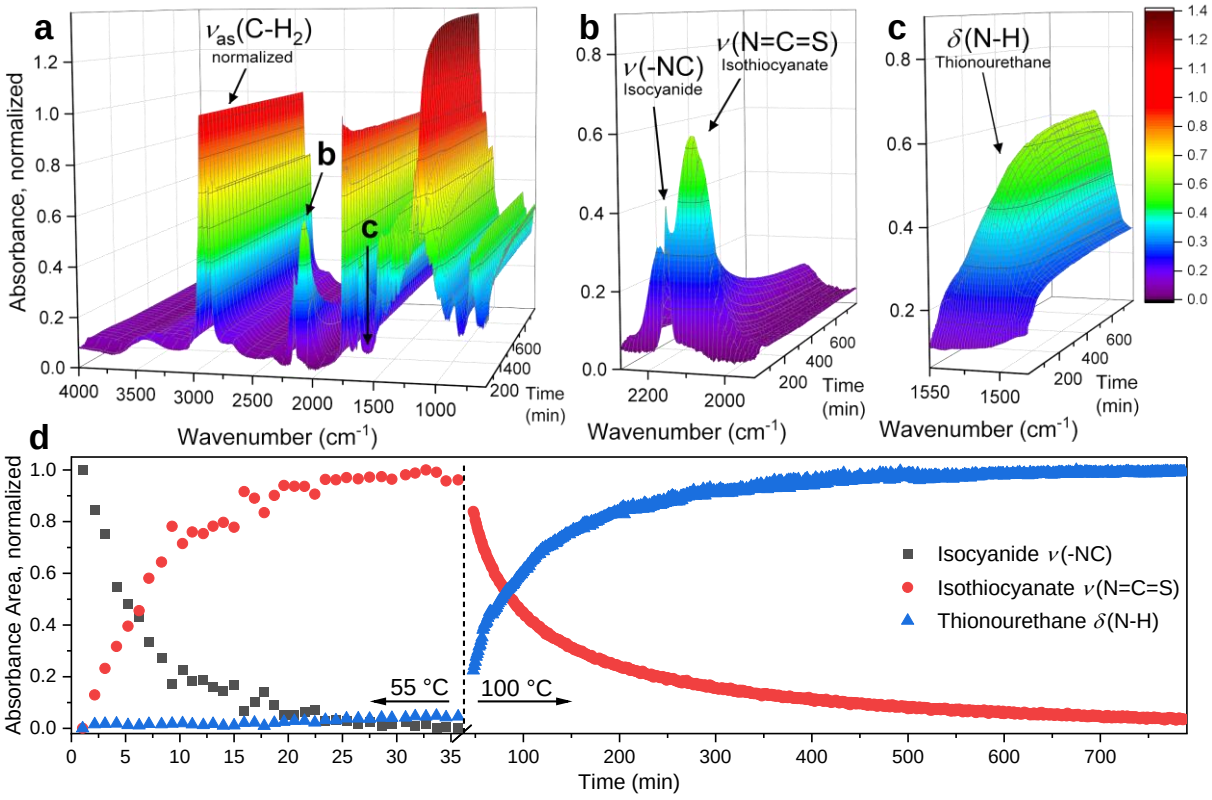

Figure 44 *(a) 3D surface plot of the IR spectra from real-time IR measurements of 1,5-diisocyano pentane with elemental sulfur and DBU as organo-base in castor oil; (b)+(c) expanded views of ν(-NC), ν(N=C=S), and δ(N-H) vibrations; (d) IR-spectroscopy absorbance area of the respective signal over time applying a peak deconvolutional method for the quantification of ν(-NC) and ν(N=C=S) as shown in* ***Figure 45****.*

Figure 44a–**b** show that the ν(-NC) and ν(N=C=S) signals overlap, which complicates a quantitative evaluation, as the peaks cannot be directly quantified *via* a simple integration. Therefore, a peak deconvolutional method was used to reliably quantify the individual signals for the first reaction step. The ν(N=C=S) signal was found as a double peak and therefore two fits (Fit 1 and Fit 3 in **Figure 45**) were used to quantify the signal, whereas the ν(-NC) signal was quantified by Fit 2 in **Figure 45** for every IR

measurement of the first reaction step. The resulting quantitative data from the peak deconvolution method are plotted in **Figure 44d** (the quantitative data of the crosslinking reaction at 100 °C was determined *via* simple integration of the signals).[330]

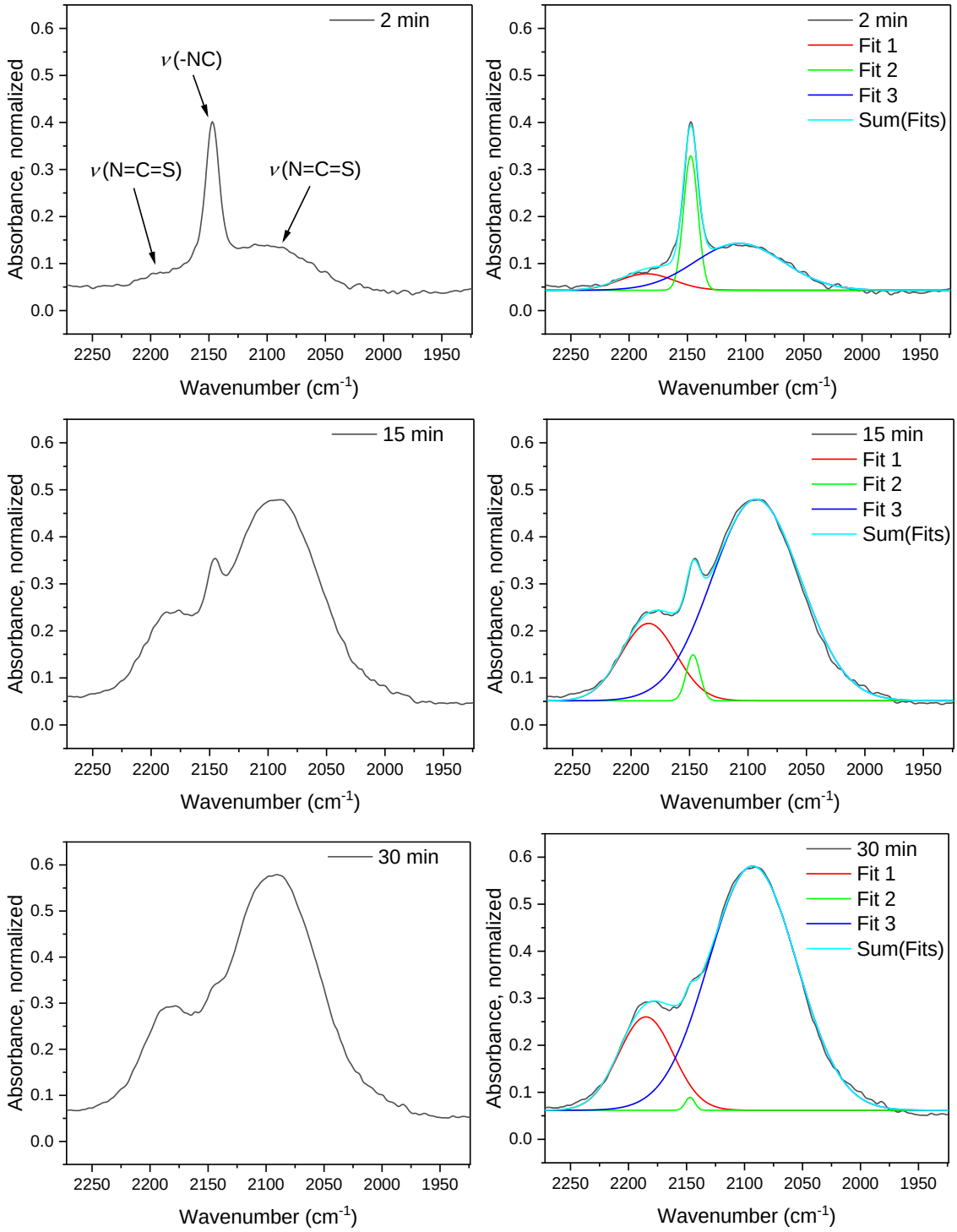

Figure 45 *Demonstration of the peak deconvolution results of three exemplary spectra at different times of the reaction of 1,5-diisocyanopentane with elemental sulfur and DBU in castor oil as a solvent, performed at T = 55 °C.*

The slight excess of elemental sulfur (1.14 eq of sulfur atoms per isocyanide functional group) is necessary for a quantitative formation of the isothiocyanate as reported previously.[266] The remaining sulfur remains in the thermoset material as no mass loss could be detected (quantitative yield), which accounts for a total weight percentage of 0.8–0.9% (depending on the used diisocyanide) of the final material. Structural analysis of the formed thermoset using NMR spectroscopy could not be performed due to its insolubility why a model reaction was performed instead to complement the IR data. Therefore, a monoisothiocyanate (*n*-dodecylisothiocyanate) instead of a diisothiocyanate was used, which led to a soluble product and could consequently be analyzed by NMR spectroscopy. The ^{1}H NMR, COSY, as well as HSQC spectra confirm the thionourethane functionality and quantitative derivatization of the OH groups were detected (Experimental Section **Figure S167**–**Figure S169**).

Kinetic Investigations

Based on the real-time IR observations, the kinetics of the two reaction steps were investigated in more detail to get a deep insight into the *in situ* generation of diisothiocyanates in castor oil, as well as the crosslinking behavior of the system. These investigations were performed using C_5-DiNC. The first reaction step, the diisothiocyanate formation from the diisocyanide with elemental sulfur in castor oil, is a heterogeneous reaction, in which the sulfur is solubilized as it reacts. The solid S_8 is first activated by DBU, forming a polysulfur chain, which is soluble in castor oil, and then reacts with the isocyanide forming the isothiocyanate functional group.[263,266] The reaction rate *r* of this reaction clearly depends on the concentration of the isocyanide as well as the one of sulfur, resulting in second order reaction kinetics (equation (13)). However, as the sulfur is being solubilized as it reacts, the concentration of activated polysulfur chains remains almost stable throughout the reaction. This results in a second order kinetics reaction with apparent first order kinetics, because the reaction rate *r* is effectively only dependent on the isocyanide concentration when the concentration of the reactive polysulfur chains remains constant (equations (14)–(15)).

$$r \propto [NC][S_x] \tag{13}$$

$$[S_X] = \text{const.} \tag{14}$$

$$r \propto [NC] \tag{15}$$

The reaction was monitored at three different temperatures and the resulting linear correlation of $\ln([NC]_0/[NC])$ with time, as shown in **Figure 46b**, was used for the determination of k_1, confirming the assumption of apparent first order kinetics. Similar peak deconvolution methods as previously explained for the quantification of the ν(-NC) signal was used again in this approach, and the resulting data are shown in **Figure 46a** and **Figure 46b**. Minor deviations from linearity at 35 and 45 °C in **Figure 46b** can be explained by slight deviations in the oil bath temperature (±1 °C), which leads to a not completely preventable fluctuation of the kinetics data. This effect has higher influence on the reaction at 35 °C compared to the reactions at 45 and 55 °C, which explains the lower fluctuation at 45 °C and no noticeable fluctuation at 55 °C. Additionally, viscosity changes, which increase with conversion, could also affect the kinetics.

The second reaction step (crosslinking) was investigated by the reaction of presynthesized 1,5-diisothiocyanato pentane (C_5-DiNCS) with castor oil in an online IR setup, monitoring the reduction of the ν(N=C=S) signal (**Figure 46c**). This homogeneous reaction follows second order kinetics, as the reaction rate *r* is proportional to the concentration of isothiocyanate and hydroxyl functional groups. This is confirmed by the linear correlation of $\ln([NCS][OH]_0/[NCS]_0[OH])$ with time for the determination of the reaction rate constant of the crosslinking reaction step k_2 as shown in **Figure 46d**. The Arrhenius plot was used for the determination of the activation energies E_a by applying a linear fit and applying the Arrhenius equation (**Figure 46e** and equation (*21*)).

$$\ln(k) = \ln(A) - \frac{E_a}{RT} \tag{16}$$

k: rate constant
A: preexponential factor
E_a: activation energy
R: universal gas constant, $R = 8.3145\ \text{J mol}^{-1}\text{K}^{-1}$
T: Temperature, $[T] = \text{K}$

Besides the calculation of E_a, this plot can furthermore be used to determine k_1 and k_2 values for any other temperature, which thus enables a prediction of the kinetics of the system for any other temperature program. For example, the k_2 value can be extrapolated for 55 °C, which enables the calculation of the reaction kinetics for the crosslinking without an elevation to higher temperatures, resulting in a theoretical time of gelation at 55 °C of t_{gel}=63 h 15 min (Experimental Section equations (*41*)–(*42*)). Furthermore, it can be predicted at which temperature both reactions proceed at the same rate, which is the intercept of the two linear fits if both reactions are of the same reaction order (k_1=k_2 at the intercept). Beyond this point would therefore correspond to the temperature range, at which the second reaction step becomes faster than the first. However, as the first reaction step follows apparent first order kinetics, and the crosslinking reaction second order kinetics, a calculative correction depending on the actual concentrations of the components has to be applied (Experimental Section equations (*43*)–(*48*)).

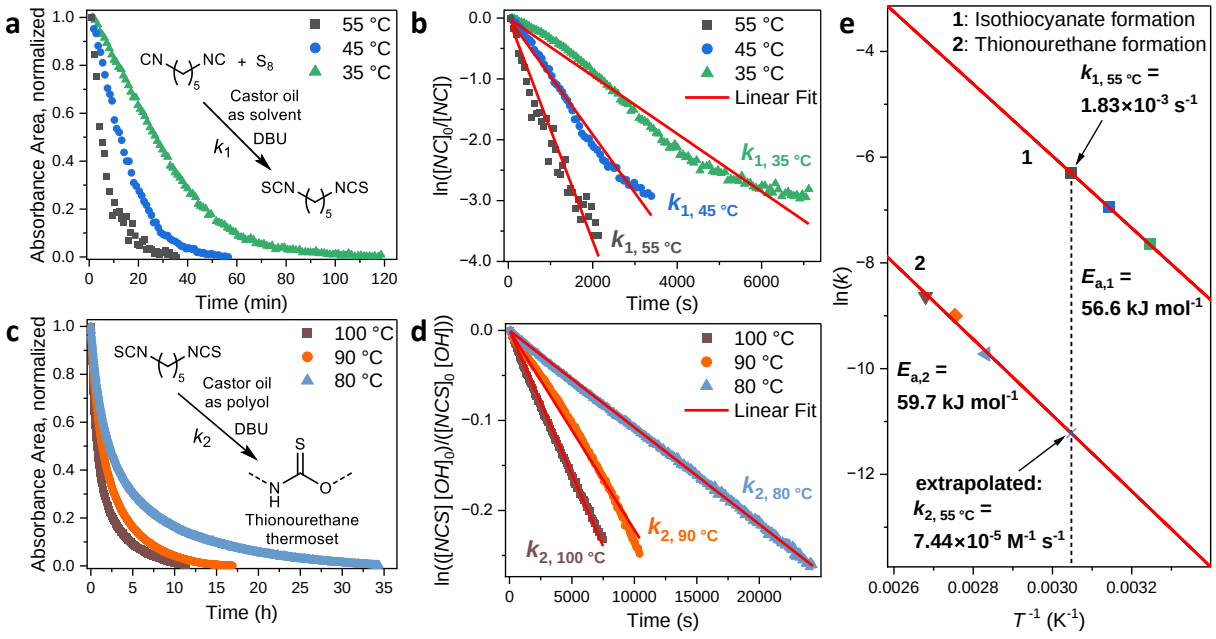

Figure 46 *(a) IR-spectroscopy absorbance area of the ν(-NC) signal for the diisothiocyanate formation reaction in castor oil at T=35, 45, and 55 °C; (b) k_1 determination applying first order kinetics for the diisothiocyanate formation reaction; (c) IR-spectroscopy absorbance area of the ν(N=C=S) signal for the polythionourethane crosslinking reaction at T=80, 90, and 100 °C; (d) k_2 determination applying second order kinetics for the polythionourethane crosslinking reaction; (e) arrhenius plot of both reaction steps for the determination of the activation energies E_a and extrapolations of k_1/k_2 values at different temperatures.*

The temperature at which both reactions proceed at the same rate was consequently calculated to a hypothetical temperature of T=-115 K. This result indicates a faster reaction rate for the first reaction step at any practically chosen temperature. All determined k_1, k_2, and E_a values are summarized in **Table 17**.

Table 17 *Determined k_1 and k_2 values of the two reaction steps (isothiocyanate and thionourethane formation, compare* ***Scheme 28****) at different temperatures and calculated activation energies E_a.*

	k_1 (s^{-1})			E_a
Isothiocyanate formation:	35 °C	45 °C	55 °C	(kJ mol^{-1})
	4.76×10^{-4}	9.58×10^{-4}	1.83×10^{-3}	56.6

	k_2 (M^{-1} s^{-1})			E_a
Thionourethane formation:	80 °C	90 °C	100 °C	(kJ mol^{-1})
	5.98×10^{-5}	1.23×10^{-4}	1.77×10^{-4}	59.7

In order to investigate the structure-property relationship on the resulting materials, a library of thionourethane thermosets was synthesized utilizing different diisocyanides applying the optimized conditions from the prior kinetic investigations. Furthermore, two reference materials based on 1,6-diisocyanatohexane (C_6-DiNCO) and isophorone diisocyanate (IP-DiNCO) were synthesized to compare the conventional polyurethane thermosets with the novel polythionourethane thermosets concerning their mechanical and thermal properties. Additionally, three thionourethane thermosets were synthesized using presynthesized diisothiocyanates for a comparison to the materials, which were synthesized *via* the multicomponent reaction approach with *in situ* generation of the diisothiocyanate (**Table 18**).

Thermal Properties

The thermal properties of all synthesized materials were analyzed using DSC and TGA measurements. DSC thermograms revealed a glass transition temperature T_g for all materials, ranging from -19 to -42 °C (**Table 18**).

Table 18 *Thermal properties of the synthesized thermoset materials as determined via DSC and TGA.*

Reagent	T_g (°C)	$T_{d,5\%}$ (°C)	$T_{d,50\%}$ (°C)	Char residue (%)[a]
C_5-DiNC + S_8	-35	207	372	3.6
C_5-DiNCS	-34	205	371	0.6
C_6-DiNC + S_8	-39	212	375	1.3
C_6-DiNCS	-31	210	377	1.4
C_6-DiNCO	-34	312	388	0.4
C_{10}-DiNC + S_8	-38	220	379	0.7
C_{12}-DiNC + S_8	-42	224	379	0.3
IP-DiNCS	-31	216	370	1.9
IP-DiNCO	-19	304	375	1.2

[a]Determined at 600 °C.

When comparing the oxourethane reference material to the thionourethane thermoset based on C_6-DiNCO/C_6-DiNCS, respectively, the observed glass transition temperatures were found to differ by 2 °C (-33 °C vs. -31 °C, **Figure 47a**), indicating that the thionourethane functionality does not have a major impact on the glass transition behavior compared to the oxourethane functionality. A slightly larger difference in T_g was obtained when comparing the thionourethane thermoset synthesized from C_6-DiNCS with the *in situ* generated isothiocyanate from C_6-DiNC + S_8. (-31 °C vs. -39 °C, **Figure 47a**). However, in the case of the C_5-analogue, a difference of just 1 °C was observed (-34 °C vs. -35 °C, **Table 18**). Thus, no considerable deviation between the *in situ* and *non in situ* approach can be concluded. Generally, the glass transition of all thermosets is in a comparable temperature range, not being substantially affected by the type of diisothiocyanate/diisocyanate, except for the IP-DiNCO based thermoset, which shows a considerably higher T_g of -19 °C.

In TGA measurements, a multi-step degradation mechanism with two major steps was found for the thionourethane thermoset materials, whereas a one-step degradation is observed for the oxourethane reference materials (**Figure 47b**). The first degradation step of the materials was characterized by the $T_{d,5\%,}$ and was found to range from 205 to 224 °C for the thionourethane materials, which is close to degradation temperatures that were found for other polymers containing the thionourethane moiety: Sun and Tang *et al*.[300] found poly(*O*-thiocarbamate)s with $T_{d,5\%}$ values in a range of 192–240 °C, depending on the substituent, and in a prior investigation in our group, we found $T_{d,5\%}$ values of 212–265 °C for thionourethane functionalized cellulose derivatives.[201] In all

these cases, a two-step degradation mechanism was observed, leading to the assumption that the thionocarbamate functional group starts degrading in these temperature ranges, followed by a second degradation step of the residual material. Similar behavior was also observed for *S*-thiocarbamate (thiolourethane) containing polymers, where the degradation of the *S*-thiocarbamate functionality to the corresponding isocyanate and thiol could be detected.[331]

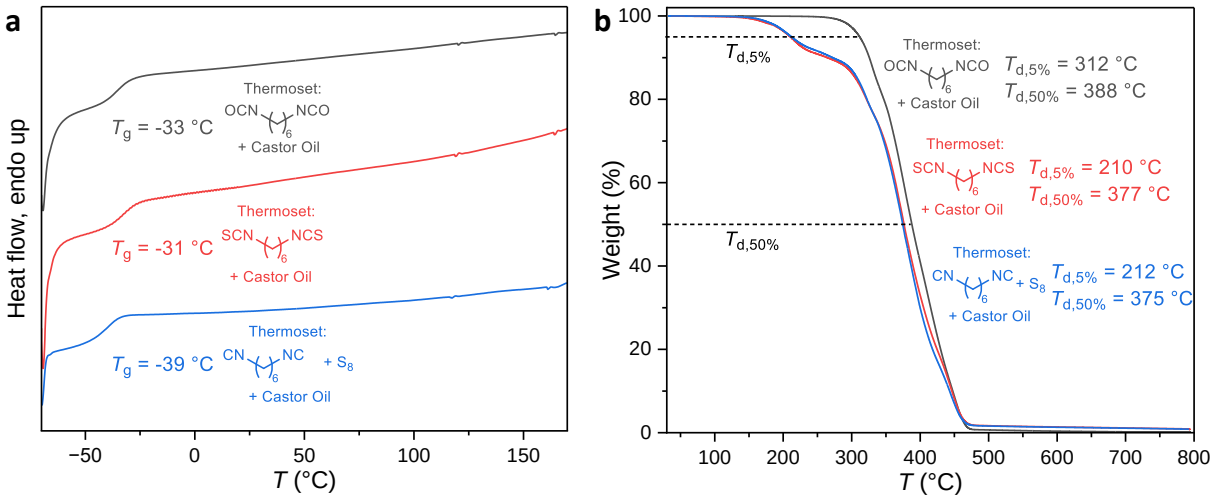

Figure 47 *(a) Stacked DSC thermograms and (b) overlaid TGA thermograms of the reference oxourethane thermoset based on C_6-DiNCO compared to the thionourethane thermosets synthesized using a presynthesized C_6-DiNCS and the in situ generated diisothiocyanate from C_6-DiNC + S_8. The data of all other materials can be found in the Experimental Section* ***Figure S174*** *and* ***Figure S175****.*

The second degradation step was evaluated at $T_{d,50\%}$, and a narrow temperature range was found for all materials (370–388 °C), especially comparing the thionourethane with the oxourethane thermoset materials (**Table 18**). Similar degradation temperatures for castor oil/isophorone diisocyanate-based oxourethane prepolymers were also reported previously by Gurunathan *et al.* with $T_{d,50\%}$=382.9–431.0 °C, depending on the chosen polyol/diisocyanate ratio.[322]

Rheological Investigations

The curing process was monitored using *in situ* rheological measurements based on the C_5-DiNCS and castor oil under three different isothermal conditions (80, 90, and 100 °C). The time of gelation t_{gel} was determined from the intercept of the loss- and storage moduli (**Figure 48a**–**c**) and ranged from 5 h 49 min at 100 °C to 17 h 56 min at 80 °C.

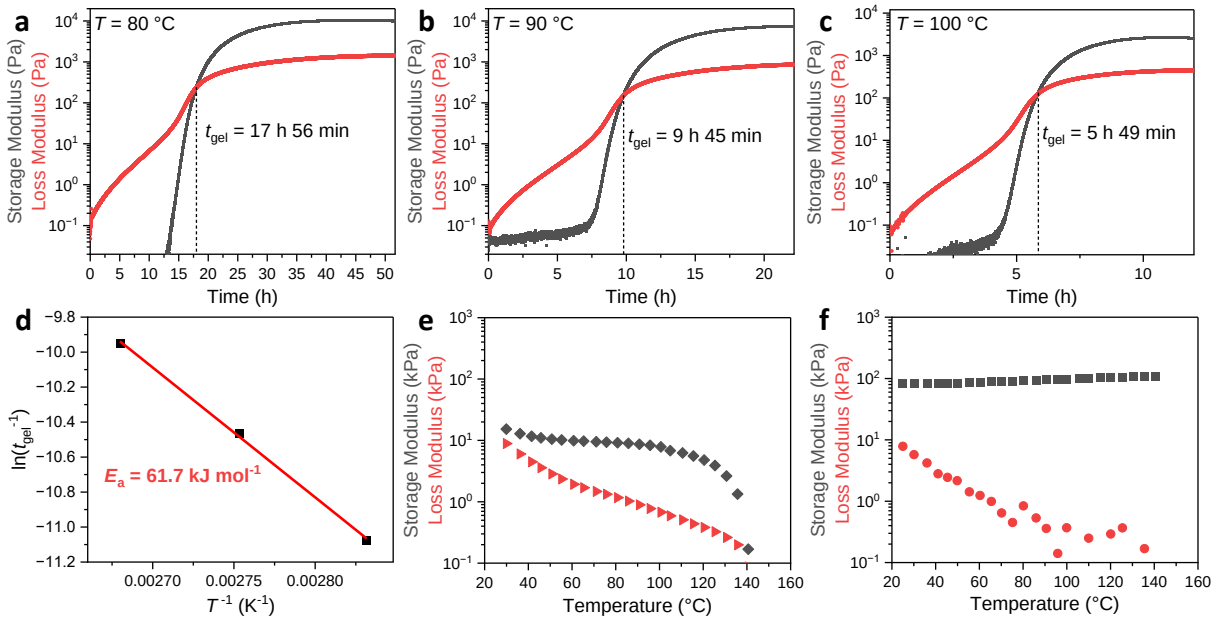

Figure 48 *(a)–(c) Rheology measurements of the isothermal in situ curing of 1,5-diisothiocyanato pentane and castor oil with DBU as organo-base at three different temperatures; (d) Arrhenius relationship applied to gelation times for the determination of E_a; (e)+(f) rheology temperature sweep measurement of a fully cured thionourethane thermoset (based on 1,6-diisothiocyanato hexane and castor oil (e)), and of a fully cured oxourethane thermoset (based on 1,6-diisocyanato hexane and castor oil (f)).*

The time of gelation can be taken as another measure of the overall rate of polymerization for the isothermal crosslinking processes, as the conversion at the gel point is constant and not dependent on the reaction temperature, according to Flory's gelation theory.[332–334] The activation Energy E_a can therefore be calculated from the t_{gel} applying the Arrhenius relationship according to equation (17).[333]

$$\ln\left(t_{\mathrm{gel}}^{-1}\right) = -\frac{E_{\mathrm{a}}}{R}\,T^{-1} + \ln A' \qquad (17)$$

The determined E_a for the crosslinking reaction from rheological measurements (**Figure 48d**) is very close to the one determined from online IR measurements ($E_{a,IR}$ = 59.7 kJ mol^{-1} vs. $E_{a,Rheometer}$ = 61.7 kJ mol^{-1}) and therefore confirm each other. Furthermore, analogous to the possible prediction of any other *k* value at different temperatures from the Arrhenius relationship in **Figure 46e**, the time of gelation for any other isothermal curing temperature can be predicted due to the linear correlation of the Arrhenius relationship (**Figure 48d**, Experimental Section equation (*49*)). The

crosslinking of the C_6-DiNCS with castor oil showed no substantial difference compared to the C_5-DiNCS concerning the time of gelation (t_{gel}=5 h 49 min vs t_{gel}=5 h 33 min) and the resulting mechanical properties (**Table 19**).

Table 19 *Mechanical properties as determined from rheological measurements.*

Reagent	$G'_{25\,°C}$ (kPa)	$G''_{25\,°C}$ (kPa)	υ_e (mol m^{-3})[a]
C_5-DiNC + S_8[b]	34.1	14.8	13.8
C_5-DiNCS[b]	17.4	11.7	7.0
C_6-DiNCS[c]	18.4	8.5	7.4
C_6-DiNCO[c]	82.0	7.9	33.1
IP-DiNCO[d]	113.9	28.3	45.9

[a]determined based on the storage moduli at 25 °C [b]Cured isothermally at 90 °C, [c]Cured isothermally at 100 °C, [d]Cured isothermally at 115 °C.

The fully cured thermoset based on C_6-DiNCS was used to compare its properties to the oxourethane reference material based on C_6-DiNCO. The thionourethane thermoset was found to have a lower storage modulus (G'=82.0 kPa vs G'=18.4 kPa), and consequently a lower crosslinking density υ_e. This is mainly expected to be a consequence of weaker hydrogen bonds in the thionourethane thermoset compared to the oxourethane material. Elongated crosslinks in the thionourethane material can also be caused by the assumed side reactions as discussed before (interposed thiourea moiety and/or dimerization of the isothiocyanate) but seem less likely, as similar side reactions also occur in classic urethane thermosets. The influence of temperature on the mechanical properties (i.e. storage and loss modulus) was investigated by a temperature sweep measurement of the fully cured material and the storage modulus remained stable up to a temperature of 130 °C (rubbery plateau), after which an irreversible drastic storage modulus decrease was found for the thionourethane material (**Figure 48e+f**). These observations are in accordance with the results from TGA measurements, as onsets of thermal degradation reactions were detected starting at 130 °C. The rapid drop in modulus also implies a stepwise degradation mechanism with a rapid decrease in molecular weight in the first step. These novel thionourethane thermosets result in softer materials with generally lower storage modulus values if compared to classic polyurethane thermosets, which usually exhibit storage moduli in the range of low MPa values at room temperature.[64,335–337] A major general advantage of polyurethanes over other polymer classes is the possibility of *in situ* foaming by the addition

of small amounts of water to the reaction mixture (which generates CO_2) for the production of polymer foams. This is theoretically also possible for the presented thionourethane system, but under the formation of COS, which should be prevented due to its toxicity, and therefore limits the system in its current research state to non-foamed thermosets. Photographs of a thionourethane thermoset sample for a basic demonstration of the optical appearance is shown in **Figure 49**.

Figure 49 *Photographs of the resulting thionourethane thermoset material.*

Conclusion

A novel multicomponent reaction based thionourethane thermoset synthesis approach from diisocyanides, elemental sulfur, and castor oil was achieved. The isothiocyanate was generated *in situ via* a DBU-catalyzed sulfurization of isocyanides, which was investigated in detail by real-time IR measurements. The kinetics for the formation of the diisothiocyanates were found to be of second order with apparent first order, likely due to the heterogeneous nature of the reaction. The crosslinking reaction was found to follow second order kinetics and proceeded considerably slower compared to the isothiocyanate formation reaction, resulting in a thermally triggerable curing of the system. These kinetic investigations enable a prediction of the diisothiocyanate formation, as well as the crosslinking process for any chosen temperature program, which could be confirmed by rheological *in situ* curing experiments. Compared to analogous oxourethane thermoset materials, similar glass transition temperatures of the thionourethane thermosets were found, whereas a two-step thermal degradation process was found for the thionourethane materials with a $T_{d,5\%}$=212 °C compared to a $T_{d,5\%}$=312 °C for an analogous oxourethane thermoset. In terms of mechanical properties, generally lower storage moduli were found for the thionourethanes compared to

the oxourethane analogues. The possibility of an *in situ* generation of the diisothiocyanate in castor oil, which acts in a dual role first as solvent and then as reactant, was found advantageous over other thermoset synthesis procedures and the presented system consequently fulfills many aspects of the *Twelve Principles of Green Chemistry*, like 100% atom economy, zero waste production (*E*-Factor = 0, all reactants remain in the final thermoset), utilization of catalysts (instead of stoichiometric amounts of base), use of renewable materials, avoidance of intermediate products, solvents, waste, and toxic chemicals. Finally, this approach with *in situ* generation of the diisothiocyanate is expected to be applicable to other liquid polyols besides castor oil, which could enable a platform for thionourethane-based thermosets.

5 Conclusion and Outlook

Based on the aim to develop novel procedures for the sustainable synthesis of polymeric materials from renewable substrates, three approaches could be achieved:

First, a novel homogeneous cellulose acetylation process in the DMSO/DBU/CO_2 switchable solvent system was established, in which vinyl acetate could be employed as a more benign acetylation agent compared to the conventionally used acetic anhydride or acetic chloride. The developed procedure resulted in high conversions (up to 99+%) under mild conditions (60 °C), and less cellulose backbone degradation due to the non-acidic conditions was detected compared to the *Acetic Acid Process*. Furthermore, a direct synthesis of cellulose acetate with lower degrees of substitution was possible by simple adjustment of the reactant equivalents, which is not possible in the *Acetic Acid Process* due to the heterogeneous reaction process. Additionally, a novel method for the degree of substitution determination of cellulose esters was developed using ATR-FTIR spectroscopy. This method facilitates the measurement process and enables a non-destructive degree of substitution determination method for cellulose acetates, butyrates, laurates, and benzoates.

Moreover, a conceptionally novel cellulose derivatization procedure was developed, in which isothiocyanate reactants were generated *in situ* in the DMSO/DBU/CO_2 switchable solvent system *via* catalytic sulfurization of isocyanides with elemental sulfur. In this tandem reaction approach, 100% atom economy was achieved, with a triple catalytic use of the superbase DBU for (i) the solubilization of cellulose, (ii) the generation of the isothiocyanate reactant, and (iii) the formation of the *O*-cellulose thiocarbamate product in a one-pot procedure. Four different bio-based isocyanides were used to form the respective isothiocyanates *in situ*, which directly reacted with cellulose, inherently preventing the exposure and handling of these potentially toxic compounds.

The *in situ* formation of isothiocyanates from isocyanides and elemental sulfur could be transferred to the formation of thionourethane thermosets based on castor oil. It was found that diisothiocyanates could be formed in a solvent-free approach, as castor oil fulfilled a dual role: acting as the solvent in the first step and subsequently as the polyol reactant in the curing process. DBU was used as the organocatalyst and found

to promote both the sulfurization reaction and the thionourethane formation. The kinetics of the two consecutive steps were studied in detail *via* real-time IR measurements, and the thionourethane crosslinking step was found to be thermally triggerable, enabling high control over the curing process.

Overall, fundamental research was performed for the development of sustainable procedures and novel bio-based polymeric materials. With the multiple use of DBU, the synthetic design for high atom economy, the coupling of multiple consecutive reactions in one pot, the use of bio-based materials, and the prevention of toxic compounds, solvents, and waste, most of the *Principles of Green Chemistry* could be implemented into the respective synthetic procedures. The established approaches are driving the transition towards more sustainable development in polymer chemistry, and the resulting novel materials hold promise as potential replacements for existing options, such as the thionourethane thermosets, offering a viable alternative to classic polyurethanes.

6 Experimental Section

6.1 Materials

Microcrystalline cellulose (MCC, dried at 100 °C under vacuum for 24 h prior to use), 2-chloro-4,4,5,5-tetramethyl-1,3,2-dioxaphospholane (TMDP) (95%), 1,6-diaminohexane (98%), 1,5-diaminopentane (95%), dimethyl acetamide (99%), 1,6-diisocyanatohexane (>98%), *n*-dodecylisocyanate (99%), *endo*-*N*-hydroxy-5-norbornene-2,3-dicarboximide (97%), glacial acetic acid (≥99%), isophorone diisocyanate (98%), *n*-hexanol (98%), oleyl amine (>98%), *para*-toluenesulfonyl chloride (>98%), silica gel (technical grade, pore size 60 Å, 230–400 mesh particle size), and vinyl laurate (>99%), were purchased from **Sigma-Aldrich**. 1,12-Diaminododecane (>98%), diazabicyclo[5.4.0]undec-7-ene (DBU) (distilled and stored over molecular sieves under Ar-atmosphere), isophorone diamine (cis- and trans- mixture, >99%), vinyl benzoate (>99%), and vinyl butyrate (TCI, >98%) were purchased from **TCI**. Butyl isocyanide (>98%), cyclohexyl isocyanide (>98%), dimethyl sulfoxide (DMSO) (dry and stored over molecular sieve, >99%), ethyl formate (>98%), trifluoroacetic acid (99%), and vinyl acetate (99%, stabilized) were purchased from **Acros Organics**. Chloroform (≥99.8%), dichloromethane (≥99.8%), pyridine (≥99.5%), and triethylamine (≥99.5%) were purchased from **Fisher Scientific**. Acetic anhydride (≥99%) was purchased from **Carl Roth**. Dodecyl amine (97%) was purchased from **Alfa Aesar**. 1,10-Diaminodecane was purchased from **Fluorochem**. Deuterated solvents DMSO-d_6 (99.8%), THF-d_8 (99%), D_2O (99%), and $CDCl_3$ (98%) were purchased from **Eurisotop**. Filter paper type MN 615 (used as cellulose source for acetylations) was purchased from **Machery-Nagel**. Castor oil (cold-pressed) was purchased from **Mea Vita**. CO_2 (99.995%) was purchased from **Air Liquide**. Sulfur (elemental, dried at 80 °C under vacuum for 24 h prior to use), acetone, and isopropanol were of technical grade.

6.2 Instrumentation

Infrared spectroscopy (IR). Infrared spectra of all cellulose samples were recorded using a Bruker Alpha-p instrument with ATR unit in a range of ν=400–4000 cm^{-1} and 24 scans per measurement at a resolution of 4 cm^{-1}. All thionourethane and oxourethane thermoset samples were measured using a PerkinElmer Spectrum 100 instrument with an attenuated total reflection (ATR) unit on a diamond crystal and an MKII Golden Gate accessory. For every spectrum, 16 scans in a range of ν = 600–4000 cm^{-1} were recorded at a resolution of 4 cm^{-1}.

Nuclear Magnetic Resonance Spectroscopy (NMR). ^{1}H NMR spectra were recorded using a Bruker Ascend 400 MHz with 128 scans for all cellulose derivatives and 16 scans for all other organic molecules, and a delay time d_1 of 5 seconds for cellulose samples and 1 second for all other samples at 298 K. The chemical shift was reported in ppm and referenced to the solvent signal of partly deuterated DMSO-d_6 at 2.50 ppm, $CDCl_3$ at 7.26 ppm, and THF-d_8 at 3.58 ppm. ^{13}C NMR spectra were recorded using a Bruker Avance DRX at 126 MHz with 26624 scans for cellulose samples and 1024 scans for all other samples and a delay time d_1 of 3 seconds at 298 K. The signals were referenced to the solvent peak of partly deuterated DMSO-d_6 at 39.52 ppm and $CDCl_3$ at 77.16 ppm. ^{31}P NMR spectra were recorded using a Bruker Ascend instrument at 162 MHz with 1024 scans, a delay time d_1 of 5 seconds, and 1 second acquisition time at 298 K.

Differential Scanning Calorimetry (DSC). DSC measurements of all cellulose acetate samples were performed on a Mettler Toledo DSC821e instrument using 100 µL aluminum crucibles under nitrogen atmosphere. The samples (20 mg) were measured in two heating cycles: 25–200 °C, 200 to -50 °C and -50 to 200 °C at a heating/cooling rate of 10 K min^{-1}. All cellulose thionocarbamate samples were measured on a TA Instruments Discovery 2500 instrument in TA TZero sample holders. The samples were measured in two heating cycles: -50 to 210 °C, 210 to -50 °C, and -50 to 210°C at a heating/cooling rate of 15 K min^{-1}. All thionourethane and oxourethane thermoset samples were measured on a Mettler Toledo DSC1 instrument equipped with a sample robot. Samples of 10–20 mg were loaded in a 100 µL aluminum crucible with pierced

lid and the measurements were performed under nitrogen atmosphere with a flow rate of 50 mL min^{-1}. The DSC thermograms were recorded at a heating/cooling rate of 10 K min^{-1} using the following heating/cooling program: First heating from 20–105 °C, hold at 105 °C for 20 min, then cooling from 105 to -70 °C, hold at -70 °C for 10 min, and a final heating step from -70 to 200 °C. The data from the last heating step is shown in all DSC curves.

Size Exclusion Chromatography (SEC). SEC analyses of cellulose acetates were performed on a Tosoh EcoSEC HLC-8320 system with three columns: PSS PFG Micro precolumn (3.0 × 0.46 cm, 10,000 Å), PSS PFG Micro (25.0 × 0.46 cm, 1000 Å), and PSS PFG Micro (25.0 × 0.46 cm, 100 Å) and a differential RI detector. Hexafluoroisopropanol (HFIP) enriched with 0.1 wt% potassium trifluoroacetate (KTFAc) was used as eluent at a temperature of 35 °C and a flow rate of 0.4 mL min^{-1}. The samples were prepared with a concentration of 1.0 mg mL^{-1} and 50 μL were injected into the system. A poly(methyl methacrylate) standard (Polymer Standard Service, M_p =102–981 kDa) was used for extrapolation of the number average molar mass (M_n). All cellulose thionocarbamate samples were measured in DMAc/LiBr on a PL-SEC 50 Plus Integrated System with a PLgel 5 μm bead-size guard column (50 × 7.5 mm) followed by three PLgel 5 μm Mixed C columns (300 × 7.5 mm) and a differential RI detector. *N*,*N*-Dimethylacetamide (DMAc) enriched with 0.03 wt% lithium bromide was used as eluent at a temperature of 70 °C and a flow rate of 1.0 mL min^{-1}. The samples were prepared with a concentration of 2.0 mg mL^{-1} and 100 μL were injected into the system. A poly(methyl methacrylate) standard was used for extrapolation of the number average molar mass (M_n).

Thermogravimetric Analysis (TGA). TGA measurements of cellulose acetate samples were carried out on a Netzsch STA 409C instrument under nitrogen atmosphere. The samples (5–10 mg) were heated in a Al_2O_3 crucible with a heating rate of 10 K min^{-1} in a temperature range of 25 to 600 °C. The cellulose thionocarbamate samples were measured on a Netzsch STA 449F3 instrument under nitrogen atmosphere. The samples (5−10 mg) were heated in a 85 μL aluminium crucible with the following temperature program: Start at 25 °C, heating to 80 °C with 10 K min^{-1}. Hold at 80 °C for 0.5 min followed by heating to 600 °C with 10 K min^{-1}. All thionourethane and

oxourethane thermoset materials were measured on a Mettler Toledo TGA/DSC1 instrument. Samples of 10–20 mg were placed in a ceramic crucible and then heated using the following program: start at 30 °C, hold for 10 min, followed by heating to 800 °C at a rate of 5 K min^{-1} and maintained isothermally at 800 °C for 10 min. All measurements were performed under nitrogen atmosphere with a flow rate of 50 mL min^{-1}.The $T_{d,5\%}$ is defined as the temperature of 5% weight loss and the $T_{d,50\%}$ as the temperature of 50% weight loss.

Tensile strength measurements. Films were prepared by dissolving 100 mg cellulose acetate sample in 2 mL acetone or chloroform and casting the solution into poly(tetraflouro ethylene) plates (40 mm diameter). The solvent was evaporated at room temperature for 48 h followed by drying in a vacuum oven for 2 h. The films were then prepared into bone shapes (16 × 2 mm) and the thickness was determined with a digital vernier caliper. Tensile strength was measured using a GABO EXPLORER instrument with a 25 N sensor. The initial speed was set to 0.5 mm min^{-1} and three measurements were performed for each sample.

Rheology Measurements. Rheology Measurements were performed using a TA Instruments DHR-2 rheometer with disposable aluminum plates (25 mm diameter) in a plate/plate configuration. All measurements were performed at an angular frequency of 1 Hz and 4% strain. For every thermoset curing experiment, 400 µL sample liquid was applied and the excess was removed after lowering to the final gap size of 300 µm.

Gas Chromatography (GC). GC chromatograms were recorded on a BRUKER 430 GC instrument with a capillary column FactorFour VF-5ms (30 m × 0.25 mm × 0.25 mm) and a flame ionization detector. Heating program: Start at 95 °C and hold for 1 min. Heating to 200 °C with 15 K min^{-1} and hold at 200 °C for 4 min. Heating to 300 °C with 15 K min^{-1} and hold at 300 °C for 2 min.

Mass Spectrometry (MS) Electrospray ionization (ESI) experiments were recorded on a Q-Exactive (Orbitrap) mass spectrometer (Thermo Fisher Scientific) equipped with a HESI II probe to record high resolution. The spectra were evaluated by molecular signals $[M–H]^+$ and indicated with their mass-to-charge ratio (*m/z*).

6.3 Experimental Procedure

6.3.1. Cellulose Acetate Synthesis – Chapter 4.1

This chapter is based on previously published results by the author of this thesis:

Wolfs, J.; Meier, M. A. R. A More Sustainable Synthesis Approach for Cellulose Acetate Using the DBU/CO_2 Switchable Solvent System. *Green Chem.* **2021**, *23* (12), 4410–4420.[140]

Text, figures, and data are reproduced from this article and were partially edited and extended with permission from the Royal Society of Chemistry.

DS Determination by ^{31}P NMR Method

DS were determined by derivatization of the CA samples using a phosphorylating agent according to the following procedure: An exact amount of 25 mg of each sample was dissolved in 1 mL of pyridine followed by the addition of 1 mL $CDCl_3$. Next, 2-chloro-4,4,5,5-tetramethyl-1,3,2- dioxaphospholane (2-Cl-TMDP, 100 µL, 0.63 mmol) was added and the solution was stirred for 15 min. Then, the internal standard *endo-N*-hydroxy-5-norbornene-2,3-dicarboximide (150 µL, 123.21 mM in pyridine/$CDCl_3$=3:2, 0.0154 mmol) was added and the solution was stirred for further 10 min. 0.6 mL of the solution was then transferred to an NMR tube and a ^{31}P NMR measurement was performed. The DS values were calculated according to equations (*18*) and (*19*) as reported by Kilpeläinen *et al*.[208]

$$\mathrm{DS}_{31\mathrm{P}} = \mathrm{DS}_{\max} \times \frac{\frac{1}{\mathrm{OH}_\mathrm{S}} - \frac{1}{\mathrm{OH}_\mathrm{C}}}{M_\mathrm{S} + \frac{1}{\mathrm{OH}_\mathrm{S}} - 1} \quad (18)$$

$$\mathrm{OH}_\mathrm{S} = \frac{c_\mathrm{IS} \times V_\mathrm{IS} \times I_\mathrm{R}}{1000000 \times m_\mathrm{S}} \quad (19)$$

$\mathrm{DS}_{\max}$: maximum achievable DS value ($\mathrm{DS}_{\max} = 3$ for unsubstituted cellulose)
OH_S: free hydroxyl groups per weight unit of substrate (mol g^{-1})
OH_C : free hydroxyl groups per weight unit of cellulose ($\mathrm{OH}_\mathrm{C} = \mathrm{DS}_{\max}/M_{\mathrm{AGU}} = 3/162.14\ \mathrm{g\ mol}^{-1}$)
M_S: molecular weight of the substituent, not including the linking oxygen atom between the substituent and the cellulose backbone (g mol^{-1})
c_IS: concentration of the used internal standard (mmol L^{-1})
V_IS: volume of the used internal standard (µL)
I_R: integration ratio of remaining functionalized cellulose hydroxyl groups against internal standard
m_S: mass of the sample (mg)

Partial DS Determination *via* ^{13}C NMR Sepctroscopy

^{13}C NMR spectra for the quantitative determination of the partial DS in C2, C3, and C6 position were acquired in an inverse gated decoupling method with 26624 scans per measurement. Peak deconvolution was performed using the software *MestReNova v12.0.0*, Method: quantitative GSD with 10 improvement cycles, peaks type: positive and negative, refinement level: 4 (20 fitting cycles).

General Procedure for the Homogeneous Synthesis of Cellulose Acetate

In a round-bottom flask, cellulose (2.00 g, 12.33 mmol) was suspended in 60 mL DMSO followed by the dropwise addition of 1,8-diazabicyclo[5.4.0]undec-7-ene (5.5 mL, 37.00 mmol, 3.0 eq. per anhydroglucose unit). After applying a CO_2 flow through the solution for 20 min at 40 °C, a clear solution was obtained and vinyl acetate (1.0–4.5 eq. per AGU, depending on the experiment) was added dropwise. The homogeneous solution was then heated to 60 °C and stirred for 4 h. Subsequently, the dark solution was added dropwise into 300 mL of isopropanol under vigorous stirring to precipitate cellulose acetate. It was then vacuum filtrated and washed with isopropanol (3 x 50 mL). The obtained precipitate was dried under high vacuum (0.02 mbar) for 24 h.

In case of residual DMSO in the product, the material was stirred with 40 mL of isopropanol (or methanol) under reflux for 1–12 h, vacuum filtrated and dried again. The final product was obtained as a white or yellow powdery substance. Yields were calculated based on the DS_{1H} (equations (*20*) and (*21*)) and ranged from 84 to 99%.

$$\text{yield} = \frac{\frac{m_{\text{CA}}}{M_{\text{repunit}}}}{\frac{m_{\text{cellulose}}}{M_{\text{AGU}}}} \tag{20}$$

$$M_{\text{repunit}} = M_{\text{AGU}} + (\overline{M_{\text{S}}} - 1.01\ \text{g mol}^{-1}) \times DS \tag{21}$$

Cellulose Acetate (CA-1): Yield: 91%

ATR-IR (cm^{-1}): 3032–3675 ν(O-H), 2819–2991 ν(C-H), 1728 ν(C=O), 1370 methyl ν(C-H), 1229 ester ν(C-O), 1023 AGU ν(C-O).
^{1}H NMR (400 MHz, DMSO-d_6) δ_H ppm: 2.78–5.30 (m, AGU, 7H), 1.69–2.27 (m, $Ac_{6,2,3}$, 9H).

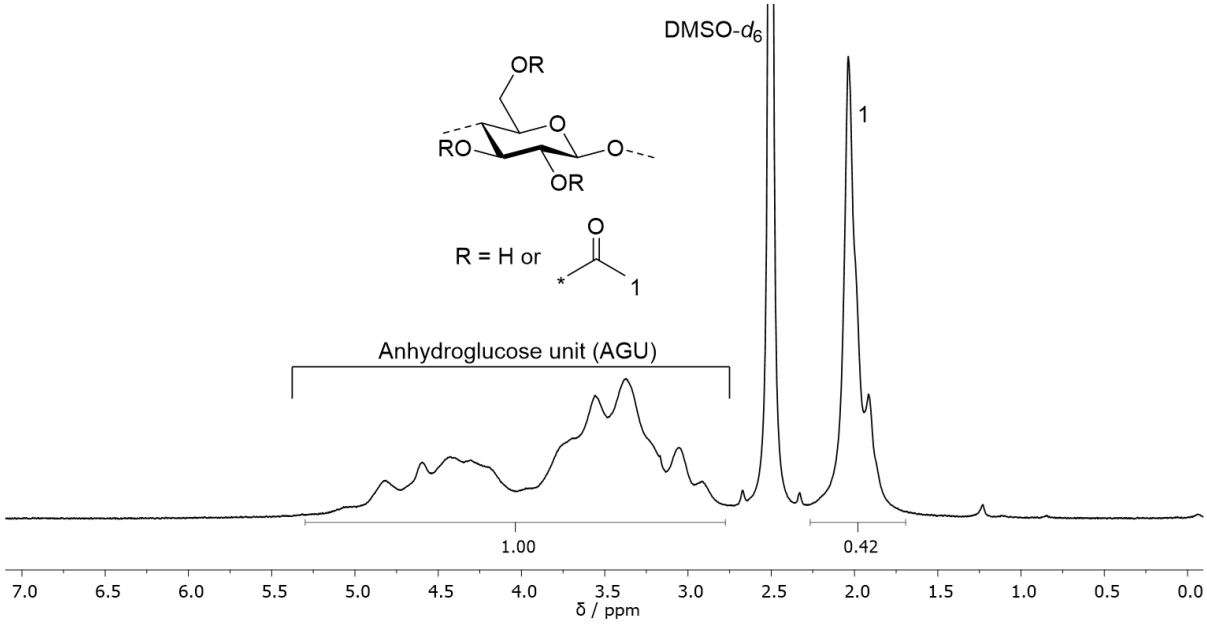

Figure S1 *^{1}H NMR (DMSO-d_6 + TFA) spectrum of CA-1.*

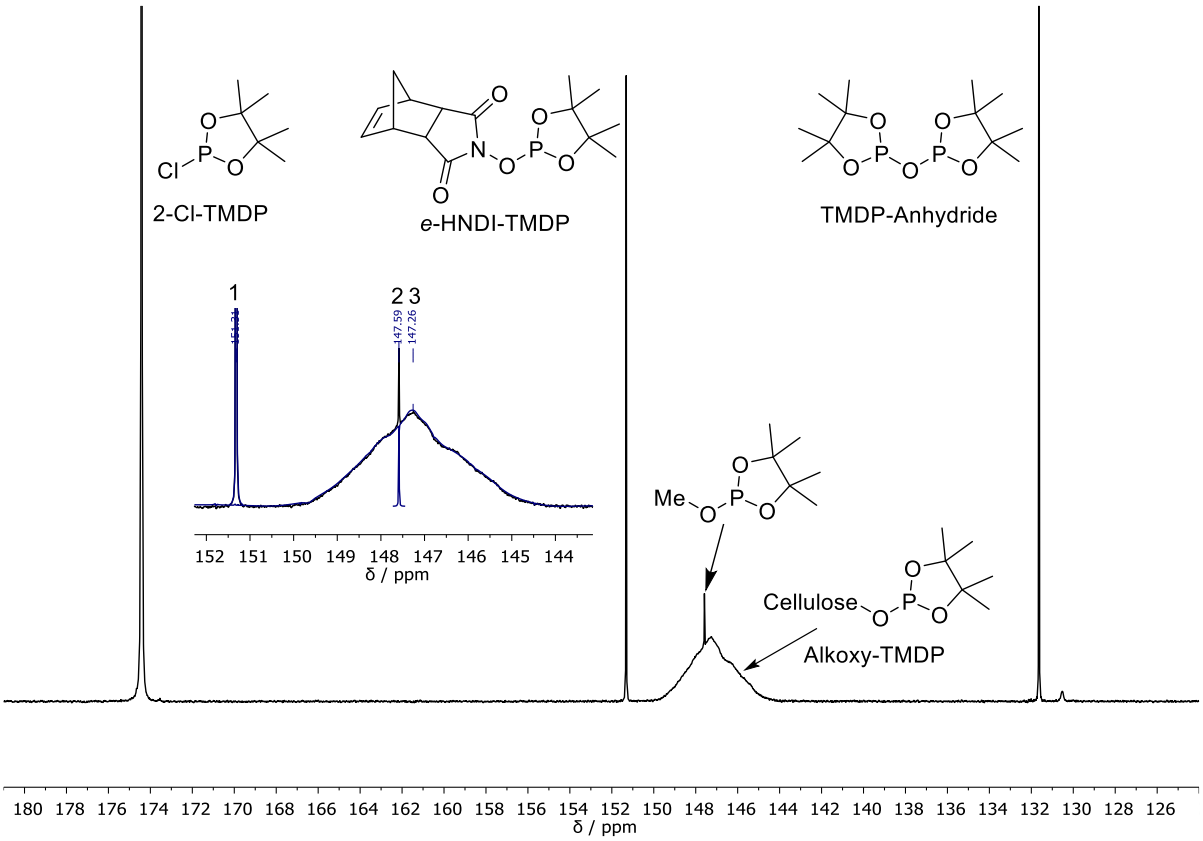

Figure S2 *^{31}P NMR ($CDCl_3$) spectrum of the phosphitylated CA-1. Peak deconvolution: blue lines in expanded view (calculated: $DS_{^{31}P}$=1.04).*

Low residual amounts of MeOH did not evaporate from CA-1 under high vacuum (0.02 mbar) and interfered with the signal for $DS_{^{31}P}$ determination. Peak deconvolution was used to correct the determined integral. The integration ratio using the data from peak deconvolution was calculated: $I_{\mathrm{R,CA-1}} = 12.86$.

Table 20 *Calculated area of the peaks in the ^{31}P NMR spectrum by peak deconvolution for sample CA-1.*

Peak	δ / ppm	Area / arb. unit
1	151.31	63598710.84
2	147.59	4674350.87
3	147.26	822819323.69

Cellulose Acetate (CA-2): Yield: 91%

ATR-IR (cm^{-1}): 3123–3689 ν(O-H), 2828–2998 ν(C-H), 1733 ν(C=O), 1371 methyl ν(C-H), 1228 ester ν(C-O), 1032 AGU ν(C-O).
^{1}H NMR (400 MHz, DMSO-d_6 + TFA) δ_H ppm: 2.79–5.51 (m, AGU, 7H), 1.72–2.26 (m, $Ac_{6,2,3}$, 9H)

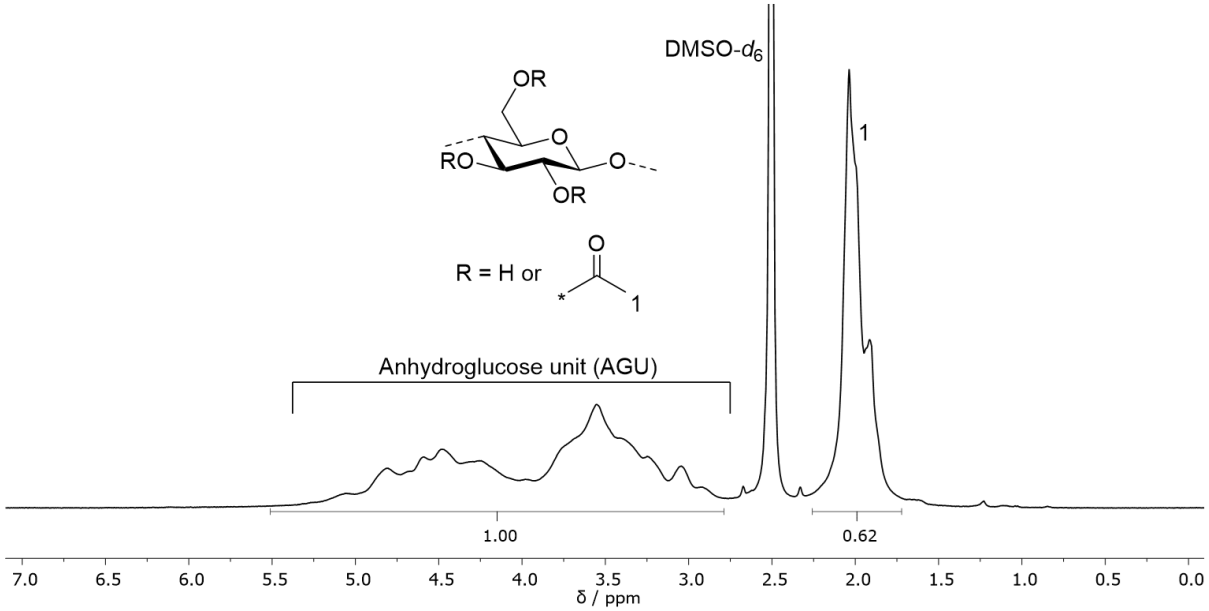

Figure S3 *^{1}H NMR (DMSO-d_6 + TFA) spectrum of CA-2.*

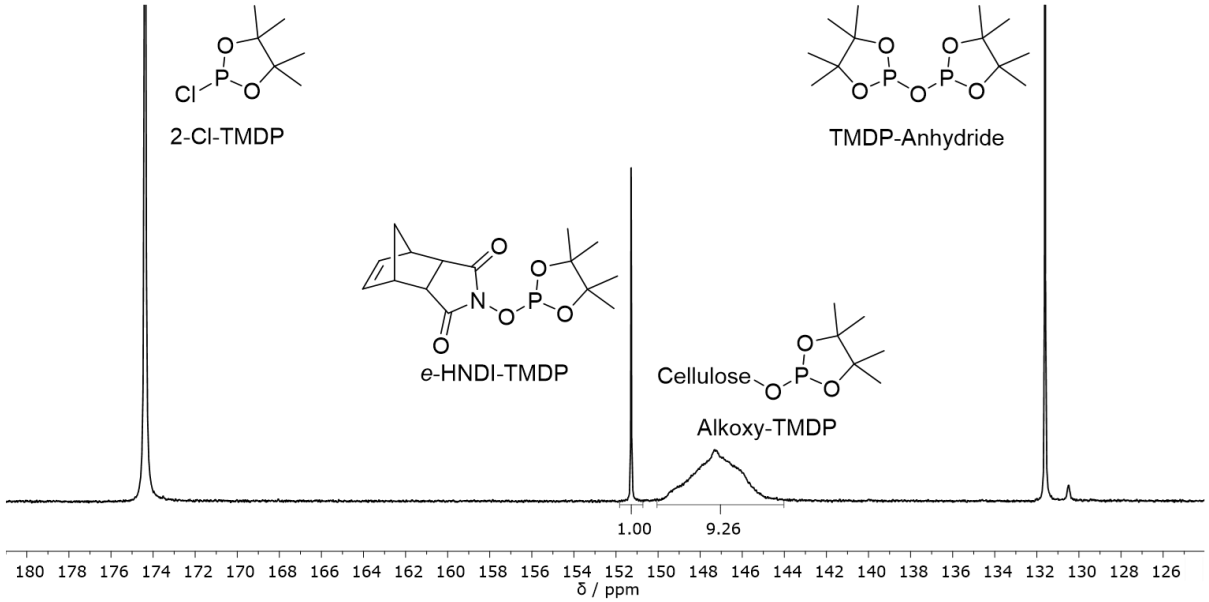

Figure S4 *^{31}P NMR ($CDCl_3$) spectrum of the phosphitylated CA-2 (calculated: DS_{31P}=1.47).*

Cellulose Acetate (CA-3): Yield: 90%

ATR-IR (cm^{-1}): 3104–3685 ν(O-H), 2819–3007 ν(C-H), 1736 ν(C=O), 1371 methyl ν(C-H), 1228 ester ν(C-O), 1035 AGU ν(C-O).
^{1}H NMR (400 MHz, DMSO-d_6 + TFA) δ_H ppm: 2.73–5.39 (m, AGU, 7H), 1.50–2.21 (m, $Ac_{6,2,3}$, 9H)

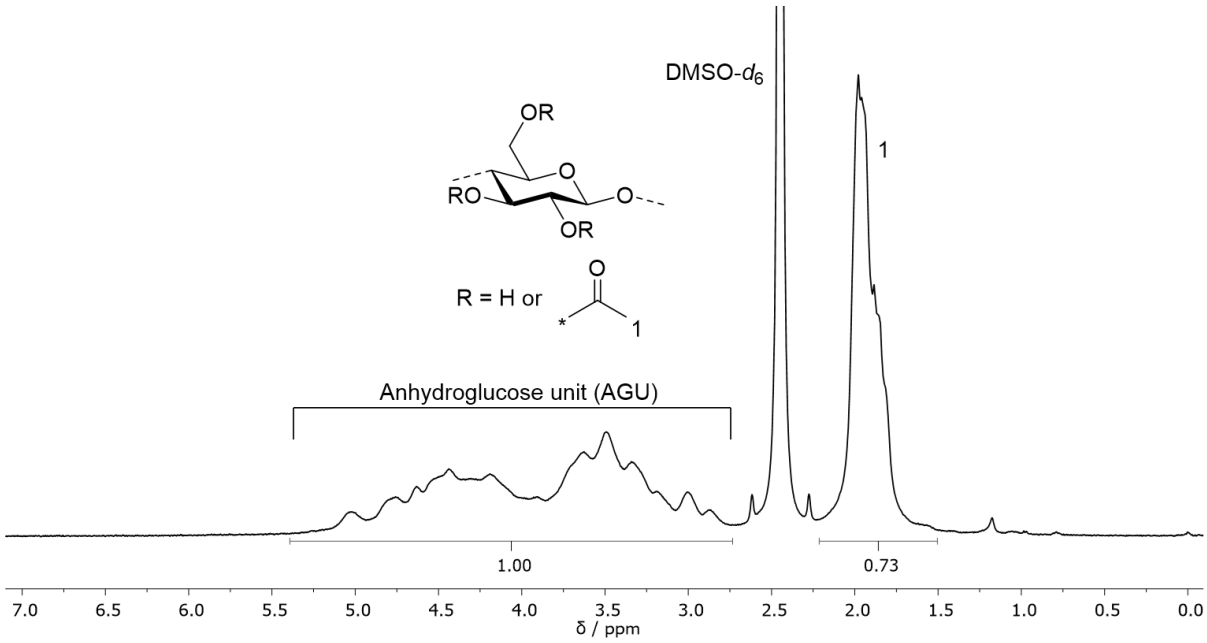

Figure S5 *^{1}H NMR (DMSO-d_6 + TFA) spectrum of CA-3.*

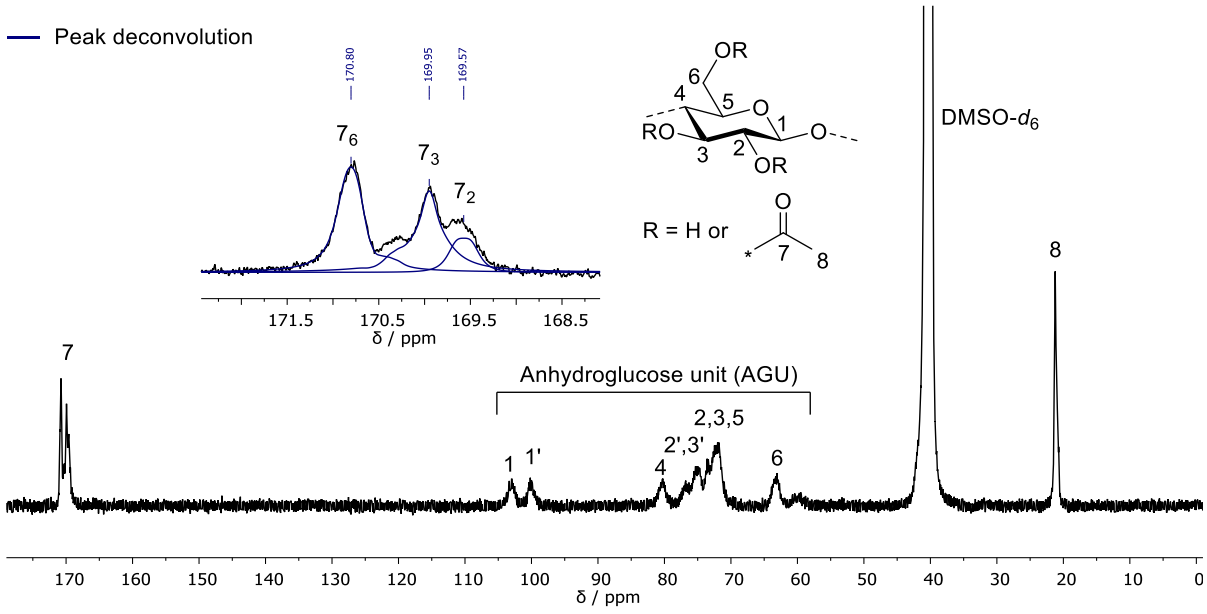

Figure S6 *^{13}C NMR (inverse gated decoupling, DMSO-d_6) spectrum of CA-3 with peak deconvolution: blue lines in expanded view.*

Table 21 *Calculated area of the carbonyl peaks via peak deconvolution for sample CA-3 (DS_{31P} = 1.73).*

Peak	δ / ppm	Area / arb. unit
7_6	170.80	186801.54
7_3	169.95	164767.94
7_2	169.57	51928.79

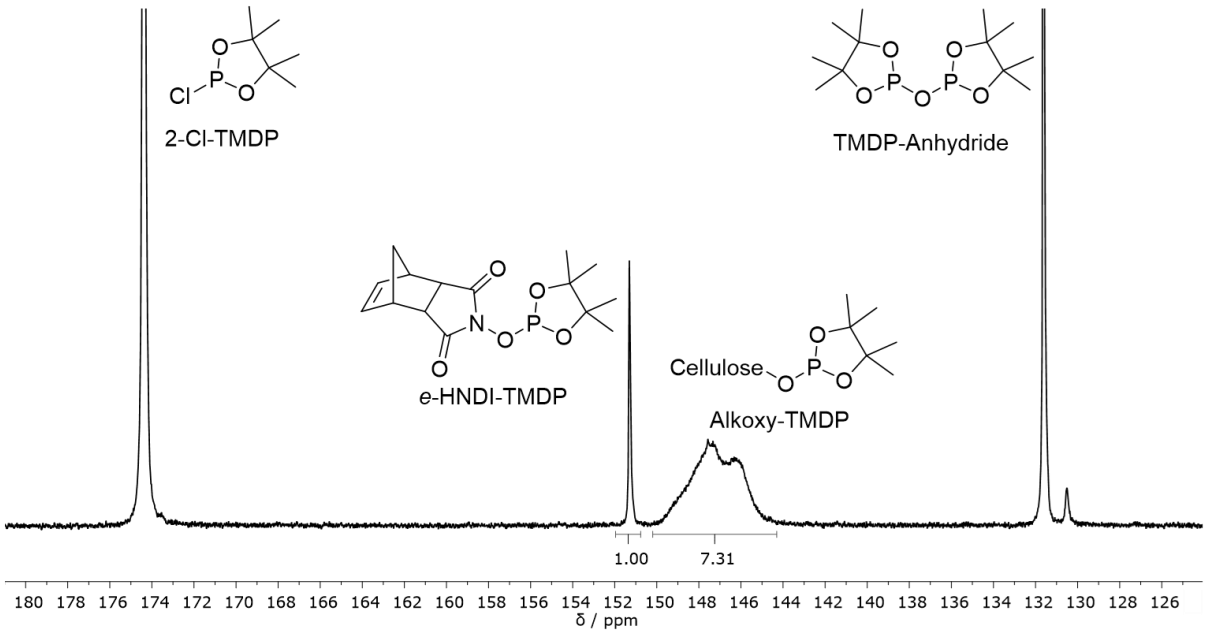

Figure S7 *^{31}P NMR ($CDCl_3$) spectrum of the phosphitylated CA-3 (calculated: DS_{31P}=1.73).*

Cellulose Acetate (CA-4): Yield: 83%

ATR-IR (cm^{-1}): 3213–3662 ν(O-H), 2813–3025 ν(C-H), 1736 ν(C=O), 1366 methyl ν(C-H), 1219 ester ν(C-O), 1028 AGU ν(C-O).
^{1}H NMR (400 MHz, DMSO-d_6 + TFA) δ_H ppm: 2.80–5.39 (m, AGU, 7H), 1.52–2.23 (m, $Ac_{6,2,3}$, 9H)

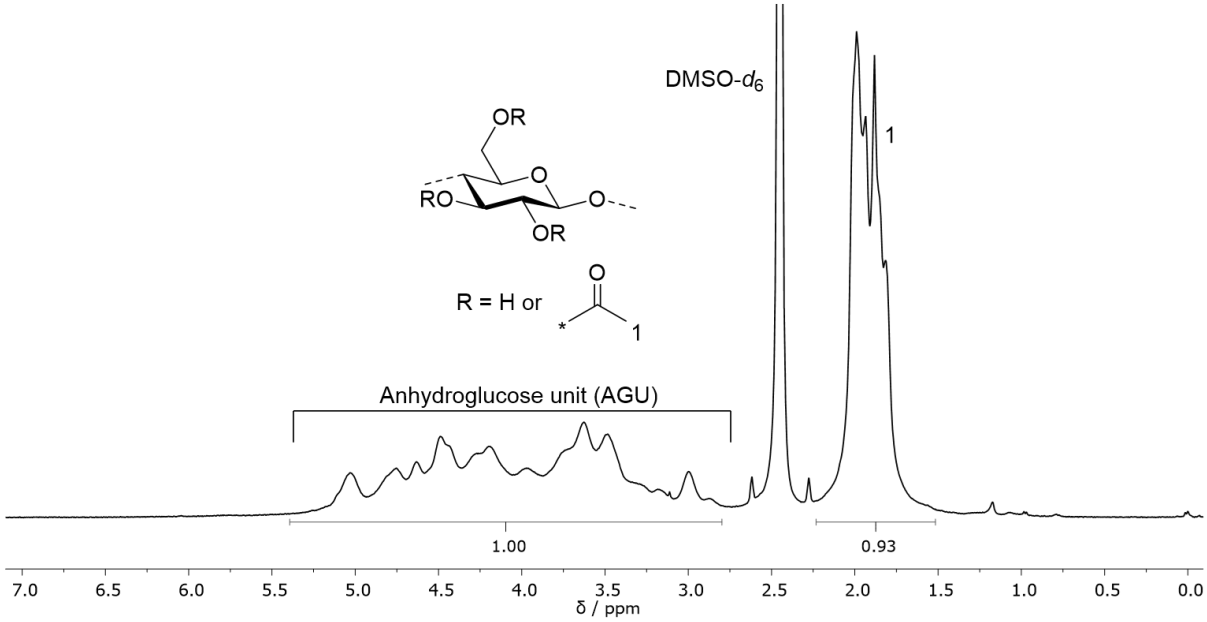

Figure S8 *^{1}H NMR (DMSO-d_6 + TFA) spectrum of CA-4.*

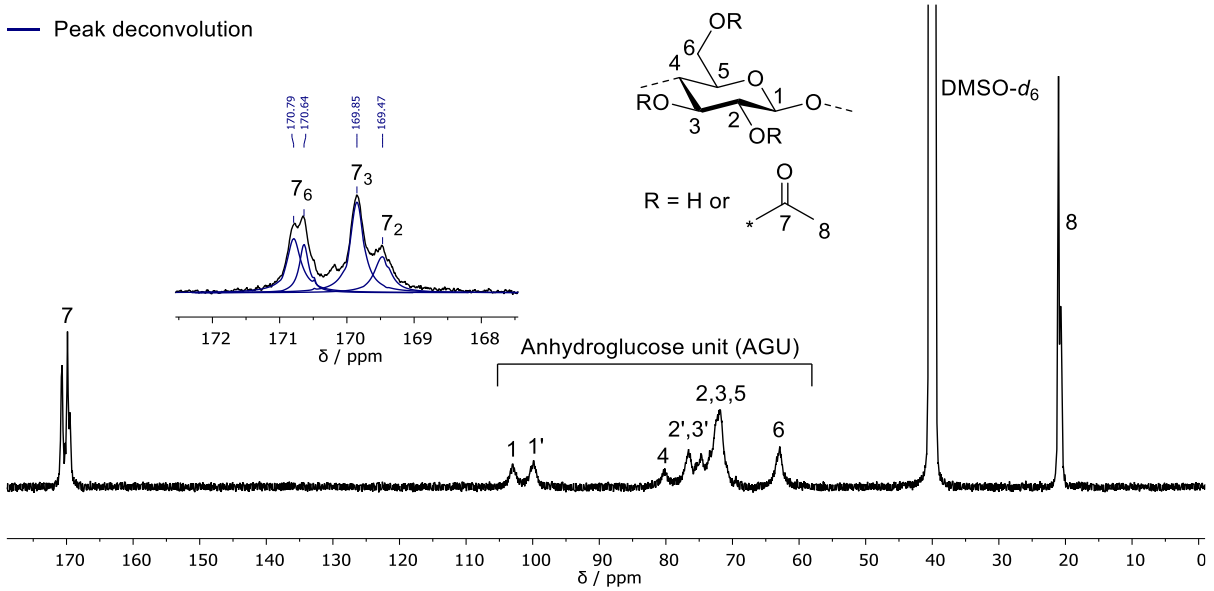

Figure S9 *^{13}C NMR (inverse gated decoupling, DMSO-d_6) spectrum of CA-4 with peak deconvolution: blue lines in expanded view.*

Table 22 *Calculated area of the carbonyl peaks via peak deconvolution for sample CA-4 (DS_{31P} = 2.18).*

Peak	δ / ppm	Area / arb. unit
7_6	170.79	151430.37
7_6	170.64	85063.47
7_3	169.85	226520.76
7_2	169.47	105902.05

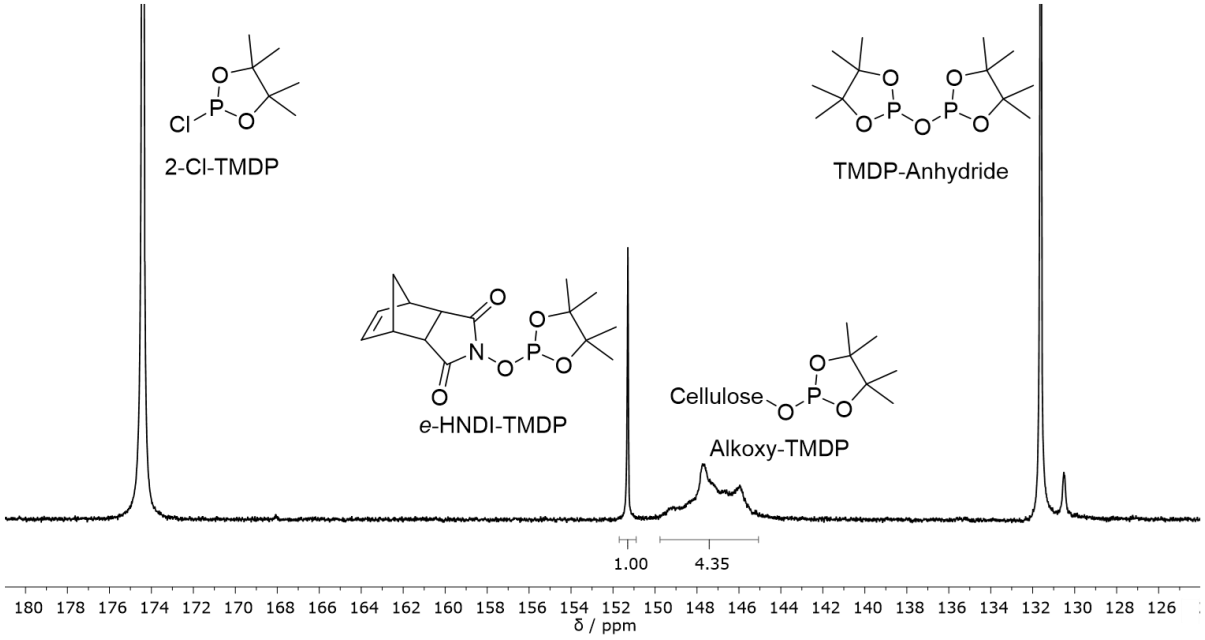

Figure S10 *^{31}P NMR ($CDCl_3$) spectrum of the phosphitylated CA-4 (calculated: DS_{31P}=2.18).*

Cellulose Acetate (CA-5): Yield: 90%

ATR-IR (cm^{-1}): 3266–3661 ν(O-H), 2824–3046 ν(C-H), 1736 ν(C=O), 1369 methyl ν(C-H), 1216 ester ν(C-O), 1030 AGU ν(C-O).
^{1}H NMR (400 MHz, DMSO-d_6 + TFA) δ_H ppm: 2.90–5.49 (m, AGU, 7H), 1.42–2.28 (m, $Ac_{6,2,3}$, 9H)

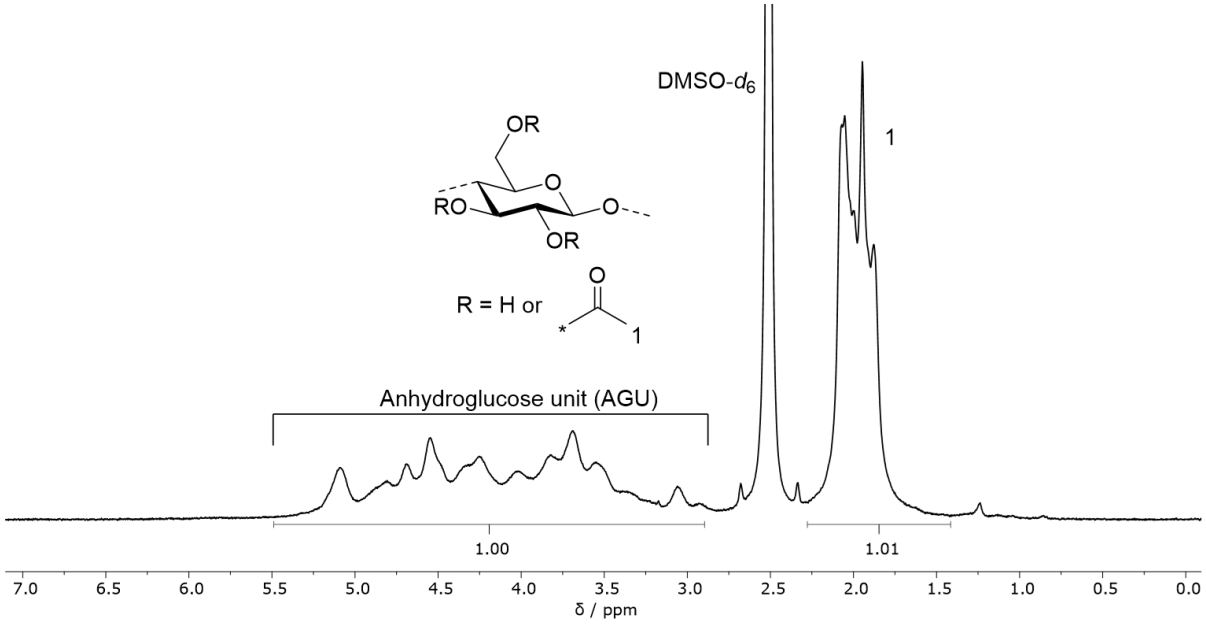

Figure S11 *^{1}H NMR (DMSO-d_6 + TFA) spectrum of CA-5.*

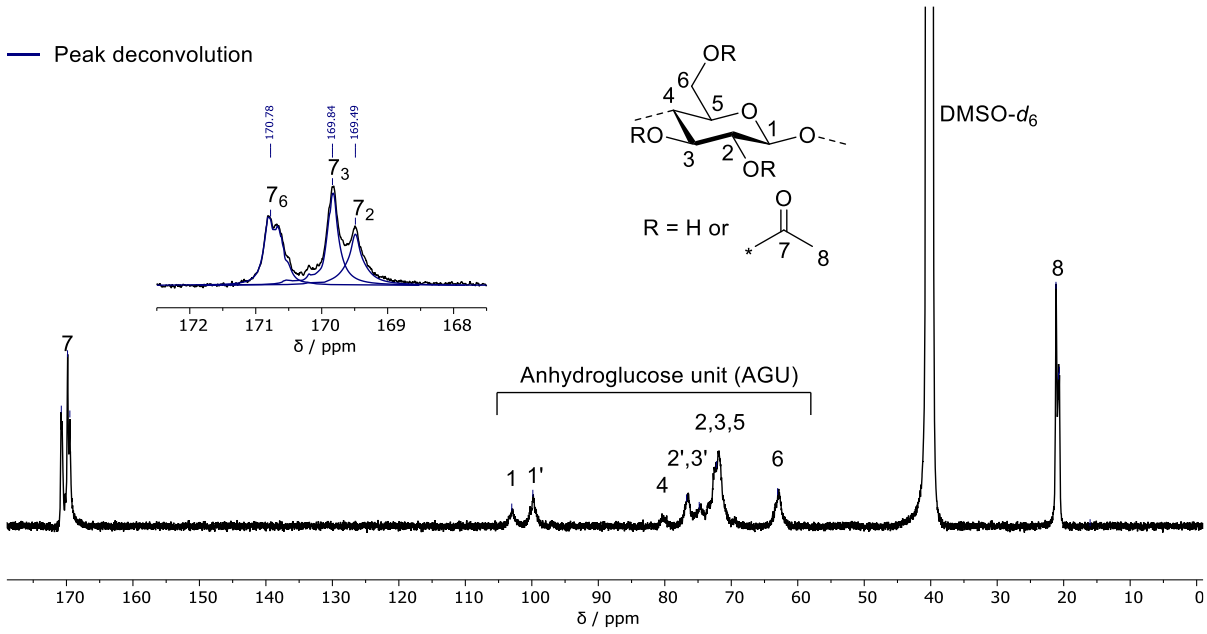

Figure S12 *^{13}C NMR (inverse gated decoupling, DMSO-d_6) spectrum of CA-5 with peak deconvolution: blue lines in expanded view.*

Table 23 *Calculated area of the carbonyl peaks via peak deconvolution for sample CA-5 (DS_{31P} = 2.50).*

Peak	δ / ppm	Area / arb. unit
7_6	170.78	208230.47
7_3	169.84	222476.37
7_2	169.49	156993.97

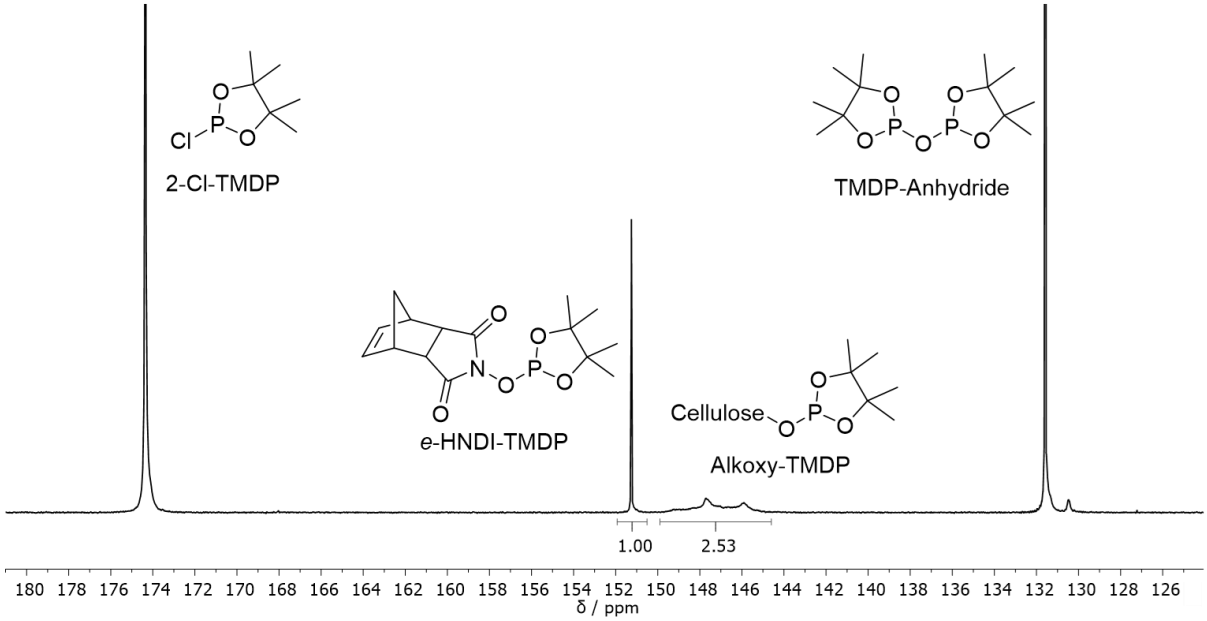

Figure S13 *^{31}P NMR ($CDCl_3$) spectrum of the phosphitylated CA-5 (calculated: DS_{31P}=2.50).*

Cellulose Acetate (CA-6): Yield: 99%

ATR-IR (cm^{-1}): 3421–3677 ν(O-H), 2828–3041 ν(C-H), 1741 ν(C=O), 1371 methyl ν(C-H), 1223 ester ν(C-O), 1037 AGU ν(C-O).
^{1}H NMR (400 MHz, $CDCl_3$) δ_H ppm: 2.76–5.44 (m, AGU, 7H), 1.78–2.26 (m, $Ac_{6,2,3}$, 9H)

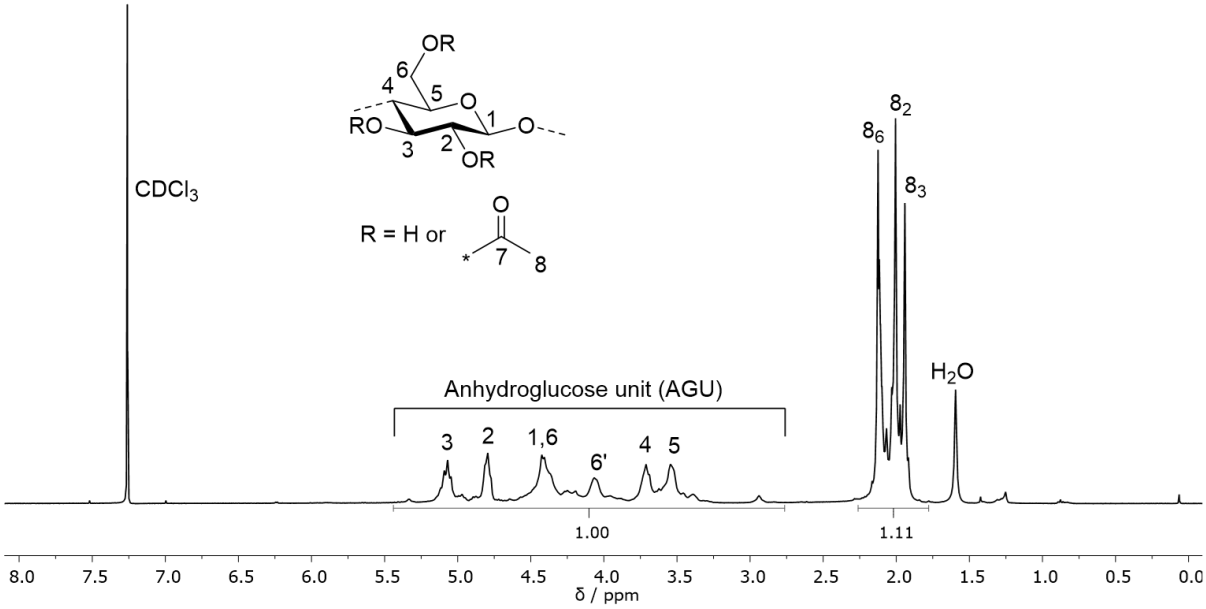

Figure S14 *^{1}H NMR ($CDCl_3$) spectrum of CA-6.*

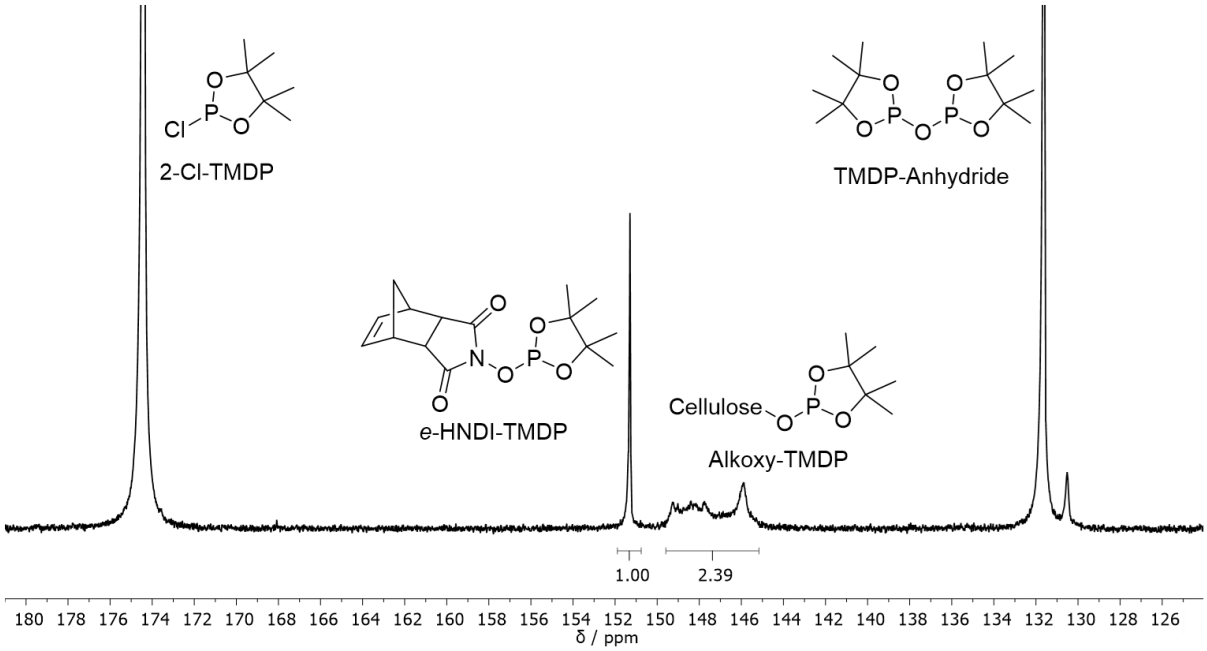

Figure S15 *^{31}P NMR ($CDCl_3$) spectrum of the phosphitylated CA-6 (calculated: DS_{31P}=2.52).*

Cellulose Acetate (CA-7): Yield: 99%

ATR-IR (cm^{-1}): 3433–3706 ν(O-H), 2836–3056 ν(C-H), 1738 ν(C=O), 1369 methyl ν(C-H), 1219 ester ν(C-O), 1037 AGU ν(C-O).
^{1}H NMR (400 MHz, $CDCl_3$) δ_H ppm: 3.20–5.45 (m, AGU, 7H), 1.75–2.47 (m, $Ac_{6,2,3}$, 9H)

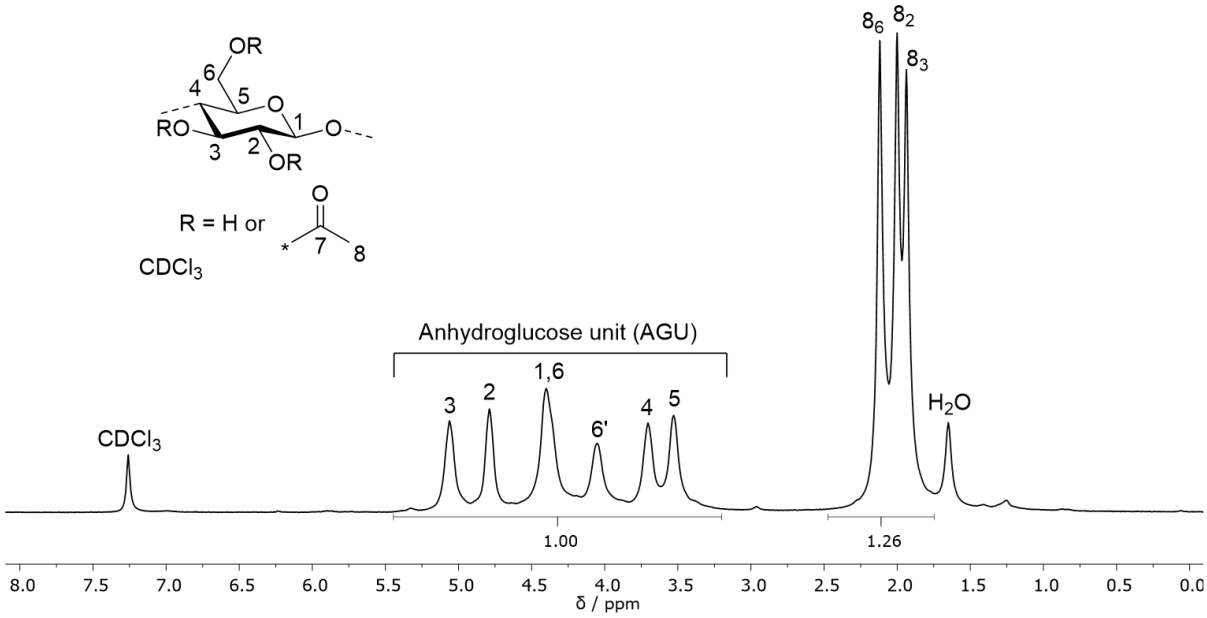

Figure S16 *^{1}H NMR ($CDCl_3$) spectrum of CA-7.*

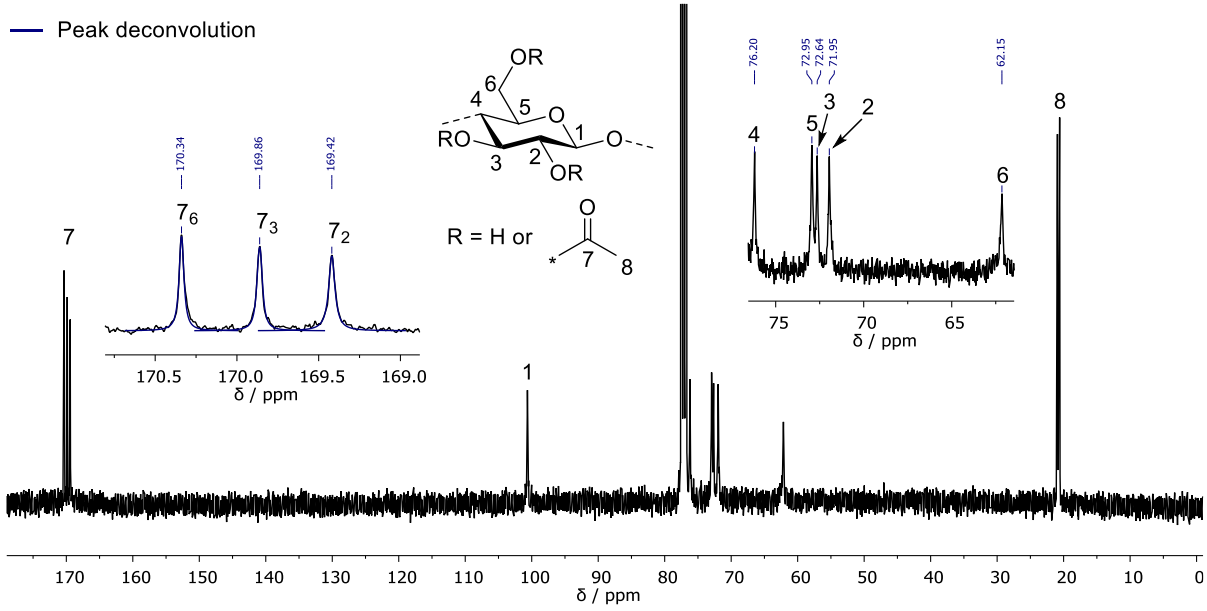

Figure S17 *^{13}C NMR (inverse gated decoupling, $CDCl_3$) spectrum of CA-7 with peak deconvolution: blue lines in expanded view.*

Table 24 *Calculated area of the carbonyl peaks via peak deconvolution for sample CA-7 (DS_{31P} = 2.97).*

Peak	δ / ppm	Area / arb. unit
7_6	170.34	17208.14
7_3	169.86	16753.88
7_2	169.42	18172.41

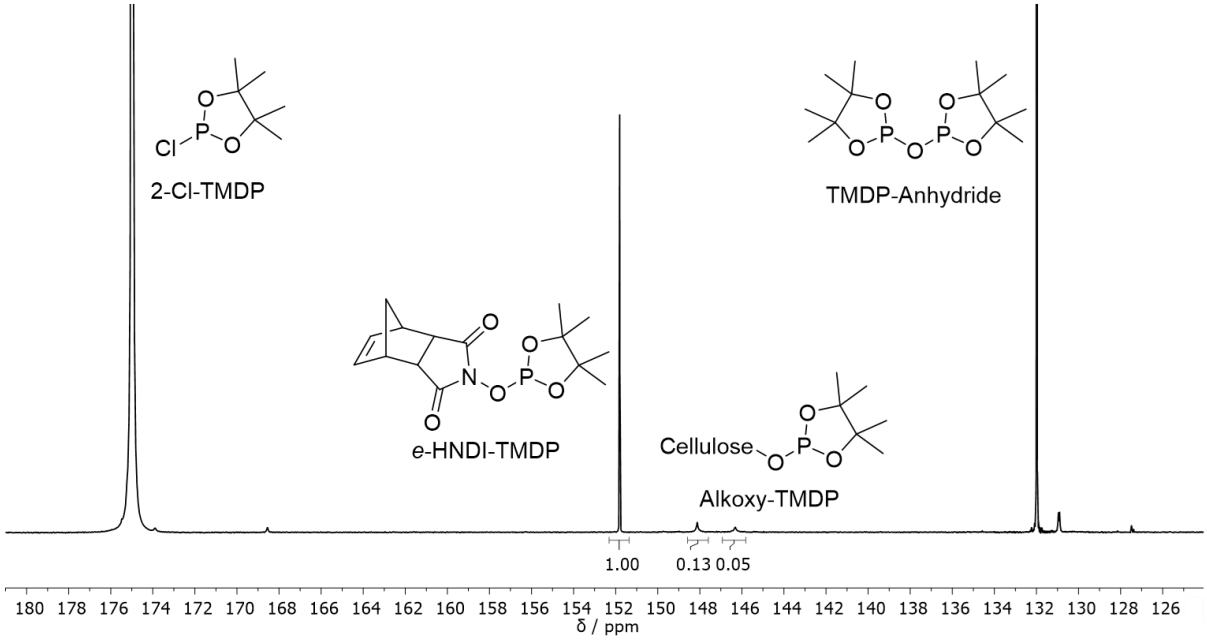

Figure S18 *^{31}P NMR ($CDCl_3$) spectrum of the phosphitylated CA-7 (calculated: DS_{31P}=2.97).*

Cellulose Acetate (CA-FP): Yield: 91%

ATR-IR (cm^{-1}): 3148–3687 ν(O-H), 2802–3032 ν(C-H), 1738 ν(C=O), 1369 methyl ν(C-H), 1216 ester ν(C-O), 1032 AGU ν(C-O).
^{1}H NMR (400 MHz, $CDCl_3$) δ_H ppm: 3.02–5.45 (m, AGU, 7H), 1.65–2.14 (m, $Ac_{6,2,3}$, 9H)

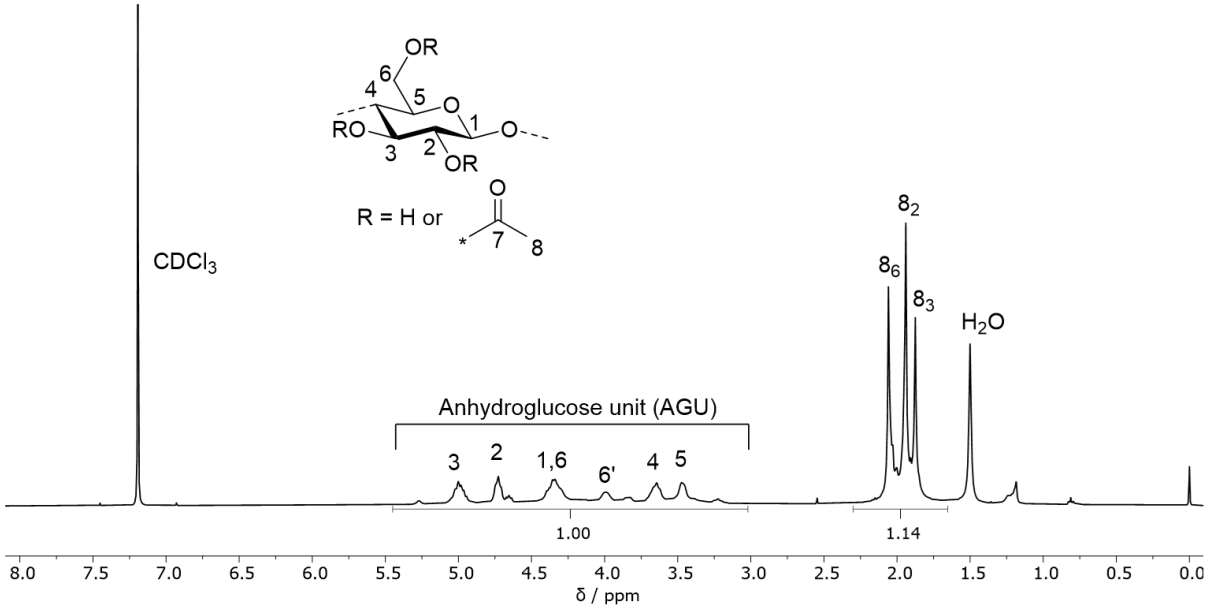

Figure S19 *^{1}H NMR ($CDCl_3$) spectrum of CA-FP.*

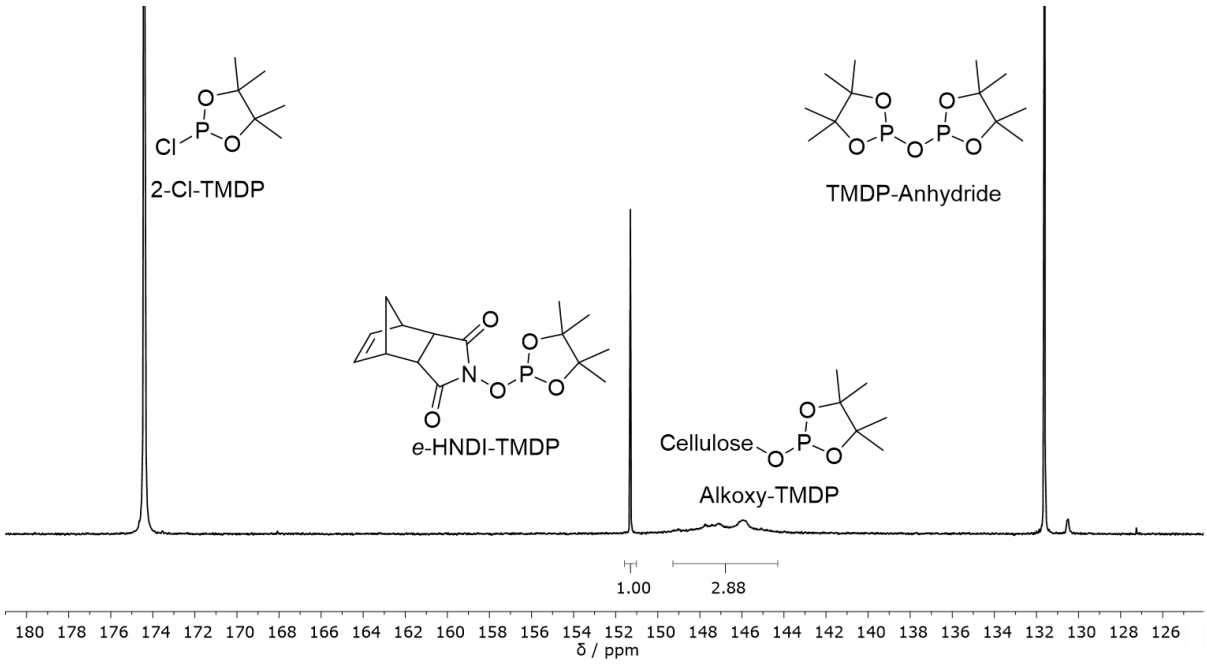

Figure S20 *^{31}P NMR ($CDCl_3$) spectrum of the phosphitylated CA-FP (calculated: DS_{31P}=2.44).*

Cellulose Acetate (CA-REC): Yield: 95%

ATR-IR (cm^{-1}): 3190–3665 ν(O-H), 2809–3018 ν(C-H), 1740 ν(C=O), 1370 methyl ν(C-H), 1225 ester ν(C-O), 1034 AGU ν(C-O).
^{1}H NMR (400 MHz, $CDCl_3$) δ_H ppm: 2.76–5.58 (m, AGU, 7H), 1.22–2.28 (m, $Ac_{6,2,3}$, 9H)

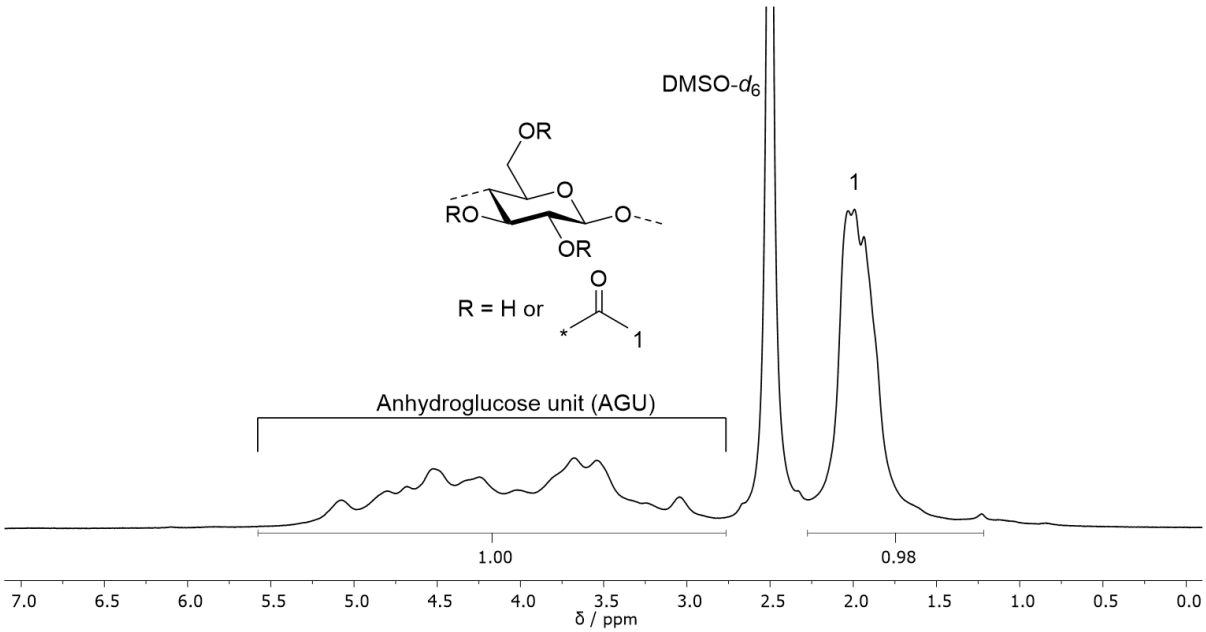

Figure S21 *^{1}H NMR (DMSO-d_6 + TFA) spectrum of CA-REC.*

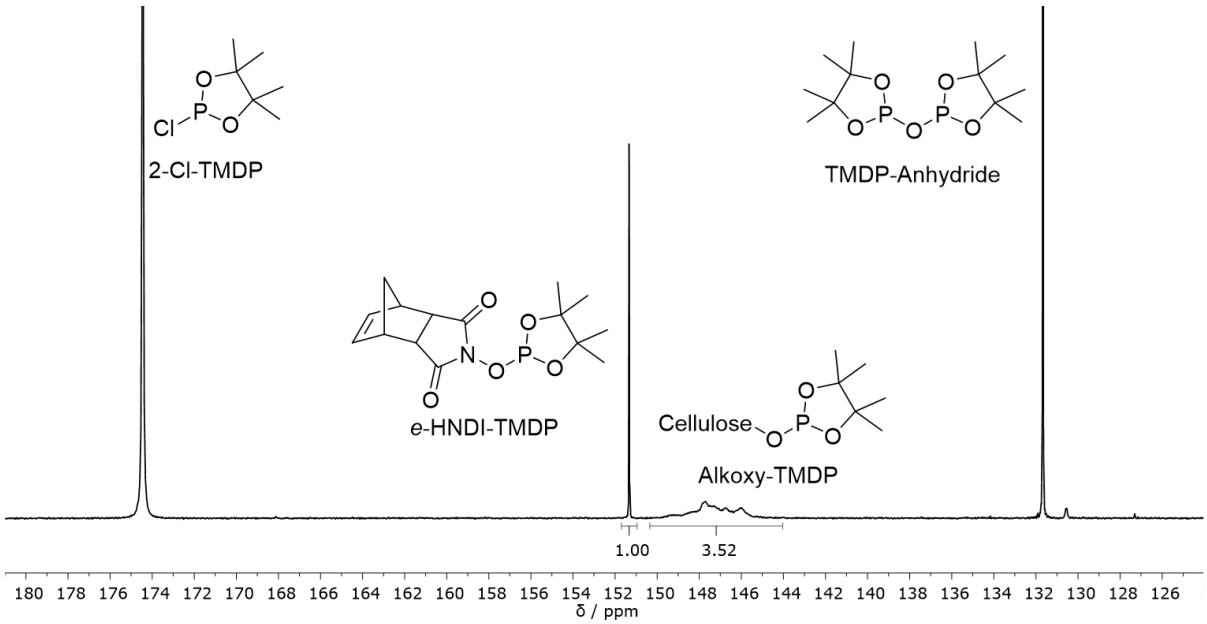

Figure S22 *^{31}P NMR ($CDCl_3$) spectrum of the phosphitylated CA-REC (calculated: DS_{31P}=2.32).*

Cellulose Acetate (CA-REC2): Yield: 99%

ATR-IR (cm^{-1}): 3272–3702 ν(O-H), 2824–3040 ν(C-H), 1740 ν(C=O), 1370 methyl ν(C-H), 1227 ester ν(C-O), 1039 AGU ν(C-O).
^{1}H NMR (400 MHz, $CDCl_3$) δ_H ppm: 2.83–5.47 (m, AGU, 7H), 1.51–2.28 (m, $Ac_{6,2,3}$, 9H)

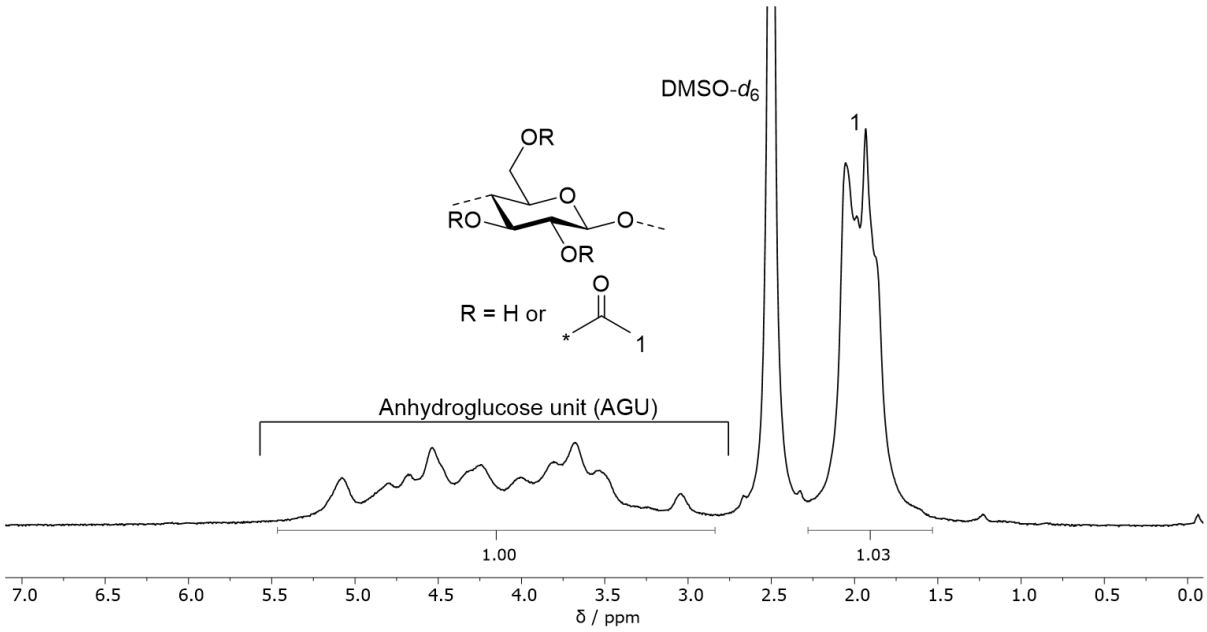

Figure S23 *^{1}H NMR (DMSO-d_6 + TFA) spectrum of CA-REC2.*

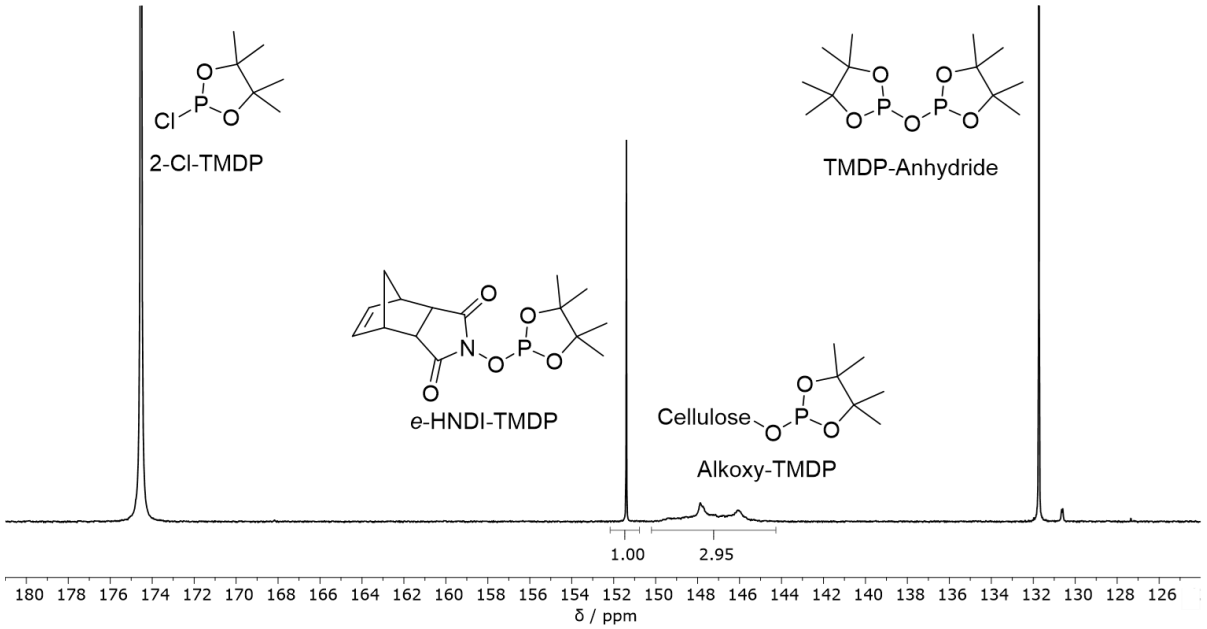

Figure S24 *^{31}P NMR ($CDCl_3$) spectrum of the phosphitylated CA-REC2 (calculated: DS_{31P}=2.42).*

General Procedure for the Heterogeneous Synthesis of Cellulose Acetate using the *Acetic Acid Process*

In a two-necked round-bottom flask equipped with a thermometer and a magnetic stirring bar, cellulose (2.00 g, 12.33 mmol) was suspended in 10 mL glacial acetic acid and stirred for 1 h at 40 °C. Afterwards, a mixture of 0.1 mL concentrated sulfuric acid in 20 mL glacial acetic acid was added dropwise and stirred at 30 °C for another 20 min. Acetic anhydride (15 mL, 159 mmol, 12.9 eq. per anhydroglucose unit) was then added dropwise and the temperature was kept below 40 °C. After 1 h stirring, the reaction mixture was added dropwise to vigorously stirred water (500 mL) and the product precipitated as a white solid. It was then vacuum filtrated, washed with excess water until the filtrate was not acidic anymore and then dried under vacuum. The yield was calculated based on the DS_{1H} using equation (*22*).

$$\text{yield} = \frac{\frac{m_{\text{CA}}}{M_{\text{repunit}}}}{\frac{m_{\text{cellulose}}}{M_{\text{AGU}}}} \tag{22}$$

$$M_{\text{repunit}} = M_{\text{AGU}} + (M_{\text{S}} - 1.01\ \text{g mol}^{-1}) \times \text{DS}_{1\text{H}} \tag{23}$$

$$DS_{1\text{H}} = \frac{7 \times I_{\text{CH3}}}{3 \times I_{\text{AGU}}} \tag{24}$$

m_{CA}: mass of the cellulose acetate product
$m_{\text{cellulose}}$: mass of the cellulose educt
M_{repunit}: average molar mass of the product's repeating unit
M_{AGU}: molar mass of the anhydroglucose unit ($M_{\text{AGU}} = 162.14\ \text{g mol}^{-1}$)
I_{CH3}: Integral of the peak of the methyl group in the ^{1}H NMR spectrum.
I_{AGU}: Integral of the peak of the anhydroglucose unit (AGU) in the ^{1}H NMR spectrum.

Cellulose Acetate (CA-HET): Yield: 91%

ATR-IR (cm^{-1}): 2826–3048 ν(C-H), 1738 ν(C=O), 1366 methyl ν(C-H), 1214 ester ν(C-O), 1032 AGU ν(C-O).
^{1}H NMR (400 MHz, $CDCl_3$) δ_H ppm: 5.07 (t, H_3, 1H), 4.79 (t, H_2, 1H), 4.28–4.50 (m, $H_{1,6}$, 2H), 3.98–4.09 (m, H_6, 1H), 3.71 (t, H_4, 1H), 3.46–3.56 (m, H_5, 1H), 2.12 (s, Ac_6, 3H), 2.01 (s, Ac_2, 3H), 1.94 (s, Ac_3, 3H).

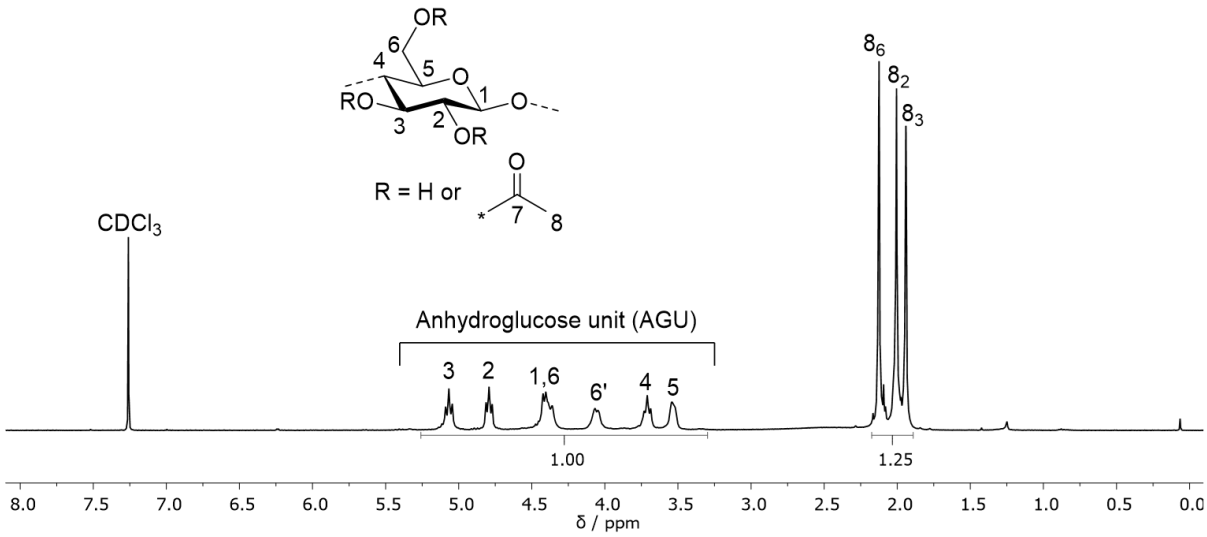

Figure S25 *^{1}H NMR ($CDCl_3$) spectrum of CA-HET.*

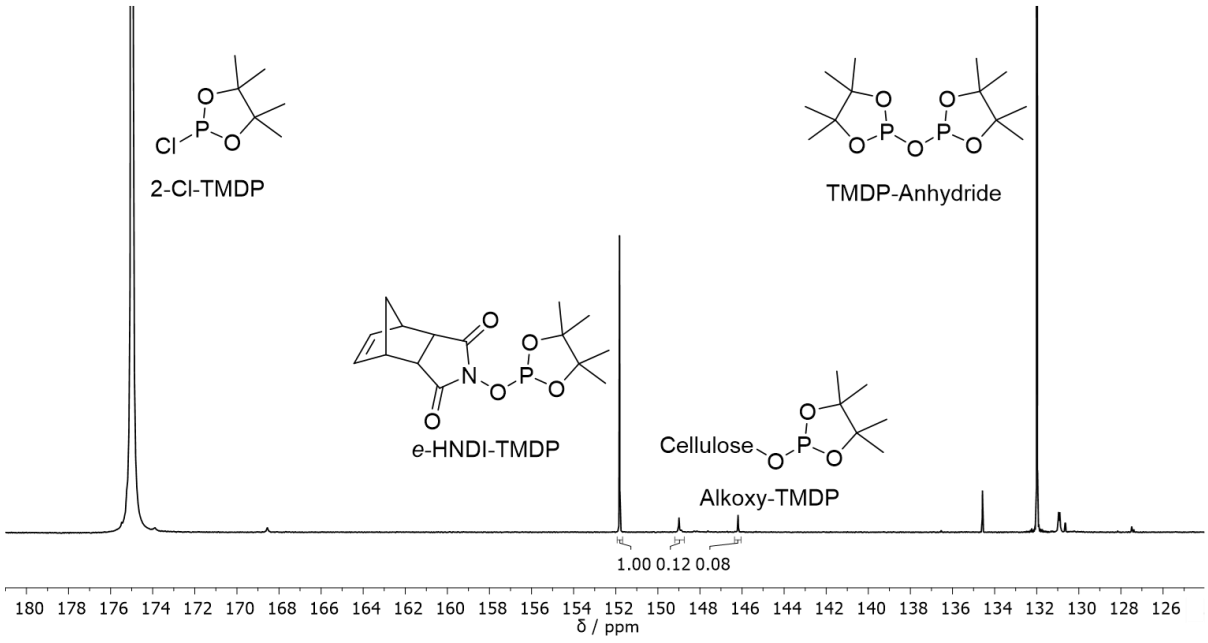

Figure S26 *^{31}P NMR ($CDCl_3$) spectrum of the phosphitylated CA-HET (calculated: DS_{31P}=2.96).*

E-Factor calculation

The *E*-factor was calculated according to equation (*25*).

$$\text{E factor} = \frac{m_{\text{starting materials}} + m_{\text{Solvent losses}} - m_{\text{Product}}}{m_{\text{Product}}} \quad (25)$$

$m_{\text{starting materials}}$: mass of the starting materials
$m_{\text{Solvent losses}}$: mass of solvent losses (including *i*PrOH, DMSO and DBU)
m_{Product}: mass of the desired product

Recycling Process

After filtration, the product was dried under vacuum and the evaporated iPrOH was captured in a cold trap. The residual filtrate containing iPrOH, DMSO and DBU was purified by distillation. First, iPrOH was recovered (50–90 mbar, 40 °C) and combined with the captured iPrOH in the cold trap. The second (intermediate) fraction was collected containing iPrOH and DMSO (30 mbar, 90 °C) to remove the iPrOH quantitatively. Then, the third fraction DMSO/DBU was distilled at 0.1 mbar and 50–150 °C oil bath temperature until dry. Recovery yield: 97.7% DMSO, 87.0% DBU, 98.9% iPrOH.

Table 25 *Used and recovered substances for the synthesis of the larger batch CA-REC (2.5 Eq VA, 60 °C, 240 min).*

Substance	Used	Recovered	Recycling ratio
DMSO	126.68 g	121.88 (+ 1.95)[a] g	96.2 (+ 1.5)[a]%
DBU	11.34 g	9.87 g	87.0%
iPrOH	364.08 g	336.44 (+ 23.62)[a] g	92.4 (+ 6.5)[a]%
VA	5.31 g	-	-
Acetaldehyde	-	0 g	0%

DS_{1H} = 2.29, DS_{31P} = 2.32, Yield: 94.8%, Conversion VA: 91.6%
[a] In brackets: DMSO and iPrOH in the intermediate (mixed) fraction. Composition of DMSO/iPrOH calculated from the integrals in the ^{1}H NMR spectrum.

25.57 g of the intermediate mixed iPrOH/DMSO fraction was recovered, composed of 23.62 g iPrOH and 1.95 g DMSO. The composition of this fraction was calculated analogously to the composition of the DMSO/DBU fraction (equation(6)–(*8*)).

5.09 g distillation residue remained in the flask, which is expected to mainly consist of degradation products of DBU and DMSO (loss of DMSO+DBU: 4.32 g). Side reactions of acetaldehyde or minor degradation products of cellulose are also possible.

Calculated *E*-factor for the whole procedure: 1.92 (23.62 g iPrOH and 1.95 g DMSO from the mixed fraction was taken into account, as the mixed fraction was added to the iPrOH fraction).

Table 26 *Used and recovered substances from a second cycle for the synthesis of CA-REC2 (3.0 Eq VA, 60 °C, 240 min).*

Substance	Used	Recovered	Recycling ratio
DMSO	32.28 (+ 1.21)[b] g	31.41 (+ 0.76)[a] g	93.8 (+ 2.3)[a][a]%
DBU	2.82 g	2.47 g	87.5%
iPrOH	171.23 (- 1.21)[b] g	160.08 (+ 3.11)[a] g	94.2 (+ 1.8)[a][a]%
VA	1.59 g	-	-
Acetaldehyde	-	0 g	0%

DS_{1H} = 2.40, Yield: 99.4%, Conversion VA: 80.0%

[a] In brackets: DMSO and iPrOH in the intermediate (mixed) fraction. Composition of DMSO/iPrOH calculated from the integrals in the ^{1}H NMR spectrum. [b] In brackets: Corrections based on the DMSO contained in the recovered iPrOH.

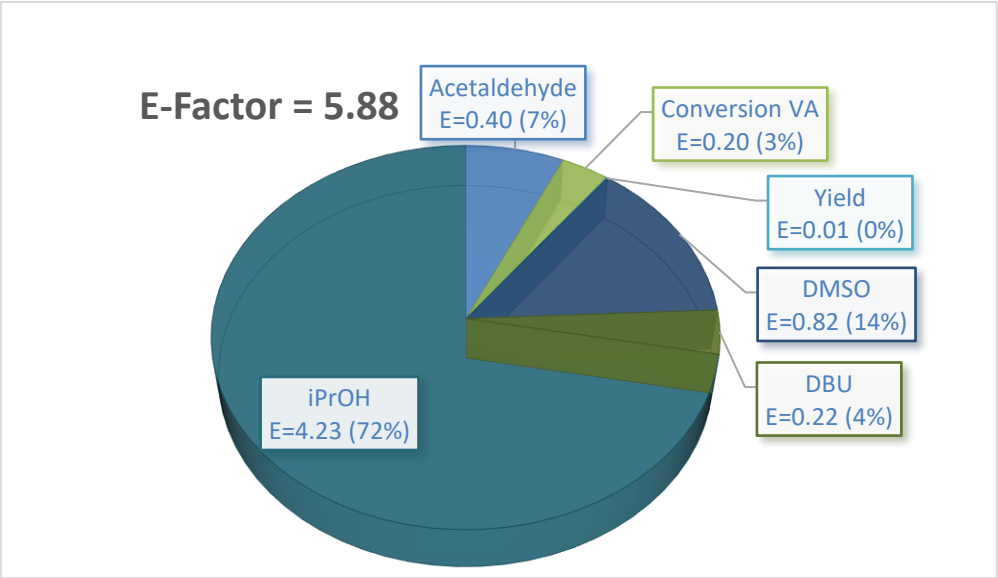

Figure S27 *Pie chart of the partial E-factors for the synthesis of CA in the second recycling cycle.*

Supporting Figures

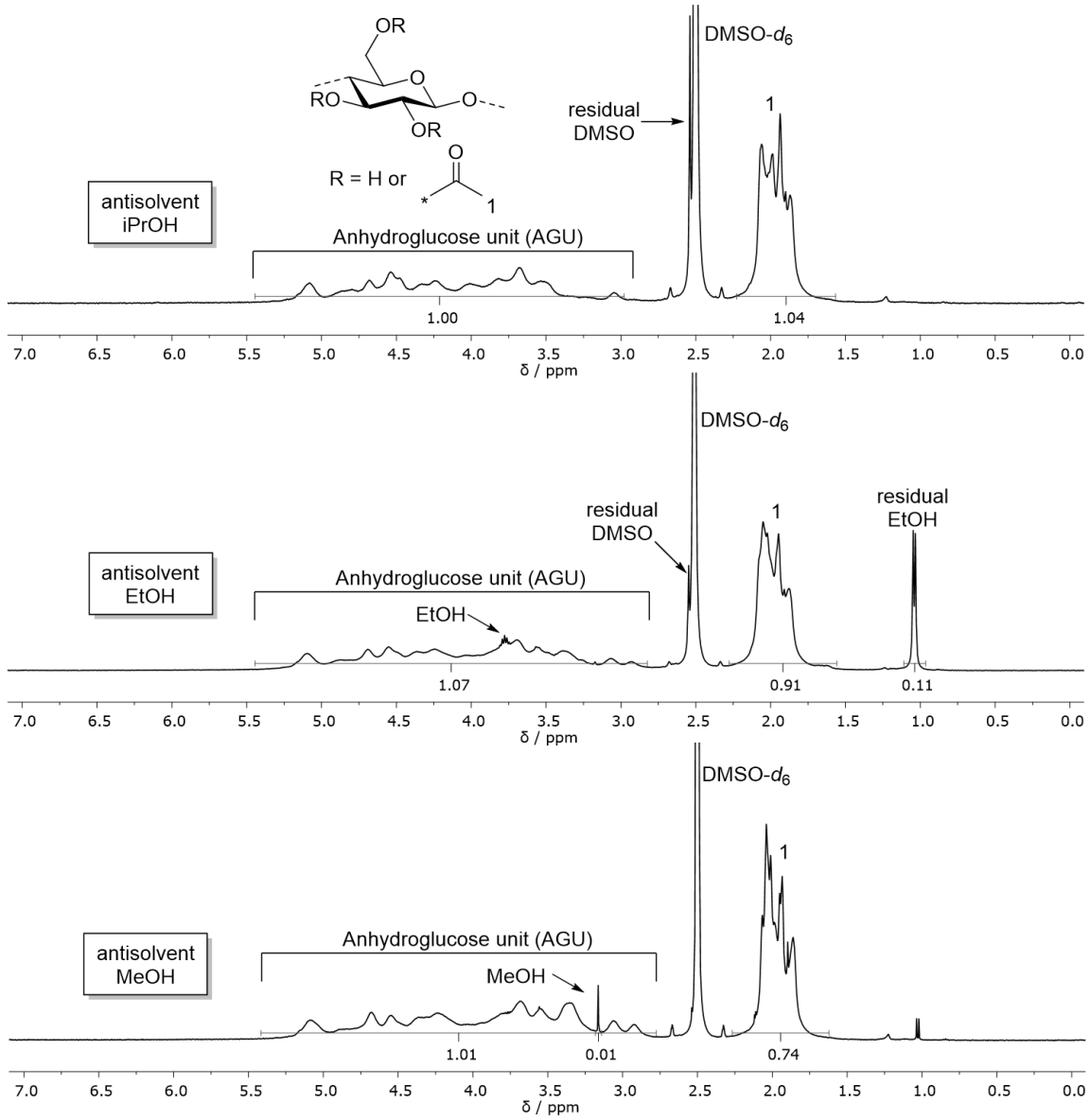

Figure S28 *^{1}H NMR (DMSO-d_6 + TFA) spectra of one homogeneous CA synthesis batch precipitated from iPrOH (top), EtOH (middle) and MeOH (bottom) with subsequent stirring for 30 min at room temperature.*

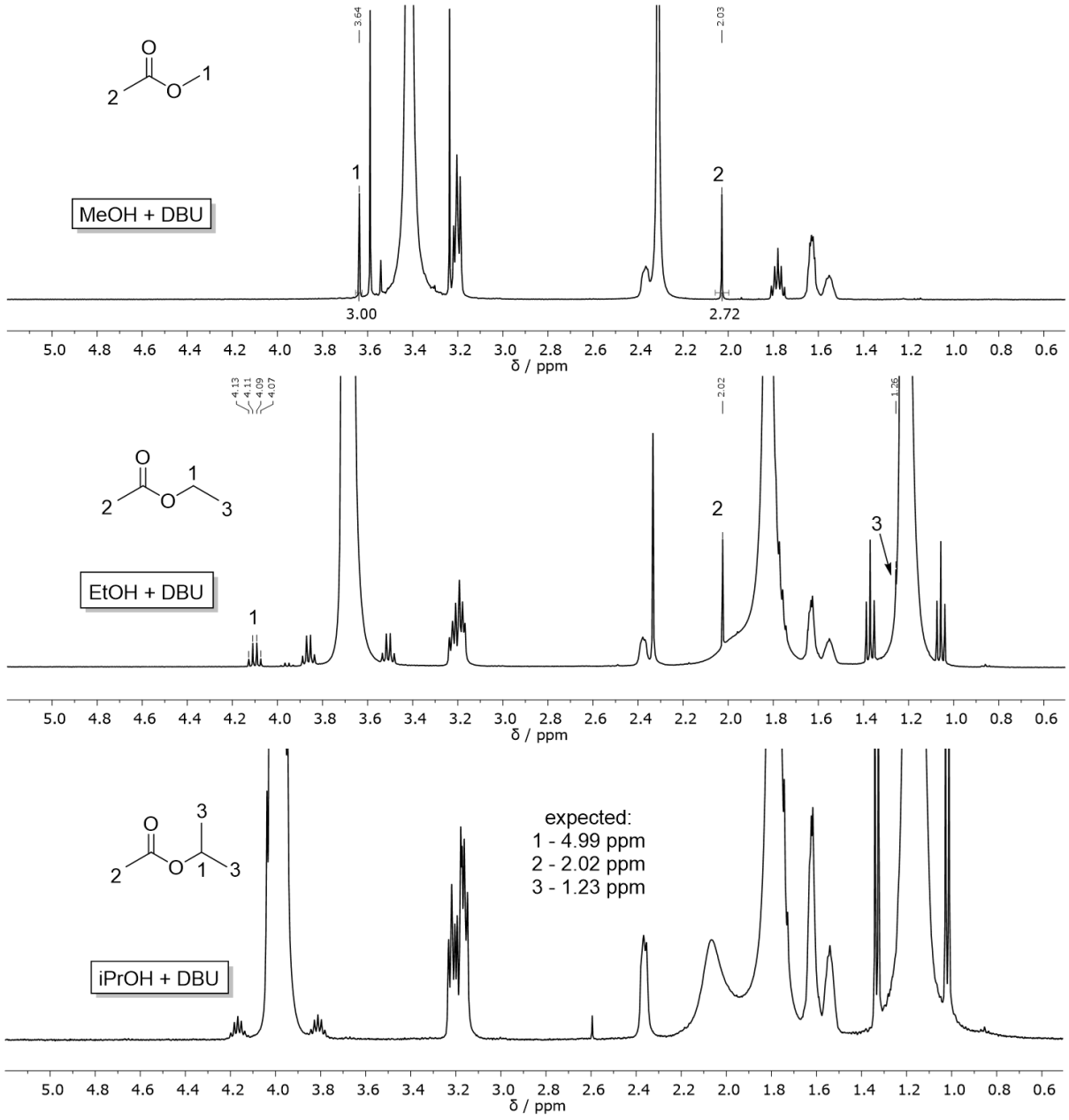

Figure S29 *^{1}H NMR ($CDCl_3$) spectra of the supernatant of a purified CA sample (DS_{1H} = 2.43) in a solution of 3 Eq. DBU (per AGU) and MeOH (top), EtOH (middle), iPrOH (bottom). The samples were stirred for 12 h at r.t. The formation of methyl acetate (top) and ethyl acetate (middle) was found whereas no formation of isopropyl acetate (bottom) was observed.*

6.3.2. Degree of Substitution Determination via ATR-FTIR Spectroscopy – Chapter 4.2

CAc-1, CAc-2, CAc-3, CAc-4, CAc-5, CAc-8, CAc-9, CAc-10, CAc-13, CBu-1, CBu-3, CBu-8, CBz-1, CBz-3, CBz-6, CL-1, CL-2, CL-4, and CL-5 were synthesized by Olga Matveyeva under supervision of the author of this thesis.

CAc-6, CAc-7, CAc-11, CAc-12, CAc-14, CAc-15, CAc-16 were synthesized by the author of this thesis.

CBu-2, CBu-4, CBu-7, CBz-4, and CL-6 were synthesized by Evelyn Hayn under supervision of the author of this thesis.

CBu-5, CBu-6, CBz-2, CBz-5, and CL-3 were synthesized by Sebastian Frentzen under supervision of the author of this thesis.

General Procedure for the Synthesis of Cellulose Esters

In a round-bottom flask, cellulose (500 mg, [monomeric unit] = 3.08 mmol) was suspended in 11 mL DMSO followed by the dropwise addition of 1,8-diazabicyclo[5.4.0]undec-7-ene (1.4 mL, 9.25 mmol, 3.0 eq. per AGU). After applying a CO_2 flow through the solution for 20 min at 40 °C, a clear solution was obtained and vinyl acetate (0.5–4.5 eq. per AGU) for cellulose acetates, vinyl butyrate (0.7–4.5 eq. per AGU) for cellulose butyrates, vinyl laurate (1.0–4.5 eq. per AGU) for cellulose laurates or vinyl benzoate (0.7–4.5 eq per AGU) for cellulose benzoates was added dropwise. The homogeneous solution was then heated to 60 °C and stirred for 4 h. Subsequently, the solution was added dropwise into 50 mL of isopropanol under vigorous stirring. The precipitate was vacuum filtrated and washed with isopropanol (2 × 20 mL), suspended in 40 mL isopropanol and heated under reflux 2× for 1–12 h, vacuum filtrated and dried. The final product was obtained as a white or yellow solid. Yields ranged from 74 to 99%.

The baseline of all ^{1}H NMR spectra was corrected manually using a multipoint baseline correction, the phase was corrected using the automatic phase correction tool from the

software MestReNova 14.2.0-26256. 30–60 μL Trifluoroacetic acid (TFA) was added to each sample before the measurement to shift the water signal downfield to allow a precise integration of the AGU protons signal. The samples were measured within 1 h after TFA addition to prevent imprecisions caused by deacetylation.

The peak assignment for all cellulose acetates is exemplarily shown for CAc-1. The standard deviation of the triple determination for the cellulose acetates DS_{1H} was calculated and is reported as the error range for every sample in the figure captions.

Cellulose Acetates:

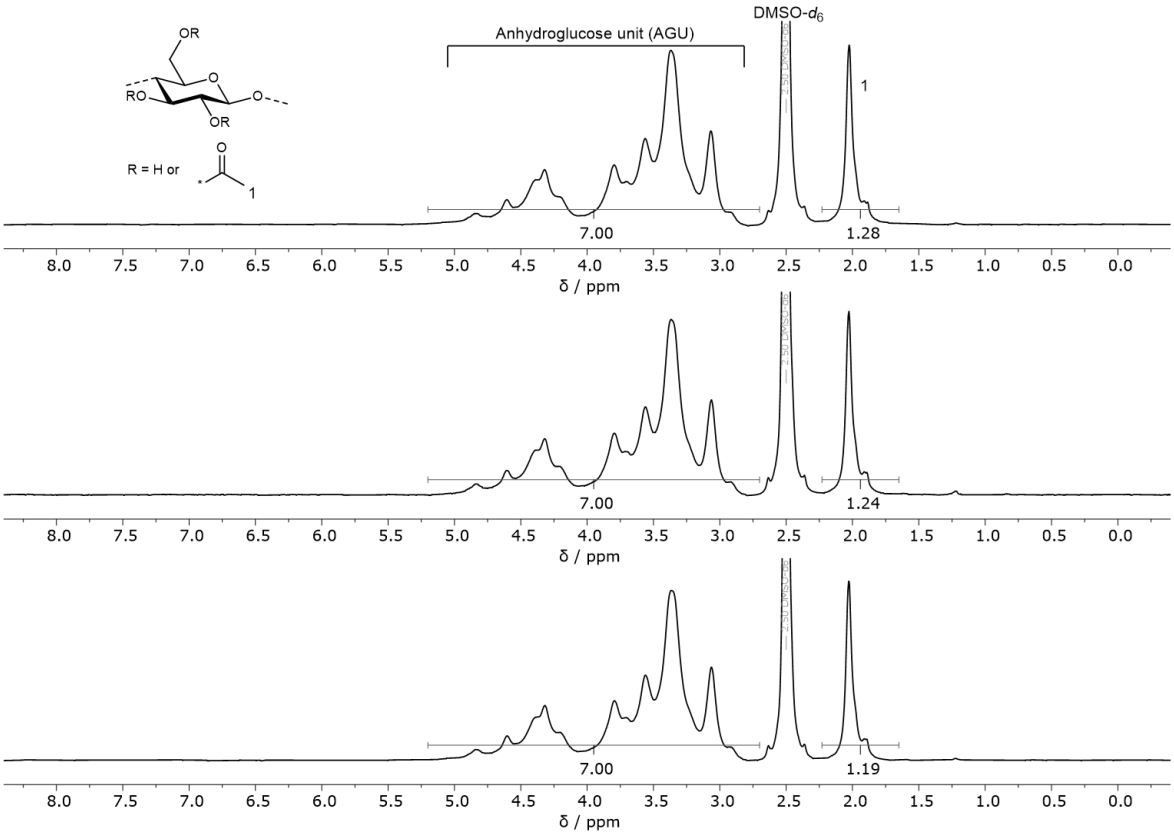

Figure S30 *^{1}H NMR (DMSO-d_6+TFA) spectra of CAc-1 (calculated average DS_{1H}=0.41±0.01).*

The DS_{31P} of CAc-1 to CAc-5 could not be determined due to insolubility.

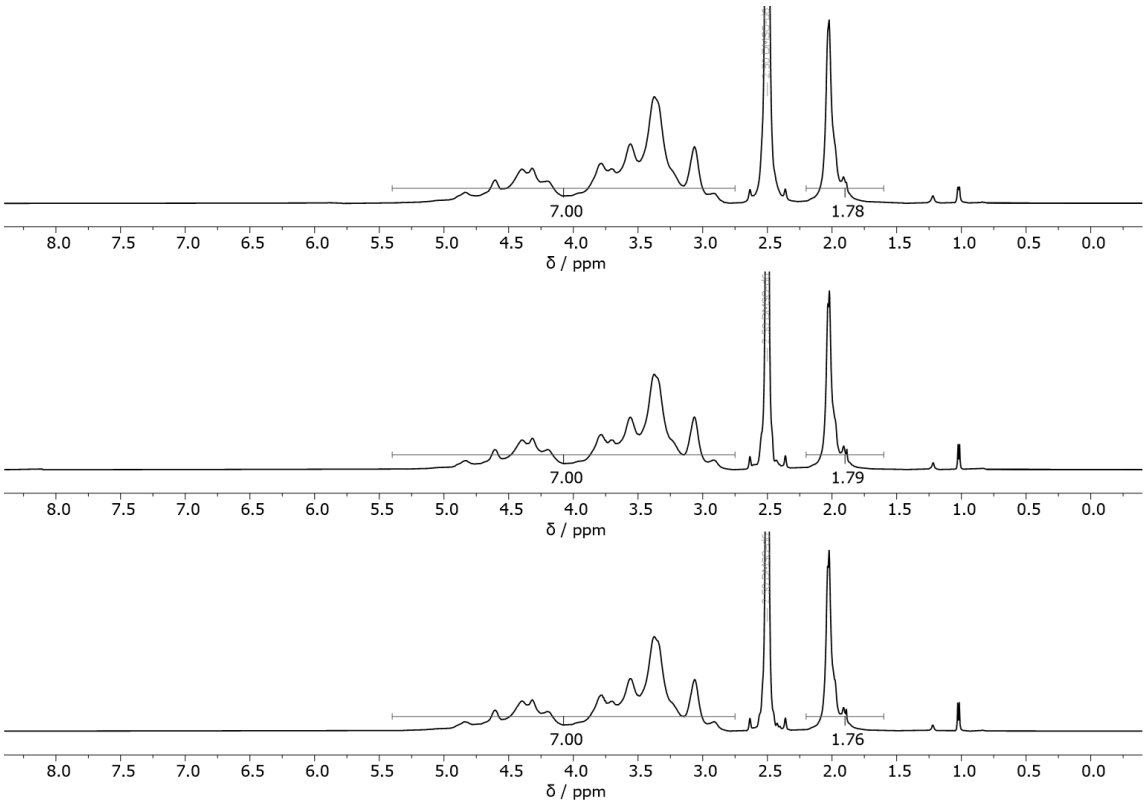

Figure S31 *^{1}H NMR (DMSO-d_6+TFA) spectra of CAc-2 (calculated average DS_{1H}=0.59±0.01).*

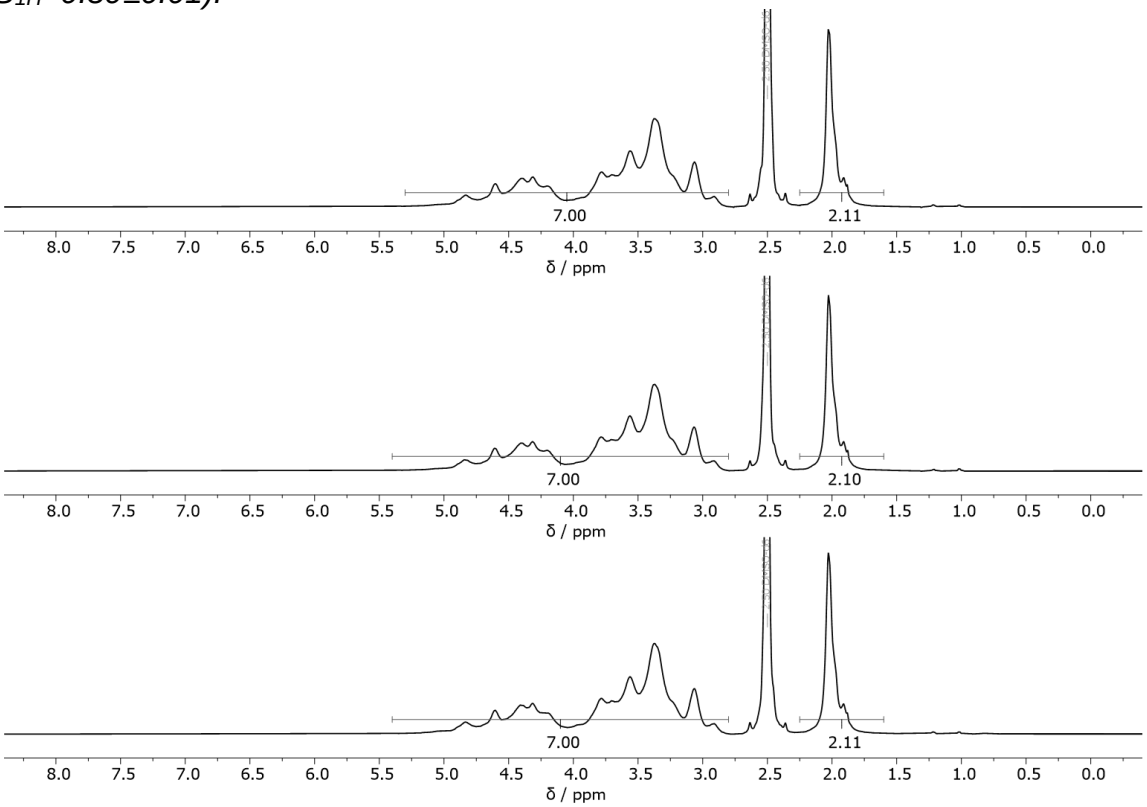

Figure S32 *^{1}H NMR (DMSO-d_6+TFA) spectra of CAc-3 (calculated average DS_{1H}=0.70±0.01).*

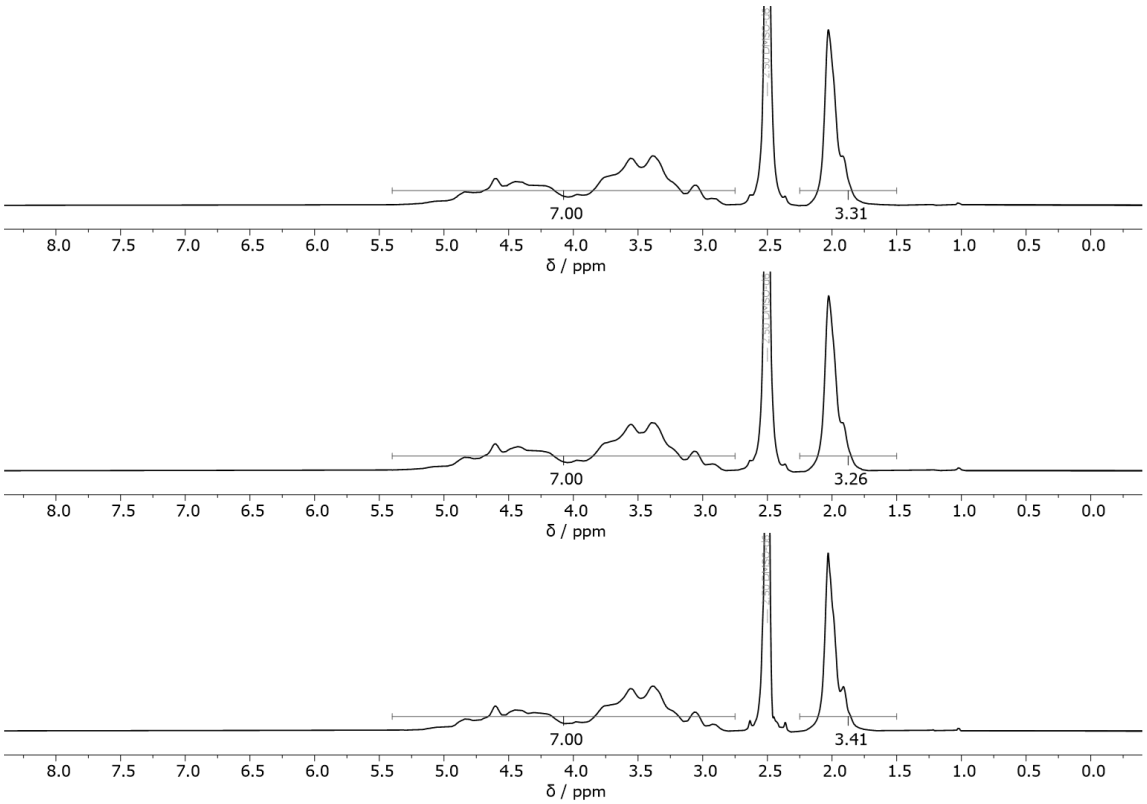

Figure S33 *^{1}H NMR (DMSO-d_6+TFA) spectra of CAc-4 (calculated average DS_{1H}=1.11±0.02).*

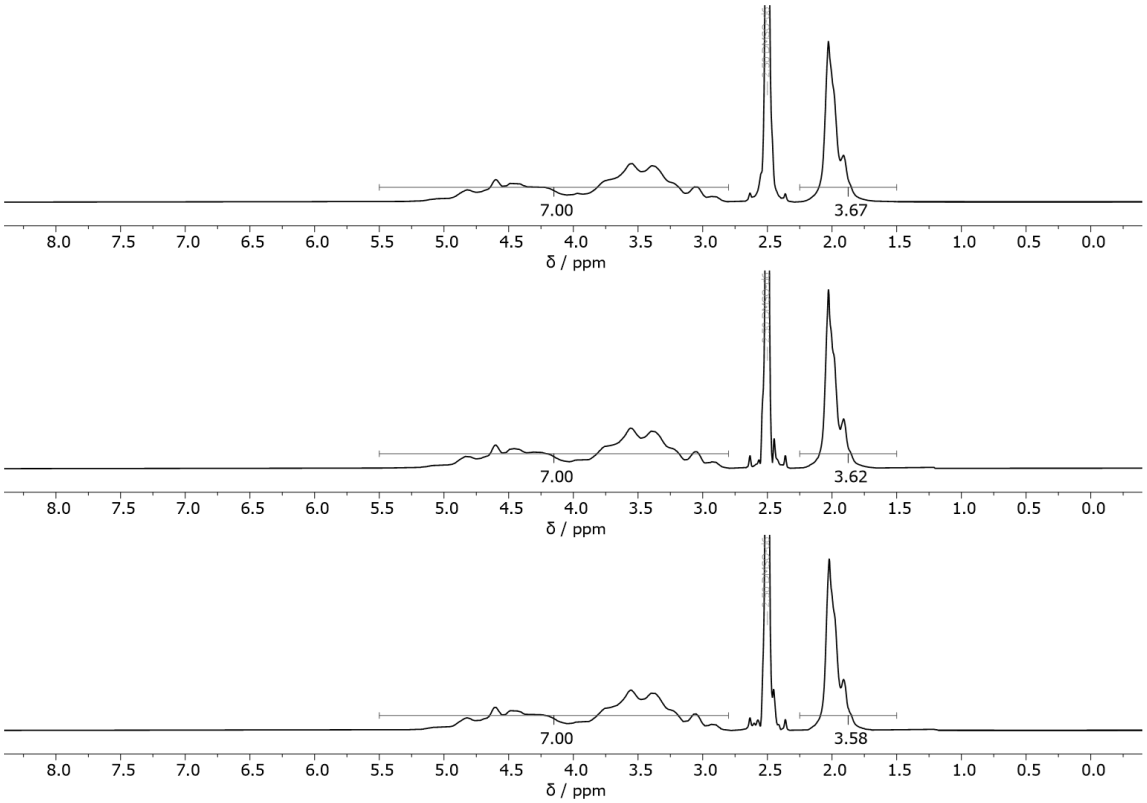

Figure S34 *^{1}H NMR (DMSO-d_6+TFA) spectra of CAc-5 (calculated average DS_{1H}=1.21±0.01).*

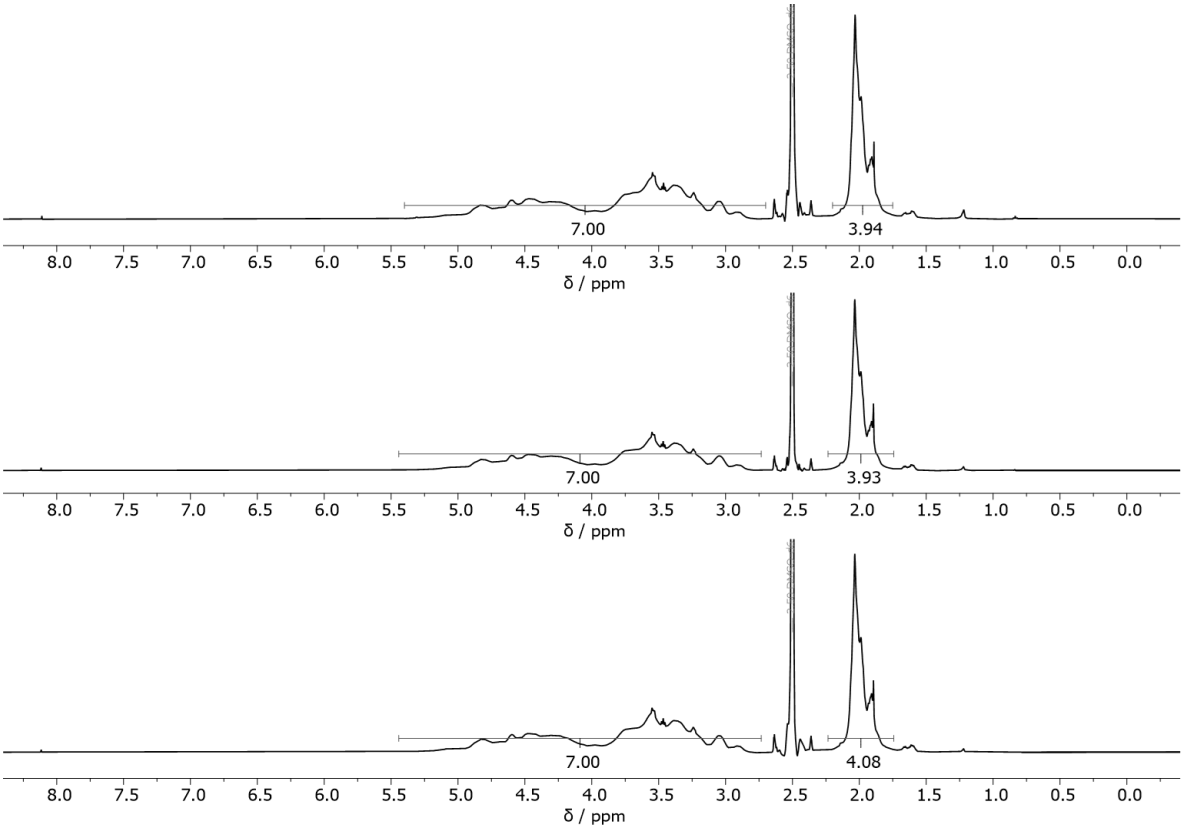

Figure S35 *^{1}H NMR (DMSO-d_6+TFA) spectra of CAc-6 (calculated average DS_{1H}=1.33±0.02).*

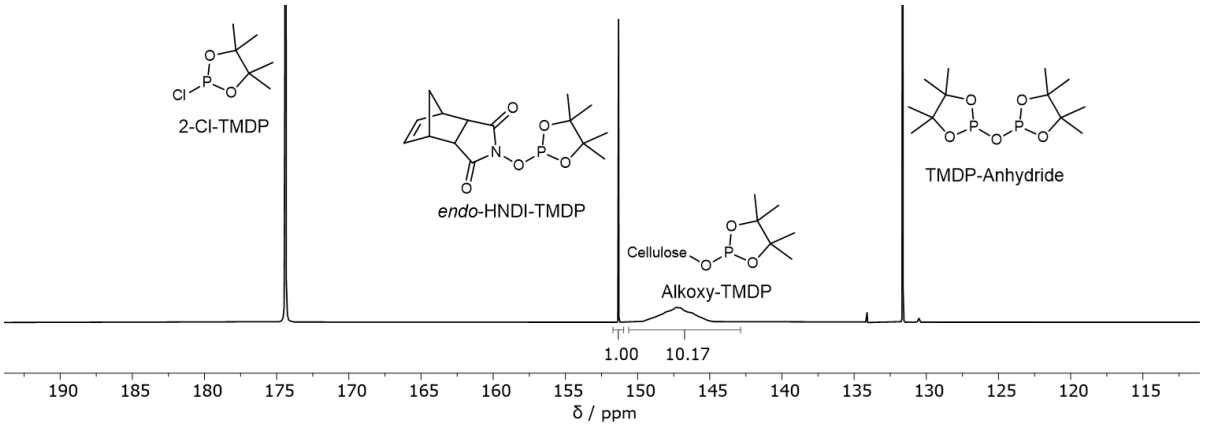

Figure S36 *^{31}P NMR ($CDCl_3$) spectrum of the phosphitylated CAc-6 (calculated: DS_{31P}=1.44).*

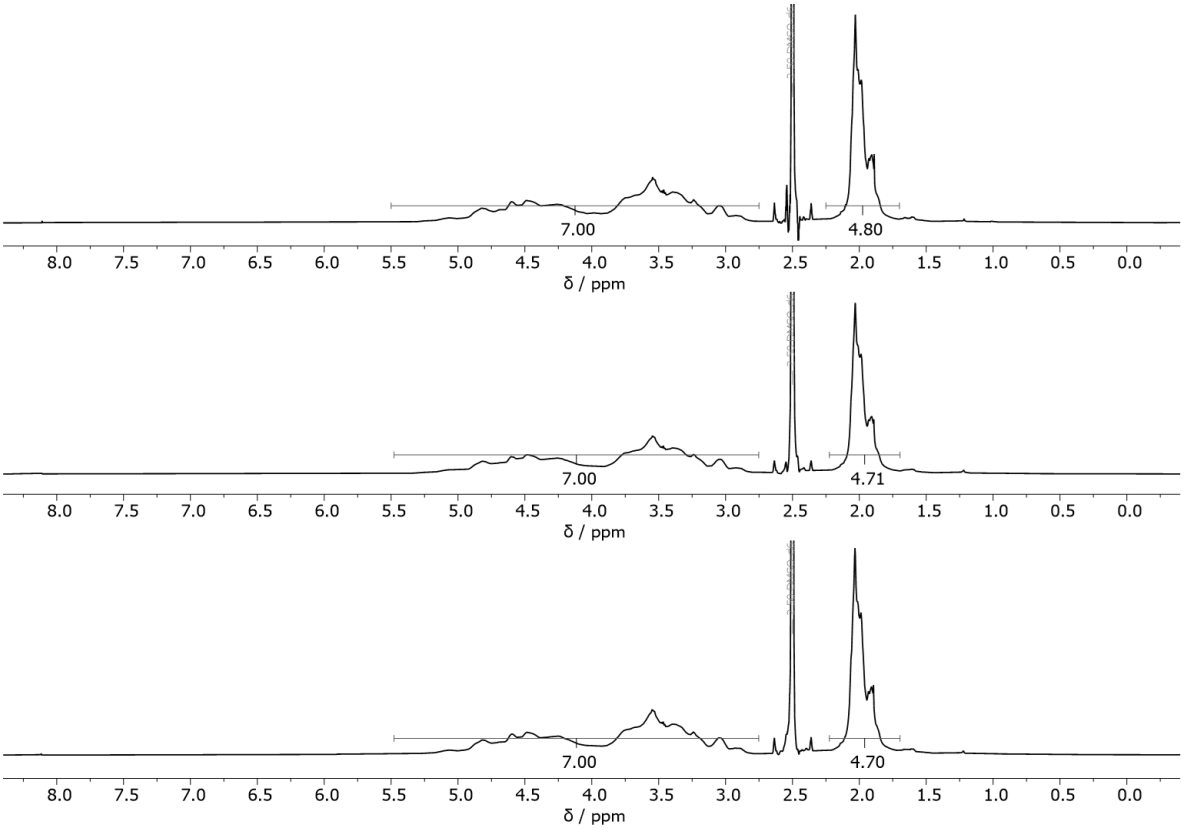

Figure S37 *^{1}H NMR (DMSO-d_6+TFA) spectra of CAc-7 (calculated average DS_{1H}=1.58±0.01).*

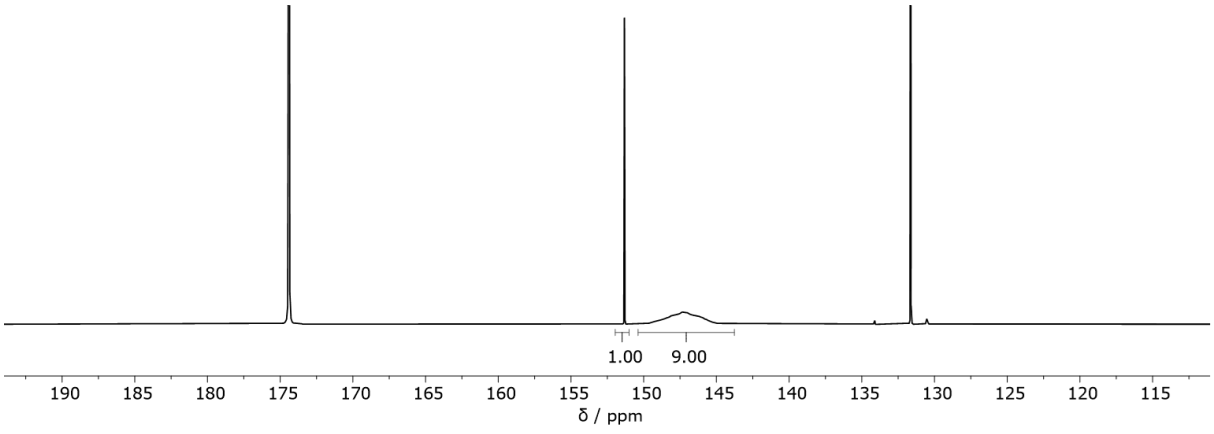

Figure S38 *^{31}P NMR ($CDCl_3$) spectrum of the phosphitylated CAc-7 (calculated: DS_{31P}=1.58). Signal assignment is analogous to* ***Figure S36****.*

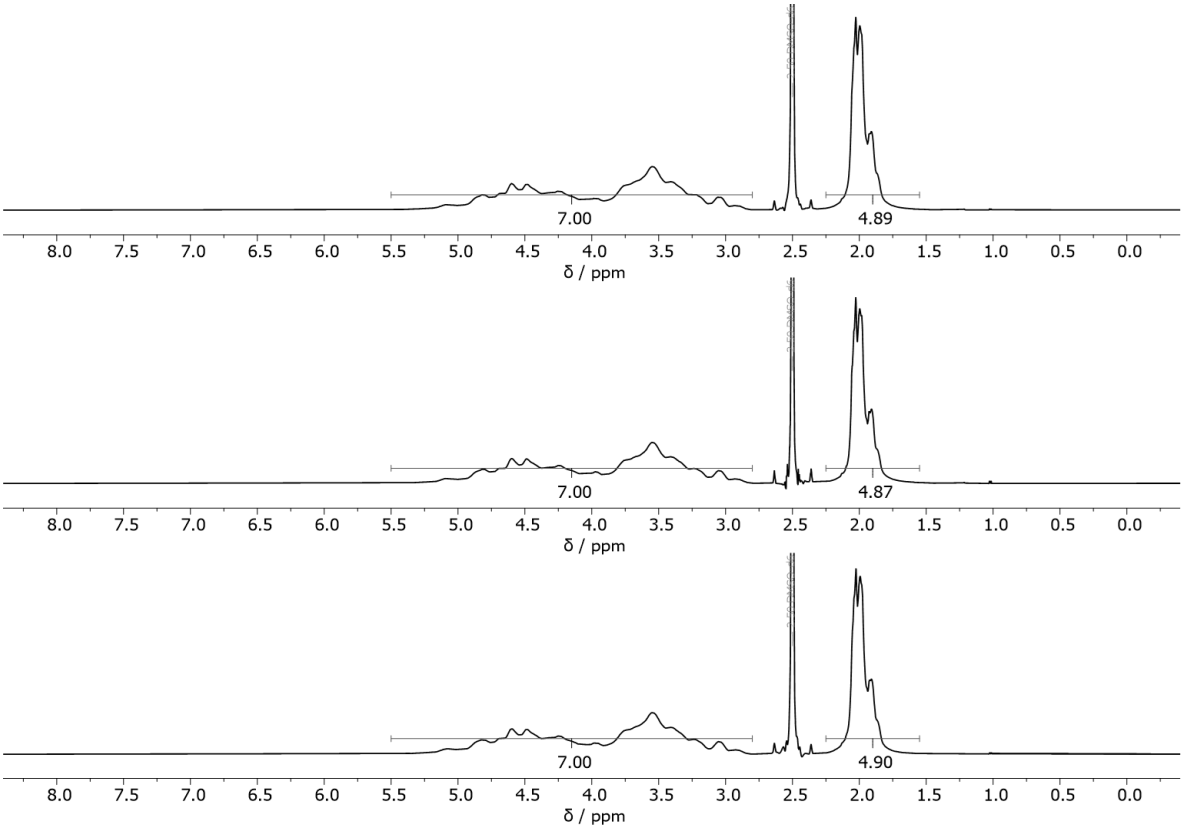

Figure S39 *^{1}H NMR (DMSO-d_6+TFA) spectra of CAc-8 (calculated average DS_{1H}=1.63±0.01).*

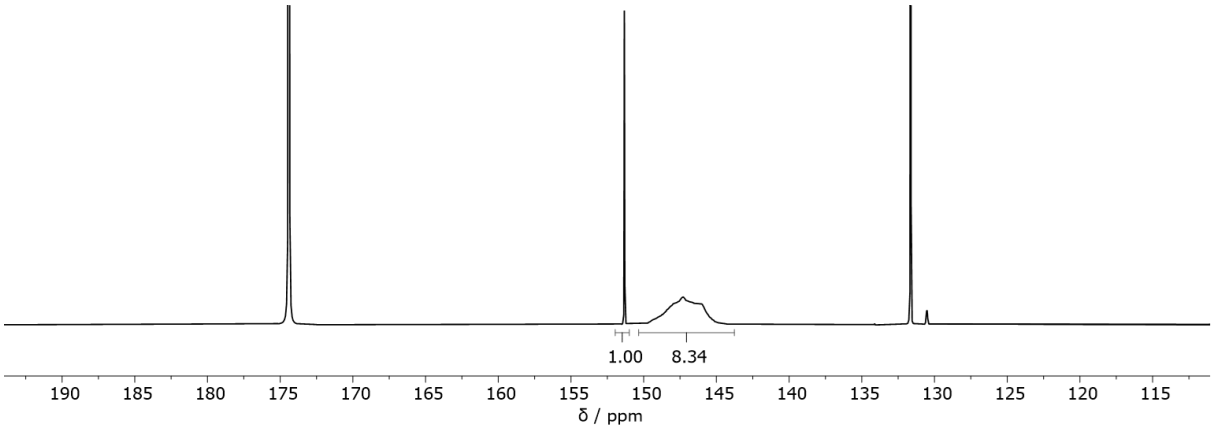

Figure S40 *^{31}P NMR ($CDCl_3$) spectrum of the phosphitylated CAc-8 (calculated: DS_{31P}=1.64). Signal assignment is analogous to* ***Figure S36****.*

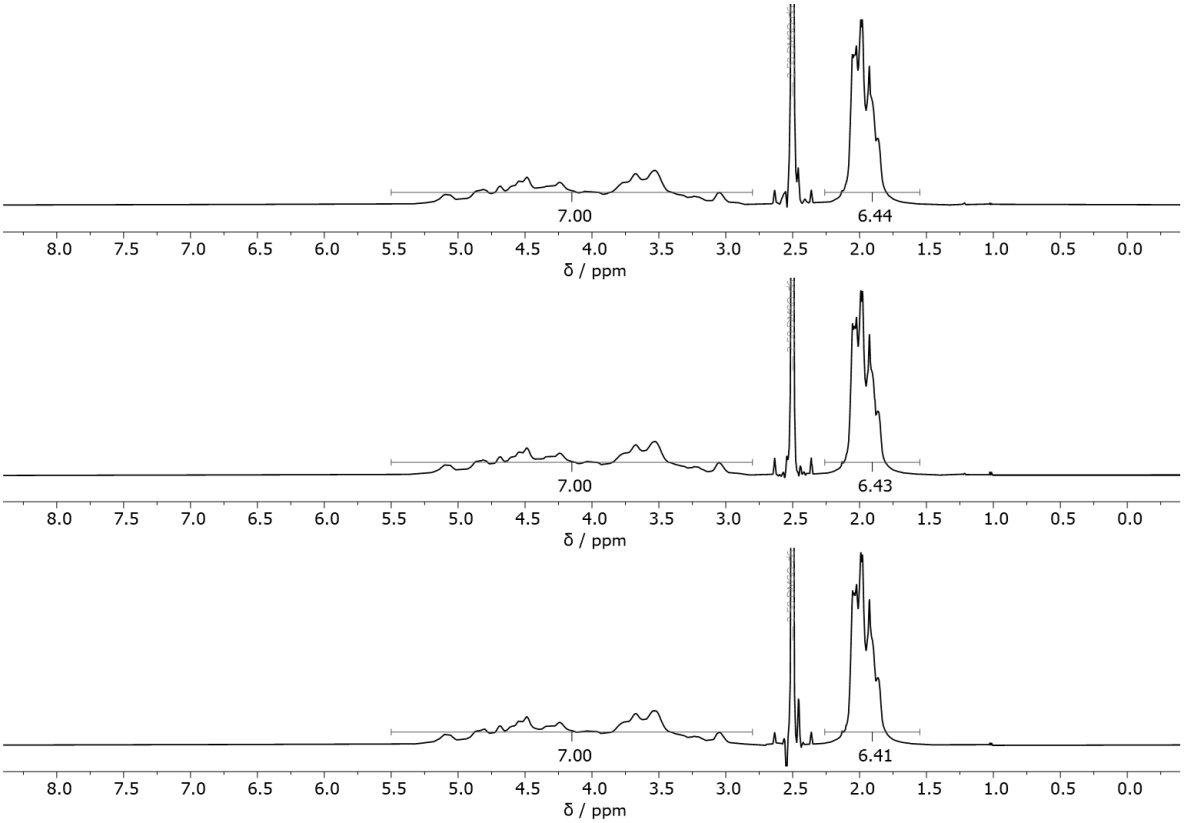

Figure S41 *^{1}H NMR (DMSO-d_6+TFA) spectra of CAc-9 (calculated average DS_{1H}=2.14±0.01).*

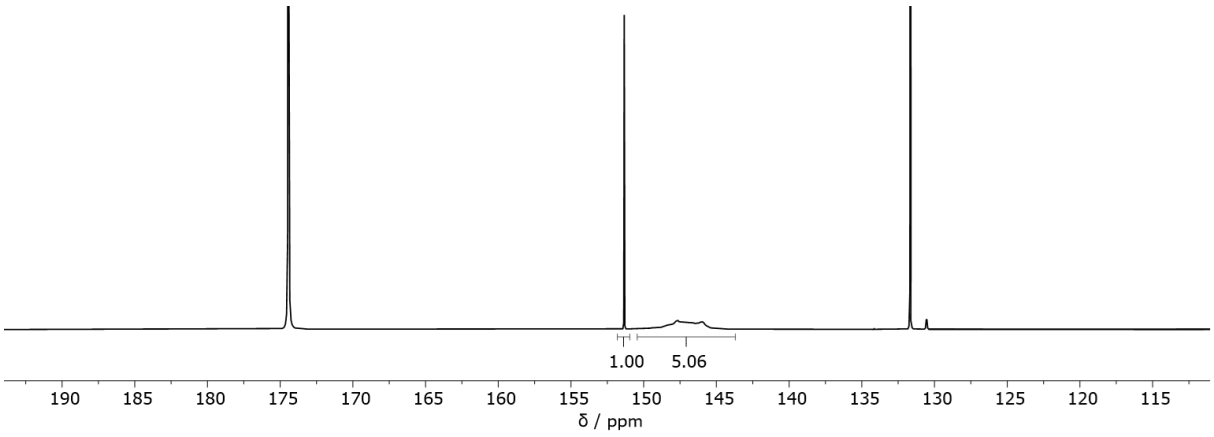

Figure S42 *^{31}P NMR ($CDCl_3$) spectrum of the phosphitylated CAc-9 (calculated: DS_{31P}=2.12). Signal assignment is analogous to* ***Figure S36****.*

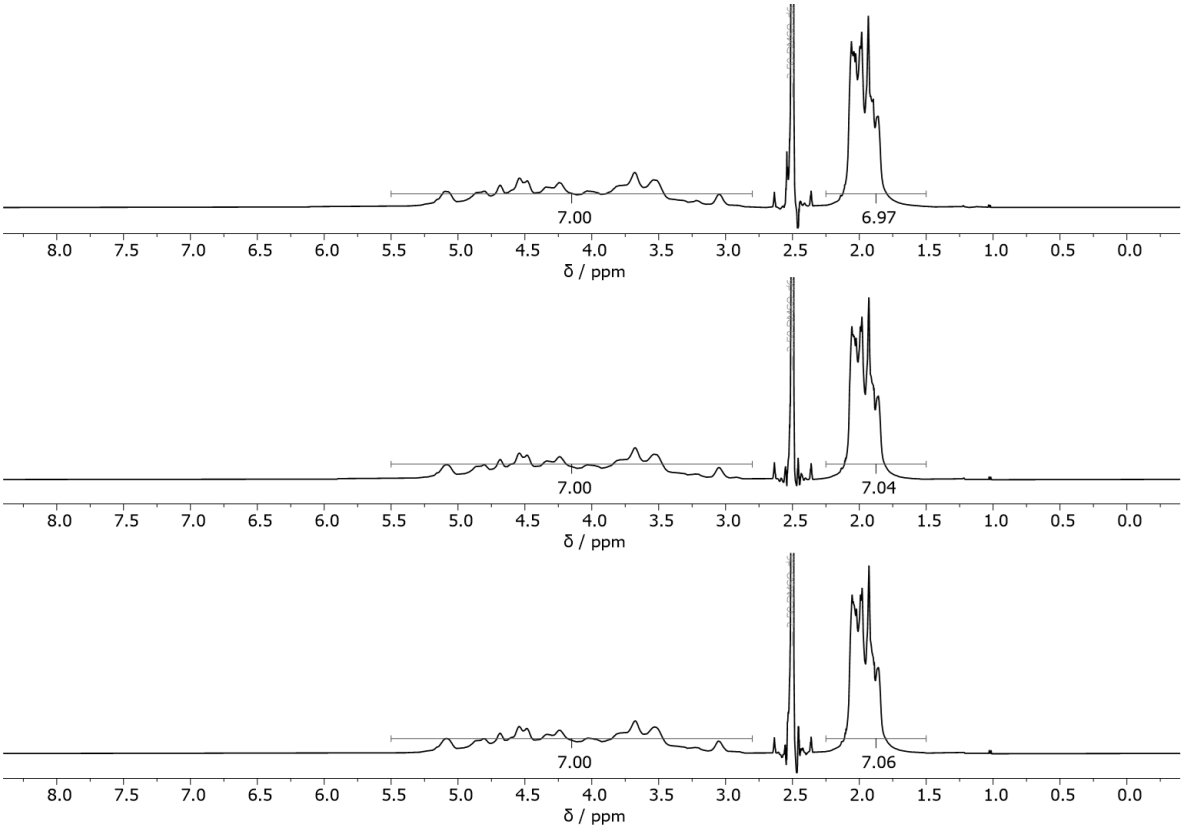

Figure S43 *^{1}H NMR (DMSO-d_6+TFA) spectra of CAc-10 (calculated average DS_{1H}=2.33±0.01).*

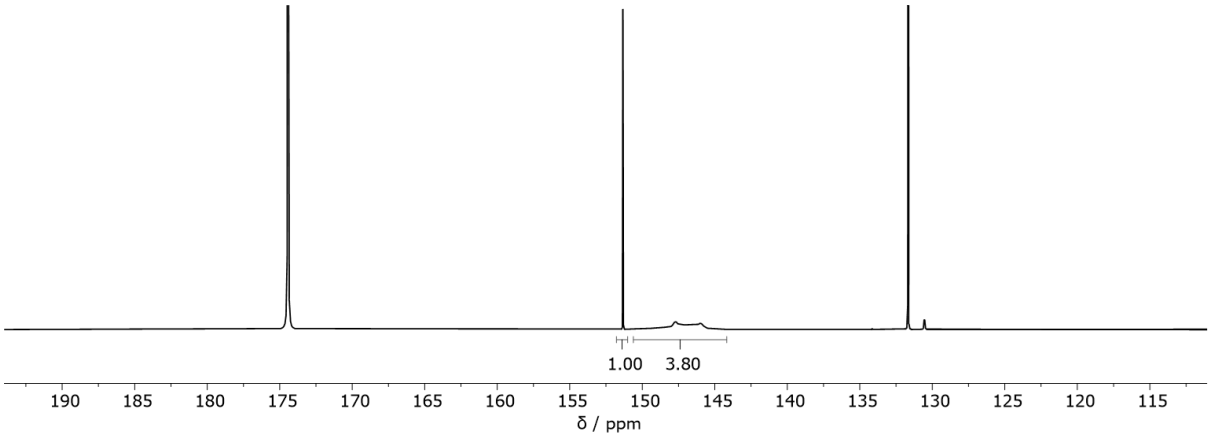

Figure S44 *^{31}P NMR ($CDCl_3$) spectrum of the phosphitylated CAc-10 (calculated: DS_{31P}=2.31). Signal assignment is analogous to* ***Figure S36****.*

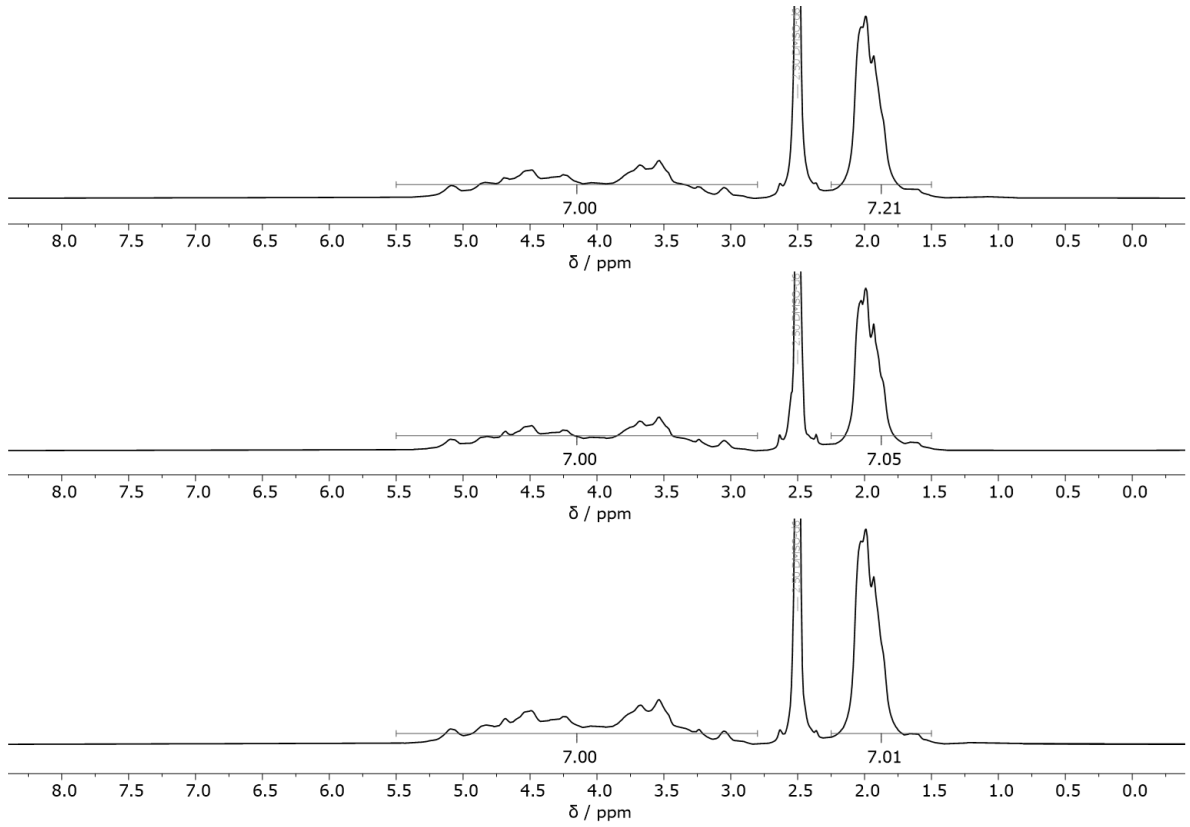

Figure S45 *^{1}H NMR (DMSO-d_6+TFA) spectra of CAc-11 (calculated average DS_{1H}=2.36±0.03).*

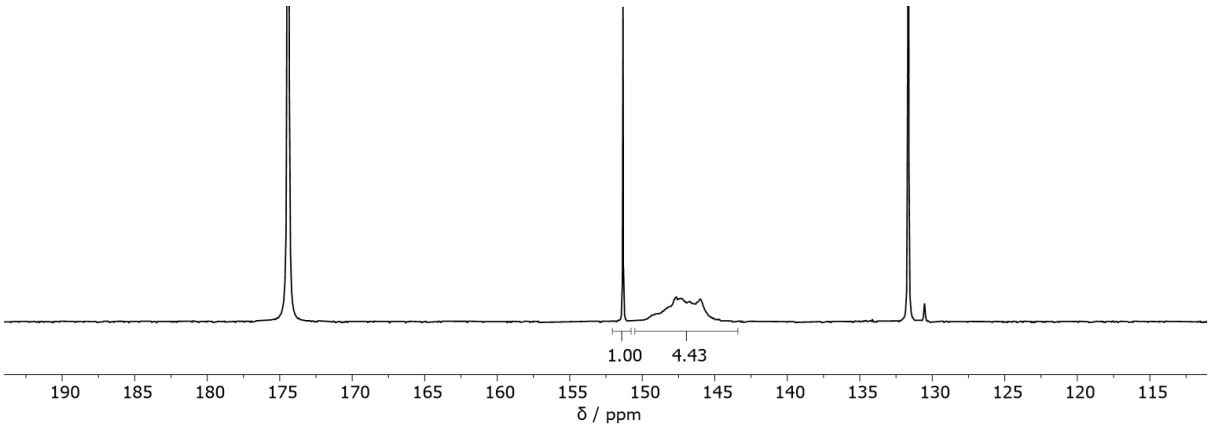

Figure S46 *^{31}P NMR ($CDCl_3$) spectrum of the phosphitylated CAc-11 (calculated: DS_{31P}=2.24). Signal assignment is analogous to* ***Figure S36****.*

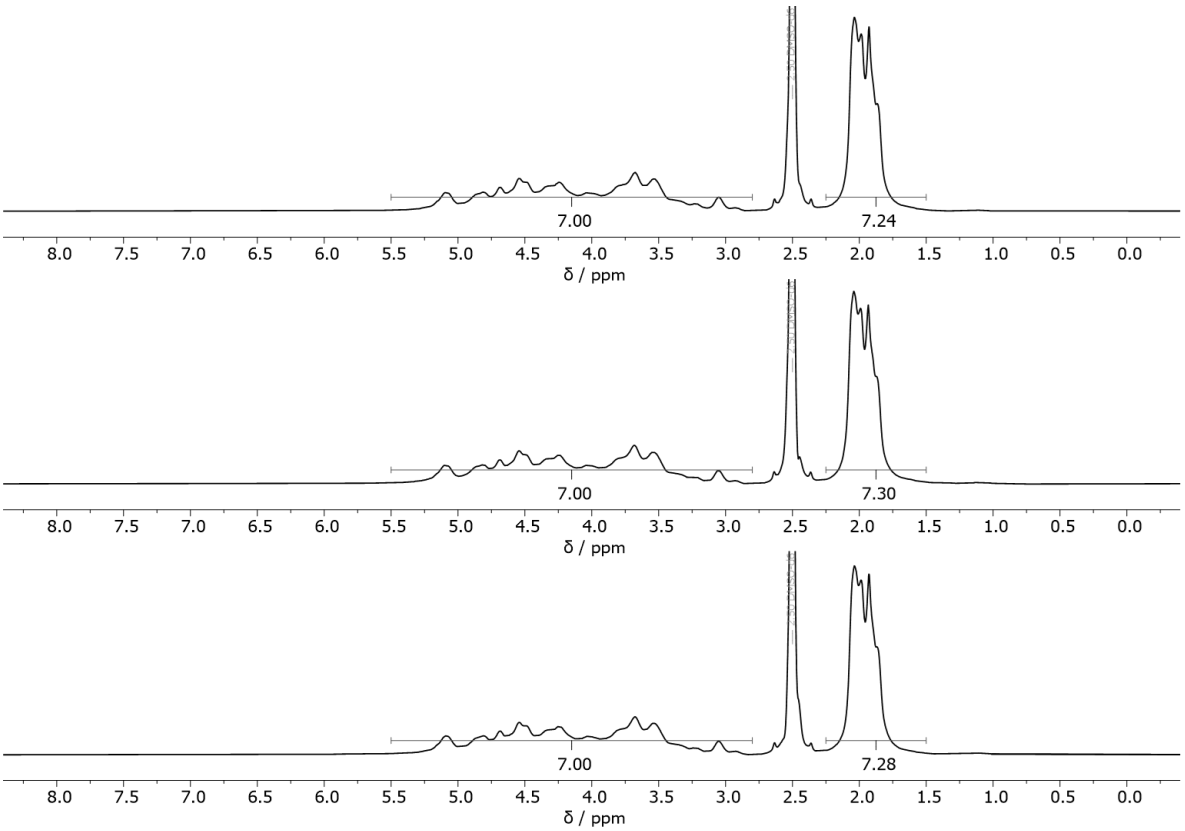

Figure S47 *^{1}H NMR (DMSO-d_6+TFA) spectra of CAc-12 (calculated average DS_{1H}=2.42±0.01).*

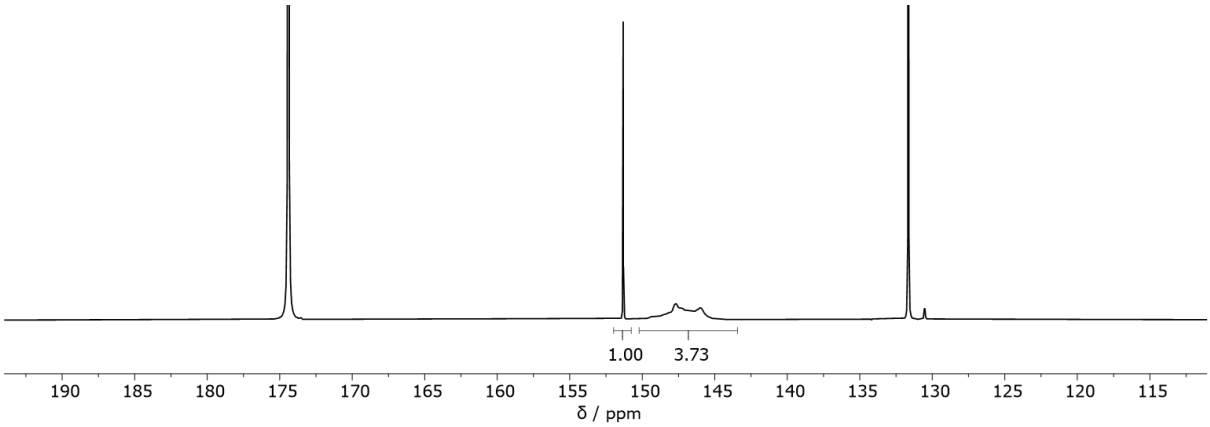

Figure S48 *^{31}P NMR ($CDCl_3$) spectrum of the phosphitylated CAc-12 (calculated: DS_{31P}=2.34). Signal assignment is analogous to* ***Figure S36****.*

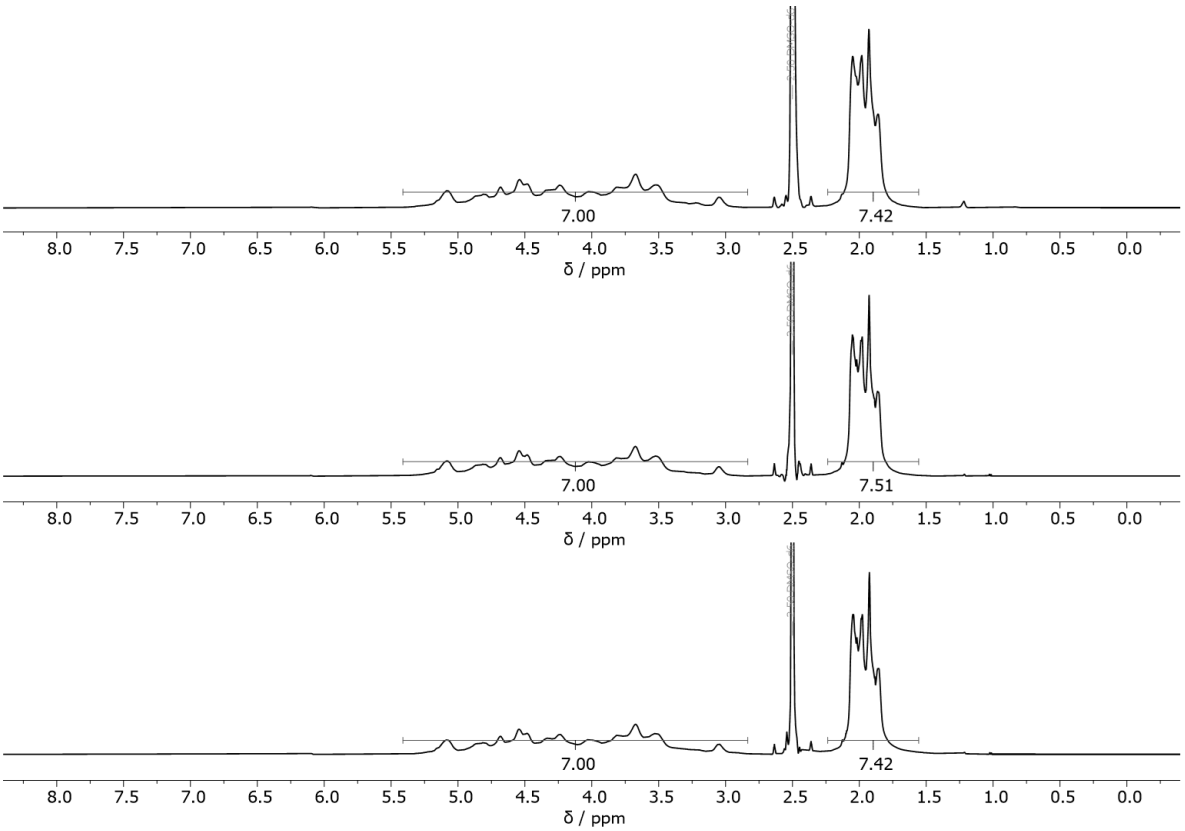

Figure S49 *^{1}H NMR (DMSO-d_6+TFA) spectra of CAc-13 (calculated average DS_{1H}=2.48±0.01).*

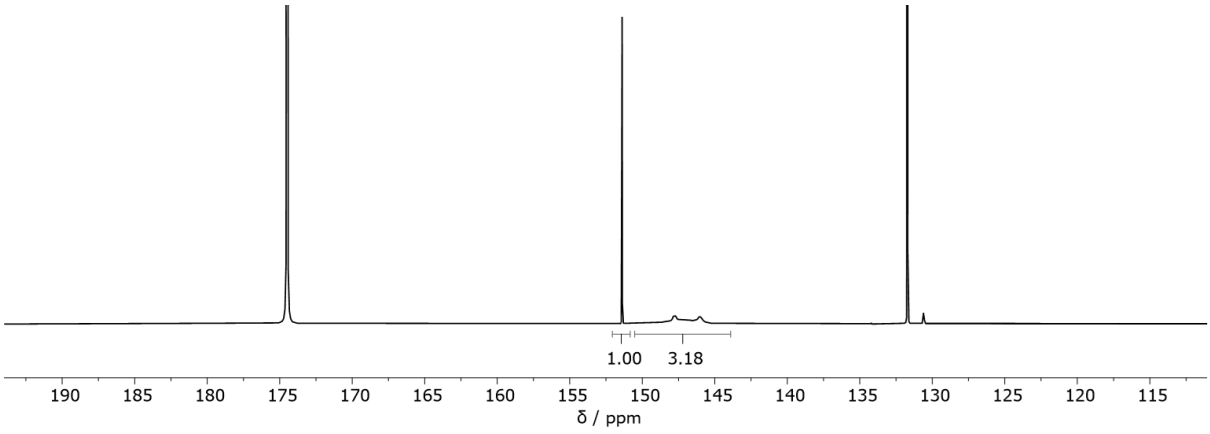

Figure S50 *^{31}P NMR ($CDCl_3$) spectrum of the phosphitylated CAc-13 (calculated: DS_{31P}=2.41). Signal assignment is analogous to* ***Figure S36****.*

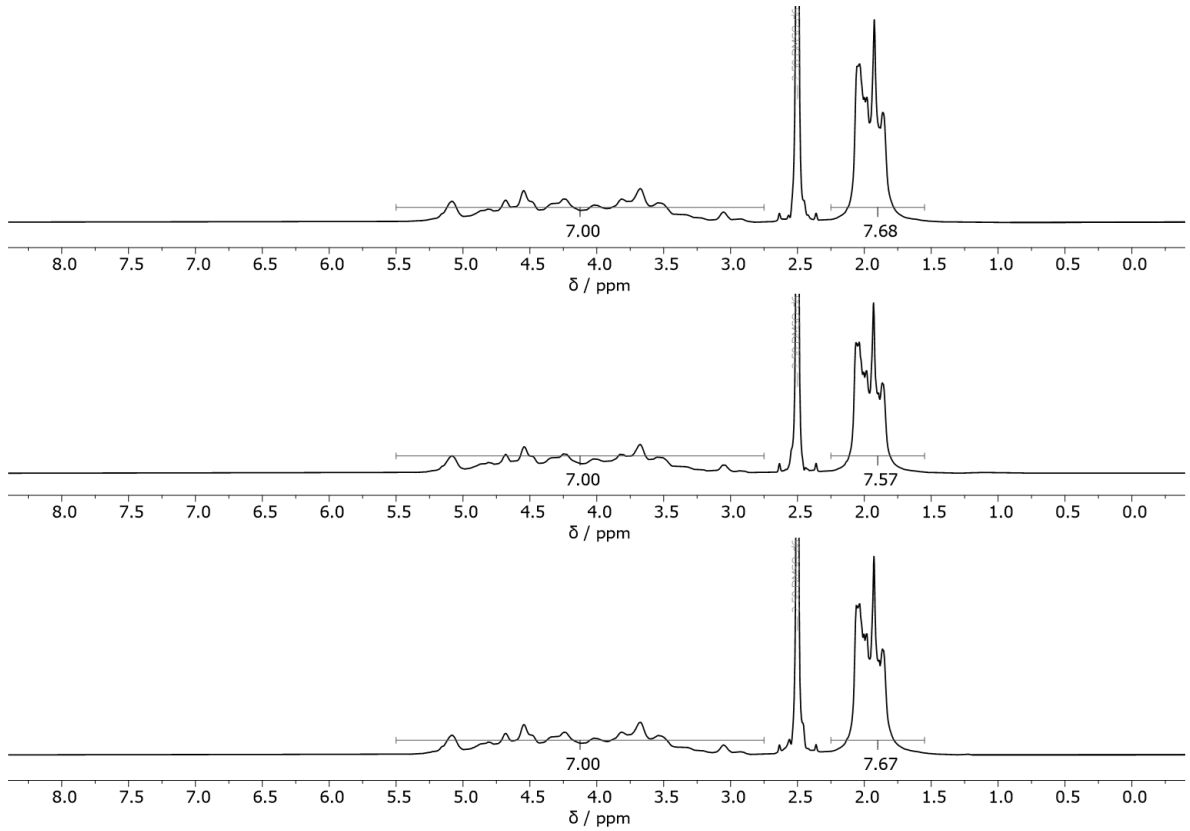

Figure S51 *^{1}H NMR (DMSO-d_6+TFA) spectra of CAc-14 (calculated average DS_{1H}=2.55±0.02).*

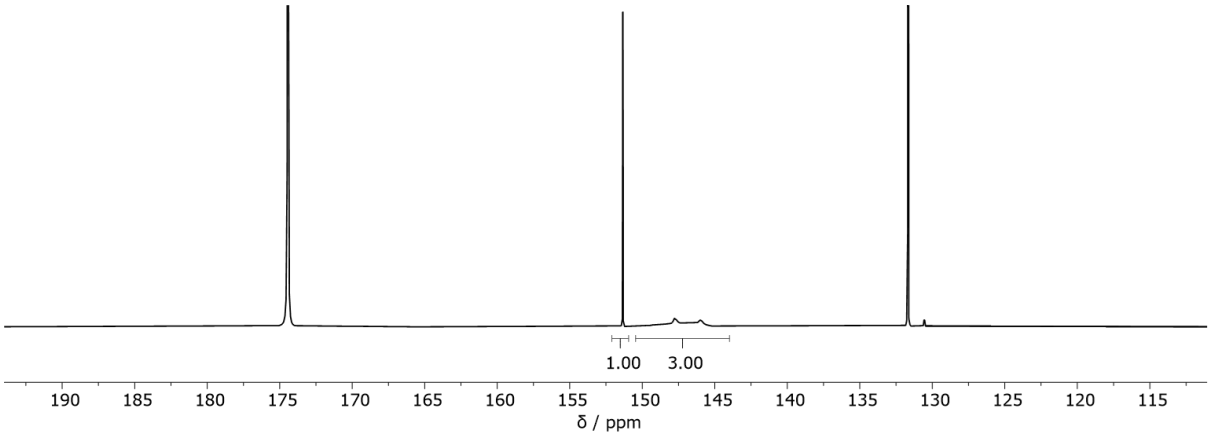

Figure S52 *^{31}P NMR ($CDCl_3$) spectrum of the phosphitylated CAc-14 (calculated: DS_{31P}=2.46). Signal assignment is analogous to* ***Figure S36****.*

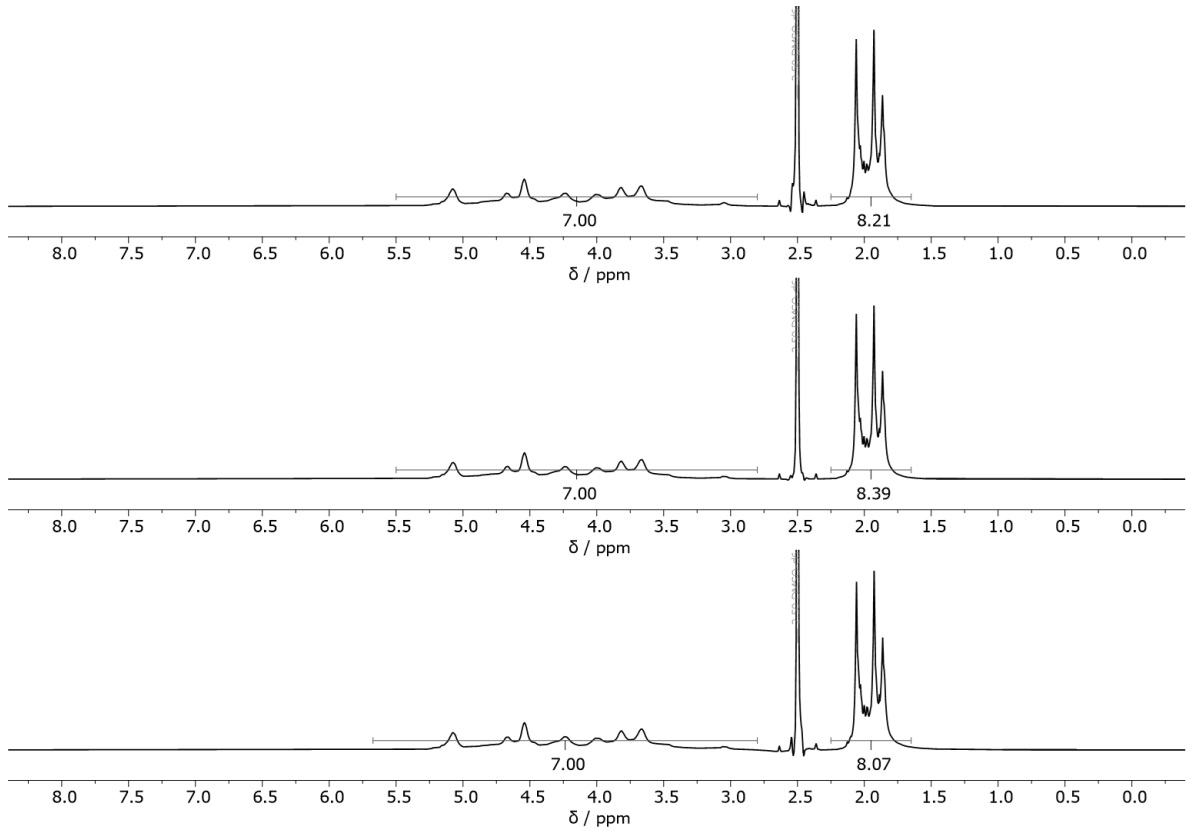

Figure S53 *^{1}H NMR (DMSO-d_6+TFA) spectra of CAc-15 (calculated average DS_{1H}=2.74±0.04).*

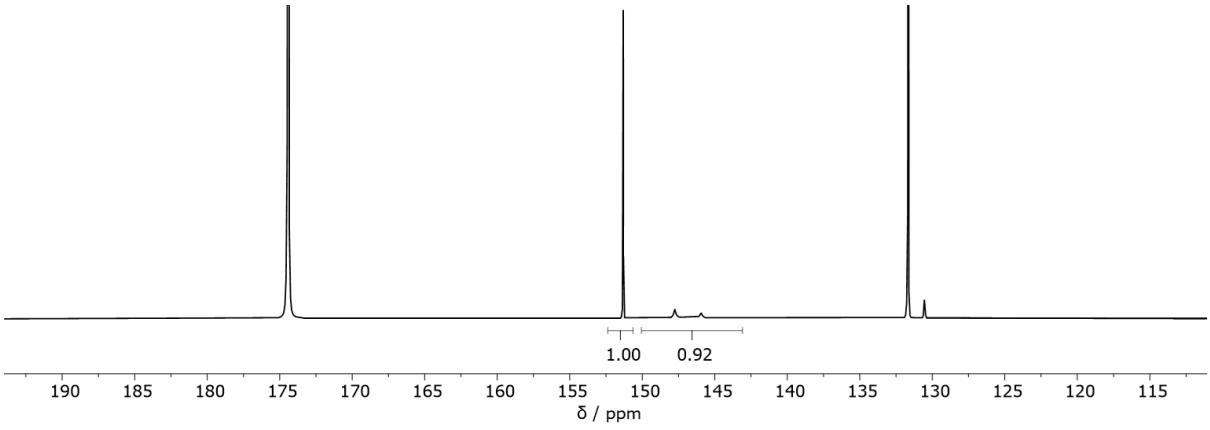

Figure S54 *^{31}P NMR ($CDCl_3$) spectrum of the phosphitylated CAc-15 (calculated: DS_{31P}=2.83). Signal assignment is analogous to* ***Figure S36****.*

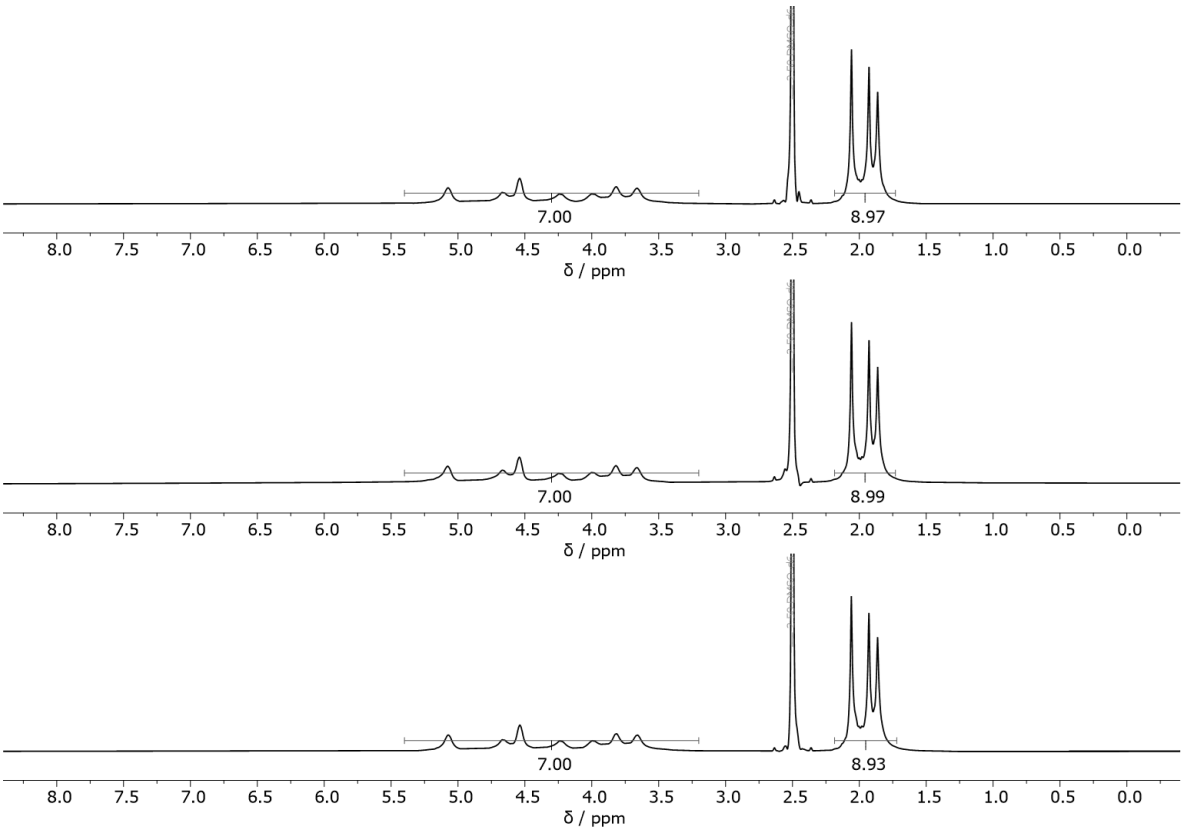

Figure S55 *^{1}H NMR (DMSO-d_6+TFA) spectra of CAc-16 (calculated average DS_{1H}=2.99±0.01).*

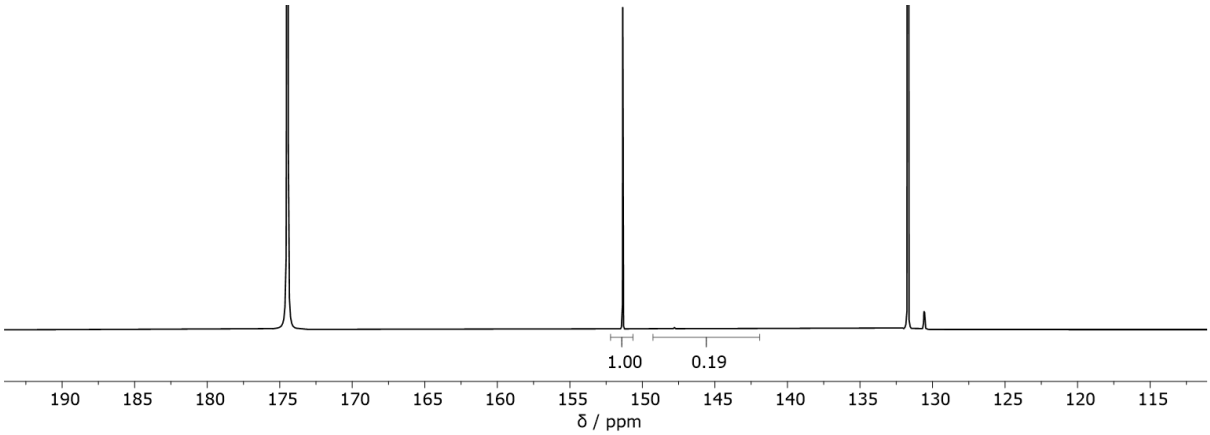

Figure S56 *^{31}P NMR ($CDCl_3$) spectrum of the phosphitylated CAc-16 (calculated: DS_{31P}=2.96). Signal assignment is analogous to* ***Figure S36****.*

Cellulose Butyrates:

The peak assignment for all cellulose butyrates is exemplarily shown for CBu-1.

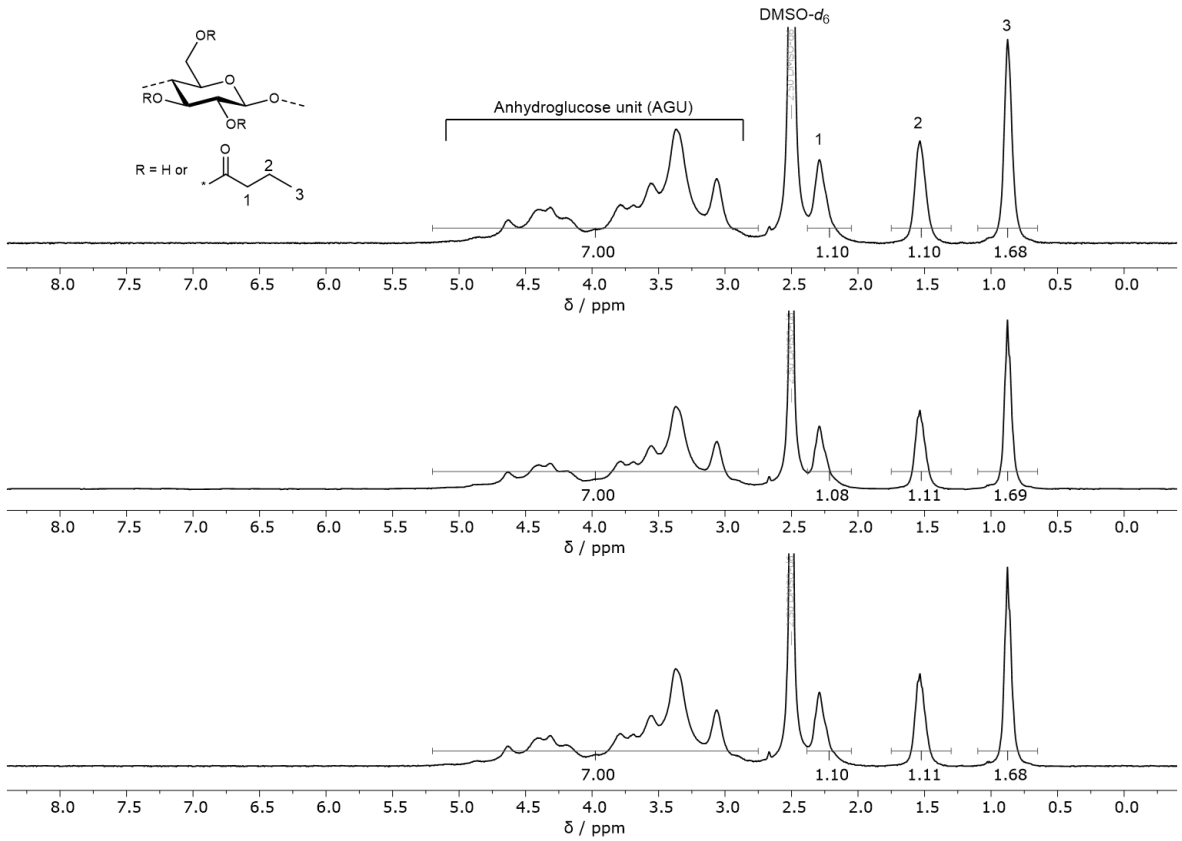

Figure S57 *^{1}H NMR (DMSO-d_6+TFA) spectra of CBu-1 (calculated average DS_{1H}=0.56±0.01).*

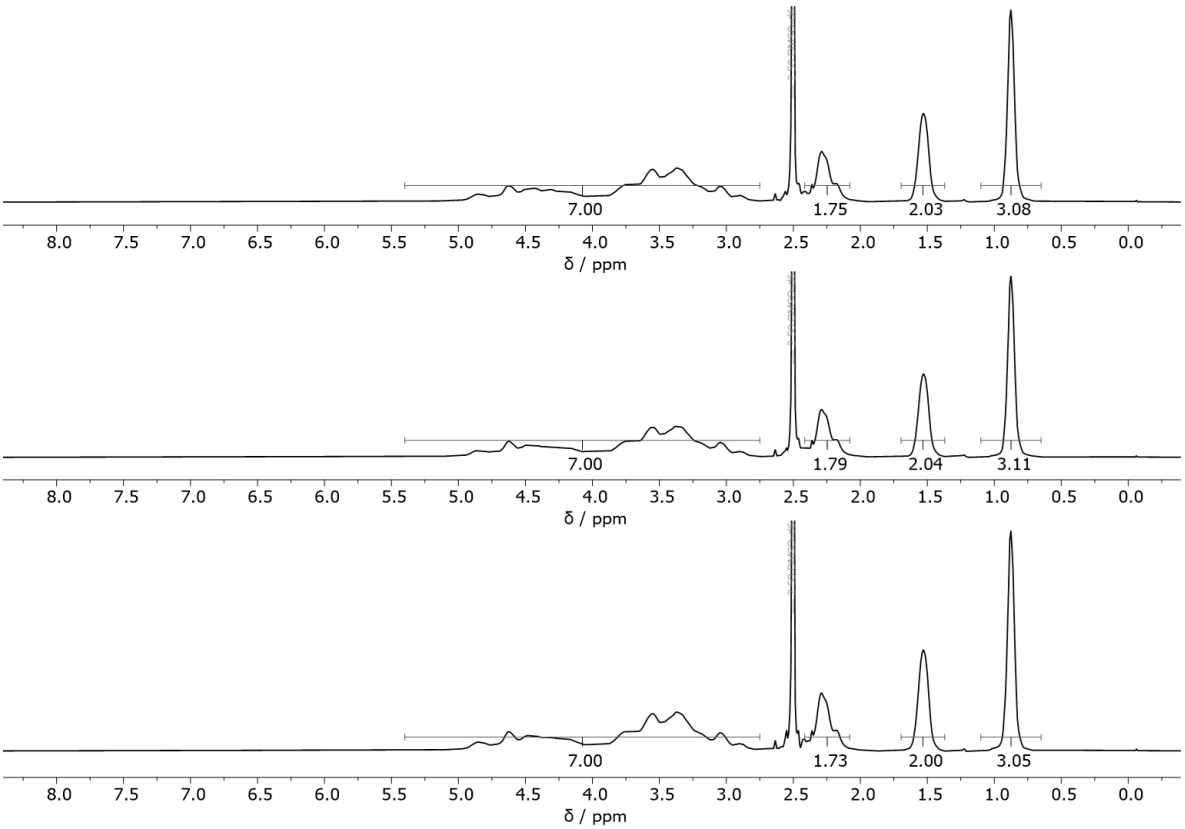

Figure S58 *^{1}H NMR (DMSO-d_6+TFA) spectra of CBu-2 (calculated average DS_{1H}=1.03±0.01).*

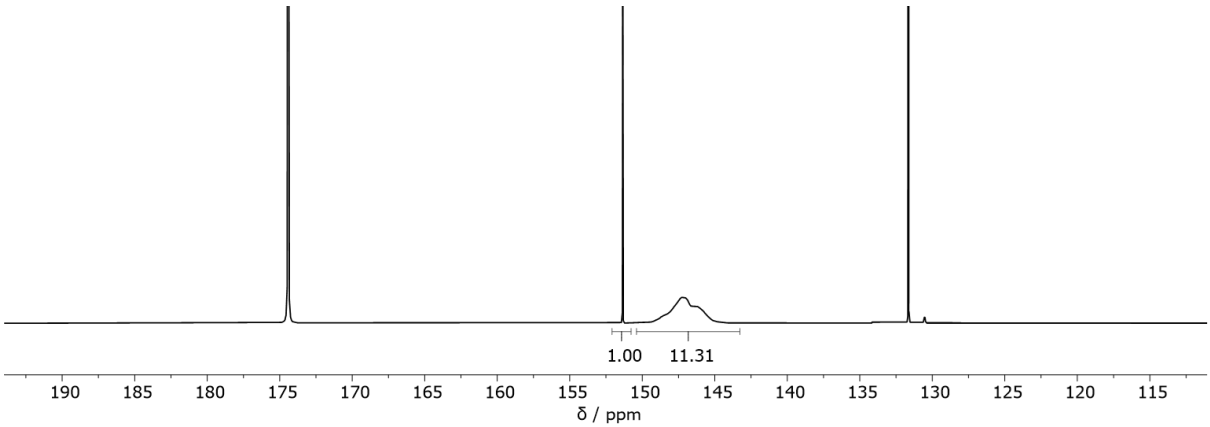

Figure S59 *^{31}P NMR ($CDCl_3$) spectrum of the phosphitylated CBu-2 (calculated: DS_{31P}=1.08). Signal assignment is analogous to* ***Figure S36****.*

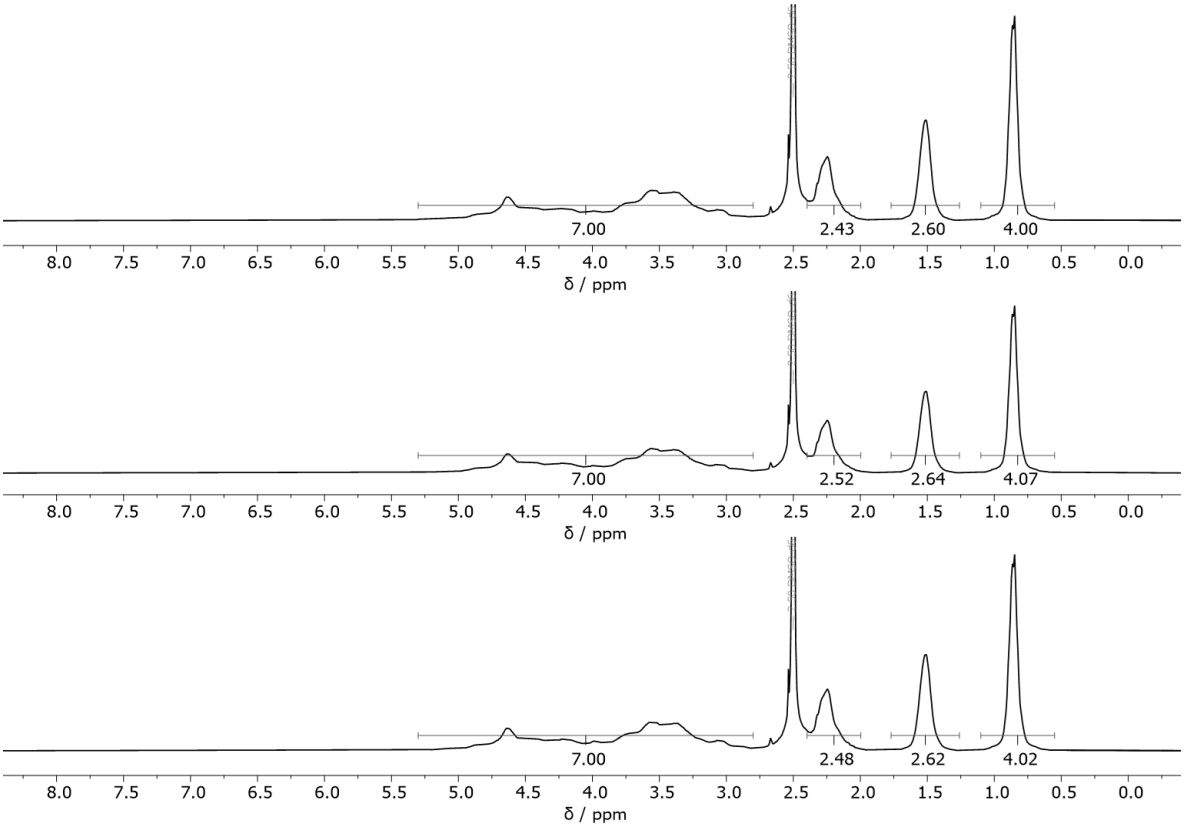

Figure S60 *^{1}H NMR (DMSO-d_6+TFA) spectra of CBu-3 (calculated average DS_{1H}=1.34±0.01).*

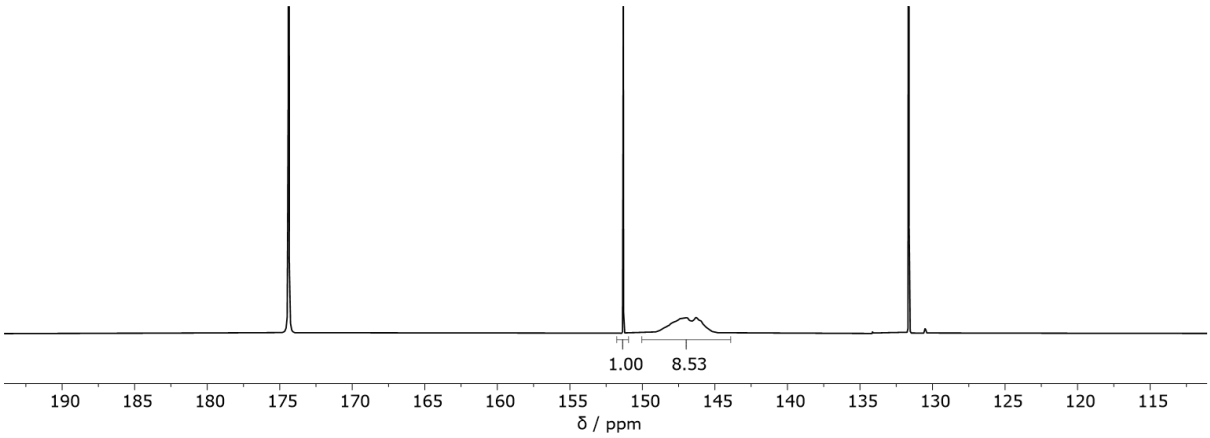

Figure S61 *^{31}P NMR ($CDCl_3$) spectrum of the phosphitylated CBu-3 (calculated: DS_{31P}=1.42). Signal assignment is analogous to* ***Figure S36****.*

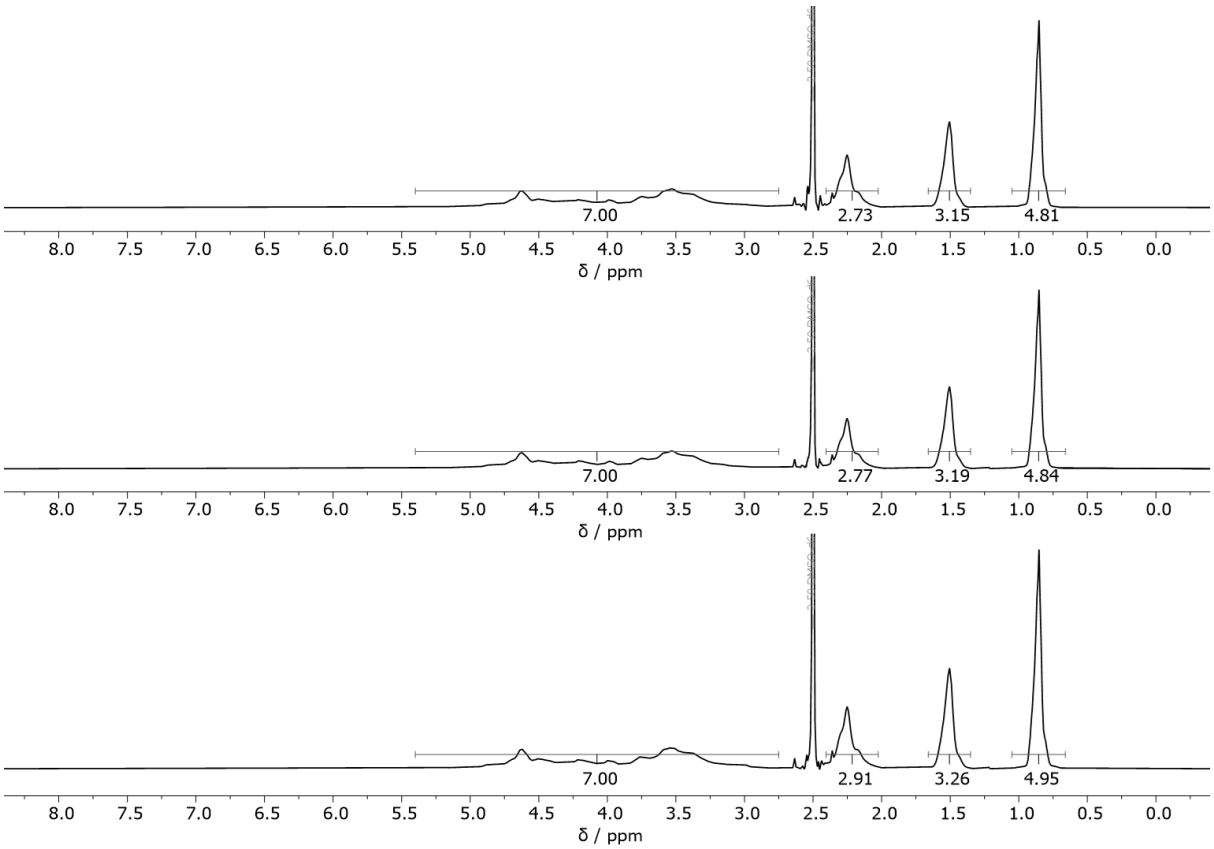

Figure S62 *^{1}H NMR (DMSO-d_6+TFA) spectra of CBu-4 (calculated average DS_{1H}=1.62±0.02).*

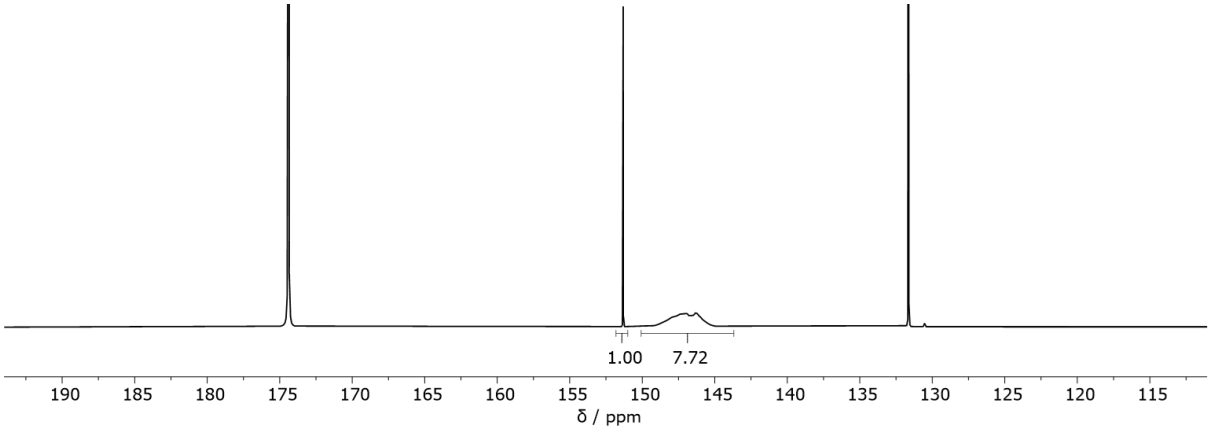

Figure S63 *^{31}P NMR ($CDCl_3$) spectrum of the phosphitylated CBu-4 (calculated: DS_{31P}=1.52). Signal assignment is analogous to* ***Figure S36****.*

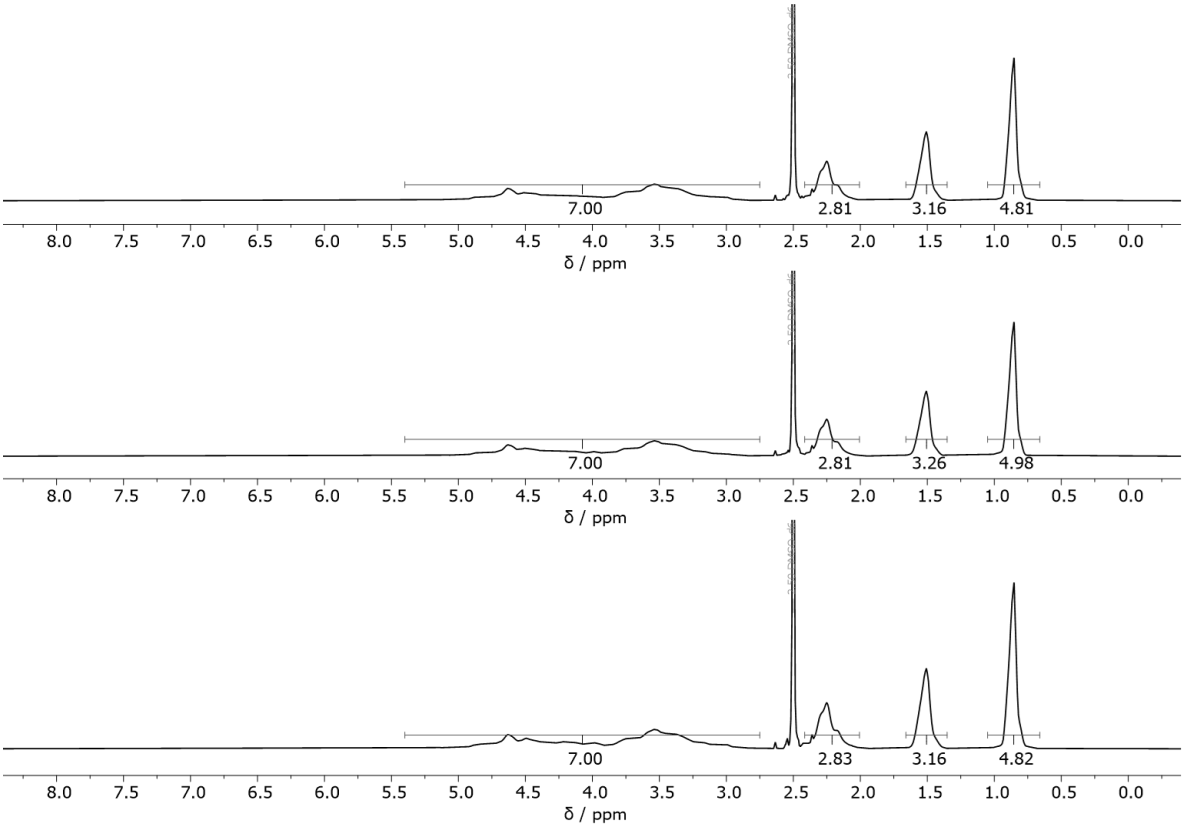

Figure S64 *^{1}H NMR (DMSO-d_6+TFA) spectra of CBu-5 (calculated average DS_{1H}=1.62±0.03).*

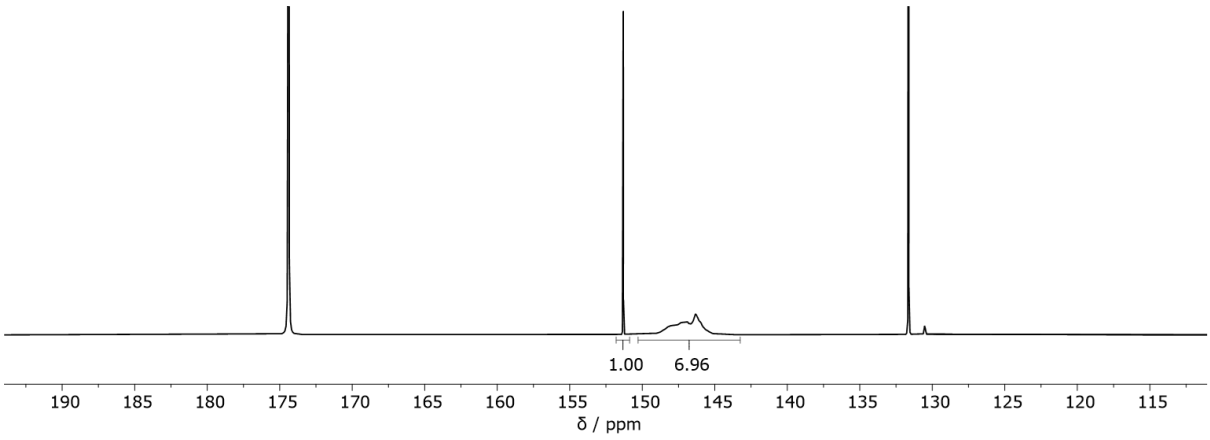

Figure S65 *^{31}P NMR ($CDCl_3$) spectrum of the phosphitylated CBu-5 (calculated: DS_{31P}=1.63). Signal assignment is analogous to* ***Figure S36****.*

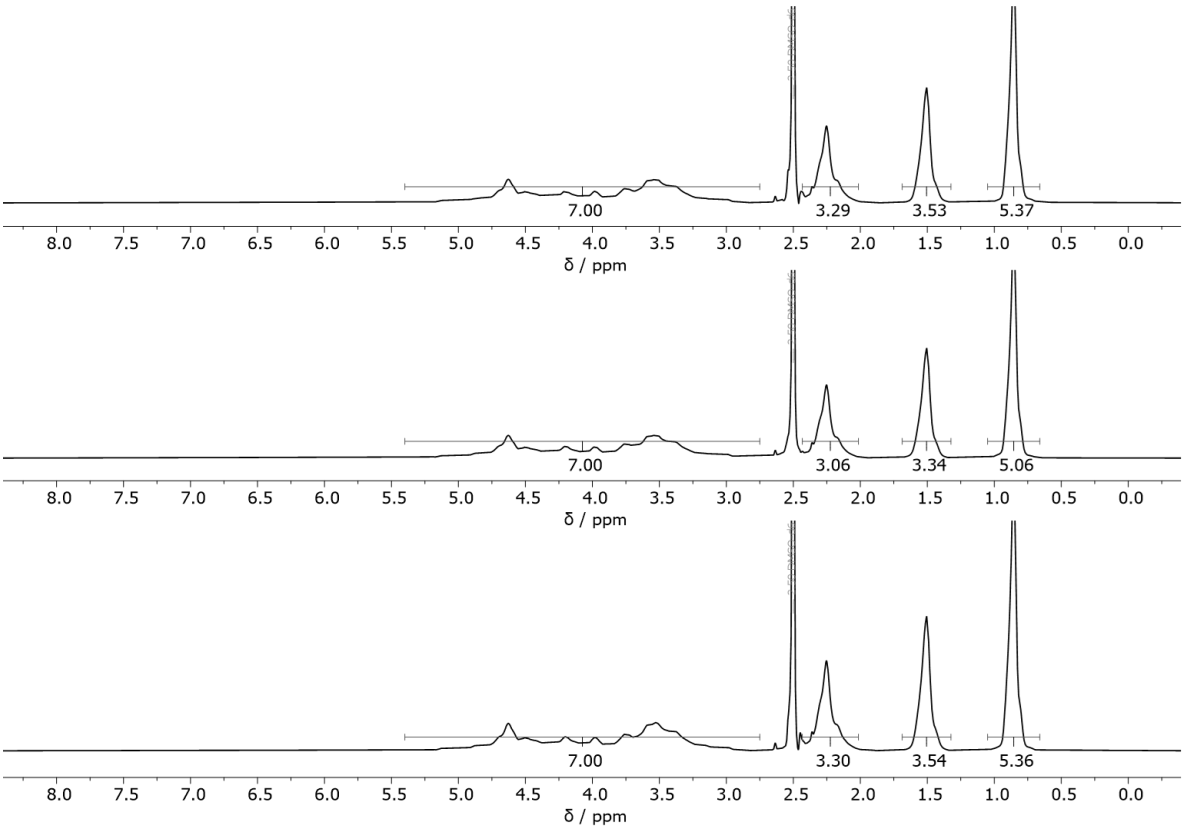

Figure S66 *^{1}H NMR (DMSO-d_6+TFA) spectra of CBu-6 (calculated average DS_{1H}=1.75±0.05).*

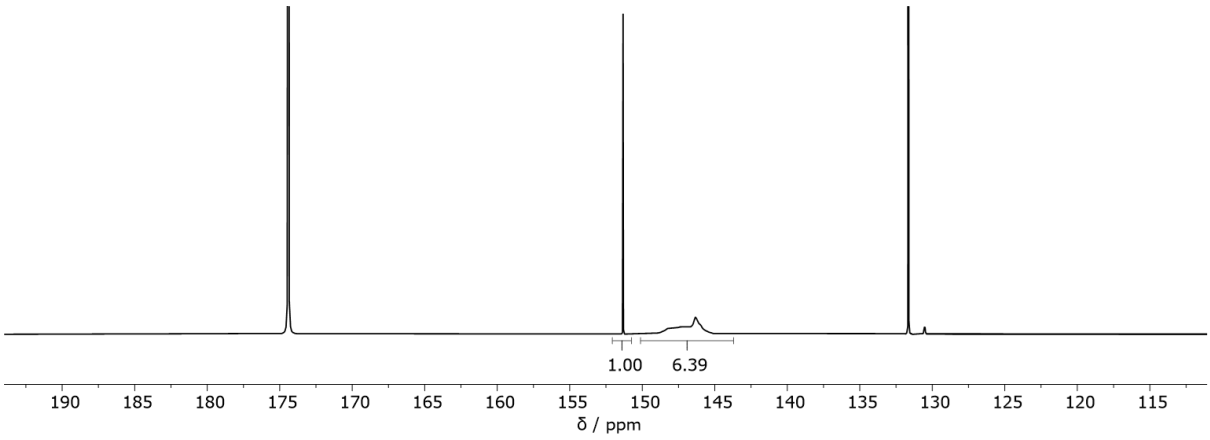

Figure S67 *^{31}P NMR ($CDCl_3$) spectrum of the phosphitylated CBu-6 (calculated: DS_{31P}=1.72). Signal assignment is analogous to* ***Figure S36****.*

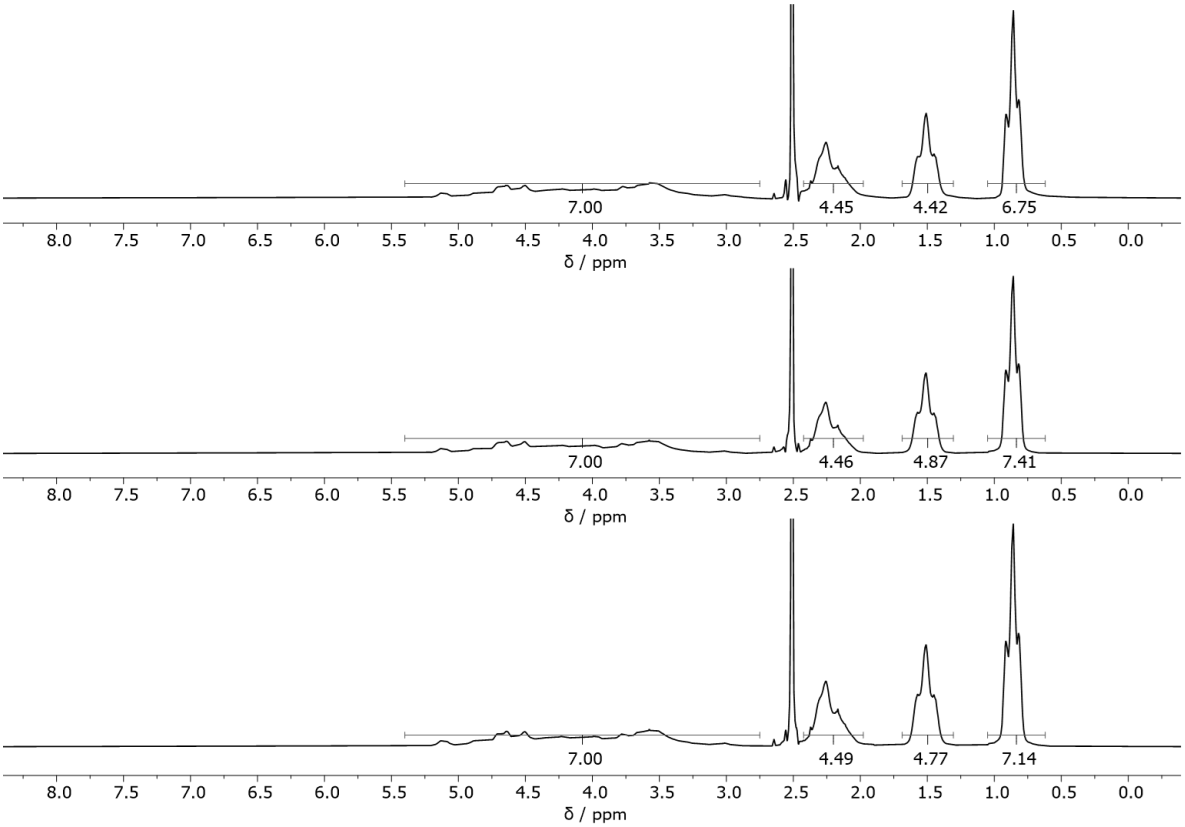

Figure S68 *^{1}H NMR (DMSO-d_6+TFA) spectra of CBu-7 (calculated average DS_{1H}=2.37±0.09).*

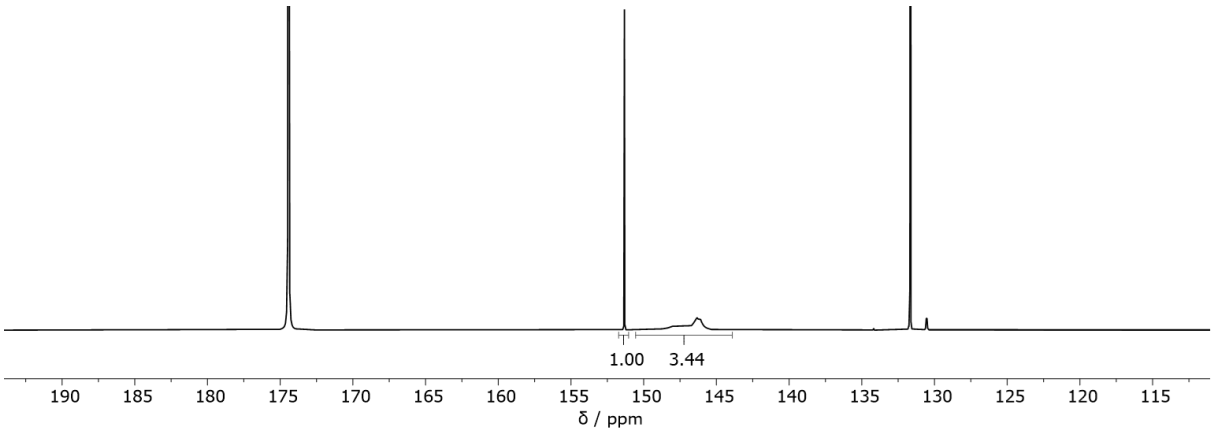

Figure S69 *^{31}P NMR ($CDCl_3$) spectrum of the phosphitylated CBu-7 (calculated: DS_{31P}=2.24). Signal assignment is analogous to* ***Figure S36****.*

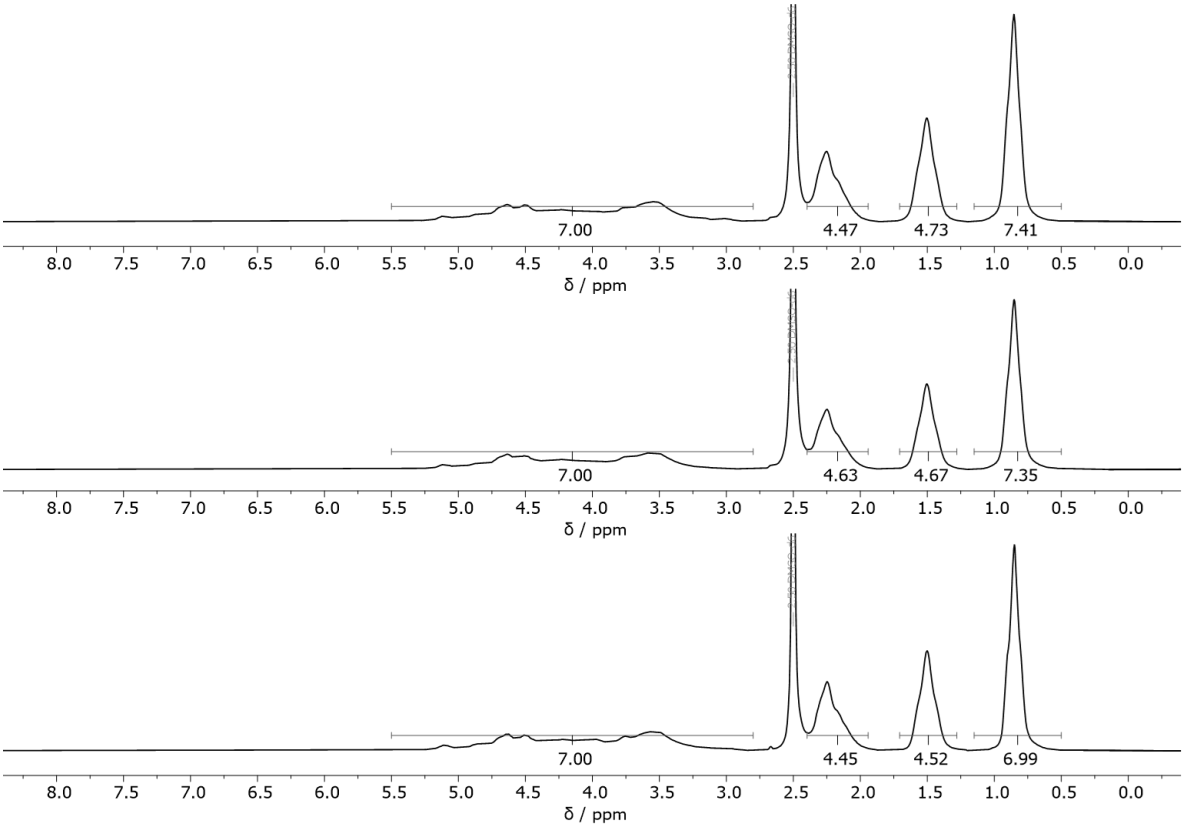

Figure S70 *^{1}H NMR (DMSO-d_6+TFA) spectra of CBu-8 (calculated average DS_{1H}=2.42±0.06).*

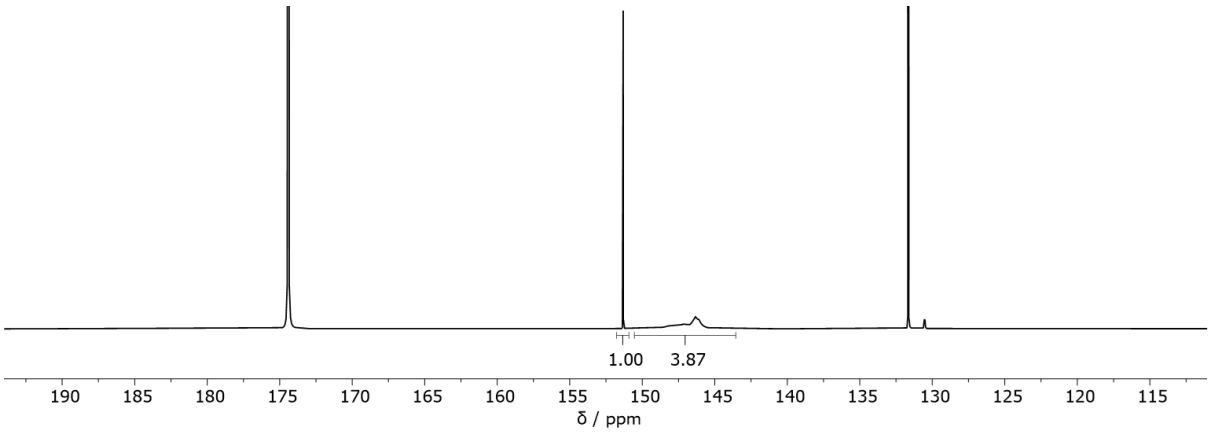

Figure S71 *^{31}P NMR ($CDCl_3$) spectrum of the phosphitylated CBu-8 (calculated: DS_{31P}=2.15). Signal assignment is analogous to* ***Figure S36****.*

Cellulose Benzoates:

The peak assignment for all cellulose benzoates is exemplarily shown for CBz-1.

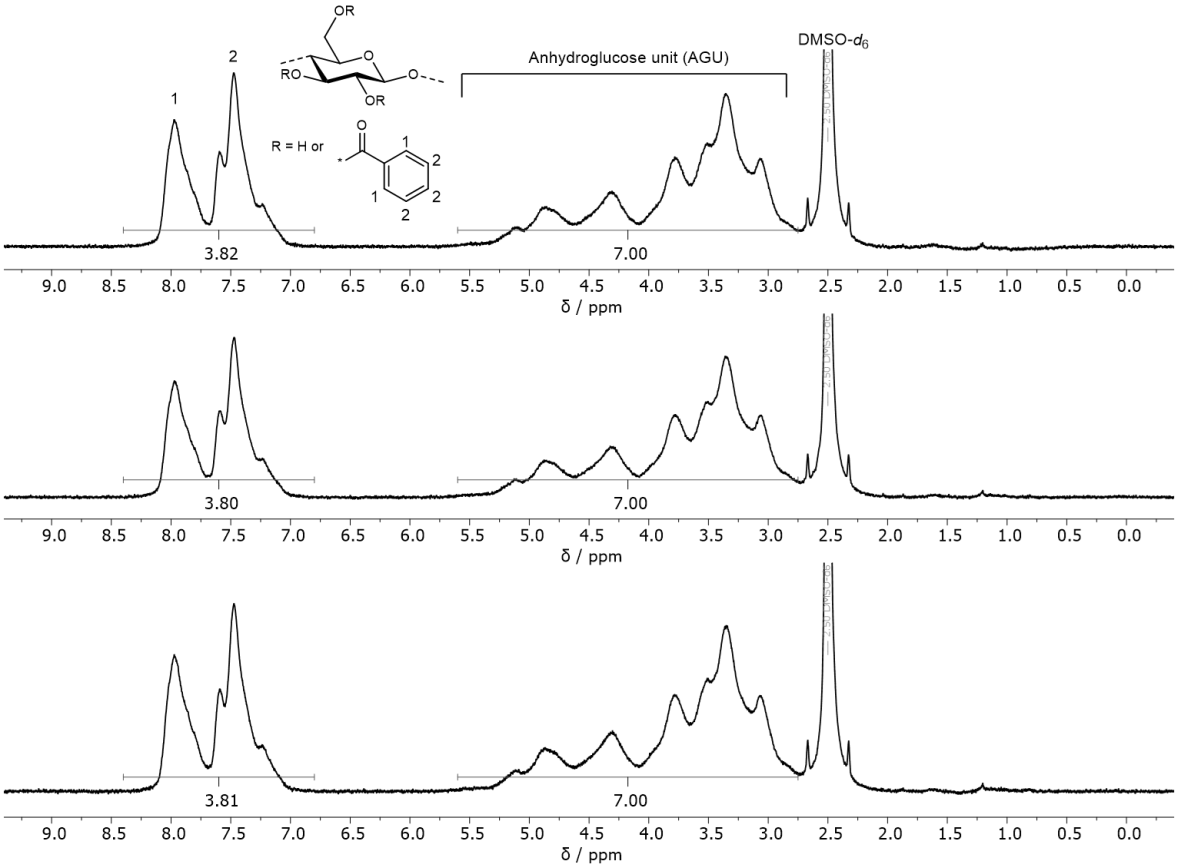

Figure S72 *^{1}H NMR (DMSO-d_6+TFA) spectra of CBz-1 (calculated average DS_{1H}=0.76±0.01).*

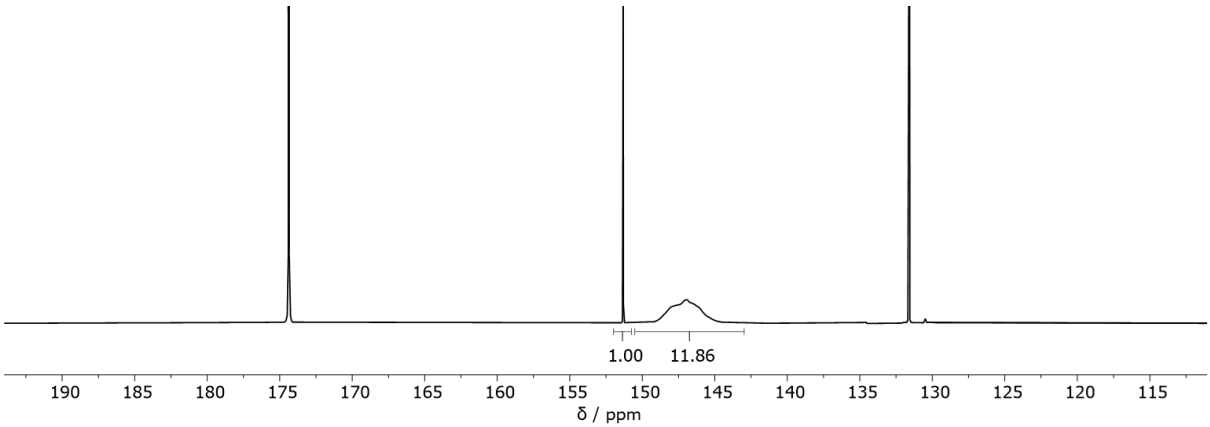

Figure S73 *^{31}P NMR ($CDCl_3$) spectrum of the phosphitylated CBz-1 (calculated: DS_{31P}=0.91). Signal assignment is analogous to* ***Figure S36****.*

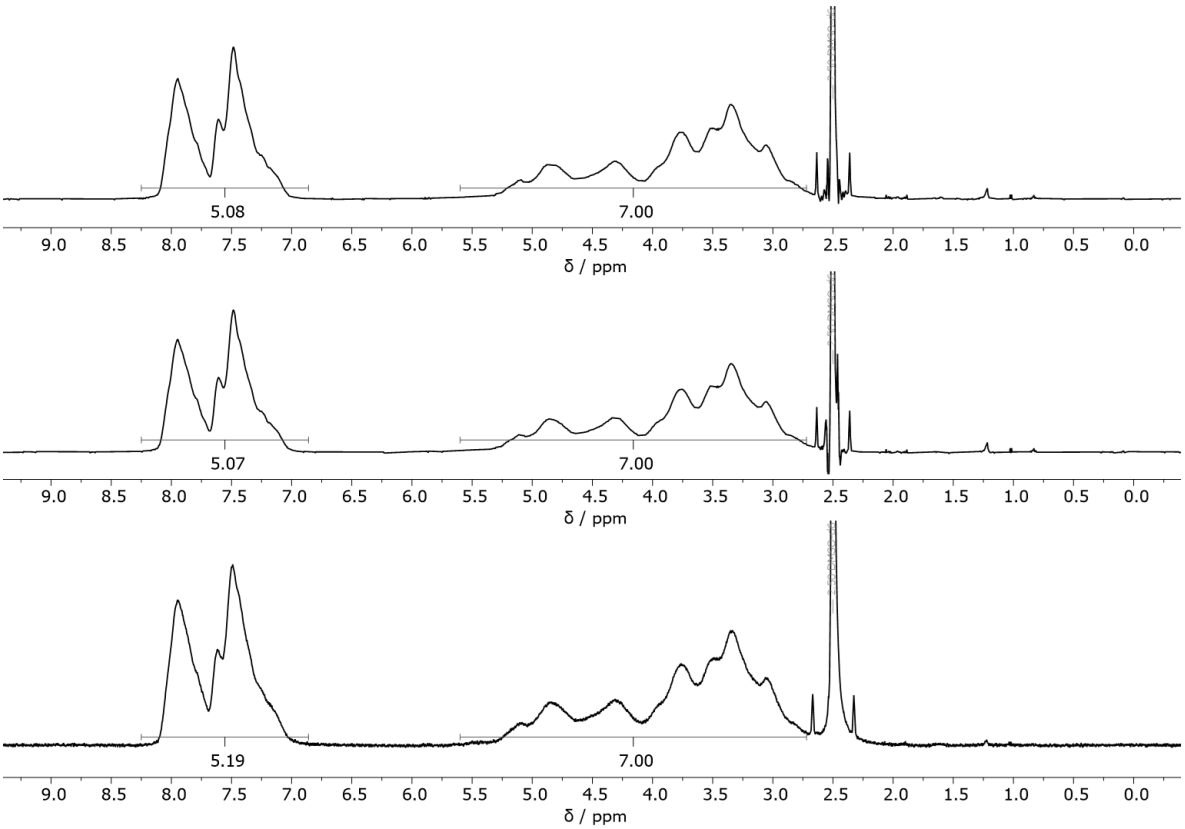

Figure S74 *^{1}H NMR (DMSO-d_6+TFA) spectra of CBz-2 (calculated average DS_{1H}=1.02±0.01).*

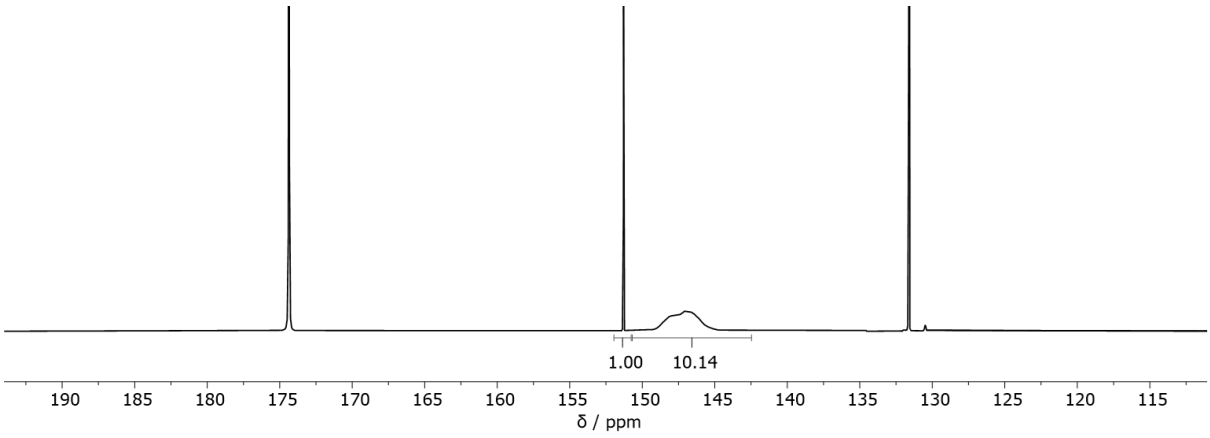

Figure S75 *^{31}P NMR ($CDCl_3$) spectrum of the phosphitylated CBz-2 (calculated: DS_{31P}=1.07). Signal assignment is analogous to* ***Figure S36****.*

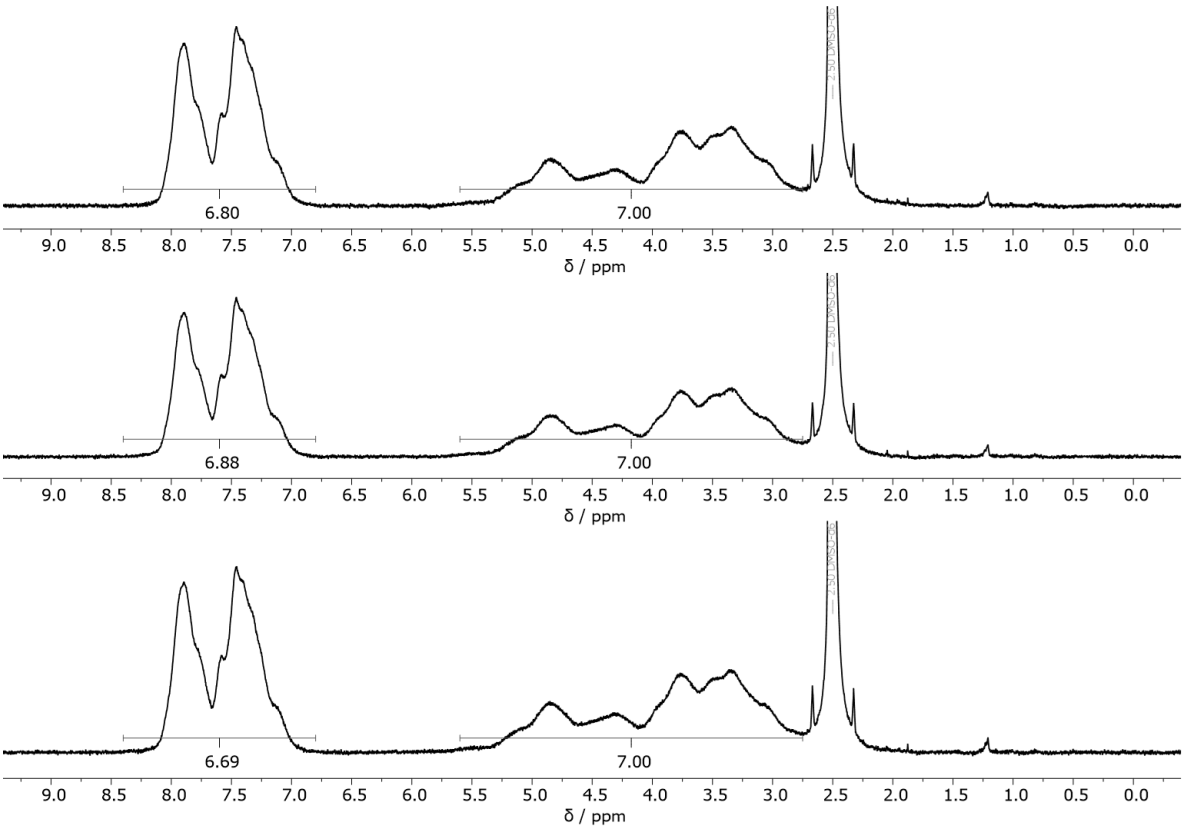

Figure S76 *^{1}H NMR (DMSO-d_6+TFA) spectra of CBz-3 (calculated average DS_{1H}=1.36±0.02).*

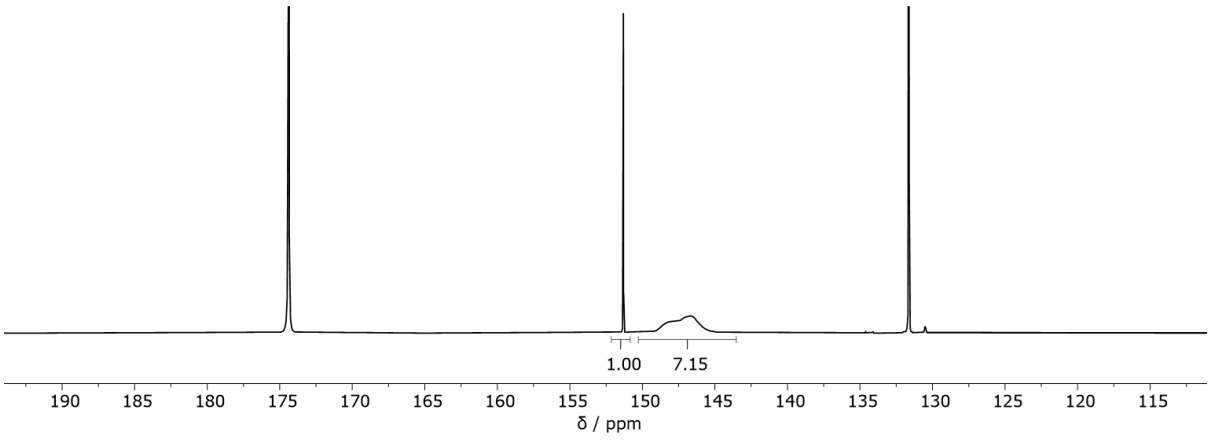

Figure S77 *^{31}P NMR ($CDCl_3$) spectrum of the phosphitylated CBz-3 (calculated: DS_{31P}=1.46). Signal assignment is analogous to* ***Figure S36****.*

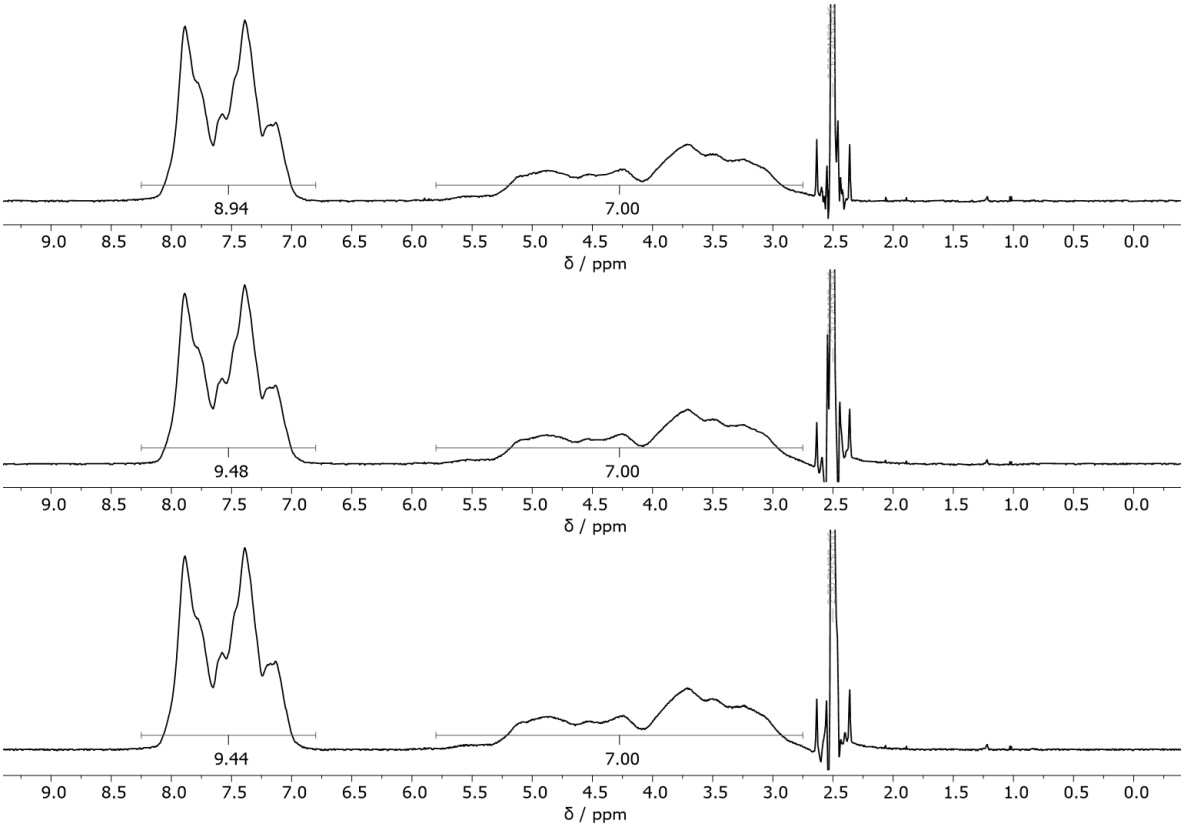

Figure S78 *^{1}H NMR (DMSO-d_6+TFA) spectra of CBz-4 (calculated average DS_{1H}=1.86±0.05).*

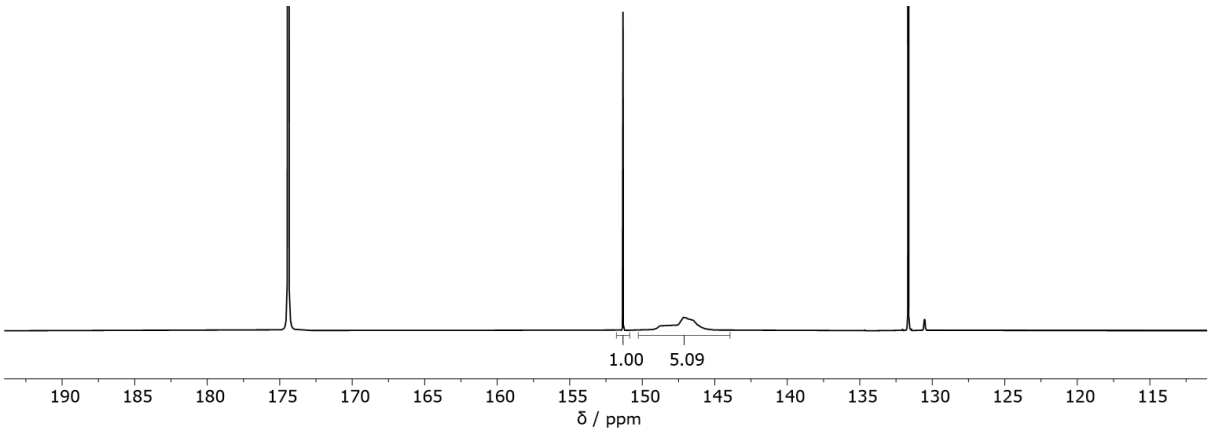

Figure S79 *^{31}P NMR ($CDCl_3$) spectrum of the phosphitylated CBz-4 (calculated: DS_{31P}=1.79). Signal assignment is analogous to* ***Figure S36****.*

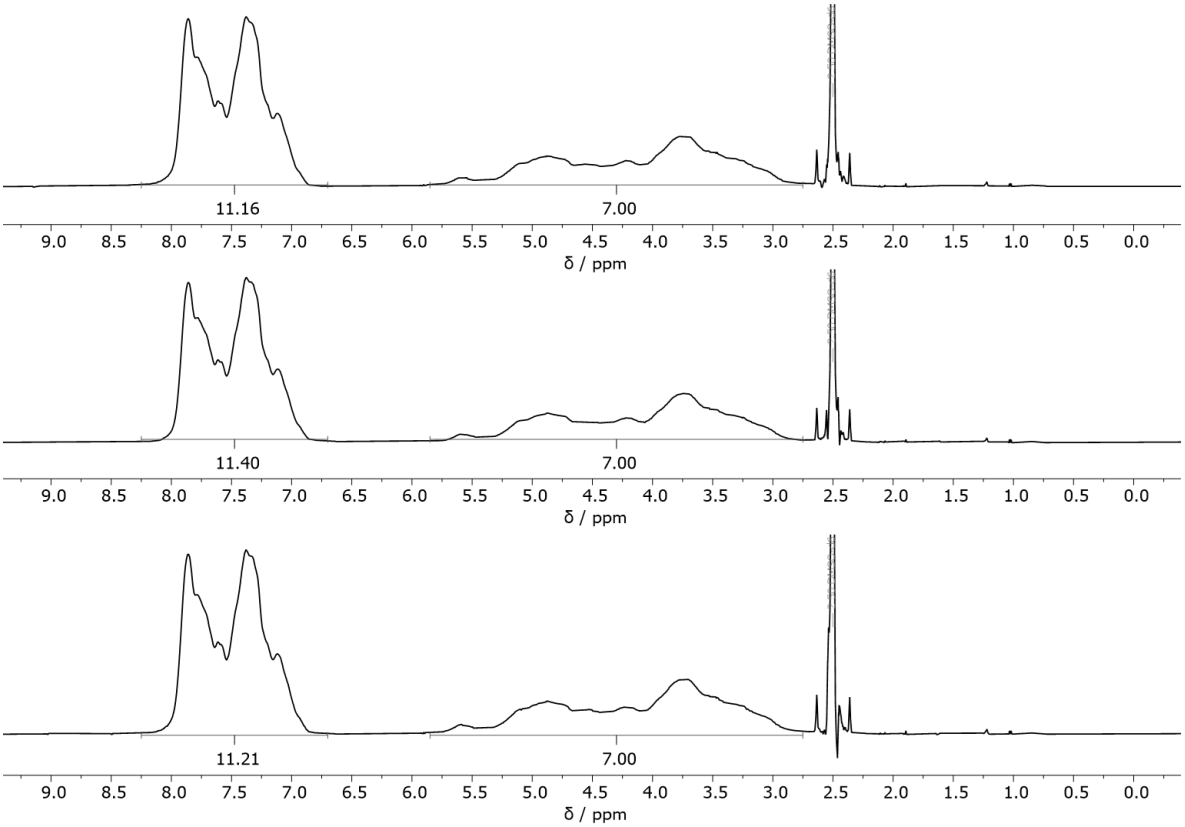

Figure S80 *^{1}H NMR (DMSO-d_6+TFA) spectra of CBz-5 (calculated average DS_{1H}=2.25±0.02).*

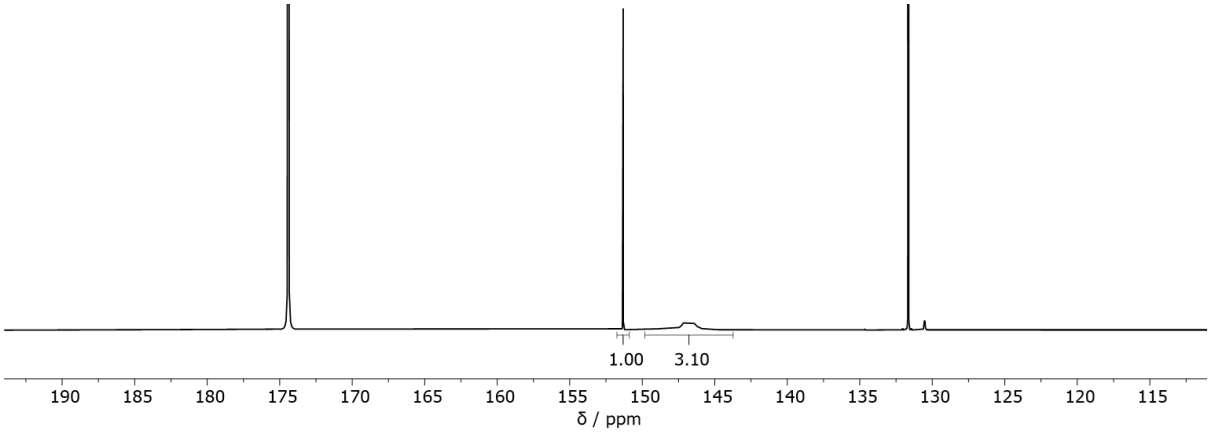

Figure S81 *^{31}P NMR ($CDCl_3$) spectrum of the phosphitylated CBz-5 (calculated: DS_{31P}=2.17). Signal assignment is analogous to* ***Figure S36****.*

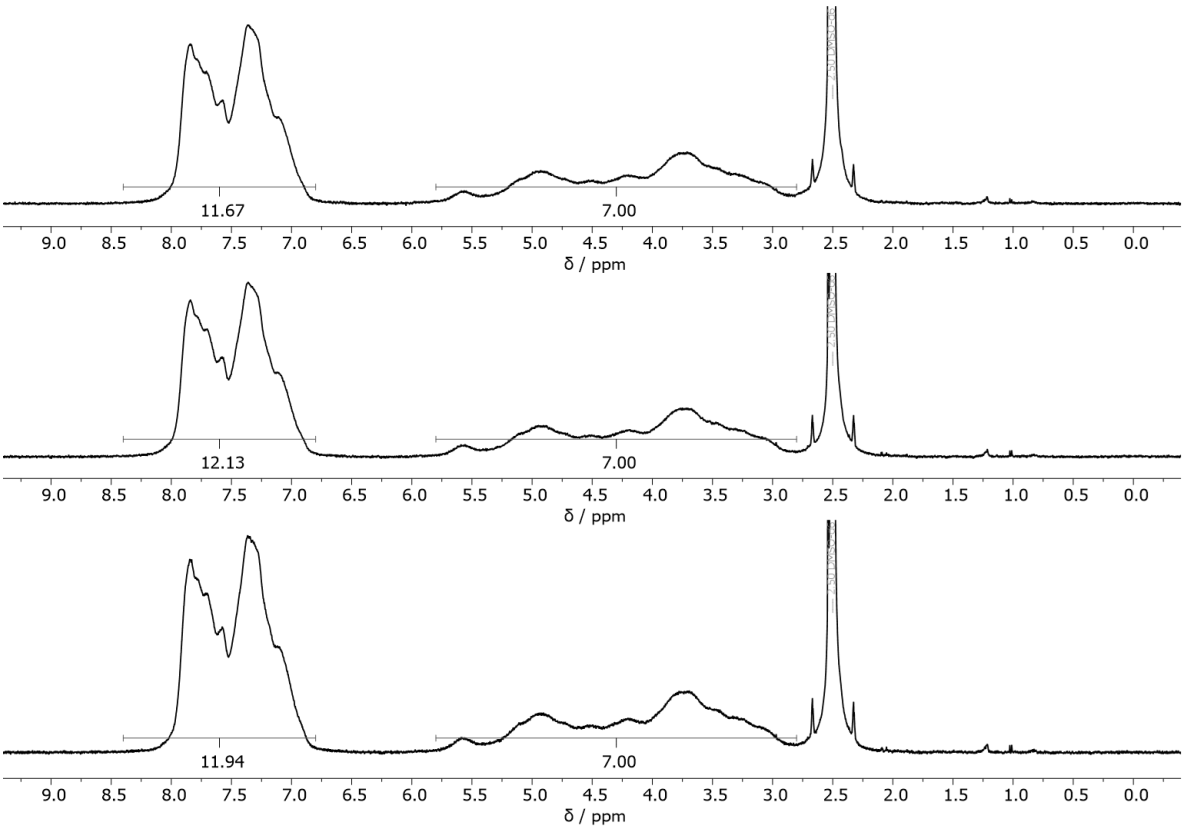

Figure S82 *^{1}H NMR (DMSO-d_6+TFA) spectra of CBz-6 (calculated average DS_{1H}=2.38±0.04).*

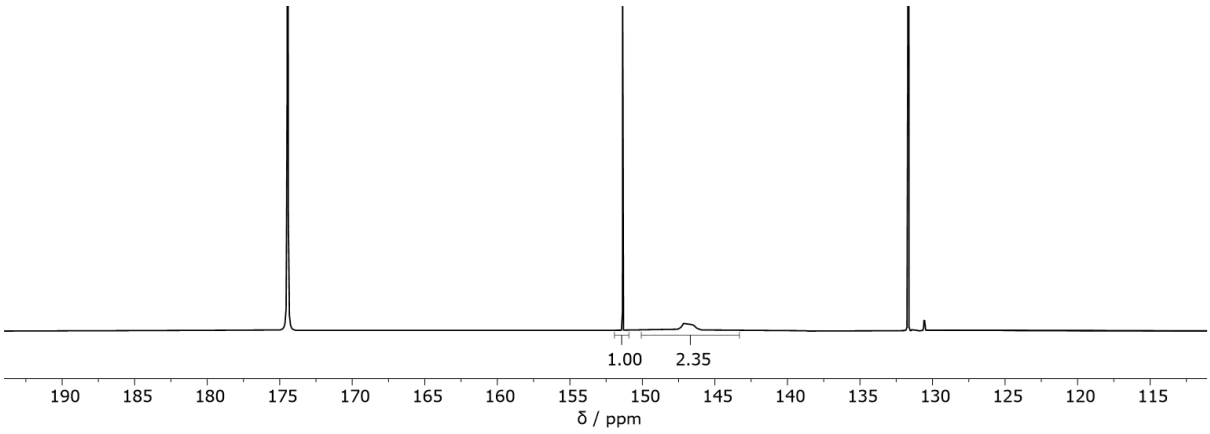

Figure S83 *^{31}P NMR ($CDCl_3$) spectrum of the phosphitylated CBz-6 (calculated: DS_{31P}=2.34). Signal assignment is analogous to* ***Figure S36****.*

Cellulose Laurates:

The peak assignment for cellulose laurates is exemplarily shown for CL-1.

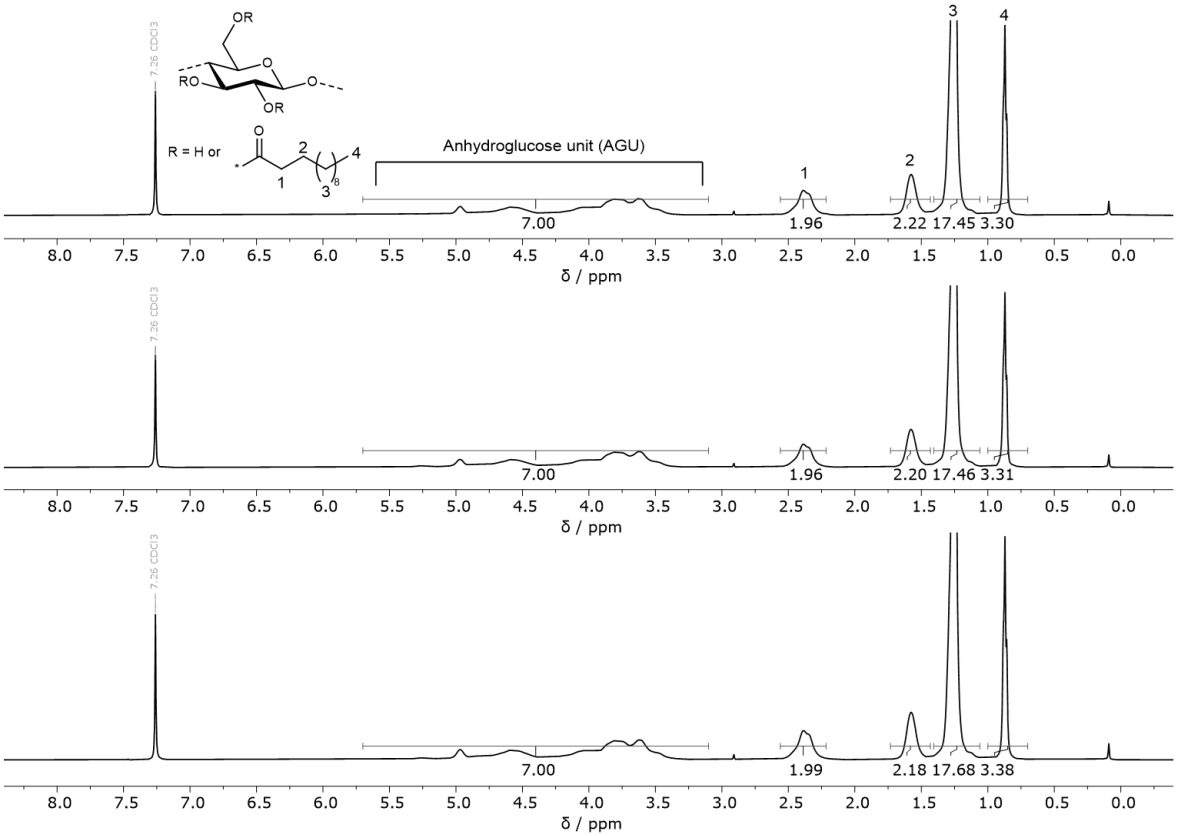

Figure S84 *^{1}H NMR ($CDCl_3$+TFA) spectra of CL-1 (calculated average DS_{1H}=1.11±0.01).*

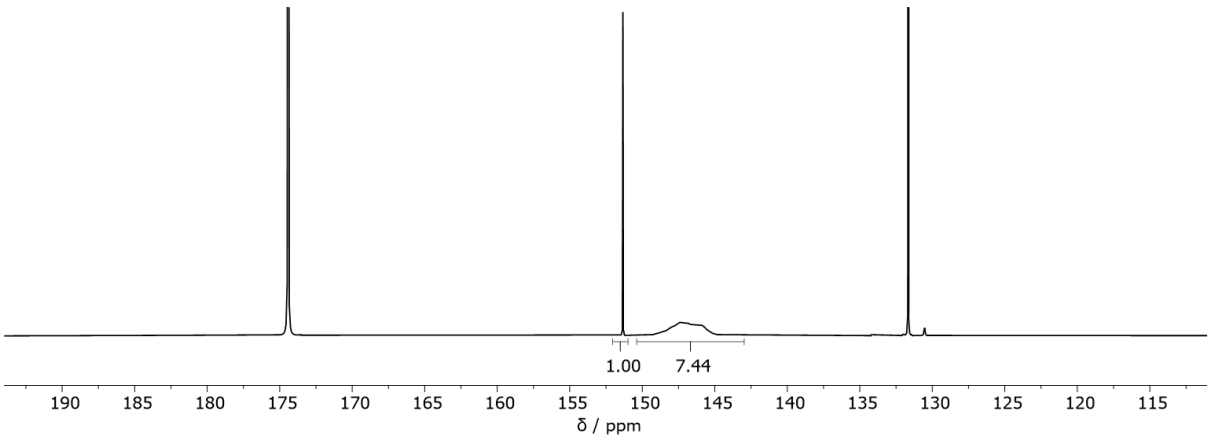

Figure S85 *^{31}P NMR ($CDCl_3$) spectrum of the phosphitylated CL-1 (calculated: DS_{31P}=1.13). Signal assignment is analogous to* ***Figure S36****.*

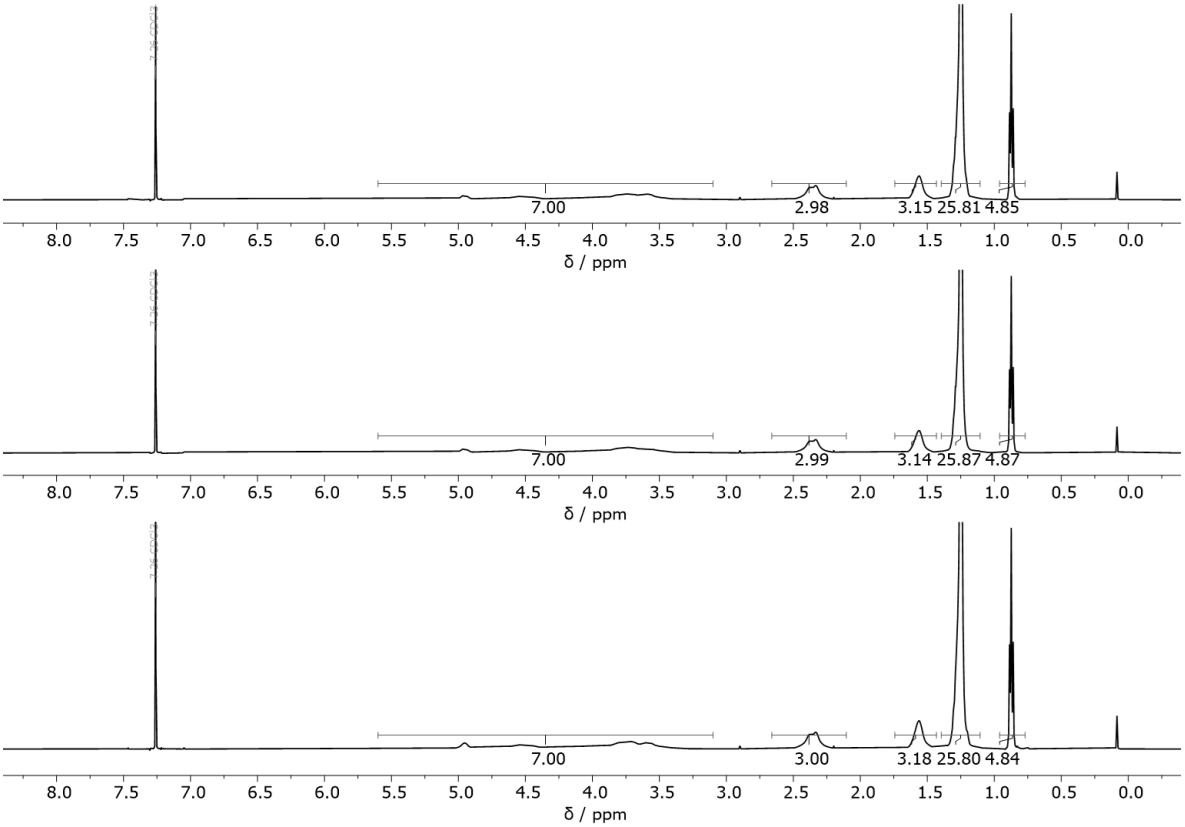

Figure S86 *^{1}H NMR ($CDCl_3$+TFA) spectra of CL-2 (calculated average DS_{1H}=1.61±0.01).*

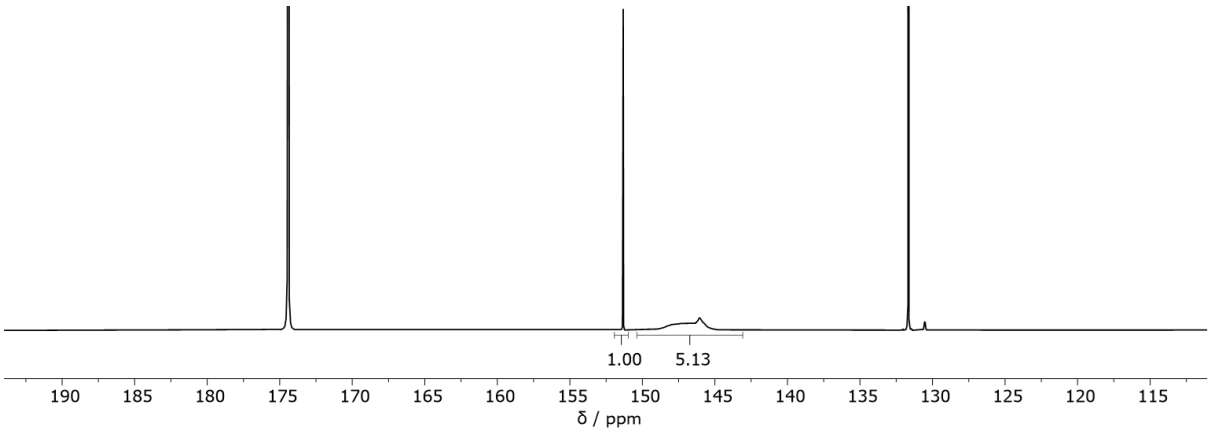

Figure S87 *^{31}P NMR ($CDCl_3$) spectrum of the phosphitylated CL-2 (calculated: DS_{31P}=1.49). Signal assignment is analogous to* ***Figure S36****.*

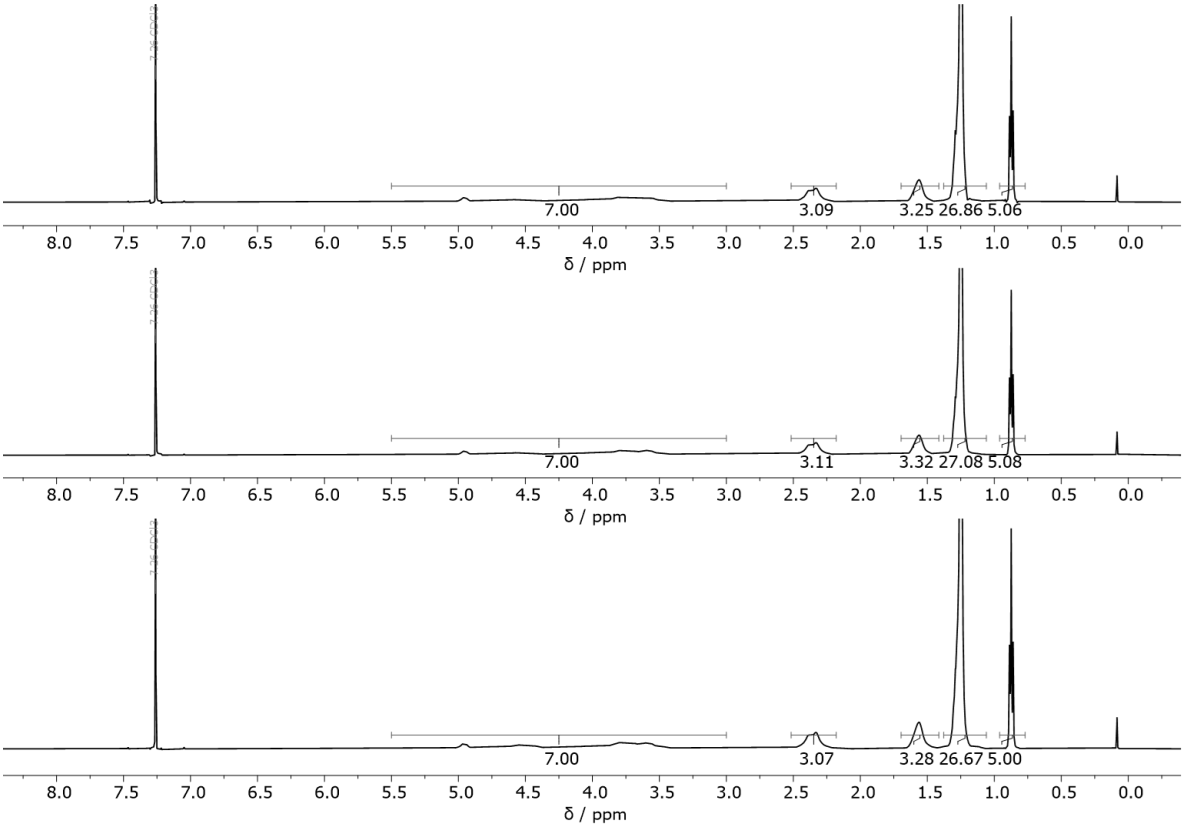

Figure S88 *^{1}H NMR ($CDCl_3$+TFA) spectra of CL-3 (calculated average DS_{1H}=1.68±0.01).*

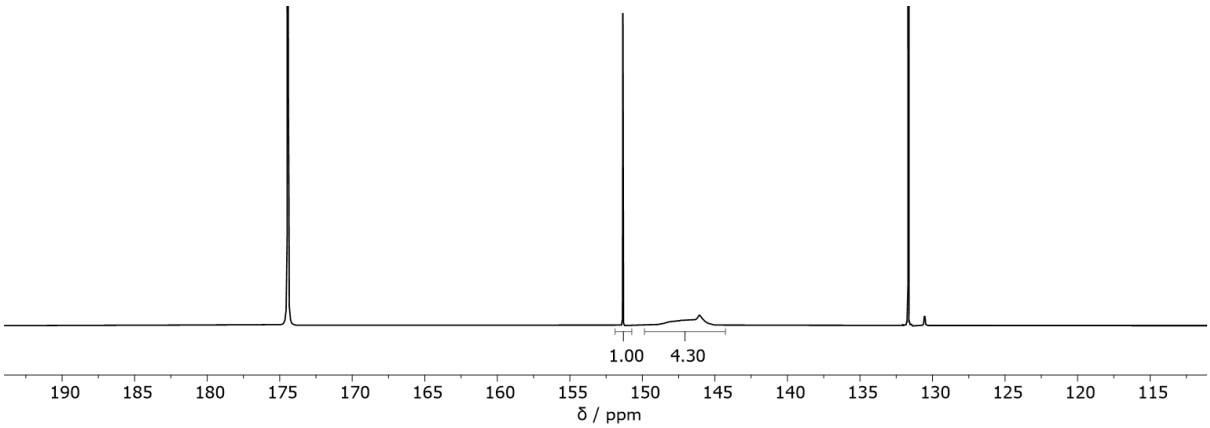

Figure S89 *^{31}P NMR ($CDCl_3$) spectrum of the phosphitylated CL-3 (calculated: DS_{31P}=1.65). Signal assignment is analogous to* ***Figure S36****.*

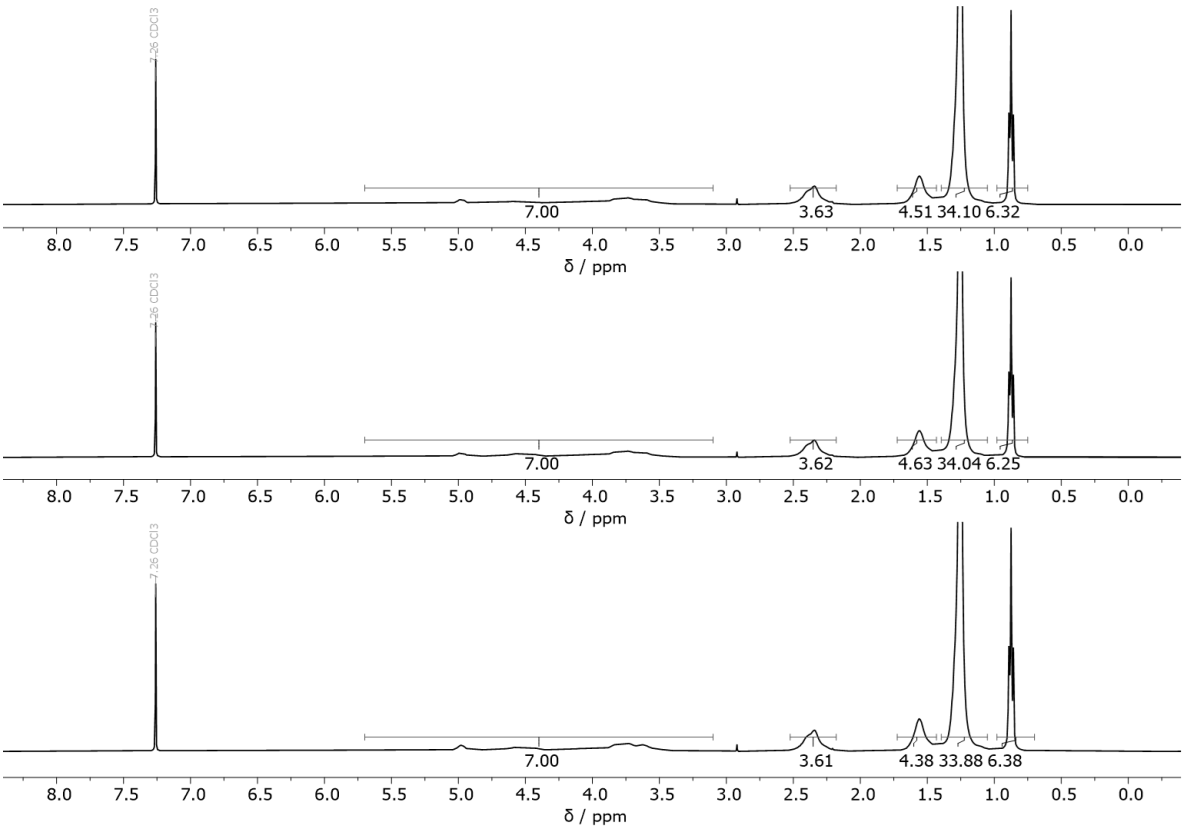

Figure S90 *^{1}H NMR ($CDCl_3$+TFA) spectra of CL-4 (calculated average DS_{1H}=2.11±0.02).*

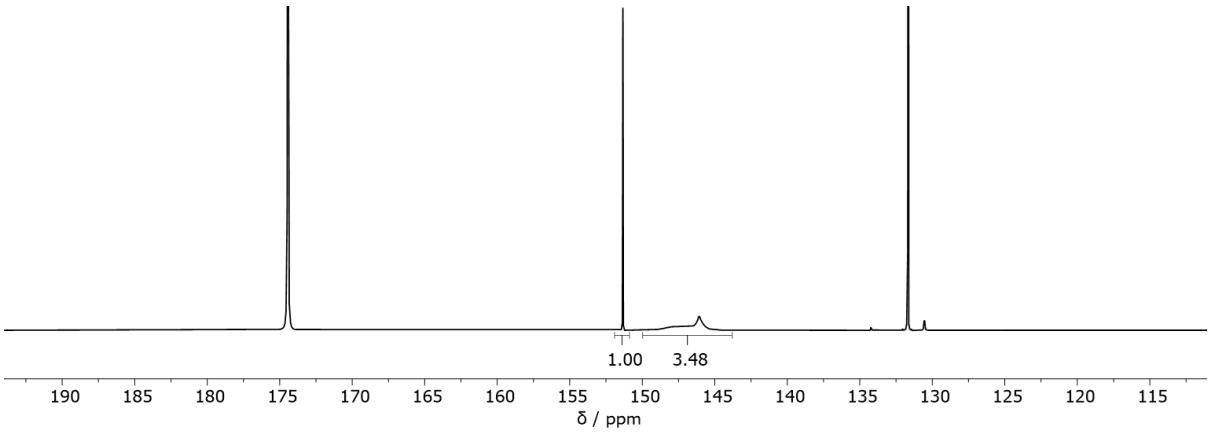

Figure S91 *^{31}P NMR ($CDCl_3$) spectrum of the phosphitylated CL-4 (calculated: DS_{31P}=1.83). Signal assignment is analogous to* ***Figure S36****.*

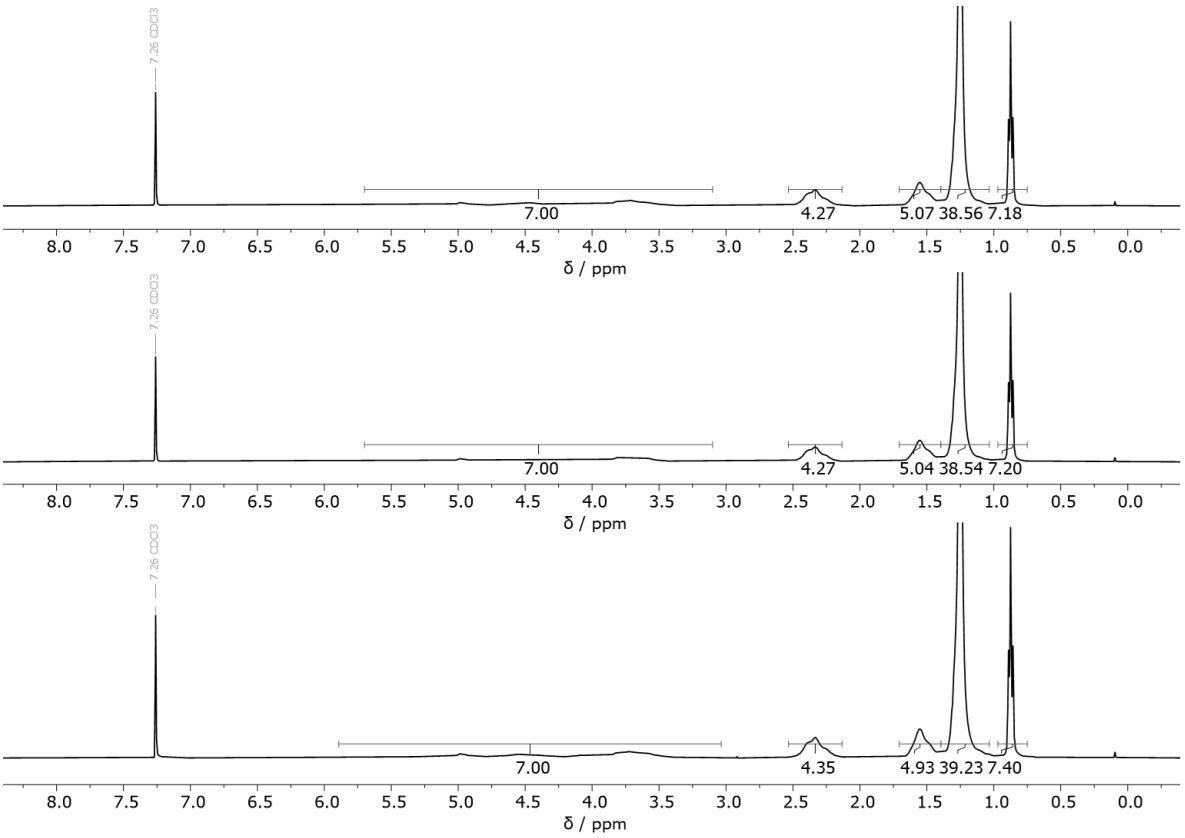

Figure S92 *^{1}H NMR ($CDCl_3$+TFA) spectra of CL-5 (calculated average DS_{1H}=2.42±0.03).*

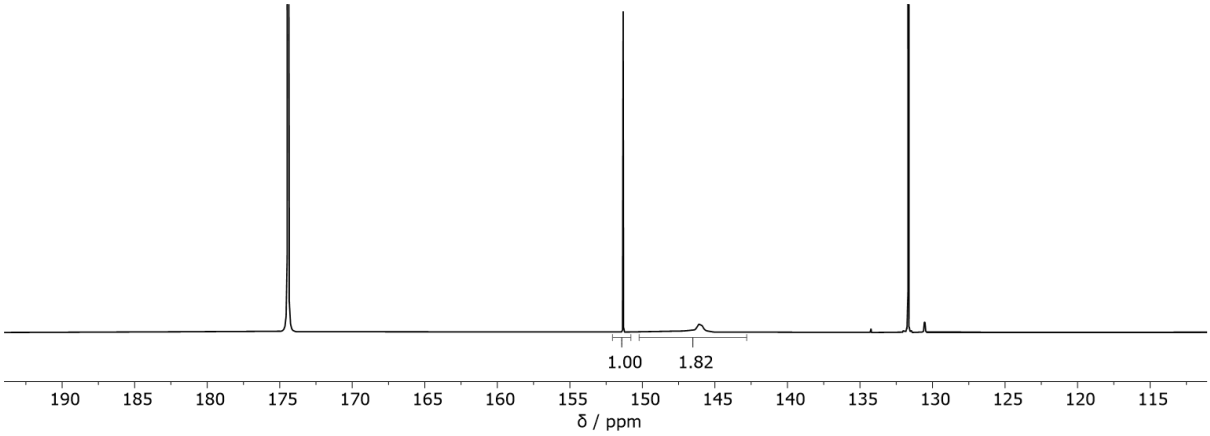

Figure S93 *^{31}P NMR ($CDCl_3$) spectrum of the phosphitylated CL-5 (calculated: DS_{31P}=2.28). Signal assignment is analogous to* ***Figure S36****.*

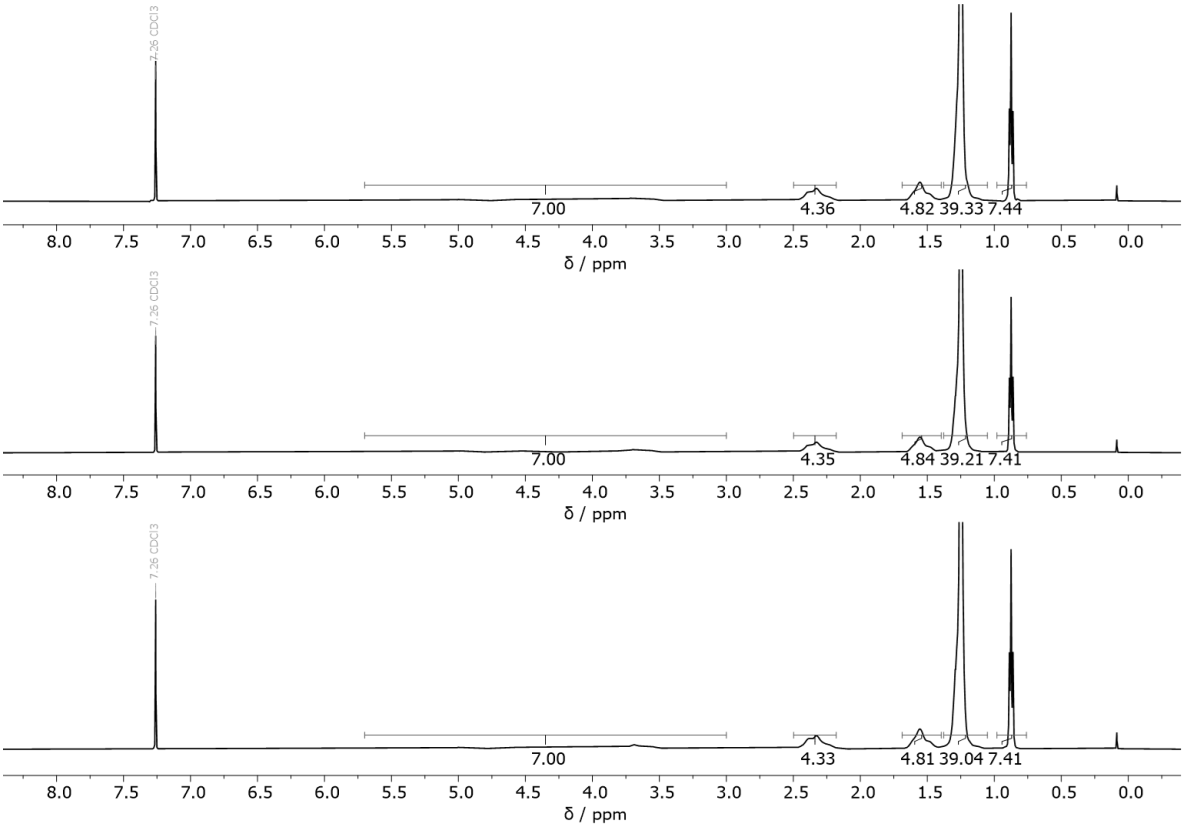

Figure S94 *^{1}H NMR ($CDCl_3$+TFA) spectra of CL-6 (calculated average DS_{1H}=2.47±0.01).*

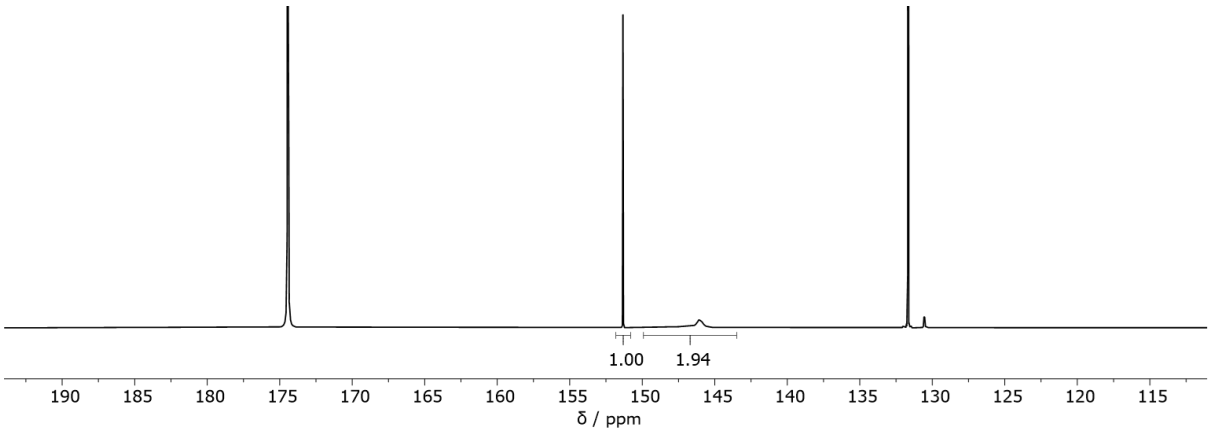

Figure S95 *^{31}P NMR ($CDCl_3$) spectrum of the phosphitylated CL-6 (calculated: DS_{31P}=2.25). Signal assignment is analogous to* ***Figure S36****.*

Procedure for the Preparation of Mixed Cellulose Acetates

The needed mass of cellulose acetate and microcrystalline cellulose to simulate different degrees of substitution were calculated according to equation (*26*). The two components were mixed and ground to a fine powder using a mortar.

$$m_{\mathrm{CAc}} = \frac{\frac{m_{\mathrm{MCC}}}{M_{\mathrm{MCC}}}}{\frac{DS_{\mathrm{CAc}}}{DS_{\mathrm{mix}}}} \times (DS_{\mathrm{CAc}} \times M_{\mathrm{Acetyl}} + M_{\mathrm{MCC}}) \qquad (26)$$

m_{CAc}: mass of cellulose acetate
m_{MCC}: mass of microcrystalline cellulose
M_{MCC}: molar mass of microcrystalline cellulose ($M_{\mathrm{MCC}} = 162.14\ \mathrm{g\,mol^{-1}}$)
DS_{CAc}: degree of substitution of cellulose acetate
DS_{mix}: intended degree of substitution of the mixture of cellulose acetate and microcrystalline cellulose
M_{Acetyl}: molar mass of the acetyl substituent $M_{\mathrm{Acetyl}} = 42.04\ \mathrm{g\,mol^{-1}}$

DS Determination by the ^{31}P NMR Method

The DS_{31P} was determined analogous as explained in chapter 6.3.1.

6.3.3. Cellulose Thionocarbamate Synthesis – Chapter 4.3

This chapter is based on previously published results by the author of this thesis:

Wolfs, J.; Nickisch, R.; Wanner, L.; Meier, M. A. R. Sustainable One-Pot Cellulose Dissolution and Derivatization via a Tandem Reaction in the DMSO/DBU/CO_2 Switchable Solvent System. *J. Am. Chem. Soc.* **2021**, *143* (44), 18693–18702.[201]

Text, figures, and data are reproduced from this article and were partially edited and extended with permission from the American Chemical Society, copyright 2021.

L. Wanner synthesized **CD-1**, **CD-2**, **CD-4**, **CD-5**, **CD-6**, **CC-1**, **CB-1**, **CB-2**, **CO-1**, **CD-2wt%**, **CD-4wt%**, **CD-5wt%**, *n*-dodecyl isocyanide, and oleyl isocyanide under supervision of the author. **CD-3**, **CC-2**, **CO-2**, **CD-REC**, and the model compounds were synthesized by the author.

Synthesis of *O*-Cellulose-*N*-*n*-Dodecyl Thiocarbamate (CD-1) Using *n*-Dodecyl Isothiocyanate

In a round-bottom flask, cellulose (300 mg, [monomeric unit]=1.85 mmol) was suspended in 8.8 mL dry DMSO under argon atmosphere followed by the dropwise addition of DBU (0.83 mL, 845 mg, 5.55 mmol, 3.0 eq. per AGU). After applying a CO_2 flow through the solution for 20 min at 40 °C using a balloon, a clear solution was obtained. *n*-Dodecyl isothiocyanate (1.26 g, 5.55 mmol, 3.0 eq. per AGU) was added dropwise over a period of 3 h. The temperature was then elevated to 70 °C and the mixture was stirred overnight. The modified cellulose precipitated during the reaction and the solid was filtrated, washed with 30 mL isopropanol, and then stirred under reflux in 50 mL isopropanol for 1 h. After vacuum filtration, the same procedure was repeated with 50 mL of water to remove residuals of DMSO and DBU and then dried under vacuum at 70 °C for 12 h. The final product was obtained as a yellow solid. The yield (71%) was calculated based on the DS_{31P} (analogous to equations (*20*) and (*21*)).

ATR-IR ν (cm^{-1}): 3672–3114 ν(O-H) and ν(N-H), 2954 ν_{as}(C-H_3), 2921 ν_{as}(C-H_2), 2851 ν_s(C-H_2), 1709 ν(C=O), 1524 δ(N-H), 1460 δ(CH_2), 1407, 1244 ν_{as}(N-(C=O)-O), 1154 ν(C=S), 1061 AGU ν(C-O).

^{1}H NMR (400 MHz, THF-d_8) δ_H (ppm): 9.07–7.22 (m, NH^{1}), 6.62–5.44 (m, NH^{2}), 5.38–2.70 (m, AGU, CH$_2^{3}$), 1.69–1.02 (m, CH$_2^{5,4}$), 0.99–0.73 (m, CH$_3^{6}$).
^{13}C NMR (126 MHz, THF-d_8) δ_C (ppm): 190.71, 46.34, 42.02, 33.09, 30.87, 30.54, 29.51, 28.15, 23.77, 14.67.

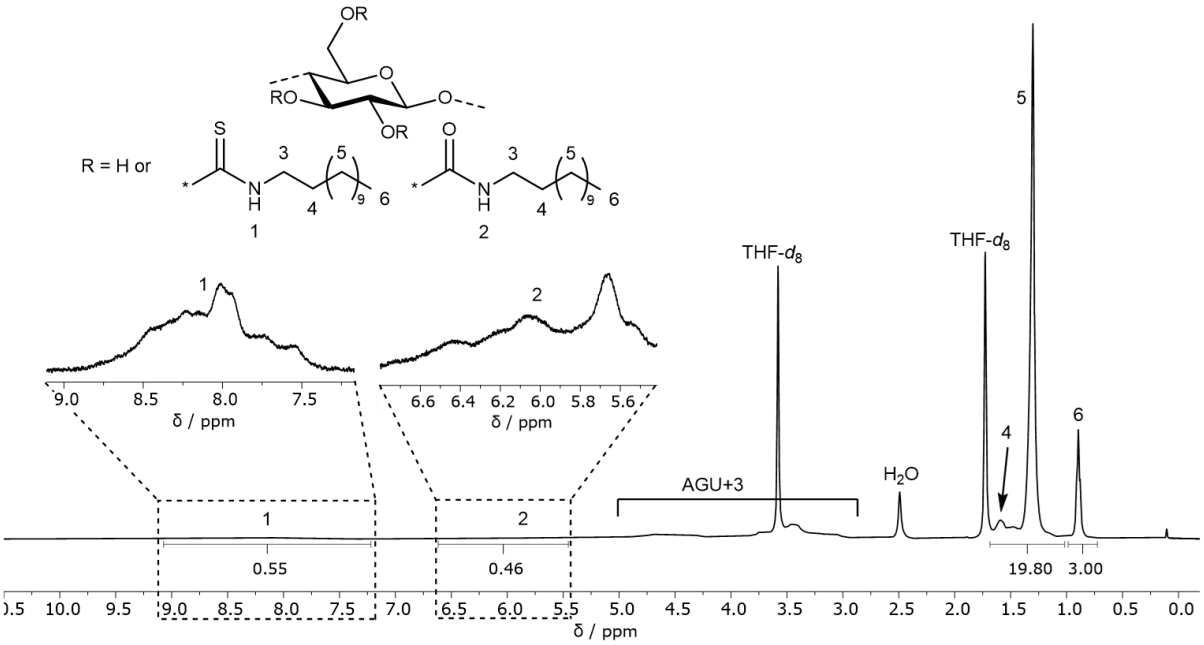

Figure S96 *^{1}H NMR spectrum (THF-d_8) of **CD-1**. AGU = Anhydroglucose unit.*

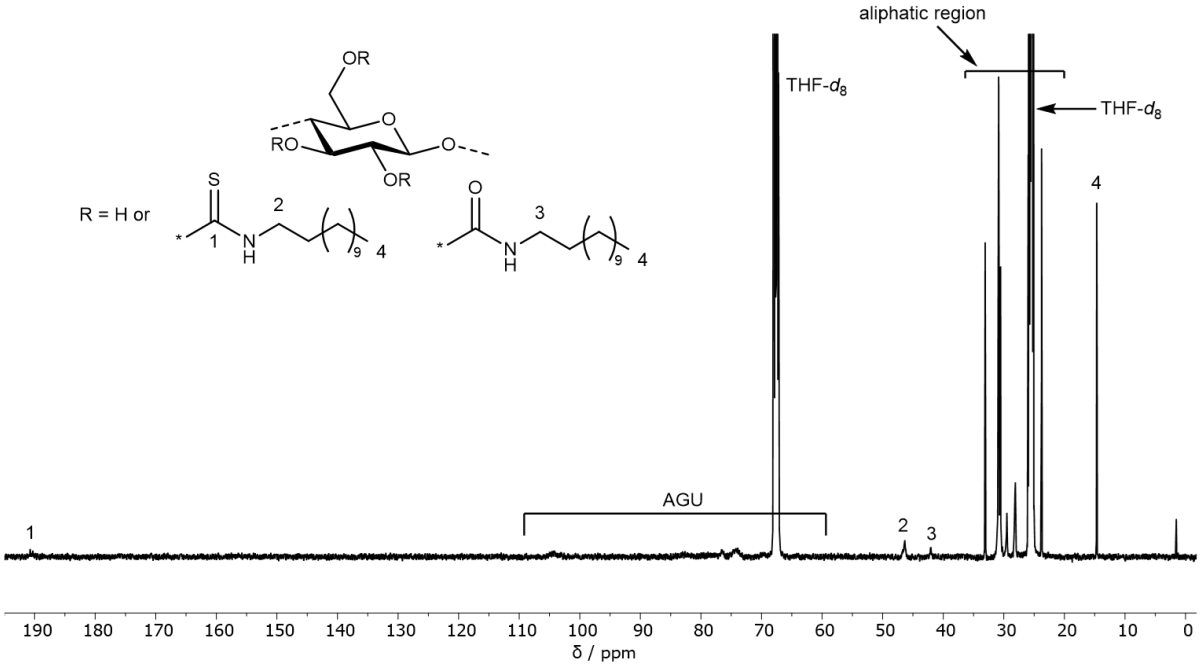

Figure S97 *^{13}C NMR spectrum (THF-d_8, 8192 scans) of **CD-1**. AGU = Anhydroglucose unit.*

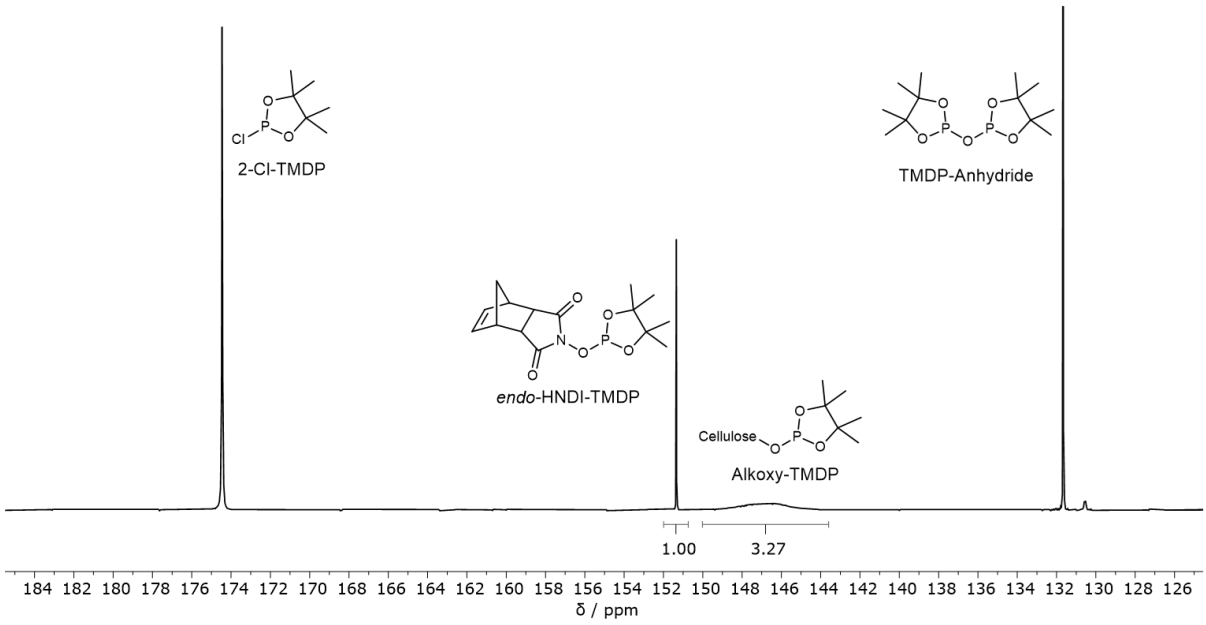

Figure S98 *^{31}P NMR ($CDCl_3$) spectrum of the phosphitylated* ***CD-1*** *(calculated: DS_{31P}=1.70).*

General Procedure for the Synthesis of *O*-Cellulose Thiocarbamates with *in situ* Generation of the Isothiocyanate

In a round-bottom flask, cellulose (250 mg, [monomeric unit]=1.54 mmol) was suspended in 7.3 mL dry DMSO under argon atmosphere, followed by the dropwise addition of DBU (0.69 mL, 705 mg, 4.63 mmol, 3.0 eq. per anhydroglucose unit (AGU)). After applying a CO_2 flow through the solution for 20 min at 40 °C using a balloon, a clear solution was obtained. In a syringe without piston, elemental sulfur (1.12 eq. of sulfur atoms per eq. isocyanide) was placed and the piston reinserted. The liquid isocyanide (1.0−6.0 eq. per AGU, depending on the experiment) was then sucked up with the prepared syringe and the resulting suspension of elemental sulfur in isocyanide was added dropwise to the reaction through a septum over a period of 3 h. The sulfur/isocyanide mixture was resuspended before every addition. The temperature was then elevated to 70 °C and the reaction was stirred overnight. The workup procedure was different, depending on the sample: Samples **CD-5**, **CD-6**, **CO-1**, **CO-2**, **CD-2wt%**, **CD-4wt%**, and **CD-5wt%** precipitated during the reaction as they became insoluble in DMSO (**Table 16**). In these cases, the precipitated solid was filtrated and washed with 30 mL isopropanol to receive the crude product. Samples **CD-2**, **CD-3**, **CD-4**, **CC-1**, **CC-2**, **CB-1**, and **CB-2** remained soluble in DMSO and therefore the homogeneous solution was added dropwise into 50 mL of isopropanol (r.t.) under vigorous stirring to precipitate the modified cellulose. The solid was filtrated and washed with 20 mL isopropanol to receive the crude product. The crude product of all samples was purified by stirring in 50 mL isopropanol under reflux for 1 h and subsequently vacuum filtrated. The same procedure was repeated with 50 mL of water to remove residuals of DMSO and DBU and the pure product was then dried under vacuum at 70 °C for 12 h. The final product was obtained as a white or yellow solid. Yields were calculated based on the DS_{31P} (analogous to equations (*20*) and (*21*)) and ranged from 51 to 81%.

***O*-Cellulose-*N*-*n*-dodecyl thiocarbamate** (**CD-2**): **Yield:** 81%

ATR-IR ν (cm^{-1}): 3659–2999 ν(O-H) and ν(N-H), 2954 ν_{as}(C-H_3), 2921 ν_{as}(C-H_2), 2853 ν_{s}(C-H_2), 1699 ν(C=O), 1532 δ(N-H), 1460 δ(CH_2), 1244 ν_{as}(N-(C=O)-O), 1154 ν(C=S), 1023 AGU ν(C-O).
^{1}H NMR (400 MHz, DMSO-d_6) δ_H (ppm): 10.25–8.67 (m, NH^1), 7.60–6.22 (m, NH^2), 5.79–2.76 (m, AGU, CH_2^3), 1.77–0.95 (m, $CH_2^{5,4}$), 0.93–0.66 (m, CH_3^6).

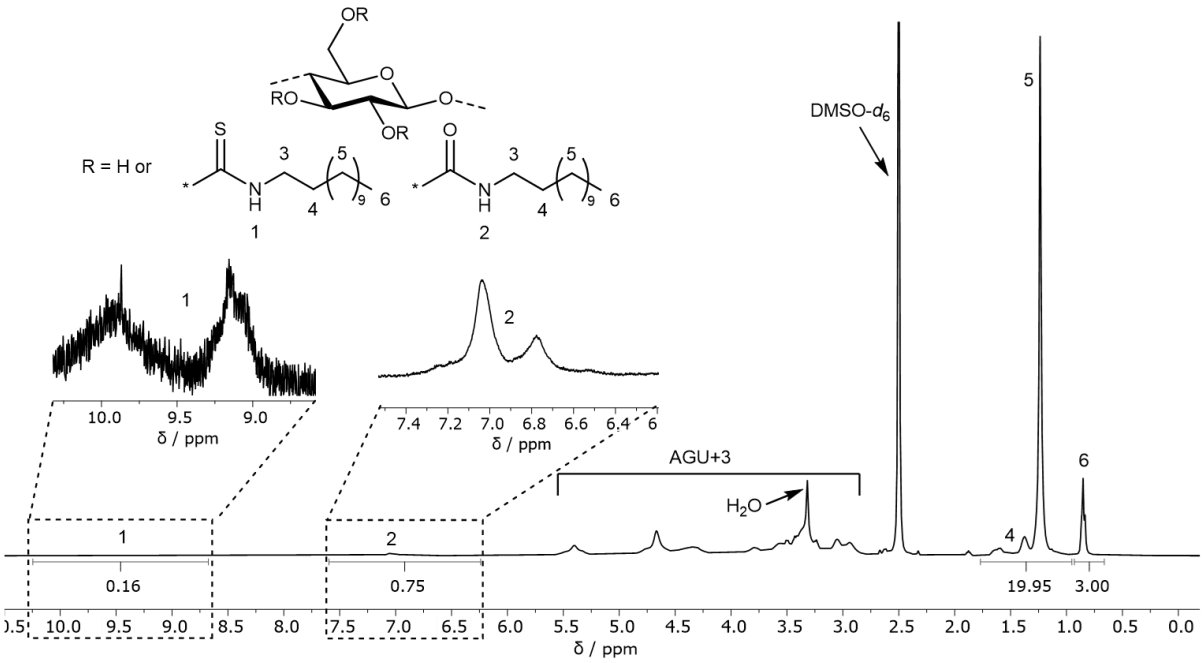

Figure S99 *^{1}H NMR spectrum (DMSO-d_6) of **CD-2**. AGU = Anhydroglucose unit.*

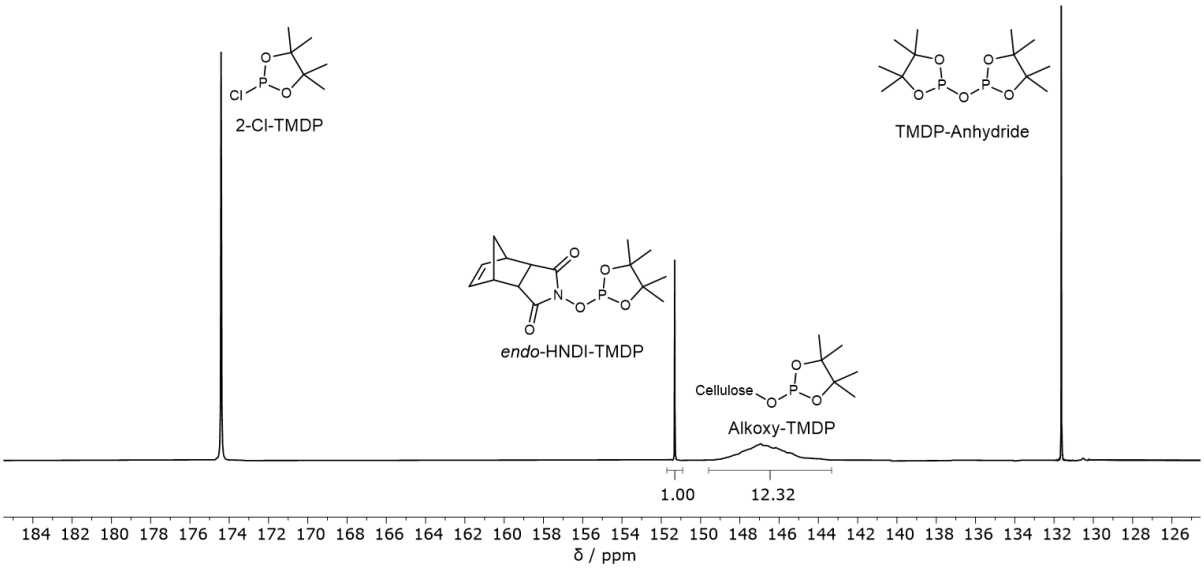

Figure S100 *^{31}P NMR ($CDCl_3$) spectrum of the phosphitylated **CD-2** (calculated: DS_{31P}=0.52).*

***O*-Cellulose-*N*-*n*-dodecyl thiocarbamate** (**CD-3**): **Yield:** 75%

ATR-IR ν (cm^{-1}): 3672–3100 ν(O-H) and ν(N-H), 2921 ν_{as}(C-H_2), 2853 ν_s(C-H_2), 1703 ν(C=O), 1528 δ(N-H), 1462 δ(CH_2), 1407, 1249 ν_{as}(N-(C=O)-O), 1150 ν(C=S), 1022 AGU ν(C-O).
^{1}H NMR (400 MHz, DMSO-d_6) δ_H (ppm): 9.39–8.65 (m, NH^1), 7.53–6.24 (m, NH^2), 5.77–2.72 (m, AGU, CH_2^3), 1.76–0.95 (m, $CH_2^{5,4}$), 0.88–0.73 (m, CH_3^6).

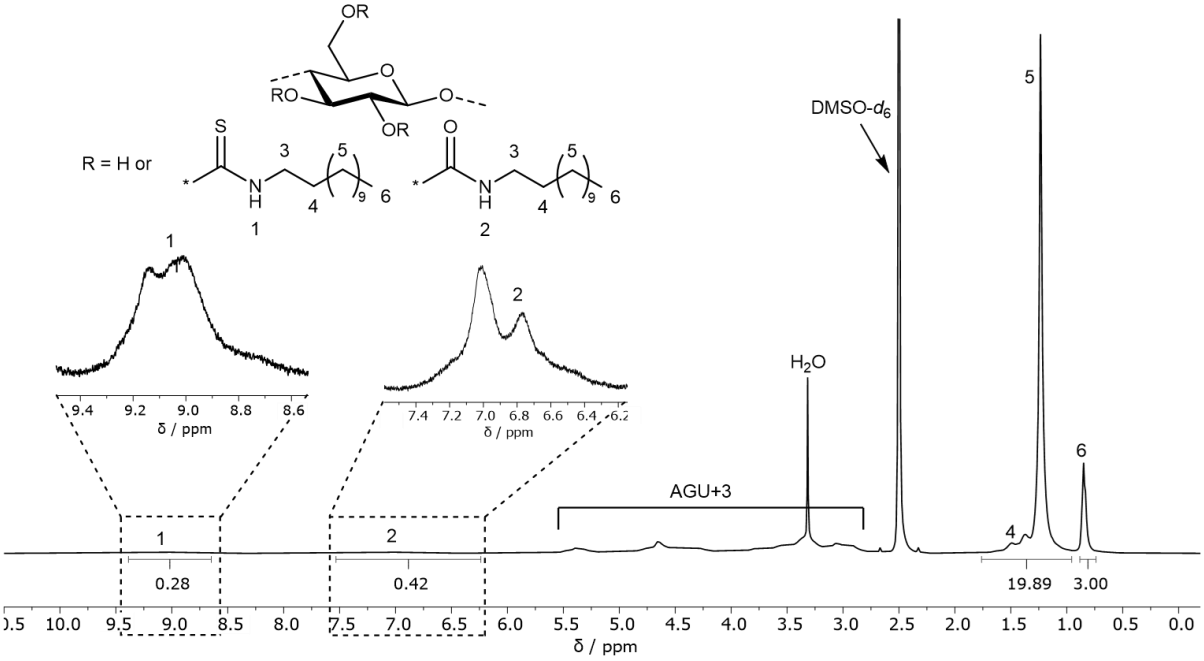

Figure S101 *^{1}H NMR spectrum (DMSO-d_6) of **CD-3**. AGU = Anhydroglucose unit.*

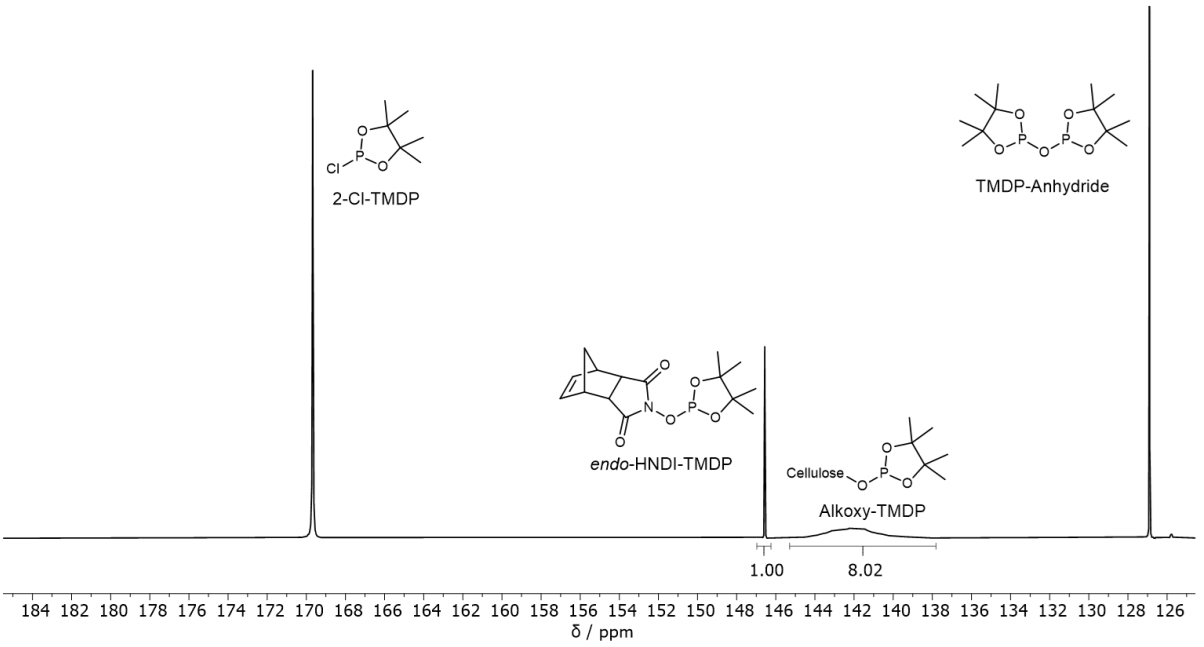

Figure S102 *^{31}P NMR ($CDCl_3$) spectrum of the phosphitylated **CD-3** (calculated: DS_{31P}=0.89).*

***O*-Cellulose-*N*-*n*-dodecyl thiocarbamate** (**CD-4**): **Yield:** 80%

ATR-IR ν (cm^{-1}): 3657–3106 ν(O-H) and ν(N-H), 2954 ν_{as}(C-H_3), 2921 ν_{as}(C-H_2), 2853 ν_s(C-H_2), 1705 ν(C=O), 1526 δ(N-H), 1460 δ(CH_2), 1409, 1249 ν_{as}(N-(C=O)-O), 1156 ν(C=S), 1057 AGU ν(C-O).
^{1}H NMR (400 MHz, DMSO-d_6) δ_H (ppm): 9.97–8.02 (m, NH^1), 7.54–6.21 (m, NH^2), 5.83–2.76 (m, AGU, CH_2^3), 1.74–0.96 (m, $CH_2^{5,4}$), 0.94–0.64 (m, CH_3^6).

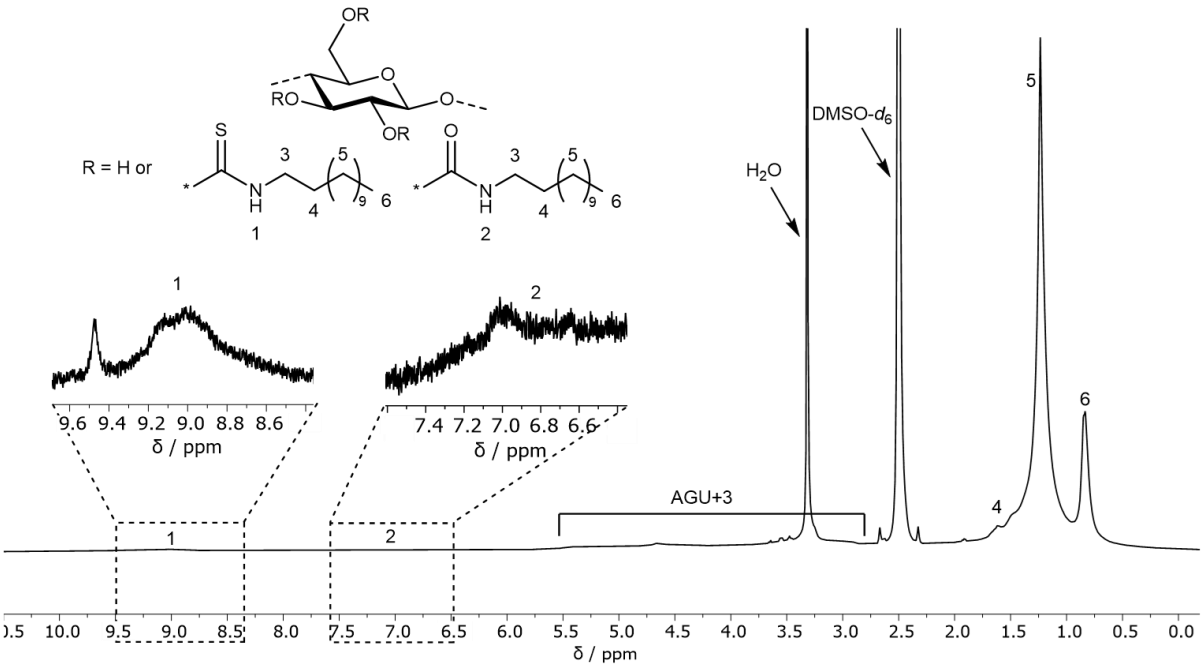

Figure S103 *^{1}H NMR spectrum (DMSO-d_6) of **CD-4**. AGU = Anhydroglucose unit.*

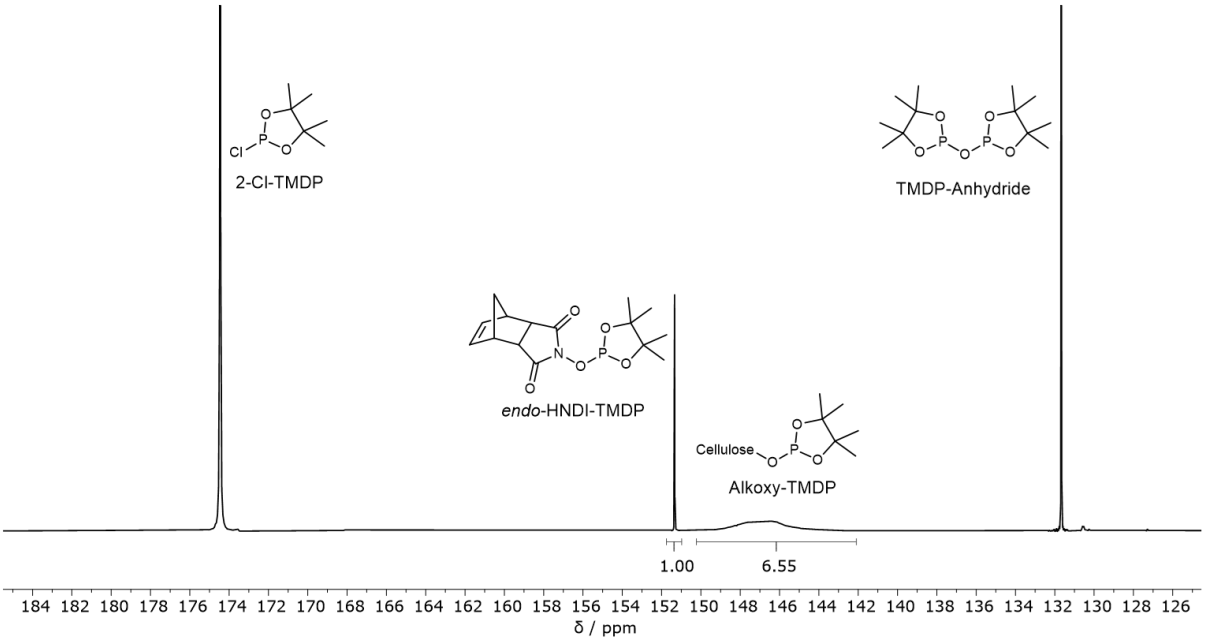

Figure S104 *^{31}P NMR ($CDCl_3$) spectrum of the phosphitylated **CD-4** (calculated: DS_{31P}=1.07).*

***O*-Cellulose-*N*-*n*-dodecyl thiocarbamate** (**CD-5**): **Yield:** 69%

ATR-IR ν (cm^{-1}): 3684–3116 ν(O-H) and ν(N-H), 2954 ν_{as}(C-H_3), 2921 ν_{as}(C-H_2), 2853 ν_s(C-H_2), 1709 ν(C=O), 1530 δ(N-H), 1458 δ(CH_2), 1409, 1246 ν_{as}(N-(C=O)-O), 1154 ν(C=S), 1063 AGU ν(C-O).
^{1}H NMR (400 MHz, THF-d_8) δ_H (ppm): 9.09–7.40 (m, NH^1), 7.12–5.51 (m, NH^2), 5.42–2.84 (m, AGU, CH_2^3), 1.64–1.08 (m, $CH_2^{5,4}$), 0.99–0.74 (m, CH_3^6).

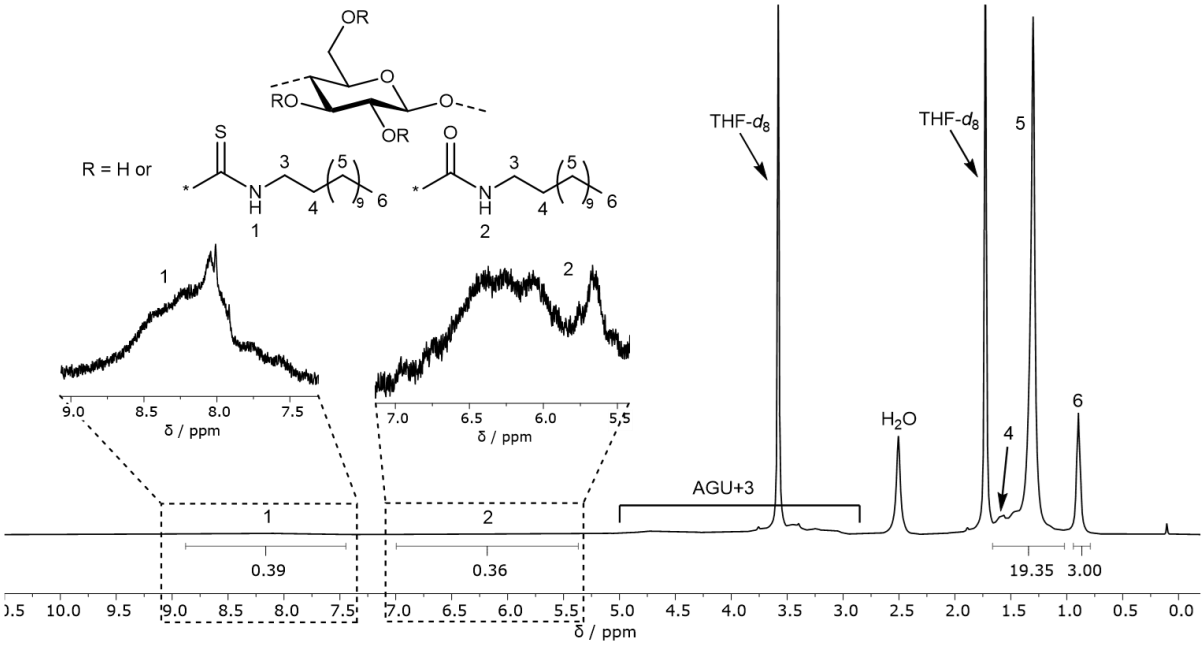

Figure S105 *^{1}H NMR spectrum (THF-d_8) of **CD-5**. AGU = Anhydroglucose unit.*

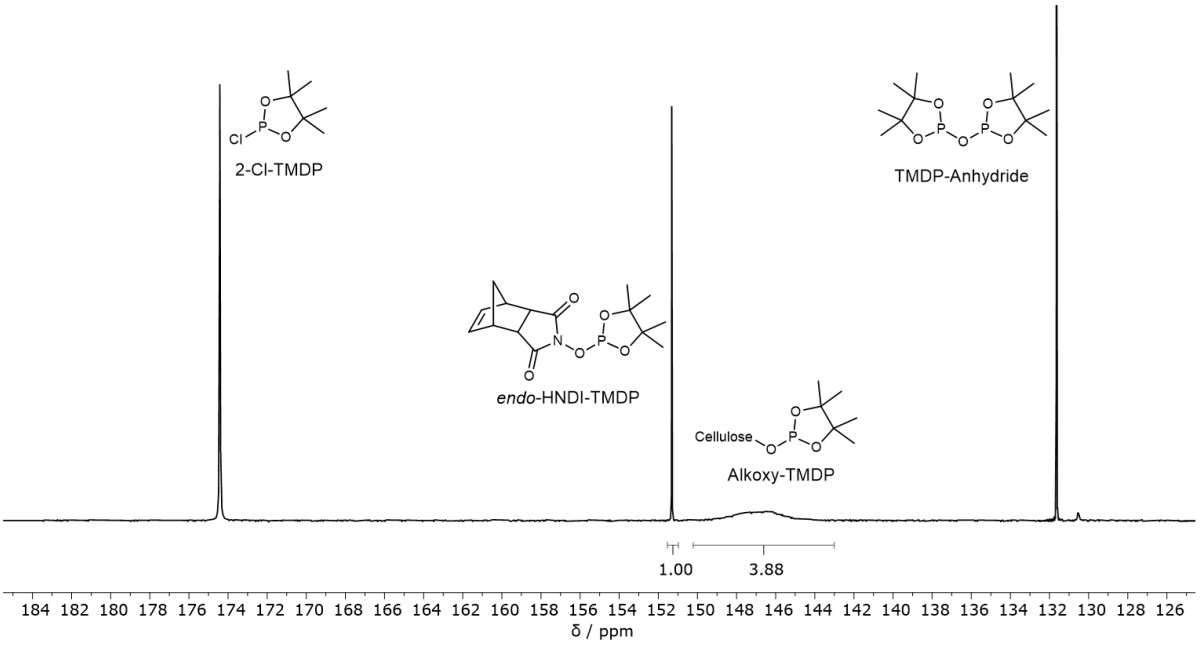

Figure S106 *^{31}P NMR ($CDCl_3$) spectrum of the phosphitylated **CD-5** (calculated: DS_{31P}=1.56).*

***O*-Cellulose-*N*-*n*-dodecyl thiocarbamate** (**CD-6**): **Yield:** 51%

ATR-IR ν (cm^{-1}): 3614–3131 ν(O-H) and ν(N-H), 2954 ν_{as}(C-H_3), 2921 ν_{as}(C-H_2), 2851 ν_{s}(C-H_2), 1720 (C=O), 1524 δ(N-H), 1465 δ(CH_2), 1407, 1246 ν_{as}(N-(C=O)-O), 1150 ν(C=S), 1061 AGU ν(C-O).
^{1}H NMR (400 MHz, THF-d_8) δ_H (ppm): 9.00–7.28 (m, NH^1), 6.48–5.36 (m, NH^2), 5.26–2.70 (m, AGU, CH_2^3), 1.65–1.09 (m, $CH_2^{5,4}$), 0.97–0.79 (m, CH_3^6).

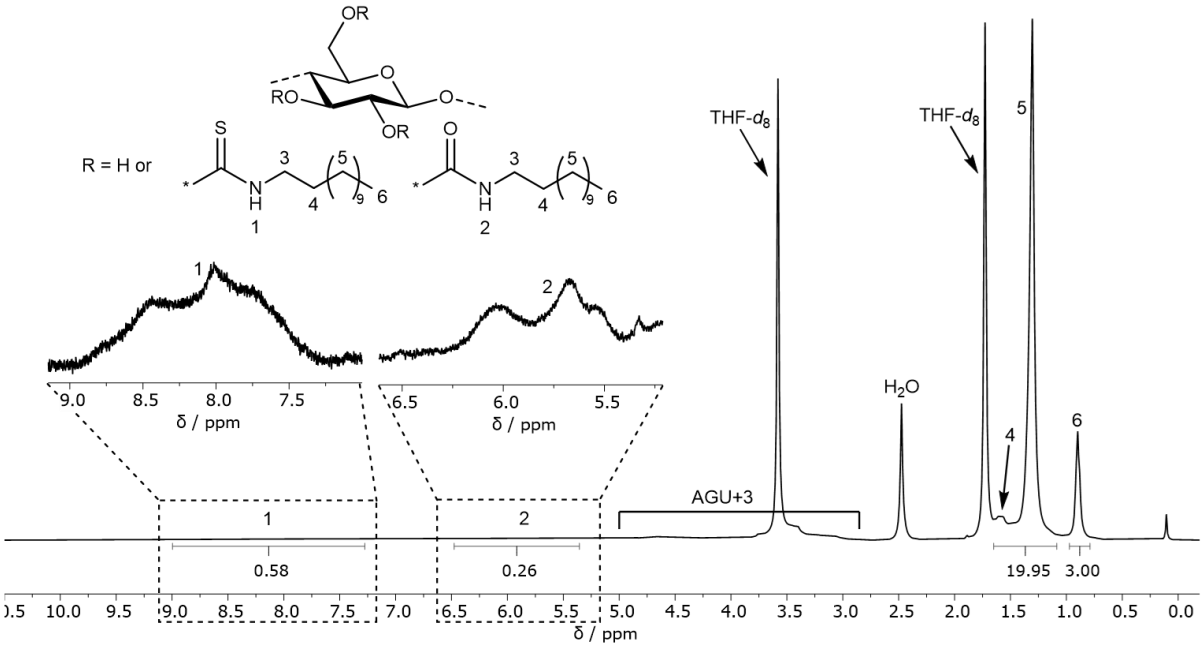

Figure S107 *^{1}H NMR spectrum (THF-d_8) of **CD-6**. AGU = Anhydroglucose unit.*

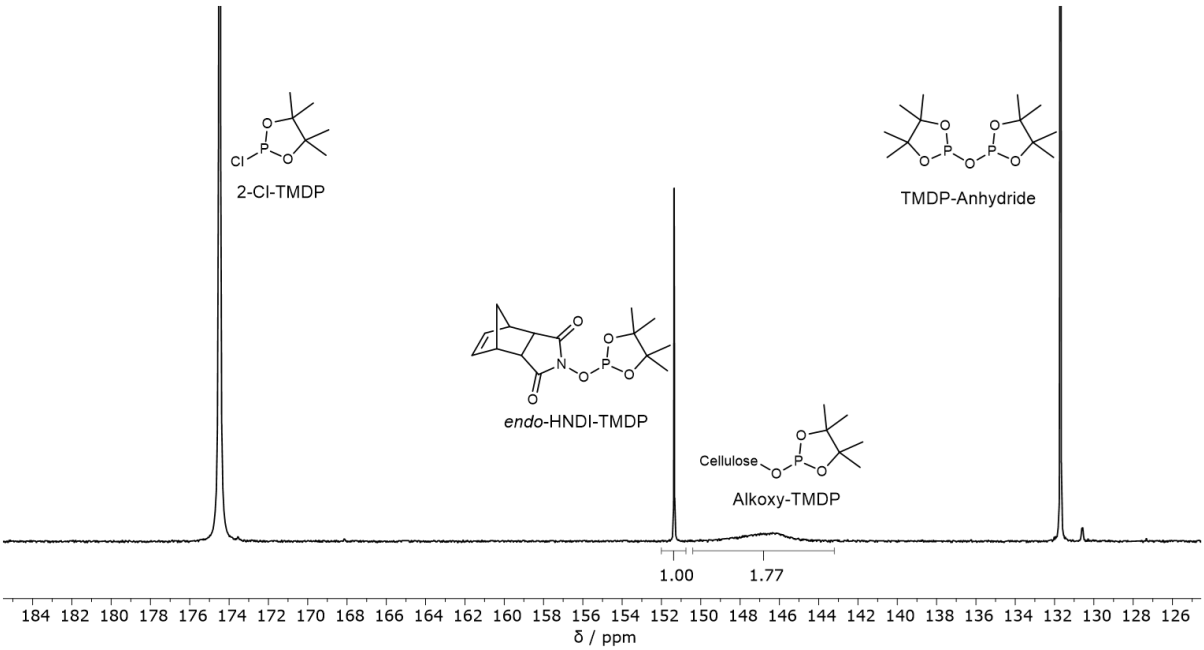

Figure S108 *^{31}P NMR ($CDCl_3$) spectrum of the phosphitylated **CD-6** (calculated: DS_{31P}=2.16).*

***O*-Cellulose-*N*-cyclohexyl thiocarbamate** (**CC-1**): **Yield:** 71%

ATR-IR ν (cm^{-1}): 3659–3059 ν(O-H) and ν(N-H), 2927 ν_{as}(C-H_2), 2855 ν_s(C-H_2), 1703 ν(C=O), 1520 δ(N-H), 1450 δ(CH_2), 1409, 1250 ν_{as}(N-(C=O)-O), 1160 ν(C=S), 1028 AGU ν(C-O).
^{1}H NMR (400 MHz, DMSO-d_6) δ_H (ppm): 9.57–8.40 (m, NH^1), 7.60–5.98 (m, NH^2), 5.74–2.79 (m, AGU, CH^3), 2.18–1.42 (m, CH_2^4), 1.42–0.65 (m, CH_2^5).

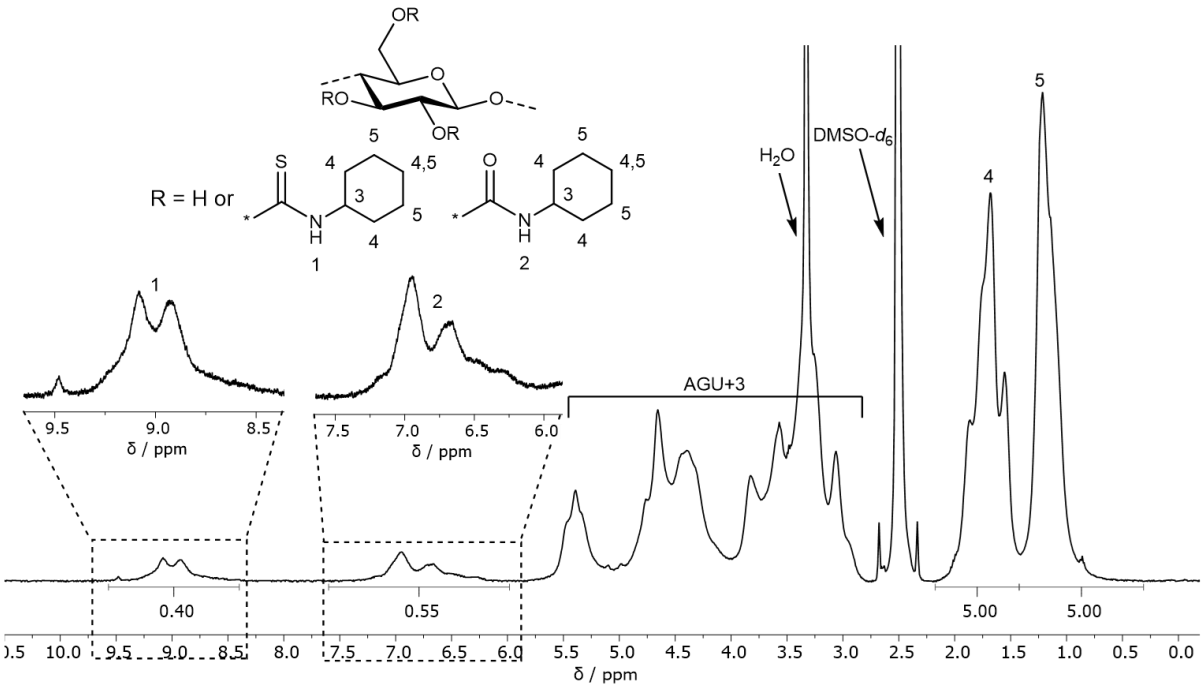

Figure S109 *^{1}H NMR spectrum (DMSO-d_6) of **CC-1**. AGU = Anhydroglucose unit.*

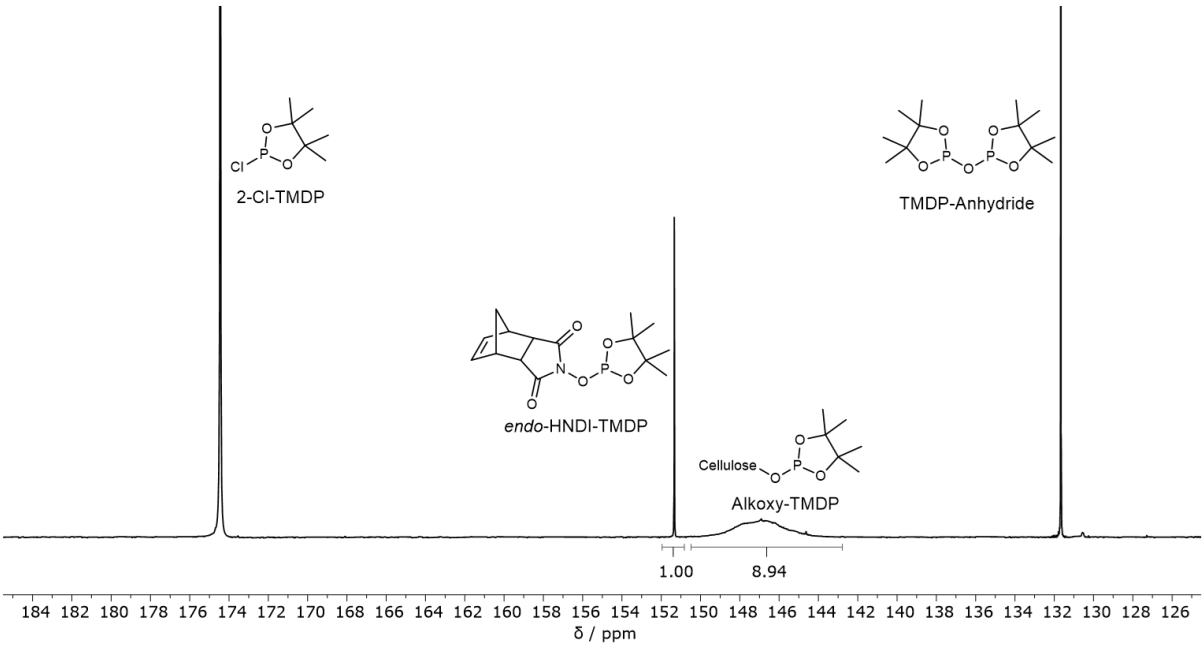

Figure S110 *^{31}P NMR ($CDCl_3$) spectrum of the phosphitylated **CC-1** (calculated: DS_{31P}=1.00).*

***O*-Cellulose-*N*-cyclohexyl thiocarbamate** (**CC-2**): **Yield:** 67%

ATR-IR ν (cm^{-1}): 3661–3106 ν(O-H) and ν(N-H), 2931 ν_{as}(C-H_2), 2855 ν_s(C-H_2), 1705 ν(C=O), 1520 δ(N-H), 1452 δ(CH_2), 1413, 1250 ν_{as}(N-(C=O)-O), 1162 ν(C=S), 1059 AGU ν(C-O).
^{1}H NMR (400 MHz, DMSO-d_6) δ_H (ppm): 9.71–8.30 (m, NH^1), 7.55–6.02 (m, NH^2), 5.85–2.77 (m, AGU, CH^3), 2.19–1.41 (m, CH_2^4), 1.41–0.63 (m, CH_2^5).
^{13}C NMR (126 MHz, THF-d_8) δ_C (ppm): 33.09, 30.86, 30.54, 29.52, 28.14, 25.98, 23.77, 14.67, 1.53.

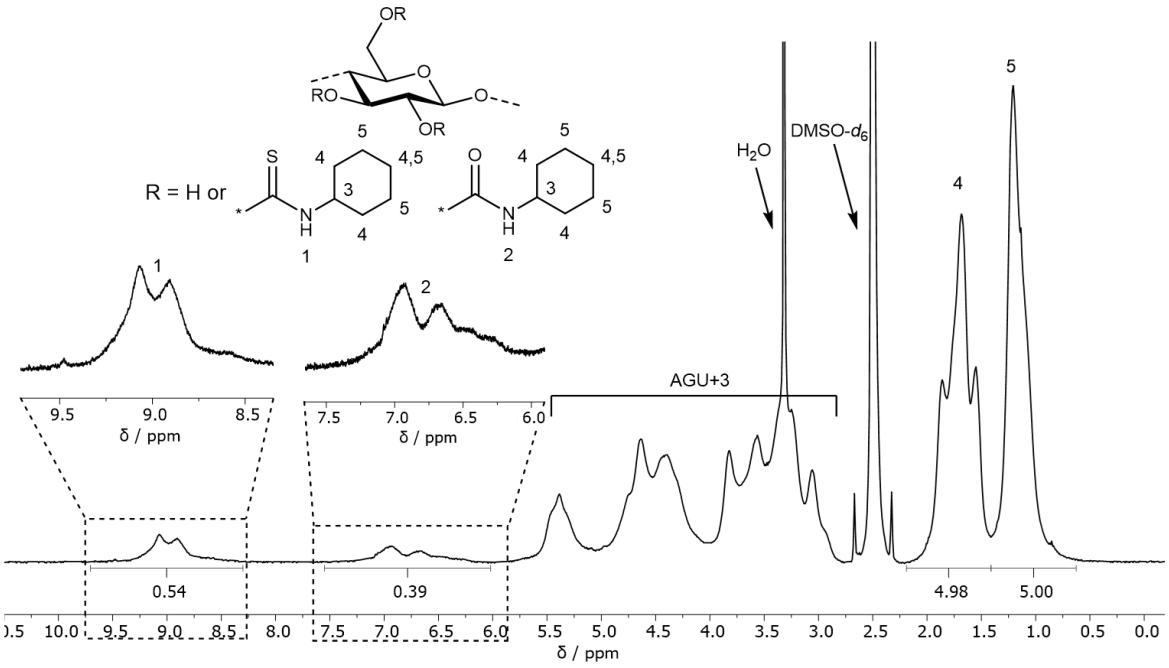

Figure S111 *^{1}H NMR spectrum (DMSO-d_6) of **CC-2**. AGU = Anhydroglucose unit.*

The ^{13}C NMR measurement was performed in THF-d_8 because of better resolution, whereas DMSO-d_6 was used as the solvent for the ^{1}H NMR measurement because of better resolution. Carbonyl and thiocarbonyl peaks could not be detected in the ^{13}C NMR spectrum.

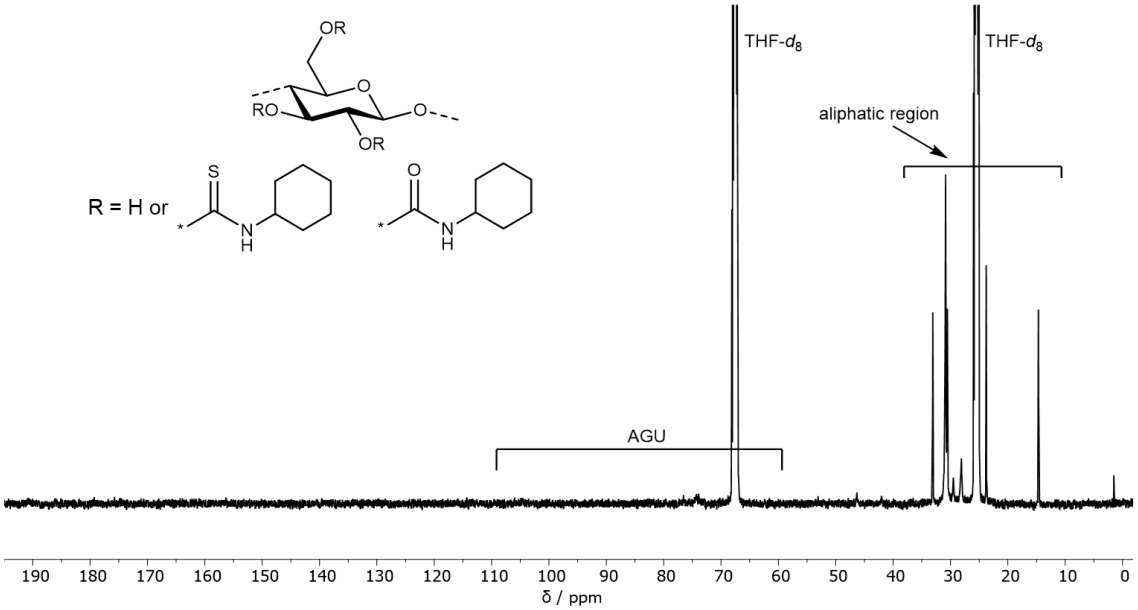

Figure S112 *^{13}C NMR spectrum (THF-d_8, 8192 scans) of* ***CC-2.*** *AGU = Anhydroglucose unit.*

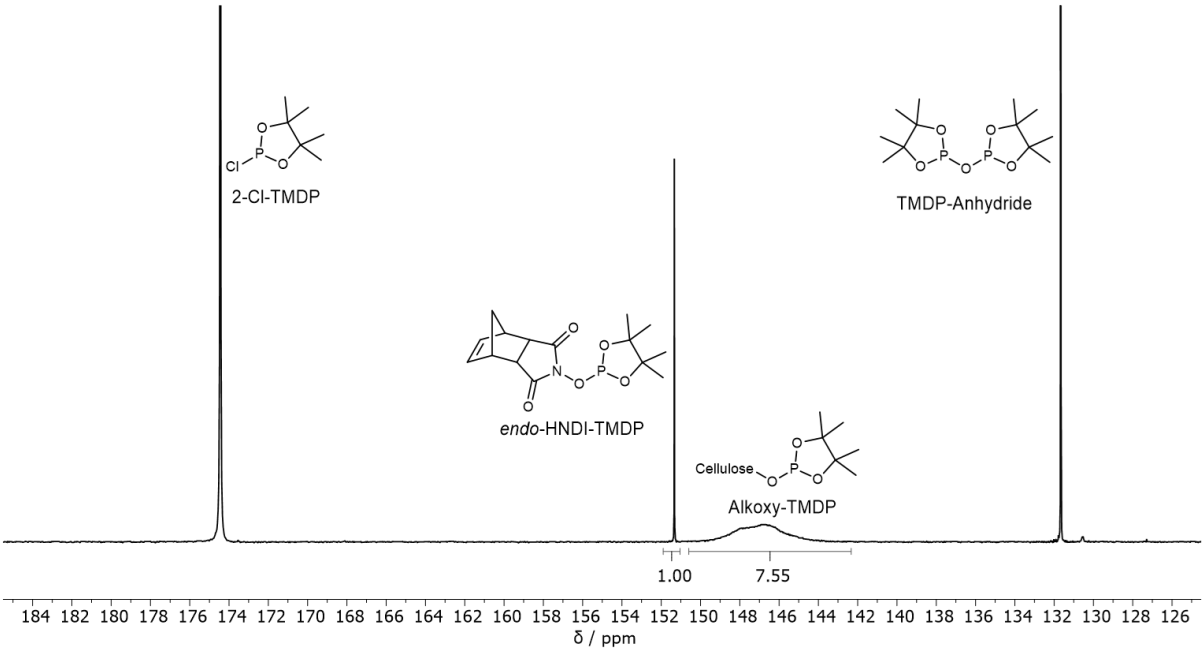

Figure S113 *^{31}P NMR ($CDCl_3$) spectrum of the phosphitylated* ***CC-2*** *(calculated: DS_{31P}=1.20).*

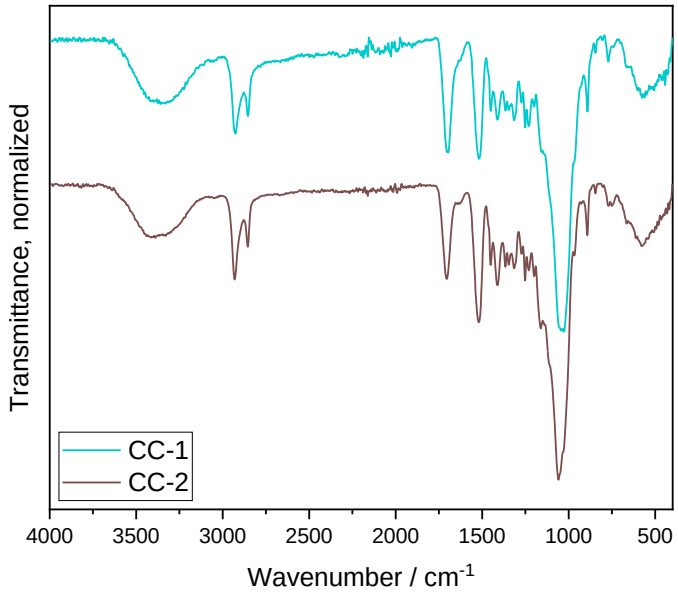

Figure S114 *IR spectra of* ***CC-1*** *and* ***CC-2****.*

***O*-Cellulose-*N*-*n*-butyl thiocarbamate** (**CB-1**): **Yield:** 65%

ATR-IR ν (cm^{-1}): 3645–3100 ν(O-H) and ν(N-H), 2958 ν_{as}(C-H_3), 2929 ν_{as}(C-H_2), 2871 ν_s(C-H_2), 1703 ν(C=O), 1528 δ(N-H), 1458 δ(CH_2), 1408, 1242 ν_{as}(N-(C=O)-O), 1146 ν(C=S), 1014 AGU ν(C-O).
^{1}H NMR (400 MHz, DMSO-d_6) δ_H (ppm): 9.83–8.24 (m, NH^1), 7.56–5.97 (m, NH^2), 5.83–2.74 (m, AGU, CH_2^3), 1.72–1.06 (m, CH_2^4), 1.09–0.61 (m, CH_3^5).

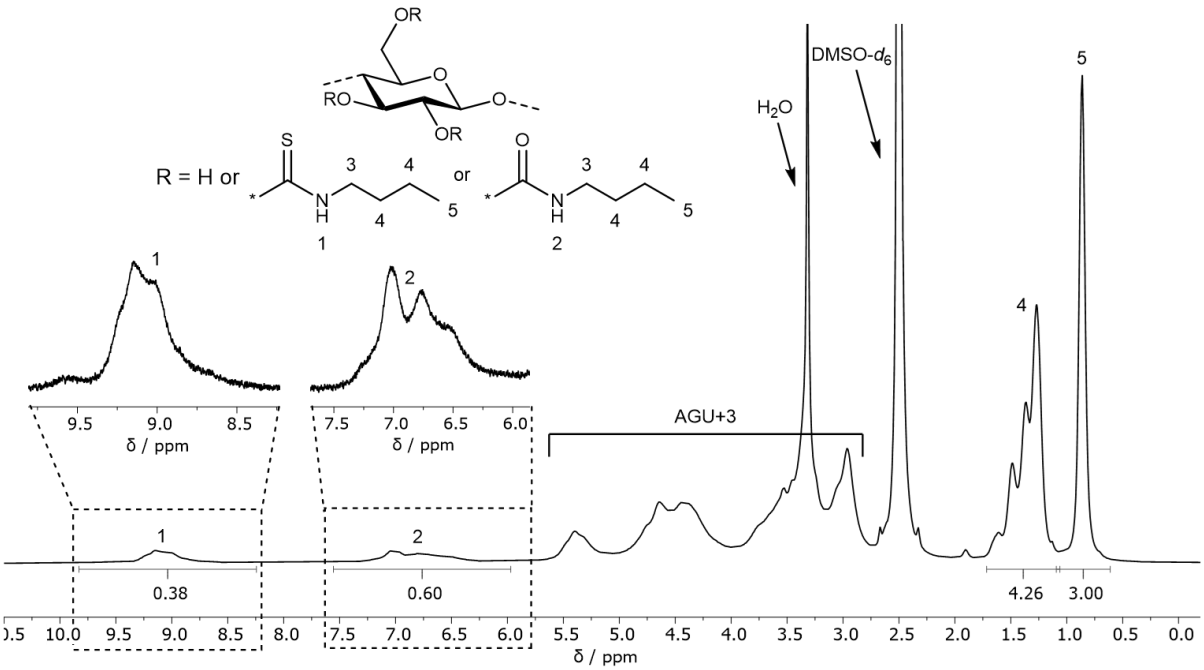

Figure S115 *^{1}H NMR spectrum (DMSO-d_6) of **CB-1**. AGU = Anhydroglucose unit.*

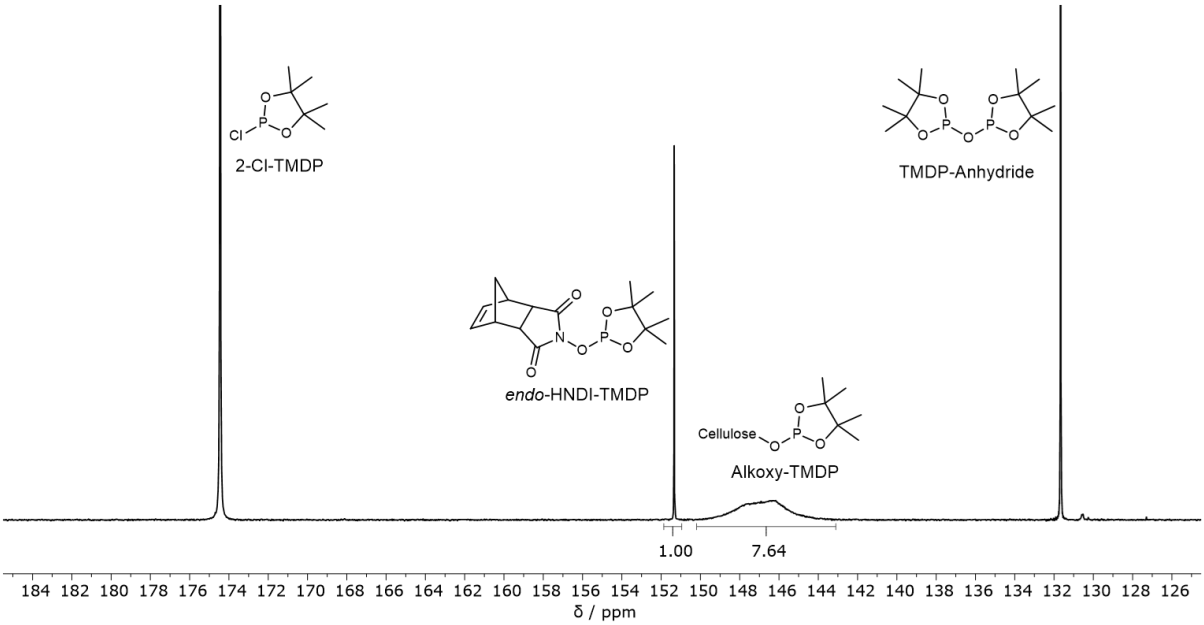

Figure S116 *^{31}P NMR ($CDCl_3$) spectrum of the phosphitylated **CB-1** (calculated: DS_{31P}=1.31).*

***O*-Cellulose-*N*-*n*-butyl thiocarbamate** (**CB-2**): **Yield:** 65%

ATR-IR ν (cm^{-1}): 3672–3102 ν(O-H) and ν(N-H), 2958 ν_{as}(C-H_3), 2931 ν_{as}(C-H_2), 2871 ν_s(C-H_2), 1707 ν(C=O), 1526 δ(N-H), 1456 δ(CH_2), 1407, 1238 ν_{as}(N-(C=O)-O), 1158 ν(C=S), 1016 AGU ν(C-O).
^{1}H NMR (400 MHz, DMSO-d_6) δ_H (ppm): 9.80–8.09 (m, NH^1), 7.61–6.05 (m, NH^2), 5.92–2.77 (m, AGU, CH_2^3), 1.83–1.09 (m, CH_2^4), 1.09–0.42 (m, CH_3^5).
^{13}C NMR (126 MHz, DMSO-d_6) δ_C (ppm): 188.99, 187.46, 65.67, 44.40, 42.17, 31.53, 30.66, 29.89, 19.59, 19.44, 13.68.

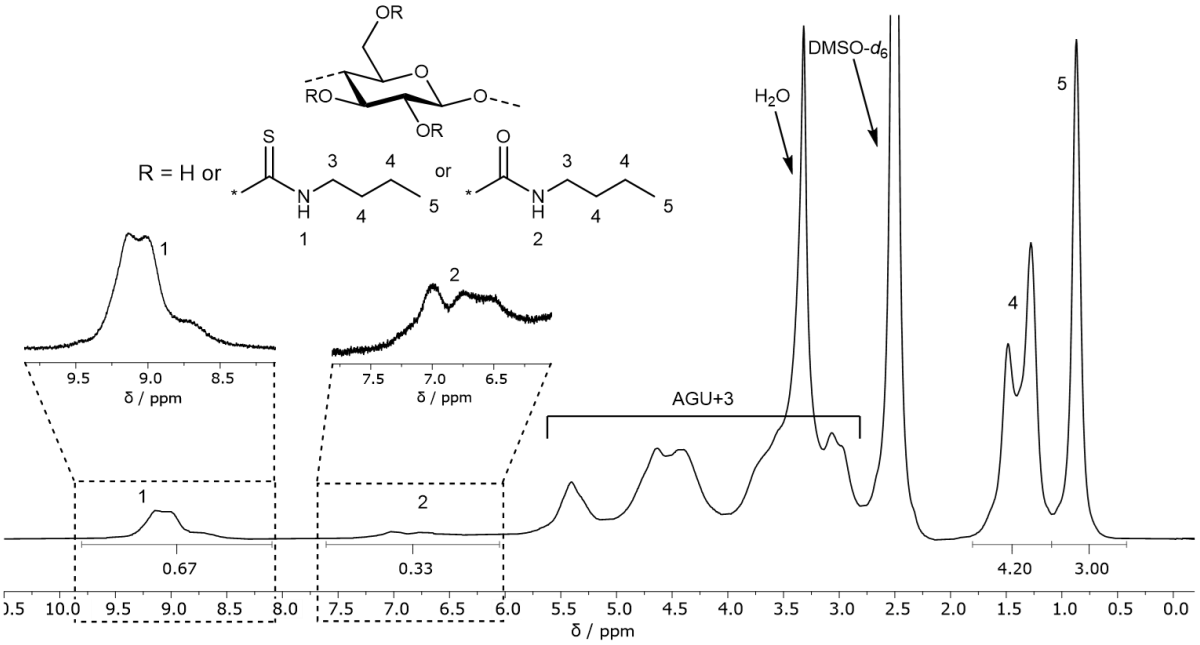

Figure S117 *^{1}H NMR spectrum (DMSO-d_6) of **CB-2**. AGU = Anhydroglucose unit.*

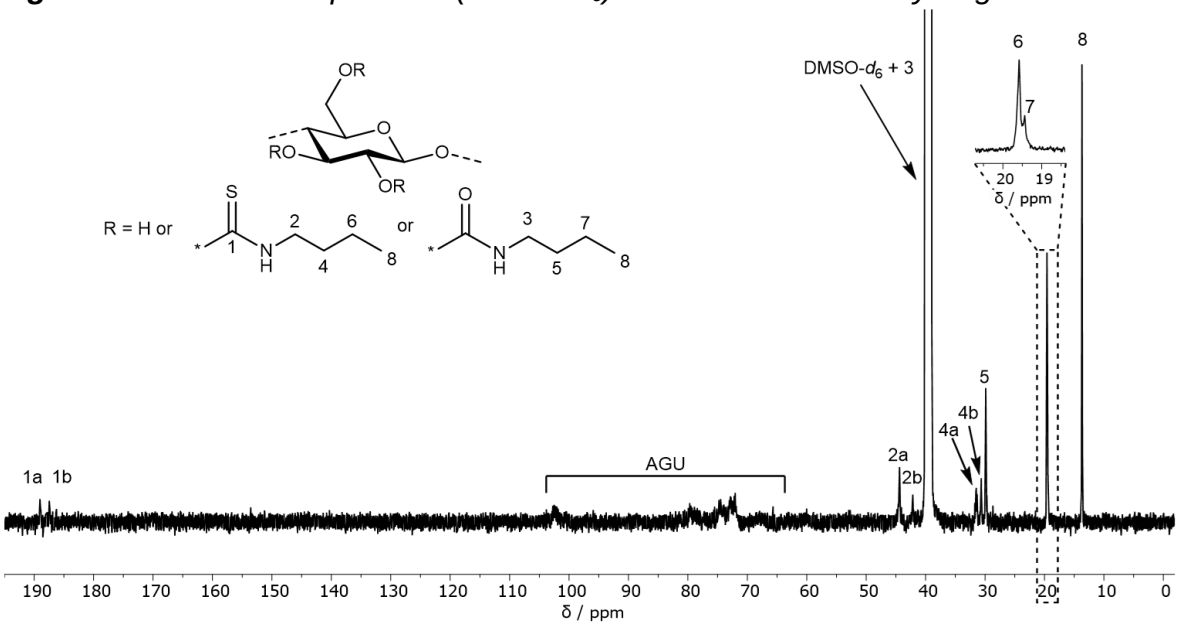

Figure S118 *^{13}C NMR spectrum (DMSO-d_6, 8192 scans) of **CB-2**. AGU = Anhydroglucose unit. Signals a and b are observed because of the cis/trans isomerism of the*

thiocarbamte moiety caused by the hindered rotation due to the partial double bond character.[313]

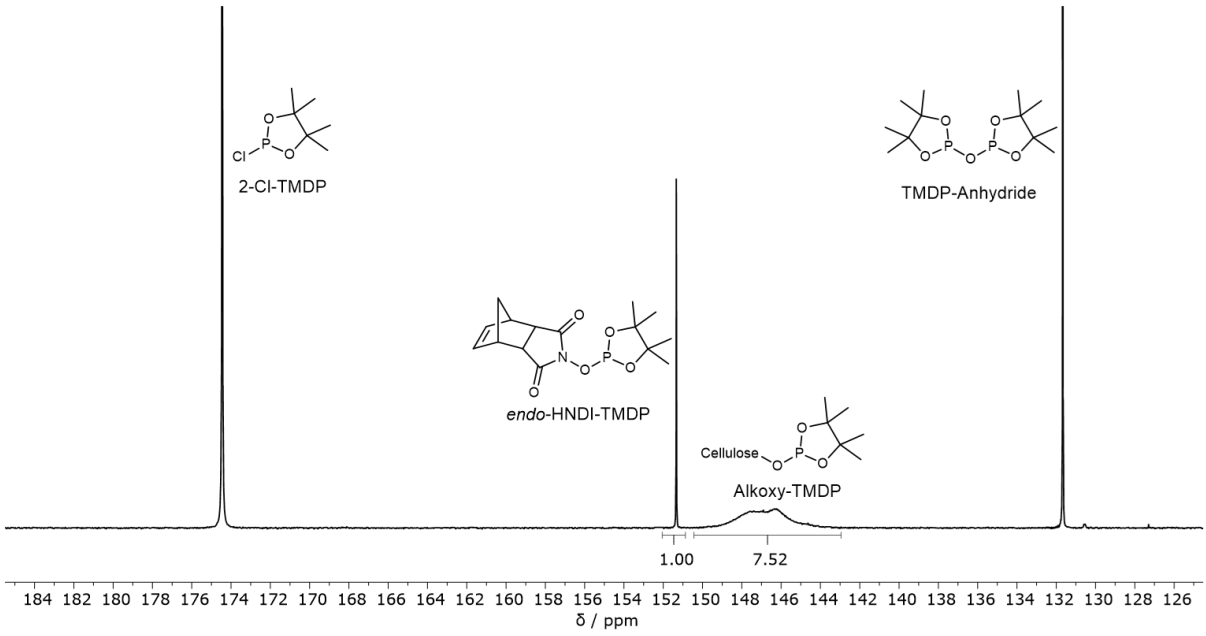

Figure S119 *^{31}P NMR ($CDCl_3$) spectrum of the phosphitylated **CB-2** (calculated: DS_{31P}=1.30).*

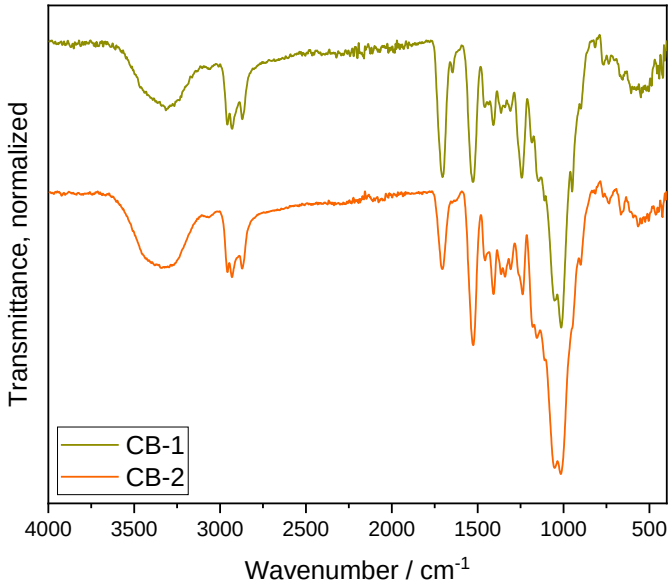

Figure S120 *IR spectra of **CB-1** and **CB-2**.*

***O*-Cellulose-*N*-oleyl thiocarbamate** (**CO-1**): **Yield:** 57%

ATR-IR ν (cm^{-1}): 3649–3129 ν(O-H) and ν(N-H), 3005 ν_{as}(C-H_3), 2921 ν_{as}(C-H_2), 2853 ν_s(C-H_2), 1711 ν(C=O), 1528 δ(N-H), 1456 δ(CH_2), 1407, 1242 ν_{as}(N-(C=O)-O), 1154 ν(C=S), 1061 AGU ν(C-O).
^{1}H NMR (400 MHz, THF-d_8) δ_H (ppm): 8.78–7.42 (NH^1), 6.86–5.55 (m, NH^2), 5.53–5.24 (m, CH^3), 5.14–2.85 (m, AGU, CH_2^4), 2.12–1.94 (m, CH_2^5), 1.61–1.48 (m, CH_2^6), 1.43–1.15 (m, CH_2^7), 1.00–0.78 (m, CH_3^8).

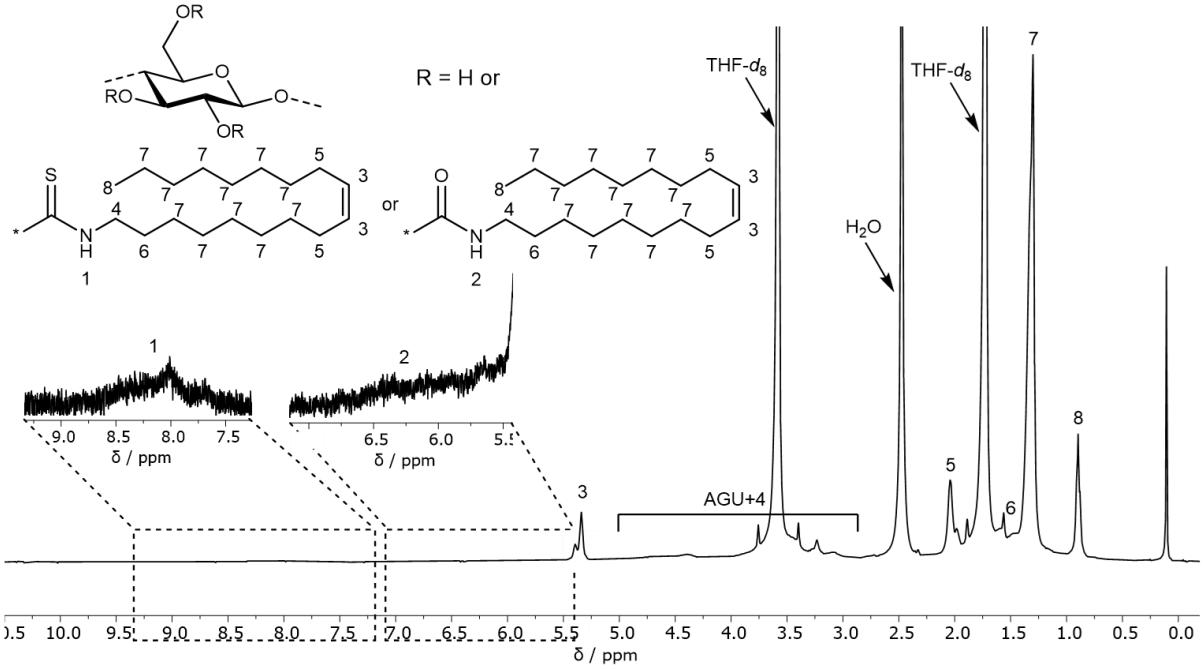

Figure S121 *^{1}H NMR spectrum (THF-d_8) of **CO-1**. AGU = Anhydroglucose unit.*

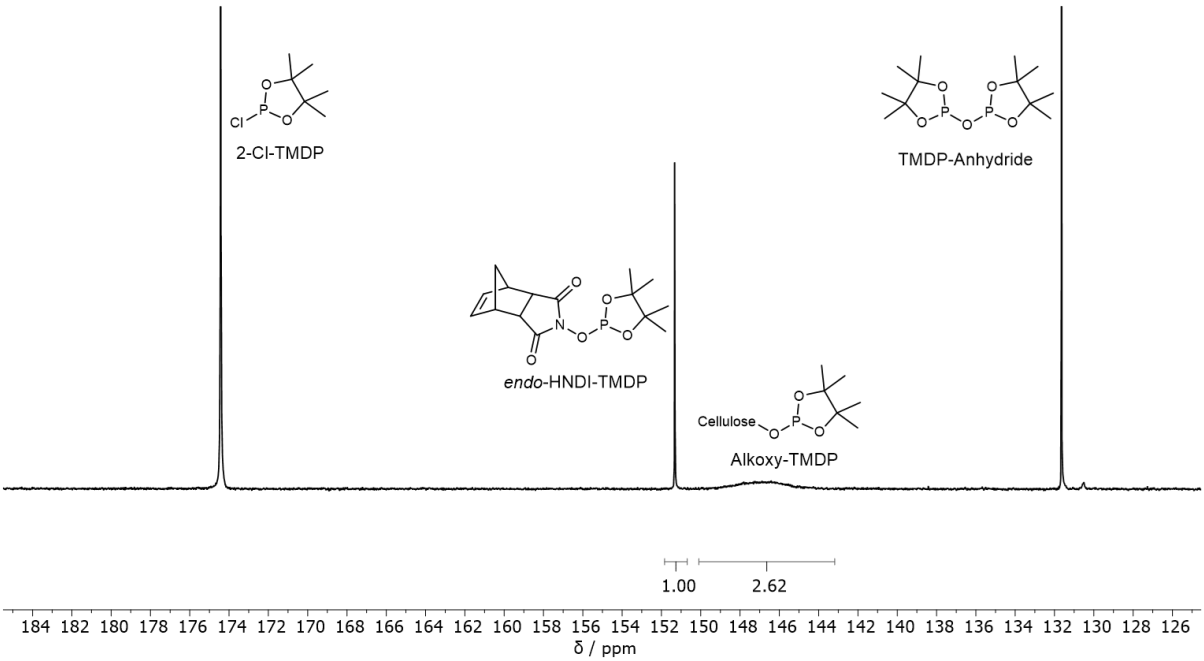

Figure S122 *^{31}P NMR ($CDCl_3$) spectrum of the phosphitylated **CO-1** (calculated: DS_{31P}=1.69).*

***O*-Cellulose-*N*-oleyl thiocarbamate** (**CO-2**): **Yield:** 59%

ATR-IR ν (cm^{-1}): 3639–3122 ν(O-H) and ν(N-H), 3005 ν_{as}(C-H_3), 2921 ν_{as}(C-H_2), 2853 ν_s(C-H_2), 1713 ν(C=O), 1526 δ(N-H), 1462 δ(CH_2), 1407, 1242 ν_{as}(N-(C=O)-O), 1156 ν(C=S), 1063 AGU ν(C-O).
^{1}H NMR (400 MHz, THF-d_8) δ_H (ppm): 8.88–7.31 (m, NH^1), 7.04–5.49 (m, NH^2), 5.48–5.23 (m, CH^3), 5.11–2.85 (m, AGU, CH_2^4), 2.22–1.91 (m, CH_2^5), 1.68–1.52 (m, CH_2^6), 1.53–1.05 (m, CH_2^7), 1.00–0.73 (m, CH_3^8).
^{13}C NMR (126 MHz, THF-d_8) δc (ppm): 189.89, 130.68, 130.07, 45.72, 41.45 33.09, 32.42, 32.30, 32.00, 31.90, 30.27, 30.14, 30.05, 29.91, 29.84, 29.81, 29.47, 28.88, 27.60, 23.12, 23.00, 14.04.

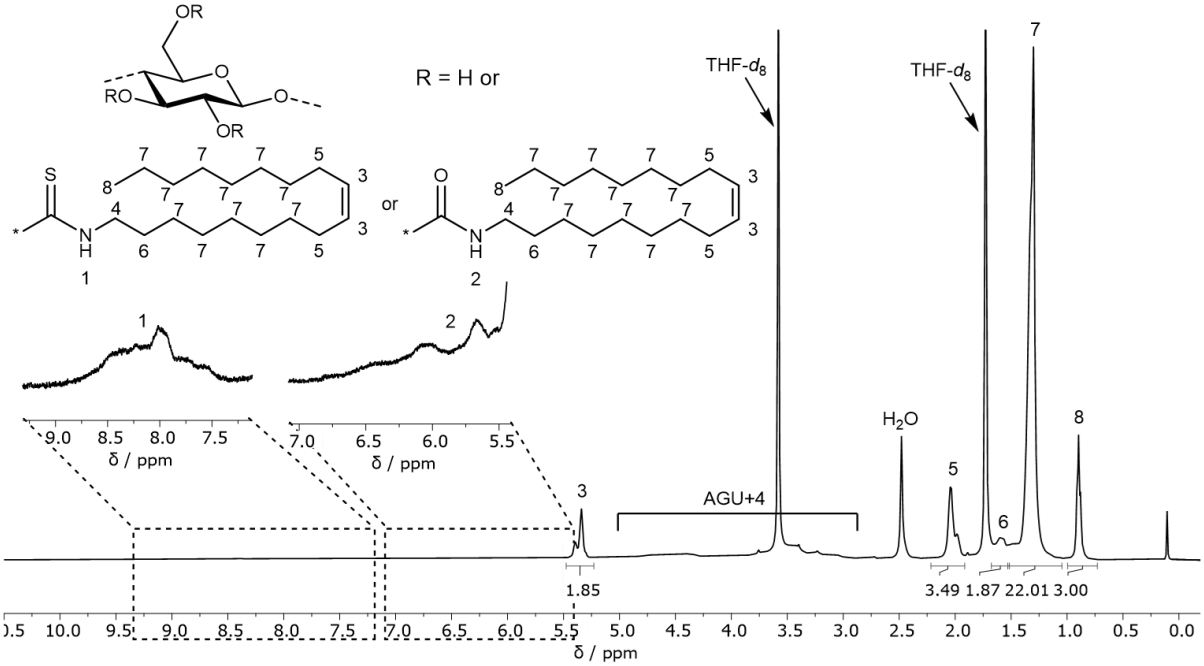

Figure S123 *^{1}H NMR spectrum (THF-d_8) of **CO-2**. AGU = Anhydroglucose unit.*

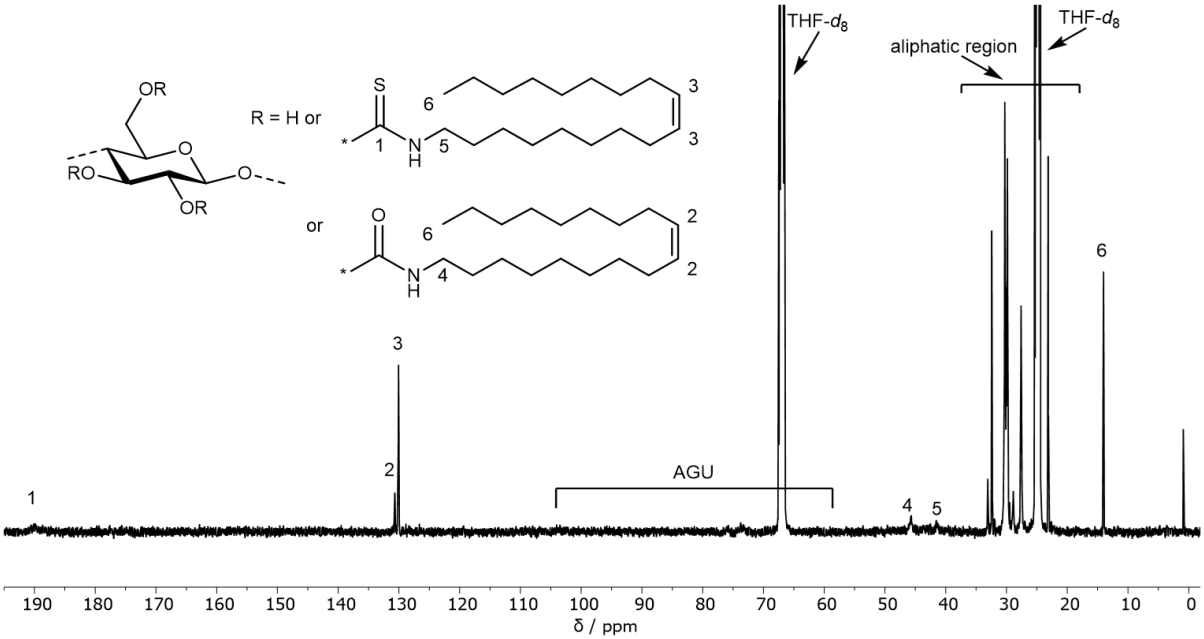

Figure S124 *^{13}C NMR spectrum (THF-d_8, 8192 scans) of **CO-2**.*

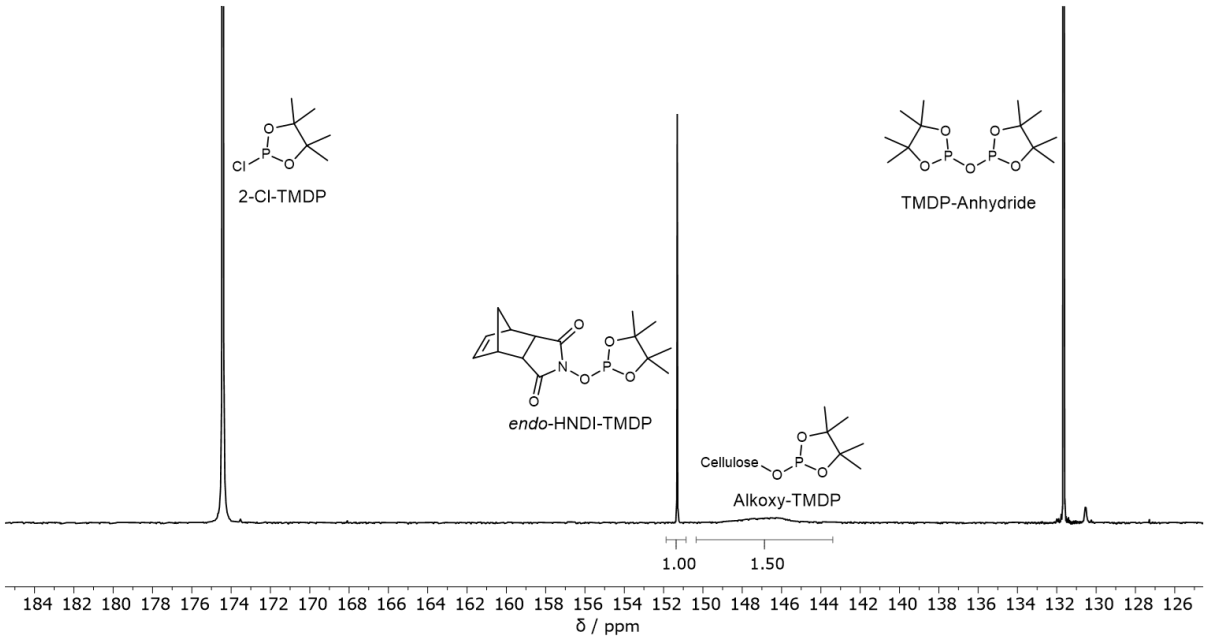

Figure S125 *^{31}P NMR ($CDCl_3$) spectrum of the phosphitylated* ***CO-2*** *(calculated: DS_{31P}=2.11).*

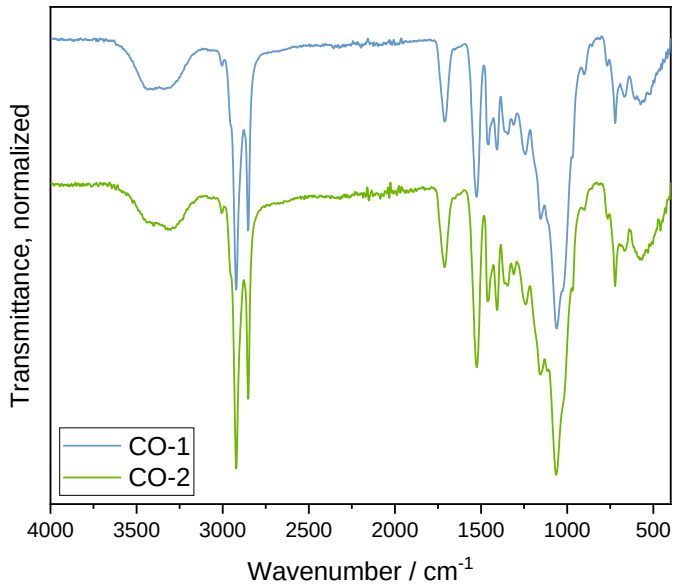

Figure S126 *IR spectra of* ***CO-1*** *and* ***CO-2****.*

O-cellulose-*N*-*n*-dodecyl thiocarbamate at a concentration of 2 wt% (CD-2wt%)

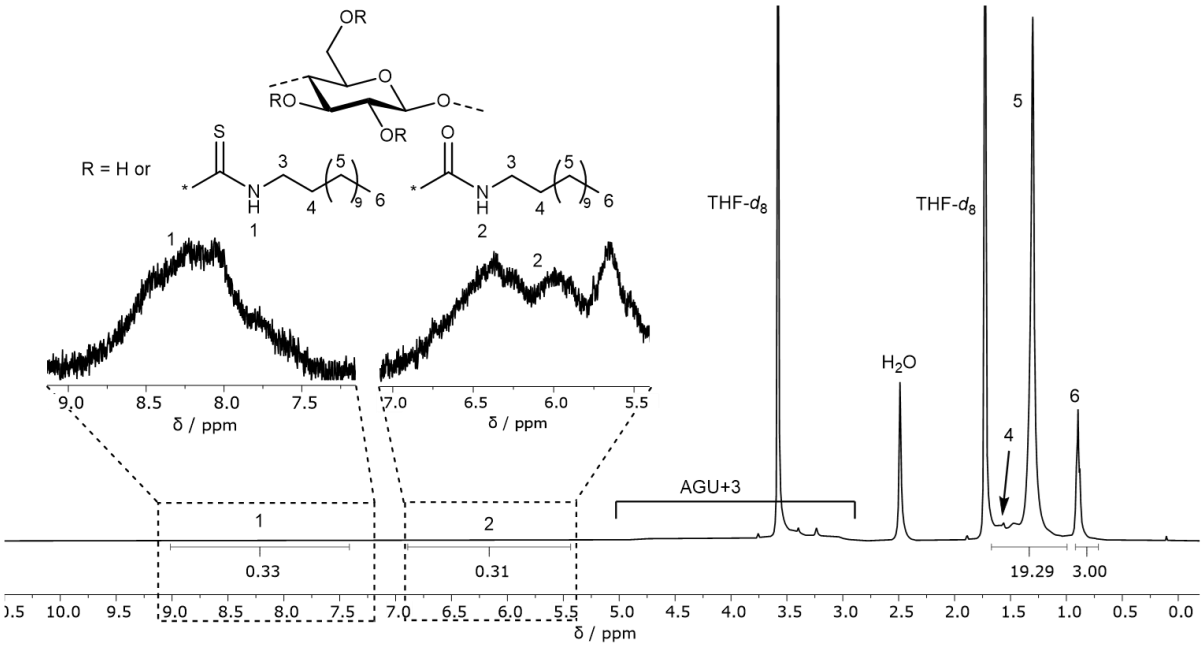

Figure S127 *^{1}H NMR spectrum (THF-d_8) of **CD-2wt%**. Calculated thiocarbamate mole fraction from ^{1}H NMR spectroscopy: $x_{S,NMR}$=51.6%.*

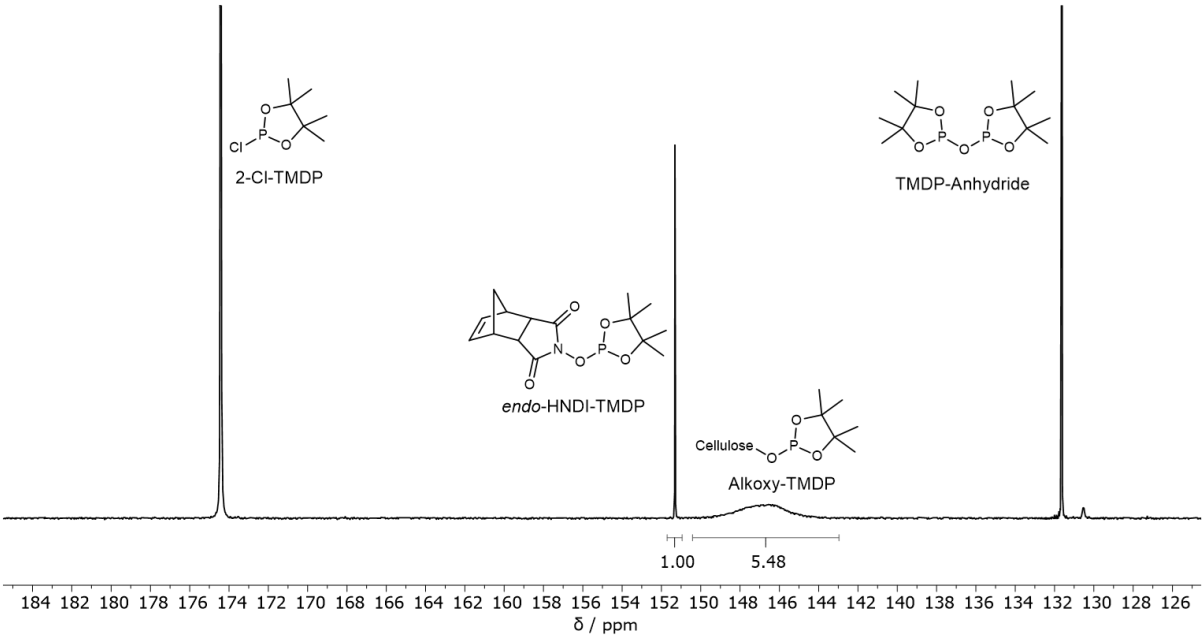

Figure S128 *^{31}P NMR ($CDCl_3$) spectrum of the phosphitylated **CD-2wt%** (calculated: DS_{31P}=1.22). The DS_{31P} was not corrected with elemental analysis data and thus, 100% thiocarbamate formation is assumed for the calculated M_S.*

O-cellulose-*N*-*n*-dodecyl thiocarbamate at a concentration of 3 wt%

See the data from **CD-5.**

_O_-cellulose-_N-n_-dodecyl thiocarbamate at a concentration of 4 wt% (CD-4wt%)

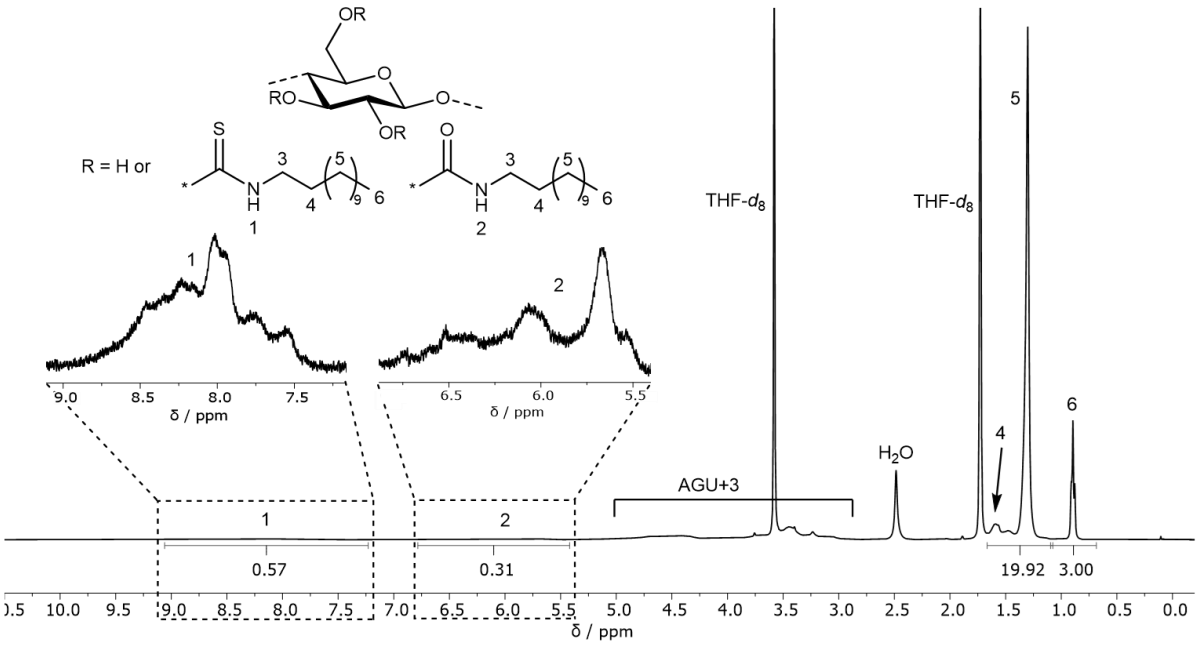

Figure S129 *^{1}H NMR spectrum (THF-d_8) of **CD-4wt%**. Calculated thiocarbamate mole fraction from ^{1}H NMR spectroscopy: $x_{S,NMR}$=64.8%.*

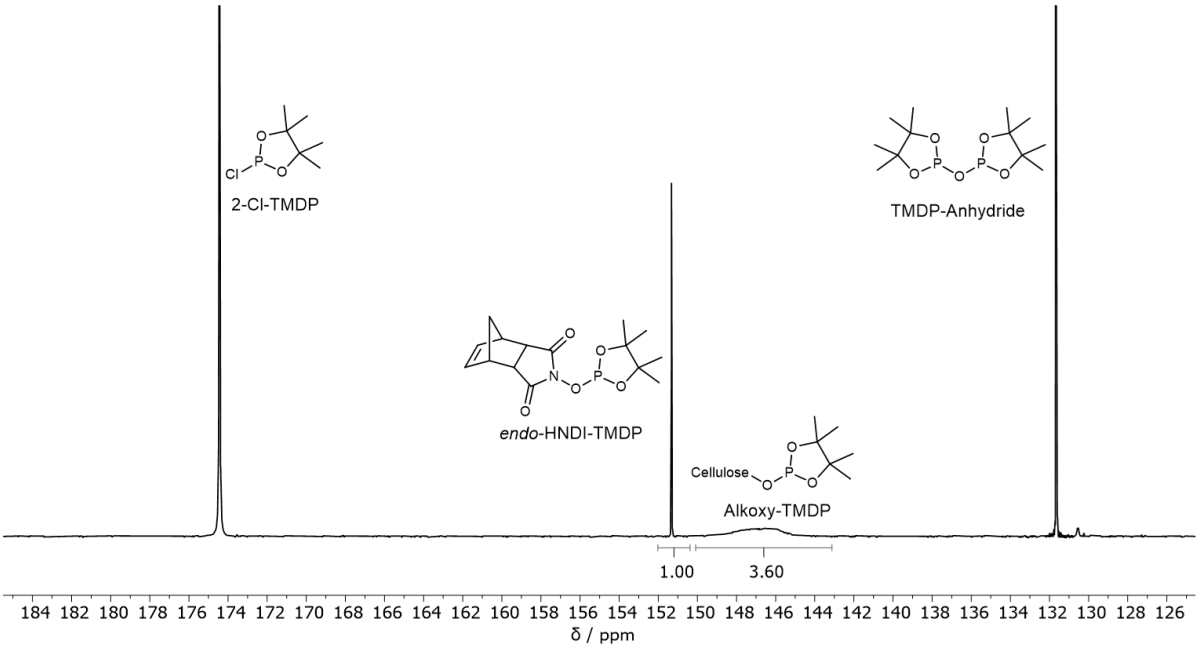

Figure S130 *^{31}P NMR ($CDCl_3$) spectrum of the phosphitylated **CD-4wt%** (calculated: DS_{31P}=1.60). The DS_{31P} was not corrected with elemental analysis data and thus, 100% thiocarbamate formation is assumed for the calculated M_S.*

_O_-cellulose-_N-n_-dodecyl thiocarbamate at a concentration of 5 wt% (CD-5wt%)

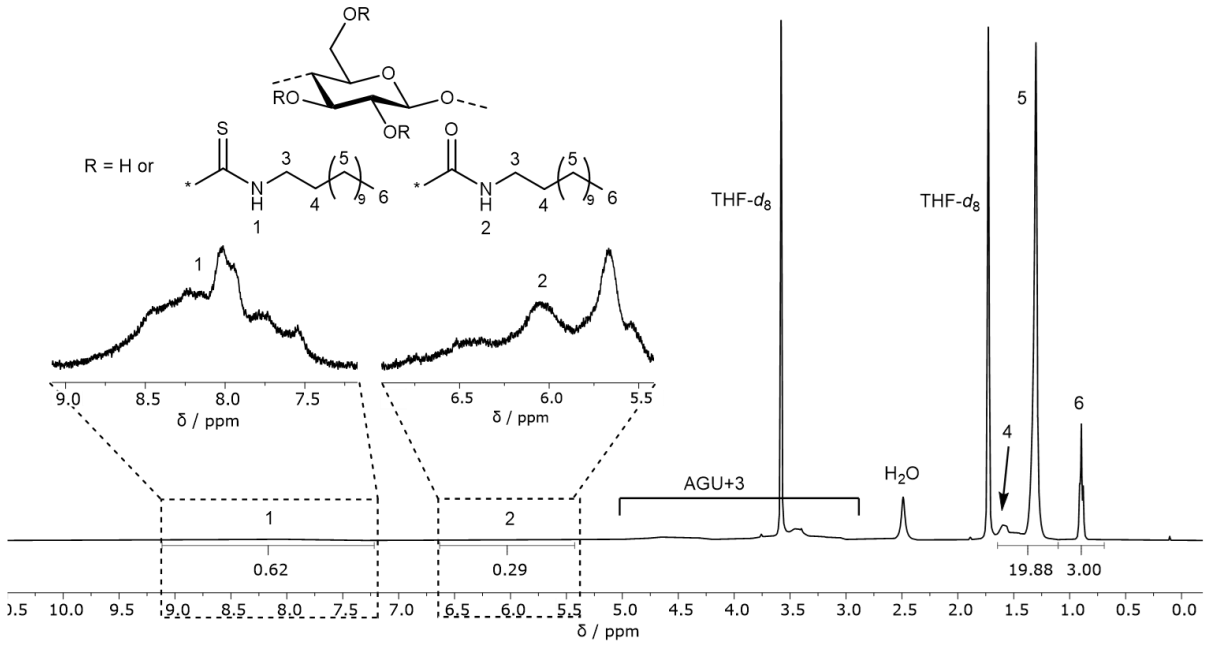

Figure S131 *^{1}H NMR spectrum (THF-d_8) of **CD-5wt%**. Calculated thiocarbamate mole fraction from ^{1}H NMR spectroscopy: $x_{S,NMR}$=68.1%.*

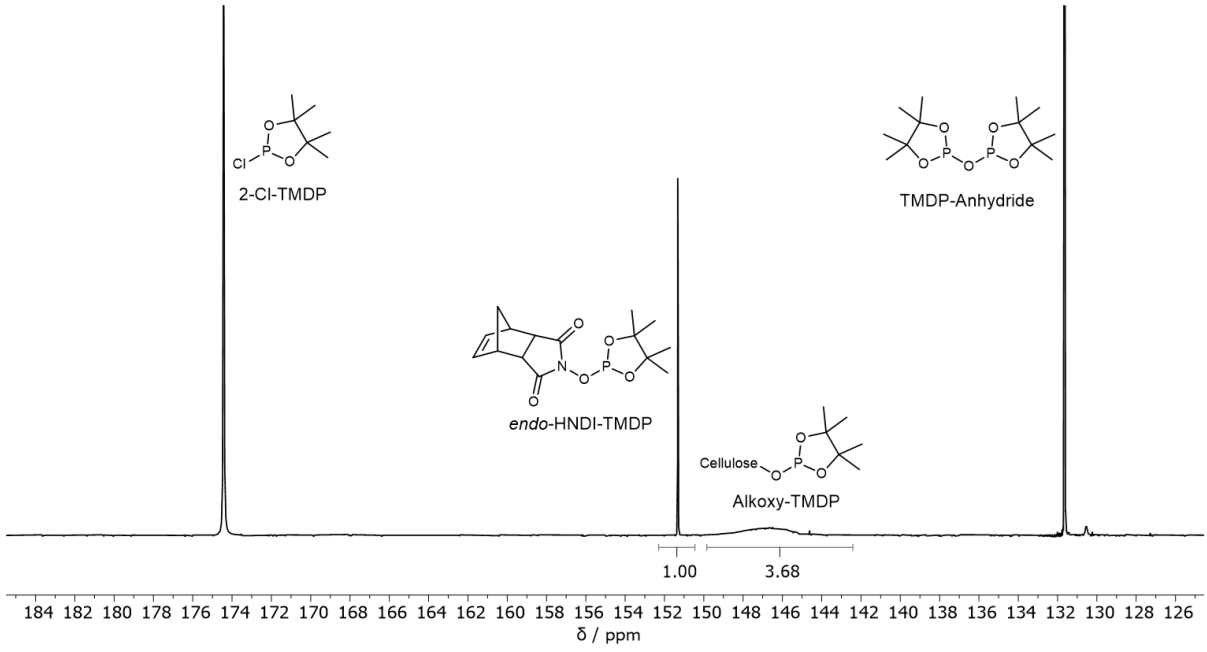

Figure S132 *^{31}P NMR ($CDCl_3$) spectrum of the phosphitylated **CD-5wt%** (calculated: DS_{31P}=1.58). The DS_{31P} was not corrected with elemental analysis data and thus, 100% thiocarbamate formation is assumed for the calculated M_S.*

Synthesis of *O*-Cellulose-*N*-*n*-Dodecyl Thiocarbamate in Larger Scale with Subsequent Recycling of the Used Solvents (CD-REC)

In a round-bottom Schlenk flask, cellulose (4.00 g, [monomeric unit]=24.67 mmol) was dried under high vacuum at 120 °C and subsequently suspended in 70 mL dry DMSO under argon atmosphere, followed by the dropwise addition of DBU (11.53 mL, 11.76 g, 77.52 mmol, 3.0 eq. per anhydroglucose unit (AGU)). After applying a CO_2 flow through the solution for 30 min at 40 °C using a balloon, a clear solution was obtained. In a syringe without piston, elemental sulfur (2.77 g, 1.12 eq. of sulfur atoms per eq. isocyanide) was placed and the piston reinserted. *n*-Dodecyl isocyanide (14.46 g, 3.0 eq. per AGU) was then sucked up with the prepared syringe and the resulting suspension of elemental sulfur in isocyanide was added dropwise to the reaction through a septum over a period of 3 h. The sulfur/isocyanide mixture was resuspended before every addition. The temperature was then elevated to 70 °C and the reaction was stirred overnight. The product precipitated during the reaction as it became insoluble in DMSO and was decanted. The crude product was purified by stirring in 150 mL isopropanol under reflux for 1 h and subsequently vacuum filtrated. The same procedure was repeated with another 150 mL of isopropanol and the pure product was then dried under high vacuum at 50 °C for 12 h. The final product was obtained as a yellow solid and the yield was calculated based on the $DS_{EA,NC}$ (Equation S10): 91.4%. **Recycling process:** The iPrOH from drying of the purified product was captured in a cold trap. The residual filtrate consisting of isopropanol, DMSO and DBU was purified by distillation. First, isopropanol was evaporated using a rotary evaporator (50 mbar, 50 °C) and this fraction was combined with the captured isopropanol from the coldtrap. In a subsequent distillation, a second fraction containing isopropanol and DMSO (0.2 mbar, 40 °C) was collected in order to remove isopropanol quantitatively, which could lead to side reactions in a second cycle. Then, the third fraction (mixed fraction consisting of DMSO and DBU) was distilled at 0.1 mbar and 50–150 °C oil bath temperature. Recovery yields are summarized in **Table 27** and the composition of fraction three was analyzed *via* ^{1}H NMR spectroscopy (**Figure S135**).

***O*-cellulose-*N*-*n*-dodecyl thiocarbamate synthesized in larger scale with recycling of the used solvents (CD-REC):** Yield: 91%.

ATR-IR ν (cm^{-1}): 3648–3112 ν(O-H) and ν(N-H), 2957 ν_{as}(C-H_3), 2921 ν_{as}(C-H_2), 2851 ν_s(C-H_2), 1709 (C=O), 1524 δ(N-H), 1456 δ(CH_2), 1409, 1249 ν_{as}(N-(C=O)-O), 1158 ν(C=S), 1063 AGU ν(C-O).
^{1}H NMR (400 MHz, THF-d_8) δ_H (ppm): 9.04–7.11 (m, NH^1), 6.43–5.41 (m, NH^2), 5.36–2.70 (m, AGU, CH_2^3), 1.57–0.95 (m, $CH_2^{5,4}$), 0.91–0.65 (m, CH_3^6).

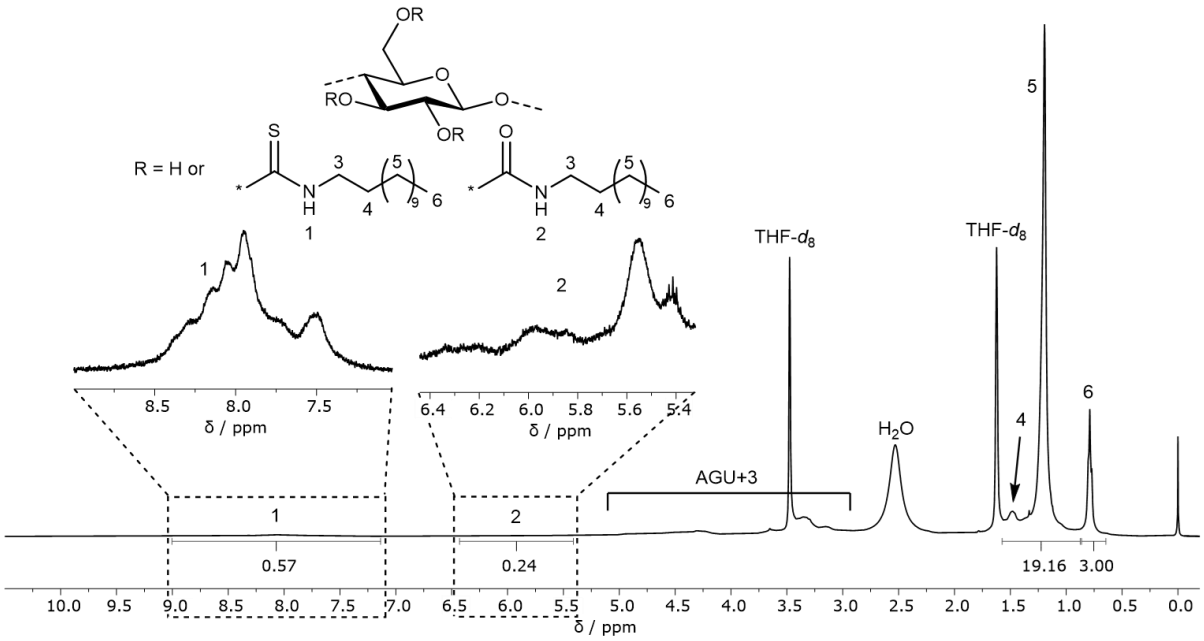

Figure S133 *^{1}H NMR spectrum (THF-d_8) of **CD-REC**. Calculated thiocarbamate mole fraction from ^{1}H NMR spectroscopy: $x_{S,NMR}$=70.4%.*

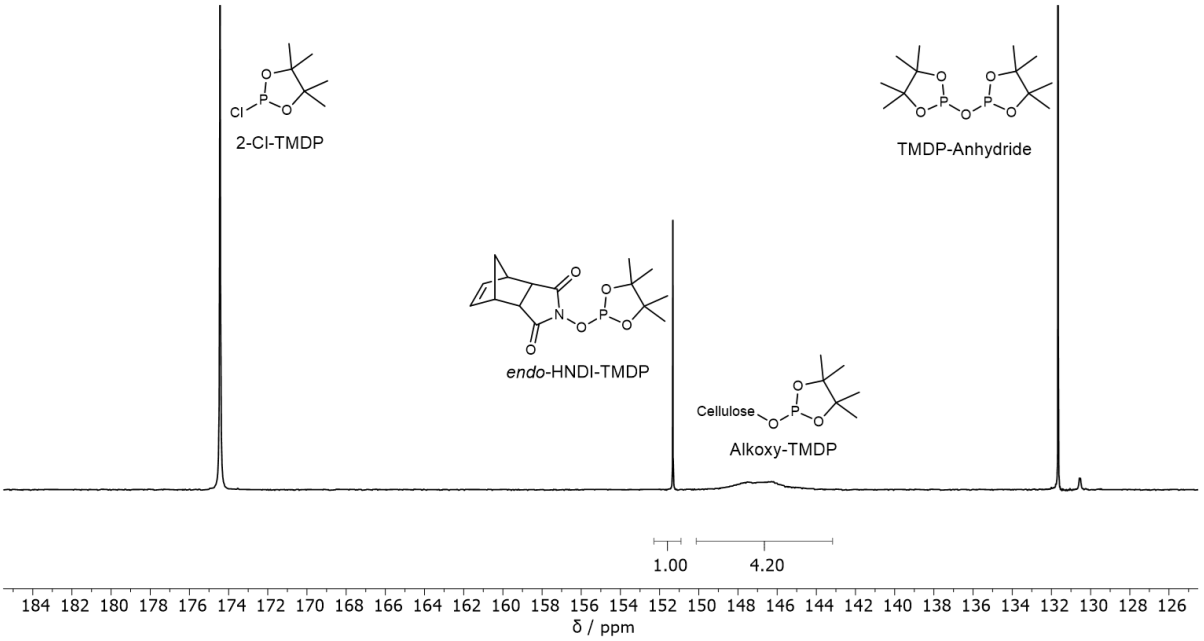

Figure S134 *^{31}P NMR ($CDCl_3$) spectrum of the phosphitylated **CD-REC** (calculated: DS_{31P}=1.47).*

Table 27 *Used and recovered substances for the synthesis of CD-REC (3.0 eq. n-dodecyl isocyanide, 0.42 eq. S_8).*

Substance	Used	Recovered	Recycling ratio
Cellulose	4.00 g	-	-
n-Dodecyl isocyanide	14.46 g	-	-
Sulfur	2.66 g	-	-
DMSO	77.03 g	70.49 g	91.5%
DBU	11.76 g	9.31 g	79.1%
iPrOH	291.16 g	278.48 g	95.6%

DS_{31P} = 1.47, $DS_{EA,NC}$ = 1.42±0.06, $DS_{EA,NH}$ = 1.44±0.09, Yield: 10.82 g (91.4%, calculated based on the $DS_{EA,NC}$), Conversion: 47.3% (calculated based on the $DS_{EA,NC}$)

The volume of CO_2 used for the solubilization was estimated to V = 2 L. Using the ideal gas law ($pV = nRT$) and the molar mass of CO_2 (M = 44.01 g mol^{-1}), the used mass of CO_2 was calculated to be m = 3.60 g. With a yield of 10.82 g, CO_2 is estimated to contribute to the E-Factor with: E-Factor$_{CO2,\ estimate}$ = 0.33. This contribution was neglected for the total E-Factor calculation due to the uncertainty in quantification and the low value. In even larger scales, the used CO_2 could be recycled as it is released during the derivatization reaction.

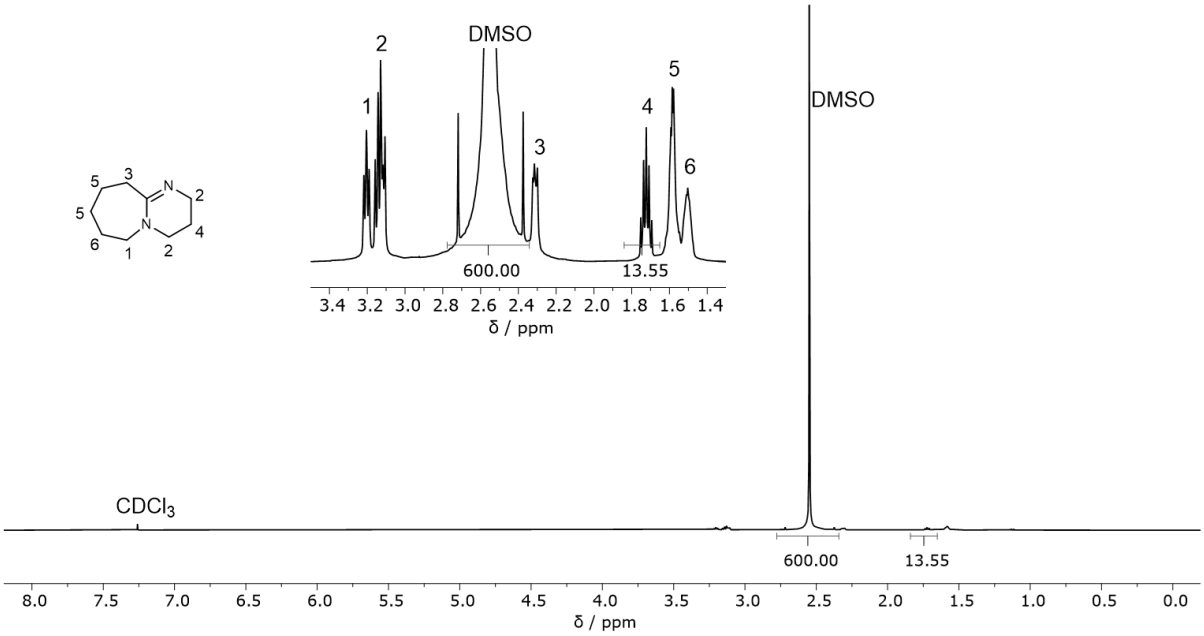

Figure S135 *^{1}H NMR ($CDCl_3$) spectrum of the redistilled DMSO/DBU mixture.*

O-Cellulose-N-oleyl thiocarbamate synthesized in larger scale with redistilled DMSO/DBU (CD-REC2): Yield: 68%.

ATR-IR ν (cm^{-1}): 3653–3107 ν(O-H) and ν(N-H), 3007 ν_{as}(C-H_3), 2921 ν_{as}(C-H_2), 2853 ν_{s}(C-H_2), 1705 ν(C=O), 1528 δ(N-H), 1465 δ(CH_2), 1407, 1246 ν_{as}(N-(C=O)-O), 1154 ν(C=S), 1055 AGU ν(C-O).
^{1}H NMR (400 MHz, THF-d_8) δ_H (ppm): 8.85–7.42 (m, NH^1), 7.02–5.59 (m, NH^2), 5.48–5.25 (m, CH^3), 5.15–2.90 (m, AGU, CH_2^4), 2.20–1.92 (m, CH_2^5), 1.69–1.55 (m, CH_2^6), 1.54–1.06 (m, CH_2^7), 0.96–0.80 (m, CH_3^8).

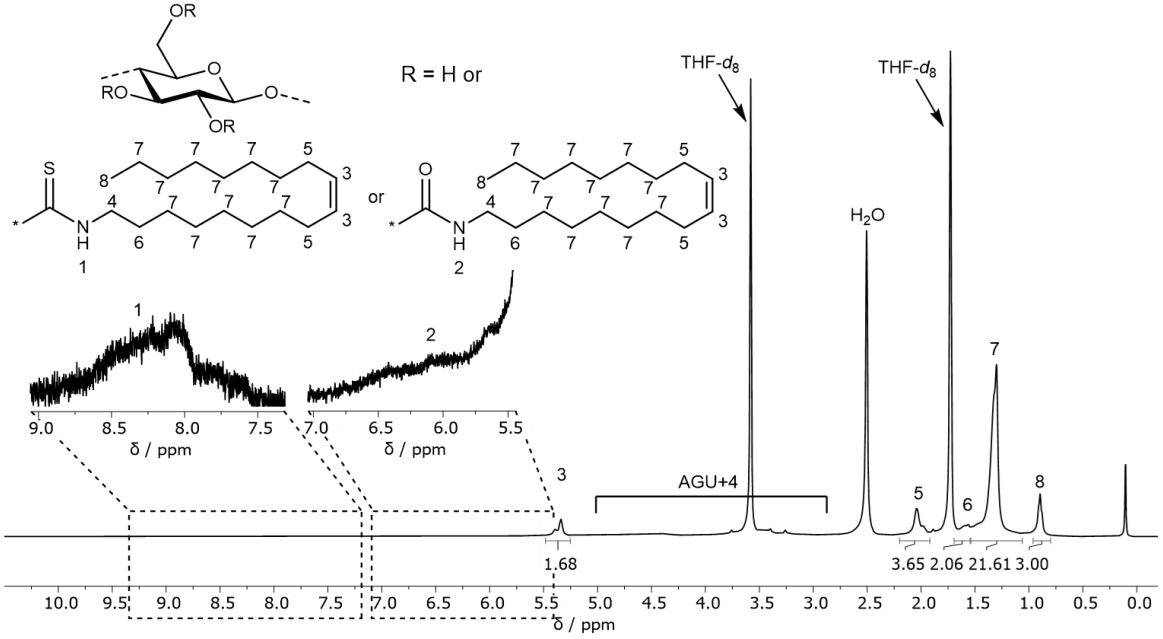

Figure S136 *^{1}H NMR spectrum (THF-d_8) of a O-Cellulose-N-oleyl thiocarbamate synthesized with redistilled DMSO and DBU. AGU = Anhydroglucose unit.*

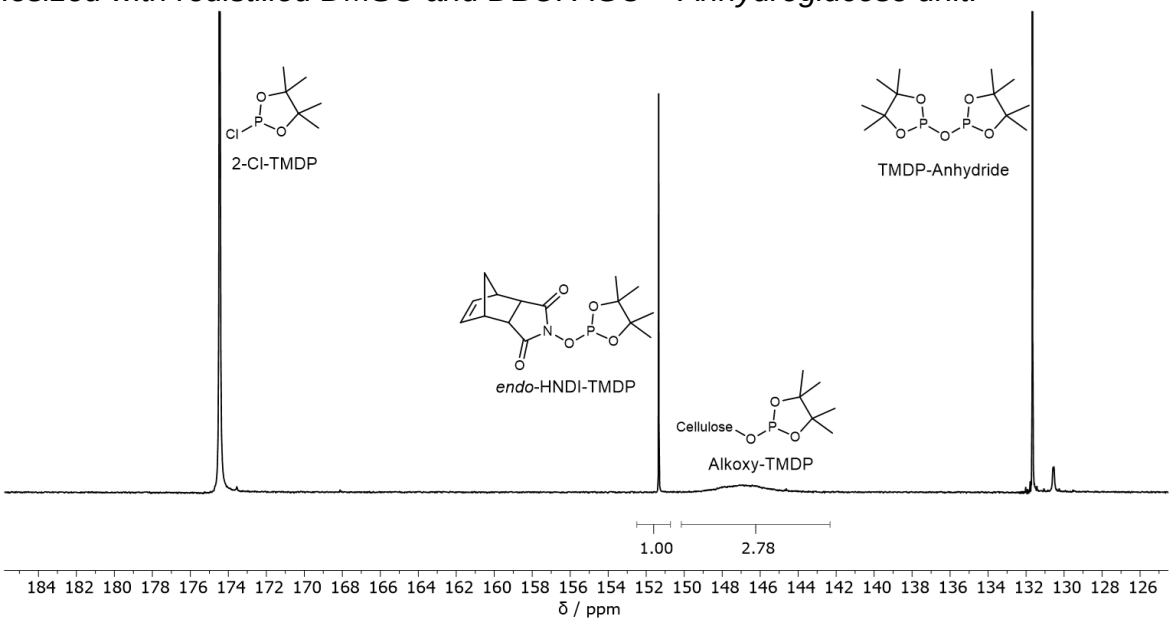

Figure S137 *^{31}P NMR ($CDCl_3$) spectrum of the phosphitylated O-Cellulose-N-oleyl thiocarbamate synthesized with redistilled DMSO and DBU (calculated: DS_{31P}=1.63). The DS_{31P} was not corrected with elemental analysis data and thus, 100% thiocarbamate formation is assumed for the calculated M_S.*

Model Compound Synthesis

In a round-bottom flask, *n*-hexanol (0.44 mL, 360 mg, 3.52 mmol, 1.0 eq.) was diluted in 10 mL DMSO followed by the dropwise addition of DBU (0.53 mL, 536 mg, 3.52 mmol, 1.0 eq.). A CO_2 flow was applied through the solution for 20 min at 40 °C using a balloon. *n*-Dodecyl isothiocyanate (800 mg, 3.52 mmol, 1.0 eq.) was added dropwise over a period of 1.5 h. The temperature was then elevated to 70 °C and stirred overnight. The organic phase was then extracted with cyclohexane, the extract was washed with water (2x) and brine (1x), and then dried over Na_2SO_4. The solution was filtered, the solvent evaporated under reduced pressure and the crude product purified *via* flash column chromatography (cyclohexane/ethyl acetate 15/1). The final products (*O*-*n*-hexyl-*N*-*n*-dodecyl thiocarbamate and *O*-*n*-hexyl-*N*-*n*-dodecyl carbamate) were obtained as colorless liquids. Yield: 49% of *O*-*n*-hexyl-*N*-*n*-dodecyl thiocarbamate, 17% of *O*-*n*-hexyl-*N*-*n*-dodecyl carbamate (combined yield: 66%).

***O-n*-Hexyl-*N-n*-dodecyl carbamate**:

ATR-IR ν (cm^{-1}): 3340 ν(N-H), 2956 ν_{as}(C-H$_3$), 2919 ν_{as}(C-H$_2$), 2849 ν_{s}(C-H$_2$), 1683 ν(C=O), 1532 δ(N-H), 1470 δ(CH$_2$), 1271, 1248 ν_{as}(N-(C=O)-O), 1145, 723, 622.
^{1}H NMR (400 MHz, DMSO-d_6) δ_H (ppm): 7.01 (t, ^3J = 5.8 Hz, 1H, NH^1), 3.91 (t, ^3J = 6.6 Hz, 2H, CH$_2^2$), 2.94 (td, ^3J = 6.6 Hz 2H, CH$_2^3$), 1.52 (p, ^3J = 6.7 Hz, 2H, CH$_2^4$), 1.44–1.34 (m, 2H, CH$_2^5$), 1.33–1.15 (m, 24H, CH$_2^6$), 0.93–0.80 (m, 6H, CH$_3^7$).
^{13}C NMR (101 MHz, DMSO-d_6) δ_C (ppm): 156.79 (C=O^1), 63.91 (CH$_2^2$), 40.47 (CH$_2^3$), 31.78 (CH$_2^4$), 31.41 (CH$_2^4$), 29.87 (CH$_2^4$), 29.52 (CH$_2^4$), 29.49 (CH$_2^4$), 29.46 (CH$_2^4$), 29.45 (CH$_2^4$), 29.19 (CH$_2^4$), 26.67 (CH$_2^4$), 25.53 (CH$_2^4$), 22.57 (CH$_2^4$), 22.51 (CH$_2^4$), 14.41 (CH$_2^5$), 14.33 (CH$_2^5$).
ASAP-MS: $C_{19}H_{39}NO_2$ $[M+H]^+$, calculated: 314.30, found: 314.4.

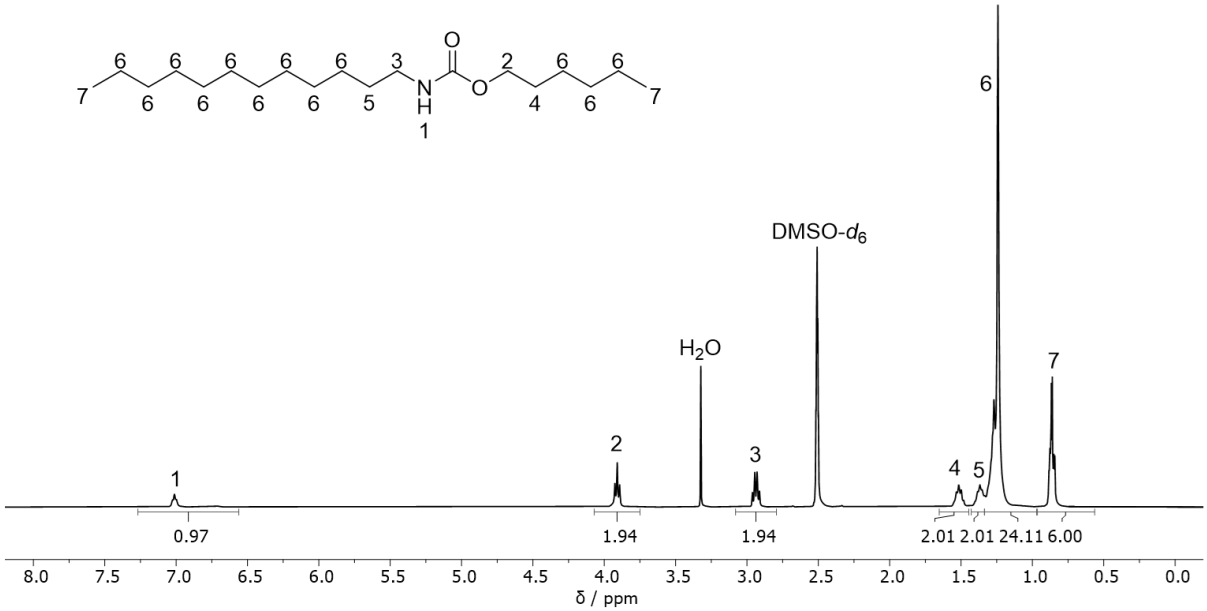

Figure S138 *^{1}H NMR spectrum (DMSO-d_6) of O-n-hexyl-N-n-dodecyl carbamate.*

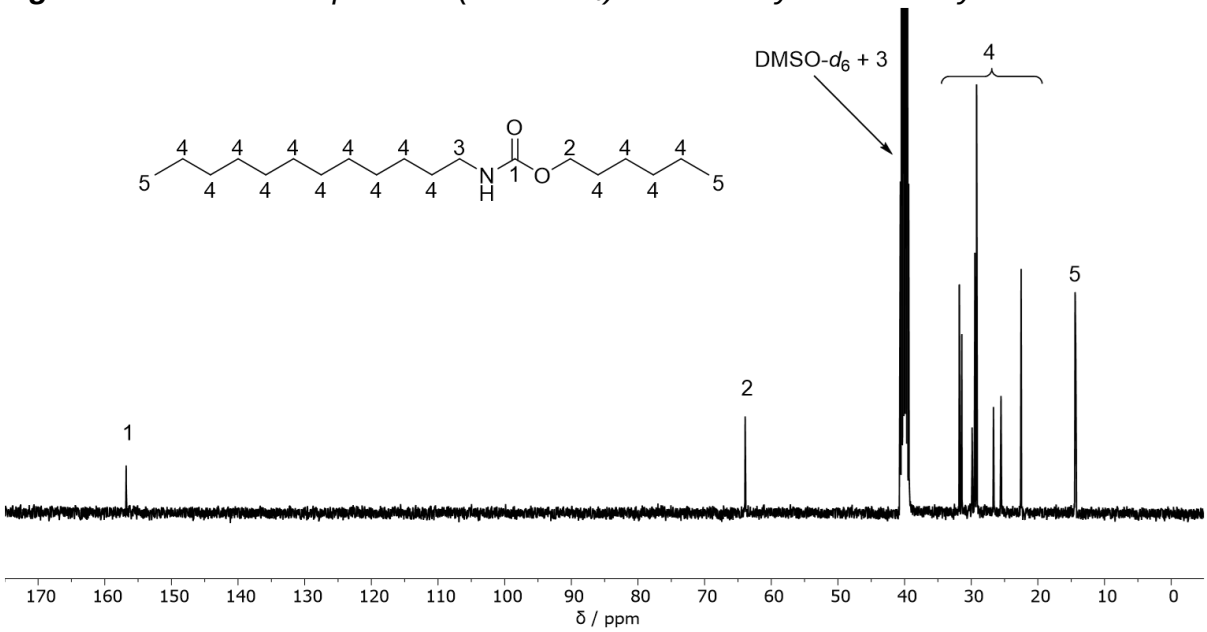

Figure S139 *^{13}C NMR spectrum (DMSO-d_6, 1024 scans) of O-n-hexyl-N-n-dodecyl carbamate.*

***O*-*n*-Hexyl-*N*-*n*-dodecyl thiocarbamate**:

ATR-IR ν (cm^{-1}): 3246 ν(N-H), 2954 ν_{as}(C-H$_3$), 2923 ν_{as}(C-H$_2$), 2851 ν_{s}(C-H$_2$), 1549 δ(N-H), 1518, 1465 δ(CH$_2$), 1403, 1337, 1164 ν(C=S), 1121, 724.
^{1}H NMR (400 MHz, CDCl$_3$) δ_H (ppm): 6.60 (s br, 1H, NH^{1a}), 6.18 (s br, 1H, NH^{1b}), 4.47 (t, ^3J = 6.6 Hz, 2H, CH$_2^{2a}$), 4.40 (t, ^3J = 6.8 Hz, 2H, CH$_2^{2b}$), 3.53 (td, ^3J = 7.3, 5.7 Hz, 2H, CH$_2^{3a}$), 3.25 (td, ^3J = 7.1, 5.8 Hz, 2H, CH$_2^{3b}$), 1.79–1.45 (m, 4H, CH$_2^{4,5}$), 1.45–1.21 (m, 24H, CH$_2^{6}$), 0.94–0.81 (m, 6H, CH$_2^{7}$).
^{13}C NMR (101 MHz, CDCl$_3$) δ_C (ppm): 190.49 (C=O^{1a}), 190.13 (C=O^{1b}), 72.12 (CH$_2^{2a}$), 70.52 (CH$_2^{2b}$), 45.26 (CH$_2^{3a}$), 43.17 (CH$_2^{3b}$), 31.92 (CH$_2^{4}$), 31.49 (CH$_2^{4}$), 31.42 (CH$_2^{4}$), 29.64 (CH$_2^{4}$), 29.62 (CH$_2^{4}$), 29.57 (CH$_2^{4}$), 29.51 (CH$_2^{4}$), 29.49 (CH$_2^{4}$), 29.34 (CH$_2^{4}$), 29.28 (CH$_2^{4}$), 29.18 (CH$_2^{4}$), 29.12 (CH$_2^{4}$), 28.68 (CH$_2^{4}$), 28.65 (CH$_2^{4}$), 28.61 (CH$_2^{4}$), 26.88 (CH$_2^{4}$), 26.77 (CH$_2^{4}$), 25.60 (CH$_2^{4}$), 25.55 (CH$_2^{4}$), 22.69 (CH$_2^{4}$), 22.56 (CH$_2^{4}$), 22.55 (CH$_2^{4}$), 14.12 (CH$_2^{5}$), 14.00 (CH$_2^{6}$).
ASAP MS: $C_{19}H_{39}NOS$ $[M+H]^+$, calculated: 330.28, found: 330.3.

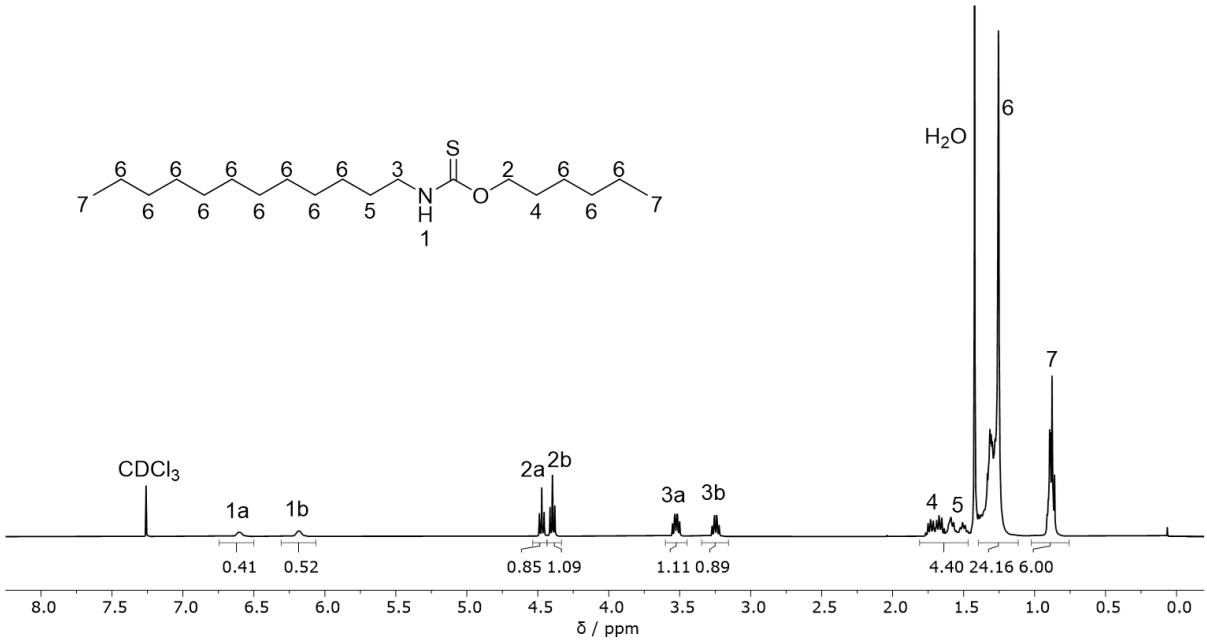

Figure S140 *^{1}H NMR spectrum (CDCl$_3$) of O-n-hexyl-N-n-dodecyl thiocarbamate. Signals a and b are observed because of the cis/trans isomerism of the thiocarbamte moiety caused by the hindered rotation due to the partial double bond character.*[313]

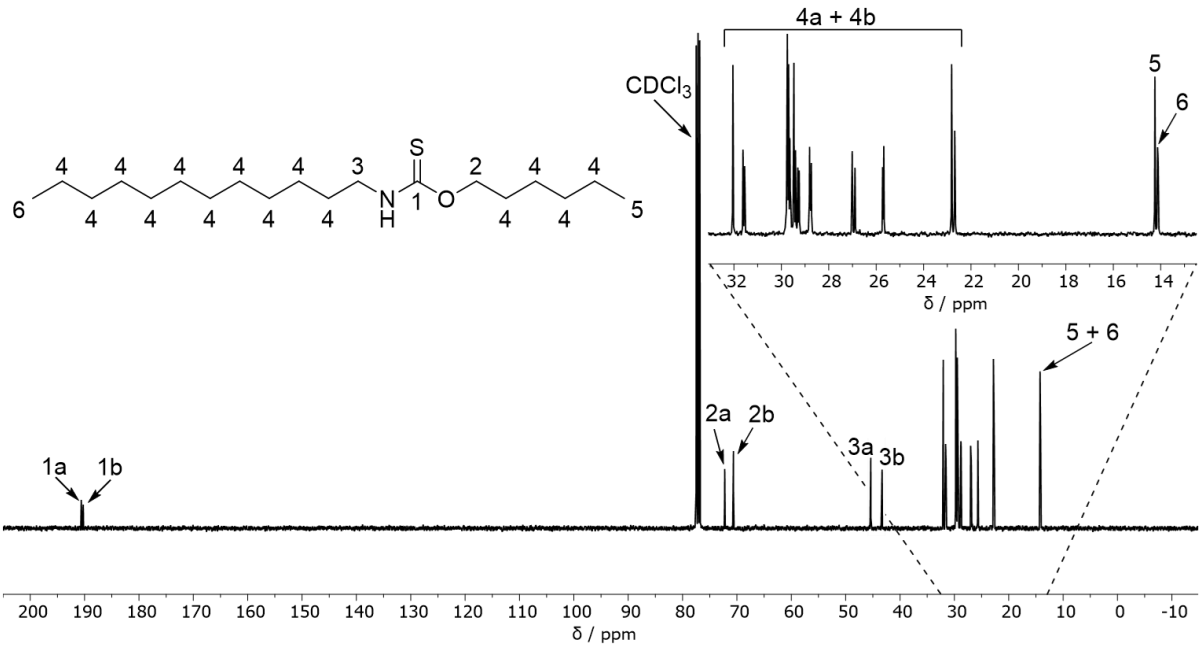

Figure S141 *^{13}C NMR spectrum ($CDCl_3$, 1024 scans) of O-n-hexyl-N-n-dodecyl thiocarbamate. Signals a and b are observed because of the cis/trans isomerism of the thiocarbamte moiety caused by the hindered rotation due to the partial double bond character.*[313]

Model Reaction Screening

The model reactions were screened using gas chromatography. Calibrations for the thionocarbamate and the (oxo-)carbamate compound were created and then used for the quantification as shown in **Figure S143**.

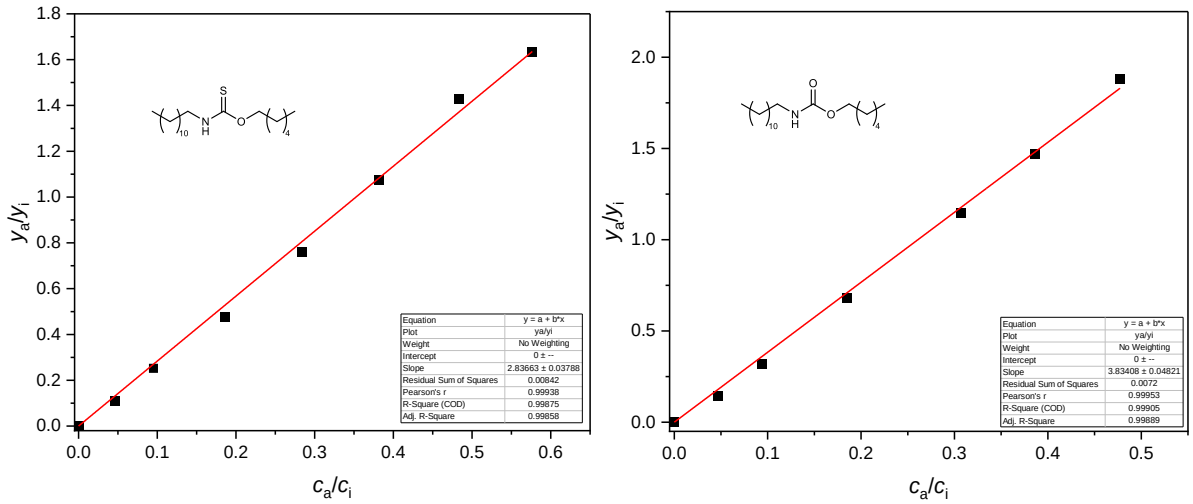

Figure S142 *Gas chromatography calibration curves of O-n-hexyl-N-n-dodecyl thiocarbamate (left) and O-n-hexyl-N-n-dodecyl carbamate (right) with 1,3,5-trimethoxybenzene as internal standard.*

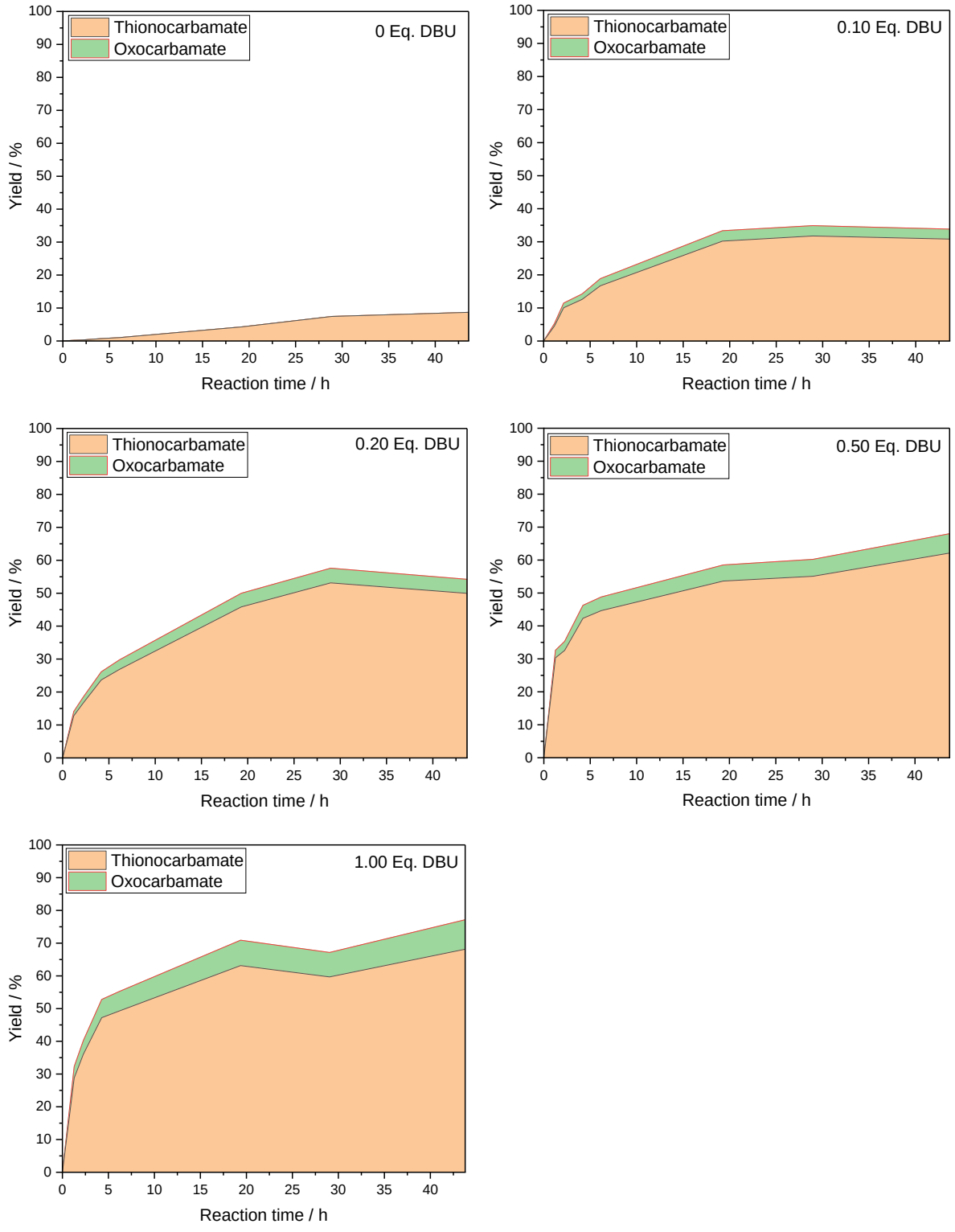

Figure S143 *Formation of O-n-hexyl-N-n-dodecyl thiocarbamate and O-n-hexyl-N-n-dodecyl carbamate over time with 0–1.00 eq. DBU at 70 °C. Determined via gas chromatography.*

***N,N'* Didodecylurea:**

ATR-IR ν (cm^{-1}): 3336 ν(N-H), 2956 ν_{as}(C-H$_3$), 2917 ν_{as}(C-H$_2$), 2849 ν_{s}(C-H$_2$), 1613 ν(C=O), 1569 δ(N-H), 1467 δ(CH$_2$), 1240, 722, 609, 588.
^{1}H NMR (400 MHz, $CDCl_3$) δ_H (ppm): 4.17 (t, ^3J = 5.7 Hz, 2H, NH^1), 3.14 (td, ^3J = 7.2, 5.6 Hz, 4H, CH$_2^2$), 1.49 (p, ^3J = 7.2 Hz, 4H, CH$_2^3$), 1.38–1.19 (m, 36H, CH$_2^4$), 0.88 (t, ^3J = 6.7 Hz, 6H, CH$_3^5$).
The analytical data is in accordance to the data reported in literature.[338]

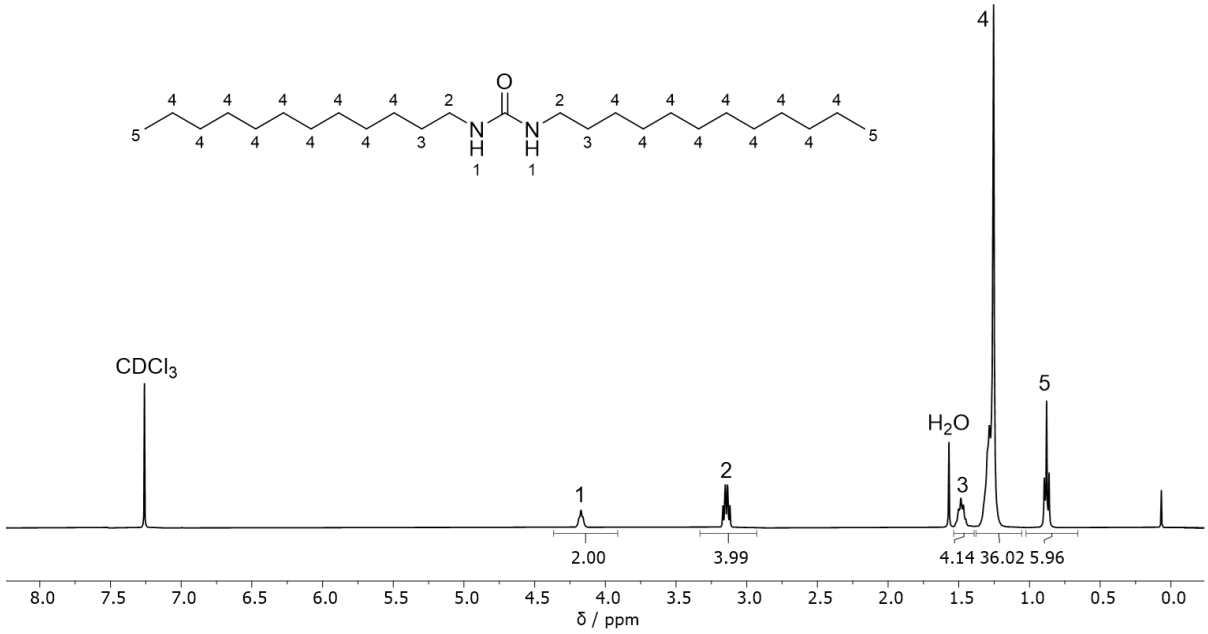

Figure S144 *^{1}H NMR spectrum ($CDCl_3$) of N,N' didodecylurea.*

Synthesis of Diisocyanides and Diisothiocyanates

Diisocyanides were synthesized according to the procedure of Meier *et al*.[327] and diisothiocyanates were synthesized according to the procedure of Meier *et al.*[266]

n-Dodecylisocyanide:

^{1}H NMR (400 MHz, $CDCl_3$) δ_H (ppm): 3.37 (tt, ^3J = 6.8 Hz, $^3J_{N\text{-}H}$ = 2.0 Hz, 2H, CH_2^1), 1.74-1.61 (m, 2H, CH_2^2), 1.42 (p, ^3J = 7.2 Hz, 2H, CH_2^3), 1.36–1.17 (m, 16H, CH_2^4), 0.88 (t, ^3J = 7.1 Hz, 3H, CH_3^5).

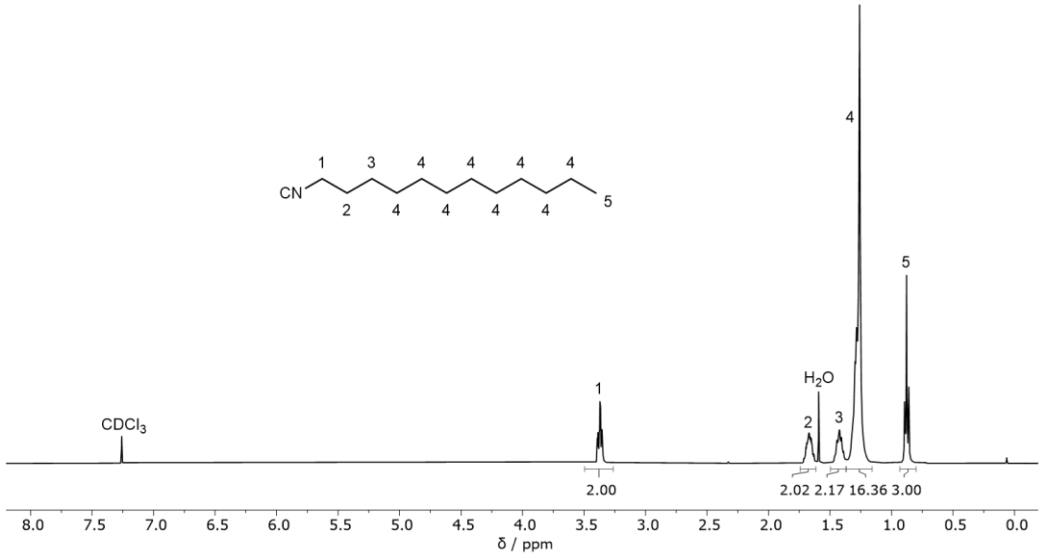

Figure S145 *^{1}H NMR spectrum ($CDCl_3$) of n-dodecylisocyanide.*

Oleylisocyanide:

^{1}H NMR (400 MHz, $CDCl_3$) δ_H (ppm): 5.44–5.29 (m, 2H, CH^1), 3.42–3.33 (m, 2H, CH_2^2), 2.06–1.92 (m, 4H, CH_2^3), 1.74–1.61 (m, 2H, CH_2^4), 1.50–1.39 (m, 2H, CH_2^5), 1.38–1.15 (m, 12H, CH_2^6), 0.88 (t, ^3J = 6.7 Hz, 3H, CH_3^7).

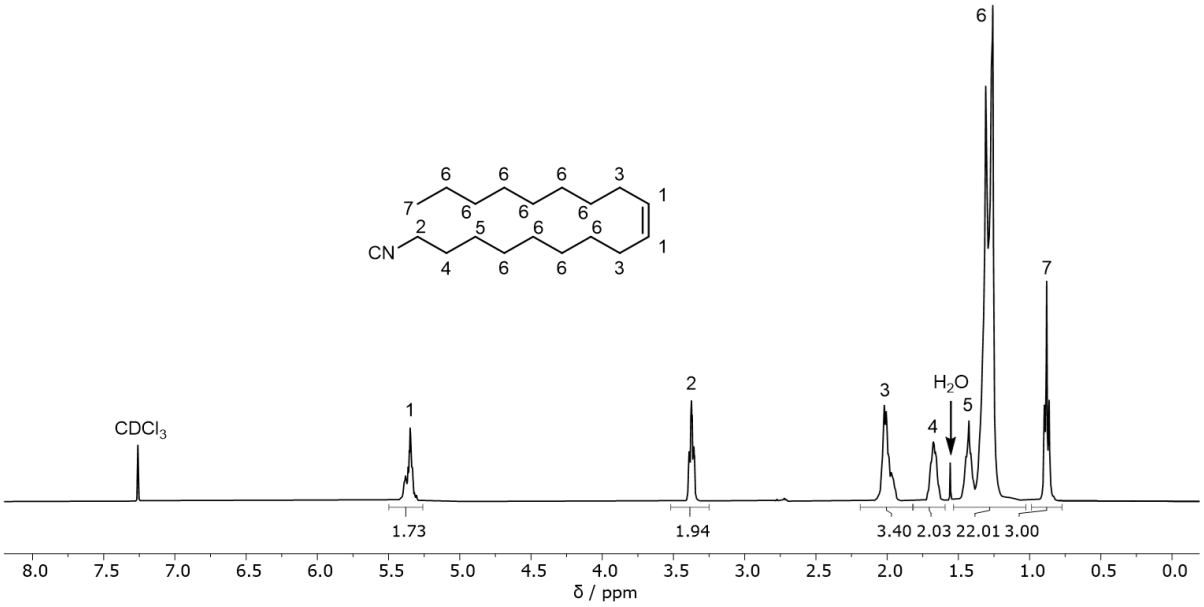

Figure S146 *^{1}H NMR spectrum ($CDCl_3$) of oleylisocyanide.*

***n*-Dodecylisothiocyanate:**

^{1}H NMR (400 MHz, $CDCl_3$) δ_H (ppm): 3.44 (t, ^{3}J = 6.7 Hz, 2H, CH_2^{1}), 1.68–1.57 (m, 2H, CH_2^{2}), 1.34 (d, ^{3}J = 7.1 Hz, 2H, CH_2^{3}), 1.28–1.12 (m, 16H, CH_2^{4}), 0.81 (t, ^{3}J = 6.8 Hz, 3H, CH_3^{5}).

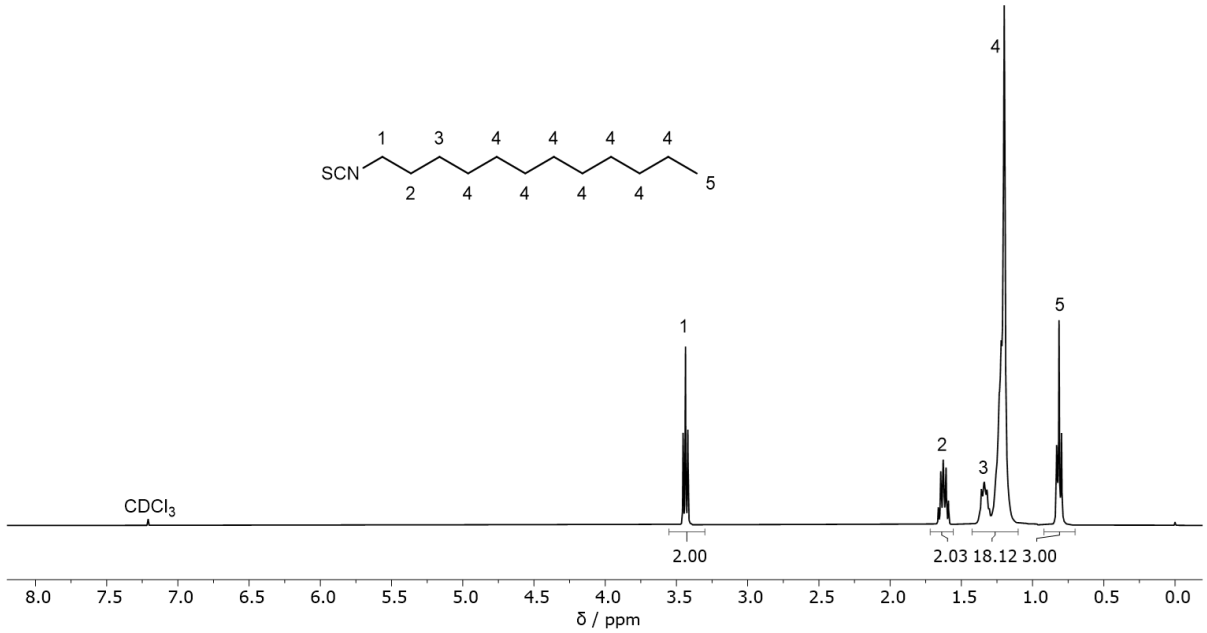

Figure S147 *^{1}H NMR spectrum ($CDCl_3$) of n-dodecylisothiocyanate.*

DS Determination by ^{31}P NMR Method

The DS was determined by derivatization of the cellulose sample using a phosphorylating agent according to a procedure developed by Kilpeläinen *et al*.[208]: An exact amount of 10 mg of each sample was dissolved in 1 mL of pyridine followed by the addition of 1 mL $CDCl_3$. Next, 2-chloro-4,4,5,5-tetramethyl-1,3,2- dioxaphospholane (2-Cl-TMDP, 50 µL, 0.63 mmol) was added and the solution was stirred for 15 min. Then, the internal standard *endo-N*-hydroxy-5-norbornene-2,3-dicarboximide (60 µL, 123.21 mM in pyridine/$CDCl_3$=3:2, 0.0074 mmol) was added and the solution was stirred for further 10 min. 0.6 mL of the solution was then transferred to an NMR tube and a ^{31}P NMR measurement was performed at 162 Mhz. The DS values were calculated analogous to equations (*18*) and (*19*).

Thiocarbamate Content Calculation from Elemental Aanalysis Data

For the quantification of thiocarbamate formation besides (oxo)carbamate formation, elemental analysis was used. From the molar ratio of sulfur (S) to nitrogen (N), the mole fraction of thiocarbamate (x_S) can be calculated according to equation (*27*).

$$x_S = \frac{S}{N} = \frac{\frac{w_S}{M(S)}}{\frac{w_N}{M(N)}} \leq 1 \tag{27}$$

w_S: mass fraction of sulfur
w_N: mass fraction of nitrogen
$M(S)$: molar mass of sulfur $M(S) = 32.0650\ \frac{g}{mol}$
$M(N)$: molar mass of nitrogen $M(N) = 14.0067\ \frac{g}{mol}$

DS Determination by Elemental Analysis

The degree of substitution determined by elemental analysis (DS_{EA}) was calculated based on the ratio of nitrogen to carbon (equation (*28*)) and on the ratio of nitrogen to hydrogen (equation (*29*)). In equation (*28*) the $DS_{EA,NC}$ multiplied by the number of nitrogen atoms of the substituent ($n_{N,S}$) equals the amount of nitrogen (N) and the amount of carbon (C) equals the number of carbon atoms of the substituent ($n_{C,S}$)

multiplied by the $DS_{\mathrm{EA,NC}}$ plus the number of carbon atoms of the anhydroglucose unit ($n_{\mathrm{C,AGU}}$).

$$\frac{\mathrm{N}}{\mathrm{C}} = \frac{n_{\mathrm{N,S}} \times DS_{\mathrm{EA,NC}}}{n_{\mathrm{C,S}} \times DS_{\mathrm{EA,NC}} + n_{\mathrm{C,AGU}}} \tag{28}$$

$DS_{\mathrm{EA,NC}}$: degree of substitution determined *via* elemental analysis based on the nitrogen to carbon ratio
$n_{\mathrm{N,S}}$: number of nitrogen atoms introduced per OH functionalization = 1
$n_{\mathrm{C,S}}$: number of carbon atoms of the substituent = 13, 5, 7, 19 for dodecyl, butyl, cyclohexyl, and oleyl moiety, respectively.
$n_{\mathrm{C,AGU}}$: number of carbon atoms of the anhydroglucose unit = 6

The calculation of the $DS_{\mathrm{EA,NH}}$ is analogous to the calculation of the $DS_{\mathrm{EA,NC}}$. In equation (*29*) the $DS_{\mathrm{EA,NH}}$ multiplied by the number of nitrogen atoms of the substituent equals the amount of nitrogen (N) and the amount of hydrogen (H) equals the number of hydrogen atoms of the substituent ($n_{\mathrm{C,S}}$) multiplied by the $DS_{\mathrm{EA,NC}}$ plus the number of hydrogen atoms of the anhydroglucose unit ($n_{\mathrm{C,AGU}}$). In addition, for the calculation of the amount of hydrogen (H) one hydrogen on the hydroxyl group is substituted per substituent.

$$\frac{\mathrm{N}}{\mathrm{H}} = \frac{n_{\mathrm{N,S}} \times DS_{\mathrm{EA,NH}}}{n_{\mathrm{H,S}} \times DS_{\mathrm{EA,NH}} + n_{\mathrm{H,AGU}} - n_{\mathrm{H}} \times DS_{\mathrm{EA,NH}}} \tag{29}$$

$DS_{\mathrm{EA,NH}}$: degree of substitution determined *via* elemental analysis based on the nitrogen to hydrogen ratio
$n_{\mathrm{N,S}}$: number of nitrogen atoms introduced per OH functionalization = 1
$n_{\mathrm{H,S}}$: number of hydrogen atoms of the substituent = 26, 10, 12, 36 for dodecyl, butyl, cyclohexyl, and oleyl moiety, respectively.
$n_{\mathrm{H,AGU}}$: number of hydrogen atoms of the anhydroglucose unit = 10
n_{H}: number of hydrogen atoms which are substituted per OH functionalization = 1

The determination of $n_{\mathrm{C,S}}$, $n_{\mathrm{C,AGU}}$, $n_{\mathrm{H,S}}$ and $n_{\mathrm{H,AGU}}$ is exemplary shown in **Figure S148** for a cellulose thiocarbamate sample.

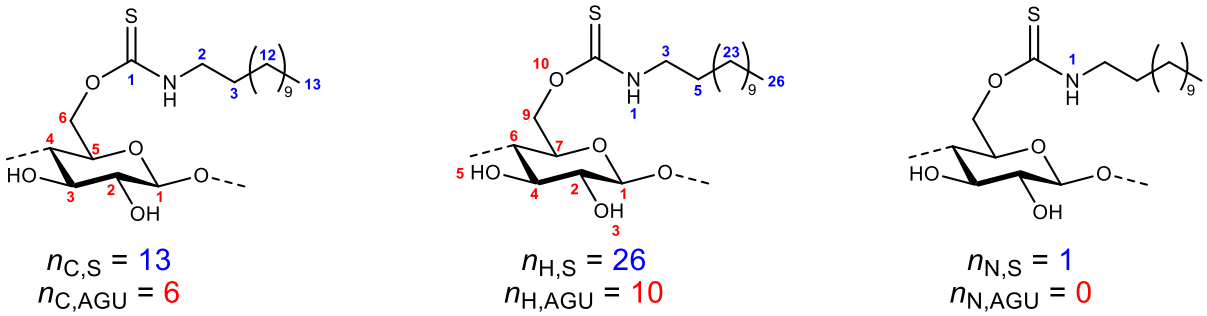

Figure S148 *Illustration for the determination of the number of carbon and hydrogen atoms ($n_{C,S}$, $n_{C,AGU}$, $n_{H,S}$ and $n_{H,AGU}$) in a monosubstituted O-cellulose-N-n-dodecyl thiocarbamate.*

From elemental analysis the mass fraction (w) is determined, which can be divided by the molar mass (M) to calculate the molar content of the respective element (N, C, H) in the measured sample. With this correlation, the equations (*28*) and (*29*) can be written as shown in equations (*30*) and (*31*) to calculate the DS_{EA}.

$$DS_{EA,NC} = \frac{n_{C,AGU} \times \frac{w_N}{M(N)}}{n_{N,S}\frac{w_C}{M(C)} - n_{C,S} \times \frac{w_N}{M(N)}} \tag{30}$$

$$DS_{\mathrm{EA,NH}} = \frac{n_{\mathrm{H,AGU}} \times \frac{w_{\mathrm{N}}}{M(\mathrm{N})}}{n_{\mathrm{N,S}}\frac{w_{\mathrm{H}}}{M(\mathrm{H})} - (n_{\mathrm{H,S}} - n_H) \times \frac{w_{\mathrm{N}}}{M(\mathrm{N})}} \tag{31}$$

w_{H}: mass fraction of hydrogen
w_{C}: mass fraction of carbon
$M(\mathrm{H})$: molar mass of hydrogen $M(\mathrm{H}) = 1.00784\ \frac{\mathrm{g}}{\mathrm{mol}}$
$M(\mathrm{C})$: molar mass of carbon $M(\mathrm{C}) = 12.0107\ \frac{\mathrm{g}}{\mathrm{mol}}$
$M(\mathrm{N})$: molar mass of nitrogen $M(\mathrm{N}) = 14.0067\ \frac{\mathrm{g}}{\mathrm{mol}}$

Table 28 *Elemental analysis raw data of the synthesized O-cellulose thiocarbamates.*

Sample	w_N	w_C	w_H	w_S
CD-1	0.0431	0.6084	0.0963	0.0657
CD-1	0.0423	0.6072	0.0993	0.0486
CD-2	0.0297	0.5326	0.0838	0.0114
CD-2	0.0304	0.5318	0.0821	0.0111
CD-3	0.0338	0.5687	0.0912	0.0268
CD-3	0.033	0.5663	0.0919	0.0247
CD-4	0.0367	0.5756	0.0941	0.049
CD-4	0.0369	0.5686	0.0893	0.0511
CD-5	0.041	0.5996	0.0962	0.0392
CD-5	0.0413	0.6033	0.0961	0.052
CD-6	0.0456	0.6212	0.1011	0.0748
CD-6	0.047	0.6263	0.1025	0.0822
CD-6	0.0448	0.6258	0.1060	0.0732
CD-REC	0.0404	0.5888	0.0914	0.0705
CD-REC	0.0396	0.5858	0.0913	0.0691
CD-REC	0.0392	0.5855	0.0915	0.0693
CC-1	0.0434	0.4996	0.0714	0.0387
CC-1	0.0434	0.5005	0.0716	0.0386
CC-2	0.0485	0.5135	0.0704	0.0568
CC-2	0.0489	0.5131	0.0718	0.057
CB-1	0.0578	0.4839	0.0727	0.0518
CB-1	0.0572	0.4787	0.0724	0.0504
CB-2	0.0578	0.4839	0.0727	0.0518
CB-2	0.0572	0.4787	0.0724	0.0504
CO-1	0.0327	0.6279	0.0983	0.0444
CO-1	0.0329	0.6344	0.1006	0.0467
CO-1	0.0325	0.6337	0.1021	0.0459
CO-2	0.0363	0.6572	0.103	0.0543
CO-2	0.0353	0.6552	0.1029	0.0552
CD-2wt%	0.0391	0.5939	0.0960	0.0502
CD-2wt%	0.0390	0.5922	0.0941	0.0492
CD-4wt%	0.0428	0.6031	0.0964	0.0701
CD-4wt%	0.0425	0.5987	0.0961	0.0692
CD-5wt%	0.0425	0.6048	0.0970	0.0724
CD-5wt%	0.0422	0.6040	0.0973	0.0727
CO-2[a]	0.0355	0.6560	0.1020	0.0543
CO-2[a]	0.0346	0.6554	0.1025	0.0566

[a]Second measurement 2 months later. Calculated: $x_{S,EA}$=69.1±2.3%.

6.3.4. Polythionourethane Thermoset Synthesis – Chapter 4.4

This chapter is based on previously published results by the author of this thesis:

Wolfs, J.; Ribca, I.; Meier, M. A. R.; Johansson, M. Polythionourethane Thermoset Synthesis via Activation of Elemental Sulfur in an Efficient Multicomponent Reaction Approach. *ACS Sustain. Chem. Eng.* **2023**, *11* (9), 3952–3962.[320]

1,5-Diisocyano pentane, 1,12-diisocyano dodecane, and 1,5-diisothiocyanato pentane was synthesized by Robin Kahler. 1,6-Diisocyano hexane and 1,6-diisothiocyanato hexane was synthesized by Xenia Kraft. 1,5-Diisocyanopentane, isophorone diisocyanide, and isophorone diisothiocyanate was synthesized by Jonas Kahler. 1,6-Diisocyano hexane was synthesized by Johanna Rietschel. 1,10-Diisocyano decane, all thionourethane, oxourethane materials, and model compounds were synthesized by the author.

Synthesis of Diisocyanides and Diisothiocyanates

Diisocyanides were synthesized according to the procedure of Meier *et al*.[327] and diisothiocyanates were synthesized according to the procedure of Meier *et al.*[266]

1,5-Diisocyano pentane:

^{1}H-NMR (400 MHz, $CDCl_3$) δ_H (ppm): 3.42 (tt, ^{3}J = 6.6 Hz, ^{2}J = 2.0 Hz, 4H, CH_2^1), 1.79–1.65 (m, 4H, CH_2^2), 1.67–1.54 (m, 2H, CH_2^3).
^{13}C-NMR (126 MHz, $CDCl_3$) δ_C (ppm): 156.3 (t), 41.3 (t), 28.2, 23.2.
ATR-IR ν (cm^{-1}): 2943, 2867, 2147, 1454 , 1353, 1026, 929, 860, 845, 733.
Purity according to GC-measurement: 99+%.
HRMS (ESI): calculated *m/z* for $C_7H_{10}N_2$ [M+H$^+$]=123.0917, found: 123.0918.

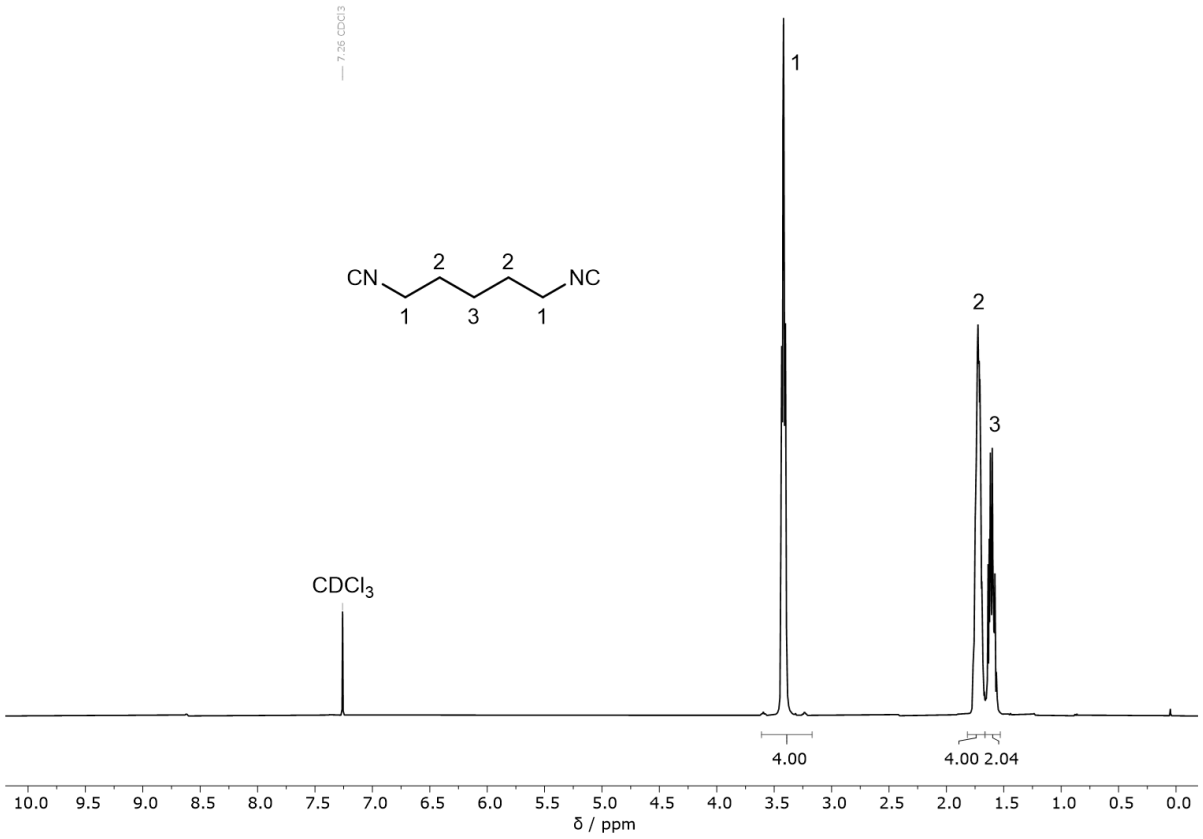

Figure S149 *^{1}H NMR spectrum (400 MHz, $CDCl_3$) of 1,5-diisocyano pentane.*

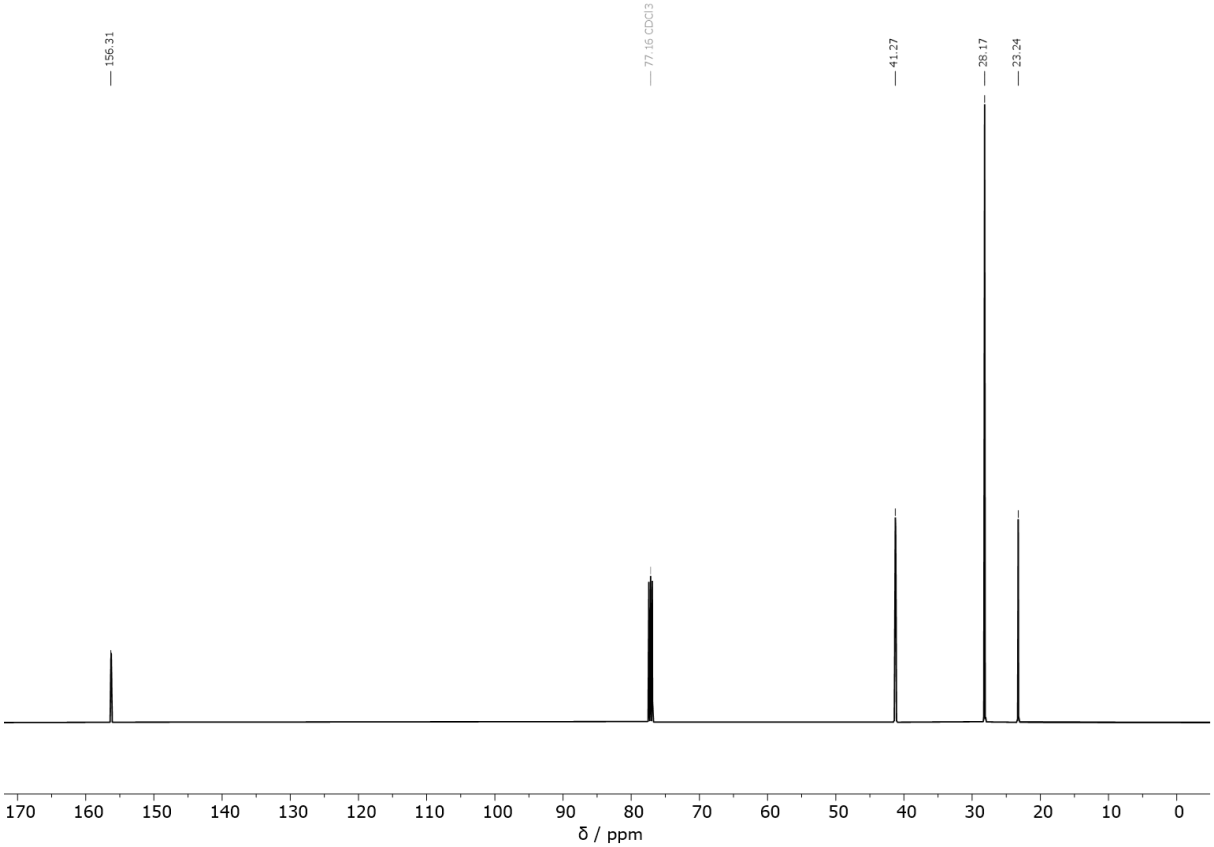

Figure S150 *^{13}C NMR spectrum (126 MHz, $CDCl_3$) of 1,5-diisocyano pentane.*

1,6-Diisocyano hexane

^{1}H-NMR (400 MHz, $CDCl_3$) δ_H (ppm): 3.41 (tt, ^{3}J = 6.7 Hz, ^{2}J = 2.0 Hz, 4H, CH_2^1), 1.78–1.64 (m, 4H, CH_2^2), 1.53–1.43 (m, 4H, CH_2^3).
^{13}C-NMR (126 MHz, $CDCl_3$) δ_C (ppm): 156.0 (t), 41.4 (t), 28.8, 25.5.
ATR-IR ν (cm^{-1}): 2938, 2863, 2147, 1454, 1352, 960, 930.
Purity according to GC-measurement: 99+%.
HRMS (ESI): calculated *m/z* for $C_8H_{12}N_2$ $[M+H^+]$=137.1073, found: 137.1072.

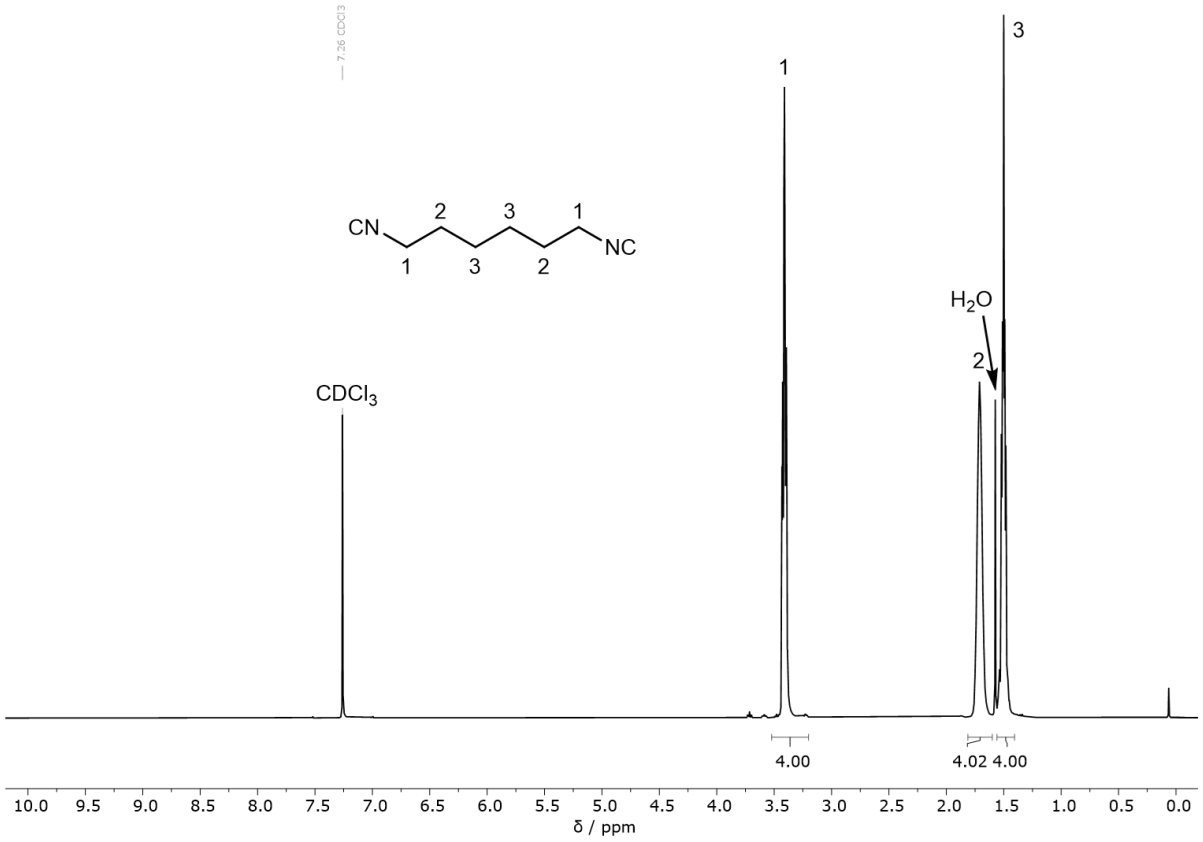

Figure S151 *^{1}H NMR spectrum (400 MHz, $CDCl_3$) of 1,6-diisocyano hexane.*

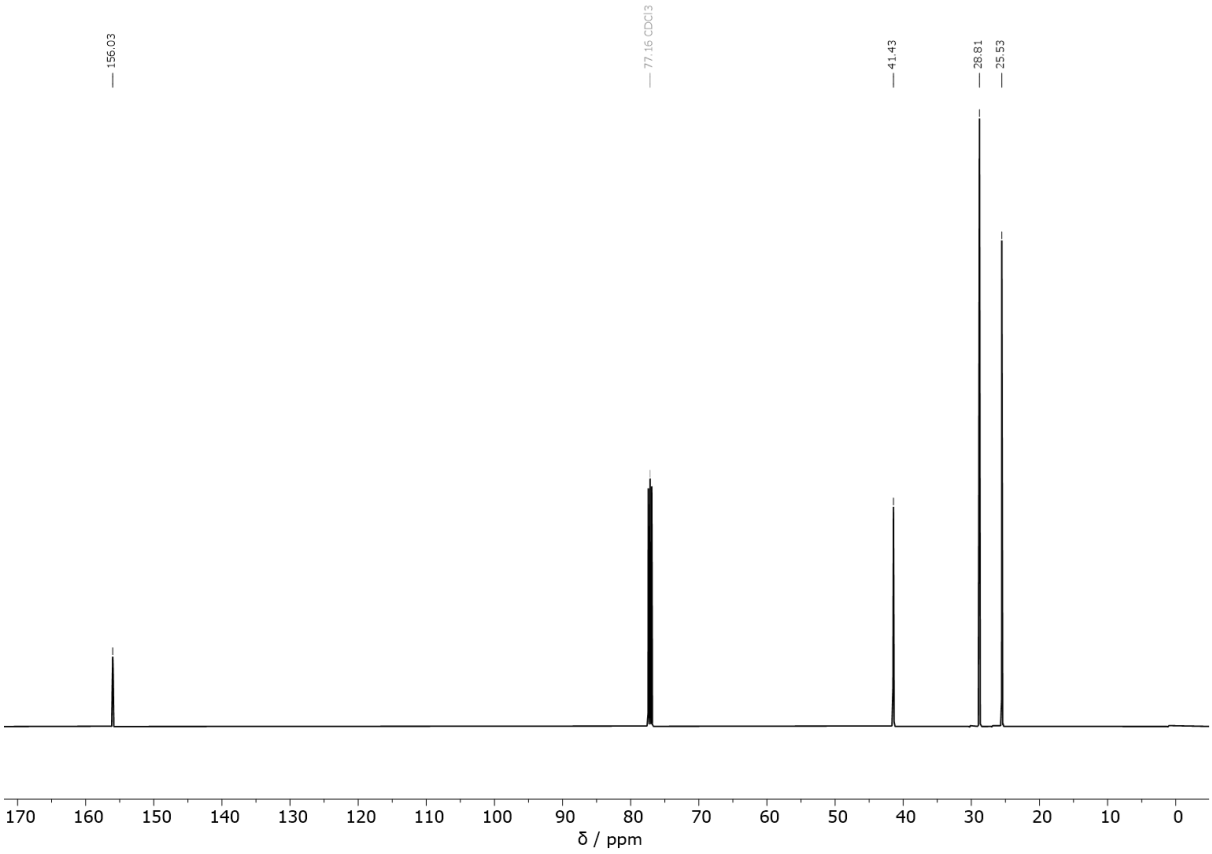

Figure S152 *^{13}C NMR spectrum (126 MHz, $CDCl_3$) of 1,6-diisocyano hexane.*

1,10 Diisocyano decane

^{1}H-NMR (400 MHz, $CDCl_3$) δ_H (ppm): 3.37 (tt, ^{3}J = 6.8 Hz, ^{2}J = 2.0 Hz, 4H, CH_2^1), 1.74–1.61 (m, 4H, CH_2^2), 1.43 (p, ^{3}J = 7.6 Hz, 4H, CH_2^3), 1.33–1.29 (m, 8H, CH_2^3).
^{13}C-NMR (126 MHz, $CDCl_3$) δ_C (ppm): 155.6 (t), 41.5 (t), 29.2, 29.0, 28.6, 26.2.
ATR-IR ν (cm^{-1}): 2927, 2857, 2146, 1454, 1440, 1351, 920, 722, 533.
Purity according to GC-measurement: 99+%.
HRMS (ESI): calculated *m/z* for $C_{12}H_{20}N_2$ $[M+H^+]$=193.1699, found: 193.1698.

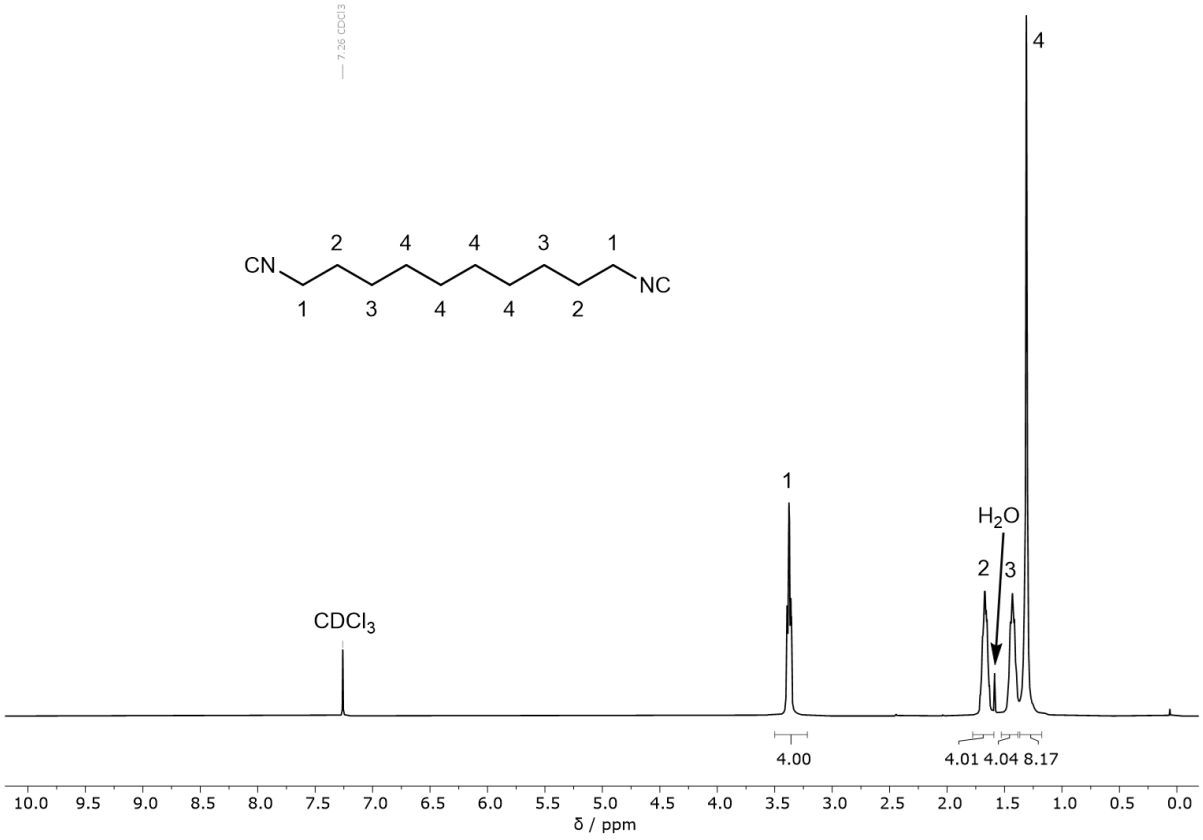

Figure S153 *^{1}H NMR spectrum (400 MHz, $CDCl_3$) of 1,10-diisocyano decane.*

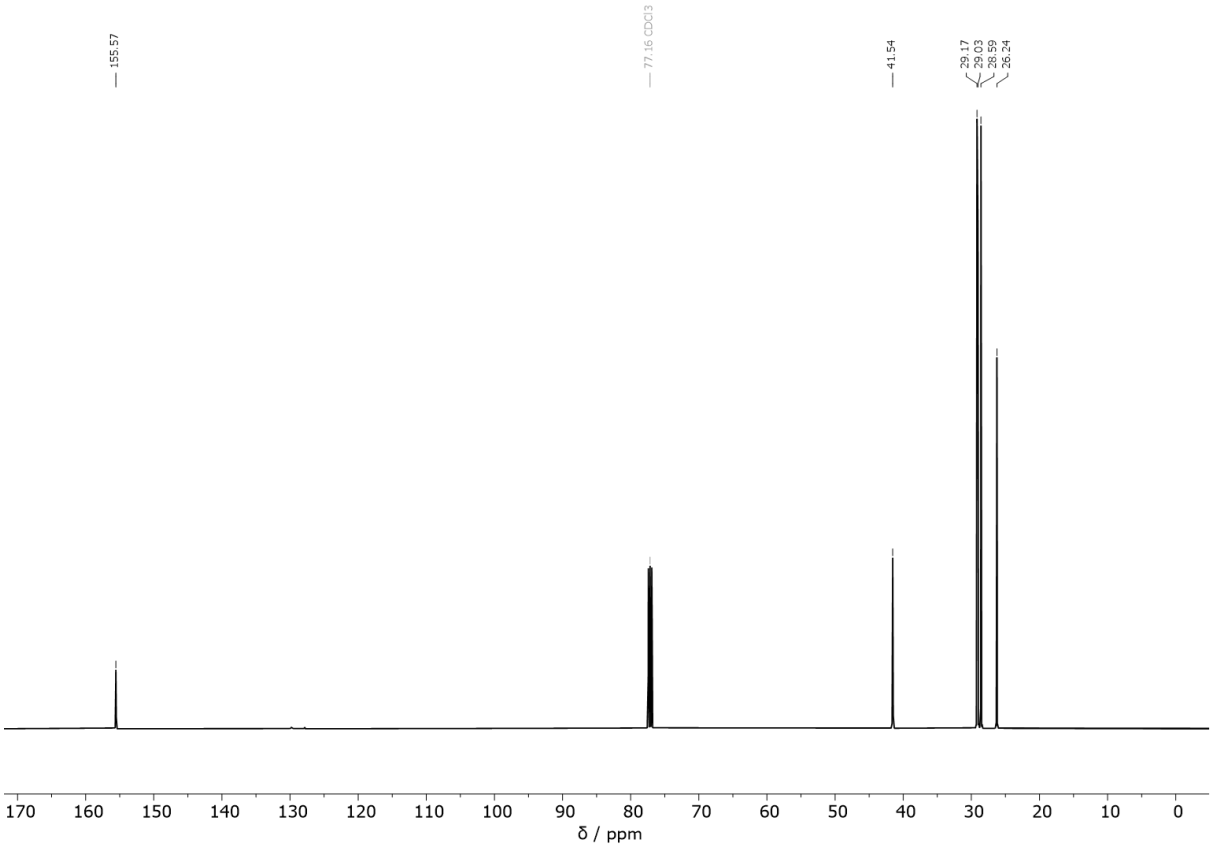

Figure S154 *^{13}C NMR spectrum (126 MHz, $CDCl_3$) of 1,10-diisocyano decane.*

1,12 Diisocyano dodecane

^{1}H-NMR (400 MHz, $CDCl_3$) δ_H (ppm): 3.38 (tt, ^{3}J = 6.9 Hz, ^{2}J = 2.0 Hz, 4H, CH_2^{1}), 1.75–1.62 (m, 4H, CH_2^{2}), 1.44 (p, ^{3}J = 7.6 Hz, 4H, CH_2^{3}), 1.34–1.28 (m, 12H, CH_2^{3}).
^{13}C-NMR (126 MHz, $CDCl_3$) δ_C (ppm): 155.6 (t), 41.6 (t), 29.4, 29.3, 29.1, 28.7, 26.3.
ATR-IR ν (cm^{-1}): 2924, 2855, 2146, 1466, 1453, 1351, 931, 846, 722, 543.
Purity according to GC-measurement: 99+%.
HRMS (ESI): calculated *m/z* for $C_{14}H_{24}N_2$ $[M+H^+]$=221.2012, found: 221.2010.

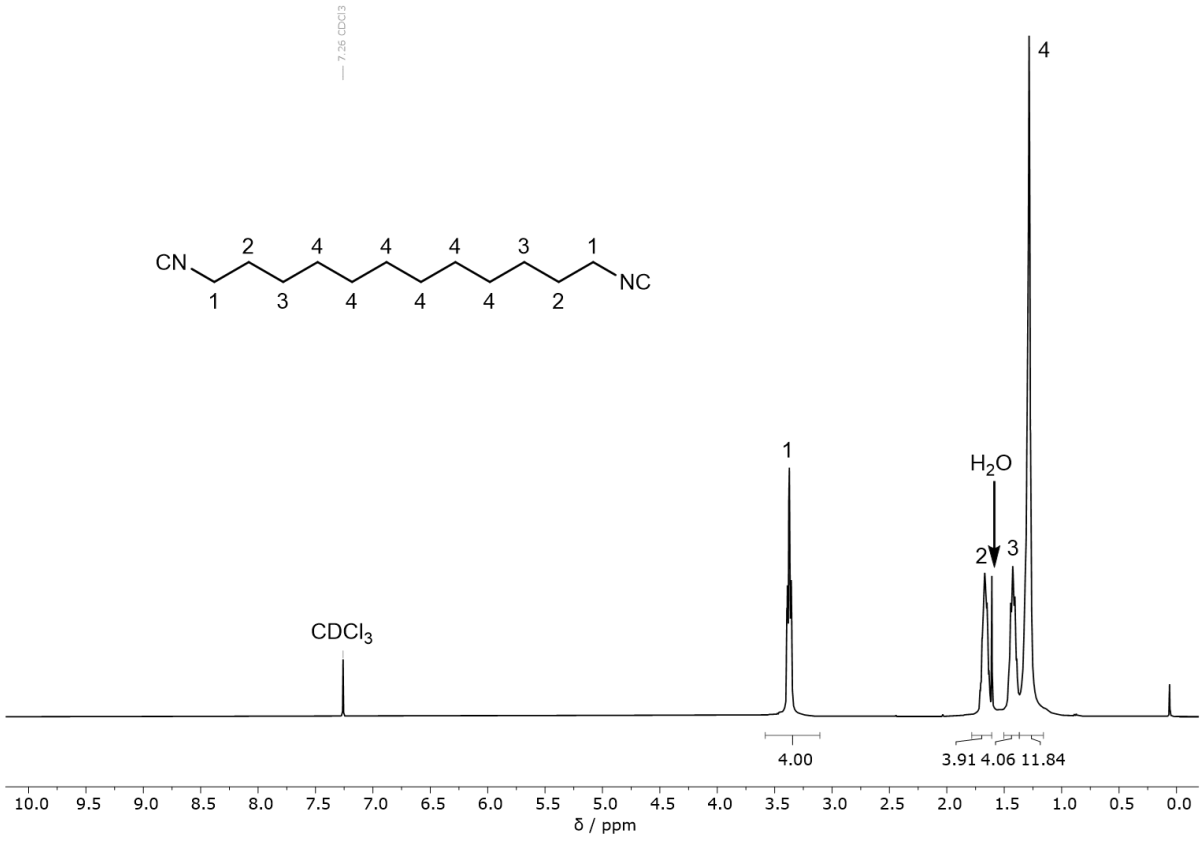

Figure S155 *^{1}H NMR spectrum (400 MHz, $CDCl_3$) of 1,12-diisocyano dodecane.*

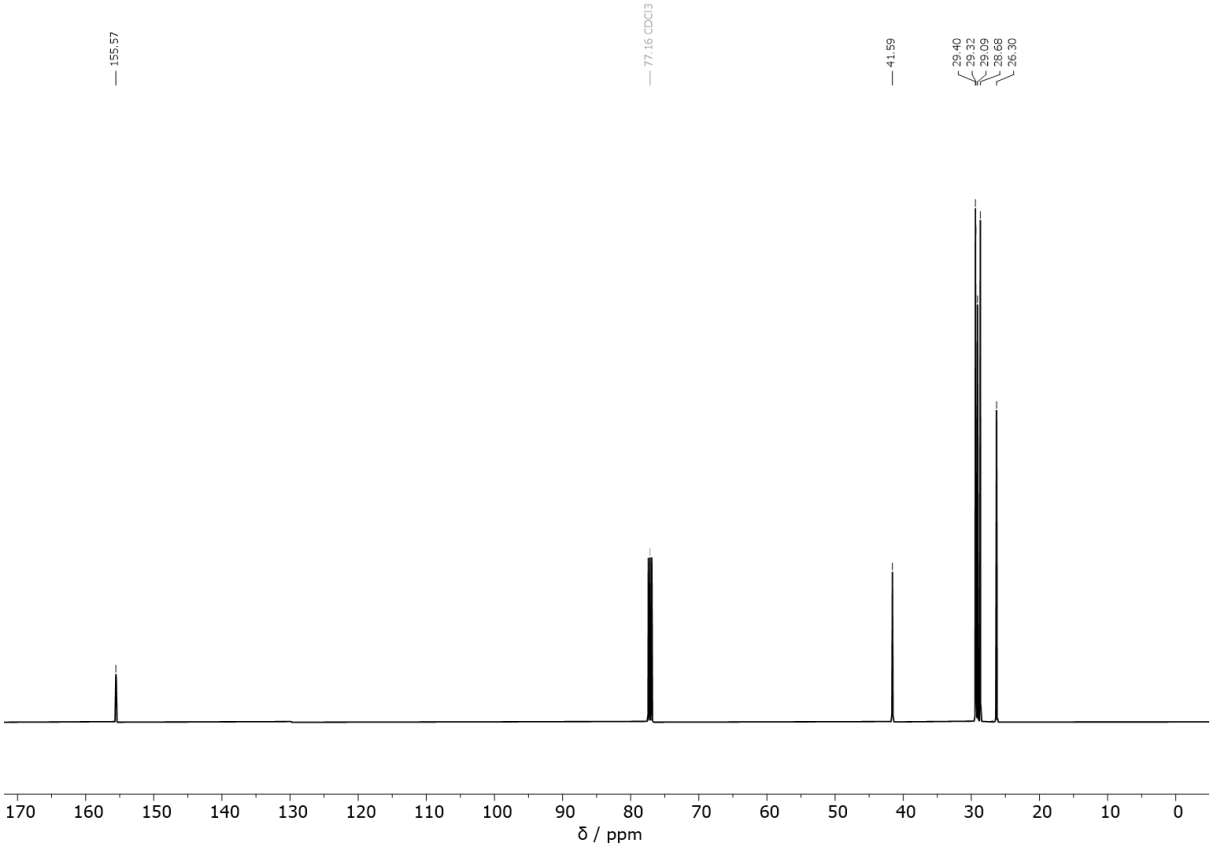

Figure S156 *^{13}C NMR spectrum (126 MHz, $CDCl_3$) of 1,12-diisocyano dodecane.*

Isophorone diisocyanide

This compound could not be purified to a satisfactory degree *via* column chromatography, which can be seen by the signals of impurities in the NMR spectra and 4% impurity according to a GC measurement.

^{1}H-NMR (400 MHz, $CDCl_3$) δ_H (ppm): 3.75–3.67 (m, 0.77H, 1a), 3.66–3.55 (m, 0.24H, 1b), 3.27 (q, 0.47H, 2b), 3.08 (s, 1.55H, 2a), 2.02–1.88 (m, 2H, 3a+b), 1.68–1.01 (m, 7H, 3a+3b+4a+4b), 1.01–0.86 (m, 6H, 5a+b)
^{13}C-NMR (126 MHz, $CDCl_3$) δ_C (ppm): 158.2, 158.0, 155.4, 155.3, 55.6, 49.9, 47.2, 46.9, 45.9, 45.8, 45.7, 41.5, 41.3, 35.2, 35.1, 34.4, 34.2, 31.5, 31.3, 29.5, 27.3, 26.8, 23.2.
ATR-IR ν (cm^{-1}): 2955, 2935, 2874, 2142, 1461, 1392, 1368, 1252, 1201, 1143, 1017, 965, 943, 921, 898, 864, 769, 620, 442
Purity according to GC-measurement: 96%.
HRMS (ESI): calculated *m/z* for $C_{12}H_{18}N_2$ $[M+H^+]$=191.1543, found: 191.1540.

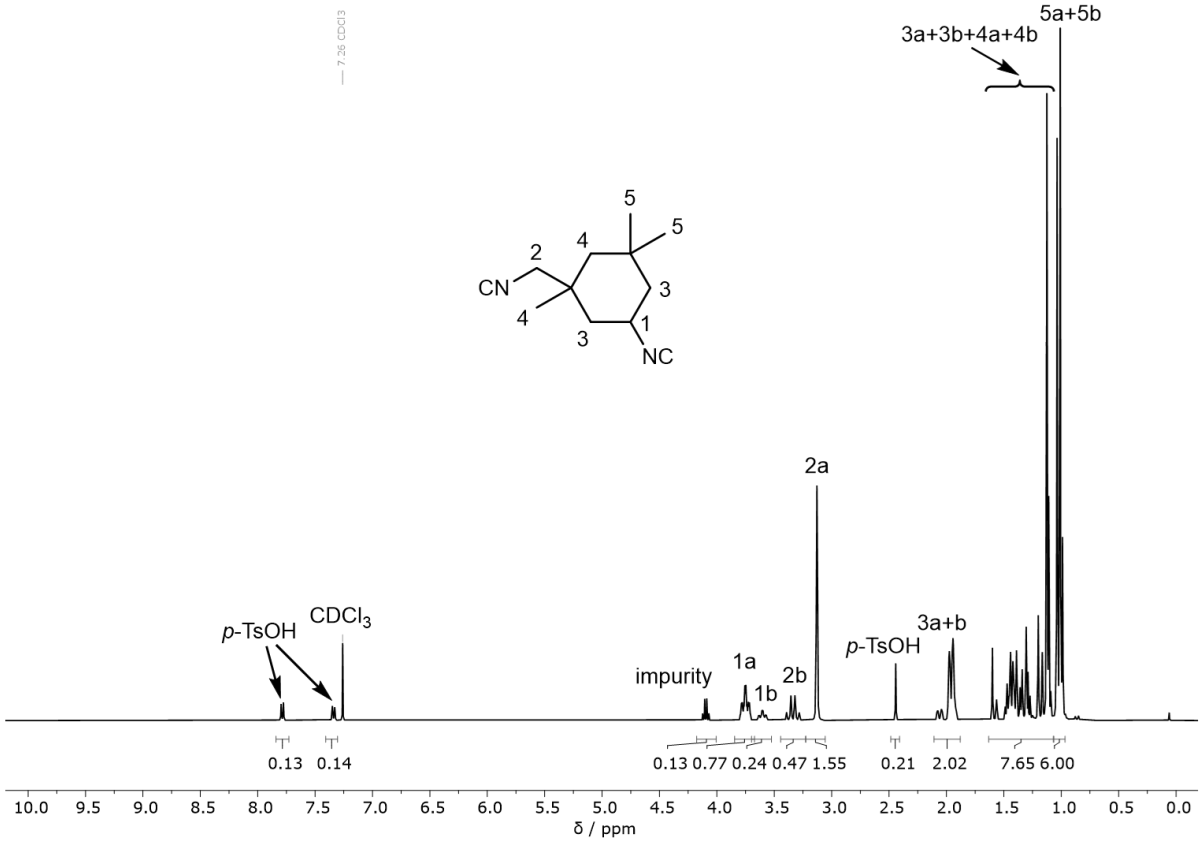

Figure S157 *^{1}H NMR spectrum (400 MHz, $CDCl_3$) of isophorone diisocyanide.*

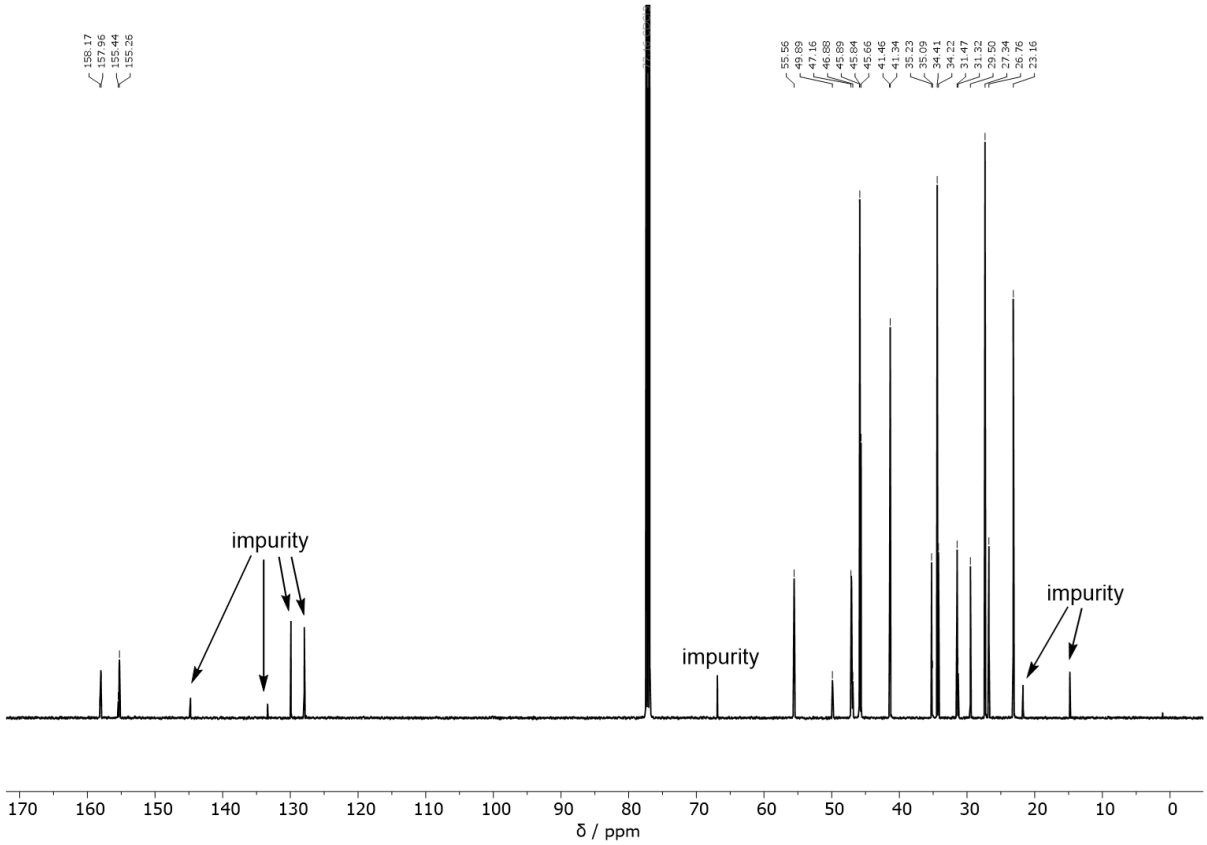

Figure S158 *^{13}C NMR spectrum (126 MHz, $CDCl_3$) of isophorone diisocyanides.*

n-Dodecyl isothiocyanate

^{1}H NMR (400 MHz, $CDCl_3$) δ_H (ppm): 3.44 (t, J = 6.7 Hz, 2H, CH_2^1), 1.68–1.57 (m, 2H, CH_2^2), 1.34 (p, J = 6.8 Hz, 2H, CH_2^3), 1.22–1.18 (m, 16H, CH_2^4), 0.81 (t, J = 6.8 Hz, 3H, CH_2^5).
^{13}C-NMR (126 MHz, $CDCl_3$) δ_C (ppm): 129.6, 45.2, 32.0, 30.1, 29.7, 29.6, 29.5, 29.5, 28.9, 26.7, 22.8, 14.3.
ATR-IR ν (cm^{-1}): 2922, 2852, 2183, 2085, 1455, 1348, 1303, 721.
HRMS (ESI): calculated *m*/*z* for $C_{13}H_{25}N_2$ [M+H$^+$]=228.1780, found: 228.1779.

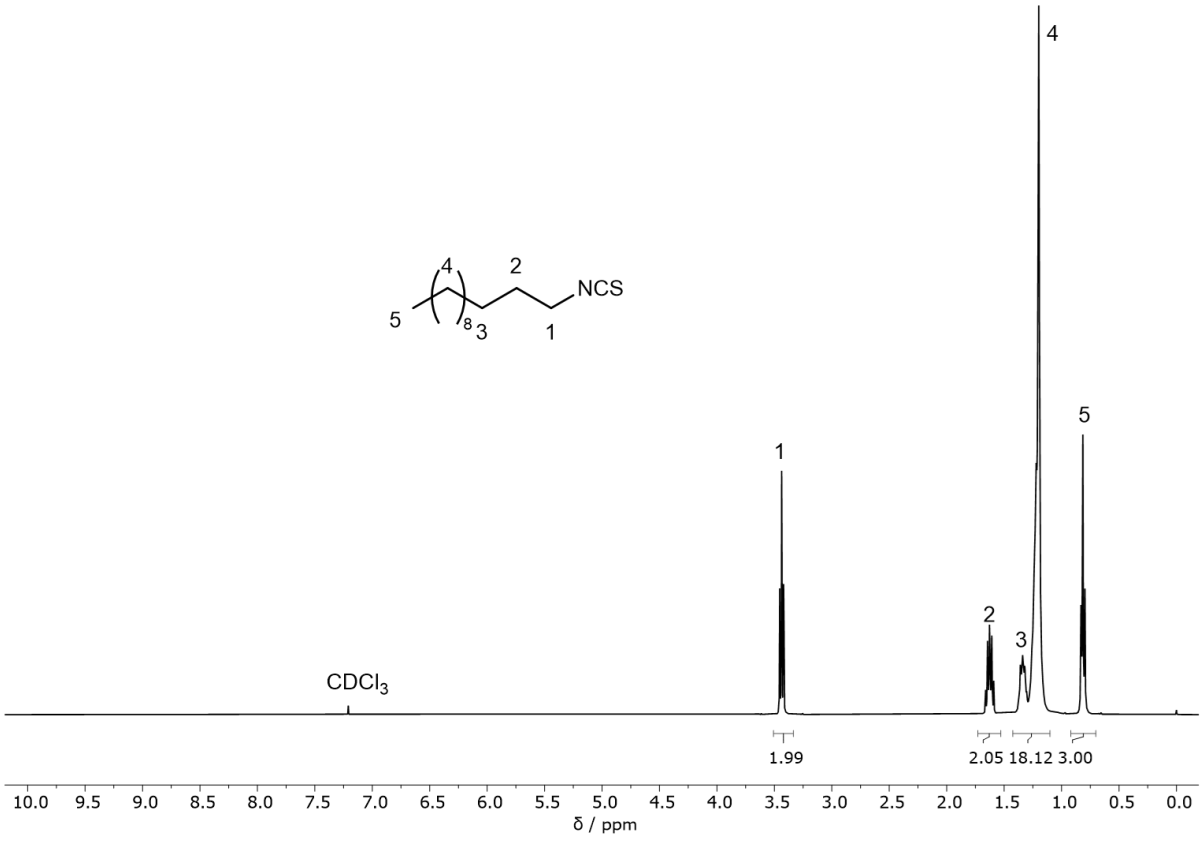

Figure S159 *^{1}H NMR spectrum (400 MHz, $CDCl_3$) of n-dodecyl isothiocyanate.*

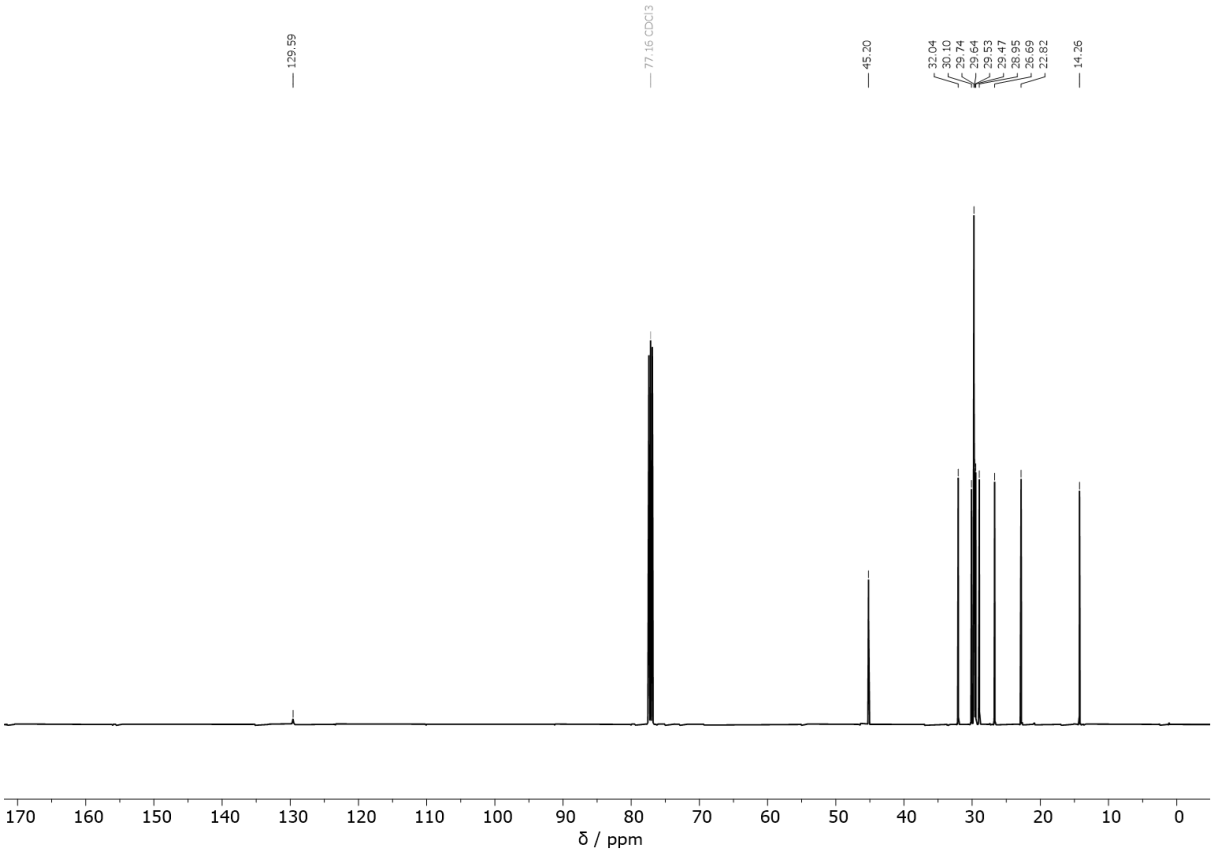

Figure S160 *^{13}C NMR spectrum (126 MHz, $CDCl_3$) of n-dodecyl isothiocyanate.*

1,5-Diisothiocyanato pentane

^{1}H-NMR (400 MHz, $CDCl_3$) δ_H (ppm): 3.56 (t, ^{3}J = 6.5 Hz, 4H, CH_2^1), 1.74 (p, ^{3}J = 6.9 Hz, 4H, CH_2^2), 1.62–1.49 (m, 2H, CH_2^3).
^{13}C-NMR (101 MHz, $CDCl_3$) δ_C (ppm): 130.37, 44.88, 29.29, 23.82.
ATR-IR ν (cm^{-1}): 2923, 2861, 2179, 2073, 1448, 1346, 1081, 728.
Purity according to GC-measurement: 97%.
HRMS (ESI): calculated *m/z* for $C_7H_{10}N_2S_2$ $[M+H^+]$=187.0358, found: 187.0359.

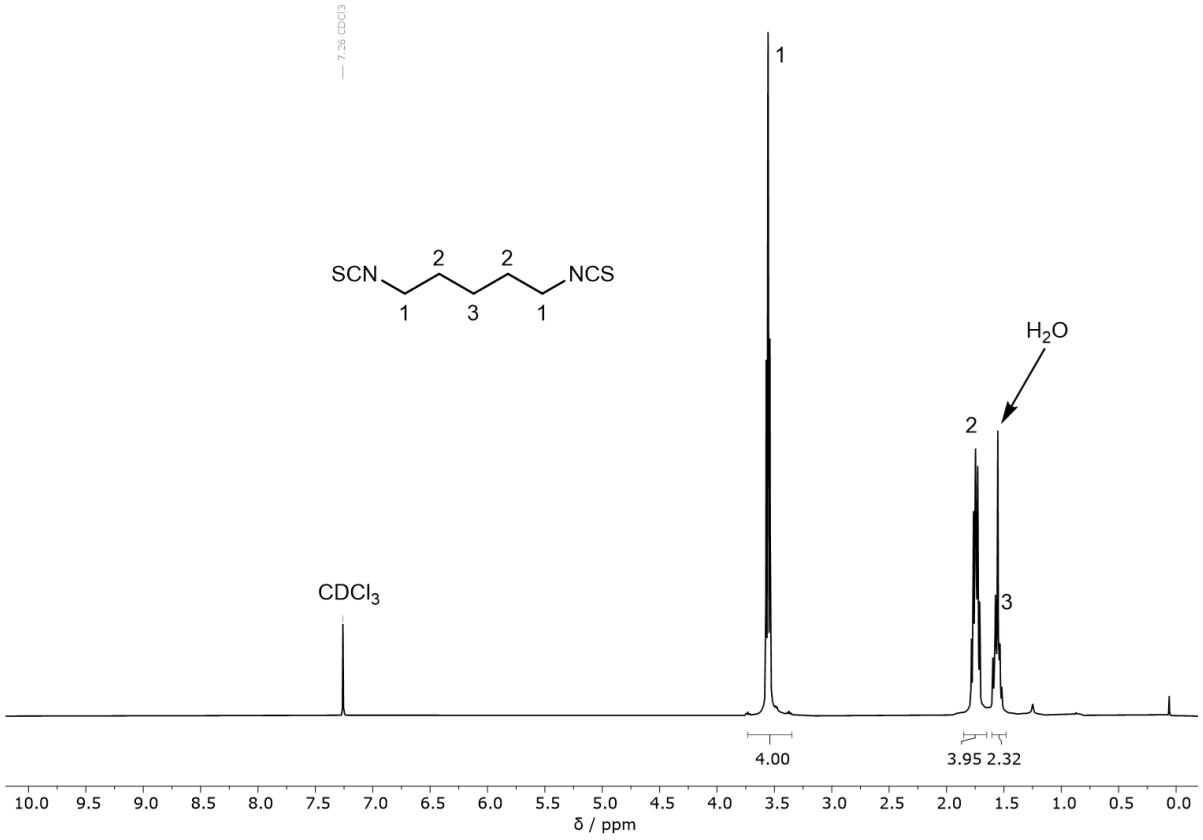

Figure S161 *^{1}H NMR spectrum (400 MHz, $CDCl_3$) of 1,5-diisothiocyanato pentane.*

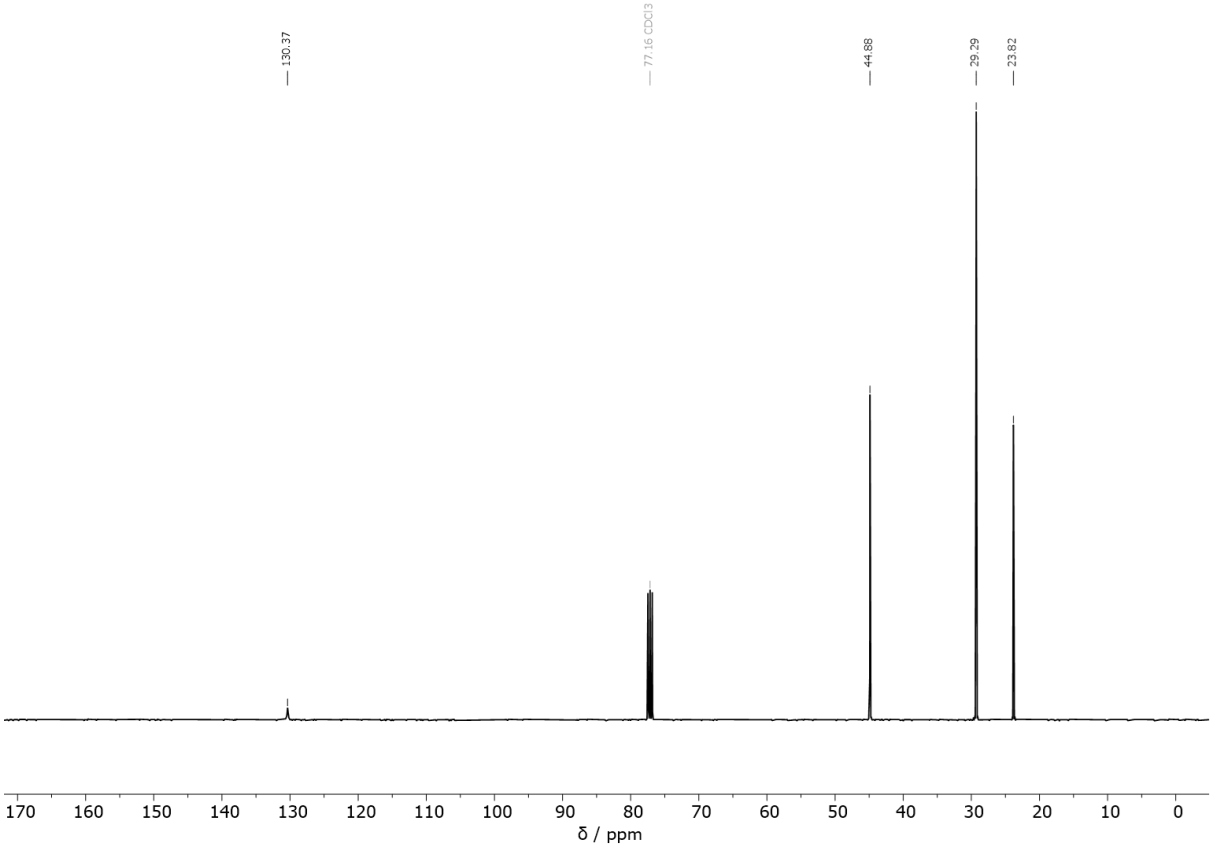

Figure S162 *^{13}C NMR spectrum (101 MHz, $CDCl_3$) of 1,5-diisothiocyanato pentane.*

1,6-Diisothiocyanato hexane

^{1}H-NMR (400 MHz, $CDCl_3$) δ_H (ppm): 3.53 (t, ^{3}J = 6.5 Hz, 4H, CH_2^1), 1.73 (p, ^{3}J = 4.0 Hz, 4H, CH_2^2), 1.53–1.39 (m, 4H, CH_2^3).
^{13}C-NMR (126 MHz, $CDCl_3$) δ_C (ppm): 129.9, 45.0, 29.8, 25.9.
ATR-IR ν (cm^{-1}): 2933, 2860, 2180, 2073, 1447, 1344, 1080, 732, 682.
Purity according to GC-measurement: 99+%.
HRMS (ESI): calculated *m/z* for $C_8H_{12}N_2S_2$ $[M+H^+]$=201.0515, found: 201.0513.

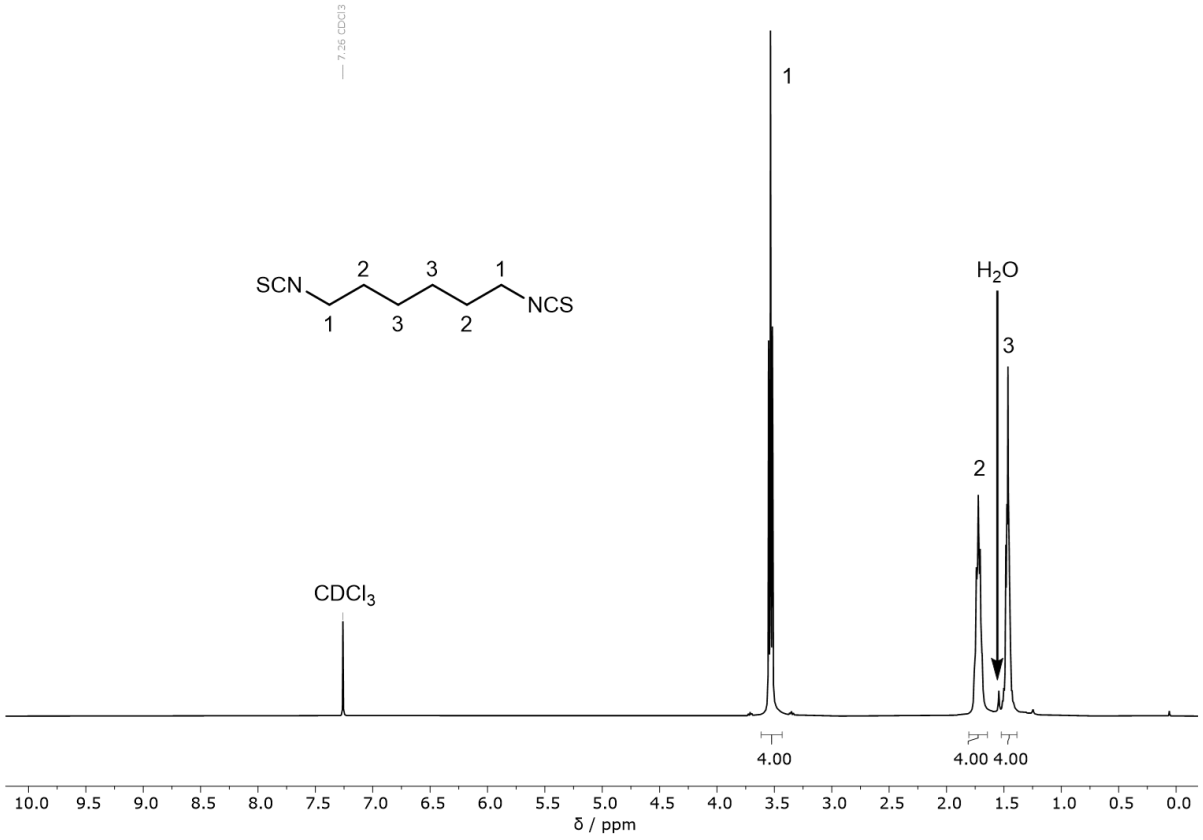

Figure S163 *^{1}H NMR spectrum (400 MHz, $CDCl_3$) of 1,6-diisothiocyanato hexane.*

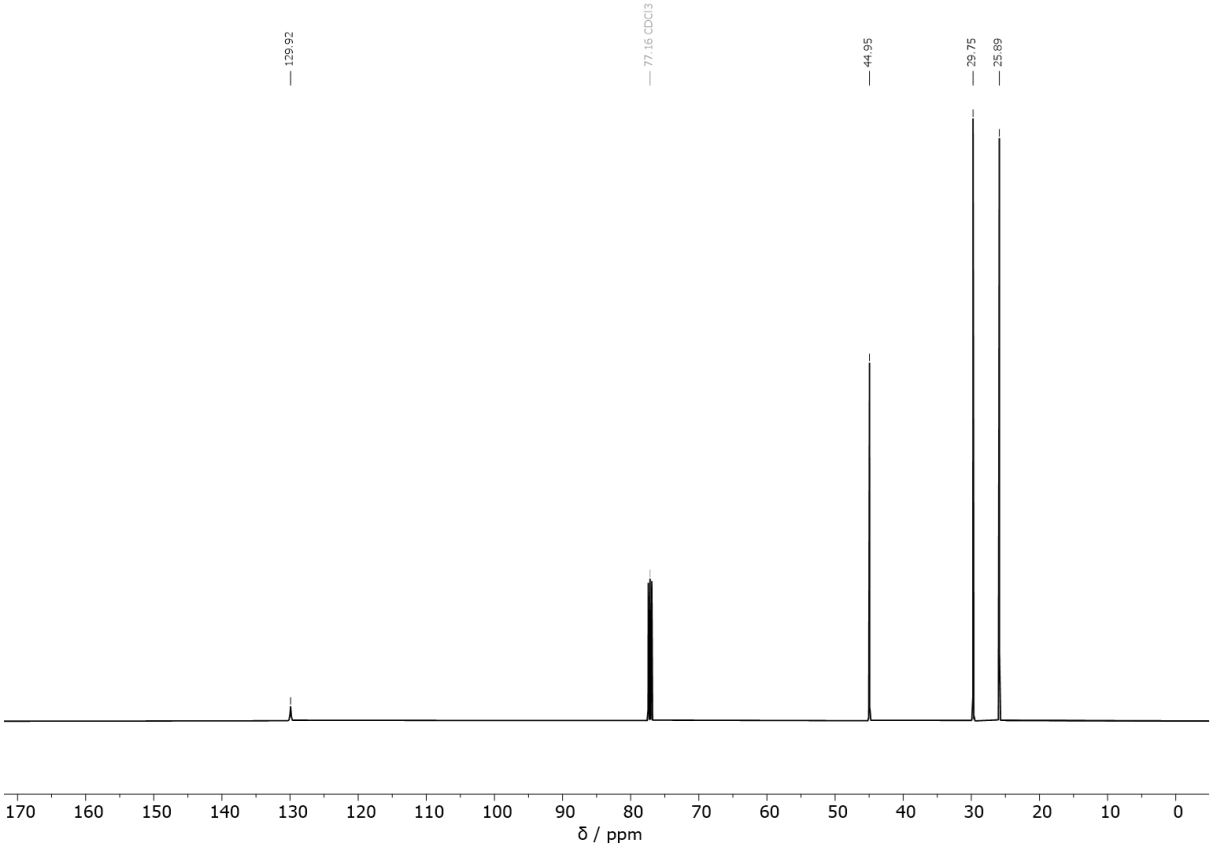

Figure S164 *^{13}C NMR spectrum (126 MHz, $CDCl_3$) of 1,6-diisothiocyanato hexane.*

Isophorone diisothiocyanate

^{1}H-NMR (400 MHz, $CDCl_3$) δ_H (ppm): 3.88 (tt, ^3J = 11.9 Hz ^2J = 3.7 Hz, 0.75H, 1a), 3.73 (tt, ^3J = 11.8 Hz ^2J = 3.8 Hz, 0.25H, 1b), 3.52 (d, ^2J = 14.3 Hz, 0.23H, 2b), 3.41 (d, ^2J = 14.3 Hz, 0.26H, 2b), 3.24 (s, 1.52H, 2a), 2.02-1.85 (m, 2H, 3a+b), 1.52 (m, 0.61H, 4b), 1.44-1.23 (m, 4H, 3a+b, 4a+b), 1.19-1.05 (m, 4H, 4a, 5), 1.07-0.95 (m, 6H, 6).
^{13}C-NMR (101 MHz, $CDCl_3$) δ_C (ppm): 131.5, 58.7, 53.1, 51.0, 50.9, 46.3, 46.0, 42.1, 41.9, 37.1, 37.1, 34.6, 34.3, 31.9, 31.6, 29.8, 27.5, 27.3, 23.5.
ATR-IR ν (cm^{-1}): 2957, 2923, 2859, 2179, 2065, 1465, 1441, 1388, 1364, 1338, 1299, 1249, 1198, 1143, 957, 922, 898, 869, 792, 713.
Purity according to GC-measurement: 98+%.
HRMS (ESI): calculated *m/z* for $C_{12}H_{18}N_2S_2$ [$M+H^+$]=255.0984, found: 255.0984.

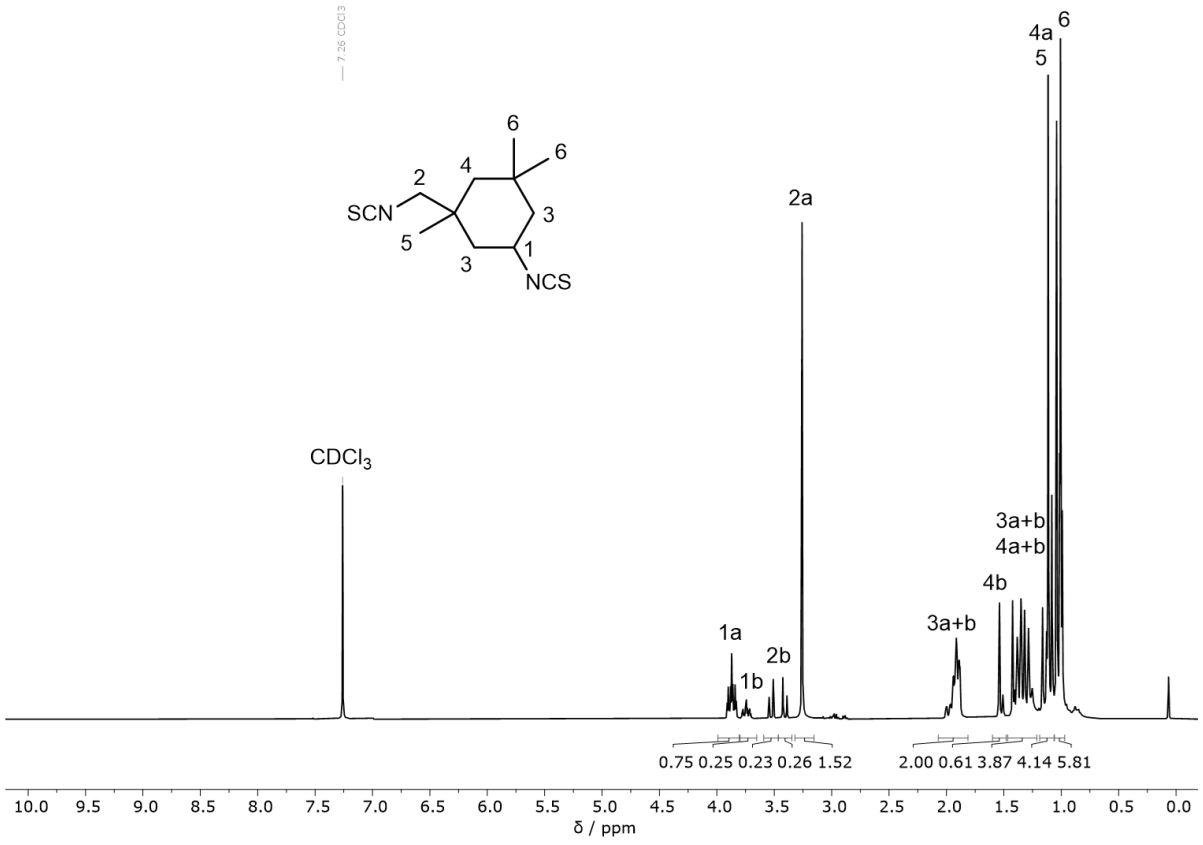

***Figure S165** ^{1}H NMR spectrum (400 MHz, $CDCl_3$) of isophorone diisothiocyanate.*

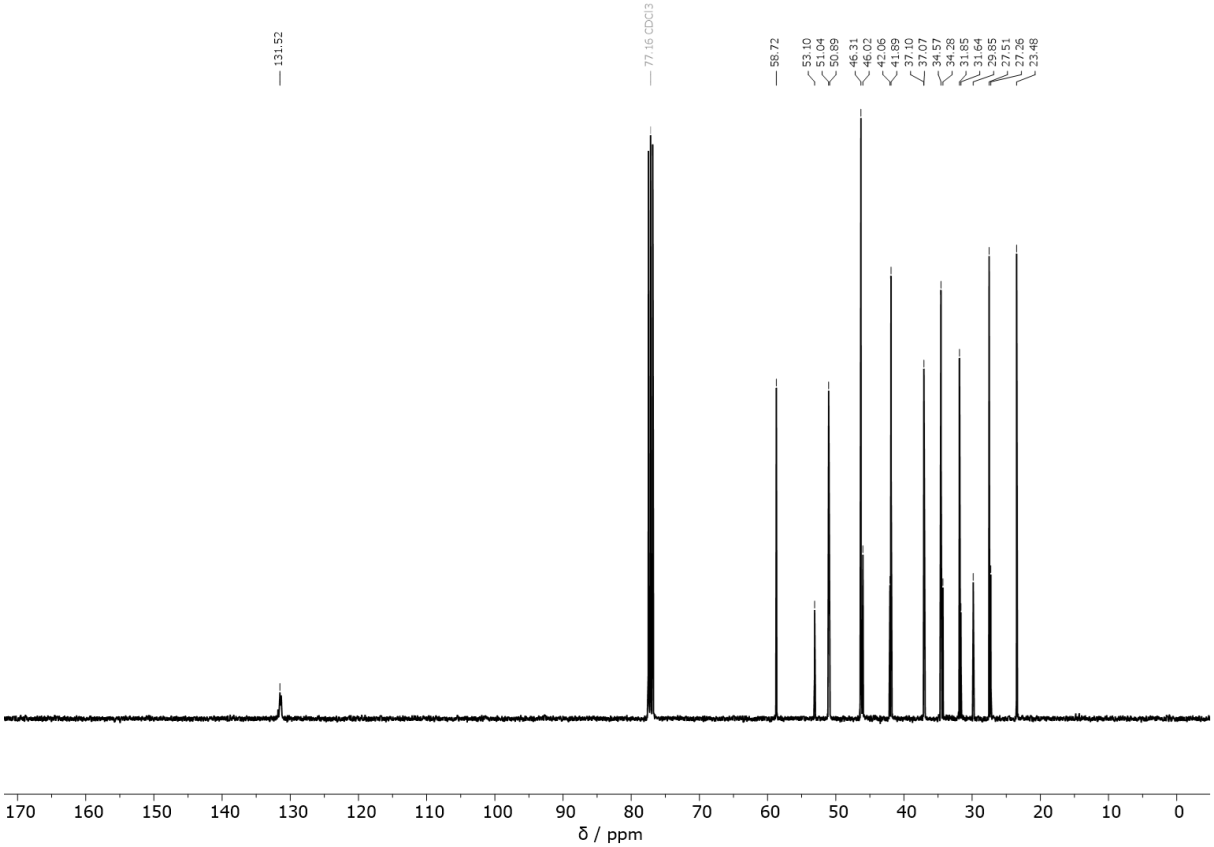

Figure S166 *^{13}C NMR spectrum (101 MHz, $CDCl_3$) of isophorone diisothiocyanate.*

Model Compound Synthesis Procedure:

In a 5 mL screw cap vial, castor oil (934 mg, $n_{OH\ groups}$=2.23 mmol), *n*-dodecyliso-thiocyanate (557 mg, 2.45 mmol, 1.10 equiv of isothiocyanate functional groups per OH group), and DBU (66.5 µL, 445.5 µmol, 0.2 equiv per OH group) were combined. The vial was sealed with a screw cap and then heated to 80 °C in an oil bath for 48 h under permanent stirring with a magnetic stirring bar. The crude product was then purified by flash column chromatography and the product was obtained as a yellow oil.

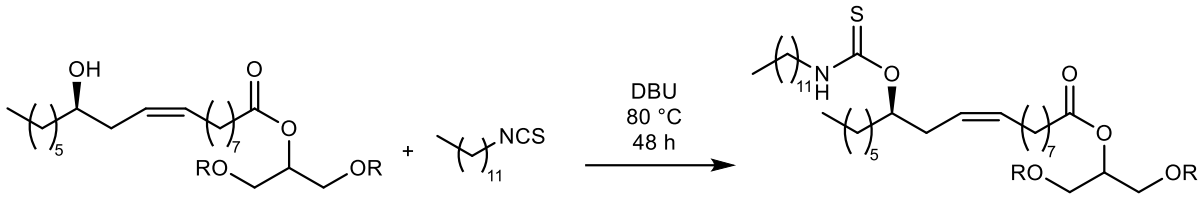

Scheme S1 *Model reaction of castor oil with n-dodecylisothiocyanate.*

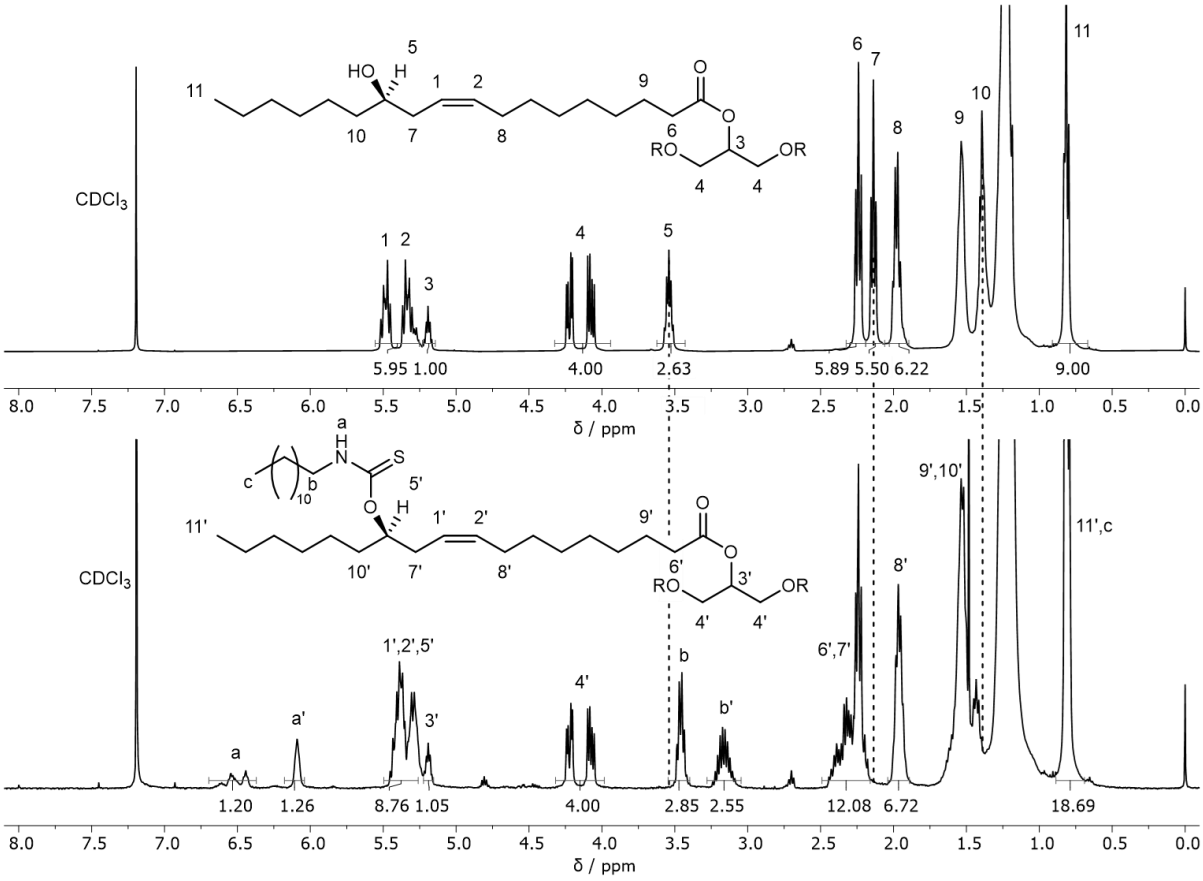

Figure S167 *^{1}H NMR spectra ($CDCl_3$) of castor oil (top) and the model compound (i.e. castor oil fully derivatized with n-dodecylisothiocyanate, bottom).Signals a/a' and b/b' are observed because of the cis/trans isomerism of the thionourethane moiety caused by the hindered rotation due to the partial double bond character as reported by Bauman.*[313]

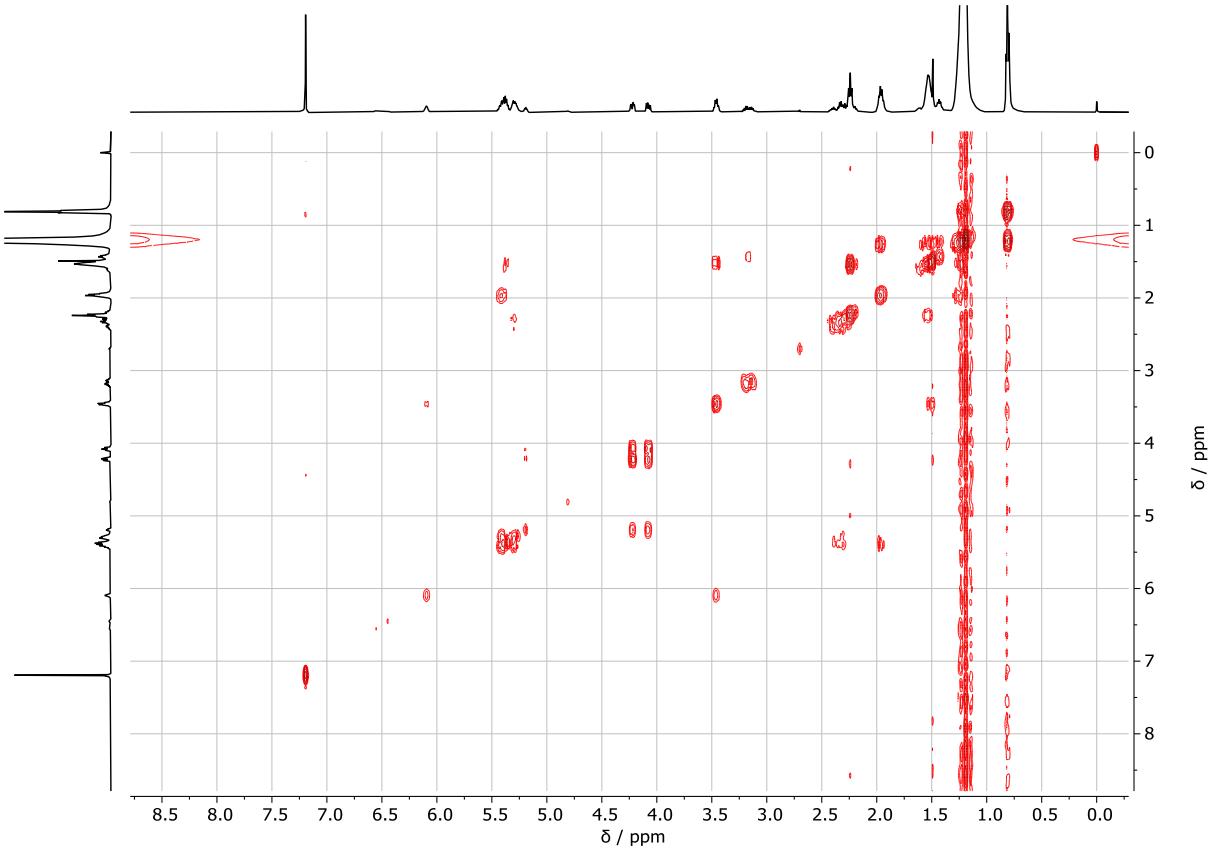

Figure S168 *^{1}H, ^{1}H COSY ($CDCl_3$) spectrum of the model compound.*

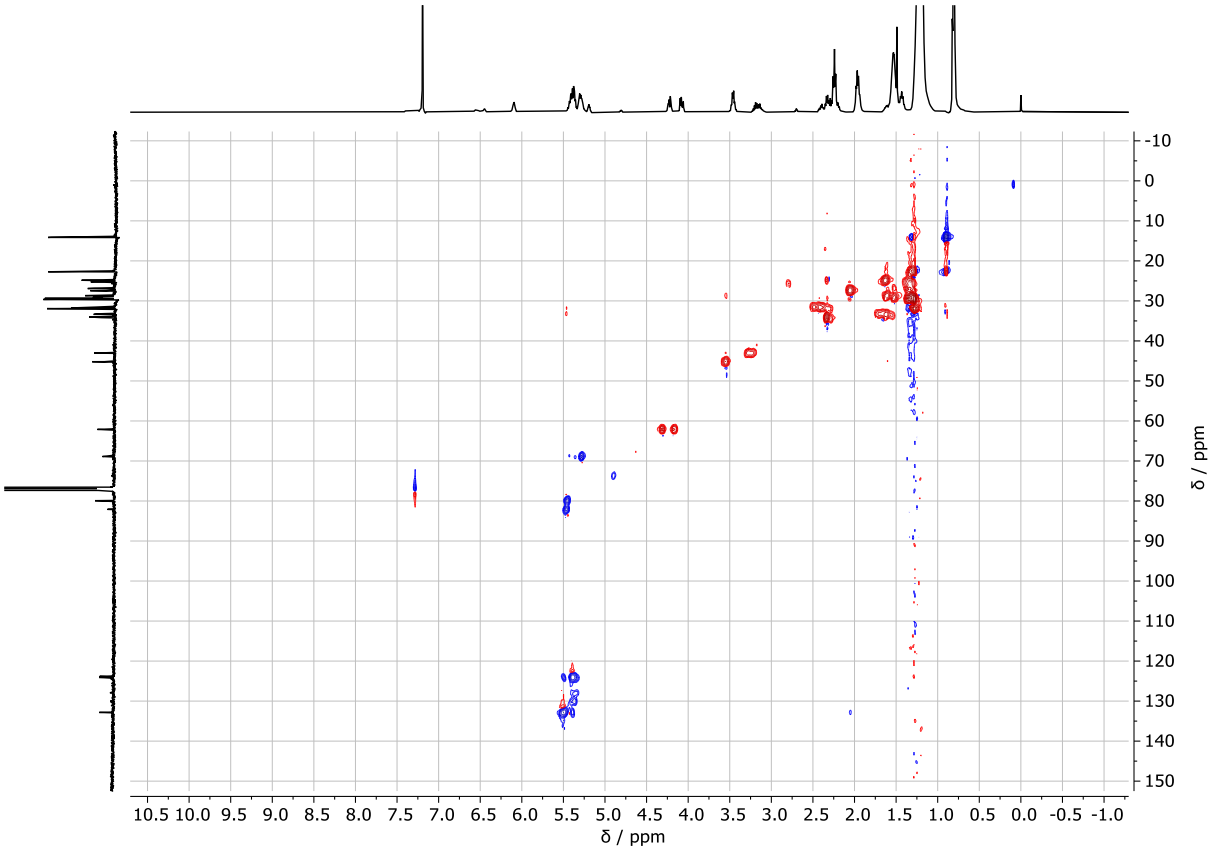

Figure S169 *^{1}H, ^{13}C HSQC ($CDCl_3$) spectrum of the model compound.*

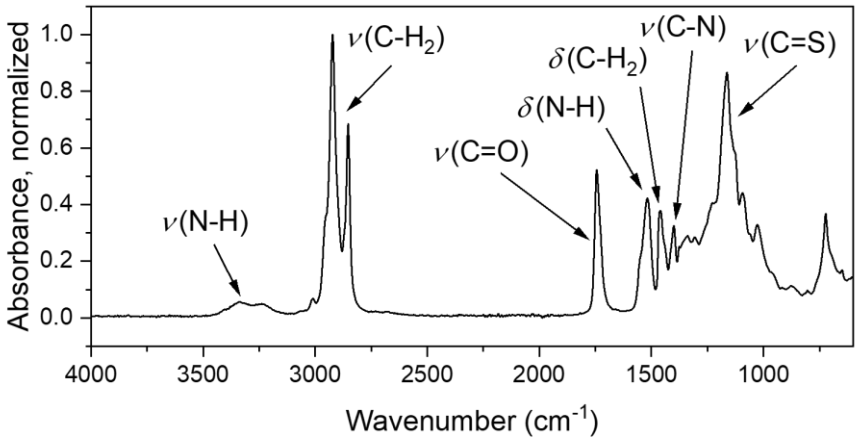

Figure S170 *ATR-IR spectrum of the model compound.*

General Procedure for the Synthesis of Polythionourethane Thermosets with *in situ* Generation of the Diisothiocyanate

In a 4 mL screw cap vial, castor oil (292 mg, $n_{\text{OH groups}}$=697.9 µmol), the diisocyanide (383.8 µmol, 1.10 equiv of isocyanide functional groups per OH group), S_8 (109.4 µmol, 1.14 equiv of sulfur atoms per isocyanide group) were combined and vortexed. Then, DBU (20.9 µL, 139.6 µmol, 0.20 equiv per OH group) was added and vortexed again. The reaction mixture was heated to 55 °C in an oil bath and stirred. After 40 min, a homogeneous solution was obtained, and the vial was flushed with nitrogen gas and sealed with a screw cap. The reaction mixture was then heated to 100 °C in an oil bath for 16 h and the fully cured thermoset was obtained as a brown rubbery solid.

General Procedure for the Synthesis of Polythionourethane Thermosets with Diisothiocyanates

In a 4 mL screw cap vial, castor oil (292 mg, $n_{\text{OH groups}}$=697.9 µmol), the diisothiocyanate (383.8 µmol, 1.10 equiv of isothiocyanate functional groups per OH group), and DBU (20.9 µL, 139.6 µmol, 0.20 equiv per OH group) were combined and vortexed to a homogeneous solution. The vial was flushed with nitrogen gas and sealed with a screw cap. The reaction mixture was then heated to 100 °C in an oil bath for 16 h and the fully cured thermoset was obtained as a brown rubbery solid.

General Procedure for the Synthesis of Polyurethane Thermosets

In an aluminum mold (2 cm in diameter), castor oil (996 mg, $n_{\text{OH groups}}$=2380.4 µmol), and the diisocyanate (200 mg, 1190 µmol, 1.00 equiv of isocyanate functional group per OH group) were combined and stirred. The mixture was then placed in an oven at 100 °C for 16 h. The fully cured thermoset was obtained as a colorless rubbery solid.

OH-value Determination of Castor Oil by ^{31}P NMR Method

For the OH-value determination of castor oil, 20–30 mg castor oil was filled in a vial and the exact mass was determined. It was then diluted in 1 mL of pyridine, followed by the addition of 1 mL of $CDCl_3$. Next, 2-chloro-4,4,5,5-tetramethyl-1,3,2- dioxaphospholane (2-Cl-TMDP, 100 µL, 0.63 mmol) was added to the mixture, and the solution was stirred for 15 min. Then, 150 µL of the internal standard solution (544.17 mg *endo*-*N*-hydroxy-5-norbornene-2,3-dicarboximide in 14.649 g pyridine and 15.050 g $CDCl_3$, OH_{IS}=100.42 mmol g^{-1}) was added and the exact mass of the added standard was weighed. The solution was stirred for another 10 min at room temperature and then 0.6 mL were transferred to an NMR tube for a subsequent ^{31}P NMR measurement. The determination was performed in triplicate and the OH-values were calculated according to equation (*32*).

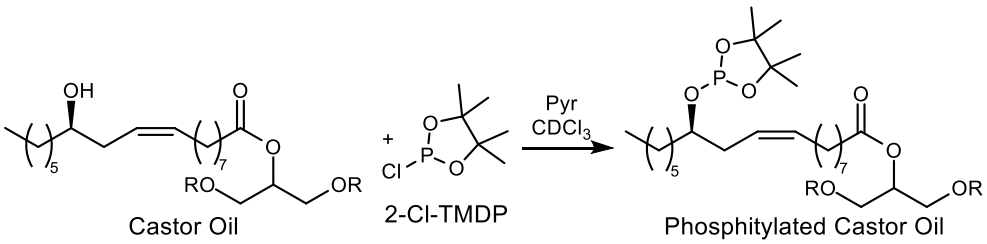

Scheme S2 *Phosphitylation reaction of castor oil.*

$$OH_S = \frac{OH_{IS} \times m_{IS} \times I_R}{m_S} \quad (32)$$

OH_S: free hydroxyl groups per weight unit of substrate (mol g^{-1})
OH_{IS}: free hydroxyl groups of the used internal standard (mol g^{-1})
m_{IS}: mass of the used internal standard (mg)
I_R: integration ratio of phosphorylated castor oil hydroxyl groups signal integral divided by the internal standard signal integral
m_S: mass of the sample (mg)

The determined integration ratios I_R and the corresponding ^{31}P NMR spectra are reported in **Figure S171**.

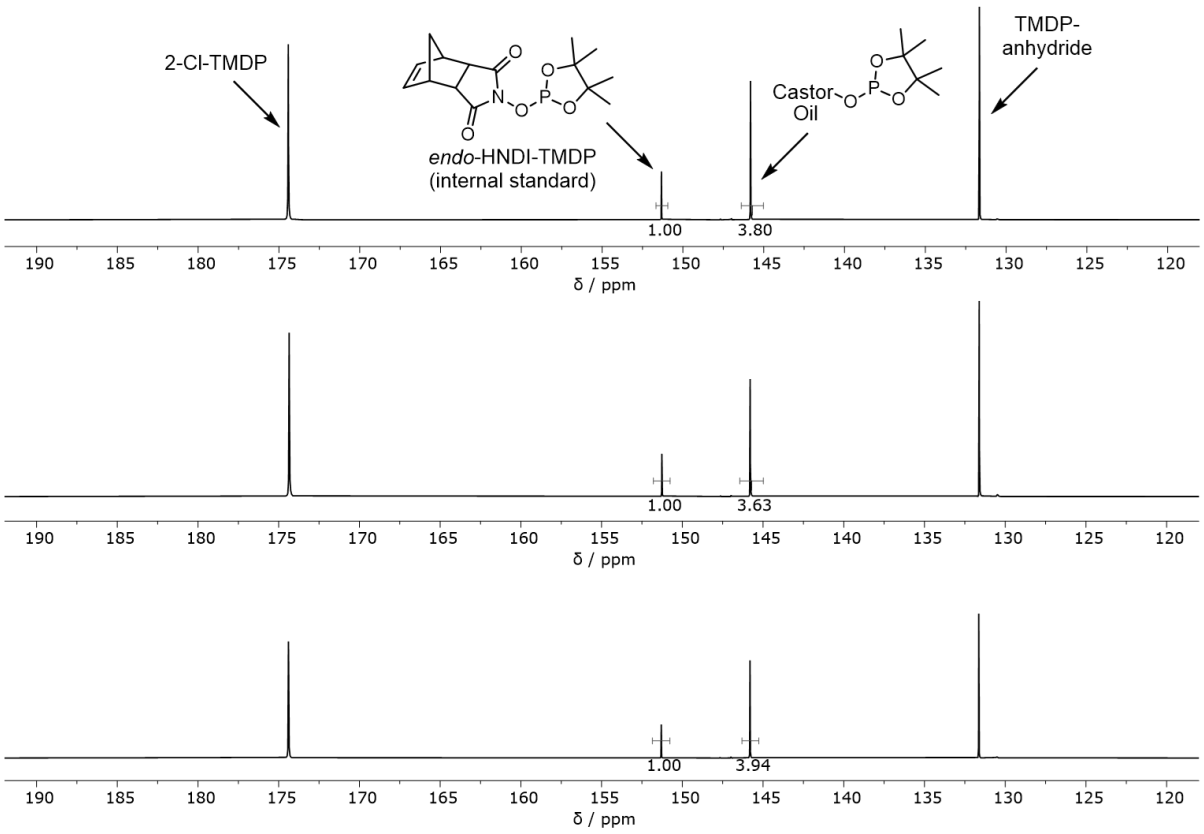

Figure S171 *^{31}P NMR ($CDCl_3$) spectra of the phosphitylated castor oil (triple determination) for the determination of the integration ratio I_R. The calculated values for OH_S can be found in* ***Table 29****.*

The OH_S value can be converted to the for polyurethane chemistry more common hydroxyl value HV by using equation (*33*).

$$HV = OH_S \times M_{KOH} \tag{33}$$

HV: hydroxyl value, $[HV] = \frac{\text{mg KOH}}{\text{g}}$

M_{KOH}: molar mass of KOH, $M_{KOH} = 56.11\ \frac{\text{g}}{\text{mol}}$

Table 29 *Values of OH_{IS}, m_{IS}, m_S, and I_R for the determination of OH_S of castor oil using equation (32) and the corresponding HV calculated applying equation* (33)*.*

Sample	OH_{IS} (µmol g^{-1})	m_{IS} (mg)	m_S (mg)	I_R	OH_S (mmol g^{-1})	HV (mg KOH g^{-1})
1	100.42	165.2	26.7	3.80	2.36	132.4
2	100.42	167.7	25.4	3.63	2.41	135.2
3	100.42	166.4	27.4	3.94	2.40	134.7

The average hydroxyl value of the triple determination was calculated to $OH_S = 2.39 \pm 0.02\ \mathrm{mmol\ g^{-1}}$ and $HV = 134.1 \pm 1.2\ \frac{\mathrm{mg\ KOH}}{\mathrm{g}}$.

The average molecular weight of castor oil was calculated based on the fatty acid composition, which was determined according to the procedure reported by Barison *et al.*[339] with the assumption of only triglycerides in the oil. The corresponding integrals are shown in **Figure S172**.

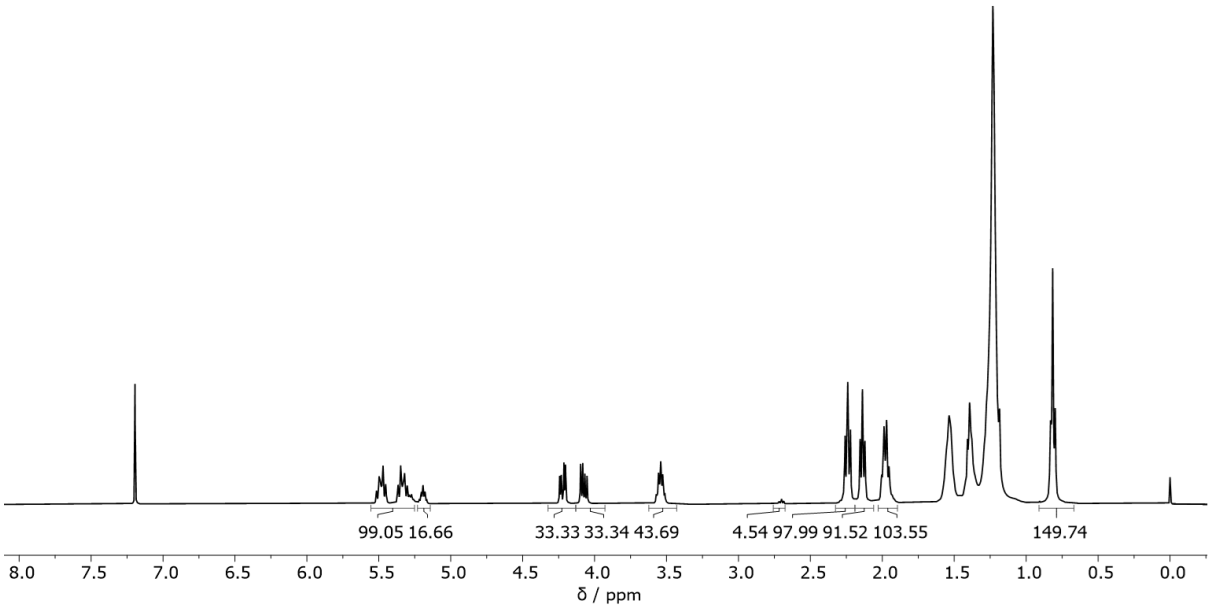

Figure S172 *^{1}H NMR spectrum of castor oil with the corresponding integrals for the evaluation of the fatty acid composition according to Barison et al.*[339]

Table 30 *Fatty acid composition determined according to the procedure reported by Barison et al..*[339]

Fatty acid	x	$M_{\mathrm{fattyacid}}$ (g mol^{-1})
Oleic acid	8.1%	282.47
Linoleic acid	4.5%	280.45
Ricinoleic acid	87.4%	298.47

The average molecular weight of castor oil $\bar{M}_{\mathrm{castor\ oil}}$ was calculated according to equation (*34*).

$$\bar{M}_{\text{castor oil}} = 3 \times \sum \left(M_{\text{fatty acid}} \times x\right) + M_{\text{glycerol}} - 3 \times M_{\text{H}_2\text{O}} = 927.12\ \text{g mol}^{-1} \quad (34)$$

$\bar{M}_{\text{castor oil}}$: average molecular weight of castor oil
$M_{\text{fatty acid}}$: molecular weight of the respective fatty acid
M_{glycerol}: molecular weight of glycerol, $M_{\text{glycerol}} = 92.09\ \text{g mol}^{-1}$
$M_{\text{H}_2\text{O}}$: molecular weight of water, $M_{\text{H}_2\text{O}} = 18.02\ \text{g mol}^{-1}$

The functionality of castor oil was calculated using equation (35) based on the estimated average molecular weight of castor oil.

$$f = OH_{\text{S}} \times \bar{M}_{\text{castor oil}} = 2.216 \quad (35)$$

f: functionality of hydroxyl groups of castor oil

Conversion of Gelation Calculation

Based on the determined hydroxyl value and the corresponding functionality f, applying the extended Carothers equation, the conversion of gelation can be calculated according to equation (36).

$$p = \frac{2}{f} - \frac{2}{f\bar{X}_n}$$

p: conversion
$\bar{X}_n$: average degree of polymerization

For $\bar{X}_n \rightarrow \infty$, the term $\frac{2}{f\bar{X}_n} \rightarrow 0$, which results in equation (*36*).

$$p_G = \frac{2}{f} = 0.903 \quad (36)$$

p_{g}: conversion of gelation

Peak Deconvolution

These deconvolutional calculations (**Figure 45**) were performed using the software Origin 2022b. A gauss fit was applied for the deconvolution process. The ν(N=C=S) stretching vibration signal results in a double peak and therefore two fits had to be applied for this signal, resulting in a total of three fits, which had to be performed (Fit 1 and Fit 3 for the ν(N=C=S) stretching vibration, and Fit 2 for the ν(-NC) stretching vibration in **Figure 45**). The following values were kept constant for the fitting calculation: Fit 1: $x_c = 2185$, $w = 47$; Fit 2: $x_c = 2147$; Fit 3: $x_c = 2093$, $w = 76$; with x_c being the center of the peak and w being the width ($w = \mathrm{FWHM}/\sqrt{\ln 4}$). These values were determined from a fit that was performed on a spectrum of the pure compounds, respectively.

Rate Constant Determination (k_1 and k_2)

For the determination of k_1, castor oil (450 mg, $n_{\text{OH groups}}$=1.076 mmol), 1,5-diisocyano pentane (72.27 mg, 591.6 µmol, 1.10 equiv of isocyanide functional groups per OH group), and S_8 (40.0 mg, 156.0 µmol, 1.14 equiv of sulfur atoms per isocyanide group) were combined and vortexed in a 4 mL screw cap vial. Then, DBU (32.1 µL, 215.1 µmol, 0.2 equiv per OH group) was added and vortexed again. The reaction mixture was placed in an oil bath at the desired temperature (35, 45, or 55 °C) and stirred manually. A sample was taken every minute and an IR spectrum was recorded. For the determination of k_2, castor oil (320 mg, $n_{\text{OH groups}}$=764.8 mmol) and 1,5-diisothiocyanato pentane (78.5 mg, 421.3 µmol, 1.10 equiv of isocyanide functional groups per OH group) were combined in a 4 mL screw cap vial and vortexed. Afterwards, DBU (22.9 µL, 153.2 µmol, 0.2 equiv per OH group) was added and vortexed again. For the online IR measurement, the reaction mixture was placed on the ATR crystal, which was heated to the desired temperature (80, 90, or 100 °C) and a spectrum was taken in time intervals of 1 min for a period of 35 h at 80 °C, 18 h at 90 °C, and 12 h at 100 °C. For the k determination, the data was plotted in **Figure 46b** and **d** according to the relationship in equations (*37*) and (*38*).

$$\ln\left(\frac{[NC]_0}{[NC]}\right) = k_1 t \tag{37}$$

$$\ln \frac{[NCS]_0[OH]}{[NCS][OH]_0} = k_2([OH]_0 - [NCS]_0)\, t \tag{38}$$

The values for $[NCS]_0$ and $[OH]_0$ are known from the starting concentration, and $[NCS]$ can be determined from the ν(N=C=S) stretching vibration signal in the IR spectra. The values for $[OH]$, however, cannot reliably be determined due to the low intensity of the ν(O-H) signal and the overlap with the arising ν(N-H) during the reaction. Therefore, the values for $[OH]$ were calculated using equation (*39*), which assumes no side reaction (1 eq of NCS reacts per 1eq of OH) and is based on the fact that one OH group reacts per NCS group. Prior experiments indicated a certain degree of side reaction of the isothiocyanate functionality (which can be approximated to $\leq$10% based on the necessary 0.10 equiv. excess of di-NCS for a successful gelation of the material). Nevertheless, this approach was pursued to estimate the $[OH]$ and consequences of the deviation caused by the side reaction were considered as explained in the following paragraph.

$$[OH] = [NCS] - ([NCS]_0 - [OH]_0) \tag{39}$$

The error for the calculation of $[OH]$ increases over time, as the extent of the side reaction increases. This results in a considerable deviation from linearity in **Figure S173a** for high conversions. The k_2 values were therefore determined based on the data until a maximum of 75% conversion, as the extent of side reaction is low until this point and was therefore assumed as a neglectable deviation from linearity as shown in **Figure S173b**.

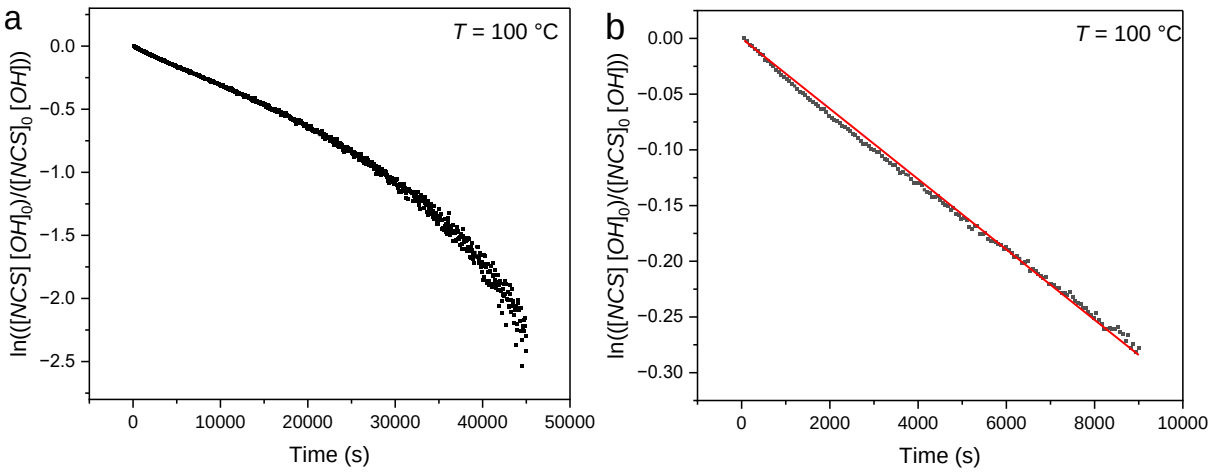

Figure S173 *Plots for the determination of k_2 based on second order kinetics.* ***a*** *Data plotted over the whole reaction time,* ***b*** *Data plotted until 75% conversion with a linear fit (red line).*

For the calculation of the concentrations, the density of the resulting reaction mixture had to be measured and was determined to be $\rho = 0.991\ \mathrm{g\,mL^{-1}}$. For the performed reaction, this results in: $[NCS]_0 = 1.98\ \mathrm{mol\,L^{-1}}$ and $[OH]_0 = 1.80\ \mathrm{mol\,L^{-1}}$. For the calculation of the k_2 values, equation (*40*) was used.

$$k = \frac{m}{[OH]_0 - [NCS]_0} \tag{40}$$

m: Slope of the linear fit from ln(([*NCS*] [*OH*]$_0$)/([*NCS*]$_0$ [*OH*])) plotted over time as shown in **Figure S173b**.

Calculations Based on Kinetics

For the calculation of the isothiocyanate concentration at any time of the reaction, equation (*41*) was used.

$$[NCS] = \frac{-[NCS]_0([NCS]_0 - [OH]_0)}{[OH]_0 \, e^{k_2([OH]_0 - [NCS]_0)t - [NCS]_0}} \tag{41}$$

This equation (*41*) can be used to calculate the concentration of isothiocyanate groups at any time of the crosslinking reaction. This can then be used to calculate the time of gelation at e.g. 55 °C, applying $k_{2,55\,^\circ\mathrm{C}} = 7.44 \times 10^{-5}\ \mathrm{M^{-1}s^{-1}}$ together with the concentration of isothiocyanate at gelation from equation (*42*).

$$[NCS]_{\mathrm{gelation}} = p_G \times [NCS]_0 \tag{42}$$

$$[NCS]_{\mathrm{gelation}} = 0.905 \times 1.98\ \mathrm{M} = 1.79\ \mathrm{M}$$

This results in a calculated time of gelation at 55 °C of $t_{\mathrm{g},55\,^\circ\mathrm{C}} = 63\ \mathrm{h}\ 15\ \mathrm{min}$.

Calculative approach because of apparent 1st order kinetics for first reaction step vs 2nd order in the second reaction step:

Equation (*43*) shows that the reaction rates have different dependencies on the concentrations of the reactants as the reactions are of a different order.

$$r_1 = k_1[NC] \quad \text{and} \quad r_2 = k_2[NCS][OH] \tag{43}$$

In order to determine the temperature at which both reactions proceed at the same rate, equation (*44*) has to be applied:

$$r_1 = r_2 \tag{44}$$

With $[NC] = 1.98\ \mathrm{mol\ L^{-1}}$, $[NCS] = 1.98\ \mathrm{mol\ L^{-1}}$, and $[OH] = 1.80\ \mathrm{mol\ L^{-1}}$

$$0.555\ k_1 = k_2 \tag{45}$$

$$-0.5878 = \ln(k_2) - \ln(k_1) \tag{46}$$

The reciprocal temperature can then be calculated, at which both reactions proceed at the same reaction rate for the given concentration.

$$T^{-1} = -0.0087321\ \mathrm{K^{-1}} \tag{47}$$

Which corresponds to:

$$T = -115\ \mathrm{K} \tag{48}$$

It should be noted that the reaction rate r_2 of the second reaction step will at some point during the reaction become slower than the reaction rate r_1 of the first reaction step due to the nature of 1st vs 2nd order kinetic reactions. Nevertheless, as the hypothetical temperature $T = -115\ \mathrm{K}$ is anyways outside of the relevant temperature range, the first reaction can practically be considered to have a higher reaction rate compared to the second reaction step.

Thermal Analysis

The thermal analysis data of the DSC and TGA measurements are monitored in **Figure S174**, **Figure S175**, and **Table 31**.

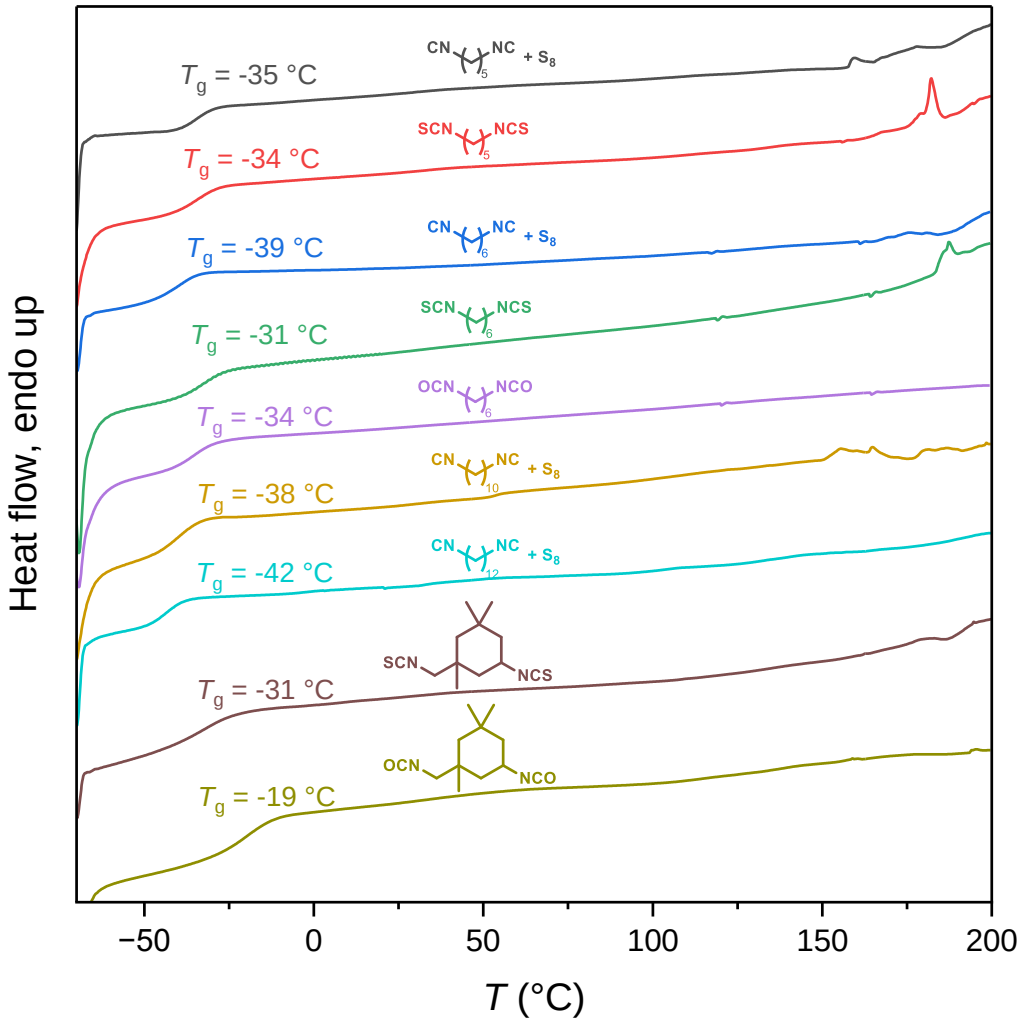

Figure S174 *Stacked DSC thermograms of all synthesized thermoset materials. Deviations in the heat flow for the thionourethane thermoset materials at above 160 °C can be explained with the onset of first degradation reactions, as confirmed by TGA measurements (**Figure S175**).*

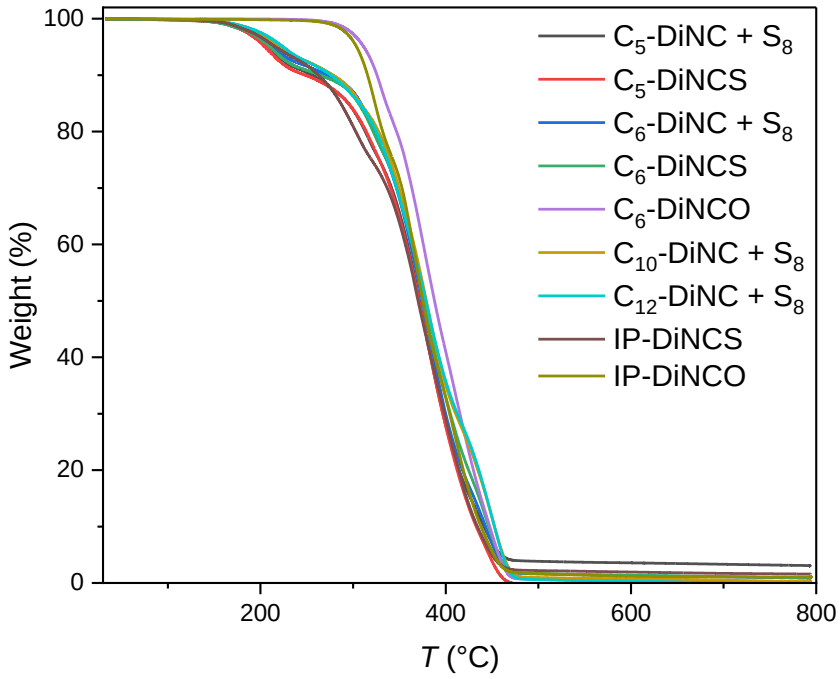

Figure S175 *Overlaid TGA thermograms of all synthesized thermoset materials.*

Table 31 *Degradation temperatures of all synthesized thermoset materials.*

Sample	$T_{d,5\%}$ **(°C)**	$T_{d,50\%}$ **(°C)**
C_5-DiNC + S_8	207	372
C_5-DiNCS	205	371
C_6-DiNC + S_8	212	375
C_6-DiNCS	210	377
C_6-DiNCO	312	388
C_{10}-DiNC + S_8	220	379
C_{12}-DiNC + S_8	224	379
IP-DiNCS	216	370
IP-DiNCO	304	375

Rheology

The linear fit equation for the Arrhenius relationship as shown in **Figure 48** was determined to: $\ln\left(t_g^{-1}\right) = -7422.40\,T^{-1} + 9.95$.

Based on the Arrhenius relationship, gelation times at other isothermal curing temperatures T can be predicted according to equation (*49*).

$$t_g = e^{7422.40\,T^{-1} - 9.95} \tag{49}$$

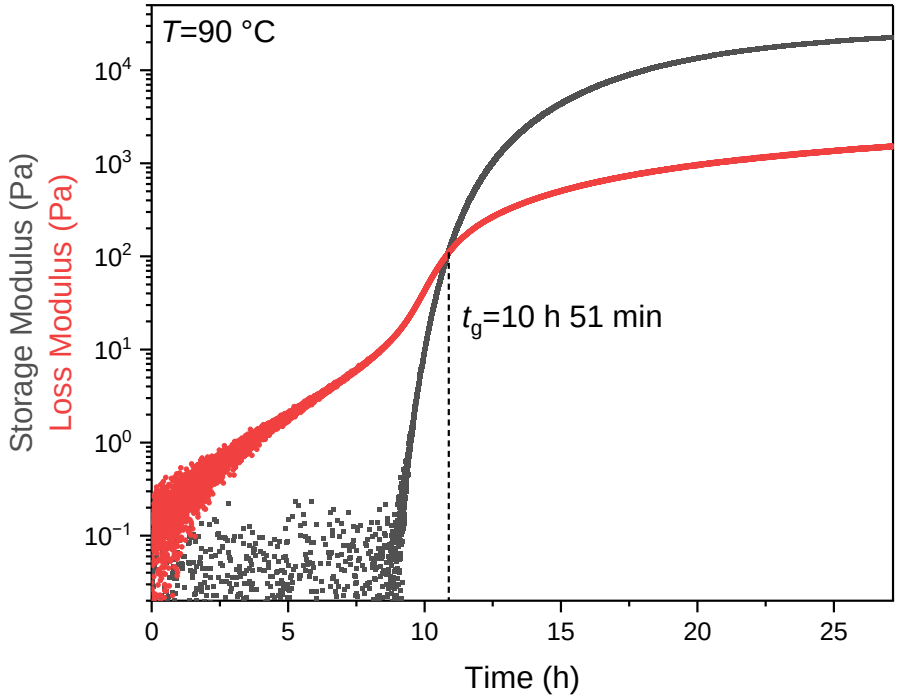

Figure S176 *Rheology measurements of the curing of 1,5-diisothiocyanato pentane, which was in situ generated from 1,5-diisocyanido pentane and sulfur in castor oil with DBU as organo-base prior to the crosslinking process. The curing was performed isothermally at 90 °C.*

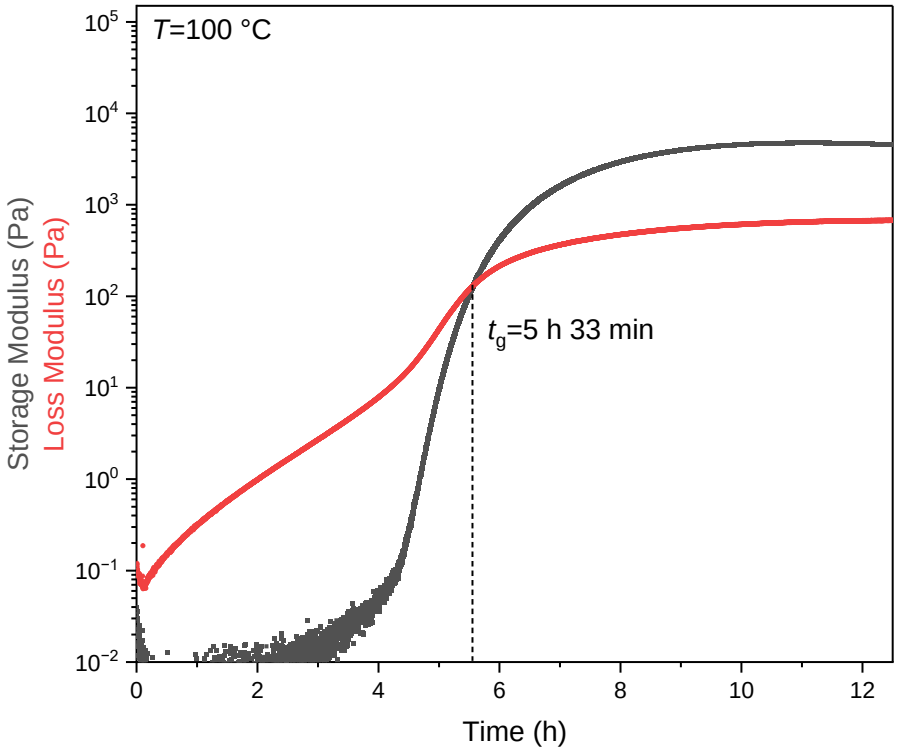

Figure S177 *Rheology measurements of the curing of 1,6-diisothiocyanato hexane with castor oil and DBU as organo-base. Curing was performed isothermally at 100 °C.*

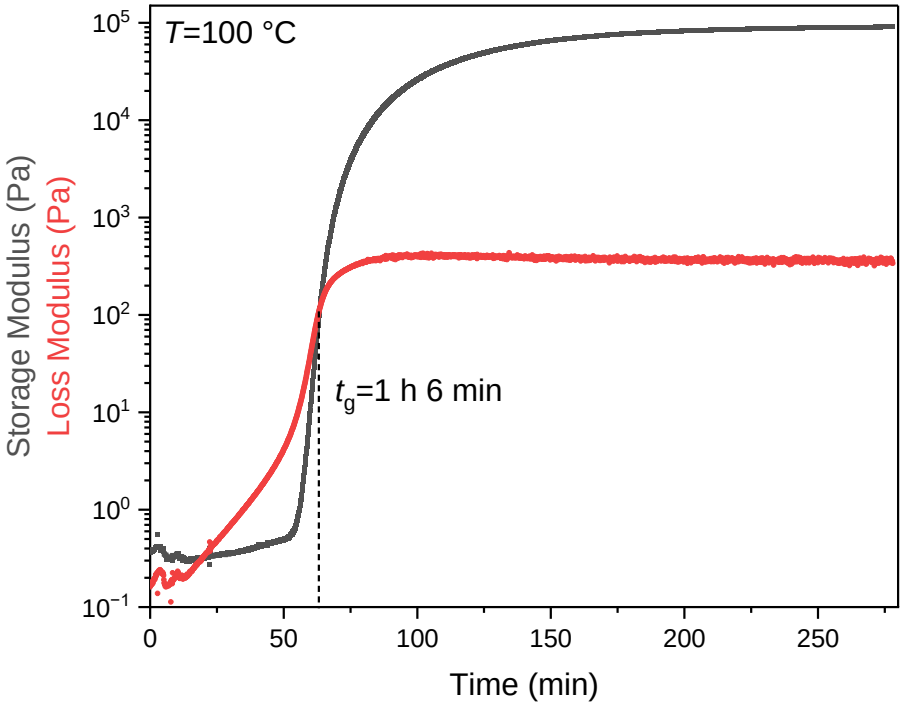

Figure S178 *Rheology measurements of the curing of 1,6-diisocyanato hexane with castor oil. The curing was performed isothermally at 100 °C.*

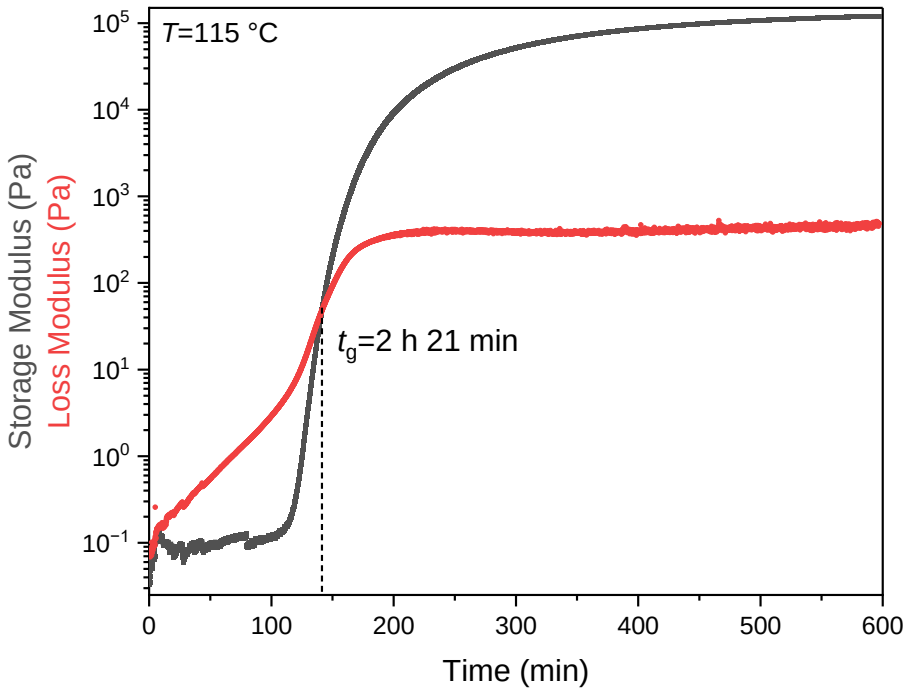

Figure S179 *Rheology measurements of the curing of isophorone diisocyanate with castor oil. The curing was performed isothermally at 115 °C.*

7 Appendix

7.1 List of Abbreviations

2-Cl-TMDP	2-Chloro-4,4,5,5-tetramethyl-1,3,2-dioxaphospholane
AAE	Actual Atom Economy
ADMIMBr	1-*N*-Allyl-2,3-dimethylimidazolium bromide
AE	Atom Economy
AGU	Anhydroglucose Unit
AMIMCl	1-Allyl-3-methylimidazolium chloride
ATR	Attenuated Total Reflection
BMIMCl	1-Butyl-3-methylimidazolium chloride
CA	Cellulose Acetate
CB	*O*-cellulose-*N*-*n*-butyl thiocarbamate
CBu	Cellulose Butyrate
CBz	Cellulose Benzoate
CC	*O*-cellulose-*N*-cyclohexyl thiocarbamate
CD	*O*-cellulose-*N*-*n*-dodecyl thiocarbamate
cEF	complete *E*-factor
CL	Cellulose Laurate
CMC	Carboxymethylcellulose
CNC	Cellulose Nano Crystal
CO	*O*-cellulose-*N*-oleyl thiocarbamate
CTA	Cellulose Triacetate
DABCO	1,4-Diazabicyclo[2.2.2]octane
DBN	1,5-Diazabicyclo[4.3.0]non-5-ene
DBU	1,8-Diazabicyclo[5.4.0]undec-7-ene
DIPEA	*N*,*N*-Diisopropylethylamine
DMAc	Dimethylacetamide
DMI	1,3-dimethyl-2-imidazolidinone
DMSO	Dimethyl sulfoxide
DP	Degree of Polymerization
DS	Degree of Substitution
DSC	Differential Scanning Calorimetry

EC	Ethyl Cellulose
EMIMOAc	1-Ethyl-3-methylimidazolium acetate
endo-HNDI	*endo*-*N*-Hydroxy-5-norbornene-2,3-dicarboximide
FACE	Fatty Acid Cellulose Ester
FTIR	Fourier Transform Infrared
GBL	gamma-Butyrolactone
GC	Gas Chromatography
HEC	Hydroxyethyl Cellulose
HFIP	Hexafluoroisopropanol
HPC	Hydroxypropyl Cellulose
HV	Hydroxyl Value
IL	Ionic Liquid
IR	Infrared
LCA	Life Cycle Assessment
MC	Methyl Cellulose
MCC	Microcrystalline Cellulose
MCR	Multicomponent Reaction
MDI	Methylene Diphenyl Isocyanate
MI	Mass Intensity
MS	Mass Spectrometry
MTBD	7-Methyl-1,5,7-triazabicyclo[4.4.0]dec-5-ene
NMMO	*N*-Methylmorpholine *N*-oxide
NMR	Nuclear Magnetic Resonance
PU	Polyurethane
RME	Reaction Mass Efficiency
SEC	Size Exclusion Chromatography
sEF	simple *E*-factor
SMCR	Sulfur-based Multicomponent Reaction
TBAF	Tetra-*n*-butylammonium fluoride
TBD	1,5,7-Triazabicyclo[4.4.0]dec-5-ene
TEMPO	2,2,6,6-Tetramethylpiperidine-*N*-oxyl
TFA	Trifluoroacetic acid
TGA	Thermogravimetric analysis

THF	Tetrahydrofuran
TMG	1,1,3,3-Tetramethylguanidine
TsCl	*p*-Toluenesulfonyl chloride
VA	Vinyl Acetate

7.2 List of Publications

Related to this work:

[7] **Wolfs, J.**, Scheelje, F. C. M., Matveyeva, O., Meier, M. A. R. Determination of the degree of substitution of cellulose esters via ATR-FTIR spectroscopy *J. Polym. Sci.*, 2023, 1–11

[6] **Wolfs, J**., Ribca, I., Meier, M. A. R., Johansson, M. Polythionourethane Thermoset Synthesis via Activation of Elemental Sulfur in an Efficient Multicomponent Reaction Approach. *ACS Sustain. Chem. Eng.* 2023, *11*, (9), 3952-3962.

[5] **Wolfs, J.**; Nickisch, R.; Wanner, L.; Meier, M. A. R. Sustainable One-Pot Cellulose Dissolution and Derivatization via a Tandem Reaction in the DMSO/DBU/CO_2 Switchable Solvent System. *J. Am. Chem. Soc.* 2021, *143* (44), 18693–18702.

[4] **Wolfs, J.**; Meier, M. A. R. A More Sustainable Synthesis Approach for Cellulose Acetate Using the DBU/CO_2 Switchable Solvent System. *Green Chem.* 2021, *23* (12), 4410–4420.

Further publications:

[3] Bohn, P.; Weisel, M. P.; **Wolfs, J.**; Meier, M. A. R. Molecular Data Storage with Zero Synthetic Effort and Simple Read-Out. *Sci. Rep.* 2022, *12* (1), 13878.

[2] Rheinberger, T.; **Wolfs, J.**; Paneth, A.; Gojzewski, H.; Paneth, P.; Wurm, F. R. RNA-Inspired and Accelerated Degradation of Polylactide in Seawater. *J. Am. Chem. Soc.* 2021, *143* (40), 16673–16681.

[1] Kunze, L.; **Wolfs, J.**; Verkoyen, P.; Frey, H. Crystalline CO_2 -Based Aliphatic Polycarbonates with Long Alkyl Chains. *Macromol. Rapid Commun.* 2018, *39* (24), 1–5.

8 References

(1) Brundtland, G. H. *Report of the World Commission on Environment and Development: Our Common Future*; Oslo, 1987.
(2) Plastics – the Facts 2022 https://plasticseurope.org/knowledge-hub/plastics-the-facts-2022/ (accessed 2022 -12 -09).
(3) Anastas, P. T.; Warner, J. C. Green Chemistry. Theory and Practice. *Oxford Univ. Press*. New York 1998, p 30.
(4) Anastas, P.; Eghbali, N. Green Chemistry: Principles and Practice. *Chem. Soc. Rev.* **2010**, *39* (1), 301–312.
(5) Horváth, I. T.; Anastas, P. T. Introduction: Green Chemistry. *Chem. Rev.* **2007**, *107* (6), 2167–2168.
(6) Alavi, S.; Thomas, S.; Sandeep, K. P.; Kalarikkal, N.; Varghese, J.; Yaragalla, S. *Polymers for Packaging Applications*; CRC press, 2014.
(7) Pham, Q.-T.; Chern, C.-S. Applications of Polymers in Lithium-Ion Batteries with Enhanced Safety and Cycle Life. *J. Polym. Res.* **2022**, *29* (4), 124.
(8) Haag, R.; Kratz, F. Polymer Therapeutics: Concepts and Applications. *Angew. Chemie Int. Ed.* **2006**, *45* (8), 1198–1215.
(9) Meyer, W. H. Polymer Electrolytes for Lithium-Ion Batteries. *Adv. Mater.* **1998**, *10* (6), 439–448.
(10) López-Rubio, A.; Almenar, E.; Hernandez-Muñoz, P.; Lagarón, J. M.; Catalá, R.; Gavara, R. Overview of Active Polymer-Based Packaging Technologies for Food Applications. *Food Rev. Int.* **2004**, *20* (4), 357–387.
(11) Sheldon, R. A. The E Factor: Fifteen Years On. *Green Chem.* **2007**, *9* (12), 1273–1283.
(12) Gallezot, P. Conversion of Biomass to Selected Chemical Products. *Chem. Soc. Rev.* **2012**, *41* (4), 1538–1558.
(13) Mülhaupt, R. Green Polymer Chemistry and Bio-Based Plastics: Dreams and Reality. *Macromol. Chem. Phys.* **2013**, *214* (2), 159–174.
(14) Centi, G.; Perathoner, S. Chemistry and Energy beyond Fossil Fuels. A Perspective View on the Role of Syngas from Waste Sources. *Catal. Today* **2020**, *342*, 4–12.
(15) Okkerse, C.; Van Bekkum, H. From Fossil to Green. *Green Chem.* **1999**, *1* (2), 107–114.
(16) Brehmer, B.; Boom, R. M.; Sanders, J. Maximum Fossil Fuel Feedstock Replacement Potential of Petrochemicals via Biorefineries. *Chem. Eng. Res. Des.* **2009**, *87* (9), 1103–1119.
(17) Zimmerman, J. B.; Anastas, P. T.; Erythropel, H. C.; Leitner, W. Designing for a Green Chemistry Future. *Science* **2020**, *367* (6476), 397–400.
(18) Fiorentino, G.; Zucaro, A.; Ulgiati, S. Towards an Energy Efficient Chemistry. Switching from Fossil to Bio-Based Products in a Life Cycle Perspective. *Energy* **2019**, *170*, 720–729.
(19) Narodoslawsky, M.; Niederl-Schmidinger, A.; Halasz, L. Utilising Renewable Resources Economically: New Challenges and Chances for Process Development. *J. Clean. Prod.* **2008**, *16* (2), 164–170.
(20) Levi, P. G.; Cullen, J. M. Mapping Global Flows of Chemicals: From Fossil Fuel Feedstocks to Chemical Products. *Environ. Sci. Technol.* **2018**, *52* (4), 1725–1734.
(21) Barthelemy, P.; Agyeman-Budu, E. European Chemical Industry's Contribution

to Sustainable Development. *Curr. Opin. Green Sustain. Chem.* **2016**, *1*, 28–32.
(22) Blum, C.; Bunke, D.; Hungsberg, M.; Roelofs, E.; Joas, A.; Joas, R.; Blepp, M.; Stolzenberg, H. C. The Concept of Sustainable Chemistry: Key Drivers for the Transition towards Sustainable Development. *Sustain. Chem. Pharm.* **2017**, *5*, 94–104.
(23) Gwehenberger, G.; Narodoslawsky, M. Sustainable Processes-The Challenge of the 21st Century for Chemical Engineering. *Process Saf. Environ. Prot.* **2008**, *86* (5), 321–327.
(24) Chen, T. L.; Kim, H.; Pan, S. Y.; Tseng, P. C.; Lin, Y. P.; Chiang, P. C. Implementation of Green Chemistry Principles in Circular Economy System towards Sustainable Development Goals: Challenges and Perspectives. *Sci. Total Environ.* **2020**, *716*, 136998.
(25) Tang, S. L. Y.; Smith, R. L.; Poliakoff, M. Principles of Green Chemistry: PRODUCTIVELY. *Green Chem.* **2005**, *7* (11), 761.
(26) Sheldon, R. A.; Bode, M. L.; Akakios, S. G. Metrics of Green Chemistry: Waste Minimization. *Curr. Opin. Green Sustain. Chem.* **2022**, *33*, 100569.
(27) Trost, B. M. The Atom Economy - A Search for Synthetic Efficiency. *Science* **1991**, *254* (5037), 1471–1477.
(28) Trost, B. M. Atom Economy—A Challenge for Organic Synthesis: Homogeneous Catalysis Leads the Way. *Angew. Chemie Int. Ed. English* **1995**, *34* (3), 259–281.
(29) Sheldon, R. A. Organic Synthesis; Past, Present and Future. *Chem. Ind.* **1992**, 903–906.
(30) Wender, P. A.; Croatt, M. P.; Witulski, B. New Reactions and Step Economy: The Total Synthesis of (±)-Salsolene Oxide Based on the Type II Transition Metal-Catalyzed Intramolecular [4+4] Cycloaddition. *Tetrahedron* **2006**, *62* (32), 7505–7511.
(31) Sheldon, R. A. Fundamentals of Green Chemistry: Efficiency in Reaction Design. *Chem. Soc. Rev.* **2012**, *41* (4), 1437–1451.
(32) Roschangar, F.; Sheldon, R. A.; Senanayake, C. H. Overcoming Barriers to Green Chemistry in the Pharmaceutical Industry – the Green Aspiration Level™ Concept. *Green Chem.* **2015**, *17* (2), 752–768.
(33) Sheldon, R. A. The: E Factor 25 Years on: The Rise of Green Chemistry and Sustainability. *Green Chem.* **2017**, *19* (1), 18–43.
(34) Andraos, J. Unification of Reaction Metrics for Green Chemistry: Applications to Reaction Analysis. *Org. Process Res. Dev.* **2005**, *9* (2), 149–163.
(35) Calvo-Flores, F. G. Sustainable Chemistry Metrics. *ChemSusChem* **2009**, *2* (10), 905–919.
(36) Albini, A.; Protti, S. Green Metrics, an Abridged Glossary. In *Paradigms in green chemistry and technology*; Springer, Cham, 2016; pp 11–24.
(37) Constable, D. J. C.; Curzons, A. D.; Cunningham, V. L. Metrics to “green” Chemistry - Which Are the Best? *Green Chem.* **2002**, *4* (6), 521–527.
(38) Curzons, A. D.; Mortimer, D. N.; Constable, D. J. C.; Cunningham, V. L. So You Think Your Process Is Green, How Do You Know? — Using Principles of Sustainability to Determine What Is Green – a Corporate Perspective. *Green Chem.* **2001**, *3* (1), 1–6.
(39) Benison, C. H.; Payne, P. R. Manufacturing Mass Intensity: 15 Years of Process Mass Intensity and Development of the Metric into Plant Cleaning and Beyond. *Curr. Res. Green Sustain. Chem.* **2022**, *5*, 100229.

(40) Finnveden, G.; Hauschild, M. Z.; Ekvall, T.; Guinée, J.; Heijungs, R.; Hellweg, S.; Koehler, A.; Pennington, D.; Suh, S. Recent Developments in Life Cycle Assessment. *J. Environ. Manage.* **2009**, *91* (1), 1–21.
(41) Kralisch, D.; Ott, D.; Gericke, D. Rules and Benefits of Life Cycle Assessment in Green Chemical Process and Synthesis Design: A Tutorial Review. *Green Chem.* **2015**, *17* (1), 123–145.
(42) Burgess, A. A.; Brennan, D. J. Application of Life Cycle Assessment to Chemical Processes. *Chem. Eng. Sci.* **2001**, *56* (8), 2589–2604.
(43) Anastas, P. T.; Lankey, R. L. Life Cycle Assessment and Green Chemistry: The Yin and Yang of Industrial Ecology. *Green Chem.* **2000**, *2* (6), 289–295.
(44) Tufvesson, L. M.; Tufvesson, P.; Woodley, J. M.; Börjesson, P. Life Cycle Assessment in Green Chemistry: Overview of Key Parameters and Methodological Concerns. *Int. J. Life Cycle Assess.* **2013**, *18* (2), 431–444.
(45) Azapagic, A.; Clift, R. The Application of Life Cycle Assessment to Process Optimisation. *Comput. Chem. Eng.* **1999**, *23* (10), 1509–1526.
(46) Guinée, J. B.; Heijungs, R.; Huppes, G.; Zamagni, A.; Masoni, P.; Buonamici, R.; Ekvall, T.; Rydberg, T. Life Cycle Assessment: Past, Present, and Future. *Environ. Sci. Technol.* **2011**, *45* (1), 90–96.
(47) Hellweg, S.; Milà i Canals, L. Emerging Approaches, Challenges and Opportunities in Life Cycle Assessment. *Science* **2014**, *344* (6188), 1109–1113.
(48) Klöpffer, W.; Grahl, B. *Life Cycle Assessment (LCA)*, 1st ed.; Wiley-VCH: Weinheim, Germany, 2014.
(49) Dodds, D. R.; Gross, R. A. Chemicals from Biomass. *Science* **2007**, *318* (5854), 1250–1251.
(50) Christensen, C. H.; Rass-Hansen, J.; Marsden, C. C.; Taarning, E.; Egeblad, K. The Renewable Chemicals Industry. *ChemSusChem* **2008**, *1* (4), 283–289.
(51) Palsson, B. O.; Fathi-Afshar, S.; Rudd, D. F.; Lightfoot, E. N. Biomass as a Source of Chemical Feedstocks: An Economic Evaluation. *Science* **1981**, *213* (4507), 513–517.
(52) Fernando, S.; Adhikari, S.; Chandrapal, C.; Murali, N. Biorefineries: Current Status, Challenges, and Future Direction. *Energy & Fuels* **2006**, *20* (4), 1727–1737.
(53) Octave, S.; Thomas, D. Biorefinery: Toward an Industrial Metabolism. *Biochimie* **2009**, *91* (6), 659–664.
(54) Fatih Demirbas, M. Biorefineries for Biofuel Upgrading: A Critical Review. *Appl. Energy* **2009**, *86* (Supplement 1), S151–S161.
(55) Cherubini, F. The Biorefinery Concept: Using Biomass Instead of Oil for Producing Energy and Chemicals. *Energy Convers. Manag.* **2010**, *51* (7), 1412–1421.
(56) Melero, J. A.; Iglesias, J.; Garcia, A. Biomass as Renewable Feedstock in Standard Refinery Units. Feasibility, Opportunities and Challenges. *Energy Environ. Sci.* **2012**, *5* (6), 7393.
(57) Huber, G. W.; Iborra, S.; Corma, A. Synthesis of Transportation Fuels from Biomass: Chemistry, Catalysts, and Engineering. *Chem. Rev.* **2006**, *106* (9), 4044–4098.
(58) Meier, M. A. R.; Metzger, J. O.; Schubert, U. S. Plant Oil Renewable Resources as Green Alternatives in Polymer Science. *Chem. Soc. Rev.* **2007**, *36* (11), 1788–1802.
(59) Meier, M. A. R.; Metzger, J. O.; Schubert, U. S. Plant Oil Renewable Resources

as Green Alternatives in Polymer Science. *Chem. Soc. Rev.* **2007**, *36* (11), 1788–1802.
(60) Gorrée, M.; Guinée, J. B.; Huppes, G.; Van Oers, L. Environmental Life Cycle Assessment of Linoleum. *Int. J. Life Cycle Assess.* **2002**, *7* (3), 158–166.
(61) Seniha Güner, F.; Yağcı, Y.; Tuncer Erciyes, A. Polymers from Triglyceride Oils. *Prog. Polym. Sci.* **2006**, *31* (7), 633–670.
(62) Zlatanić, A.; Lava, C.; Zhang, W.; Petrović, Z. S. Effect of Structure on Properties of Polyols and Polyurethanes Based on Different Vegetable Oils. *J. Polym. Sci. Part B Polym. Phys.* **2004**, *42* (5), 809–819.
(63) Mutlu, H.; Meier, M. A. R. Castor Oil as a Renewable Resource for the Chemical Industry. *Eur. J. Lipid Sci. Technol.* **2010**, *112* (1), 10–30.
(64) Petrovic, Z. Polyurethanes from Vegetable Oils. *Polym. Rev.* **2008**, *48* (1), 109–155.
(65) Annual Ethanol Production, Renewable Fuels Association https://ethanolrfa.org/markets-and-statistics/annual-ethanol-production (accessed 2023 -02 -28).
(66) Balat, M.; Balat, H.; Öz, C. Progress in Bioethanol Processing. *Prog. Energy Combust. Sci.* **2008**, *34* (5), 551–573.
(67) Sarkar, N.; Ghosh, S. K.; Bannerjee, S.; Aikat, K. Bioethanol Production from Agricultural Wastes: An Overview. *Renew. Energy* **2012**, *37* (1), 19–27.
(68) Kim, S.; Dale, B. E. Global Potential Bioethanol Production from Wasted Crops and Crop Residues. *Biomass and Bioenergy* **2004**, *26* (4), 361–375.
(69) Zimmermann, H.; Walzl, R. Ethylene. In *Ullmann's Encyclopedia of Industrial Chemistry*; Wiley-VCH Verlag GmbH & Co. KGaA: Weinheim, Germany, 2009; pp 465–526.
(70) Le Berre, C.; Serp, P.; Kalck, P.; Torrence, G. P. Acetic Acid. In *Ullmann's Encyclopedia of Industrial Chemistry*; Wiley: Weinheim, Germany, 2014; pp 1–34.
(71) Arpe, H. J. *Industrielle Organische Chemie: Bedeutende Vor- Und Zwischenprodukte*, 6th ed.; Wiley, 2007.
(72) Bienewald, F.; Leibold, E.; Tužina, P.; Roscher, G. Vinyl Esters. In *Ullmann's Encyclopedia of Industrial Chemistry*; Wiley, 2019; pp 1–16.
(73) Ott, J.; Gronemann, V.; Pontzen, F.; Fiedler, E.; Grossmann, G.; Kersebohm, D. B.; Weiss, G.; Witte, C. Methanol. In *Ullmann's Encyclopedia of Industrial Chemistry*; Wiley: Weinheim, Germany, 2012.
(74) Klemm, D.; Heublein, B.; Fink, H. P.; Bohn, A. Cellulose: Fascinating Biopolymer and Sustainable Raw Material. *Angew. Chemie - Int. Ed.* **2005**, *44* (22), 3358–3393.
(75) Heinze, T. Cellulose: Structure and Properties. *Adv. Polym. Sci.* **2015**, *271*, 1–52.
(76) Payen, A. Sur Un Moyen d'isoler Le Tissue Élémentaire Des Bois. *CR Hebd. Seances Acad. Sci* **1838**, *7* (1125), 26.
(77) Brongniart, A.; Pelouze, T. J.; Dumas, A. B. Rapport Sur Un Mémoire de M. Payen, Relatif à La Composition de La Matière Ligneuse. *CR Hebd Seances Acad Sci* **1839**, *8*, 51–53.
(78) Staudinger, H. On Polymerization. In *A Source Book in Chemistry, 1900-1950*; Harvard University Press, 1968; pp 259–264.
(79) Heise, K.; Delepierre, G.; King, A. W. T.; Kostiainen, M. A.; Zoppe, J.; Weder, C.; Kontturi, E. Chemical Modification of Reducing End-Groups in Cellulose

Nanocrystals. *Angew. Chemie Int. Ed.* **2021**, *60* (1), 66–87.
(80) Heise, K.; Koso, T.; Pitkänen, L.; Potthast, A.; King, A. W. T.; Kostiainen, M. A.; Kontturi, E. Knoevenagel Condensation for Modifying the Reducing End Groups of Cellulose Nanocrystals. *ACS Macro Lett.* **2019**, *8* (12), 1642–1647.
(81) Tao, H.; Lavoine, N.; Jiang, F.; Tang, J.; Lin, N. Reducing End Modification on Cellulose Nanocrystals: Strategy, Characterization, Applications and Challenges. *Nanoscale Horizons* **2020**, *5* (4), 607–627.
(82) Kobayashi, S.; Sakamoto, J.; Kimura, S. In Vitro Synthesis of Cellulose and Related Polysaccharides. *Prog. Polym. Sci.* **2001**, *26* (9), 1525–1560.
(83) Trache, D.; Hussin, M. H.; Hui Chuin, C. T.; Sabar, S.; Fazita, M. R. N.; Taiwo, O. F. A.; Hassan, T. M.; Haafiz, M. K. M. Microcrystalline Cellulose: Isolation, Characterization and Bio-Composites Application—A Review. *Int. J. Biol. Macromol.* **2016**, *93*, 789–804.
(84) Battista, O. A.; Smith, P. A. Microcrystalline Cellulose. *Ind. Eng. Chem.* **1962**, *54* (9), 20–29.
(85) Vora, R. S.; Shah, Y. D. Production of Microcrystalline Cellulose from Corn Husk and Its Evaluation as Pharmaceutical Excipient. *Int. J. Res. Sci. Innov.* **2015**, *2* (11), 69–74.
(86) Katakojwala, R.; Mohan, S. V. Microcrystalline Cellulose Production from Sugarcane Bagasse: Sustainable Process Development and Life Cycle Assessment. *J. Clean. Prod.* **2020**, *249*, 119342.
(87) Nobles, D. R.; Romanovicz, D. K.; Brown, R. M. Cellulose in Cyanobacteria. Origin of Vascular Plant Cellulose Synthase? *Plant Physiol.* **2001**, *127* (2), 529–542.
(88) Brown, R. M. Cellulose Structure and Biosynthesis: What Is in Store for the 21st Century? *J. Polym. Sci. Part A Polym. Chem.* **2004**, *42* (3), 487–495.
(89) Kobayashi, S.; Kashiwa, K.; Kawasaki, T.; Shoda, S. Novel Method for Polysaccharide Synthesis Using an Enzyme: The First in Vitro Synthesis of Cellulose via a Nonbiosynthetic Path Utilizing Cellulase as Catalyst. *J. Am. Chem. Soc.* **1991**, *113* (8), 3079–3084.
(90) Kobayashi, S.; Shoda, S.; Uyama, H. Enzymatic Polymerization and Oligomerization. *Polym. Synth. Eng.* **1995**, 1–30.
(91) Kobayashi, S.; Uyama, H.; Ohmae, M. Enzymatic Polymerization for Precision Polymer Synthesis. *Bull. Chem. Soc. Jpn.* **2001**, *74* (4), 613–635.
(92) Nakatsubo, F.; Kamitakahara, H.; Hori, M. Cationic Ring-Opening Polymerization of 3,6-Di-O-Benzyl-α-D-Glucose 1,2,4-Orthopivalate and the First Chemical Synthesis of Cellulose. *J. Am. Chem. Soc.* **1996**, *118* (7), 1677–1681.
(93) Heinze, T.; El Seoud, O. A.; Koschella, A. *Cellulose Derivatives*; Springer Series on Polymer and Composite Materials; Springer International Publishing: Cham, 2018.
(94) Forestry Production and Trade, Food and Agriculture Organization of the United Nations https://www.fao.org/faostat/en/#data/FO (accessed 2023 -02 -28).
(95) Zhou, C. H.; Xia, X.; Lin, C. X.; Tong, D. S.; Beltramini, J. Catalytic Conversion of Lignocellulosic Biomass to Fine Chemicals and Fuels. *Chem. Soc. Rev.* **2011**, *40* (11), 5588–5617.
(96) Ragauskas, A. J.; Williams, C. K.; Davison, B. H.; Britovsek, G.; Cairney, J.; Eckert, C. A.; Frederick, W. J.; Hallett, J. P.; Leak, D. J.; Liotta, C. L.; Mielenz, J. R.; Murphy, R.; Templer, R.; Tschaplinski, T. The Path Forward for Biofuels and

Biomaterials. *Science* **2006**, *311* (5760), 484–489.
(97) Davda, R. R.; Dumesic, J. A. Renewable Hydrogen by Aqueous-Phase Reforming of Glucose. *Chem. Commun.* **2004**, *4* (1), 36–37.
(98) Davda, R. R.; Shabaker, J. W.; Huber, G. W.; Cortright, R. D.; Dumesic, J. A. A Review of Catalytic Issues and Process Conditions for Renewable Hydrogen and Alkanes by Aqueous-Phase Reforming of Oxygenated Hydrocarbons over Supported Metal Catalysts. *Appl. Catal. B Environ.* **2005**, *56* (1–2), 171–186.
(99) Tsuchiya, Y.; Sumi, K. Thermal Decomposition Products of Cellulose. *J. Appl. Polym. Sci.* **1970**, *14* (8), 2003–2013.
(100) Cao, F.; Schwartz, T. J.; McClelland, D. J.; Krishna, S. H.; Dumesic, J. A.; Huber, G. W. Dehydration of Cellulose to Levoglucosenone Using Polar Aprotic Solvents. *Energy Environ. Sci.* **2015**, *8* (6), 1808–1815.
(101) He, J.; Huang, K.; Barnett, K. J.; Krishna, S. H.; Alonso, D. M.; Brentzel, Z. J.; Burt, S. P.; Walker, T.; Banholzer, W. F.; Maravelias, C. T.; Hermans, I.; Dumesic, J. A.; Huber, G. W. New Catalytic Strategies for a,u-Diols Production from Lignocellulosic Biomass. **2017**.
(102) Ragnar, M.; Henriksson, G.; Lindström, M. E.; Wimby, M.; Blechschmidt, J.; Heinemann, S. Pulp. In *Ullmann's Encyclopedia of Industrial Chemistry*; Wiley-VCH Verlag GmbH & Co. KGaA: Weinheim, Germany, 2014; pp 1–92.
(103) Ek, M.; Gellerstedt, G.; Henriksson, G. *Pulping Chemistry and Technology*; Ek, M., Gellerstedt, G., Henriksson, G., Eds.; Walter de Gruyter, 2009; Vol. 2.
(104) Kleinert, T. N. Organosolv Pulping and Recovery Process. *Pat. US3585104* **1971**.
(105) Sjostrom, E. *Wood Chemistry*; Elsevier, 1993.
(106) Schweizer, E. Das Kupferoxyd-Ammoniak, Ein Auflösungsmittel Für Die Pflanzenfaser. *Vierteljahrsschrift der Züricher Naturf. Gesellschaft* **1857**, 109–111.
(107) Weißl, M.; Hobisch, M. A.; Johansson, L. S.; Hettrich, K.; Kontturi, E.; Volkert, B.; Spirk, S. Cellulose Carbamate Derived Cellulose Thin Films: Preparation, Characterization and Blending with Cellulose Xanthate. *Cellulose* **2019**, *26* (12), 7399–7410.
(108) Fink, H. P.; Ganster, J.; Lehmann, A. Progress in Cellulose Shaping: 20 Years Industrial Case Studies at Fraunhofer IAP. *Cellulose* **2014**, *21* (1), 31–51.
(109) Heinze, T.; Dicke, R.; Koschella, A.; Kull, A. H.; Klohr, E.-A.; Koch, W. Effective Preparation of Cellulose Derivatives in a New Simple Cellulose Solvent. *Macromol. Chem. Phys.* **2000**, *201* (6), 627–631.
(110) Ciacco, G. T.; Liebert, T. F.; Frollini, E.; Heinze, T. J. Application of the Solvent Dimethyl Sulfoxide/Tetrabutyl-Ammonium Fluoride Trihydrate as Reaction Medium for the Homogeneous Acylation of Sisal Cellulose. *Cellulose* **2003**, *10* (2), 125–132.
(111) McCormick, C. L.; Callais, P. A. Derivatization of Cellulose in Lithium Chloride and N-N-Dimethylacetamide Solutions. *Polymer (Guildf).* **1987**, *28* (13), 2317–2323.
(112) Chrapava, S.; Touraud, D.; Rosenau, T.; Potthast, A.; Kunz, W. The Investigation of the Influence of Water and Temperature on the LiCl/DMAc/Cellulose System. *Phys. Chem. Chem. Phys.* **2003**, *5* (9), 1842–1847.
(113) Dawsey, T. R.; McCormick, C. L. The Lithium Chloride/Dimethylacetamide Solvent for Cellulose: A Literature Review. *J. Macromol. Sci. Part C* **1990**, *30* (3–4), 405–440.

(114) Potthast, A.; Rosenau, T.; Buchner, R.; Röder, T.; Ebner, G.; Bruglachner, H.; Sixta, H.; Kosma, P. The Cellulose Solvent System N,N-Dimethylacetamide/Lithium Chloride Revisited: The Effect of Water on Physicochemical Properties and Chemical Stability. *Cellulose* **2002**, *9* (1), 41–53.
(115) Fink, H. P.; Weigel, P.; Purz, H. J.; Ganster, J. Structure Formation of Regenerated Cellulose Materials from NMMO-Solutions. *Prog. Polym. Sci.* **2001**, *26* (9), 1473–1524.
(116) Firgo, H.; Eibl, M.; Eichinger, D. Lyocell: Eine Ökologische Alternative. *Lenzinger Berichte* **1996**, *75* (96), 47ff.
(117) Cardoso, I. S.; Pedro, A. Q.; Silvestre, A. J. D.; Freire, M. G. Ionic Liquids and Deep Eutectic Solvents in the Field of Environmental Monitoring. In *Green Chemistry and Sustainable Technology*; Springer, Singapore, 2019; pp 203–240.
(118) Dupont, J.; De Souza, R. F.; Suarez, P. A. Z. Ionic Liquid (Molten Salt) Phase Organometallic Catalysis. *Chem. Rev.* **2002**, *102* (10), 3667–3692.
(119) Dong, K.; Liu, X.; Dong, H.; Zhang, X.; Zhang, S. Multiscale Studies on Ionic Liquids. *Chem. Rev.* **2017**, *117* (10), 6636–6695.
(120) Graenacher, C. Cellulose Solution. US1943176A, September 16, 1931.
(121) Wu, J.; Zhang, J.; Zhang, H.; He, J.; Ren, Q.; Guo, M. Homogeneous Acetylation of Cellulose in a New Ionic Liquid. *Biomacromolecules* **2004**, *5* (2), 266–268.
(122) Cao, Y.; Wu, J.; Meng, T.; Zhang, J.; He, J.; Li, H.; Zhang, Y. Acetone-Soluble Cellulose Acetates Prepared by One-Step Homogeneous Acetylation of Cornhusk Cellulose in an Ionic Liquid 1-Allyl-3-Methylimidazolium Chloride (AmimCl). *Carbohydr. Polym.* **2007**, *69* (4), 665–672.
(123) Kakuchi, R.; Yamaguchi, M.; Endo, T.; Shibata, Y.; Ninomiya, K.; Ikai, T.; Maeda, K.; Takahashi, K. Efficient and Rapid Direct Transesterification Reactions of Cellulose with Isopropenyl Acetate in Ionic Liquids. *RSC Adv.* **2015**, *5* (88), 72071–72074.
(124) Chen, M.; Li, R. M.; Runge, T.; Feng, J.; Feng, J.; Hu, S.; Shi, Q. S. Solvent-Free Acetylation of Cellulose by 1-Ethyl-3-Methylimidazolium Acetate-Catalyzed Transesterification. *ACS Sustain. Chem. Eng.* **2019**, *7* (20), 16971–16978.
(125) Van Nguyen, Q.; Nomura, S.; Hoshino, R.; Ninomiya, K.; Takada, K.; Kakuchi, R.; Takahashi, K. Recyclable and Scalable Organocatalytic Transesterification of Polysaccharides in a Mixed Solvent of 1-Ethyl-3-Methylimidazolium Acetate and Dimethyl Sulfoxide. *Polym. J.* **2017**, *49* (11), 783–787.
(126) Barthel, S.; Heinze, T. Acylation and Carbanilation of Cellulose in Ionic Liquids. *Green Chem.* **2006**, *8* (3), 301–306.
(127) Gericke, M.; Fardim, P.; Heinze, T. Ionic Liquids — Promising but Challenging Solvents for Homogeneous Derivatization of Cellulose. *Molecules* **2012**, *17* (6), 7458–7502.
(128) Köhler, S.; Liebert, T.; Schöbitz, M.; Schaller, J.; Meister, F.; Günther, W.; Heinze, T. Interactions of Ionic Liquids with Polysaccharides 1. Unexpected Acetylation of Cellulose with 1-Ethyl-3-Methylimidazolium Acetate. *Macromol. Rapid Commun.* **2007**, *28* (24), 2311–2317.
(129) Jessop, P. G.; Heldebrant, D. J.; Li, X.; Eckert, C. A.; Liotta, C. L. Reversible Nonpolar-to-Polar Solvent. *Nature* **2005**, *436* (7054), 1102–1102.
(130) Zhang, Q.; Oztekin, N. S.; Barrault, J.; De Oliveira Vigier, K.; Jérôme, F. Activation of Microcrystalline Cellulose in a CO 2 -Based Switchable System. *ChemSusChem* **2013**, *6* (4), 593–596.

(131) Xie, H.; Yu, X.; Yang, Y.; Zhao, Z. K. Capturing CO2 for Cellulose Dissolution. *Green Chem.* **2014**, *16* (5), 2422–2427.
(132) Onwukamike, K. N.; Tassaing, T.; Grelier, S.; Grau, E.; Cramail, H.; Meier, M. A. R. R. Detailed Understanding of the DBU/CO2 Switchable Solvent System for Cellulose Solubilization and Derivatization. *ACS Sustain. Chem. Eng.* **2018**, *6* (1), 1496–1503.
(133) Gunnarsson, M.; Bernin, D.; Hasani, M.; Lund, M.; Bialik, E. Direct Evidence for Reaction between Cellulose and CO2from Nuclear Magnetic Resonance. *ACS Sustain. Chem. Eng.* **2021**, *9* (42), 14006–14011.
(134) Kirchberg, A.; Meier, M. A. R. Regeneration of Cellulose from a Switchable Ionic Liquid: Toward More Sustainable Cellulose Fibers. *Macromol. Chem. Phys.* **2021**, *222* (6), 2000433.
(135) Henderson, R. K.; Jiménez-González, C.; Constable, D. J. C.; Alston, S. R.; Inglis, G. G. A.; Fisher, G.; Sherwood, J.; Binks, S. P.; Curzons, A. D. Expanding GSK's Solvent Selection Guide – Embedding Sustainability into Solvent Selection Starting at Medicinal Chemistry. *Green Chem.* **2011**, *13* (4), 854–862.
(136) Prat, D.; Hayler, J.; Wells, A. A Survey of Solvent Selection Guides. *Green Chem.* **2014**, *16* (10), 4546–4551.
(137) Yang, Y.; Song, L.; Peng, C.; Liu, E.; Xie, H. Activating Cellulose via Its Reversible Reaction with CO 2 in the Presence of 1,8-Diazabicyclo[5.4.0]Undec-7-Ene for the Efficient Synthesis of Cellulose Acetate. *Green Chem.* **2015**, *17* (5), 2758–2763.
(138) Onwukamike, K. N.; Grelier, S.; Grau, E.; Cramail, H.; Meier, M. A. R. Sustainable Transesterification of Cellulose with High Oleic Sunflower Oil in a DBU-CO 2 Switchable Solvent. *ACS Sustain. Chem. Eng.* **2018**, *6* (7), 8826–8835.
(139) Pei, M.; Peng, X.; Shen, Y.; Yang, Y.; Guo, Y.; Zheng, Q.; Xie, H.; Sun, H. Synthesis of Water-Soluble, Fully Biobased Cellulose Levulinate Esters through the Reaction of Cellulose and Alpha-Angelica Lactone in a DBU/CO2/DMSO Solvent System. *Green Chem.* **2020**, *22* (3), 707–717.
(140) Wolfs, J.; Meier, M. A. R. A More Sustainable Synthesis Approach for Cellulose Acetate Using the DBU/CO2 Switchable Solvent System. *Green Chem.* **2021**, *23* (12), 4410–4420.
(141) Chen, H.; Yang, F.; Du, J.; Xie, H.; Zhang, L.; Guo, Y.; Xu, Q.; Zheng, Q.; Li, N.; Liu, Y. Efficient Transesterification Reaction of Cellulose with Vinyl Esters in DBU/DMSO/CO2 Solvent System at Low Temperature. *Cellulose* **2018**, *25* (12), 6935–6945.
(142) Xu, Q.; Song, L.; Zhang, L.; Hu, G.; Du, J.; Liu, E.; Zheng, Q.; Liu, Y.; Li, N.; Xie, H. Organocatalytic Cellulose Dissolution and In Situ Grafting of ϵ-Caprolactone via ROP in a Reversible DBU/DMSO/CO $_2$ System. *ChemistrySelect* **2017**, *2* (24), 7128–7134.
(143) Söyler, Z.; Meier, M. A. R. Sustainable Functionalization of Cellulose and Starch with Diallyl Carbonate in Ionic Liquids. *Green Chem.* **2017**, *19* (16), 3899–3907.
(144) Yang, Y.; Xie, H.; Liu, E. Acylation of Cellulose in Reversible Ionic Liquids. *Green Chem.* **2014**, *16* (6), 3018–3023.
(145) Onwukamike, K. N.; Lapuyade, L.; Maillé, L.; Grelier, S.; Grau, E.; Cramail, H.; Meier, M. A. R. Sustainable Approach for Cellulose Aerogel Preparation from the DBU–CO 2 Switchable Solvent. *ACS Sustain. Chem. Eng.* **2019**, *7* (3), 3329–3338.

(146) Esen, E.; Hädinger, P.; Meier, M. A. R. Sustainable Fatty Acid Modification of Cellulose in a CO2-Based Switchable Solvent and Subsequent Thiol-Ene Modification. *Biomacromolecules* **2021**, *22* (2), 586–593.
(147) Balser, K.; Hoppe, L.; Eicher, T.; Wandel, M.; Astheimer, H.; Steinmeier, H.; Allen, J. M. Cellulose Esters. In *Ullmann's Encyclopedia of Industrial Chemistry*; Wiley, 2004.
(148) Abel, F. A. Researches on Gun-Cotton.—On the Manufacture and Composition of Gun-Cotton. *Philos. Trans. R. Soc. London* **1866**, *156*, 269–308.
(149) Hummel, A. Industrial Processes. *Macromol. Symp.* **2004**, *208*, 61–80.
(150) Fischer, S.; Thümmler, K.; Volkert, B.; Hettrich, K.; Schmidt, I.; Fischer, K. Properties and Applications of Cellulose Acetate. *Macromol. Symp.* **2008**, *262* (1), 89–96.
(151) Steinmeier, H. 3. Acetate Manufacturing, Process and Technology 3.1 Chemistry of Cellulose Acetylation. *Macromol. Symp.* **2004**, *208* (1), 49–60.
(152) Malm, C. J.; Tanghe, L. J.; Laird, B. C. Preparation of Cellulose Acetate - Action of Sulfuric Acid. *Ind. Eng. Chem.* **1946**, *38* (1), 77–82.
(153) Heinze, T.; Liebert, T. Celluloses and Polyoses/Hemicelluloses. In *Polymer Science: A Comprehensive Reference*; Elsevier, 2012; Vol. 10, pp 83–152.
(154) Fordyce, Charles, R. Hydrolyzed Cellulose Acetate. US2129052A, February 4, 1938.
(155) Law, R. C. 5. Applications of Cellulose Acetate 5.1 Cellulose Acetate in Textile Application. *Macromol. Symp.* **2004**, *208* (1), 255–266.
(156) Law, R. C. 5. Applications of Cellulose Acetate 5.1 Cellulose Acetate in Textile Application. *Macromol. Symp.* **2004**, *208* (1), 255–266.
(157) Shibata, T. 5.6 Cellulose Acetate in Separation Technology. *Macromol. Symp.* **2004**, *208* (1), 353–370.
(158) Carollo, P.; Grospietro, B. 5.5 Plastic Materials. *Macromol. Symp.* **2004**, *208* (1), 335–352.
(159) Sata, H.; Murayama, M.; Shimamoto, S. 5.4 Properties and Applications of Cellulose Triacetate Film. *Macromol. Symp.* **2004**, *208* (1), 323–334.
(160) Law, P. W.; Longdon, A.; Willins, G. G. 5.3 Solvent Cast Cellulose Diacetate Film. *Macromol. Symp.* **2004**, *208* (1), 293–322.
(161) Rustemeyer, P. 5.2 CA Filter Tow for Cigarette Filters. *Macromol. Symp.* **2004**, *208* (1), 267–292.
(162) Suzuki, S.; Yada, R.; Hamano, Y.; Wada, N.; Takahashi, K. Green Synthesis and Fractionation of Cellulose Acetate by Controlling the Reactivity of Polysaccharides in Sugarcane Bagasse. *ACS Sustain. Chem. Eng.* **2020**, *8* (24), 9002–9008.
(163) Kakko, T.; King, A. W. T.; Kilpeläinen, I. Homogenous Esterification of Cellulose Pulp in [DBNH][OAc]. *Cellulose* **2017**, *24* (12), 5341–5354.
(164) Heinze, T.; Liebert, T. Unconventional Methods in Cellulose Functionalization. *Prog. Polym. Sci.* **2001**, *26* (9), 1689–1762.
(165) Schenzel, A.; Hufendiek, A.; Barner-Kowollik, C.; Meier, M. A. R. Catalytic Transesterification of Cellulose in Ionic Liquids: Sustainable Access to Cellulose Esters. *Green Chem.* **2014**, *16* (6), 3266.
(166) Marson, G. A.; El Seoud, O. A. Novel, Efficient Procedure for Acylation of Cellulose under Homogeneous Solution Conditions. *J. Appl. Polym. Sci.* **1999**, *74* (6), 1355–1360.
(167) Würfel, H.; Kayser, M.; Heinze, T. Efficient and Catalyst-Free Synthesis of

Cellulose Acetoacetates. *Cellulose* **2018**, *25* (9), 4919–4928.
(168) Yao, Z.; Mi, S.; Chen, B.; Liu, F.; Na, H.; Zhu, J. Rapid Homogeneous Acylation of Cellulose in a CO 2 Switchable Solvent by Microwave Heating. *ACS Sustain. Chem. Eng.* **2022**, *10* (51), 17327–17335.
(169) Klug, E. D.; Tinsley, J. S. Preparation of Carboxyalkylethers of Cellulose. US2517577A, December 10, 1950.
(170) Felcht, U.-H.; Perplies, E. Method for Producing Cellulose Ethers with Dimethoxyethane as Dispersing Agents. DE3147434A1, November 30, 1981.
(171) Pope, B. G. Hydroxyalkylation of Polysaccharides. US4474951A, September 27, 1983.
(172) Thielking, H.; Schmidt, M. Cellulose Ethers. In *Ullmann's Encyclopedia of Industrial Chemistry*; Wiley, 2006.
(173) Isogai, A.; Ishizu, A.; Nakano, J. Preparation of Tri-O-Alkylcellulose by the Use of a Nonaqueous Cellulose Solvent and Their Physical Characteristics. *J. Appl. Polym. Sci.* **1986**, *31* (2), 341–352.
(174) Isogai, A.; Ishizu, A.; Nakano, J. Preparation of Tri-O-Substituted Cellulose Ethers by the Use of a Nonaqueous Cellulose Solvent. *J. Appl. Polym. Sci.* **1984**, *29* (12), 3873–3882.
(175) Isogai, A.; Ishizu, A.; Nakano, J. Preparation of Tri-O-Benzylcellulose by the Use of Nonaqueous Cellulose Solvents. *J. Appl. Polym. Sci.* **1984**, *29* (6), 2097–2109.
(176) Petruš, L.; Gray, D. G.; BeMiller, J. N. Homogeneous Alkylation of Cellulose in Lithium Chloride/Dimethyl Sulfoxide Solvent with Dimsyl Sodium Activation. A Proposal for the Mechanism of Cellulose Dissolution in LiCl/Me2SO. *Carbohydr. Res.* **1995**, *268* (2), 319–323.
(177) Takaragi, A.; Minoda, M.; Miyamoto, T.; Liu, H. Q.; Zhang, L. N. Reaction Characteristics of Cellulose in the LiCl/1,3-Dimethyl-2-Imidazolidinone Solvent System. *Cellulose* **1999**, *6* (2), 93–102.
(178) Takahashi, S.-I.; Fujimoto, T.; Miyamoto, T.; Inagaki, H. Relationship between Distribution of Substituents and Water Solubility of O-Methyl Cellulose. *J. Polym. Sci. Part A Polym. Chem.* **1987**, *25* (4), 987–994.
(179) Kondo, T.; Gray, D. G. The Preparation of O-Methyl- and O-Ethyl-Celluloses Having Controlled Distribution of Substituents. *Carbohydr. Res.* **1991**, *220* (C), 173–183.
(180) Floor, M.; Hofsteede, L. P. M.; Kieboom, A. P. G.; van Bekkum, H.; Greenland, W. P. T.; Verhaar, L. A. T. Preparation and Calcium Complexation of Oxidized Polysaccharides. II: Hydrogen Peroxide as Co-Reactant in the Chlorite Oxidation of Dialdehyde Glucans. *Recl. des Trav. Chim. des Pays-Bas* **2010**, *108* (10), 384–392.
(181) Kasai, W.; Morooka, T.; Ek, M. Mechanical Properties of Films Made from Dialcohol Cellulose Prepared by Homogeneous Periodate Oxidation. *Cellulose* **2014**, *21* (1), 769–776.
(182) Simon, J.; Fliri, L.; Sapkota, J.; Ristolainen, M.; Miller, S. A.; Hummel, M.; Rosenau, T.; Potthast, A. Reductive Amination of Dialdehyde Cellulose: Access to Renewable Thermoplastics. *Biomacromolecules* **2023**, *24* (1), 166–177.
(183) Esen, E.; Meier, M. A. R. Sustainable Functionalization of 2,3-Dialdehyde Cellulose via the Passerini Three-Component Reaction. *ACS Sustain. Chem. Eng.* **2020**, *8* (41), 15755–15760.
(184) de Nooy, A. E. J.; Besemer, A. C.; van Bekkum, H. Highly Selective Tempo Mediated Oxidation of Primary Alcohol Groups in Polysaccharides. *Recl. des*

Trav. Chim. des Pays-Bas **1994**, *113* (3), 165–166.
(185) Gomez-Bujedo, S.; Fleury, E.; Vignon, M. R. Preparation of Cellouronic Acids and Partially Acetylated Cellouronic Acids by TEMP/NaClO Oxidation of Water-Soluble Cellulose Acetate. *Biomacromolecules* **2004**, *5* (2), 565–571.
(186) Isogai, A.; Kato, Y. Preparation of Polyuronic Acid from Cellulose by TEMPO-Mediated Oxidation. *Cellulose* **1998**, *5* (3), 153–164.
(187) Isogai, A.; Saito, T.; Fukuzumi, H. TEMPO-Oxidized Cellulose Nanofibers. *Nanoscale* **2011**, *3* (1), 71–85.
(188) Tahiri, C.; Vignon, M. R. TEMPO-Oxidation of Cellulose: Synthesis and Characterisation of Polyglucuronans. *Cellulose* **2000**, *7* (2), 177–188.
(189) Bailey, W. F.; Bobbitt, J. M.; Wiberg, K. B. Mechanism of the Oxidation of Alcohols by Oxoammonium Cations. *J. Org. Chem.* **2007**, *72* (12), 4504–4509.
(190) Matsumura, S.; Nishioka, M.; Shigeno, H.; Tanaka, T.; Yoshikawa, S. Builder Performance in Detergent Formulations and Biodegradability of Partially Dicarboxylated Cellulose and Amylose Containing Sugar Residues in the Backbone. *Angew. Makromol. Chemie* **1993**, *205* (1), 117–129.
(191) Varma, A. J.; Chavan, V. B. Some Preliminary Studies on Polyelectrolyte and Rheological Properties of Sodium 2,3-Dicarboxy-Cellulose. *Carbohydr. Polym.* **1995**, *27* (1), 63–67.
(192) Kolb, H. C.; Finn, M. G.; Sharpless, K. B. Click Chemistry: Diverse Chemical Function from a Few Good Reactions. *Angew. Chemie - Int. Ed.* **2001**, *40* (11), 2004–2021.
(193) Hafrén, J.; Zou, W.; Córdova, A. Heterogeneous 'Organoclick' Derivatization of Polysaccharides. *Macromol. Rapid Commun.* **2006**, *27* (16), 1362–1366.
(194) Pierre-Antoine, F.; François, B.; Rachida, Z. Crosslinked Cellulose Developed by CuAAC, a Route to New Materials. *Carbohydr. Res.* **2012**, *356*, 247–251.
(195) Peng, P.; Cao, X.; Peng, F.; Bian, J.; Xu, F.; Sun, R. Binding Cellulose and Chitosan via Click Chemistry: Synthesis, Characterization, and Formation of Some Hollow Tubes. *J. Polym. Sci. Part A Polym. Chem.* **2012**, *50* (24), 5201–5210.
(196) Fenn, D.; Pohl, M.; Heinze, T. Novel 3-O-Propargyl Cellulose as a Precursor for Regioselective Functionalization of Cellulose. *React. Funct. Polym.* **2009**, *69* (6), 347–352.
(197) Koschella, A.; Hartlieb, M.; Heinze, T. A "Click-Chemistry" Approach to Cellulose-Based Hydrogels. *Carbohydr. Polym.* **2011**, *86* (1), 154–161.
(198) Jogunola, O.; Eta, V.; Hedenström, M.; Sundman, O.; Salmi, T.; Mikkola, J. P. Ionic Liquid Mediated Technology for Synthesis of Cellulose Acetates Using Different Co-Solvents. *Carbohydr. Polym.* **2016**, *135*, 341–348.
(199) Chen, J.; Xu, J.; Wang, K.; Cao, X.; Sun, R. Cellulose Acetate Fibers Prepared from Different Raw Materials with Rapid Synthesis Method. *Carbohydr. Polym.* **2016**, *137*, 685–692.
(200) Chen, C. Y.; Chen, M. J.; Zhang, X. Q.; Liu, C. F.; Sun, R. C. Per-O-Acetylation of Cellulose in Dimethyl Sulfoxide with Catalyzed Transesterification. *J. Agric. Food Chem.* **2014**, *62* (15), 3446–3452.
(201) Wolfs, J.; Nickisch, R.; Wanner, L.; Meier, M. A. R. Sustainable One-Pot Cellulose Dissolution and Derivatization via a Tandem Reaction in the DMSO/DBU/CO_2 Switchable Solvent System. *J. Am. Chem. Soc.* **2021**, *143* (44), 18693–18702.
(202) Yuan, C.; Shi, W.; Chen, P.; Chen, H.; Zhang, L.; Hu, G.; Jin, L.; Xie, H.; Zheng,

Q.; Lu, S. Dissolution and Transesterification of Cellulose in γ-Valerolactone Promoted by Ionic Liquids. *New J. Chem.* **2019**, *43* (1), 330–337.
(203) Guo, Y.; Li, L.; Guo, G.; Pei, M.; Zhang, L.; Xie, H.; Sun, H.; Zheng, Q. Synthesis of a Fully Biobased Cellulose-3-(2-Hydroxyphenyl) Propionate Ester with Antioxidant Activity and UV-Resistant Properties by the DBU/CO 2 /DMSO Solvent System. *Green Chem.* **2021**, *23* (6), 2352–2361.
(204) Hinner, L. P.; Wissner, J. L.; Beurer, A.; Nebel, B. A.; Hauer, B. Homogeneous Vinyl Ester-Based Synthesis of Different Cellulose Derivatives in 1-Ethyl-3-Methyl-Imidazolium Acetate. *Green Chem.* **2016**, *18* (22), 6099–6107.
(205) Kono, H.; Hashimoto, H.; Shimizu, Y. NMR Characterization of Cellulose Acetate: Chemical Shift Assignments, Substituent Effects, and Chemical Shift Additivity. *Carbohydr. Polym.* **2015**, *118*, 91–100.
(206) Tezuka, Y.; Tsuchiya, Y. Determination of Substituent Distribution in Cellulose Acetate by Means of a 13C NMR Study on Its Propanoated Derivative. *Carbohydr. Res.* **1995**, *273* (1), 83–91.
(207) Da Ros, S.; Aliev, A. E.; del Gaudio, I.; King, R.; Pokorska, A.; Kearney, M.; Curran, K. Characterising Plasticised Cellulose Acetate-Based Historic Artefacts by NMR Spectroscopy: A New Approach for Quantifying the Degree of Substitution and Diethyl Phthalate Contents. *Polym. Degrad. Stab.* **2021**, *183*.
(208) King, A. W. T.; Jalomäki, J.; Granström, M.; Argyropoulos, D. S.; Heikkinen, S.; Kilpeläinen, I. A New Method for Rapid Degree of Substitution and Purity Determination of Chloroform-Soluble Cellulose Esters, Using 31P NMR. *Anal. Methods* **2010**, *2* (10), 1499.
(209) Söyler, Z.; Onwukamike, K. N.; Grelier, S.; Grau, E.; Cramail, H.; Meier, M. A. R. Sustainable Succinylation of Cellulose in a CO 2 -Based Switchable Solvent and Subsequent Passerini 3-CR and Ugi 4-CR Modification. *Green Chem.* **2018**, *20* (1), 214–224.
(210) Asaadi, S.; Kakko, T.; King, A. W. T.; Kilpeläinen, I.; Hummel, M.; Sixta, H. High-Performance Acetylated Ioncell-F Fibers with Low Degree of Substitution. *ACS Sustain. Chem. Eng.* **2018**, *6* (7), 9418–9426.
(211) Kakko, T.; King, A. W. T.; Kilpeläinen, I. Homogenous Esterification of Cellulose Pulp in [DBNH][OAc]. *Cellulose* **2017**, *24* (12), 5341–5354.
(212) Freire, C. S. R.; Silvestre, A. J. D.; Neto, C. P.; Rocha, R. M. A. An Efficient Method for Determination of the Degree of Substitution of Cellulose Esters of Long Chain Aliphatic Acids. *Cellulose* **2005**, *12* (5), 449–458.
(213) Samaranayake, G.; Glasser, W. G. Cellulose Derivatives with Low DS. II. Analysis of Alkanoates. *Carbohydr. Polym.* **1993**, *22* (2), 79–86.
(214) Casarano, R.; Fidale, L. C.; Lucheti, C. M.; Heinze, T.; Seoud, O. A. E. Expedient, Accurate Methods for the Determination of the Degree of Substitution of Cellulose Carboxylic Esters: Application of UV-Vis Spectroscopy (Dye Solvatochromism) and FTIR. *Carbohydr. Polym.* **2011**, *83* (3), 1285–1292.
(215) Peydecastaing, J.; Vaca-Garcia, C.; Borredon, E. Accurate Determination of the Degree of Substitution of Long Chain Cellulose Esters. *Cellulose* **2009**, *16* (2), 289–297.
(216) Vaca-Garcia, C.; Borredon, M. E.; Gaseta, A. Determination of the Degree of Substitution (DS) of Mixed Cellulose Esters by Elemental Analysis. *Cellulose* **2001**, *8*, 225–231.
(217) Hou, D.-F.; Li, M.-L.; Yan, C.; Zhou, L.; Liu, Z.-Y.; Yang, W.; Yang, M.-B. Mechanochemical Preparation of Thermoplastic Cellulose Oleate by Ball Milling.

Green Chem. **2021**, *23* (5), 2069.
(218) Fei, P.; Liao, L.; Cheng, B.; Song, J. Quantitative Analysis of Cellulose Acetate with a High Degree of Substitution by FTIR and Its Application. *Anal. Methods* **2017**, *9* (43), 6194–6201.
(219) Nunes, S.; Ramacciotti, F.; Neves, A.; Angelin, E. M.; Ramos, A. M.; Roldão, É.; Wallaszkovits, N.; Armijo, A. A.; Melo, M. J. A Diagnostic Tool for Assessing the Conservation Condition of Cellulose Nitrate and Acetate in Heritage Collections: Quantifying the Degree of Substitution by Infrared Spectroscopy. *Herit. Sci.* **2020**, *8* (1), 1–14.
(220) Li, W.; Cai, G.; Zhang, P. A Simple and Rapid Fourier Transform Infrared Method for the Determination of the Degree of Acetyl Substitution of Cellulose Nanocrystals. *J. Mater. Sci.* **2019**, *54* (10), 8047–8056.
(221) Räisänen, J. Sulfur. In *Encyclopedia of Analytical Science: Second Edition*; Elsevier Inc., 2004; pp 415–423.
(222) Mineral Commodity Summaries 2022. *U.S. Geological Survey* **2022**, 162–163.
(223) Rappold, T. A.; Lackner, K. S. Large Scale Disposal of Waste Sulfur: From Sulfide Fuels to Sulfate Sequestration. *Energy* **2010**, *35* (3), 1368–1380.
(224) Wu, X.; Zhou, Q.; Xu, K. Are Isothiocyanates Potential Anti-Cancer Drugs? *Acta Pharmacol. Sin.* **2009**, *30* (5), 501–512.
(225) Gupta, P.; Kim, B.; Kim, S.-H.; Srivastava, S. K. Molecular Targets of Isothiocyanates in Cancer: Recent Advances. *Mol. Nutr. Food Res.* **2014**, *58* (8), 1685–1707.
(226) Choudhari, A. S.; Mandave, P. C.; Deshpande, M.; Ranjekar, P.; Prakash, O. Phytochemicals in Cancer Treatment: From Preclinical Studies to Clinical Practice. *Front. Pharmacol.* **2020**, *10*, 1614.
(227) Hanschen, F. S.; Lamy, E.; Schreiner, M.; Rohn, S. Reactivity and Stability of Glucosinolates and Their Breakdown Products in Foods. *Angew. Chemie Int. Ed.* **2014**, *53* (43), 11430–11450.
(228) Sugiyama, R.; Li, R.; Kuwahara, A.; Nakabayashi, R.; Sotta, N.; Mori, T.; Ito, T.; Ohkama-Ohtsu, N.; Fujiwara, T.; Saito, K.; Nakano, R. T.; Bednarek, P.; Hirai, M. Y. Retrograde Sulfur Flow from Glucosinolates to Cysteine in Arabidopsis Thaliana. *Proc. Natl. Acad. Sci. U. S. A.* **2021**, *118* (22), 2017890118.
(229) Lawson, A. P.; Long, M. J. C.; Coffey, R. T.; Qian, Y.; Weerapana, E.; El Oualid, F.; Hedstrom, L. Naturally Occurring Isothiocyanates Exert Anticancer Effects by Inhibiting Deubiquitinating Enzymes. *Cancer Res.* **2015**, *75* (23), 5130–5142.
(230) Dufour, V.; Stahl, M.; Baysse, C. The Antibacterial Properties of Isothiocyanates. *Microbiology* **2015**, *161* (2), 229–243.
(231) Németh, A.; Ábrányi-Balogh, P. Recent Advances in the Synthesis of Isothiocyanates Using Elemental Sulfur. *Catalysts* **2021**, *11* (9), 1081.
(232) Kulkarni, P. M.; Kulkarni, A. R.; Korde, A.; Tichkule, R. B.; Laprairie, R. B.; Denovan-Wright, E. M.; Zhou, H.; Janero, D. R.; Zvonok, N.; Makriyannis, A.; Cascio, M. G.; Pertwee, R. G.; Thakur, G. A. Novel Electrophilic and Photoaffinity Covalent Probes for Mapping the Cannabinoid 1 Receptor Allosteric Site(S). *J. Med. Chem.* **2016**, *59* (1), 44–60.
(233) Abdeldayem, A.; Raouf, Y. S.; Constantinescu, S. N.; Moriggl, R.; Gunning, P. T. Advances in Covalent Kinase Inhibitors. *Chem. Soc. Rev.* **2020**, *49* (9), 2617–2687.
(234) Petri, L.; Szijj, P. A.; Kelemen, Á.; Imre, T.; Gömöry, Á.; Lee, M. T. W.; Hegedus, K.; Ábrányi-Balogh, P.; Chudasama, V.; Keseru, G. M. Cysteine Specific

Bioconjugation with Benzyl Isothiocyanates. *RSC Adv.* **2020**, *10* (25), 14928–14936.
(235) Tamura, T.; Hamachi, I. Chemistry for Covalent Modification of Endogenous/Native Proteins: From Test Tubes to Complex Biological Systems. *J. Am. Chem. Soc.* **2019**, *141* (7), 2782–2799.
(236) Mukerjee, A. K.; Ashare, R. Isothiocyanates in the Chemistry of Heterocycles. *Chem. Rev.* **1991**, *91* (1), 1–24.
(237) Sharma, S. Thiophosgene in Organic Synthesis. *Synth.* **1978**, *1978* (11), 803–820.
(238) Eschliman, K.; Bossmann, S. H. Synthesis of Isothiocyanates: An Update. *Synth.* **2019**, *51* (8), 1746–1752.
(239) Hull, R.; Seden, T. P. The Preparation Of Vinylenedi-Isothiocyanate. *Synth. Commun.* **1980**, *10* (6), 489–493.
(240) Ian Grayson, J. Industrial Scale Synthesis of Thiophosgene and Its Derivatives. *Org. Process Res. Dev.* **1997**, *1* (3), 240–246.
(241) Németh, A. G. Application of Elemental Sulfur in Multicomponent Reactions, Budapest University of Technology and Economics, 2021.
(242) Fu, Z.; Yuan, W.; Chen, N.; Yang, Z.; Xu, J. Na2S2O8-Mediated Efficient Synthesis of Isothiocyanates from Primary Amines in Water. *Green Chem.* **2018**, *20* (19), 4484–4491.
(243) Sun, N.; Li, B.; Shao, J.; Mo, W.; Hu, B.; Shen, Z.; Hu, X. A General and Facile One-Pot Process of Isothiocyanates from Amines under Aqueous Conditions. *Beilstein J. Org. Chem.* **2012**, *8* (1), 61–70.
(244) Munch, H.; Hansen, J. S.; Pittelkow, M.; Christensen, J. B.; Boas, U. A New Efficient Synthesis of Isothiocyanates from Amines Using Di-Tert-Butyl Dicarbonate. *Tetrahedron Lett.* **2008**, *49* (19), 3117–3119.
(245) Janczewski, Ł.; Gajda, A.; Gajda, T. Direct, Microwave-Assisted Synthesis of Isothiocyanates. *European J. Org. Chem.* **2019**, *2019* (14), 2528–2532.
(246) Fujiwara, S. ichi; Shin-Ike, T.; Sonoda, N.; Aoki, M.; Okada, K.; Miyoshi, N.; Kambe, N. Novel Selenium Catalyzed Synthesis of Isothiocyanates from Isocyanides and Elemental Sulfur. *Tetrahedron Lett.* **1991**, *32* (29), 3503–3506.
(247) Fujiwara, S. ichi; Shin-Ike, T.; Okada, K.; Aoki, M.; Kambe, N.; Sonoda, N. A Marvelous Catalysis of Tellurium in the Formation of Isothiocyanates from Isocyanides and Sulfur. *Tetrahedron Lett.* **1992**, *33* (46), 7021–7024.
(248) Tanaka, S.; Uemura, S.; Okano, M. The Thallium(I) Salt-Catalyzed Formation of Isothiocyanates from Isocyanides and Disulfides. *Bull. Chem. Soc. Jpn.* **1977**, *50* (10), 2785–2788.
(249) Baumann, M.; Baxendale, I. R. The Rapid Generation of Isothiocyanates in Flow. *Beilstein J. Org. Chem.* **2013**, *9* (1), 1613–1619.
(250) Li, Z. Y.; Ma, H. Z.; Han, C.; Xi, H. T.; Meng, Q.; Chen, X.; Sun, X. Q. Synthesis of Isothiocyanates by Reaction of Amines with Phenyl Chlorothionoformate via One-Pot or Two-Step Process. *Synth.* **2013**, *45* (12), 1667–1674.
(251) Nath, J.; Ghosh, H.; Yella, R.; Patel, B. K. Molecular Iodine Mediated Preparation of Isothiocyanates from Dithiocarbamic Acid Salts. *European J. Org. Chem.* **2009**, *2009* (12), 1849–1851.
(252) Zhang, X.; Lee, Y. K.; Kelley, J. A.; Burke, T. R. Preparation of Aryl Isothiocyanates via Protected Phenylthiocarbamates and Application to the Synthesis of Caffeic Acid (4-Isothiocyanato)Phenyl Ester. *J. Org. Chem.* **2000**, *65* (19), 6237–6240.

(253) Wong, R.; Dolman, S. J. Isothiocyanates from Tosyl Chloride Mediated Decomposition of in Situ Generated Dithiocarbamic Acid Salts. *J. Org. Chem.* **2007**, *72* (10), 3969–3971.
(254) Shaw, W. H. R.; Walker, D. G. Kinetic Studies of Thiourea Derivatives. IV. The Methylated Thioureas. Conclusions1. *J. Am. Chem. Soc.* **1958**, *80* (20), 5337–5342.
(255) Párkányi, C.; Al-Salamah, M. A. Thermal Decomposition of Aromatic Thioureas. *Zeitschrift fur Naturforsch. - Sect. B J. Chem. Sci.* **1986**, *41* (1), 101–104.
(256) Kim, S.; Yi, K. Y. Di-2-Pyridyl Thionocarbonate. A New Reagent for the Preparation of Isothiocyanates and Carbodiimides. *Tetrahedron Lett.* **1985**, *26* (13), 1661–1664.
(257) Larsen, C.; Steliou, K.; Harpp, D. N. Thiocarbonyl Transfer Reagents. *J. Org. Chem.* **1978**, *43*, 337–339.
(258) Valette, L.; Poulain, S.; Fernandez, X.; Lizzani-Cuvelier, L. Efficient and Solvent-Free Microwave-Accelerated Synthesis of Isothiocyanates Using Lawesson's Reagent. *J. Sulfur Chem.* **2005**, *26* (2), 155–161.
(259) Birchall G E; Haszeldine, R N, J. M. C. No Title. *Proc. Chem. Soc., London* **1960**, 81.
(260) Wang, F.; Luo, T.; Hu, J.; Wang, Y.; Krishnan, H. S.; Jog, P. V.; Ganesh, S. K.; Prakash, G. K. S.; Olah, G. A. Synthesis of Gem-Difluorinated Cyclopropanes and Cyclopropenes: Trifluoromethyltrimethylsilane as a Difluorocarbene Source. *Angew. Chemie Int. Ed.* **2011**, *50* (31), 7153–7157.
(261) Wang, F.; Zhang, W.; Zhu, J.; Li, H.; Huang, K. W.; Hu, J. Chloride Ion-Catalyzed Generation of Difluorocarbene for Efficient Preparation of Gem.-Difluorinated Cyclopropenes and Cyclopropanes. *Chem. Commun.* **2011**, *47* (8), 2411–2413.
(262) Ni, C.; Hu, J. Recent Advances in the Synthetic Application of Difluorocarbene. *Synthesis (Germany)*. Georg Thieme Verlag 2014, pp 842–863.
(263) Németh, A. G.; Keserű, G. M.; Ábrányi-Balogh, P. A Novel Three-Component Reaction between Isocyanides, Alcohols or Thiols and Elemental Sulfur: A Mild, Catalyst-Free Approach towards O -Thiocarbamates and Dithiocarbamates . *Beilstein J. Org. Chem.* **2019**, *15* (1), 1523–1533.
(264) Németh, A. G.; Szabó, R.; Domján, A.; Keserű, G. M.; Ábrányi-Balogh, P. Chromatography-Free Multicomponent Synthesis of Thioureas Enabled by Aqueous Solution of Elemental Sulfur. *ChemistryOpen* **2021**, *10* (1), 16–27.
(265) Nguyen, T. B.; Ermolenko, L.; Al-Mourabit, A. Three-Component Reaction between Isocyanides, Aliphatic Amines and Elemental Sulfur: Preparation of Thioureas under Mild Conditions with Complete Atom Economy. *Synth.* **2014**, *46* (23), 3172–3179.
(266) Nickisch, R.; Conen, P.; Gabrielsen, S. M.; Meier, M. A. R. A More Sustainable Isothiocyanate Synthesis by Amine Catalyzed Sulfurization of Isocyanides with Elemental Sulfur. *RSC Adv.* **2021**, *11* (5), 3134–3142.
(267) Ugi, I.; Dömling, A.; Hörl, W. Multicomponent Reactions in Organic Chemistry. *Endeavour* **1994**, *18* (3), 115–122.
(268) Gu, Y. Multicomponent Reactions in Unconventional Solvents: State of the Art. *Green Chemistry*. Royal Society of Chemistry August 1, 2012, pp 2091–2128.
(269) Cioc, R. C.; Ruijter, E.; Orru, R. V. A. Multicomponent Reactions: Advanced Tools for Sustainable Organic Synthesis. *Green Chem.* **2014**, *16* (6), 2958–2975.
(270) Jung, G. *Combinatorial Chemistry: Synthesis, Analysis, Screening*; John Wiley & Sons, 2008.

(271) Strecker, A. Ueber Die Künstliche Bildung Der Milchsäure Und Einen Neuen, Dem Glycocoll Homologen Körper. *Justus Liebigs Ann. Chem.* **1850**, *75* (1), 27–45.
(272) Mannich, C.; Krösche, W. Ueber Ein Kondensationsprodukt Aus Formaldehyd, Ammoniak Und Antipyrin. *Arch. Pharm. (Weinheim).* **1912**, *250* (1), 647–667.
(273) Hantzsch, A. Condensationsprodukte Aus Aldehydammoniak Und Ketonartigen Verbindungen. *Berichte der Dtsch. Chem. Gesellschaft* **1881**, *14* (2), 1637–1638.
(274) Passerini, M. Isonitriles. II. Compounds with Aldehydes or with Ketones and Monobasic Organic Acids. *Gazz. chim. ital* **1921**, *51*, 181–189.
(275) Ugi, I.; Steinbrückner, C. Über Ein Neues Kondensations-Prinzip. *Angew. Chemie* **1960**, *72* (7-8), 267–268.
(276) Ugi, I. The A-addition of Immonium Ions and Anions to Isonitriles Accompanied by Secondary Reactions. *Angew. Chemie Int. Ed. English* **1962**, *1* (1), 8–21.
(277) Meier, M. A. R.; Hu, R.; Tang, B. Z. Multicomponent Reactions in Polymer Science. *Macromol. Rapid Commun.* **2021**, *42* (6), 2100104.
(278) Tang, Q.; Yin, X.; Kuchukulla, R. R.; Zeng, Q. Recent Advances in Multicomponent Reactions with Organic and Inorganic Sulfur Compounds. *Chem. Rec.* **2021**, *21* (4), 893–905.
(279) Liu, S.; Deng, G. J.; Huang, H. Recent Advances in Sulfur-Containing Heterocycle Formation via Direct C-H Sulfuration with Elemental Sulfur. *Synlett* **2021**, *32* (2), 142–158.
(280) Kindler, K. Studien Über Den Mechanismus Chemischer Reaktionen. Erste Abhandlung. Reduktion von Amiden Und Oxydation von Aminen. *Justus Liebigs Ann. Chem.* **1923**, *431* (1), 187–230.
(281) Willgerodt, C. Ueber Die Einwirkung von Gelbem Schwefelammonium Auf Ketone Und Chinone. *Berichte der Dtsch. Chem. Gesellschaft* **1887**, *20* (2), 2467–2470.
(282) Willgerodt, C.; Merk, F. H. Darstellung von Säuren Und Säureamiden Aus Phenylalkylketonen Durch Behandlung Mit Gelbem Schwefelammonium. *J. für Prakt. Chemie* **1909**, *80* (1), 192–200.
(283) Priebbenow, D. L.; Bolm, C. Recent Advances in the Willgerodt–Kindler Reaction. *Chem. Soc. Rev.* **2013**, *42* (19), 7870–7880.
(284) Asinger, F. Über Die Gemeinsame Einwirkung von Schwefel Und Ammoniak Auf Ketone. *Angew. Chemie* **1956**, *68* (12), 413–413.
(285) Sternlieb, I.; Scheinberg, I. H. Penicillamine Therapy for Hepatolenticular Degeneration. *JAMA* **1964**, *189* (10), 748–754.
(286) Crawhall, J. C.; Scowen, E. F.; Watts, R. W. E. Effect of Penicillamine on Cystinuria. *Br. Med. J.* **1963**, *1* (5330), 588.
(287) Henkin, R.; Keiser, H.; Jaffe, I.; Sternlieb, I.; Scheinberg, I. H. Decreased Taste Sensitivity after D-Penicillamine Reversed by Copper Administration. *Lancet* **1967**, *290* (7529), 1268–1271.
(288) Drauz, K.; Koban, H. G.; Martens, J.; Schwarze, W. Phosphonic and Phosphinic Acid Analogs of Penicillamine. *Liebigs Ann. der Chemie* **1985**, *1985* (3), 448–452.
(289) Harris JR, E.; Sjoerdsma, A. Effect of Penicillamine on Human Collagen and Its Possible Application to Treatment of Scleroderma. *Lancet* **1966**, *288* (7471), 996–999.
(290) Gewald, K.; Schinke, E.; Böttcher, H. Heterocyclen Aus CH-aciden Nitrilen, VIII. 2-Amino-thiophene Aus Methylenaktiven Nitrilen, Carbonylverbindungen Und

Schwefel. *Chem. Ber.* **1966**, *99* (1), 94–100.
(291) Chen, Z.; Liang, P.; Xu, F.; Qiu, R.; Tan, Q.; Long, L.; Ye, M. Lewis Acid-Catalyzed Intermolecular Annulation: Three-Component Reaction toward Imidazo[1,2- a]Pyridine Thiones. *J. Org. Chem.* **2019**, *84* (14), 9369–9377.
(292) Saito, M.; Murakami, S.; Nanjo, T.; Kobayashi, Y.; Takemoto, Y. Mild and Chemoselective Thioacylation of Amines Enabled by the Nucleophilic Activation of Elemental Sulfur. *J. Am. Chem. Soc.* **2020**, *142* (18), 8130–8135.
(293) Kozlov, M.; Kozlov, A.; Komkov, A.; Lyssenko, K.; Zavarzin, I.; Volkova, Y. Synthesis of Phosphoryl Thioamides *via* Three-Component Reaction of Phosphinic Chlorides with Amines and Sulfur. *Adv. Synth. Catal.* **2019**, *361* (12), 2904–2915.
(294) Huang, H.; Xu, Z.; Ji, X.; Li, B.; Deng, G. J. Thiophene-Fused Heteroaromatic Systems Enabled by Internal Oxidant-Induced Cascade Bis-Heteroannulation. *Org. Lett.* **2018**, *20* (16), 4917–4920.
(295) Theato, P.; Dilcher, J.-P. *Multi-Component and Sequential Reactions in Polymer Synthesis*; Springer, 2015; Vol. 269.
(296) Kreye, O.; Tóth, T.; Meier, M. A. R. Introducing Multicomponent Reactions to Polymer Science: Passerini Reactions of Renewable Monomers. *J. Am. Chem. Soc.* **2011**, *133* (6), 1790–1792.
(297) Kanbara, T.; Kawai, Y.; Hasegawa, K.; Morita, H.; Yamamoto, T. Preparation of Polythioamides from Dialdehydes and Diamines with Sulfur by the Willgerodt-Kindler Type Reaction. *J. Polym. Sci. Part A Polym. Chem.* **2001**, *39* (21), 3739–3750.
(298) Lu, Q. L.; Li, X. Y.; Tang, L. R.; Lu, B. L.; Huang, B. One-Pot Tandem Reactions for the Preparation of Esterified Cellulose Nanocrystals with 4-Dimethylaminopyridine as a Catalyst. *RSC Adv.* **2015**, *5* (69), 56198–56204.
(299) Tian, T.; Hu, R.; Tang, B. Z. Room Temperature One-Step Conversion from Elemental Sulfur to Functional Polythioureas through Catalyst-Free Multicomponent Polymerizations. *J. Am. Chem. Soc.* **2018**, *140* (19), 6156–6163.
(300) Zhang, J.; Zang, Q.; Yang, F.; Zhang, H.; Sun, J. Z.; Tang, B. Z. Sulfur Conversion to Multifunctional Poly(O-Thiocarbamate)s through Multicomponent Polymerizations of Sulfur, Diols, and Diisocyanides. *J. Am. Chem. Soc.* **2021**, *143* (10), 3944–3950.
(301) Nickisch, R.; Conen, P.; Meier, M. A. R. Polythiosemicarbazones by Condensation of Dithiosemicarbazides and Dialdehydes. *Macromolecules* **2022**, *55* (8), 3267–3275.
(302) Robertson, R. M.; Thomas, W. C.; Suthar, J. N.; Brown, D. M. Accelerated Degradation of Cellulose Acetate Cigarette Filters Using Controlled-Release Acid Catalysis. *Green Chem.* **2012**, *14* (8), 2266–2272.
(303) Allen, N. S.; Edge, M.; Appleyard, J. H.; Jewitt, T. S.; Horie, C. V.; Francis, D. Degradation of Historic Cellulose Triacetate Cinematographic Film: The Vinegar Syndrome. *Polym. Degrad. Stab.* **1987**, *19* (4), 379–387.
(304) Sookne, A. M.; Harris, M. Polymolecularity and Mechanical Properties of Cellulose Acetate. *Ind. Eng. Chem.* **1945**, *37* (5), 478–482.
(305) Sookne, A. M.; Harris, M. *Mechanical Properties of Cellulose Acetate as Related to Molecular Chain Length*; 1943; Vol. 30.
(306) Kamide, K.; Saito, M. Thermal Analysis of Cellulose Acetate Solids with Total Degrees of Substitution of 0.49, 1.75, 2.46, and 2.92. *Polym. J.* **1985**, *17* (8), 919–928.

(307) El Seoud, O. A.; Marson, G. A.; Ciacco, G. T.; Frollini, E. An Efficient, One-Pot Acylation of Cellulose under Homogeneous Reaction Conditions. *Macromol. Chem. Phys.* **2000**, *201* (8), 882–889.
(308) Hanabusa, H.; Izgorodina, E. I.; Suzuki, S.; Takeoka, Y.; Rikukawa, M.; Yoshizawa-Fujita, M. Cellulose-Dissolving Protic Ionic Liquids as Low Cost Catalysts for Direct Transesterification Reactions of Cellulose. *Green Chem.* **2018**, *20* (6), 1412–1422.
(309) King, A. W. T.; Asikkala, J.; Mutikainen, I.; Järvi, P.; Kilpeläinen, I. Distillable Acid-Base Conjugate Ionic Liquids for Cellulose Dissolution and Processing. *Angew. Chemie Int. Ed.* **2011**, *50* (28), 6301–6305.
(310) Onwukamike, K. N.; Grelier, S.; Grau, E.; Cramail, H.; Meier, M. A. R. Critical Review on Sustainable Homogeneous Cellulose Modification: Why Renewability Is Not Enough. *ACS Sustain. Chem. Eng.* **2019**, *7* (2), 1826–1840.
(311) Wolfs, J.; Scheelje, F. C. M.; Matveyeva, O.; Meier, M. A. R. Determination of the Degree of Substitution of Cellulose Esters via ATR-FTIR Spectroscopy. *J. Polym. Sci.* **2023**, No. May, 1–11.
(312) Minnes, R.; Nissinmann, M.; Maizels, Y.; Gerlitz, G.; Katzir, A.; Raichlin, Y. Using Attenuated Total Reflection-Fourier Transform Infra-Red (ATR-FTIR) Spectroscopy to Distinguish between Melanoma Cells with a Different Metastatic Potential. *Sci. Rep.* **2017**, *7* (1), 1–7.
(313) Bauman, R. A. Cis-Trans Isomerism of Thioncarbamate Esters. *J. Org. Chem.* **1967**, *32* (12), 4129–4132.
(314) Tandel, S. K.; Rajappa, S.; Pansare, S. V. Conversion of Thiocarbamates to Carbamates. *Tetrahedron* **1993**, *49* (34), 7479–7486.
(315) Boudebouz, I.; Arrous, S.; Parunov, I. V. Oxidation of Thioamides to Amides with Tetrachloro- and Tetrabromoglycolurils. *Russ. J. Org. Chem.* **2019**, *55* (12), 1874–1877.
(316) Alper, H.; Kwiatkowska, C.; Petrignani, J. F.; Sibtain, F. An Exceptionally Mild, Phase Transfer Catalyzed Method for the Conversion of Thiocarbonyl Compounds to Carbonyls. *Tetrahedron Lett.* **1986**, *27* (45), 5449–5450.
(317) Wu, C.; Cheng, H.; Liu, R.; Wang, Q.; Hao, Y.; Yu, Y.; Zhao, F. Synthesis of Urea Derivatives from Amines and CO2 in the Absence of Catalyst and Solvent. *Green Chem.* **2010**, *12* (10), 1811–1816.
(318) Zhang, G.; Yi, H.; Chen, H.; Bian, C.; Liu, C.; Lei, A. Trisulfur Radical Anion as the Key Intermediate for the Synthesis of Thiophene via the Interaction between Elemental Sulfur and NaO t Bu. *Org. Lett.* **2014**, *16* (23), 6156–6159.
(319) Waibel, K. A.; Barther, D.; Malliaridou, T.; Moatsou, D.; Meier, M. A. R. One-Pot Synthesis of Thiocarbamates. *European J. Org. Chem.* **2021**, *2021* (31), 4508–4516.
(320) Wolfs, J.; Ribca, I.; Meier, M. A. R.; Johansson, M. Polythionourethane Thermoset Synthesis via Activation of Elemental Sulfur in an Efficient Multicomponent Reaction Approach. *ACS Sustain. Chem. Eng.* **2023**, *11* (9), 3952–3962.
(321) Park, C. K.; Lee, J. H.; Kim, I. S.; Kim, S. H. Castor Oil-Based Polyols with Gradually Increasing Functionalities for Biopolyurethane Synthesis. *J. Appl. Polym. Sci.* **2020**, *137* (4), 1–11.
(322) Gurunathan, T.; Mohanty, S.; Nayak, S. K. Isocyanate Terminated Castor Oil-Based Polyurethane Prepolymer: Synthesis and Characterization. *Prog. Org. Coatings* **2015**, *80*, 39–48.

(323) Sardon, H.; Mecerreyes, D.; Basterretxea, A.; Avérous, L.; Jehanno, C. From Lab to Market: Current Strategies for the Production of Biobased Polyols. *ACS Sustain. Chem. Eng.* **2021**, *9* (32), 10664–10677.
(324) Sreenivasan, B.; Kamath, N. R.; Kane, J. G. Studies on Castor Oil. I. Fatty Acid Composition of Castor Oil. *J. Am. Oil Chem. Soc.* **1956**, *33* (2), 61–66.
(325) Nekhavhambe, E.; Mukaya, H. E.; Nkazi, D. B. Development of Castor Oil–Based Polymers: A Review. *J. Adv. Manuf. Process.* **2019**, *1* (4), 1–13.
(326) Yeganeh, H.; Hojati-Talemi, P. Preparation and Properties of Novel Biodegradable Polyurethane Networks Based on Castor Oil and Poly(Ethylene Glycol). *Polym. Degrad. Stab.* **2007**, *92* (3), 480–489.
(327) Waibel, K. A.; Nickisch, R.; Möhl, N.; Seim, R.; Meier, M. A. R. A More Sustainable and Highly Practicable Synthesis of Aliphatic Isocyanides. *Green Chem.* **2020**, *22* (3), 933–941.
(328) Taguchi, Y.; Yasumoto, M.; Tsuchiya, T.; Oishi, A.; Shibuya, I. A Novel Synthesis of 1,3,5-Triazine Derivative under High Pressure. *Chem. Lett.* **1993**, *22* (7), 1097–1100.
(329) Taguchi, Y.; Yasumoto, M.; Tsuchiya, T.; Shibuya, I.; Yonemoto, K. The Trimerization of Isothiocyanates under High Pressure. *Nippon Kagaku Kaishi* **1992**, *1992* (4), 383–387.
(330) Wu, L.; Glebe, U.; Böker, A. Synthesis of Hybrid Silica Nanoparticles Densely Grafted with Thermo and PH Dual-Responsive Brushes via Surface-Initiated ATRP. *Macromolecules* **2016**, *49* (24), 9586–9596.
(331) Waibel, K. A.; Barther, D.; Malliaridou, T.; Moatsou, D.; Meier, M. A. R. One-Pot Synthesis of Thiocarbamates. *European J. Org. Chem.* **2021**, *2021* (31), 4508–4516.
(332) Echeverri, D. A.; Jaramillo, F.; Rios, L. A. Curing Copolymerization Kinetics of Styrene with Maleated Castor Oil Glycerides Obtained from Biodiesel-Derived Crude Glycerol. *J. Appl. Polym. Sci.* **2015**, *132* (4), 1–9.
(333) Gough, L. J.; Smith, I. T. A Gel Point Method for the Estimation of Overall Apparent Activation Energies of Polymerization. *J. Appl. Polym. Sci.* **1960**, *3* (9), 362–364.
(334) Flory, P. J. *Principles of Polymer Chemistry*; Cornell University Press: New York, 1953.
(335) Cao, S.; Li, S.; Li, M.; Xu, L.; Ding, H.; Xia, J.; Zhang, M.; Huang, K. A Thermal Self-Healing Polyurethane Thermoset Based on Phenolic Urethane. *Polym. J.* **2017**, *49* (11), 775–781.
(336) Kanbur, Y.; Tayfun, U. Development of Multifunctional Polyurethane Elastomer Composites Containing Fullerene: Mechanical, Damping, Thermal, and Flammability Behaviors. *J. Elastomers Plast.* **2019**, *51* (3), 262–279.
(337) Swartz, J. L.; Sheppard, D. T.; Haugstad, G.; Dichtel, W. R. Blending Polyurethane Thermosets Using Dynamic Urethane Exchange. *Macromolecules* **2021**, *54* (23), 11126–11133.
(338) Li, J.; Guo, X.; Wang, L.; Ma, X.; Zhang, Q.; Shi, F.; Deng, Y. Co(Acac)3/BMMImCl as a Base-Free Catalyst System for Clean Syntheses of N,N′-Disubstituted Ureas from Amines and CO2. *Sci. China Chem.* **2010**, *53* (7), 1534–1540.
(339) Barison, A.; Pereira da Silva, C. W.; Campos, F. R.; Simonelli, F.; Lenz, C. A.; Ferreira, A. G. A Simple Methodology for the Determination of Fatty Acid Composition in Edible Oils through 1H NMR Spectroscopy. *Magn. Reson. Chem.*

2010, *48* (8), 642–650.